

LEVEL

40  
2

AGARD-LS-97

AGARD-LS-97

**AGARD**

ADVISORY GROUP FOR AEROSPACE RESEARCH & DEVELOPMENT

7 RUE ANCELLE 92200 NEUILLY SUR SEINE FRANCE

AGARD LECTURE SERIES No. 97

**Fracture Mechanics Design  
Methodology**

This document has been approved  
for public release and sale; its  
distribution is unlimited.

DDC  
DECEMBER  
APR 4 1979  
MUSULI

NORTH ATLANTIC TREATY ORGANIZATION



DISTRIBUTION AND AVAILABILITY  
ON BACK COVER

79 04 03 050

LS 97

FRACTURE MECHANICS DESIGN METHODOLOGY

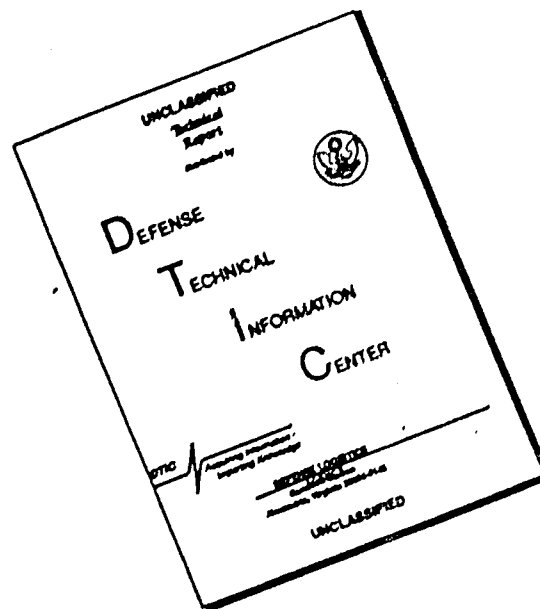
AD A0 66808

DDC FILE COPY



SMP/DPP

# DISCLAIMER NOTICE



THIS DOCUMENT IS BEST QUALITY AVAILABLE. THE COPY FURNISHED TO DTIC CONTAINED A SIGNIFICANT NUMBER OF PAGES WHICH DO NOT REPRODUCE LEGIBLY.



(2)

14  
AGARD-LS-97

NORTH ATLANTIC TREATY ORGANIZATION  
ADVISORY GROUP FOR AEROSPACE RESEARCH AND DEVELOPMENT  
(ORGANISATION DU TRAITE DE L'ATLANTIQUE NORD)

6 AGARD Lecture Series No.97  
FRACTURE MECHANICS DESIGN METHODOLOGY.

11 1979  
12 242p.

DDC  
APR 4 1979  
R  
C

The material in this publication was assembled to support a Lecture Series under the sponsorship of the Structures and Materials Panel and the Consultant and Exchange Programme of AGARD, presented on 5-6 October 1978 in Delft, The Netherlands, 9-10 October 1978 in München, Germany, and 12-13 October 1978 in Sacavem, Portugal.

400049 01 00 050 13

## THE MISSION OF AGARD

The mission of AGARD is to bring together the leading personalities of the NATO nations in the fields of science and technology relating to aerospace for the following purposes:

- Exchanging of scientific and technical information;
- Continuously stimulating advances in the aerospace sciences relevant to strengthening the common defence posture;
- Improving the co-operation among member nations in aerospace research and development;
- Providing scientific and technical advice and assistance to the North Atlantic Military Committee in the field of aerospace research and development;
- Rendering scientific and technical assistance, as requested, to other NATO bodies and to member nations in connection with research and development problems in the aerospace field;
- Providing assistance to member nations for the purpose of increasing their scientific and technical potential;
- Recommending effective ways for the member nations to use their research and development capabilities for the common benefit of the NATO community.

The highest authority within AGARD is the National Delegates Board consisting of officially appointed senior representatives from each member nation. The mission of AGARD is carried out through the Panels which are composed of experts appointed by the National Delegates, the Consultant and Exchange Programme and the Aerospace Applications Studies Programme. The results of AGARD work are reported to the member nations and the NATO Authorities through the AGARD series of publications of which this is one.

Participation in AGARD activities is by invitation only and is normally limited to citizens of the NATO nations.

A large part of the content of this publication has been reproduced directly from material supplied by AGARD or the authors; the remainder has been set by Technical Editing & Reproduction Ltd.

Published January 1979

Copyright © AGARD 1979  
All Rights Reserved

ISBN 92-835-1294-4



Printed by Technical Editing and Reproduction Ltd  
Harford House, 7-9 Charlotte St, London, W1P 1HD

## PREFACE

This lecture series presents a review of the state of the art of damage tolerance analysis of airplanes. It shows that damage tolerance and fail safety assessment are out of the stage that tests were the only means to get answers to the pertinent questions regarding crack growth and residual strength. It also shows that tests are still indispensable, so that the question can be raised what has been gained by the development of analysis procedures.

Tests only give information for a few specific areas: e.g., in a full scale test only one representative spectrum and load history are applied and only a limited number of critical locations can be evaluated. Analysis provides the means to evaluate spectrum variations, different airplane usage, other critical locations, and most important, design alternatives.

Analysis still has shortcomings, but many of these apply equally much to experiments insomuch as the reliability of test data and analysis results depend largely upon spectrum evaluation, flight load analysis, stress history, etc. Other shortcomings of the analysis can be largely overcome by using the tests to adjust predictions of crack growth and residual strength.

Every engineer who has been actively involved in damage tolerance analysis of real airplane structures, has experienced that possible inaccuracies in the results of the analysis are generally due more to assumptions and approximations used to generate input information than to shortcomings of fracture mechanics procedures. Further improvement of fracture mechanics methods will not significantly alter this situation. Therefore, there is no justification for the further postponement of damage tolerance analysis.

The compilation of this Lecture Series was only possible through the co-operation of my three fellow lecturers — Mr T.Swift, Dr W.Schütz and especially Prof. D.P.Wilhem who kindly agreed to participate at very short notice.

DAVID BROEK  
Lecture Series Director  
Columbus, 1978

ACCESSION for	
NTIS	Section <input checked="" type="checkbox"/>
DOC	Section <input type="checkbox"/>
UNANNOUNCED	<input type="checkbox"/>
DATE	
BY	
DISTRIBUTION/AVAILABILITY CODES	
Di	or SPECIAL
A	

## LIST OF SPEAKERS

Lecture Series Director: Dr D. Broek  
Section 626  
Battelle Memorial Institute  
505 King Avenue  
Columbus  
Ohio 43201  
USA

Dr W. Schütz  
Industrie Anlagen Betriebs Gesellschaft, IABG  
Einsteinstrasse  
9012 Ottobrun bei München  
Germany

Mr T. Swift  
Douglas Aircraft Company  
Structural Mechanics Subdivision  
McDonnell Douglas Corporation  
Long Beach  
California 90801  
USA

Dr D.P. Wilhem  
Northrop Corporation,  
*Aircraft Group*  
3901 West Broadway  
Hawthorne  
California 90250  
USA



## CONTENTS

	Page
PREFACE	iii
LIST OF SPEAKERS	iv
	Reference
 <u>SESSION I: PRINCIPLES</u>	
INTRODUCTION TO FRACTURE MECHANICS by D.Broek	1
FRACTURE by D.Broek	2
FATIGUE CRACK GROWTH by W.Schütz	3
 <u>SESSION II: DAMAGE TOLERANCE ANALYSIS</u>	
STRESS INTENSITY ANALYSIS: ANALYTICAL, FINITE ELEMENT FOR SURFACE FLAWS, HOLES by D.P.Wilhem	4
DAMAGE TOLERANCE ANALYSIS OF REDUNDANT STRUCTURES by T.Swift	5
FATIGUE CRACK GROWTH ANALYSIS by D.Broek	6
 <u>SESSION III: DAMAGE TOLERANCE DESIGN</u>	
DESIGN OF HEAVY SECTIONS by W.Schütz	7
TREATMENT OF SCATTER OF FRACTURE TOUGHNESS DATA FOR DESIGN PURPOSES by W.Schütz	8
DESIGN OF REDUNDANT STRUCTURES by T.Swift	9
ANALYSIS OF AIRCRAFT STRUCTURE USING APPLIED FRACTURE MECHANICS by D.P.Wilhem	10
DAMAGE TOLERANCE IN PRACTICE by D.Broek	11
BIBLIOGRAPHY	B

**SESSION I**

**PRINCIPLES**



## INTRODUCTION TO FRACTURE MECHANICS

David Broek  
Battelle's Columbus Laboratories  
505 King Avenue  
Columbus, Ohio 43201

### 1. INTRODUCTION

Fatigue loading of aircraft structures may eventually lead to the development of cracks. Provisions for fail safety and damage tolerance are intended to ensure safe operation in the event that cracks do occur. Thus, these provisions require an analysis of the growth of cracks and of the consequences of cracks for the strength of the structure. The fracture control plan includes the scheduling of inspections, repairs, and retirement, based on predictions of crack growth and fracture, made possible by recent developments in the mechanics of cracks. The fracture control plan permits operational management decisions on usage, repair, and replacement to provide the lowest failure risk at the lowest cost.

The basis for the damage tolerance analysis is the mathematics to compute and predict the behavior of flaws and cracks which is called FRACTURE MECHANICS. The discipline of fracture mechanics was developed during the last 20 years. It enables quantitative predictions that were hitherto impossible.

Catastrophic failures of T-2 tankers and Liberty-ships during World War II and many ship failures thereafter instigated extensive research into the problem of brittle fracture. Some basic concepts of present-day fracture mechanics stem from this work. Later, the failure of missiles and aircraft (in particular the Comet accidents) gave a new boost to fracture research in the late 50's and early 60's. New concepts of fatigue analysis and fracture were established and refined. The hazard of potential failures in the nuclear industry was a stimulus for the extension of these concepts to structural steels during the last decade. New developments will be seen in the future, but present day technology is ready for cautious application.

Although far from complete, fracture mechanics now offers quantitative solutions to many crack growth and fracture problems that could not be handled a decade ago. Several areas require further refinements, but many of the limitations of the technology are due to engineering judgments associated with any technical design procedure. The application to a new area of technology usually requires some development of specific data and techniques, but most of the principles are available for use by knowledgeable engineers.

Advocates of fracture mechanics encounter much skepticism. The three main reasons for this are believed to be

- Shortcomings and limitations of the procedure
- The lack of long-time experience showing that the method has resulted in safer structures and lower failure risk at reasonable cost
- The psychological threshold to apply new methods.

The shortcomings and limitations of fracture mechanics, which are dealt with in detail in this Lecture Series, are in many instances quantifiable, so that safety factors can be taken appropriately. But even if some parts are not ideal, the method can give information that cannot be obtained otherwise. In the hands of a knowledgeable engineer the method is a useful tool.

Probably the most important difficulty in the application of fracture mechanics is the variability of the relevant material properties. However, this can hardly be considered a deficiency of the methodology. If crack growth properties can vary by a factor of two, a prediction of crack growth may later appear to be a factor of two in error. It is unjust to blame this on the predictive method, since it is due to erratic material behavior. The theory of elasticity is considered very sophisticated; however, its accurate predictions of stresses and strains are by virtue of the fact that the elastic modulus of most materials is practically invariant. If the modulus would generally vary by a factor of two, even the theory of elasticity would have serious limitations. Further developments and refinements in fracture mechanics will not greatly alter the situation, because material variability will remain. The method can give useful answers now or later. However, safety factors will have to be used.

The two other reasons for skepticism (the lack of experience and the psychological threshold) are strongly related. Engineers have no reservations to use a simple bending formula to predict bending strength, because experience with many structures during the last century has shown that adequate answers are obtained. Despite the adequacy of static strength design procedures many structures have failed unexpectedly, but this was due to flaws and cracks and inadequate detail designs. It is this hazard that can be substantially reduced by using fracture mechanics. Naturally, there will be reluctance to rely fully on the answers, but if the method is not applied, the necessary experience will never be obtained. Cautious application will gradually build experience and more adequate safety factors can be established.

Despite sophisticated stress analysis techniques and a wealth of past experience with static strength design methods, no engineer has the confidence that the static strength of a complex structure can be calculated to a great accuracy. Where full scale static strength experiments are carried out, a difference of 10 percent between predicted and actual strength is not considered surprising. For this reason safety factors are necessary, but not for this reason alone. Substantial safety factors are applied because of unknowns in loading and environmental conditions. Thus, conventional methods do not have a large advantage over the new fracture mechanics procedures.

In conclusion, it can be stated that fracture mechanics is almost as good a tool as it will ever be. Further developments and refinements are welcome, but what is available is ready for cautious application. The method provides information that cannot be obtained otherwise; safety factors are necessary, but this the method has in common with all other design procedures.

This Lecture Series will provide an overview of the state of the art of the application of fracture mechanics to fail safety and damage tolerance analysis of airplane structures. In order to facilitate understanding, the first few lectures will present a brief review of the most elementary principles of fracture mechanics. Since many participants are already somewhat familiar with these principles, the review will only touch upon the most essential details. For a more extensive treatise a textbook<sup>(1)</sup> is recommended.

## 2. MECHANICS OF CRACKS

### 2.1. The Stress Intensity Factor

A crack in a solid can be stressed in three different modes, denoted Modes I, II, and III, as depicted in Figure 1. Superposition of the three modes constitutes the general case of crack loading. Mode I is technically the most important. Cracks in some aircraft structural parts are subjected to combinations of Modes I and II, or Modes I and III. Because of its technical significance, Mode I will be assumed throughout the discussions.

Taking a coordinate system as in Figure 2, the stresses at the crack tip can be calculated<sup>(1-5)</sup> by conventional theory of elasticity as

$$\sigma_{ij} = A_1 \left(\frac{r}{a}\right)^{-\frac{1}{2}} f_{1ij}(\theta) + A_2 \left(\frac{r}{a}\right)^0 f_{2ij}(\theta) + A_3 \left(\frac{r}{a}\right)^{\frac{1}{2}} f_{3ij}(\theta) + \dots \quad (1)$$

where  $a$  denotes the crack size. In the vicinity of the crack tip, the first term in Equation (1) dominates because of the singularity. The non-singular terms then can be neglected, leading to

$$\sigma_{ij} = A_1 \sqrt{\frac{a}{r}} f_{ij}(\theta) = \frac{K_I}{\sqrt{2\pi r}} f_{ij}(\theta) \quad (2)$$

The parameter  $K_I$  is called the STRESS-INTENSITY FACTOR. It is a measure of the strength of the crack-tip-stress singularity. The subscript I stands for Mode I. Similar expressions can be derived for Modes II and III.

For the Mode I case, the crack tip stresses can be developed from Equation (2) as:

$$\begin{aligned} \sigma_c &= \frac{K_I}{\sqrt{2\pi r}} \cos \frac{\theta}{2} \left[ 1 - \sin^2 \frac{3\theta}{2} \right] , \\ \sigma_y &= \frac{K_I}{\sqrt{2\pi r}} \cos \frac{\theta}{2} \left[ 1 + \sin^2 \frac{3\theta}{2} \right] , \\ \sigma_z &= 0 \text{ (plane stress) or } \sigma_z = \nu(\sigma_u + \sigma_y) \text{ (plane strain)} , \\ \tau_{xy} &= \frac{K_I}{\sqrt{2\pi r}} \sin \frac{\theta}{2} \cos \frac{\theta}{2} \cos \frac{3\theta}{2} , \end{aligned} \quad (3)$$

and

$$\tau_{xz} = \tau_{yz} = 0 .$$

The stresses for any Mode I case can be calculated by substituting the appropriate expression for  $K_I$ . The solution to a crack tip problem is in finding an expression for  $K_I$ . For any Mode I problem  $K_I$  can ALWAYS be written as:

$$K_I = \beta \sigma \sqrt{\pi a} \quad (4)$$

so that the solution really amounts to finding an expression for  $\beta$ , which is a nondimensional function of crack size and structural geometry. The stress  $\sigma$  in Equation (4) is the remote stress. For a small central crack of size  $2a$  in a plate remotely loaded by a tensile stress  $\sigma$ , the factor  $\beta = 1$ , so that:

$$K_I = \sigma \sqrt{\pi a} \quad (5)$$

However, if the crack is not small compared to the width  $W$  of the plate, the stress intensity is given<sup>(6)</sup> as:

$$K_I = \sigma \sqrt{\pi a} \sqrt{\sec \frac{\pi a}{W}} \quad (6)$$

Handbooks<sup>(7-9)</sup> provide expressions for  $\beta$  for many standard crack cases. In its usual form, the function is a series expression.

### 2.2. The Parameter for Crack Growth and Fracture

The stress field given by Equation (3) depends upon the distance  $r$  and the angle  $\theta$  in the same way for all cracks. Thus, the stress field is governed completely by the stress intensity factor,  $K_I$ . The equation shows that two different cracks in the same material subjected to the same stress intensity have exactly identical crack-tip stress fields. If the stress fields are equal, the two cracks will show the same

behavior if their stress intensities are equal. They will grow at equal rate and they are equally liable to cause a failure. Thus the stress intensity seems to be the governing parameter for crack growth and fracture. However, the elastic stress field solutions show a stress singularity at the crack tip, which implies that the stresses at the crack tip will always be infinite. Since structural materials deform plastically above the yield stress, there will be a plastic zone at the crack tip. As a consequence, the elastic solutions are not unconditionally applicable.

A rough guess of the magnitude of the plastic zone easily can be made. The elastic stress in the Y-direction along  $\theta = 0$ , is given as [see Equation (3)]

$$\sigma_y = \frac{K}{\sqrt{2\pi r}}; \text{ For center crack: } \sigma_y = \frac{\alpha\sqrt{\pi a}}{\sqrt{2\pi r}} \quad (7)$$

This stress distribution is shown diagrammatically in Figure 3. It is assumed that nowhere can the stress be higher than the yield stress,  $\sigma_{ys}$ . The distance from the crack tip,  $r_p$ , to which the elastic stresses are above yield is found by substituting  $\sigma_y = \sigma_{ys}$  in Equation (16),

$$\sigma_{ys} = \frac{\alpha\sqrt{\pi a}}{\sqrt{2\pi r_p}} \quad \text{or} \quad r_p = \frac{\sigma^2 a}{2\sigma_{ys}^2} = \frac{K^2}{2\pi\sigma_{ys}^2} = \frac{K^2}{\alpha\sigma_{ys}^2} \quad (8)$$

More accurate calculations of the size and shape of the plastic zone have been made<sup>(1)</sup>, however if the plastic zone is small with respect to the crack size Equation (8) is still valid with a constant  $\alpha$  in the denominator.

When the applied stress is half the yield stress and  $\alpha = 2\pi$ , the plastic zone size,  $r_p$  is  $0.125a$ . As long as the plastic zone is small compared to the crack size, the stress distribution will be affected only slightly by the plastic zone. Particularly, the stress distribution outside the plastic zone is still governed by  $K$ . Since the same  $K$  always gives rise to the same plastic zone size [Equation (7)], the stresses and strains inside the plastic zone will be a direct function of the stress intensity factor. Hence,  $K$  still can be used.

Since  $K$  determines the entire crack tip stress field and the plastic zone if small, it must be the governing parameter, not only for fracture, but also for other crack growth processes. The rate of fatigue crack propagation under cyclic load applications as well as the rate of stress corrosion cracking are a function of  $K$ . The higher the stress intensity, the higher is the rate of crack growth. Thus, crack growth and fracture are determined by the same stress field parameter. Hence, all damage tolerance calculations can conveniently be based on the stress intensity factor.

### 2.3. Plane Stress and Plane Strain

According to Equation (3), the state of stress at the crack tip is at least biaxial, which is plane stress. In that case, the stress  $\sigma_z$  in thickness direction is zero. The stresses  $\sigma_x$  and  $\sigma_y$  at the crack tip are extremely high, much more so than in the rest of the plate. Thus the material at the crack tip wants to undergo more Poisson's contraction than the rest of the plate: There is a tendency to the formation of a dimple in the plate surface at the crack tip, as shown in Figure 4. If the plate is thick, this contraction will be constrained by the surrounding material that undergoes less contraction. Clearly, the constraint will be larger if the required displacements are larger (i.e., if the plate is thicker).

In the ultimate case, the contraction is fully constrained (i.e., the strain in the thickness direction is zero). This means that there will be a stress acting in the thickness direction, given by (see also Equation (3))

$$E_z = \sigma_z/E - \nu(\sigma_x + \sigma_y)/E = 0 \quad \text{or} \quad \sigma_z = \nu(\sigma_x + \sigma_y) \quad (9)$$

which represents a condition of plane strain. Since the thickness of the plate governs the constraint, there is a tendency for a change from plane stress to plane strain when going to thicker plates.

It can easily be shown that the state of stress affects the plastic zone size, plane strain being associated with a smaller plastic zone than plane stress. At the same time, the size of the plastic zone largely affects the state of stress. The material in the plastic zone wants to contract in thickness direction, more than in the elastic case, because of the condition of constant volume during plastic flow. When the plastic zone is large compared with the plate thickness, yielding in the thickness direction can take place freely. This promotes plane stress. If the plastic zone is small compared with the thickness, yielding in the thickness direction will be constrained. As a result, a small plastic zone is under plane strain. Plane stress can develop when the plastic zone is of the order of the plate thickness.

When two plates of equal thickness but with the same size of crack, are loaded to a different stress, the one with the highest stress exhibits the larger plastic zone. The latter may be in plane stress and the other in plane strain. Apparently, at low stresses, even a fairly thin plate may show plane strain behavior. If two plates of unequal thickness but with the same size of crack are loaded to the same stress they can both be in plane strain. In that case, they will have equal plastic zones (same  $K$ ). With further increase of the stress, the plastic zone will grow in size. When it attains a size of the order of the thickness of the thinner plate, the latter will turn into plane stress. This implies that its plastic zone will grow further to the plane stress size.

The surface of a plate always will be in plane stress because a stress perpendicular to the free surface cannot exist. As a result, the plastic zone at the surface always will be larger than in the interior of the plate if the interior is in plane strain. This is depicted in Figure 5.



If the plate is very thick, the plane strain region in the interior will be large with respect to the plane-stress surface regions. Thus plane strain behavior dominates. As a general rule, this is the case when the (plane strain) plastic zone is only about 2 percent of the plate thickness. The plastic zone size can be expressed in terms of  $K$ . For plane strain, it is approximately  $K^2/6\sigma_{ys}^2$ . Hence, the plane strain condition is that  $B \geq 2.5K^2/\sigma_{ys}^2$ , where  $B$  is the plate thickness.

Increase of the stress increases the plastic zone size. Full plane stress can develop when the plastic zone size is on the order of the plate thickness (i.e.,  $B \approx \alpha K^2/\sigma_{ys}^2$ , where  $\alpha$  is on the order of 0.1 - 0.2). Between these two thickness conditions, there will be a gradual transition from full plane strain to full plane stress.

The above criteria for the state of stress are not applicable to cracks with a curved front (i.e., corner cracks and surface flaws). The curvature maintains a stress tangential to the crack front. As a result, the greater part of the crack front is always in plane strain.

### 3. TOUGHNESS AND RESIDUAL STRENGTH

It was concluded in Section 2.2 that  $K$  governs the fracture behavior of a cracked body. Fracture will occur when the stresses and strain reach a critical state, described by  $K$ . This implies that fracture takes place if  $K$  exceeds a critical value. The critical  $K$  for fracture is denoted as  $K_{IC}$  for plane strain conditions and  $K_{IC}$  or  $K_c$  for plane stress conditions. Within the limitations discussed in subsequent sections,  $K_{IC}$  and  $K_{IC}$  can be considered a material property called fracture toughness (with adjectives plane strain or plane stress, respectively). They can be determined by experiment.

One can take a large, thick plate with a small crack of known size  $a$ , fracture the specimen in a testing machine and measure the stress  $\sigma$  at which it fails. Then Equation (5) can be used to calculate the stress intensity at failure  $K_{IC}$ . As an example, suppose the size of the crack is 50 mm and the specimen fails at a stress of 12 kg/mm<sup>2</sup>. The strain intensity at failure follows from  $K_{IC} = 12 \times \sqrt{25\pi} = 106$  kg/mm<sup>3/2</sup>. Other cracks in the same material will also cause fracture if  $K = K_{IC} = 30$  ksi/in. The unit of  $K_{IC}$  is somewhat unusual, but it follows directly from the multiplication of stress and square root of crack size. In a strength analysis the fracture toughness would be analogous to the ultimate tensile strength,  $\sigma_u$ , of the material ( $\sigma_u$  is the value of the stress  $\sigma$  at failure,  $K_{IC}$  is the value of the stress intensity  $K_I$  at failure).

The fracture toughness found in the above example would be typical for a high-strength aluminum alloy with an ultimate tensile strength of the order of 50 kg/mm<sup>2</sup>. Apparently, an undamaged structure made out of this material would fail at a stress of 50 kg/mm<sup>2</sup>. If the structure would contain a crack of 10 mm, the failure stress would be much lower. Since the fracture toughness is 106 kg/mm<sup>3/2</sup>, the stress at failure is

$$\sigma = \frac{106}{\sqrt{5\pi}} = 27 \text{ kg/mm}^2$$

The presence of a 10 mm crack has reduced the strength of the structure by almost a factor of two. This failure stress under the presence of cracks is called the RESIDUAL STRENGTH.

If the structure is normally loaded to a stress of 15 kg/mm<sup>2</sup>, it follows that it may contain a crack of a size

$$2a = \frac{2}{\pi} \left( \frac{106}{15} \right)^2 = 32 \text{ mm}$$

This is called the CRITICAL CRACK SIZE at the given stress.

A high strength steel with an ultimate tensile strength of 180 kg/mm<sup>2</sup> would have a fracture toughness of the order of 150 kg/mm<sup>3/2</sup>. Under the presence of a 32 mm long crack the residual strength would be

$$\sigma = \frac{150}{\sqrt{\pi \times 16}} = 21 \text{ kg/mm}^2$$

which is only about 10 percent of the original strength.

Experiments to measure the plane strain fracture toughness of a material are usually carried out in accordance with the specification<sup>(10-12)</sup> for such tests issued by the American Society for Testing and Materials (ASTM). Compliance with this standard will ensure that plane strain conditions are met, so that valid  $K_{IC}$  data are obtained.

The plane strain fracture toughness of a material depends strongly upon yield strength, for most alloy systems. Variations in toughness also occur as a result of anisotropy. Usually there are appreciable differences in toughness for different crack directions. The toughness in the short transverse direction is always the lowest. For an aluminum-zinc-magnesium alloy, toughness values are reported<sup>(13)</sup> of 36 ksi/in., 19 ksi/in., and 15 ksi/in. for the longitudinal, transverse, and short transverse direction, respectively. Data for many aerospace materials can be found in the Damage Tolerance Data Handbook<sup>(14)</sup>.

As shown above, the residual strength can be calculated for any crack size, given the fracture toughness of the material. The residual strength can be plotted as a function of crack size in a residual strength diagram, as shown in Figure 6. This diagram further illustrates the rapid decay of residual strength for materials with low toughness.

The above equations predict that the residual strength goes to infinity if the crack size approaches zero. Obviously, the strength of the material at zero crack size is limited by the yield or tensile strength.

The discrepancy is a result of the fact that the above equations are based on elasticity considerations. Therefore, they should not be applied when the stresses are higher than the yield stress of the material. This need not be a severe limitation since aircraft operational stresses are generally lower than the yield stress and there exist ways to handle the case of very small cracks in low-toughness materials in a satisfactory way, (1,6) as will appear later in this Lecture Series.

#### 4. SUBCRITICAL CRACK GROWTH

In the previous sections it was shown how to deal with fracture caused by cracks that have reached the critical size. The following sections will consider the problem of how cracks reach the critical size and after what period of time. The growth of very small material defects and machining or welding defects into cracks and the further growth of these cracks until imminent fracture is called SUBCRITICAL CRACK GROWTH. The two prevalent mechanisms by which subcritical crack growth takes place are fatigue crack propagation and stress corrosion cracking.

Since the stress intensity factor governs the stress field at the crack tip, it is the decisive factor for the behavior of the crack. Thus, if two cracks in the same material are subjected to the same stress intensity, they will show the same rate of fatigue crack growth. (This statement is not formulated precisely enough as will be shown in Lecture 3.) Since most of the subcritical crack growth takes place at stress intensity factors far below the critical stress intensity (fracture toughness), the plastic zone sizes are generally very small.

Consider a crack in a structure or specimen that is subjected to a remote stress that cyclically varies between zero and certain maximum (i.e., constant amplitude with a lower stress equal to zero), so that the range of stress variation is  $\Delta\sigma$ . Recalling the equation for the stress intensity factor  $K = \sigma\sqrt{\pi a}$ , it follows that the stress intensity is zero when the stress is zero, and that during cyclic loading the stress intensity varies over a range  $\Delta K$  as

$$\Delta K = \Delta\sigma \sqrt{\pi a} \quad (10)$$

The rate of fatigue propagation is defined as the crack extension,  $\Delta a$ , during a small number of cycles,  $\Delta N$ , i.e., the rate of propagation is  $\Delta a/\Delta N$ . In the limit this rate of growth can be written as a differential  $da/dN$ , and the rate is given in inches/cycle.

The rate of fatigue crack propagation is governed by the stress intensity. The larger the cyclic range,  $\Delta K$ , the larger the growth rate  $da/dN$ . Apparently, the growth rate will be some function of  $\Delta K$ :

$$\frac{da}{dN} = f(\Delta K) \quad (11)$$

Many attempts have been made to predict  $f(\Delta K)$  on the basis of theoretical arguments. In practice  $f(\Delta K)$  is determined empirically, by simply measuring the rate of growth in a test. To this end a cracked specimen is cyclically loaded in a fatigue machine and the length of the growing crack is measured periodically. This enables calculation of the growth rate  $da/dN$  by taking the crack growth increment for a certain number of cycles and dividing. Since the crack size is known as well as the stress range  $\Delta\sigma$ , the range  $\Delta K$  can be calculated. Then  $da/dN$  can be plotted versus  $\Delta K$  in a growth rate diagram such as Figure 7. The plot is usually made on double-logarithmic paper.

In itself this plot does not prove that  $da/dN$  is a unique function of  $\Delta K$ . This proof can only be obtained if specimens tested under different stress ranges and of different configurations all give the same results, which would mean that two specimens with different cracks and cycled at different stress levels, but with the same  $\Delta K$ , exhibit the same rate of growth. This is what appears to be the case.

Stress corrosion cracking is governed also by the stress-intensity factor. The rate of growth of a stress corrosion crack as a function of time,  $da/dt$ , in a certain corrosive environment is a function of the stress intensity,

$$\frac{da}{dt} = f(K) \quad (12)$$

As in the case of fatigue crack propagation  $f(K)$  has to be established empirically (Figure 8).

As a consequence of the above equation, the time to failure depends upon the initial value of  $K$ . If a number of similar cracked specimens are loaded to different stresses (different initial  $K$ ), the times to failure will vary as shown in Figure 9. If the stress intensity is below a certain threshold, usually denoted by  $K_{IScc}$ , the crack growth rate is zero and failure does not occur. If the initial  $K$  is larger than  $K_{IScc}$ , the crack will grow thus increasing  $K$ . This in turn causes a higher growth rate, and so on, until  $K$  reaches  $K_{IC}$ . At that point, the stress intensity becomes equal to the fracture toughness and failure occurs.

In principle, the above relations permit a prediction of the time to failure for a structural crack. In practice, a design will usually be aimed at prevention of stress corrosion cracking. It should then be assured that the stress intensity remains below  $K_{IScc}$ .

#### 5. ENERGY RELEASE RATE

A sometimes useful alternative to the stress-intensity concept is the energy criterion for fracture. Basically, it states that a crack can propagate if sufficient energy is made available to supply the work required for cracking. The condition for crack growth is

$$\frac{d}{da} (F - U) = \frac{dW}{da} \quad (13)$$

where  $U$  is the elastic energy contained in the plate,  $F$  is the work done by the external force,  $W$  is the energy for crack formation, and  $a$  is the crack size. Usually,  $d/da (F - U)$  is called the energy release rate, denoted by  $G$ . The term at the right hand side of the equation is called the crack resistance,  $R$ . Then Equation (13) becomes

$$G = R \quad (14)$$

Both  $G$  and  $R$  are based on unit thickness.

Consider a cracked plate of thickness  $B$  under a load  $P$ . The load application points undergo a relative displacement,  $v$ . When the crack increases in size by  $da$ , the displacement will increase by  $dv$  (the stiffness decreases with increasing crack size). Hence, the work done by the external force is  $Pdv$ . It follows that

$$G = \frac{d}{da} (F - U) = \frac{1}{B} \left( P \frac{dv}{da} - \frac{dU}{da} \right) \quad (15)$$

As long as there is no crack growth, the displacement is proportional to load:  $v = CP$ . Here  $C$  is the compliance of the plate. The elastic energy is given by

$$U = \frac{1}{2} P v = \frac{1}{2} C P^2 \quad (16)$$

Then  $G$  can be further evaluated as

$$G = \frac{1}{B} \left( P^2 \frac{\partial C}{\partial a} + C P \frac{dP}{da} - \frac{1}{2} P^2 \frac{\partial C}{\partial a} - C P \frac{dP}{da} \right) = \frac{P^2}{2B} \frac{\partial C}{\partial a} \quad (17)$$

The terms with  $dP/da$  cancel. Thus,  $G$  is independent of whether or not the load is constant. From a comparison of Equations (16) and (17), it follows that

$$G = \frac{1}{B} \left( \frac{dU}{da} \right)_v \quad (18)$$

Hence, the energy release rate is equal to the reduction in strain energy in the case of crack propagation at constant displacement.

It follows that the energy release rate can be determined from the compliance or from the elastic energy. Thus calculated, it appears that for a center-cracked plate in plane strain:

$$G = \frac{\pi \sigma_c^2 a}{E} (1 - \nu^2) \quad (19)$$

Hence, the fracture condition of Equation (14) becomes

$$\sigma_c = \sqrt{\pi a_c} = \sqrt{ER} \quad (20)$$

Note that this equation is equivalent to  $K = K_{IC}$ , with  $K_{IC} = \sqrt{ER}$ . Apparently, the stress-intensity concept and the energy concept lead to the same result.

It follows from Equation (19) that  $G = (1 - \nu^2) K^2/E$ , which can be shown in many ways<sup>(1)</sup> to be generally true. For plane stress  $G = K^2/E$ . This provides a means to determine the stress-intensity factor from the compliance or the strain energy by Equations (17) and (18),

$$K = P \sqrt{\frac{E}{2B} \frac{\partial C}{\partial a}} = \sqrt{\frac{E}{B} \left( \frac{dU}{da} \right)_v} \quad (21)$$

This provides a basis to derive  $K$  from a finite element analysis or from an experiment. For example, the compliance of a plate can be measured by measuring  $v$  as a function of  $P$  for various crack sizes. This permits determination of  $C = v/P$ . Differentiation to  $a$  and use of Equation (21) provides  $K$ .



## 6. REFERENCES

1. Broek, D., Elementary Engineering Fracture Mechanics, Noordhoff, Leyden Holland (1974).
2. Paris, P. C., and Sih, G. C., "Stress Analysis of Cracks", ASTM STP 381 (1965) pp 30-81.
3. Rice, G. R., "Mathematical Analysis in Mechanics of Fracture", Fracture II, H. Liebowitz, Ed., Academic Press (1969) pp 192-308.
4. Goodier, J. N., "Mathematical Theory of Equilibrium of Cracks", Fracture II, H. Liebowitz, Ed., Academic Press (1969) pp 2-67.
5. Mushkelishvili, N. I., Some Basic Problems of the Mathematical Theory of Elasticity, (1933) English Translation, Noordhoff (1953).
6. Feddersen, C. E., "Discussion", ASTM STP 410 (1967) pp 77-79.
7. Tada, H., Paris, P. C., and Irwin, G. R., "The Stress Analysis of Cracks Handbook", Del Research Corporation (1973).
8. Sih, G. C., Handbook of Stress Intensity Factors, Inst. of Fract. and Solid Mech., Lehigh University (1973).
9. Rooke, D. P., "Compendium of Stress Intensity Factors", Her Majesty's Stationary Office, London (1976).
10. Anon., "The Standard  $K_{IC}$  Test", ASTM Standards 31, (1969) pp 1099-1114.
11. Anon., "The Standard  $K_{IC}$  Test", ASTM STP 463, (1970) pp 249-269.
12. Brown, W. F., and Frawley, Y. I., "Plane Strain Crack Toughness Testing of High Strength Metallic Materials", ASTM STP 410 (1966).
13. Tetelman, A. S., and McEvily, A. J., "Fracture of High Strength Materials", Fracture VI, H. Liebowitz, Ed., Academic Press (1969) pp 137-180.
14. Anon., Damage Tolerant Design Handbook (Data), MCIC HB-01, Vols. I and II (1972).
15. Staehle, R. W., Wang, M. T., and Kerns, G. E., "Stress-Corrosion Cracking and Hydrogen Embrittlement in High-Strength Steels", International Conference on Stress Corrosion Cracking and Hydrogen Embrittlement of Iron Base Alloys, NACE, Firminy, France (1973).
16. Colangelo, V. J., and Ferguson, M. S., "Susceptibility of Gun Steels to Stress Corrosion Cracking", Technical Report WVT-7012, Watervliet Arsenal, U. S. Government Report AD 717 553 (November 1970).

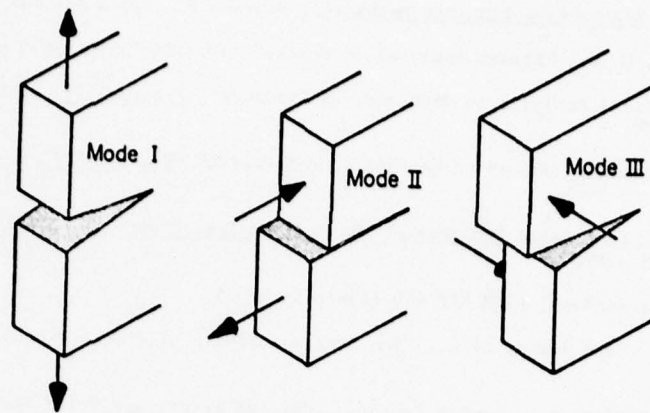


FIGURE 1. MODES OF LOADING

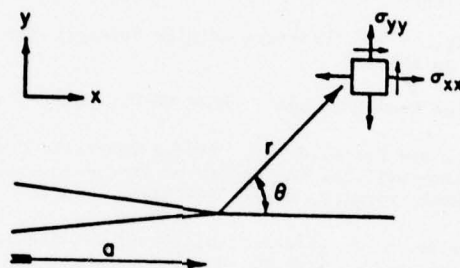


FIGURE 2. CRACK TIP COORDINATE SYSTEM

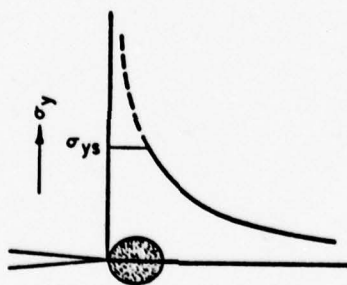


FIGURE 3. CRACK TIP STRESS DISTRIBUTION AND PLASTIC ZONE

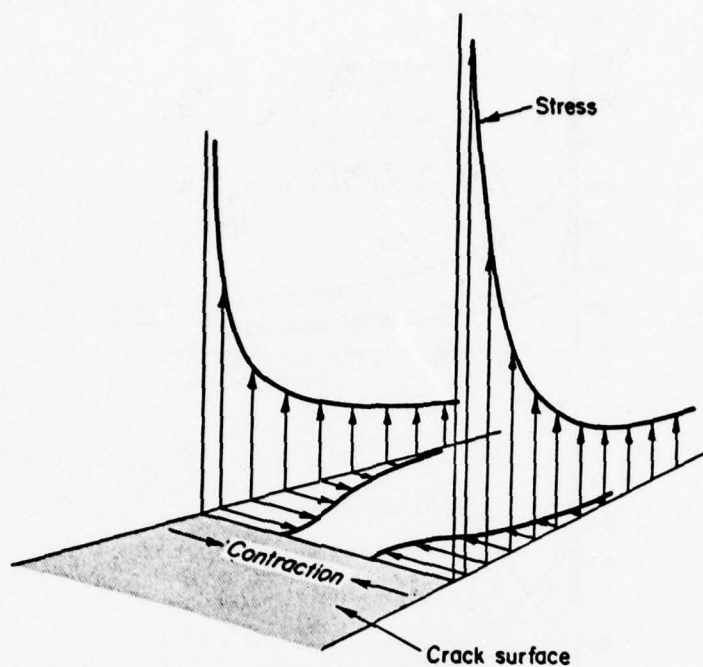


FIGURE 4. CONTRACTION IN THICKNESS DIRECTION DUE TO HIGH CRACK TIP STRESSES

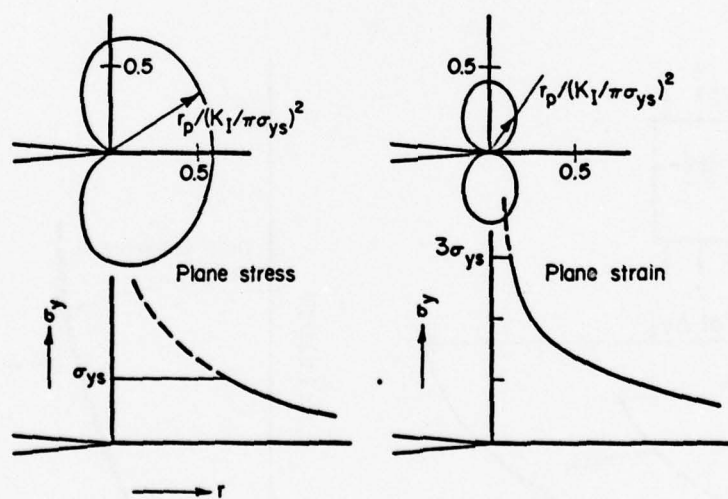


FIGURE 5. PLASTIC ZONES IN PLANE STRESS AND PLANE STRAIN

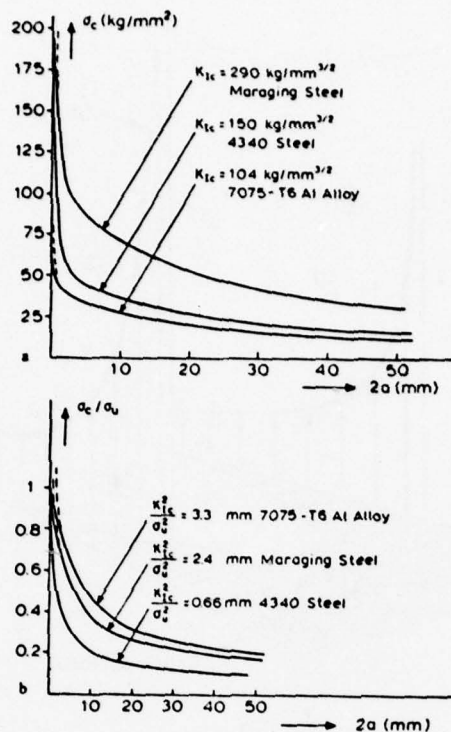


FIGURE 6. RESIDUAL STRENGTH AND CRITICAL CRACK SIZE

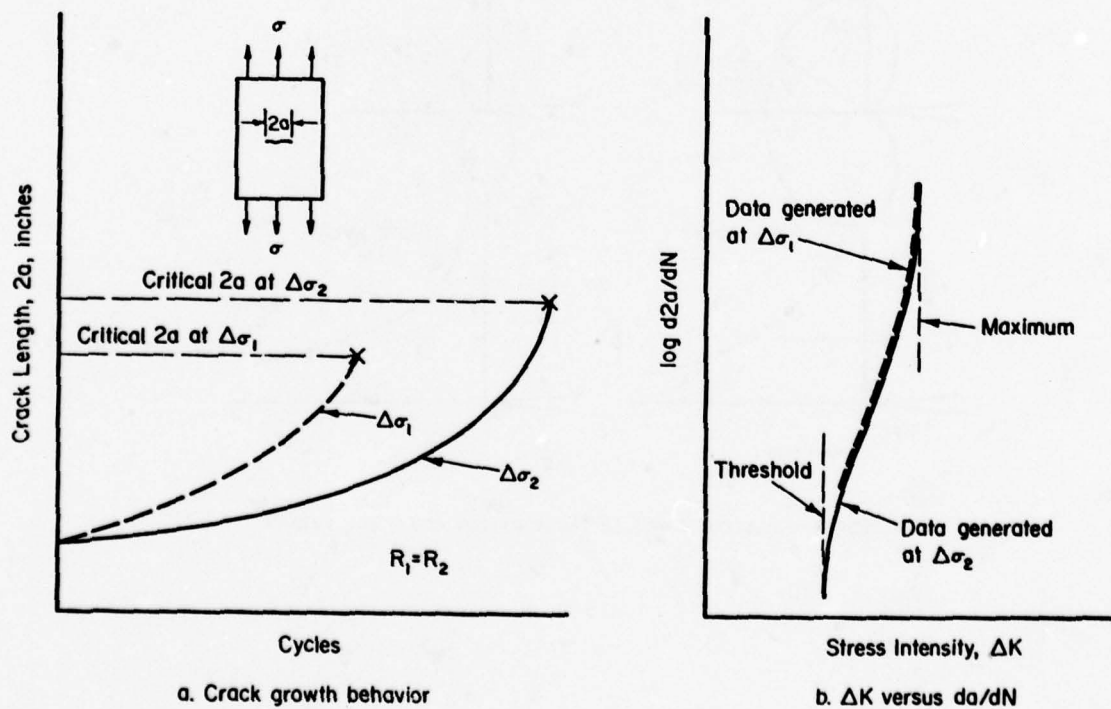
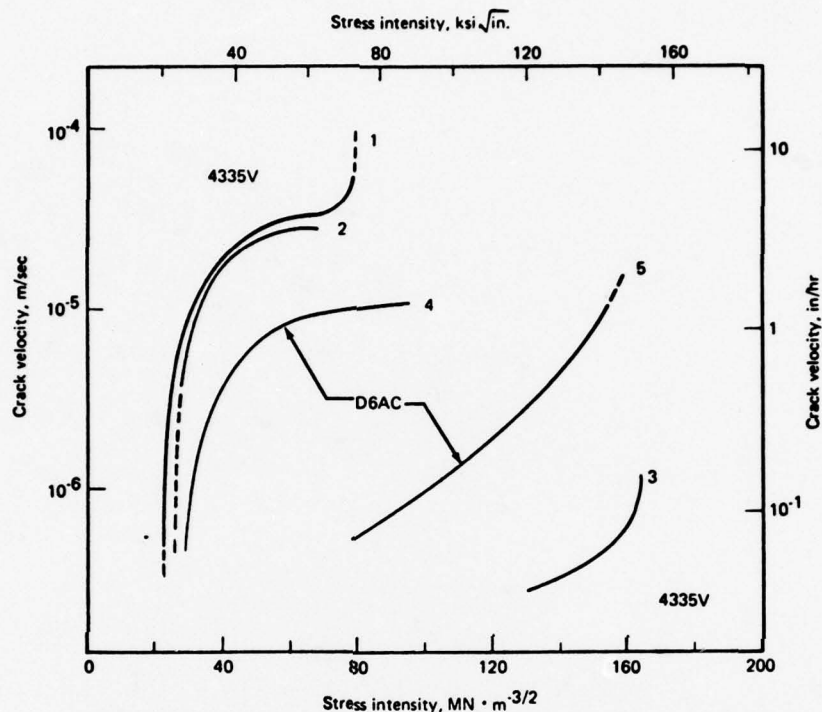
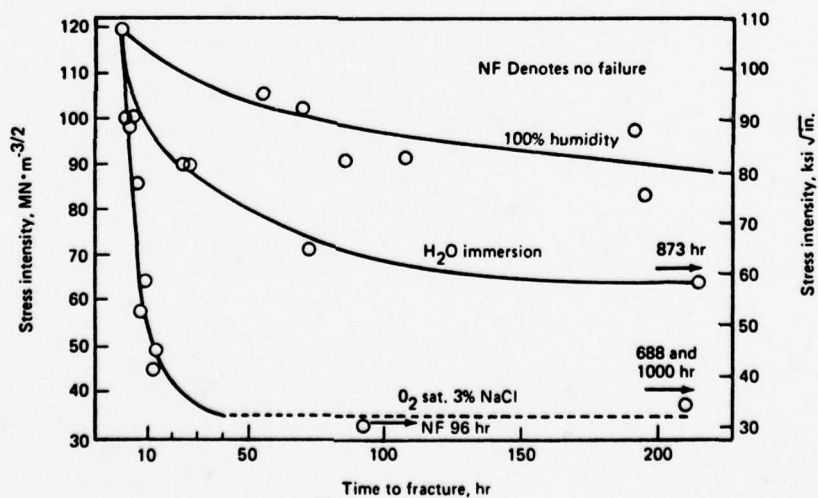


FIGURE 7. BASIC CORRELATION OF CRACK GROWTH BEHAVIOR



Environment: 300 torr hydrogen gas

Steel	Curve	Ultimate tensile strength	Tempering temperature
4335V	1	1660 MN · m <sup>-2</sup> (241 ksi)	315° C (600° F)
	2	1925 MN · m <sup>-2</sup> (279 ksi)	205° C (400° F)
	3	1280 MN · m <sup>-2</sup> (186 ksi)	540° C (1000° F)
D6AC	4	1540 MN · m <sup>-2</sup> (223 ksi)	540° C (1000° F)
	5	1510 MN · m <sup>-2</sup> (219 ksi)	595° C (1100° F)

FIGURE 8. STRESS CORROSION CRACK GROWTH RATE AS A FUNCTION OF STRESS INTENSITY<sup>(15)</sup>FIGURE 9. TIME TO FAILURE OF A FUNCTION OF INITIAL STRESS INTENSITY<sup>(16)</sup>

## FRACTURE

David Broek  
 Battelle's Columbus Laboratories  
 505 King Avenue  
 Columbus, Ohio 43201

## 1. INTRODUCTION

In particular in the case of large civil airplanes, the larger part of the primary aircraft structure consists of reinforced thin plate. Therefore, unlike in many other structures, plane stress fracture is of vital importance for all major aircraft components. In view of this the behavior of thin plates and the analysis of plane stress fracture will be extensively discussed during this Lecture Series.

Plane stress behavior is more difficult to analyze than plane strain behavior and has received relatively little attention in the literature. Fracture under plane stress conditions is more complex than plane strain fracture, and no rigorous analysis procedures exist. However, for most practical purposes useful engineering methods can provide approximative answers to plane stress fracture problems. The following is a review of plane stress and transitional fracture.

## 2. THE THICKNESS EFFECT

Associated with the state of stress is a strong variation in fracture toughness. In the case of plane stress, the toughness (critical value of  $K$ ) can be 2 to 3 times as high as that under plane strain conditions. A thick plate under plane strain will fracture when the stress intensity reaches the critical value,  $K_{Ic}$ . When the plate thickness,  $B$ , exceeds  $2.5 K_{Ic}^2 / \sigma_{ys}^2$ , the critical value will be essentially independent of plate thickness, because the plane strain part is large compared with the plane stress region.

When a thin plate is loaded to  $K_{Ic}$ , the plastic zone is already of the order of the plate thickness. Plane stress develops, the plastic zone becomes large, and deformation becomes easier. Therefore  $K_{Ic}$  is not enough for fracture and the plate can be loaded to much further before  $K$  reaches the critical value. This plane stress fracture toughness is usually denoted as  $K_{Ic}$  or  $K_c$ . Plates of intermediate thickness become critical at  $K$  values somewhere between  $K_{Ic}$  and  $K_c$ .

The fracture toughness as a function of plate thickness is shown diagrammatically in Figure 1. Usually there is a small decay in toughness for thin sheets, below the full plane stress thickness. The transition from plane stress fracture to plane strain fracture is associated with a change in fracture plane.<sup>(1)</sup> This is also shown in Figure 1. In the case of plane stress, the crack plane is at an angle of 45 degrees to the plate surface and to the loading direction. In plane strain, the crack surface is perpendicular to the plate surface and the loading direction. The plane stress fracture is sometimes described as slant fracture or shear fracture, the plane strain fracture as square or tensile mode fracture.

At the surface of the plate there will always be plane stress, because the stress  $\sigma_{zz}$  cannot exist at the free surface (there is no reaction). Therefore, along the edges of a plane strain fracture, there are always small regions of the slant, plane stress, and fracture. These regions are called shear lips. In thinner plates, the square fracture becomes smaller, the shear lips covering more and more of the fracture surface until they meet to form the slant plane stress fracture.

Actual data, distinctly showing the behavior depicted in Figure 1, are scarce. The scatter in the transitional region is usually so large that a reliable curve hardly can be drawn. Some data<sup>(2)</sup> are compiled in Figure 2. Plates of different thickness are usually from different heats of material. As a result, their yield stress will be different. The strong dependence of toughness on yield strength then is responsible for the scatter in the data<sup>(1,2)</sup>. If the plates would be machined from the same stock, scatter likely would be less.

Various models have been proposed<sup>(1-5)</sup> to account for the thickness effect. Except for the engineering approach suggested by Anderson<sup>(2)</sup>, most of these models predict a much stronger dependence of toughness on thickness than actually observed. Anderson proposed a linear decay of toughness between the maximum (plane stress) value and  $K_{Ic}$ , as shown in Figure 2. For the time being, this seems to be a reasonable way to estimate the toughness for a given thickness as an orientational value. For reliable residual strength predictions, it is a prerequisite to measure the toughness on plates of the heats and thickness that will actually be used in the design.

## 3. PLANE STRESS AND TRANSITIONAL BEHAVIOR

Consider a thin plate under plane stress with a central crack  $2a_i$ , loaded in tension (Figure 3). Upon reaching a stress  $\sigma_i$ , the crack will begin to extend. However, fracture will not yet occur. In order to maintain crack growth, the stress has to be further increased. This crack growth is stable: the crack will stop growing if the load is kept constant, it will continue to grow upon load increase.

Slow crack growth continues until a critical crack size  $2a_c$  is reached at a stress  $\sigma_c$ . Then the crack becomes unstable and fracture occurs. If the initial crack is longer, crack growth starts at a lower stress, the amount of slow crack growth is larger, but  $\sigma_c$  is lower. This is shown in Figure 3.

Slow stable crack growth is a phenomenon that is observed particularly in plane stress and transitional stress states. In the ideal case of plane strain, unstable fracture follows immediately upon crack growth initiation. Sometimes, however, some slow growth is observed. Its occurrence depends upon the testing system stiffness. In a hard testing system, a sharp drop in load may occur when the crack starts propagating. As a result, the stress may fall below the critical value (i.e.,  $K < K_{Ic}$ ), which causes crack arrest.



In plane stress, the slow stable crack growth is also dependent upon testing system stiffness and specimen geometry. However, it will still occur in a soft testing system where no drop of load takes place when the crack propagates. Slow crack growth may be of the order of 20 to 50 percent of the initial crack size<sup>(1,6)</sup> depending upon alloy type and testing conditions.

According to the energy concept, there is a continuous energy balance, i.e.,

$$\frac{d}{da} (F - U) = \frac{dU}{da} \quad \text{or} \quad G = R \quad (1)$$

If there were no energy balance, the crack would not propagate ( $G < R$ ) or it would become unstable ( $G > R$ ).

The instantaneous value of  $G$  during slow crack growth in plane stress is

$$G = \frac{\pi \sigma^2 a}{E} = \frac{K^2}{E} \quad (2)$$

Since both  $\sigma$  and  $a$  increase during slow growth, the energy release rate increases. Because  $G = R$ , it appears that the resistance to crack growth,  $R$ , increases. From a simultaneous measurement of  $\sigma$  and  $a$  during slow growth,  $G$  can be calculated; hence, the increase of crack growth resistance can be measured indirectly. The resulting curve, called the  $R$ -curve, is depicted in Figure 4.

Also shown in Figure 4 are straight lines representing  $G = K^2/E$  for a central crack under constant stress. The quantity  $K^2/E = \pi \sigma^2 a/E$  is a straight line as a function of crack size if the stress  $\sigma$  is constant. So one can draw a straight line  $K^2/E = \pi \sigma_1^2 a/E$ . On this line, there is a point  $a = a_1$  where  $K_1^2/E = \pi \sigma_1^2 a_1/E$ . This is the point of crack initiation (point A in Figure 4). At that point, the released energy is equal to the instantaneous crack growth resistance,  $R_1$ .

During slow crack growth  $K^2/E$  remains equal to  $R$ . Thus successive points on the curve can be found by drawing straight lines. For example, at a stress  $\sigma_1$ , the instantaneous crack size is  $a_1$ , and  $\pi \sigma_1^2 a_1/E = R_1$ .

Finally, if the stress is equal to  $\sigma_c$ , the line  $\pi \sigma_c^2 a/E$  is tangent to the  $R$ -curve. If the crack propagates at constant stress, the value of  $K^2/E$  will remain larger than  $R$ . Hence, no further stress increase is necessary to maintain crack growth, which means that the fracture condition is reached. Apparently, the condition for instability is given (point of tangency) by

$$\frac{\partial G}{\partial a} = \frac{\partial R}{\partial a} \quad (3)$$

The  $R$ -curve is supposed to be a characteristic of the material at the given thickness (state of stress). It is reasonably independent of specimen geometry<sup>(7)</sup>. It is also assumed independent of the initial crack size<sup>(8)</sup>. The energy release rate,  $G$ , depends upon specimen geometry and loading condition. However, given the shape of the  $G$  line for a certain geometry, the instability condition would still follow from Equation (3) with the same  $R$ -curve. The  $R$ -curve can be determined experimentally by measuring stress and crack size during slow growth. This allows calculation of  $K$  and of  $K^2/E$  (which is equal to  $R$ ).

#### 4. ENGINEERING ANALYSIS OF PLANE STRESS

The  $R$ -curve approach is sometimes used for residual strength predictions. However, the procedure may be rather cumbersome. Also, as yet there is no proper understanding of its significance. Several engineering methods have been proposed<sup>(1,2,9)</sup> to treat the plane stress and transitional problem. Only Feddersen's approach<sup>(9)</sup> has the versatility required for structural design. Therefore, only this method will be discussed.

It can be assumed that all events described in the foregoing paragraphs are governed by the stress intensity factor. Each event can be labeled by a stress-intensity expression, i.e.,

$$\begin{aligned} K_1 &= \sigma_1 \sqrt{\pi a_1} \\ K_c &= \sigma_c \sqrt{\pi a_c} \\ K_a &= \sigma_c \sqrt{\pi a_1} \end{aligned} \quad (4)$$

$K_1$  is the critical stress intensity for the onset of crack growth,  $K_c$  is the critical stress intensity for fracture.  $K_a$  is an apparent stress intensity. It is not a physical quantity, because it relates the initial crack size to the fracture stress and the two are not coincident. However,  $K_a$  does have engineering significance. It gives the residual strength of a plate that contains a (fatigue) crack of a given size. Whether or not this crack shows stable growth before fracture is immaterial from an engineering point of view.

Tests have shown that  $K_1$ ,  $K_c$ , and  $K_a$  are not material constants with general validity like  $K_{IC}$ . But to a first approximation, they are constant for a given thickness and for a limited range of crack sizes. For a given material with an apparent toughness,  $K_a$ , the relation between the residual strength and crack size of a center cracked panel is given by  $\sigma_c = K_a / \sqrt{\pi a}$ . This residual strength is plotted as a function of total crack size as in Figure 5.

For small crack sizes,  $\sigma_c$  tends to infinity, but the residual strength at  $a = 0$  cannot be larger than the material's yield stress. Therefore, Feddersen<sup>(9)</sup> proposed to construct two tangents to the curve, one from the stress axis starting at  $\sigma_{ys}$ , the other from the crack axis starting at  $W_1$  (where  $W_1$  is the

panel width). In the region between the points of tangency  $K_a$  is approximately constant. This piece of the curve plus the two tangents constitute the residual strength diagram.

Now consider a panel of smaller size  $W_{min}$ . The tangent from  $W_{min}$  is coincident with the tangent from  $\sigma_{ys}$ . Hence, with a panel of size  $W_{min}$  or smaller, one cannot determine a point on the  $K_a$  curve. Therefore, the panel would be too small to measure  $K_a$ . A tangent to any point at the curve is given by

$$\frac{d\sigma}{d(2a)} = \frac{d}{d(2a)} \left( \frac{K}{\sqrt{\pi a}} \right) = - \frac{\sigma}{4a} \quad (5)$$

For the tangent through  $(\sigma_{ys}, 0)$ , this yields (Figure 5)

$$- \frac{\sigma_1}{4a_1} = - \frac{\sigma_{ys} - \sigma_1}{2a_1} \quad \text{or} \quad \sigma_1 = \frac{2}{3} \sigma_{ys} \quad (6)$$

Equation (5) shows that the left hand tangency point is always at  $2/3 \sigma_{ys}$ , independent of  $K$ . The tangent through  $(0, W)$  is defined by (Figure 5)

$$- \frac{\sigma_2}{4a_2} = - \frac{\sigma_2}{W - 2a_2} \quad \text{or} \quad 2a_2 = W/3 \quad (7)$$

This means that the right hand point of tangency is always at  $W/3$ .

Consequently, the complete residual strength diagram can be constructed for any panel size if  $K_a$  is known. Two points can be taken at the curve, one at  $\sigma = 2/3 \sigma_{ys}$ , the other at  $W/3$  and the tangents can be drawn to  $(\sigma_{ys}, 0)$  and  $(0, W/3)$ , respectively. The two points of tangency coincide when  $\sigma_c = 2/3 \sigma_{ys}$  for  $2a = W/3$ , i.e.,

$$\frac{2}{3} \sigma_{ys} \sqrt{\pi W/6} = K_a \quad \text{or} \quad W = \frac{27}{2\pi} \left( \frac{K_a}{\sigma_{ys}} \right)^2 \quad (8)$$

Hence, panels smaller than this will fail by net section yield. Their failure point will be below the  $K_a$ -curve, which means that they cannot be used to measure  $K_a$ . Obviously, the screening criteria for a valid test would be that the failure stress  $\sigma_c < 2/3 \sigma_{ys}$  and the crack size  $2a < W/3$ . If a test panel fails at  $\sigma_c \geq 2/3 \sigma_{ys}$  while the crack size,  $2a = W/3$ , the panel is too small to determine  $K_a$ . Similar arguments can be used for  $K_I$  and  $K_{IC}$ .

Figure 6 shows that Feddersen's approach gives a fair representation of the data. The versatility of the method is in the fact that it allows a simple characterization of plane stress and transitional residual strength. Presentation of  $K_a$  and/or  $K_{IC}$  is sufficient to determine the residual strength for any crack size and panel size. Also, the method is based on stress intensity which makes it more universal and compatible with fatigue crack analysis.

The crack tip plasticity gives rise to slightly larger displacement than in the elastic case. This is sometimes accounted for by using an apparent crack size,  $a^* = a + r_p$ . The stress intensity then becomes

$$K_I = \beta \alpha \sqrt{\pi a^*} = \beta \alpha \sqrt{\pi(a + r_p)} = \beta \alpha \sqrt{\pi a} + \alpha K_{I1}^2 / \sigma_{ys}^2 \quad (9)$$

Since this correction would be used in the determination of the critical stress-intensity factor as well as in the reverse operation to calculate the fracture stress or critical crack size, it would practically cancel out. Therefore, it is recommended that this artificial correction not be used.

Plane stress fracture toughness tests should preferably be performed on center-cracked panels. Fatigue precracking is advisable, but not necessary if the notch is sharp enough to start slow crack growth long before fracture. The maximum load in the test should be taken as the fracture load. Slow crack growth should be measured, preferably by means of a movie camera (16 frames per second is usually sufficient). Taking a load COD as record is advisable. A load time record synchronized with the crack growth record is indispensable.

Due to the compressive stresses acting along the crack edge, the plate may locally buckle. Then, a reduced toughness is found.<sup>(1)</sup> If such buckling would be constrained in service (i.e., due to reinforcements) antibuckling guides may be applied in the test. If buckling can occur freely in service, antibuckling guides should not be used. The above procedure is applicable to plane stress but also to intermediate thickness with transitional behavior.

## 5. FRACTURE AT NET SECTION YIELD

Consider a material with a plane stress fracture toughness  $K_a$ . The residual strength as a function of crack size can be calculated and plotted and the residual strength diagram for a panel of size  $W$  is found by drawing the two tangents. Similarly one finds the residual strength for other panel sizes. However, panel size  $W_1$  (Figure 7) does not behave according to  $K_a$ . It always fails at net section yield (or slightly above yield in case of extremely tough materials not used in airframes). The net section stress is the nominal engineering stress in the cracked section:

$$\sigma_{net} = \frac{\text{Load}}{(W_1 - 2a)B} \quad (10)$$

If  $\sigma_{net} = \sigma_{ys}$ , the net section can yield freely and will tear apart. The critical stress is always defined as

$$\sigma_c = \frac{\text{Load}}{W_1 B} = \sigma_{net} \cdot \left( \frac{W_1 - 2a}{W_1} \right) \quad (11)$$

Hence, for  $\sigma_{net} = \sigma_{ys}$ , the failure stress  $\sigma_c$  will be given by a straight line from  $\sigma_{ys}$  to  $W_1$ , as shown in Figure 7. This is consistent with the Peddersen approach discussed in the previous section: when the two tangents to the curve coincide, the fracture condition becomes automatically a net section yield criterion.

It is worthwhile noting that the fracture stress of small panels obeying the net section yield criterion is considerably below the fracture stress that would be predicted on the basis of  $K_a$ . Conversely, if  $K_a$  were derived from tests on these small panels, its value would be lower than the real  $K_a$ , however this practice is ruled out by the size requirements presented in the previous section.

Consider two materials with low and high toughness as in Figure 8. Low toughness materials usually have a higher yield strength, which is assumed in the figure. For a crack of size  $2a_1$ , the low toughness material will have the lowest residual strength. However, for small cracks ( $2a_2$ ) in small panels  $W_2$ , the high toughness material may have the lower strength. Although this is of little consequence for large structures, it may be of some consequence in plane stress cases of strips and reinforcements.

## 6. HIGH TOUGHNESS MATERIALS

Airframe materials in general belong to the low and medium toughness categories. Therefore, the previous methodology is usually applicable. In the case of materials with very high toughness (most low and medium strength structural steels for general engineering, 5000 series aluminum alloy, copper alloys) the methods break down.

As an example, consider a medium strength steel sheet with a yield stress of  $80 \text{ kg/mm}^2$  and a plane stress fracture toughness of  $K_a = 2000 \text{ kg/mm}^{3/2}$ . Then the minimum panel size to determine  $K_a$  would be

$$W = \frac{27}{2\pi} \left( \frac{2000}{80} \right)^2 \approx 2700 \text{ mm}$$

Any size of panel smaller than this would behave according to the net section stress criterion. Thus, a fracture mechanics calculation on the basis of  $K$  would never be applicable.

As was shown in the foregoing small panels of low toughness materials fail at a net stress equal to yield. The high toughness materials usually have much reserve strength beyond net section yield, because they always have a low  $\sigma_{ys}$  as compared to  $\sigma_u$ . This is illustrated in Figure 9, showing the residual strength data for 12-inch wide panels of 304 stainless steel. The net section failure stress is somewhere between  $\sigma_{ys}$  and  $\sigma_u$ . It is important though that fracture is still determined by a net section stress criterion. The net section failure stress can be determined from an experiment on a cracked plate, after which predictions for other crack sizes and panel sizes can be made (Figure 9). The procedure is limited however to the center crack case.

Attempts are under way to extend fracture mechanics to the regime of high toughness materials. Two approaches are being pursued intensively, namely COD and J-integral. The COD approach assumes that fracture will occur when the crack tip opening displacement CTOD exceeds a critical value. It can be shown rigorously that this assumption is equivalent to the  $K_{Ic}$  approach if the plastic zone is small. Therefore, it may be applicable also to cases with large scale plasticity. A difficulty is that CTOD cannot be measured in an experiment. Therefore, one measures COD.

Small specimens (essentially cracked Charpy specimens) are loaded to fracture while the crack mouth opening (COD) is measured. CTOD is then determined from a linear extrapolation to the crack tip. The CTOD at fracture is the critical value. It is difficult to apply the result in a residual strength calculation, because it requires that one can compute CTOD and equate it to the critical value. Moreover, CTOD values are often ambiguous, because there is usually slow crack growth before fracture.

The J-integral is a path independent contour integral around the crack tip. In the elastic case, it can be shown that  $J = K^2/E$ . It can also be shown that  $J = \sigma_{ys} \text{ CTOD}$ . Hence, J is equivalent to K and CTOD in the linear elastic case. The J-integral can be readily calculated in elastic-plastic finite element analysis. Therefore, J would be a more suitable criterion than CTOD for quantitative predictions of fracture in structures. It should be noted however, that so far the J-criterion is strictly limited to plane strain. Aircraft parts in which plane strain prevails are invariably built of low to medium toughness alloys, so that  $K_{Ic}$  is applicable. The J-integral cannot be applied to growing cracks. Therefore its application to plane stress fracture - where it would be needed most for aerospace applications - is highly questionable.

## 6. PRACTICAL CASES

### 6.1. Scope

In practice cracks will often start at a hole or grow as a surface crack. Analysis of these two cases is considered briefly in the following subsections. An in-depth treatment of the behavior of crack at holes and of surface flaws is presented in Reference 1.



### 6.2. Cracks at Holes

On the basis of the work by Bowie, the stress-intensity factor for a through crack at a hole in an infinite plate (Figure 10) is given<sup>(1)</sup> by

$$K = \alpha \sqrt{\pi} f_B \left( \frac{a}{D} \right) \quad (12)$$

where  $a$  is the size of the crack as measured from the edge of the hole and  $D$  is the hole diameter. The function  $f_B(a/D)$  can be given in tabular or graphical form as  $f_{B1}$  for a single crack and  $f_{B2}$  for the symmetric case with two cracks.

If the crack is not too small with respect to the hole size, the hole may be considered part of the crack. The total defect size is then given by the physical crack length plus the hole diameter. The stress intensity is simply

$$K = \alpha \sqrt{\pi a_{\text{eff}}} \quad (13)$$

By developing Equation (13) as

$$K = \alpha \sqrt{\pi a} \sqrt{\frac{D}{2a} + \frac{1}{2}} = \alpha \sqrt{\pi a} f_{E1} (a/D) \quad (14)$$

for the asymmetric case, and

$$K = \alpha \sqrt{\pi a_{\text{eff}}} = \alpha \sqrt{\pi a} \sqrt{\frac{D}{2a} + 1} = \alpha \sqrt{\pi a} f_{E2} (a/D) \quad (15)$$

for the symmetric case, it follows that  $f_{B1}$  and  $f_{B2}$  in the Bowie equation are replaced by  $f_{E1}$  and  $f_{E2}$ . A comparison of these functions is made in Figure 10. It appears that the differences between the exact functions and the engineering functions are small. If  $a/D > 0.1$ , Equation (13) can be used in many applications. This gives a feeling for the significance of a crack at a hole. It behaves as if the total damage size is equal to the hole plus the crack.

Results of residual strength tests<sup>(10)</sup> are shown in Figure 11. The material (7075-T6) had a toughness  $K_{IC} = 204 \text{ kg/mm}^{3/2}$  ( $= 58 \text{ ksi/in.}$ ). The results show that the residual strength for the cracks at the holes fall almost exactly on the curve for normal center cracks. This indicates that the crack, indeed, behaves as if the total damage was equal to the size of the hole plus the crack.

### 6.3. Surface Flaws

A surface flaw is generally treated in the same way as an embedded elliptical crack. For the latter, the solution developed by Irwin<sup>(11)</sup> is almost always used. It gives the stress intensity as

$$K = \frac{\sigma}{\sqrt{2}} \sqrt{\pi a \left( \frac{a^2}{c^2} \cos^2 \theta + \sin^2 \theta \right)^{1/2}} \quad (16)$$

with

$$\frac{\pi}{2} = \int_0^{\pi/2} (1 - k^2 \sin^2 \phi)^{1/2} d\phi \quad \text{with } k^2 = 1 - \frac{a^2}{c^2} \quad (17)$$

In these equations,  $a$  is the semiminor axis of the ellipse,  $c$  is the semimajor axis, and  $\theta$  is the angular coordinate. The elliptical integral,  $\frac{\pi}{2}$ , is evaluated for the relevant values of  $a/c$ . It is given in graphical form in Figure 12(a). Series expansion of the elliptical integral shows that

$$\frac{\pi}{2} = \frac{3\pi}{8} + \frac{\pi}{8} \frac{a^2}{c^2} \quad (18)$$

is a very good approximation (Figure 12(a)) of its value for ratios of  $a/2c$  between 0.3 and 0.5, which technically is the most important range.

The stress intensity varies along the crack front. It is maximum at the end of the major axis where  $\theta = \pi/2$ ,

$$K = \frac{\sigma}{\sqrt{2}} \sqrt{\pi a} \quad (19)$$

Its minimum value is at the end of the major axis ( $\theta = 0$ ) where

$$K = \frac{\sigma}{\sqrt{2}} \sqrt{\pi \frac{a^3}{c}} \quad (20)$$

Due to the free surface, a correction to  $K$  is necessary. This front-free-surface correction is usually taken at 1.12. If the crack protrudes deeply inward, the proximity of the back-free surface also requires a correction to  $K$ . This back-free-surface correction,  $M_k$ , was determined by Shah and Kobayashi<sup>(12)</sup> for flaws under pure tension. It depends upon the ratio between crack depth and thickness and upon flaw shape as shown in Figure 12(b). Consequently, the maximum stress intensity is

$$K = 1.12 M_k \frac{\sigma}{\sqrt{2}} \sqrt{\pi a} \quad (21)$$

According to the foregoing, fracture will occur if  $K_I = K_{IC}$ . Thus, one would assume that fracture is determined by the highest stress intensity, i.e.,

$$\sigma_c = \frac{\phi K_{IC}}{1.12 M_k \sqrt{\pi a}} \quad (22)$$

The highest stress intensity occurs only at one point, namely at the end of the semimajor axis of the surface flaw. When this point is ready for fracture, the stress intensity everywhere else along the flaw is still lower than  $K_{IC}$ . Generally speaking, it must be conservative to assume that fracture of the surface flaw is determined by its highest stress intensity, as is shown by Figure 13.

## 7. REFERENCES

1. Broek, D., Elementary Engineering Fracture Mechanics, Noordhoff, Leyden Holland (1974).
2. Anderson, W. E., "Some Designer-Oriented Views on Brittle Fracture", Battelle Northwest Laboratories Report SA-2290 (1969).
3. Bluhm, Z. I., "A Model for the Effect of Thickness on Fracture Toughness", ASTM Proc. 61 (1961), pp 1324-1331.
4. Sih, G. C., and Hartranft, R. J., "Variation of Strain Energy Release Rate with Thickness; Int. J. Fracture 9 (1973) pp 75-82.
5. Broek, D., and Vlieger, H., "The Thickness Effect in Plane Stress Fracture Toughness", National Aerospace Inst., Amsterdam, Report TR 74032 (1974).
6. Broek, D., "The Residual Strength of Light Alloy Sheets Containing Fatigue Cracks", Aerospace Proc. 1966, McMillan (1967), pp 811-835.
7. Heyer, R. H., and McCabe, D. E., "Crack Growth Resistance in Plane-Stress Fracture Testing", Engn. Fract. Mech. 4 (1972), pp 413-430.
8. Krafft, J. M., Sullivan, A. M., and Boyle, R. W., "Effect of Dimensions on Fast Fracture Instability of Notched Sheets", Cranfield Symposium 1961, I, The College of Aeronautics (1961) pp 8-28.
9. Feddersen, C. E., "Evaluation and Prediction of the Residual Strength of Center Cracked Tension Panels", ASTM STP 486 (1971) pp 50-78.
10. Broek, D., and Vlieger, H., "Cracks Emanating from Holes in Plane Stress", Int. J. Fracture Mechanics, 8 (1972) pp 353-356.
11. Irwin, G. R., "Crack Extension Force for a Part-Through Crack in a Plate", J. Appl. Mech. (December 1962) pp 651-654.
12. Shah, R. C., and Kobayashi, A. S., "Stress-Intensity Factors for an Elliptical Crack Approaching the Surface of a Semi-Infinite Solid", Int. J. Fract., 9 (1973) p 2.

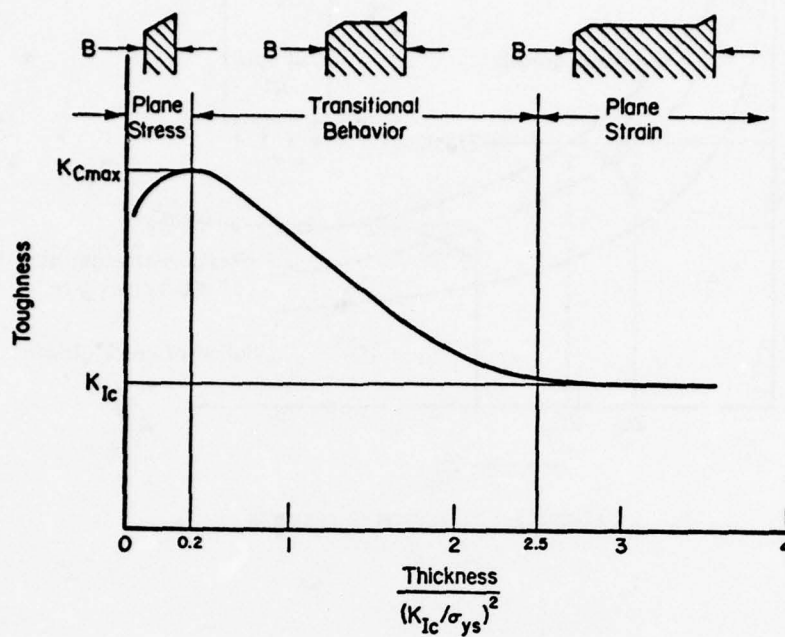


FIGURE 1. THE THICKNESS EFFECT

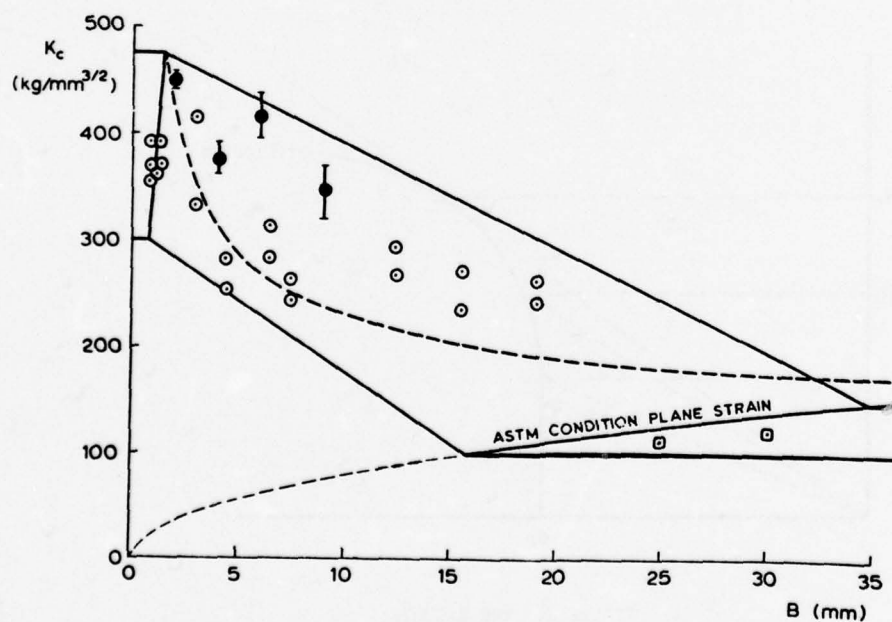


FIGURE 2. THE THICKNESS EFFECT IN 2024-T3 ALUMINUM ALLOYS. MISCELLANEOUS DATA POINTS SHOWN. STRAIGHT LINES: ANDERSON(2) MODEL. DASHED LINE OTHER MODELS(3,5)



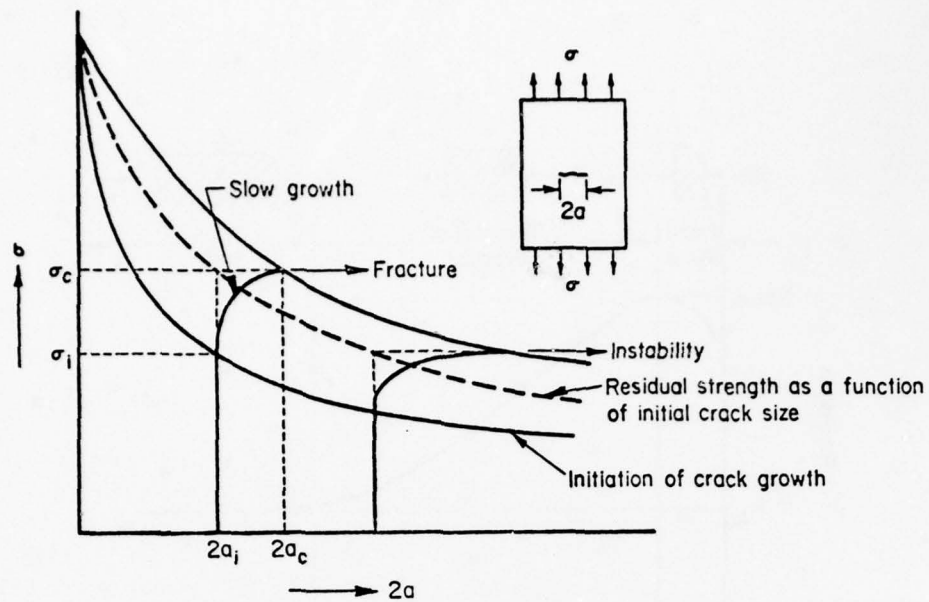


FIGURE 3. PLANE STRESS BEHAVIOR

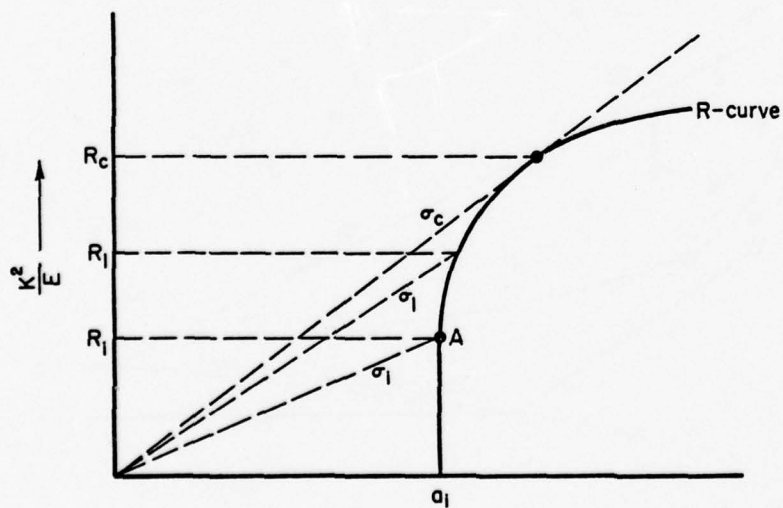


FIGURE 4. THE R-CURVE

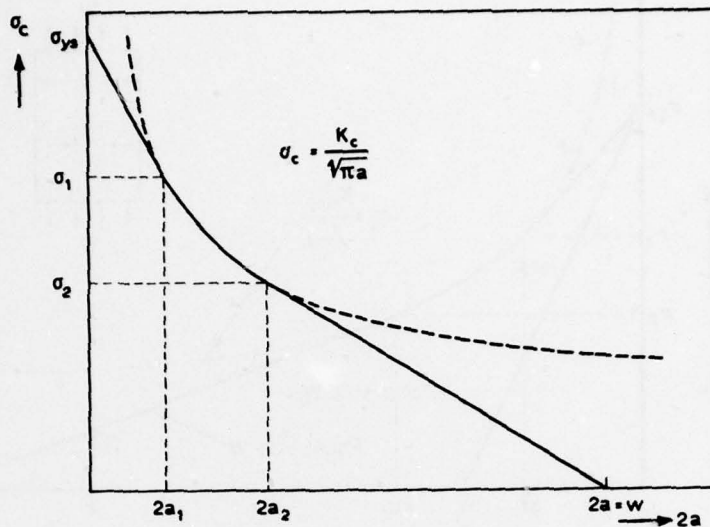
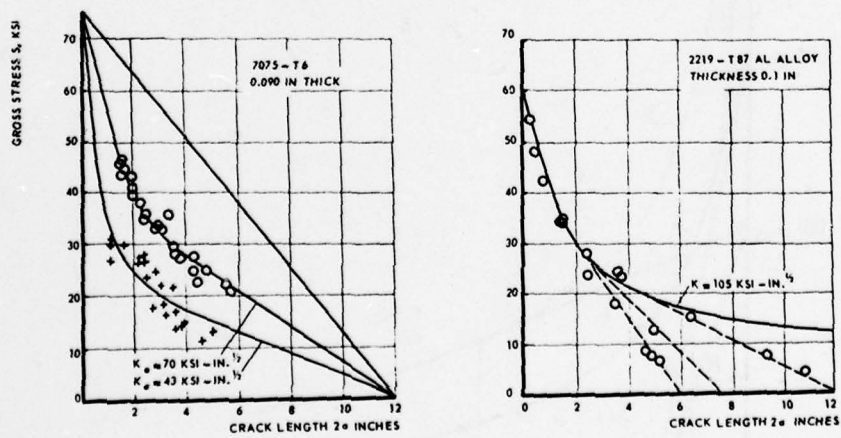


FIGURE 5. THE RESIDUAL STRENGTH DIAGRAM

FIGURE 6. TEST DATA COMPARED WITH FEDDERSEN'S METHOD<sup>(9)</sup>

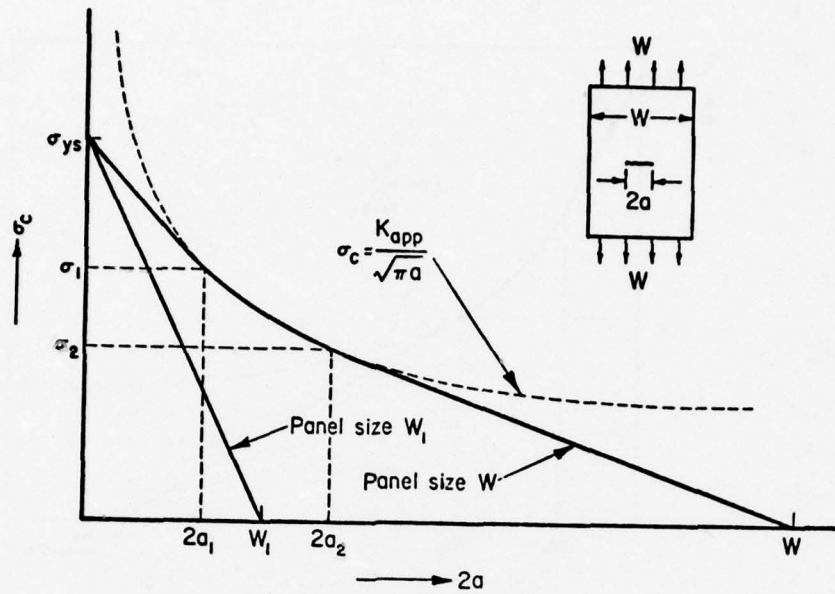


FIGURE 7. NET SECTION YIELD OF SMALL PANELS

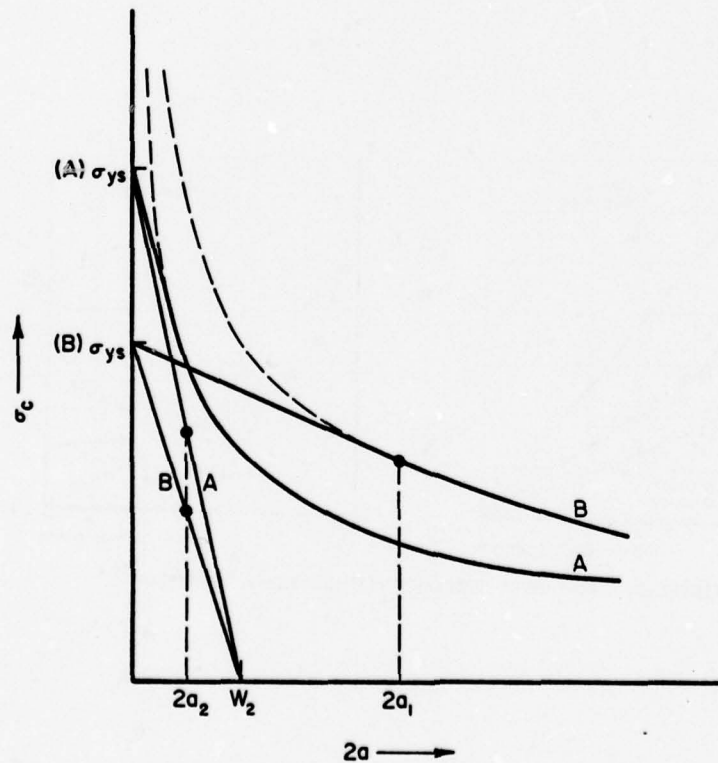


FIGURE 8. THE RESIDUAL-STRENGTH DIAGRAM II



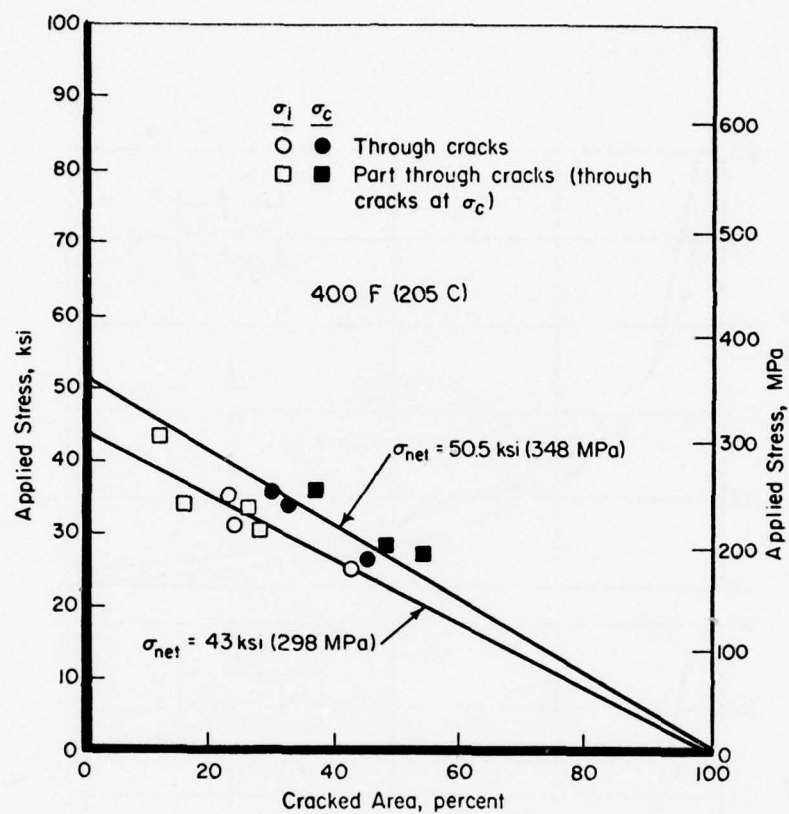


FIGURE 9. RESIDUAL STRENGTH OF 304 STAINLESS STEEL

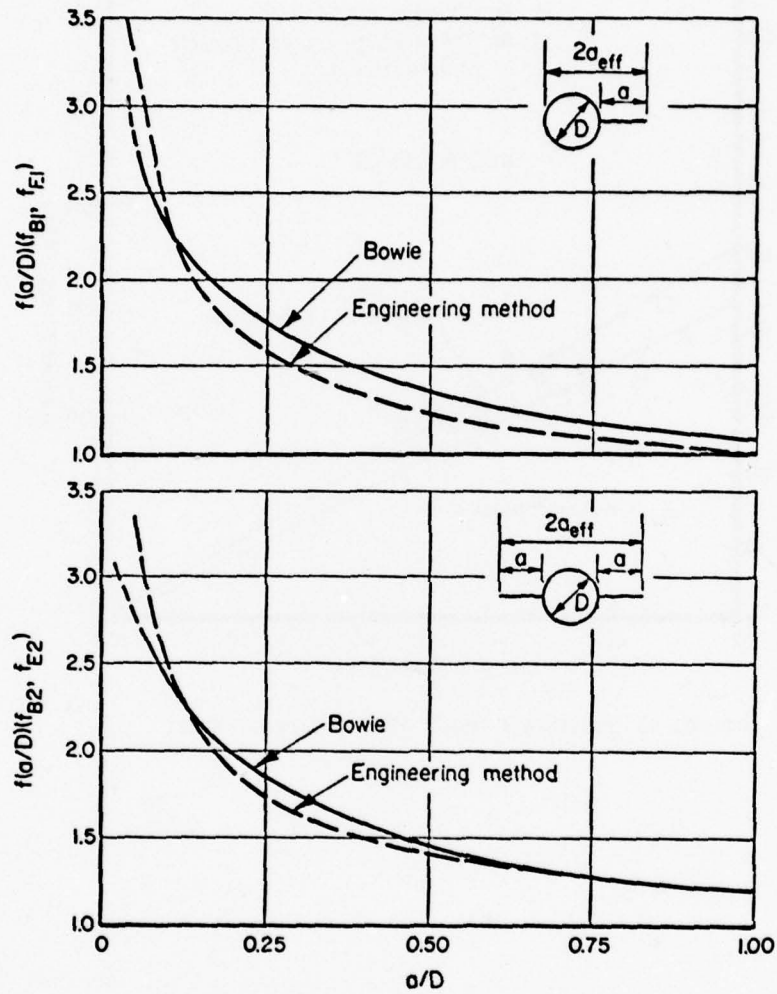


FIGURE 10. THROUGH-THICKNESS CRACKS AT HOLES

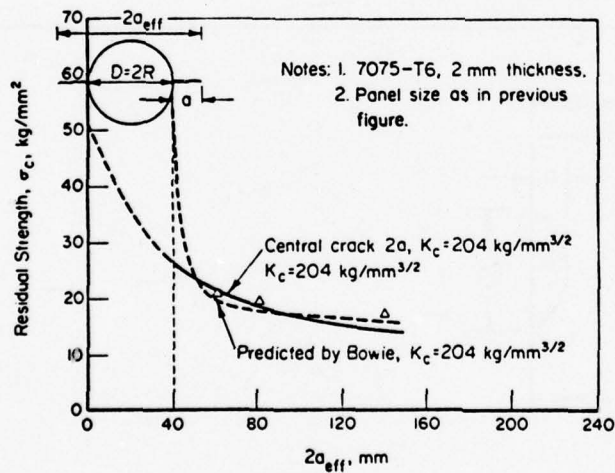
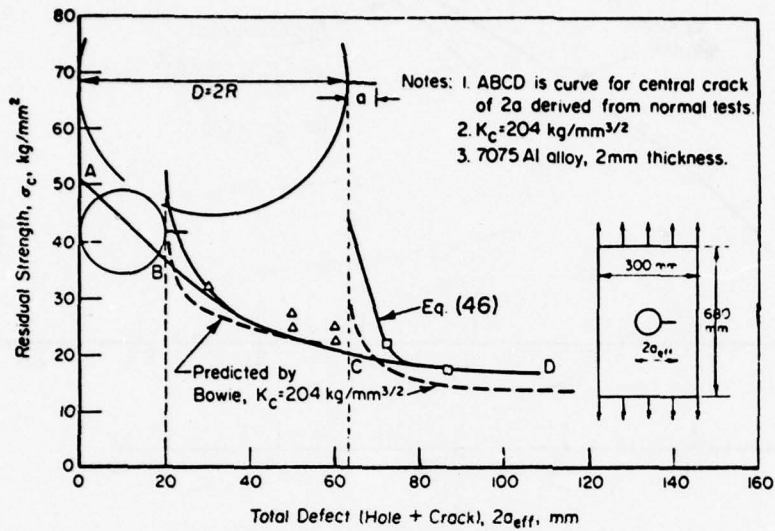


FIGURE 11. THROUGH-CRACKS AT HOLES; RESIDUAL STRENGTH

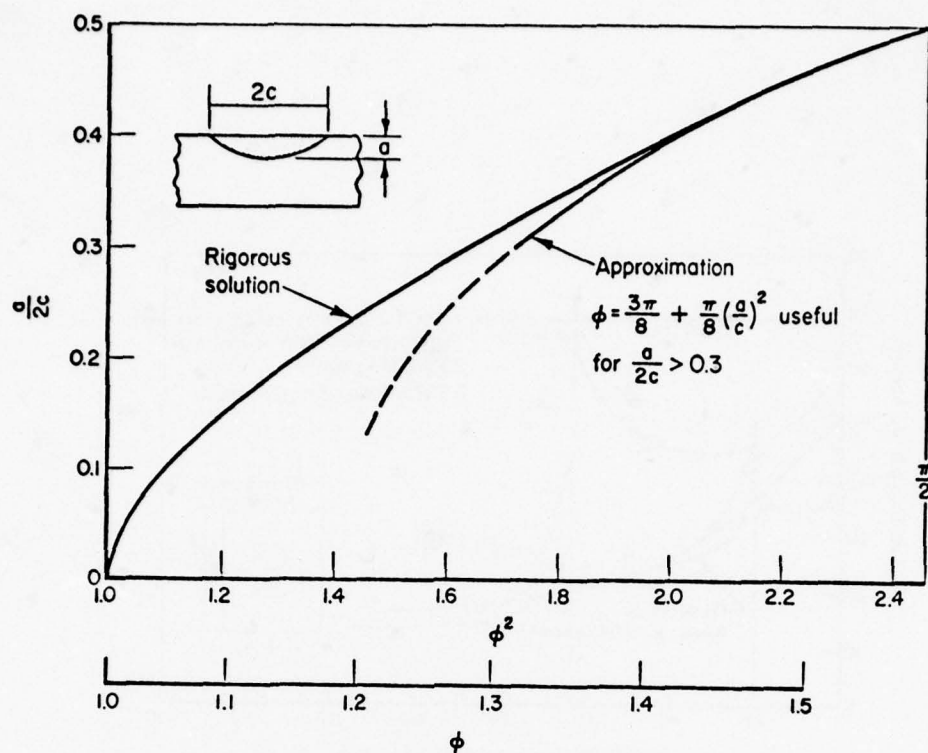


FIGURE 12(a). ELLIPTICAL FLAW PARAMETER

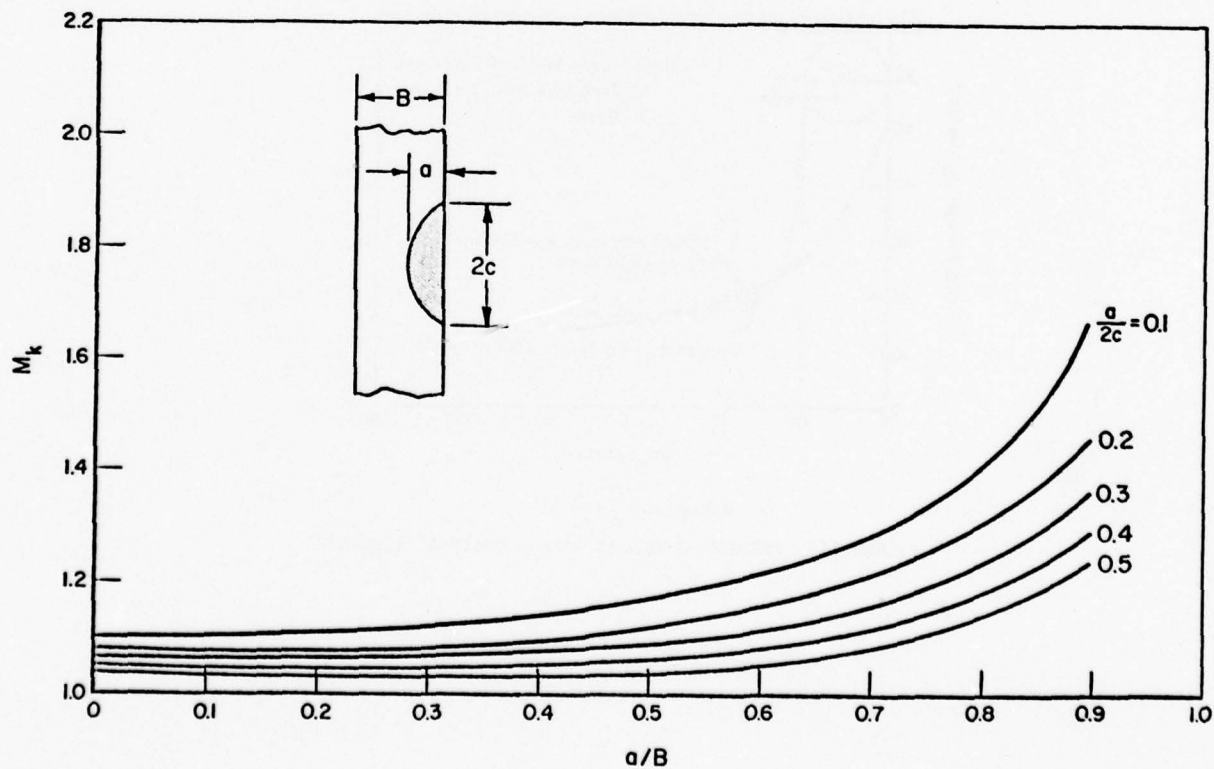


FIGURE 12(b). BACK-FREE SURFACE CORRECTION



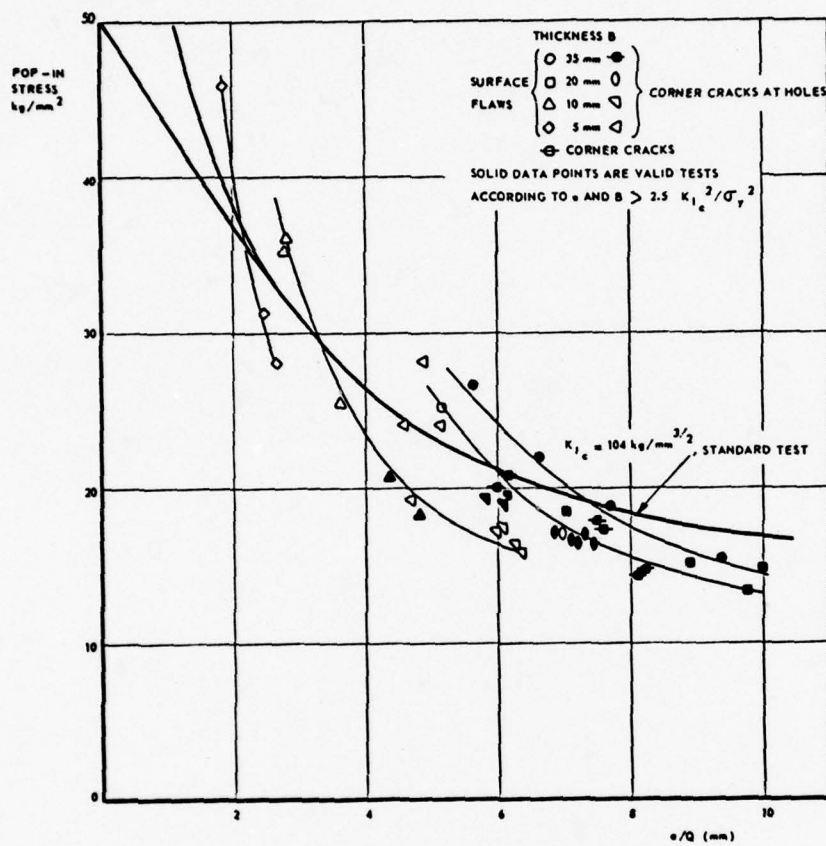


FIGURE 13. SURFACE FLAWS

## FATIGUE CRACK GROWTH

BY

Dr.-Ing. Walter Schütz

Industrieanlagen-Betriebsgesellschaft mbH  
Einsteinstraße 20, 8012 Ottobrunn, Germany

## 1. INTRODUCTION

It is now an established fact that structures may go into service containing crack-like manufacturing defects. However, only in very rare cases these cracks are so large that immediate static failure occurs when the first high service loads occur; rather, it is the service loads themselves which produce crack growth starting either from the small manufacturing cracks or from notches which are unavoidable in a structure. In the first case, the whole life of the structure consists of crack growth; it ends when the remaining cross section can no longer sustain the service loads and fails statically. In the second case, at the notch root a crack must first be initiated which then grows to failure and the life consists of the crack initiation and the crack propagation phase. In both cases, crack propagation and its calculation is therefore an important task - at least as important as the calculation of residual static strength and much more difficult. This is so because fatigue crack propagation is a cyclic phenomenon and is therefore much more complex and difficult than a static phenomenon. One reason is the very large number of parameters; therefore experimental verification of calculation methods, hypotheses etc. is very time-consuming and expensive.

## 2. PARAMETERS CONTROLLING FATIGUE CRACK GROWTH

Reading across from fatigue test experience one can list the parameters of influence on fatigue crack growth:

- The amplitude of nominal stress  $\pm \sigma_a$  or (better) of local stress or strain at the crack tip. For fracture mechanics purposes the double amplitude (or range) of the stress intensity factor  $\Delta K$  is normally used. This is the most significant parameter.
- The mean stress  $\sigma_m$ . Depending on the material in question, this may be an almost negligible or a significant parameter. Usually it is found that the crack propagation behavior of high-strength materials like 7075-T6 or a maraging steel is very sensitive to mean stress, higher tensile mean stress giving faster crack propagation (1-11), see Figure 1.  
For medium or low strength materials like 2024-T3 or shipbuilding steels, mean stress has less influence on crack propagation rate.

There is an additional mean stress effect: When the minimum stress in a cycle goes into compression, i.e. when  $R < 0$ , the crack closes (neglecting for the moment crack closure effects) and the stress intensity is zero; this would mean that the compressive part of a cycle has no effect on crack propagation and should be correspondingly neglected in calculation. That this is too simplistic a view has been shown by many experiments (12,13,39); Due to crack closure effects the compressive part of a cycle does have an effect on crack propagation. To make matters more difficult, different materials react differently, as can be seen from Figure 2:

For high strength materials the compressive part can be neglected; for example with 7075-T6 the crack propagation is very similar for stresses of  $0 \pm 140 \text{ N/mm}^2$  or  $70 \pm 70 \text{ N/mm}^2$ ; for medium strength materials like 2024-T3 or 1.7734.5 there is a detrimental influence of the compressive portion of the cycle.

- As the stress intensity range is decreased a characteristic lower limit is reached, below which the crack does not grow even at very high numbers of cycles. This is the fatigue crack propagation threshold or "fracture mechanics fatigue limit" (14), a most important parameter for components loaded by high frequency constant stress amplitudes, for example turbine blades or certain machinery parts. If crack-like machining defects must be assumed to be present, the service stresses must be below this threshold, otherwise failure is unavoidable. The threshold may be less important for typical structures of military aircraft loaded by relatively few cycles of a severe spectrum. In the literature, a growing amount of numerical data on the threshold  $\Delta K_{th}$  is becoming available (3,15-30), the most comprehensive compilation probably being in (3). As was to be expected from fatigue testing experience,  $\Delta K_{th}$  also depends on the stress ratio  $R$  (24) and this dependence is again different for different materials (28).

Both these effects mean that  $\Delta K_{th}$  can be determined only by timeconsuming and expensive tests because one must apply a large number of cycles before  $K_{th}$  can be assumed to have been reached. In this respect there are some disturbing new data from Speidel and Scarlin (20). Their  $\Delta K_{th}$ -values are about half as large (1) as those in (3). Speidel

ascribes these low numbers to exacting test procedures and patience. because this tests were run down to a crack propagation rate of  $10^{-8}$  mm/cycle.

Under variable load amplitudes  $\Delta K$ , obviously will also be influenced by preceding larger loads, as was found in (30).<sup>th</sup>

### 3. REQUIREMENTS TO BE MET BY A FORMULA FOR CALCULATING FATIGUE CRACK GROWTH

In principle all present and future formulae for calculating fatigue crack growth behavior of materials must be hypotheses by which one tries to describe some or all of the phenomena observed in corresponding experiments. These formulae must therefore contain materials "constants", which, being determined by test, have an inherent scatter like all other similar "constants". However, it is not enough to just carry out some tests and fit their results by a formula with the help of one or more constants. This would be just a data fitting technique, easy in the case of fatigue crack growth because of the "regular" shape of the crack propagation curve.

There are some additional requirements to be fulfilled before such a formula can be considered to be a useful model:

- The materials "constants" determined by a few tests at one particular set of  $\sigma_m$  and  $\sigma$  must be suitable, for other sets of  $\sigma_m$  and  $\sigma$ . In other words: The determination of the necessary constants must not require the tests which the calculation method is supposed to replace.
- All parameters influencing crack growth (as discussed in chapter 2) must be contained in the model. This requirement may sound trivial, but most of the models published so far do not meet it completely.
- The increase of the crack propagation rate when  $K_{max}$  approaches  $K_C$  or  $K_{IC}$  must be incorporated, as well as the decrease when  $\Delta K_{th}$  is near.
- The model should be generally applicable, that is it should give the correct prediction, within the limits of scatter, for any stress amplitude  $\sigma_a$  and mean stress  $\sigma_m$ , material, component, type of loading, environment etc.
- If possible it should be applicable down to very small crack lengths.

It should be noted that the above requirements are valid for constant stress amplitude loading. The (much more difficult) case of realistic load sequences will not be covered here.

### 4. AVAILABLE SOLUTIONS

In this chapter some published formulae for the calculation and prediction of crack propagation under constant stress amplitudes will be discussed. It was not the aim of the author to enumerate the countless models found in the literature; the reader is referred to the references (31 - 34); in (31) no less than thirtythree different formulae are tabulated! Rather, the few models actually used in design and verified by test will be judged against their only criterium - how well did they predict experimental results.

There was one serious attempt on a crack propagation model before the advent of fracture mechanics, that of Mc Evily and Illg (35) based on Neubers' notch strength theory.

Beginning with 1960 many crack propagation models appeared in the literature, mostly based on fracture mechanics principles. The first and still best known was published by Paris (36) and coworkers (37). Paris postulated that the cyclic change in the stress field surrounding the crack tip, the range of the stress intensity  $K$ , determined crack propagation according to the formula

$$\frac{da}{dN} = C \cdot \Delta K^n$$

For Aluminium alloys  $n = 4$  was proposed. This formula is still being used in design, for example in the pressure vessel industry, where all the load changes occur at  $R = 0$ , in spite of its obvious shortcomings; it accounts neither for mean stress effects, nor for  $K_{th}$  nor for  $K_C$ . If the effect of mean stress is taken into consideration by different constants  $C$ , as is sometimes suggested, we have a classic example of data fitting, because exactly those tests are required for determining  $C$  which the formula is supposed to replace. In 1967 Forman and coworkers (38) published an improved Paris equation

$$\frac{da}{dN} = C \frac{\Delta K^n}{(1-R) \cdot K_C - \Delta K}$$

in which at least mean stress effects and  $K_C$  were incorporated. This formula has been proved by many laboratories (7,32,40-42) to give a reasonable approximation to crack pro-



pagation test results for many different materials. Some examples are presented in Figs. 3 and 4, taken from (2), in which it is shown that it is possible to determine the constants  $C$  and  $n$  by tests at one particular set of stress amplitude  $\sigma_a$  and mean stress  $\sigma_m$  and to calculate crack propagation at other  $\sigma_a$  and  $\sigma_m$  values, using these constants. It was also shown by other IABG tests that this was also true at low temperatures (43), see Fig. 5 and under seawater corrosion (44). This is valid for  $R \geq 0$ . If the minimum stress of the cycle goes into compression, i.e. if  $R < 0$ , new tests at  $R < 0$  are necessary to determine new constants  $C$  and  $n$ .

Within the German Aircraft Industry the Forman equation is widely used; it has been incorporated as well in the German aircraft structural handbook (45). A commonly agreed computer program developed by MBB is used to calculate the constants  $C$  and  $n$  from the test data at hand.  $K_C$  is determined from the residual static strength of the fatigue crack propagation specimens themselves, using the Feddersen concept (46) and assuming no stable crack growth during the residual static strength test. In other words: The crack length present at the end of the fatigue crack propagation test is input into the  $K_C$  calculation.

Crack propagation for different sheet widths, stress amplitudes  $\sigma_a$  and mean stresses  $\sigma_m$  are then to be calculated using these  $C$ ,  $n$  and  $K_C$  values. This is obviously not quite correct because  $K_C$  depends among other things on sheet width. However, the Forman equation is not too sensitive to small variations in  $K_C$ , so the procedure described can be considered as an adequate engineering approximation.

The above equation does not contain  $\Delta K_{th}$  and therefore implies fatigue crack propagation even at infinitely small  $\Delta K$ . Klesnil and Lukas (47) modified the original Paris equation in the following way

$$\frac{da}{dN} = C \cdot (\Delta K^n - \Delta K_{th}^n),$$

while Hartmann and Schijve (40) suggested a slightly different version:

$$\frac{da}{dN} = C \cdot (\Delta K - \Delta K_{th})^n$$

In (28) the IABG incorporated both proposals into the Forman equation and found the Klesnil and Lukas solution

$$\frac{da}{dN} = \frac{C \cdot (\Delta K^n - \Delta K_{th}^n)}{(1-R) K_C - \Delta K}$$

to be a better fit to the experimental data available. Two examples are shown in Figs. 6 and 7. However, the numerical values for  $\Delta K_{th}$  must be determined by test.

Other formulae for calculation crack propagation have appeared in large numbers. To the author's knowledge none has, however, been so thoroughly investigated and judged against its only criterion - how well did it predict crack propagation under different  $\sigma_a$  and  $\sigma_m$  - as the Forman equation. The models of Walker (10) and the NEL (48) found a certain utilisation.

To conclude, it is suggested that the Forman equation, preferably in the modified form presented above, is a good enough approximation for engineering purposes. Any real improvement would certainly require

- a disproportionate effort and
- yet more "constants"

and thus might not be cost effective. In the opinion of the author, any future effort should be directed towards other problem areas, such as

- a method to correctly calculate  $K_C$  for different sheet widths and
- the determination of the variability of constants  $C$ ,  $n$ ,  $\Delta K_{th}$  and  $K_C$  within one heat and between different heats of a material.

## 5. RETARDATION EFFECTS

The above discussion dealt exclusively with crack propagation under constant stress amplitudes - a condition not often met in service. Rather, an irregular mixture of deterministically and stochastically varying stress amplitudes occurs in most engineering structures and the real design problem is to predict crack propagation in such conditions.

In this section, only some basic phenomena are covered, while the available semi-empirical models for the calculation of crack propagation under realistic load sequences will be treated in another lecture of this series.

Already in the very simple case of a single overload in a constant amplitude sequence some very complex events take place in the most highly stressed volume around the crack tip:



- The crack grows a certain amount  $\Delta a$ , increasing the stress intensity factor.
- A plastic zone develops in front of the crack tip, the size of which depends on the maximum stress of the overload, the crack length  $l$ , the yield stress at this moment in time, which is most probably not the original yield strength of the material and so on.
- In addition residual compressive stresses are set up, changing the effective mean stress.
- The crack tip is also blunted, resulting in a lower notch effect.
- The crack also closes before the load has reached zero and it takes a portion of the following tensile load cycle to open it again, decreasing the effective stress amplitude or stress intensity.
- Finally the plastic deformation of the material at the crack tip results in a cyclic strain hardening or softening, changing the relevant material properties.

Thus all the parameters affecting crack propagation, namely stress intensity (or stress amplitude), mean stress, crack tip acuity and the relevant material properties have been altered by just this one high load and the crack propagation rate will certainly have changed.

In most cases, the crack will have been slowed or retarded. The retardation effects in such simple load sequences have been treated extensively in the literature (49 - 59).

If one simply considers that in real load sequences, some of the effects of one high load will still be present to an unknown degree when the next high load of equal or different size occurs, one can imagine the difficulties in developing a model for predicting crack propagation under realistic load sequences: All of these events should be quantitatively accounted for in their synergistic effects on crack propagation. So even the most sophisticated of the presently available models are based on highly simplified assumptions (60 - 64).

## 6. REFERENCES

1. Leis, H. and W. Schütz: Bruchzähigkeit und Rißfortschritt von Titanlegierungen. Luftfahrttechnik - Raumfahrttechnik, Bd. 15, 1969, Nr. 7, pp. 180 - 184
2. Oberparleiter, W. and W. Schütz: Rißfortschritts- und Restfestigkeitsverhalten von Flugzeugbauwerkstoffen. IABG-Versuchsbericht TF 236, 1971
3. Frost, N.E., L. P. Pook and K. Denton: A Fracture Mechanics Analysis of Fatigue Crack Growth Data for Various Materials. Engineering Fracture Mechanics, Vol. 3, 1971, pp. 109 - 126
4. Frost, E. and A. F. Greenan: Effect of Tensile Mean Stress on the Alternating Stress Required to Propagate an Edge Crack in Mild Steel. Journal of Engineering Science, Vol. 9, No. 3, 1967, pp. 234 - 240
5. Mantz, J. and V. Weiss: Mean Stress and Environmental Effects on Near Threshold Fatigue Crack Growth, in: ASTM 601, 1976
6. Chu, H. P.: Effect of Mean Stress Intensity on Fatigue Crack Growth in a 5456-H117 Aluminum Alloy, in: ASTM STP 539, 1974
7. Hudson, C. M.: Effect of Stress Ratio on Fatigue Crack Growth in 7075-T6 and 2024-T3 Aluminum Alloy Specimens. NASA TN-D 5390, 1969
8. Katcher, M. and M. Kaplan: Effects of R-Factor and Crack Closure on Fatigue Crack Growth for Aluminum and Titanium Alloys, in: ASTM STP 559, 1974
9. Broek, D. and J. Schijve: The Influence of Mean Stress on the Propagation of Fatigue Cracks in Aluminum Alloy Sheet. NLR-TR M 2111, 1973
10. Walker, K.: The Effect of Stress Ratio During Crack Propagation and Fatigue for 2024-T3 and 7075-T6 Aluminum, in: ASTM STP 462, 1970
11. Sullivan, A. M. and T. W. Crooker: Analysis of Fatigue Crack Growth in a High-Strength Steel, Part I. ASME Paper 75-WA -PVP 22
12. Hubbard, R. P.: Crack Growth under Cyclic Compression. ASME Journal of Basic Engineering, December 1969, pp. 626 - 631
13. Schütz, W.: Fatigue Life Prediction of Aircraft Structures - Past, Present and Future. Engineering Fracture Mechanics, Vol. 6, No. 3, pp. 671 - 699, 1974
14. Hobbacher, A.: Zur Betriebsfestigkeit der Schweißkonstruktionen auf der Grundlage der Dauerfestigkeit. Thesis, Technical University Aachen, 1975
15. Lindner, B. M.: Extremely Slow Crack Growth Rates in Aluminum Alloy 7075-T6. M.S. Thesis, Lehigh University 1965
16. Cooke, R. J. and C. J. Beevers: The Effect of Load Ratio on the Threshold Stresses for Fatigue Crack Growth in Medium Carbon Steels. Engineering Fracture Mechanics, 1973, Vol. 5, pp. 1061 - 1071
17. Paris, P. C., R. J. Bucci, E. T. Wessel, W. G. Clark and R. T. Mager: An Extensive Study on Low Fatigue Crack Growth Rates in A 533 and A 508 Steels. ASTM STP 513, 1972
18. Masounave, J. and J. P. Bailon: The Dependence of the Threshold Stress Intensity Factor on the Cyclic Stress Ratio on Fatigue of Ferritic-Perlitic Steels. Scripta Metallurgica, Vol. 9, 1975, pp. 723 - 730
19. Pook, L. P. and A. F. Greenan: Fatigue Crack Growth Threshold for Mild Steel, a Low Alloy Steel and a Grey Cast Iron. NEL-Report No. 571, July 1974
20. Speidel, M. and R. B. Scarlin: Auswirkungen des Gefüges auf das Wachstum von Ermüdungsrisen, in: Gefüge und Bruch. Internationale Werkstoffprüftagung Leoben, November 1976. Bornträger, Berlin - Stuttgart 1977
21. Frost, E. and A. F. Greenan: Cyclic Stress Required to Propagate Edge Cracks in 8 Materials. Journal of Mechanical Engineering Science, Vol. 6, No. 3, 1964, pp. 203 - 210
22. Bucci, R. J., W. G. Clark and P. C. Paris: Fatigue Crack Propagation Growth Rates under a Wide Variation of  $\Delta K$  for an ASTM A 517 Grade F (T-1) Steel. ASTM STP 513, 1972

23. Paris, P. C., W. Weiss, E. T. Wessel and A. F. Anderson: On the Threshold for Fatigue Crack Growth. Presented at the 5th Int. Symp. on Fracture Mechanics, 1971
24. Schmidt, R. A. and P. C. Paris: Threshold for Fatigue Crack Propagation and the Effects of Load Ratio and Frequency, in: ASTM STP 536, 1973
25. Bucci, R. J., P. C. Paris, R. W. Hertzberg, R. A. Schmidt and A. F. Anderson: Fatigue Threshold Crack Propagation in Air and Dry Argon for a Ti6 Al4V Alloy, in: ASTM STP 513, 1972
26. Pook, L. P.: Fatigue Crack Growth Data for Various Materials Deduced from the Fatigue Lives of Precracked Plates, in: ASTM STP 513, 1972
- 26a. Frost, N. E. and D. S. Dugdale: Fatigue Tests on Notched Mild Steel Plates with Measurements of Fatigue Cracks. Jour. Med. Phys. Solids, Vol. 5, No. 3, 1957
27. Cooke, R. J. and C. J. Beevers: Slow Fatigue Crack Propagation in Pearlitic Steels. Material Science and Engineering, 13 (1974) pp. 201 - 210
- 27a. Mc Evily, A. J. Jr. and W. Illg: An Investigation of Nonpropagating Fatigue Cracks. NASA Technical Note D-208, December 1959
28. Schütz, W. and W. Oberparleiter: Ermittlung des unteren Grenzwertes für den Rißfortschritt bei Flugzeugbauwerkstoffen. IABG-Bericht B-TF-583
- 28a. Harrison, J. D.: An Analysis of Data on Non-propagating Fatigue Cracks on a Fracture Mechanics Basis. IIW-Doc XIII-591-70
29. Tu, L. K. and B. B. Seth: Threshold Corrosion Fatigue Crack Growth in Steels. Journal of Testing and Evaluation, Vol. 6, No. 1, Jan. 1978, pp. 66 - 74
- 29a. Hagn, L., R. Frank and P.-H. Effertz: Schwingungsbruch in Vergütungsstählen, in: Angewandte Bruchuntersuchung und Schadensklärung, Allianz-Zentrum für Technik, 20.-21.11.1975
30. Noack, H. G., K. Seifert und H. D. Steffens: Rißfortschrittsverhalten in Schweißnähten des Schiffbaustahls Gütegrad A im 8-Stufen-Programmversuch, in: Anwendung bruchmechanischer Verfahren auf Fragen der Betriebsfestigkeit. DVM, 1978
31. Hoepfner, P. W. and W. E. Krupp: Prediction of Component Life by Application of Fracture Crack Growth Knowledge. Engineering Fracture Mechanics, 1974, Vol. 6, pp. 47 - 70
32. Toor, P. M.: A Review of Some Damage Tolerance Design Approaches for Aircraft Structures. Engineering Fracture Mechanics, Vol. 5, pp. 837 - 880, 1973
33. Pelloux, R. M.: Review of Theories and Laws of Fatigue Crack Propagation. Air Force Conference on Fatigue and Fracture, 1969, AFFDL-TR-70-144, 1970, pp. 409 - 416
34. Erdogan, F.: Crack Propagation Theories. NASA CR-901, 1967
35. Mc Evily, A.J. and W. Illg: The Rate of Crack Propagation in two Aluminum Alloys. NASA TN-4396, 1958
36. Paris, P. C.: The Growth of Cracks due to Variations on Load. Dissertation, Leigh-University, 1960
37. Paris, P.C., M. P. Gomez and W. E. Anderson: A Rational Analytic Theory of Fatigue. The Trend in Engineering, University of Washington, Vol. 13, No. 1, 1961
38. Forman, F. G., V. E. Kearney and R. M. Engle: Numerical Analysis of Crack Propagation in Cyclic Loaded Structures. Journal of Basic Engineering, Sept. 1967, pp. 459 - 464
39. Crooker, T. W.: Effects of Tension Compression Cycling on Fatigue Crack Growth in High Strength Alloys. Journal of Engineering for Industry. Nov. 1971, pp. 893 - 896
40. Hartmann, A., and J. Schijve: The Effect of Environment and Load Frequency on the Crack Propagation Law for Macro Fatigue Crack Growth in Aluminum Alloys. Engineering Fracture Mechanics, Vol. 1, 1970, p. 615
41. Feddersen, C. E., and W. S. Hyler: Fracture and Fatigue Crack Propagation Characteristics of 7075-T7351 Aluminum Alloy Sheet and Plate. Report No. G 8902, Battelle Memorial Institute, Columbia, Ohio
42. Odorico, J.: Application de la Mécanique de la Rupture à la Sélection des Alliages d'Aluminium, in: AGARD-CP-221, 1977



43. Mertens, D. and W. Schütz: Rißfortschritts- und Restfestigkeitsverhalten von Flugzeugbauwerkstoffen bei tiefen Temperaturen. IABG-Versuchsbericht TF 365, 1973
44. Bär, S., W. Oberparleiter and W. Schütz: Einfluß korrosiver Umgebungsbedingungen auf zulässige Spannungen in Flugzeugstrukturen. IABG-Versuchsbericht B-TF-528, September 1975
45. Luftfahrttechnisches Handbuch: Handbuch Struktur Berechnung - HSB
46. Feddersen, C. E.: Evaluation and Prediction of Residual Static Strength of Center Cracked Tension Panels. ASTM STP 486, 1971
47. Klesnil, M. and P. Lukas: Influence of Strength and Stress History on Growth and Stabilisation on Fatigue Cracks. Engineering Fracture Mechanics, 1972, Vol. 4, pp. 77 - 92
48. Pook, L. P. and N. E. Frost: A Fatigue Crack Growth Theory. International Journal of Fracture, March 1973
49. Mills, W. J., R. W. Hertzberg, and R. Roberts: Load Interaction Effects on Fatigue Crack Growth in A514F Steel Alloy. Engineering Fracture Mechanics, Vol. 8, 1976, pp. 657-667
50. Mills, W. J. and R. W. Hertzberg: The Effect of Sheet Thickness on Fatigue Crack Retardation in 2024-T3 Aluminum Alloy. Engineering Fracture Mechanics, Vol. 7, 1975, pp. 705 - 711
51. Mills, W. J. and R. W. Hertzberg: Load Interaction Effects on Fatigue Crack Propagation in 2024-T3 Aluminum Alloy. Engineering Fracture Mechanics, Vol. 8, 1976
52. Katcher, M.: Crack Growth Retardation Under Aircraft Spectrum Loads. Engineering Fracture Mechanics, Vol. 5, 1973, pp. 793 - 818
53. Rice, R. C. and R. I. Stephens: Overload Effects on Subcritical Crack Growth in Austenitic Manganese Steel, Progress in Flaw Growth and Fracture Toughness Testing. ASTM STP 536, 1973, pp. 95 - 113
54. Gallagher, J. P. and T. F. Hughes: Influence of Yield Strength on Overload Affected Fatigue Crack Growth Behavior in 4340 Steel. AFFDL-TR-74-27, Air Force Flight Dynamics Lab, 1974
55. Corbly, D. M. and P. F. Packman: On The Influence of Single and Multiple Peak Overloads on Fatigue Crack Propagation in 7075-T6511 Aluminum. Engineering Fracture Mechanics, Vol. 5, 1973, pp. 479 - 497
56. Von Euw, E. F. J., R. W. Hertzberg, and R. Roberts: Delay Effects in Fatigue Crack Propagation, Stress Analysis and Growth of Cracks. ASTM STP 513, 1972
57. Trebules, V. W. Jr., R. Roberts, and R. W. Hertzberg: Effects of Multiple Overloads on Fatigue Crack Propagation in 2024-T3 Aluminum Alloy, in: Progress in Flaw Growth and Fracture Toughness Testing. ASTM STP 536, 1973, pp. 115 - 139
58. Probst, E. P. and B. M. Hillberry: Fatigue Crack Delay and Arrest Due to Single Peak Overloads. AIAA Journal, Vol. 12, No. 3, March 1974, p. 330
59. Jones, R. E.: Fatigue Crack Growth Retardation After Single - Cycle Peak Overload in Ti-6Al-4V Titanium Alloy. Engineering Fracture Mechanics, Vol. 5, 1973, pp. 585-604
60. Nelson, D. V.: Review of Fatigue-Crack-Growth Prediction Under Irregular Loading. Paper at the 1975 SESA Spring Meeting, Chicago, Illinois
61. Broek, D.: The Prediction of Crack Propagation. Chapter V B.1 in: Fracture Mechanics of Aircraft Structures, Editor H. Liebowitz, AGARD-AG-176
62. Oberparleiter, W. and W. Schütz: Berechnung des Rißfortschrittes an Bauteilen bei veränderlichen Spannungsamplituden. IABG-Bericht B-TF-508, 1976
63. Wood, H. A.: A Summary of Crack Growth Prediction Techniques, in: AGARD LS-62, 1972
64. Schütz, W.: Calculation Methods for Fatigue Life and Crack Propagation, in: Fatigue Design of Fighters, AGARD AG 231



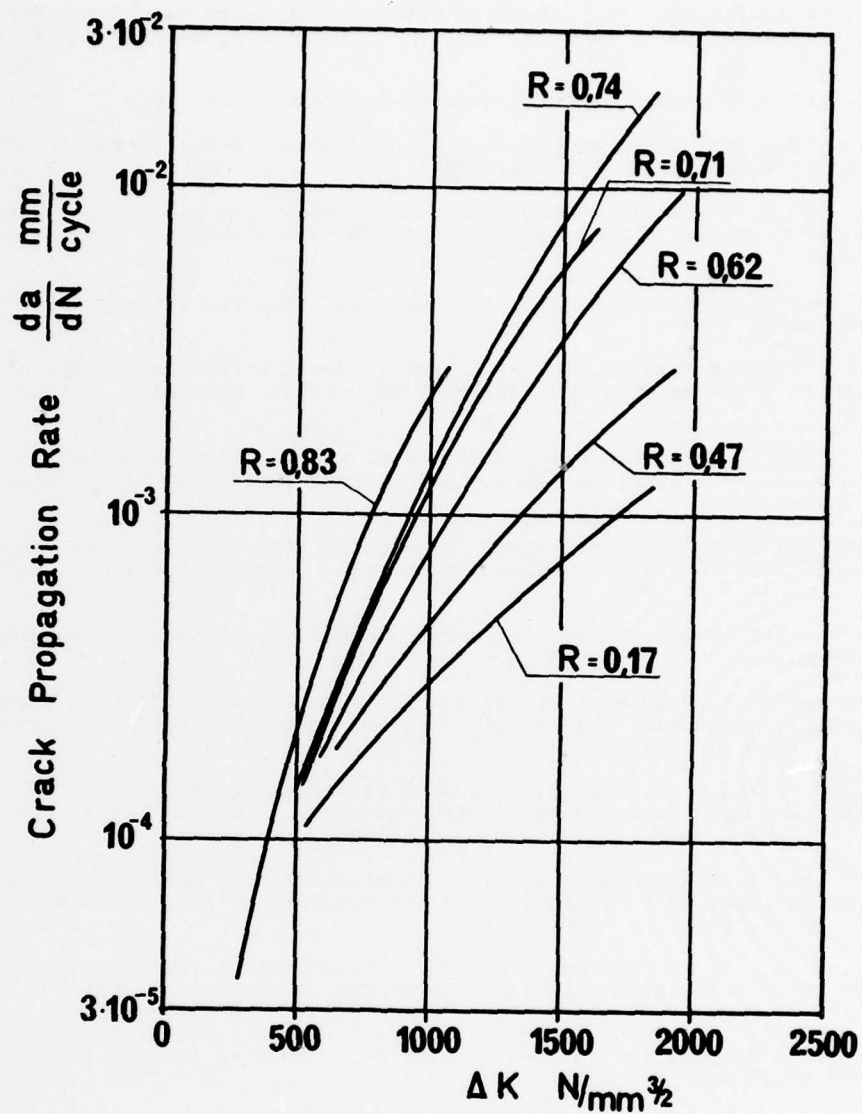


FIGURE 1. INFLUENCE OF STRESS RATIO  $R$   
ON CRACK PROPAGATION RATE  
MATERIAL: NICOMO MARAGING STEEL

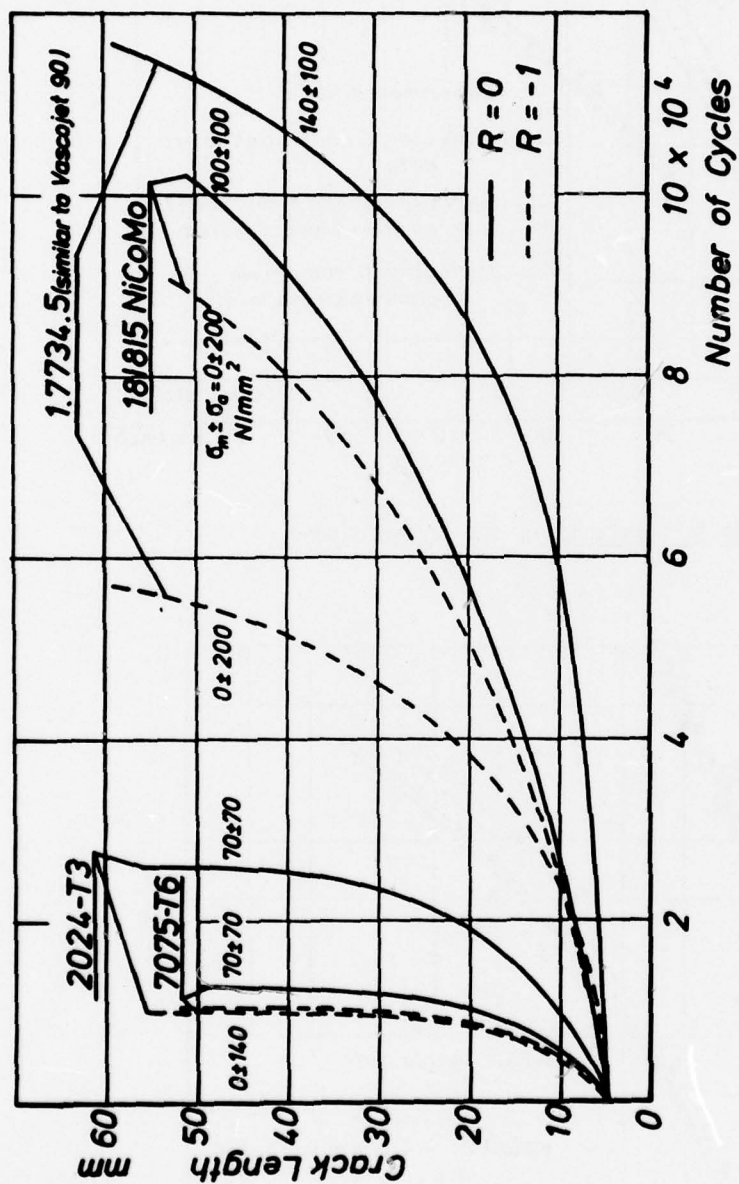


FIGURE 2. INFLUENCE OF TENSION-COMPRESSION LOADING ON CRACK PROPAGATION OF DIFFERENT MATERIALS

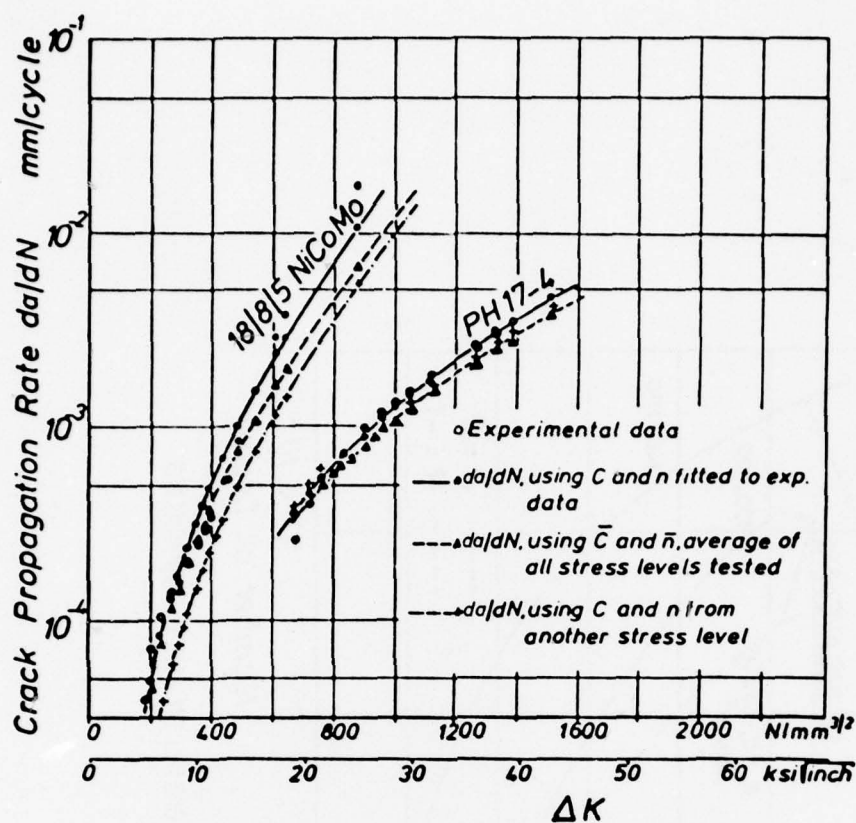


FIGURE 3. CHECKING OF THE FORMAN FORMULA

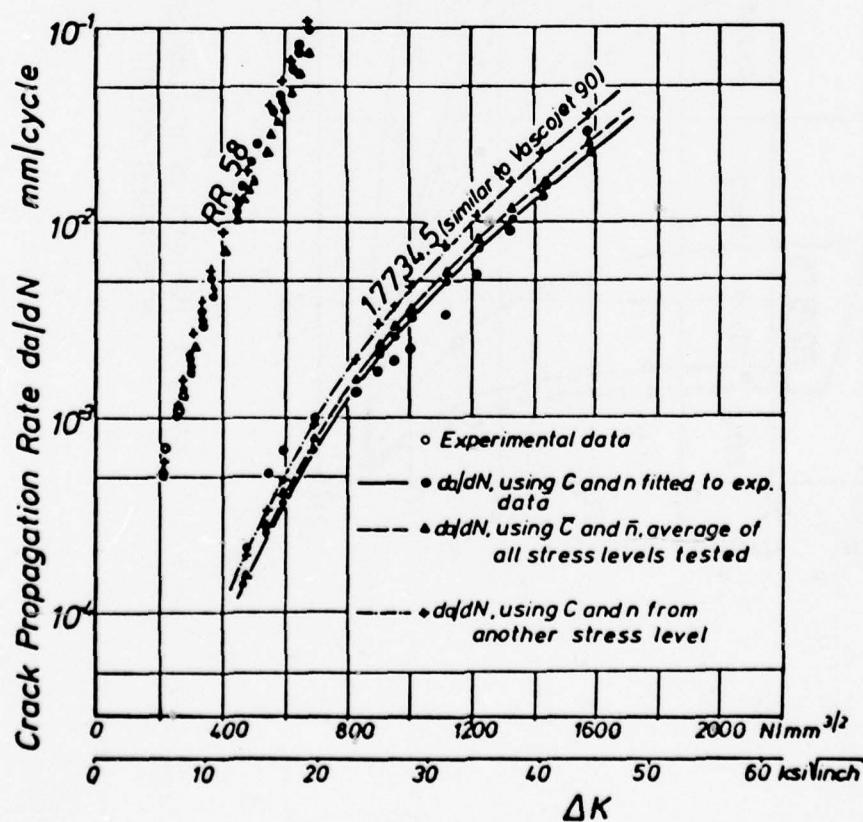


FIGURE 4. CHECKING OF THE FORMAN FORMULA

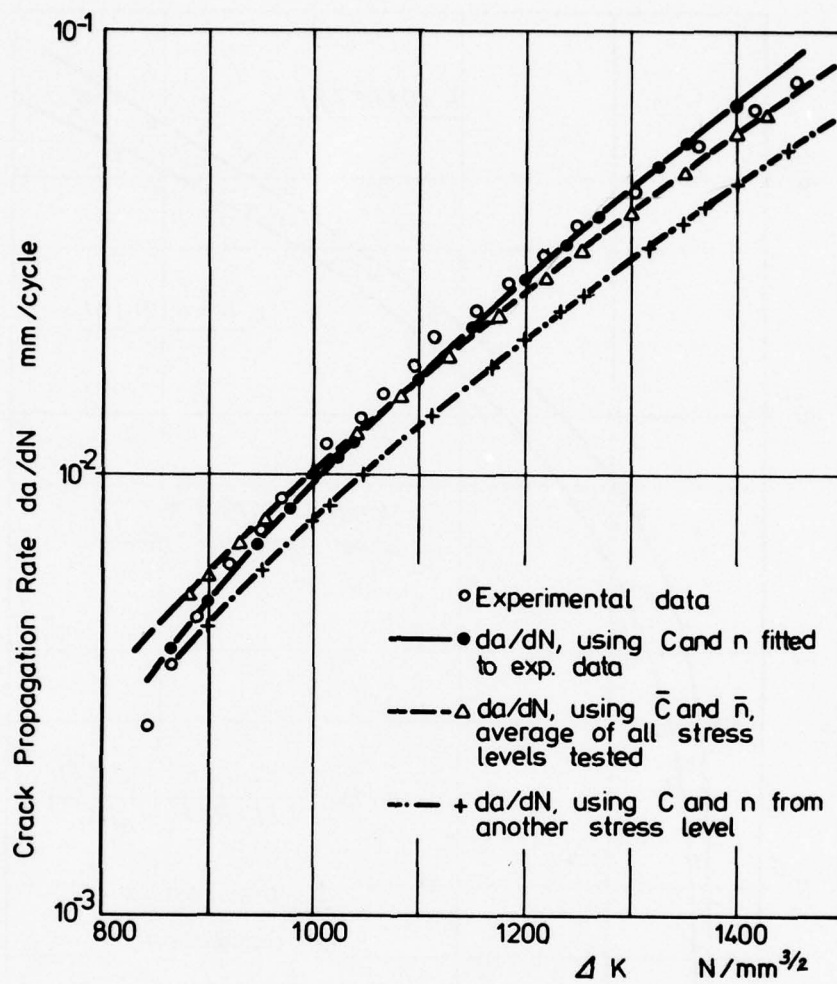


FIGURE 5. CHECKING OF THE FORMAN FORMULA AT  $-50^{\circ}C$ .  
MATERIAL: TI6AL4V



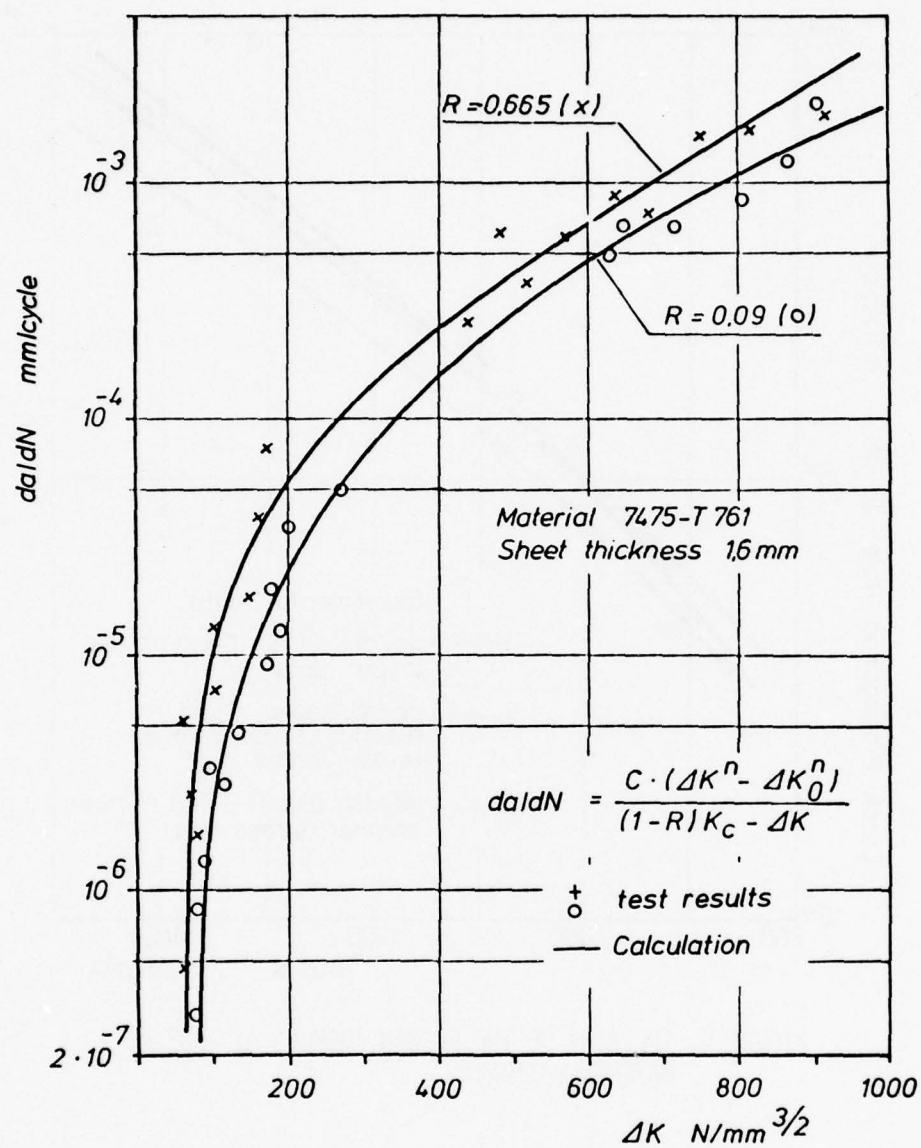


FIGURE 6. CHECKING OF THE IMPROVED FORMAN FORMULA

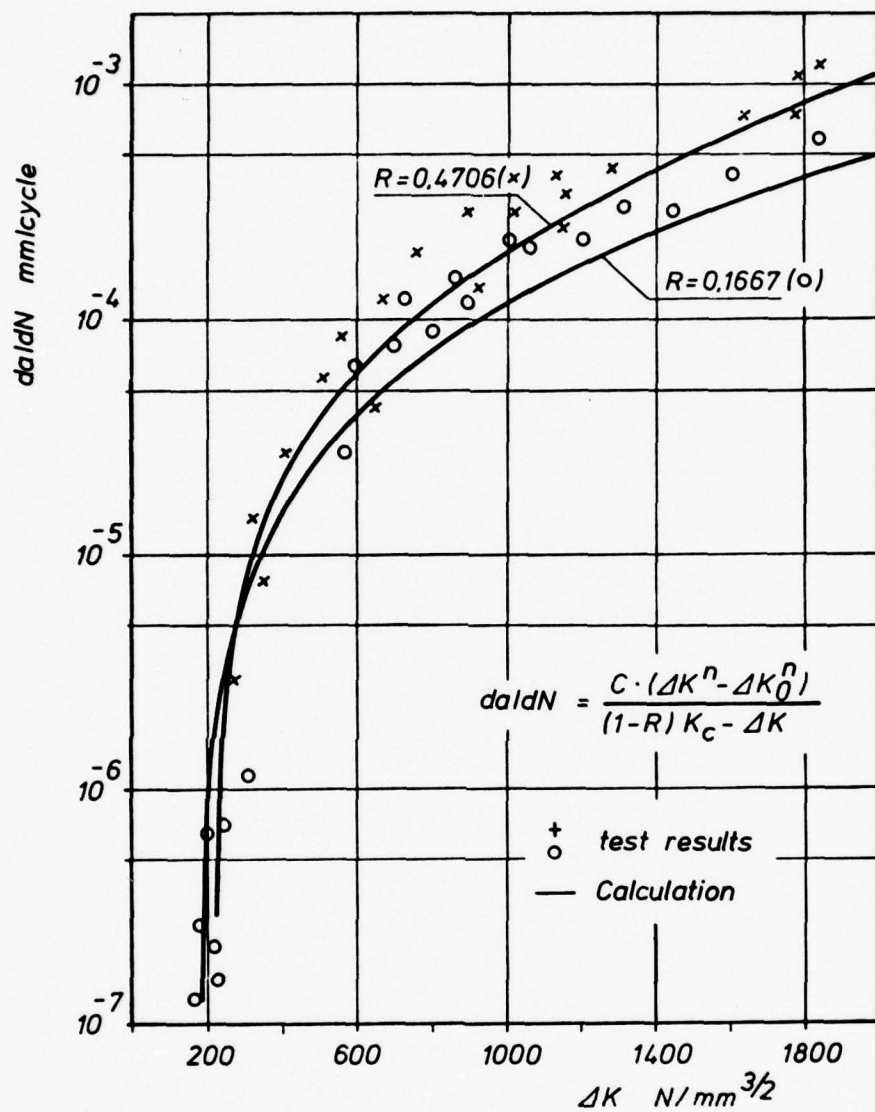


FIGURE 7. CHECKING OF THE IMPROVED FORMAN FORMULA  
MATERIAL: MARAGING STEEL

**SESSION II**

**DAMAGE TOLERANCE ANALYSIS**

STRESS INTENSITY ANALYSIS:  
ANALYTICAL, FINITE ELEMENT FOR SURFACE FLAWS, HOLES

D.P. Wilhem  
Northrop Corporation  
Aircraft Group  
3901 West Broadway  
Hawthorne, California 90250

SUMMARY

Several methods are available to obtain stress intensity factors for developing cracks in structure where uniform loading and symmetric cracks prevail. Unfortunately in all aircraft structure both loading (stress) and crack geometries are far from ideal. These factors combined with localized plasticity require the use of more sophisticated means of obtaining stress intensity factors. Finite element analysis, both with and without special cracked elements, can be used to obtain stress intensity values. Careful attention must be paid in modeling to account for various factors, i.e., fasteners, etc., which affect the stress field. In many cases where elastic-plastic behavior is evident those finite element programs with nonlinear capability can be effectively used to compute J-integral values for use in both fatigue and fracture studies. A case study will be shown which involves a cutout in the wing in a highly stressed region the root. Other cases will deal with part-through-cracks at holes and countersinks and other design details. Recently, the use of three dimensional finite element models to obtain stress intensities for cracks at holes provided an opportunity to evaluate the merits of each method of analysis; analytical, finite element and semi-empirical. Comparisons are presented for several cases.

## 1. INTRODUCTION

In most structural cracking, the most common site for cracks are at holes which are used for fastening the structure together. If nominal loading is applied, it is well known that a stress concentration for an unfilled hole is on the order of three. Thus, if nominal maximum anticipated stress is  $2/3$  of the ultimate strength, local stresses near the hole can be extremely large and with time cause local cracking. Tear-down inspections indicate numerous cracks radiating from the holes. In particular, countersunk holes show predominant cracking at the intersection of the bore and countersink. Recent research has concentrated on obtaining stress intensity factors for crack(s) at holes. An accurate representation of the stress intensity for part-through-cracks at holes is now available and can be used with confidence in predicting the fatigue crack growth from holes. Another situation occurring in structure is the change in usage resulting in a new spectrum of loads, usually more severe than originally intended. An example of this is shown for a PTC at a radius which required a finite element analysis of the structure that had to be verified by a coupon test in the nonlinear fracture mechanics range. Much can be determined about the local elastic-plastic region, e.g., plastic zone sizes, stress gradient, etc., using a J-integral approach. Comparisons can be made with strain gradients obtained from fatigue and static tests of the full scale structure. Examples are given for several cases as applied to a high performance aircraft structure.

## 2. STRESS INTENSITY ANALYSIS

### 2.1 General Discussion

In calculating stress intensity factors, the limitations of linear elastic fracture mechanics apply. In general, the solutions that are available are for "ideal" crack geometries and loading conditions. Corrections can be applied to K to treat limited plasticity (i.e., small scale yielding) and are a function of K and hence have limited utility in real life situations, i.e., short cracks in loaded holes. The problem exists when a structure intended for a given external loading environment is placed in one that is more severe than the design load conditions. Cracks develop in areas which were known to be fatigue sensitive, and due to the change in load environment, now become fatigue critical. Estimates must still be made of spectrum fatigue crack growth and critical fracture stresses for these situations. In addition, rework designs must be evaluated for their adequacy in extending structural life for these higher than anticipated loads. An examination of what is currently available, and how new fracture mechanics techniques may be useful in obtaining reasonable life estimates, will be the starting point.

### 2.2 Developments in K - Stress Influence

In stress intensity factor development the basic equation is:

$$K = \sigma \sqrt{\pi a} \quad \beta \quad (1)$$

The stress term,  $\sigma$ , is normally the gross area stress based on remotely applied load. In a structure, the magnitude and direction of applied load is not always obvious. The seriousness or criticality of the part or structure will generally dictate the type of analysis for determining local loads. New and evolving structures have finite element analyses performed to determine the optimum weight/strength combination. This is particularly true in aircraft structures as noted in other lectures of this series. But, in most cases the potential or existing crack in a structure requires a more detailed stress field description than that obtained from large area, finite element models. The gradients, due to local structural details, fillets, holes, radii, lugs, etc., must be described in a fair amount of detail. If confirmative testing is to be accomplished, this is a definite requirement so that gradients can be properly matched. This requires the use of local finite element models. The boundary stresses obtained from the larger models can then be applied to the local model. In many situations the individual performing the modeling is not versed in fracture mechanics. To properly interpret the local model results then requires close



cooperation between the FM specialist and finite element modeler.

In analytical assessments of stress gradients there are mathematical techniques available to properly evaluate  $\sigma$  in Equation (1). Superposition of stress intensities, Green's function matching, and others can be used to obtain reasonable estimates of  $K$  and are particularly useful in preliminary design, where frequent changes are made to sizing resulting in stress alterations. However, stress is not the only controlling factor in Equation (1).

### 2.3 Developments in $K$ - Boundary Corrections (Betas)

The basic stress intensity solutions are primarily developed for infinite boundary problems such that Beta in Equation (1) is unity. This implies that the boundaries of the crack are far removed from the specimen or structural boundaries. However, this is not the case in structural hardware problems where part-through cracks predominate, holes are nominally 2D in edge distance, and radii are on free edges. Based on past experience, it is known that without accounting for these influences, it becomes difficult to accurately predict fatigue crack growth.

In summary, the following are a must if stress intensity factor solutions are to be used successfully in structural analysis:

- Loading must be accurately represented;
- Plasticity must be accounted for;
- Boundary corrections must be incorporated.

In current finite element techniques it is possible to accurately determine local stress and influence of boundaries. However, the description of any elastic-plastic behavior requires something newer than LEFM  $K$ 's, and the J-integral approach looks promising.

### 2.4 Obtaining Structural Stress Intensity Factors

Numerous procedures are available to determine  $K$ . In all cases, the solution is normalized and compared to some existing solution (usually classical). The basic means of obtaining  $K$  are numerical, finite element, and empirical or semi-empirical. For most structural crack geometries where cracking has occurred in service, the semi-empirical fatigue crack growth matching procedure (see e.g. Reference 1) is most reliable, but limited to matching in-service structural behavior by test.

Of the several techniques available, numerical analyses is the most popular. These consist of collocation, boundary integral equations, conformal mapping, complex variables, eigenfunction expansion, boundary collocation, and others. In most of these methods, ideal loading, along with crack symmetry, is a must. They are ideally situated to treat test coupon type of cracking when crack symmetry is not a problem.

Finite element analysis was first employed several years ago to develop stress intensity factors for various through-the-thickness crack configurations. These were determined from linear extrapolation of displacements toward the crack tip. This extrapolated displacement was then used in calculating  $K$  from the normal LEFM displacement equations. Recently, the development of both two and three dimensional cracked elements (treating the singularity at the crack tip) have been used with a high degree of success for determining specimen-type, crack stress intensities, (e.g. center cracked & edge cracked geometries). The use of these hybrid elements in conjunction with existing structural finite element analysis, becomes immediately apparent. However, the ultimate use of these special elements should be planned during the initial modeling stages to prevent excessive computer time and cost. The use of the finite element in the analysis of structural crack problems will follow the trend already established in its use in structural analysis.

In the case of fatigue crack growth in structure, one of the most accurate means of obtaining stress intensities for crack geometries without existing solutions is by using semi-empirical methods. Those described in Reference (1) are typical of the technique in which matching of unknown structural  $K$ 's (knowing the fatigue crack growth rates ( $da/dN$ )) is accomplished by applying appropriate Betas to match the classic  $da/dN$  versus  $K$  or  $\Delta K$  data. Comparison of data obtained from both numerical solutions for  $K$  with those obtained using this technique have been found to be excellent (see Reference 2) for complex structural arrangements. Other empirical methods which have been used with confidence are energy techniques, such as determining  $\mathcal{H}$  for the structure at given crack lengths, and the use of photoelastic (stress freezing) techniques for the crack geometry of interest.

## 3. APPLICATIONS OF $K$ TO A CRACK AT A STRUCTURAL HOLE

### 3.1 Comparison of Existing $K$ Solutions - Thru and Part-Thru Thickness Cracks at Open Holes

The numerical solutions which are available for determining  $K$ 's for a crack at a hole are limited to the ideal crack geometry. However, if a crack at a hole is to be analyzed, a comparison of existing solutions would be a useful exercise, and indicate both trends and limitations of the analytical methods. For the open hole case, Bowie analyzed the through-the-thickness crack (TTC) at a remotely loaded open hole (Reference 3). Equations have been fit to the tabular data of Bowie, namely Reference 4 & 5, and describe this TTC situation quite well. Other solutions use the stress concentration ( $K_t$ ) approach for an uncracked hole and decay the stress away from the hole (typical Green's function matching) for the cracked geometry. An example of this approach is shown in Figure 1 where the data of Hsu (Reference 6) agrees quite accurately with the classic solution of Bowie for a TTC.

In service the TTC is not the usual crack geometry as indicated from numerous inspections of aircraft as described in Reference 7.

Since most naturally occurring cracks are PTC and edge distance (finite width) becomes important, a

comparison of PTC, K solutions should be made. The basic K solution applies (Equation 1) where the Beta terms can best describe each individual solution. Beta generally being a function of crack depth,  $a$ , and hole diameter (D) or radius (r). As the importance of other factors such as crack length,  $c$ , (on the surface) and flaw shape were realized, they were included in the basic K equation. For example, Liu (Reference 8) indicated that Beta was a function of the ratio of depth to length and length to hole radius as well as part geometry, i.e., width. W. Hsu (Reference 6) included the effect of flaw shape parameter,  $Q$ , and crack depth to hole radius as a Beta function. Newman, using a semi-empirical approach (Reference 9) included the back surface correction as a function of depth of crack to thickness (B) ratio and crack eccentricity (for single cracks at holes) for a more complete description of K. Recently, Raju and Newman (Reference 10) using a three dimensional finite element approach, have indicated that in addition to those factors already discussed, the stress intensity varies along the crack front as a function of  $\theta$ , the angular position along the front.

A comparison of these solutions for the case of a symmetrical crack ( $a/c = 1.0$ ) for a given geometry, is shown in Figure 2 for PTC at a 0.26 inch diameter hole. Several trends are evident. The solutions of Liu (Reference 8) and Hsu (Reference 6) bracket those of Newman (Reference 9) and Wilhem (Reference 11). The latter was determined using the Reference 1 approach to the data of Schijve and Jacobs (Reference 12), developing semi-empirical K's for the PTC geometry, since crack symmetry ( $a/c = 1.0$ ) was evident in that data. Interestingly, the results of Reference 9 and 11 merge. The data used in the Reference 9 approach were from stress freezing results and aluminum fatigue crack growth for Reference 11. Note that the three dimensional results of Reference 10 falls within the band of these data. A variation is noted for the given crack size which reflects the change in K with position along the crack front ( $\theta$ ). For comparison, the severity of the Bowie (Reference 3) solution for a TTC is noted, which emphasizes that a severe penalty is paid by not properly modeling the primary structural cracking behavior at holes, i.e., as a PTC.

With comparative, normalized K data (Beta in this case) like those shown in Figure 2, a judgement can then be made as to the proper solution to use in any fracture or fatigue analysis for that crack geometry. In this symmetrical case, the solution of Reference 9 would be adequate for estimating K.

### 3.2 Influence of Random and Constant Amplitude Loading on Crack Shape

As part of an extensive damage tolerance assessment program performed in Reference 13, numerous PTC specimens were tested to several random spectra. Post fracture examination of the fracture faces indicate the less than symmetrical crack growth, i.e.,  $a/c$  varies with depth of crack (see Figure 3). Note that the growth from both countersunk and noncountersunk hole is not symmetrical in surface length and depth. To further verify these changing crack aspect ( $a/c$ ) ratios, several specimens of 7075-T651 aluminum were tested to a given spectrum. Post fracture examination of the photomacrographs (similar to Figure 3) were used to measure initial and half thickness  $a/c$  ratios. These data are shown in Table 1.

Table 1 Measured Crack Aspect Ratios for Random Spectrum Loaded PTC at Hole

HOLE CONDITION	INITIAL $a/c$	$a/c$ AT HALF-THICKNESS
No Countersink	6.48	1.40
	3.74	2.05
	2.67	1.00
Countersunk 100°	2.00	1.06
	2.18	1.38
	2.00	1.36
Thickness - 0.410 inches (1.04 cm)      Hole Diameter - 0.260 inches (0.66 cm) Width - 3.0 inches (7.62 cm)      Maximum Spectrum Stress - 48 ksi (331 MPa)		

Although large variations of crack aspect ratio are noted for initial cracking, once the crack grows to half-thickness, a fairly uniform  $a/c$  ratio develops, regardless of hole condition. With this information in hand, it was thought that these trends may be a peculiarity of spectrum loading. As an indication of the unpredictable nature of even constant amplitude data, refer to Figure 4. These data obtained from holes (Ref. 14) on 7075-T6 aluminum, 0.635 cm thick with 0.635 cm diameter holes spaced  $> 10$  diameter apart, show two different trends in  $a/c$  within the same specimen.

### 3.3 Factors Influencing Crack Growth From Open Holes

Several questions arose from the information provided thus far; 1) are there estimates of K available to predict  $a/c$  changes with length; 2) how important are these changes in shape to life prediction; and 3) must the countersink be included in the Beta corrections to account for early life crack acceleration?

Normalized, three dimensional finite element results of Reference 10 can provide some insight into the predictable trends of change in crack aspect ratio ( $a/c$ ) with crack length,  $a$ . Polar plots of these data are shown in Figure 5 for  $a/c = 1.0$  and Figure 6 for  $a/c = 2.0$  at three values of crack depth to thickness ratio ( $a/t$ ). Note the varying shape of normalized  $K_I$  with crack length. The maximum value of K changes in angular position ( $\theta$ ) with crack depth. Interestingly, the shape of the crack front of Figure 3 (open hole) at an  $a/t = 0.2$  looks very similar to that curve shown in Figure 6 for the same  $a/t$  ratio. If predictions of crack front shape were required, then the use of the method described in Reference 10 could be used with confidence. However, as inferred from that reference cost considerations do not warrant further refinements since the limits of these data agree quite well with the Reference 9 solutions for both  $a/c$  ratios.

In all fatigue crack growth tests of Reference 13 initial, accelerated crack growth occurred from the



PTC located at the bottom of the countersink. This acceleration was quite rapid and results from the increase in stress concentration known to exist at the bore/countersink intersection. Previous data (Reference 15) indicated a 20% increase in stress for that intersection. Recent data (Reference 16) shows increases as large as 25 to 35% using stress freezing techniques for uniaxially loaded holes.

It is now possible to develop the complete model for fatigue crack growth at holes. Those factors required for an accurate analysis would be to account for:

- ° Countersink
- ° Changing Crack Shape
- ° Fatigue Life Improvement (Cold work, Interference Fit, etc.)
- ° Load Transfer

The test of any stress intensity solution is how well it will repredict the measured fatigue crack growth data. Use of these solutions in predicting growth will be discussed next.

### 3.4 Correlation of Constant and Random Loaded Fatigue Crack Growth at Holes

A prediction was made of one, constant amplitude fatigue crack growth data set from Reference 14, where crack symmetry prevailed to failure. The data and prediction using the Reference 9, K solution are shown in Figure 7. Note that all datasets are plotted in terms of surface length,  $c$ , (rather than depth) as this dimension is more readily accessible during structural inspections. The prediction is conservative, which is very desirable for life prediction purposes. More importantly the trend matches the data quite well.

Data from spectrum loading of an open hole are noted in Figure 8 for duplicate tests. The solution of Reference 9 was employed in conjunction with a retardation model proposed in Reference 17. This retardation model was selected over others since it treats the higher spectrum stresses in a more consistent manner for those spectra which are high stress dominant, as in this case. An in-house computer code was used to predict the flight-by-flight growth of the crack using the proper retardation model, and the various crack aspect ratios noted in Figure 8. Note that good correlation is obtained only for the early life portion. If a variable  $a/c$  (with "a") were available to account for the changes occurring during test, then a closer fit to the data would occur.

The influence of countersink on both early and overall life crack growth for two (2) alloys of 7075 aluminum is shown in Figure 9 for identical spectrum. Notice the rapid, initial crack growth for the countersunk specimens of both -T651 and -T7351. One anomaly is obvious from these data. Contrary to constant amplitude fatigue crack growth data which show slower rates for 7075-T7351, these spectrum data show a reversal, i.e., the -T651 material has a slower growth rate. Examination of the literature revealed that these reversals in trends for constant amplitude and spectrum loading, have been observed by others (Reference 18) for aluminum alloys. To further verify this trend, two (2) center cracked tension (CCT) specimens of identical geometry were spectrum loaded to failure. One coupon was 7075-T651 and the other 7075-T7351. An initial constant amplitude fatigue crack was started from a 0.031 inch diameter hole with small jeweler's sawcuts. From the data shown in Figure 10, it is evident that the only difference is in total life for the spectrum environment. The consistency noted here for these two (2) materials obviously negated the use of a retardation model for prediction of the 7075-T7351 material, since the constant amplitude fatigue crack growth constants are different for these two alloys.

In the actual hardware application there are influences which can override any of those discussed thus far. In addition to load transfer, the condition of the hole and structural arrangements are most important.

## 4. A FINITE ELEMENT SOLUTION FOR STRUCTURAL CRACK PROBLEMS

### 4.1 A Crack at a Highly Stressed Radius

A typical problem encountered in high performance aircraft is a crack in an area which is highly stressed due to a combination of factors (wing sweep, new spectra, etc.). Knowing the structural description, a finite element model can be developed as shown in Figure 11. By proper planning, a local model of the problem area can be made at the same time. Two (2) such models were made using the NASTRAN program and included the skin, rib, and spars in the region of the skin radius. Making NASTRAN calculations of overall and local stresses for the critical fatigue conditions produces plots (on the local level) as shown in Figure 12. The build-up in stress at the radius is evident. The skin is tapered in thickness forward in this region. From data such as these, a gradient is established for the radius which can be used to produce test matching, and in the analysis. If stresses are large enough, then plastic behavior of the radius must also be considered. Several studies were performed examining this elastic-plastic fatigue crack growth problem. Detail results are reported elsewhere (Reference 19) and will be summarized here.

The problem was to predict fatigue crack growth from a PTC at a half inch radius, compare the results with test data, and evaluate the "fix" which consisted of increased thickness, radius (to 3 inches), and changing alloy. First step was to properly match the local model stress gradient in test. This required a finite element model of the test coupon. The NASTRAN model is shown in Figure 13. Provisions were made for elastic-plastic analysis using J-integral calculations. The details of the procedure used for calculating J are described in Reference 20. Square root of J values (in the elastic sense  $J = K^2/E$ ) for given TTC lengths, are shown in Figure 14 for two alloys of 7075. Cross plots of these data with applied stress, can be made which follow the trends noted in Figure 15. Normalized values can then be determined and used in a corrective sense (as a Beta factor), which is now a function of applied stress since the  $\sqrt{J}$  is a function of stress (see Figure 14).

The elastic gradient of the specimen can be analytically predicted and is a function of the position of the loading hole seen in Figure 13. Using this information a plot can be made of stress gradient with load hole location. This variation in gradient is shown in Figure 16. The "fix" consisted, as mentioned,

of increasing radius and thickness as well as changing alloy. The gradient for this larger radius is shown in Figure 17. To match the local NASTRAN model gradient of the wing, a load point 1 1/2 inches away from the centerline is indicated by the data. Other information can also be obtained from these elastic-plastic analyses. By assuming that flow stress ( $\bar{\sigma}$ ) equals the elastic proportional limit of the material, the individual elements are considered yielded under those conditions. A map can then be made of the elastic-plastic boundary for each TTC length. The flow stress is computed from the following equation for elements near the crack.

$$\bar{\sigma} = \left[ \sigma_x^2 - \sigma_x \sigma_y + \sigma_y^2 + 3 \tau_{xy}^2 \right]^{1/2} \quad (2)$$

A map of the computed zones using Equation (2) is shown in Figure 18 for the 7.62 cm radius loaded 1 1/2 inches off-center.

#### 4.2 A Crack at a Cutout

The structural description is shown for a typical cockpit area in Figure 19. Cutouts are provided in the upper longeron to permit latching of the canopy. A local model of the cutout with detail in the corner is shown in Figure 20 which shows cross sectional detail. Primary loading is due to cockpit pressurization and fuselage bending. Once again, a model of the coupon which will be tested must be furnished, and comparisons made of gradients prior to test, with both full scale and local area models. Since the region of interest is similar to a chord rather than a radius, the specimen was designed containing a chord. The comparison of the fuselage gradient from the Figure 19 model, with that from the Figure 20 local model (at a slightly different longeron location) is shown in Figure 21. Note a slight difference in depth of radius between test coupon and local model. However, the gradients match quite well between test and analysis (which also agree with the static test data on the full scale aircraft). Differences do occur in  $K_t$ 's at the radius edge, therefore, care must be exercised in applying the proper loads to the test coupon, to match service loading.

The accuracy of the analytical procedures developed in this lecture will be discussed in the second lecture by the author of this series.

#### 5. REFERENCES

1. James, L.A. and Anderson, W.E., "A Simple Experimental Procedure for Stress Intensity Factor Calibration," in Compendium to Engineering Fracture Mechanics, Volume I, 1969.
2. Ratwani, M.M., "Characterization of Fatigue Crack Growth in Bonded Structures, Volume I: Crack Growth Prediction in Bonded Structure," AFFDL TR-77-31, Volume I, June 1977.
3. Bowie, O.L., "Analysis of an Infinite Plate Containing Radial Cracks Originating from the Boundary of an Internal Circular Hole," Journal of Mathematics and Physics, Volume 35, 1956.
4. Newman, J.C. Jr., "Fracture Analysis of Various Cracked Configurations in Sheet and Plate Materials", NASA TM X-72709, 1975.
5. Brussat, T.R., et. al., "Flaw Growth in Complex Structure," AFFDL TR-77-79, December 1977.
6. Hsu, T.M., et. al., "Extended Study of Flaw Growth at Fastener Holes," Volume I, AFFDL TR-77-83, April 1978.
7. AGARD, "Northrop/United States Air Force Durability and Damage Tolerance Assessment of the F-5E/F Aircraft," presented at the 43rd Meeting of the AGARD Structures and Materials Panel, London, September 1976.
8. Liu, A.F., "Stress Intensity Factor for a Corner Flaw," Engineering Fracture Mechanics, Volume 4, 1972.
9. Newman, Jr. J.C., "Predicting Failure of Specimens with Either Surface Cracks or Corner Cracks at Holes," NASA TND-8244, June 1976.
10. Raju, I.S., and Newman, Jr. J.C., "Stress Intensity Factors for Corner Cracks at the Edge of a Hole," NASA Memo 78728, June 1978.
11. Wilhem, D.P., Internal Northrop Aircraft Group Communication, July 1977.
12. Schijve, J. and Jacobs, F.A., "Fatigue Crack Propagation in Unnotched and Notched Aluminum Alloy Specimens," National Aero and Astronautical Research Institute Report, NLR-TR-M.2128, May 1964.
13. Northrop Corporation, Aircraft Group Report, "T-38 Damage Tolerance Assessment Program NPN 3347 - Crack Growth Test Summary Report," Report No. NOR 77-17, Hawthorne, California, October 1978.
14. Private communication, Boeing Aerospace, January 1978.
15. Whaley, R.E., "Stress Concentration Factors for Countersunk Holes," SESA Experimental Mechanics, August 1965.
16. Cheng, Y.F., "Stress Concentration Factors for a Countersunk Hole in a Flat Bar in Tension and Transverse Bending," presented to 8th U.S. National Congress of Applied Mechanics, Los Angeles, California, June 26-30, 1978, (to be published in Journal of Appl. Mech., ASME).



17. North American - Rockwell, Report No. NA-72-94, "Crack Propagation Analysis by G. Vroman's Model - Computer Analysis Summary, Program EFFGRO, Los Angeles Division, Rockwell International, dated February 1972.
18. Sippel, K.O. and Weisgerber, D., "Crack Propagation in Flight by Flight Tests on Different Materials," paper presented to the 1975 ICAF Colloquium, Lausanne, 5 June 1975.
19. Northrop Corporation, Aircraft Group Report No. NOR 78-79, "Nonlinear Fracture Mechanics Analysis of the T-38 Wing Root Radius," Northrop Corporation, Hawthorne, California, July 1978.
20. Ratwani, M.M., and Wilhem, D.P., "Development and Evaluation of Methods of Plane Stress Fracture Analysis -- Part II Volume I, A Technique for Predicting Residual Strength of Structure," AFFDL-TR-73-42, Part II, Volume I, August 1977.

#### 6. ACKNOWLEDGEMENTS

The author wishes to thank Dr. M.M. Ratwani and J.P. Carter for their analytical efforts performing the parametric elastic/plastic study. This manuscript was diligently typed by Phyllis Yokley which is gratefully acknowledged.

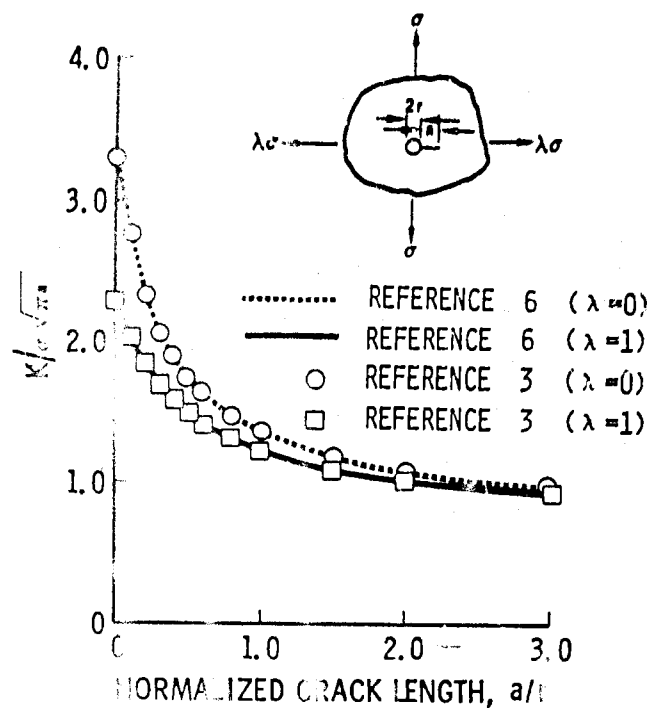


FIGURE 1. COMPARISON OF TTC AT A HOLE SOLUTIONS FROM REFERENCES 3 &amp; 6

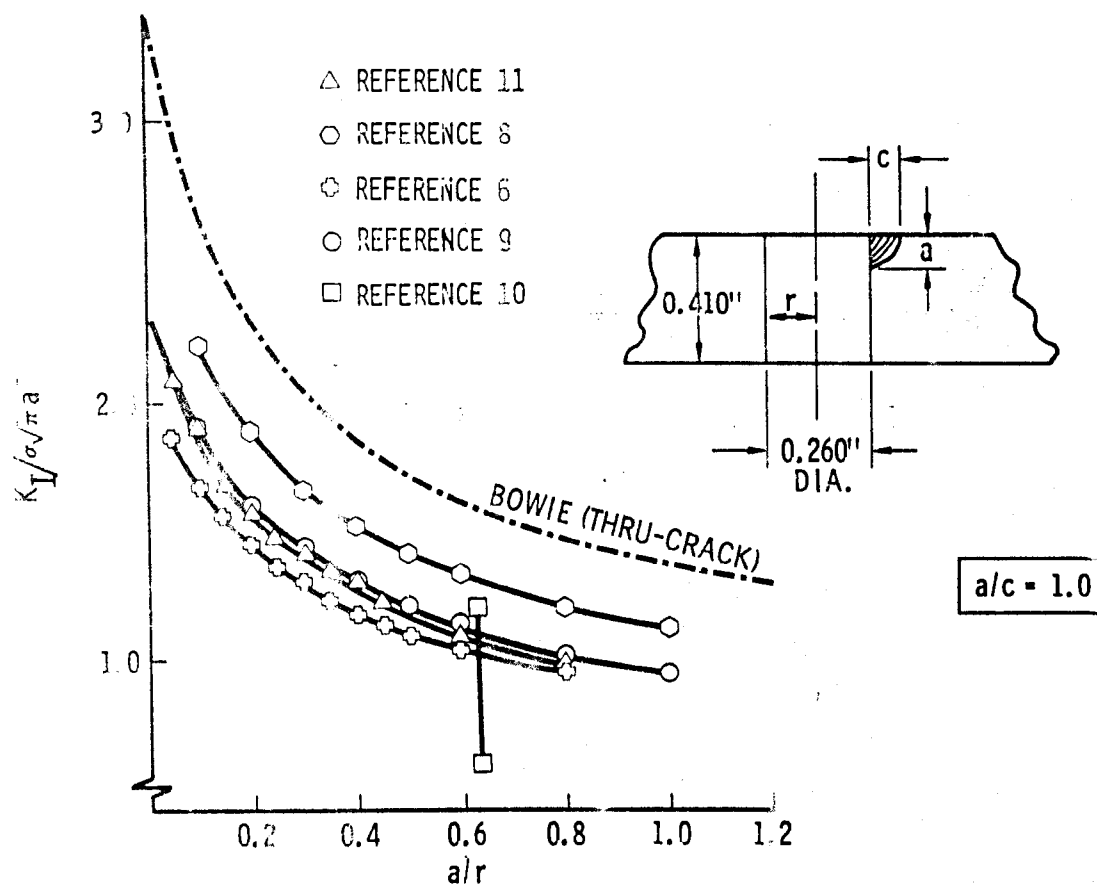
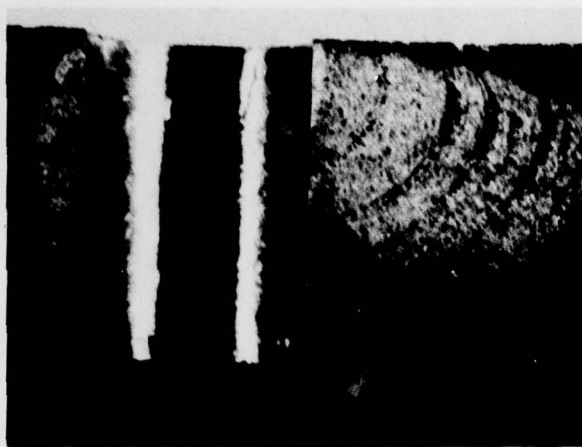
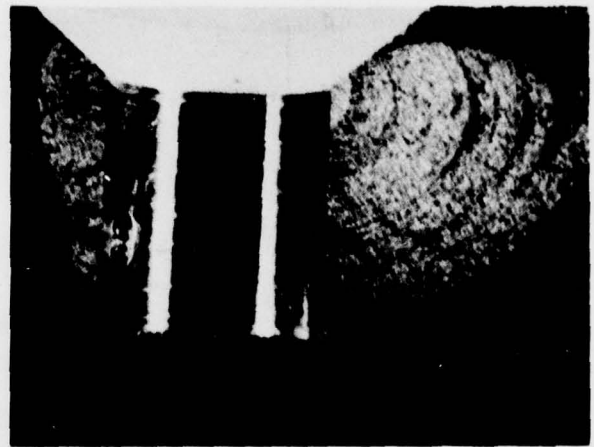


FIGURE 2. COMPARISON OF NORMALIZED STRESS INTENSITIES - PTC AT A HOLE



NONCOUNTERSUNK



COUNTERSUNK

FIGURE 3. SPECTRUM CRACK GROWTH IN 7075-T651, 0.42 INCH THICK

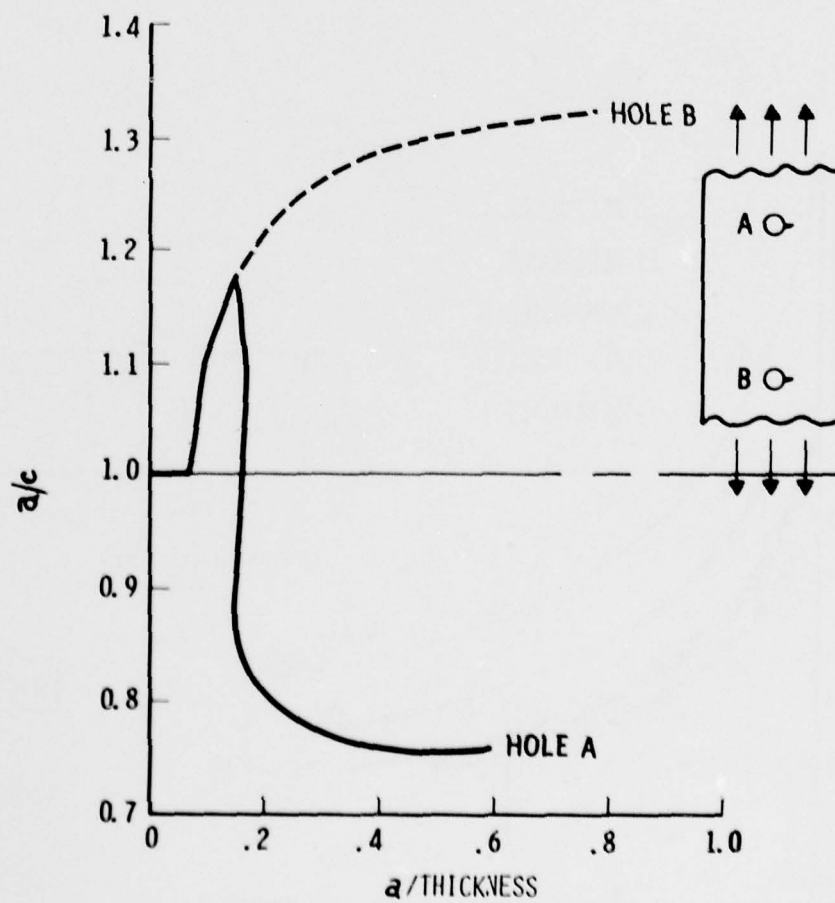


FIGURE 4. VARIATION IN CRACK ASPECT RATIO WITH CONSTANT AMPLITUDE GROWTH

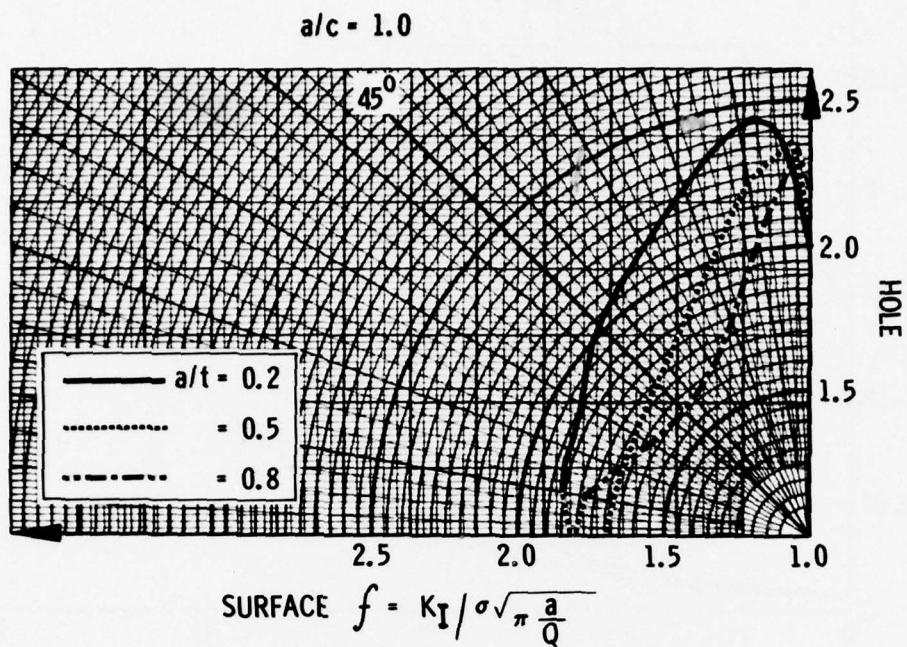


FIGURE 5. NORMALIZED THREE DIMENSIONAL K's AT  $a/c = 1.0$  (REF.10)

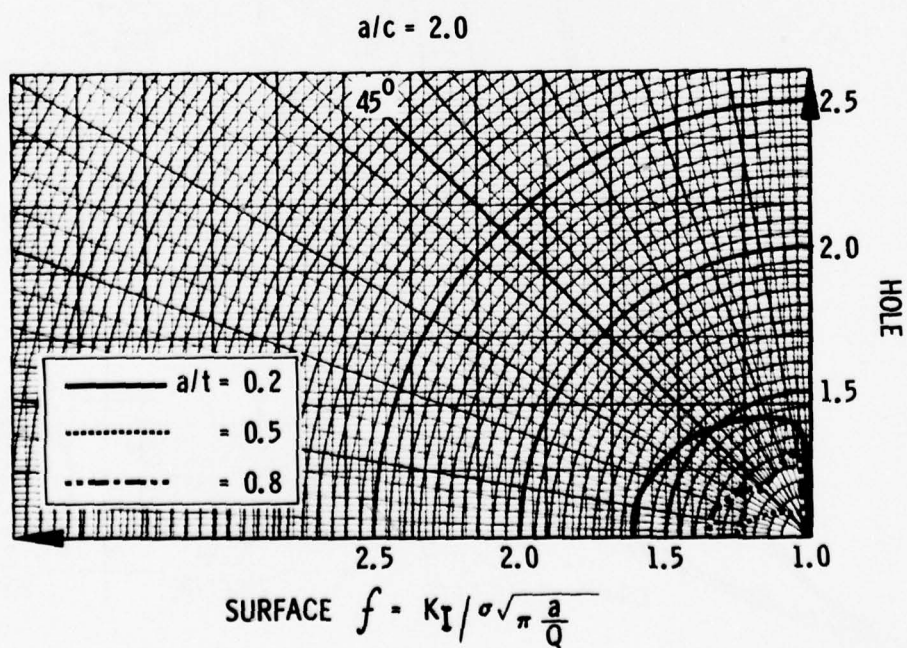


FIGURE 6. NORMALIZED THREE DIMENSIONAL K's AT  $a/c = 2.0$  (REF. 10)



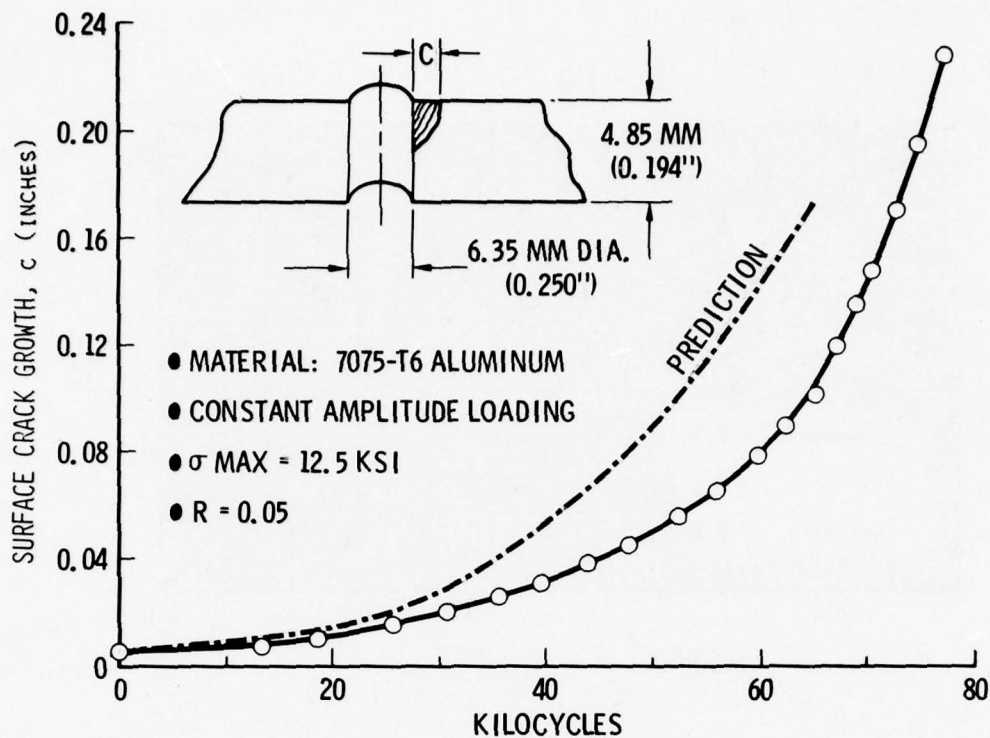


FIGURE 7. PREDICTION OF CONSTANT AMPLITUDE FATIGUE CRACK GROWTH

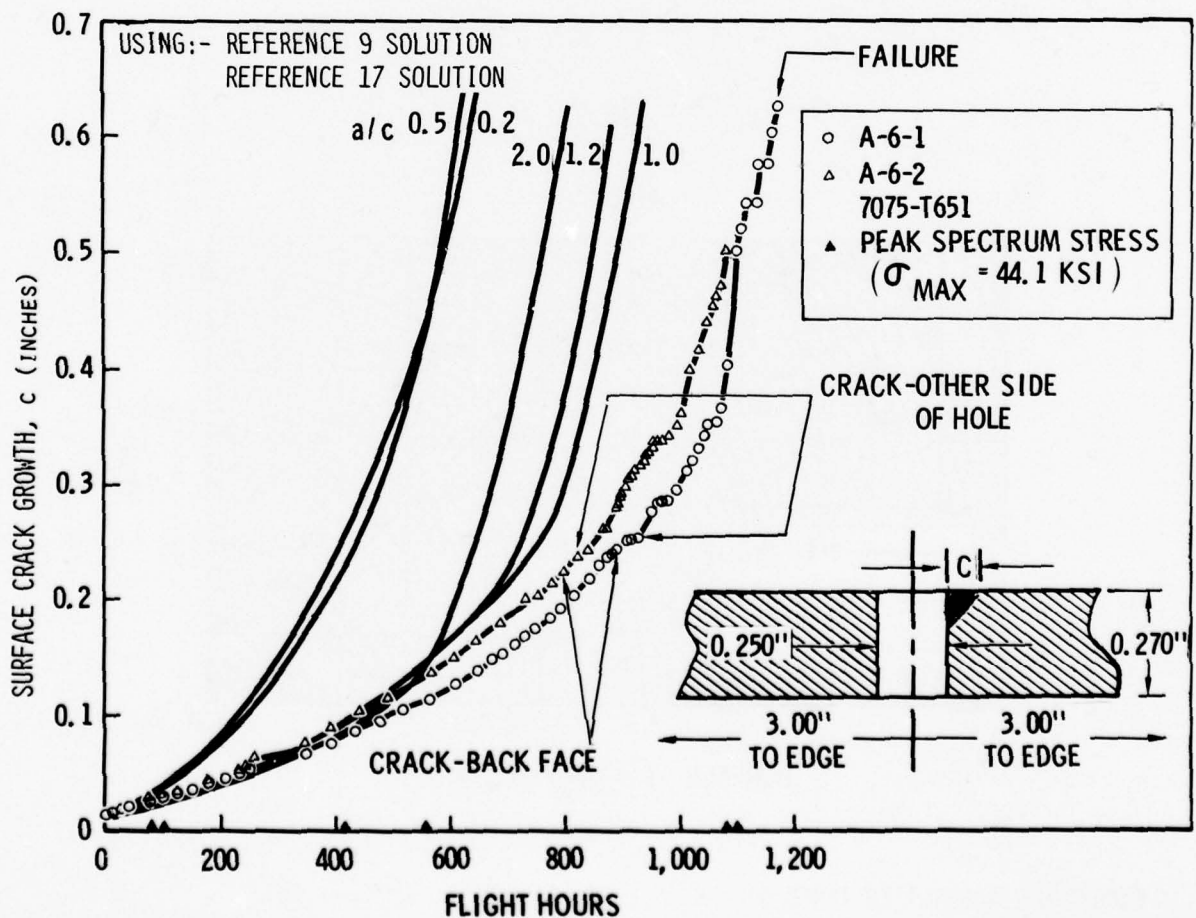


FIGURE 8. PREDICTION OF SPECTRUM FATIGUE CRACK GROWTH

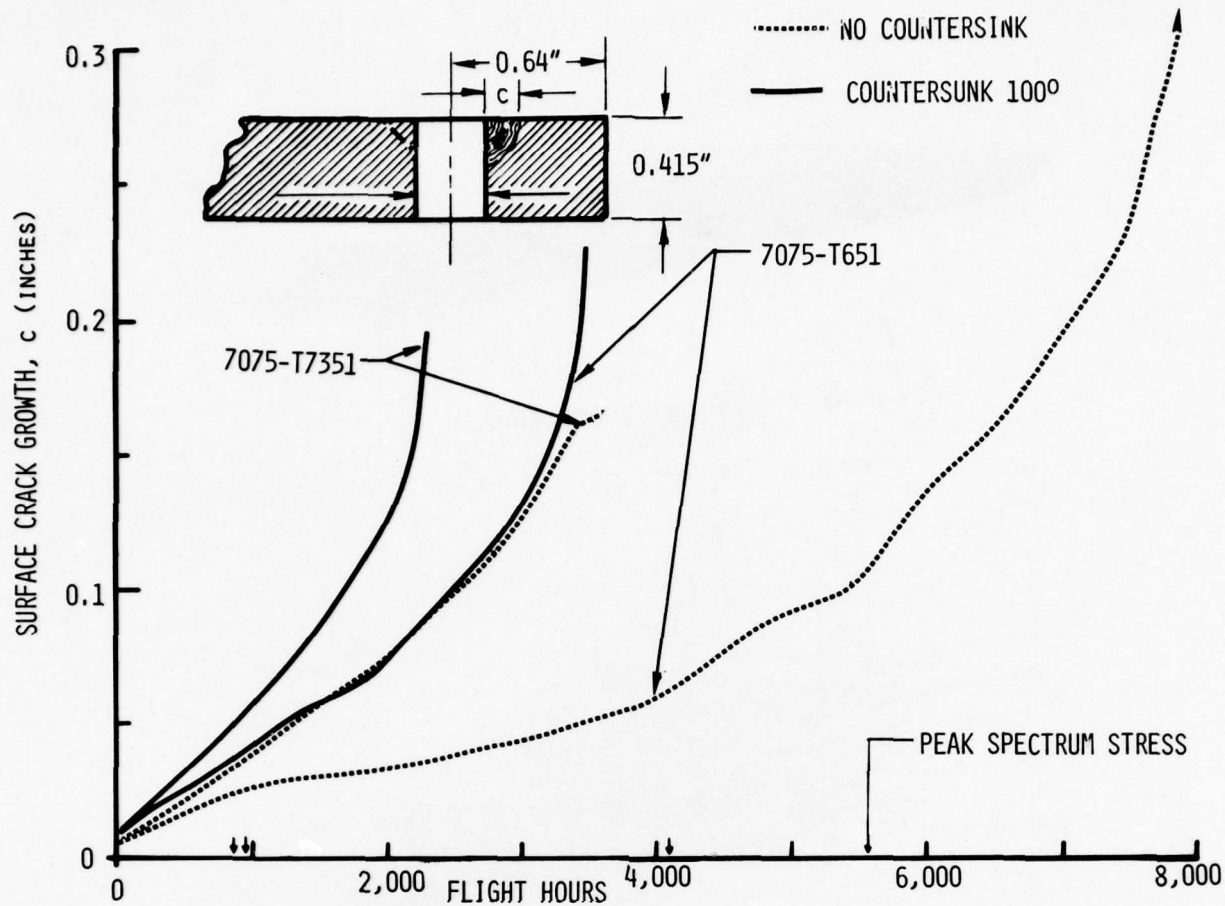


FIGURE 9. COMPARISON OF SPECTRUM GROWTH FROM COUNTERSUNK AND NONCOUNTERSUNK HOLES

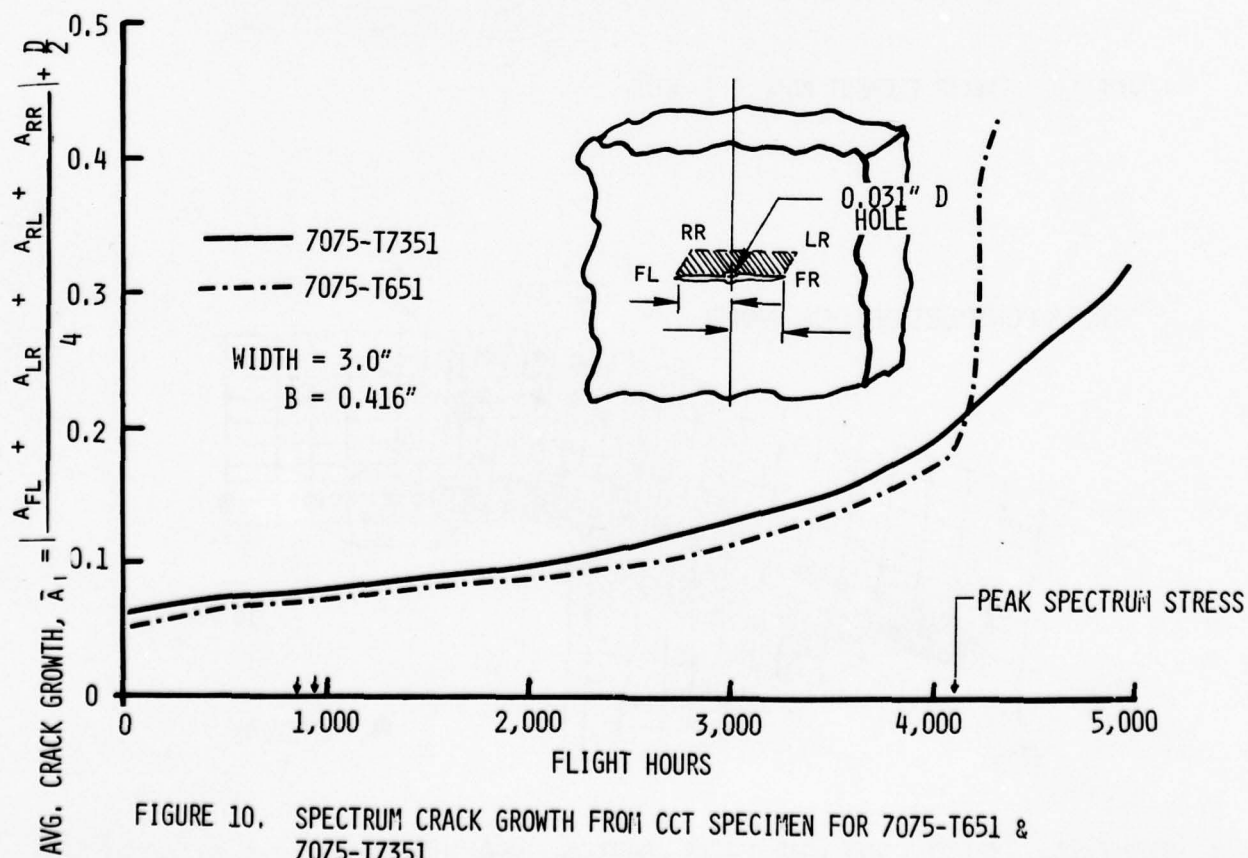


FIGURE 10. SPECTRUM CRACK GROWTH FROM CCT SPECIMEN FOR 7075-T651 &amp; 7075-T7351

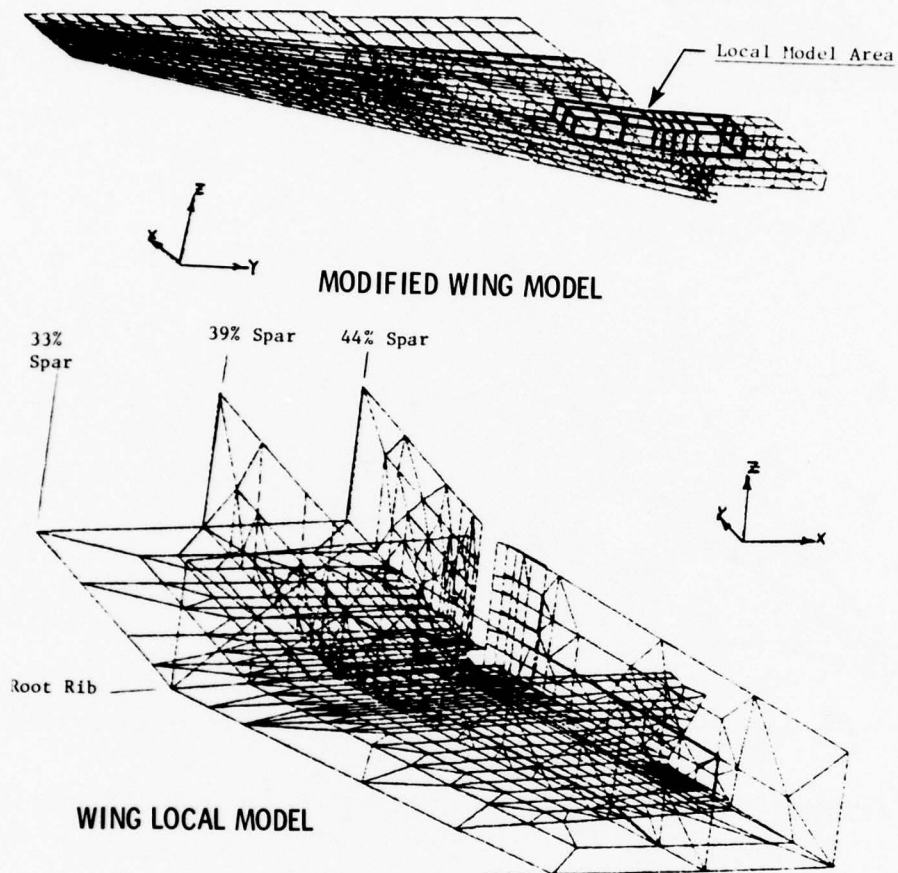


FIGURE 11. FINITE ELEMENT MODELS OF WING

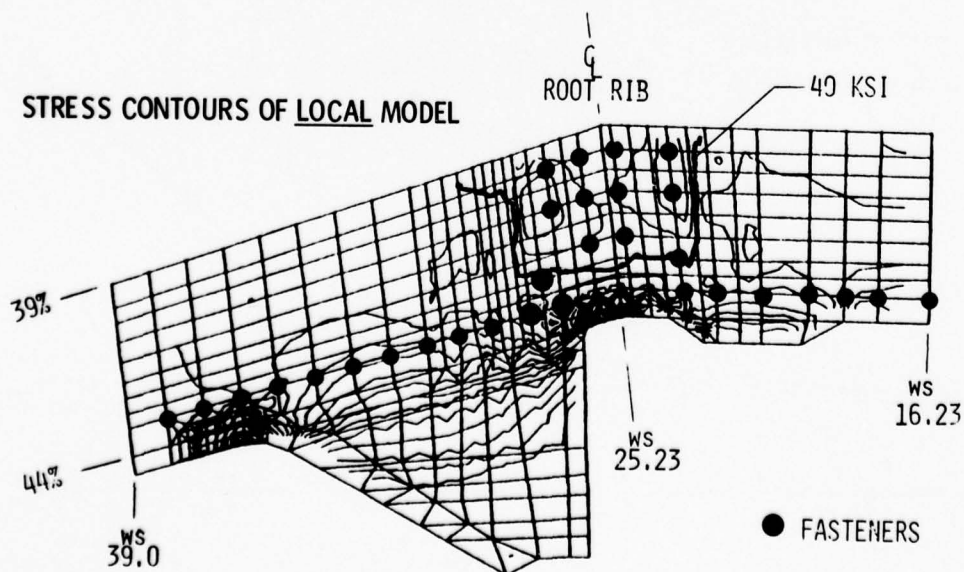


FIGURE 12. TYPICAL LIMIT LOAD STRESS CONTOURS FOR RADIUS STUDY

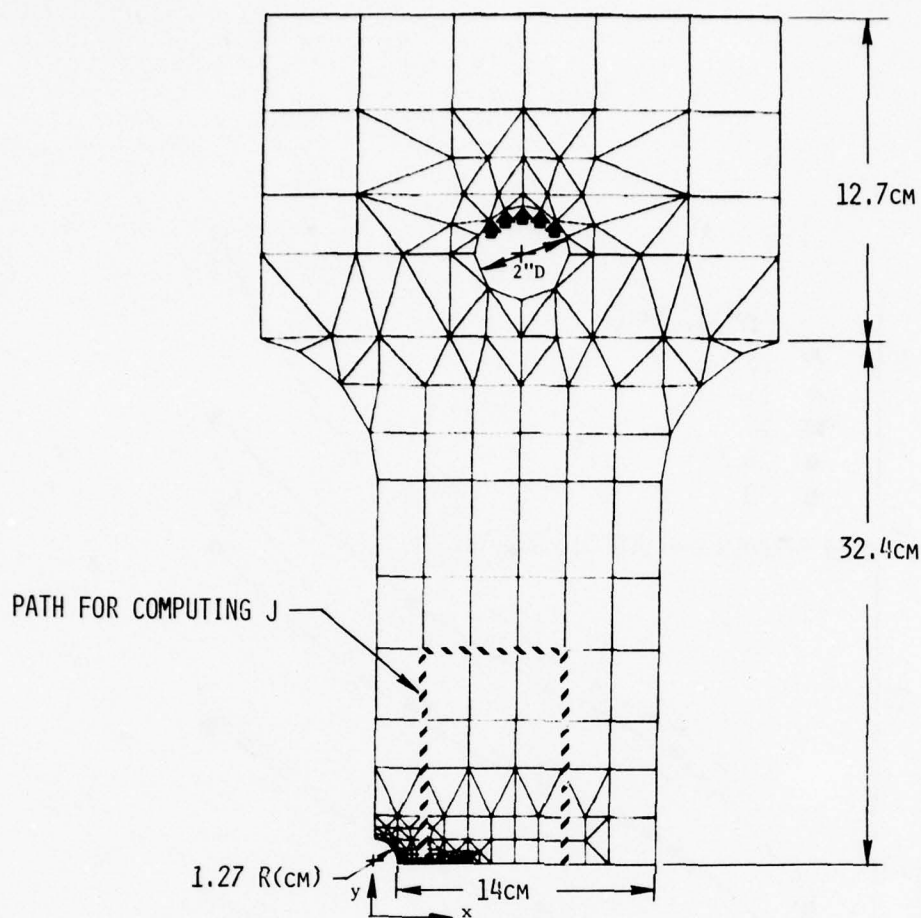


FIGURE 13. FINITE ELEMENT MODEL OF THE 1.27cm RADIUS COUPON

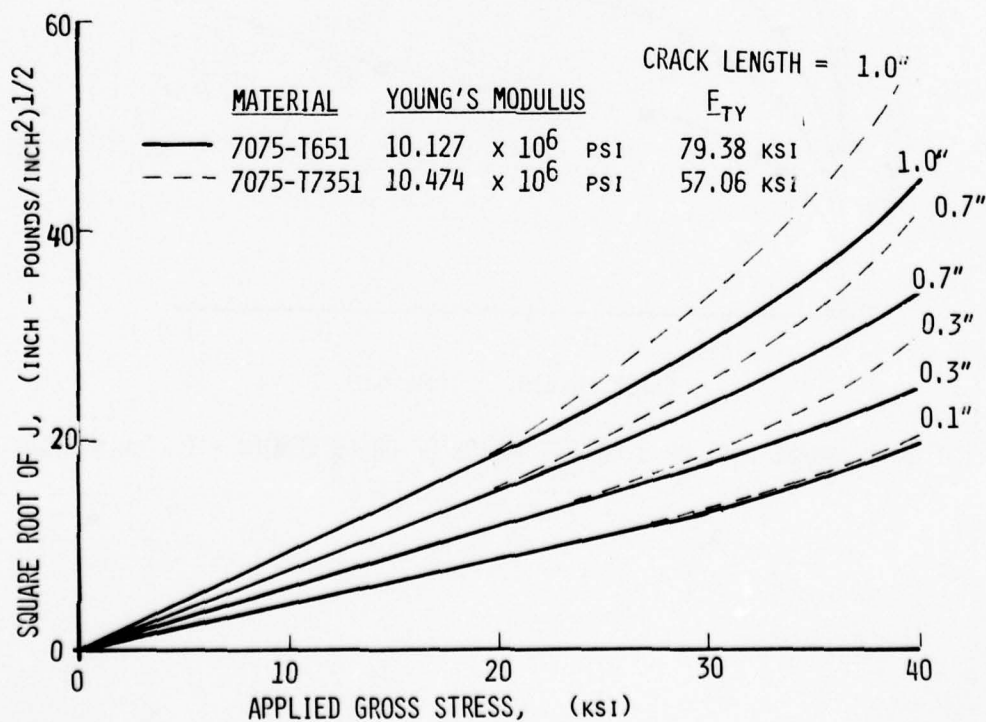


FIGURE 14. SQUARE ROOT OF J AS A FUNCTION OF APPLIED STRESS - 1.27cm RADIUS



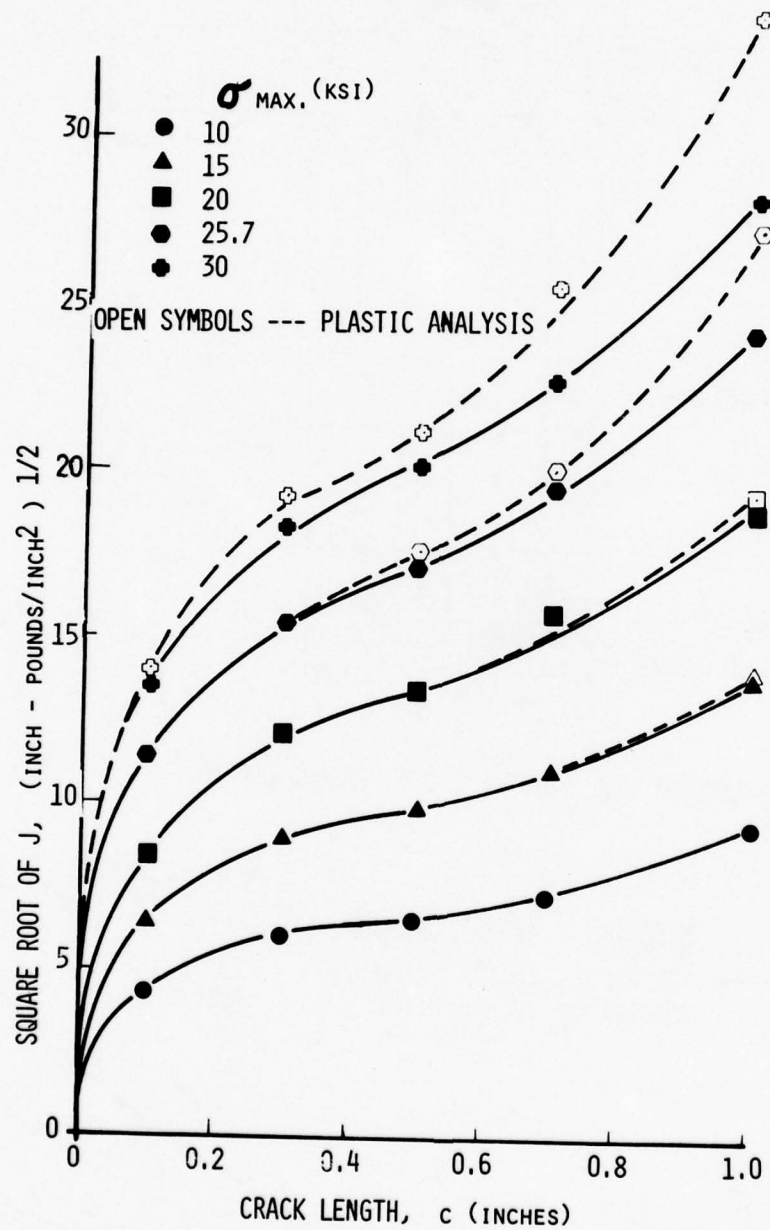


FIGURE 15. SQUARE ROOT OF J AS A FUNCTION OF CRACK LENGTH - 1.27cm RADIUS

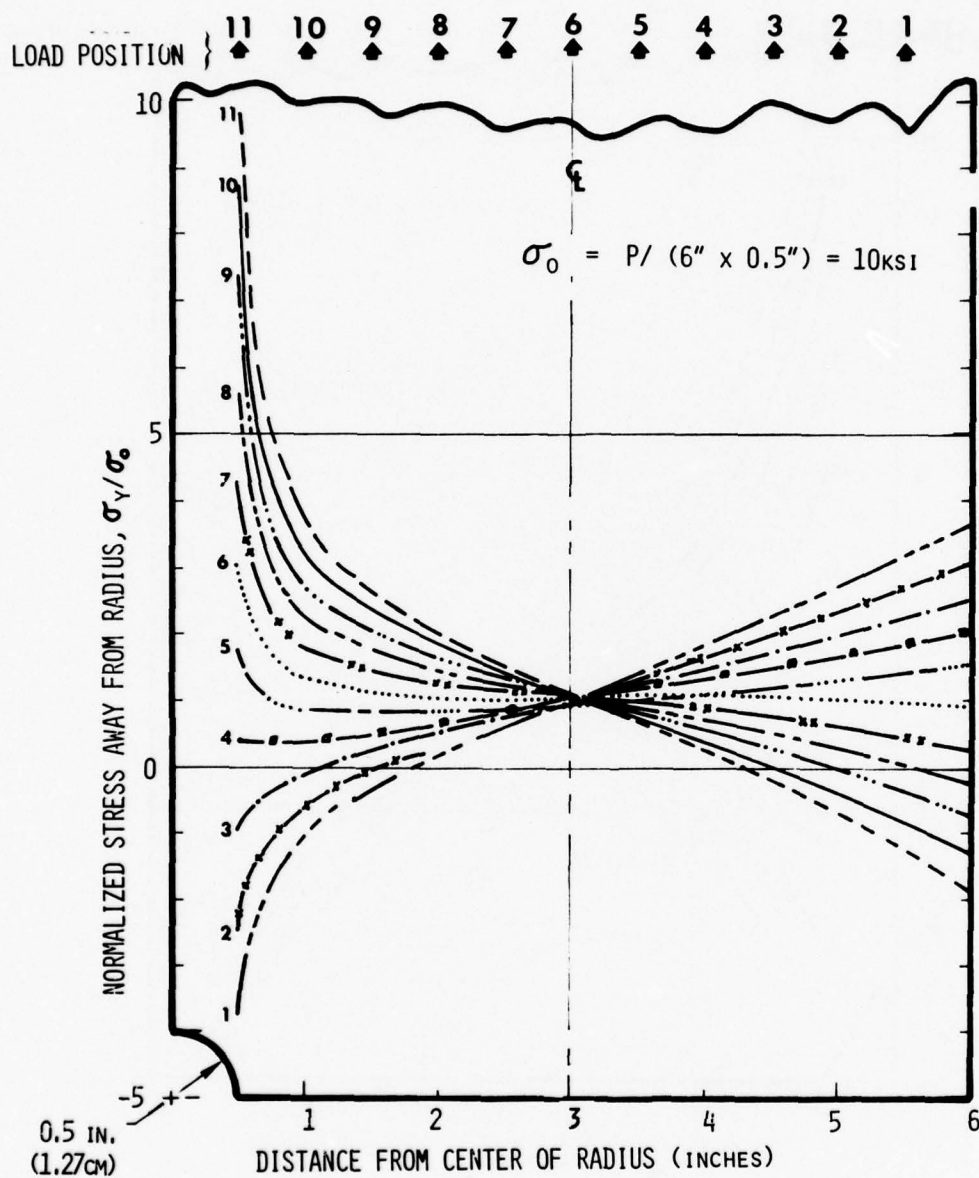


FIGURE 16. COMPARISON OF STRESS GRADIENT FOR 1.27cm RADIUS COUPON

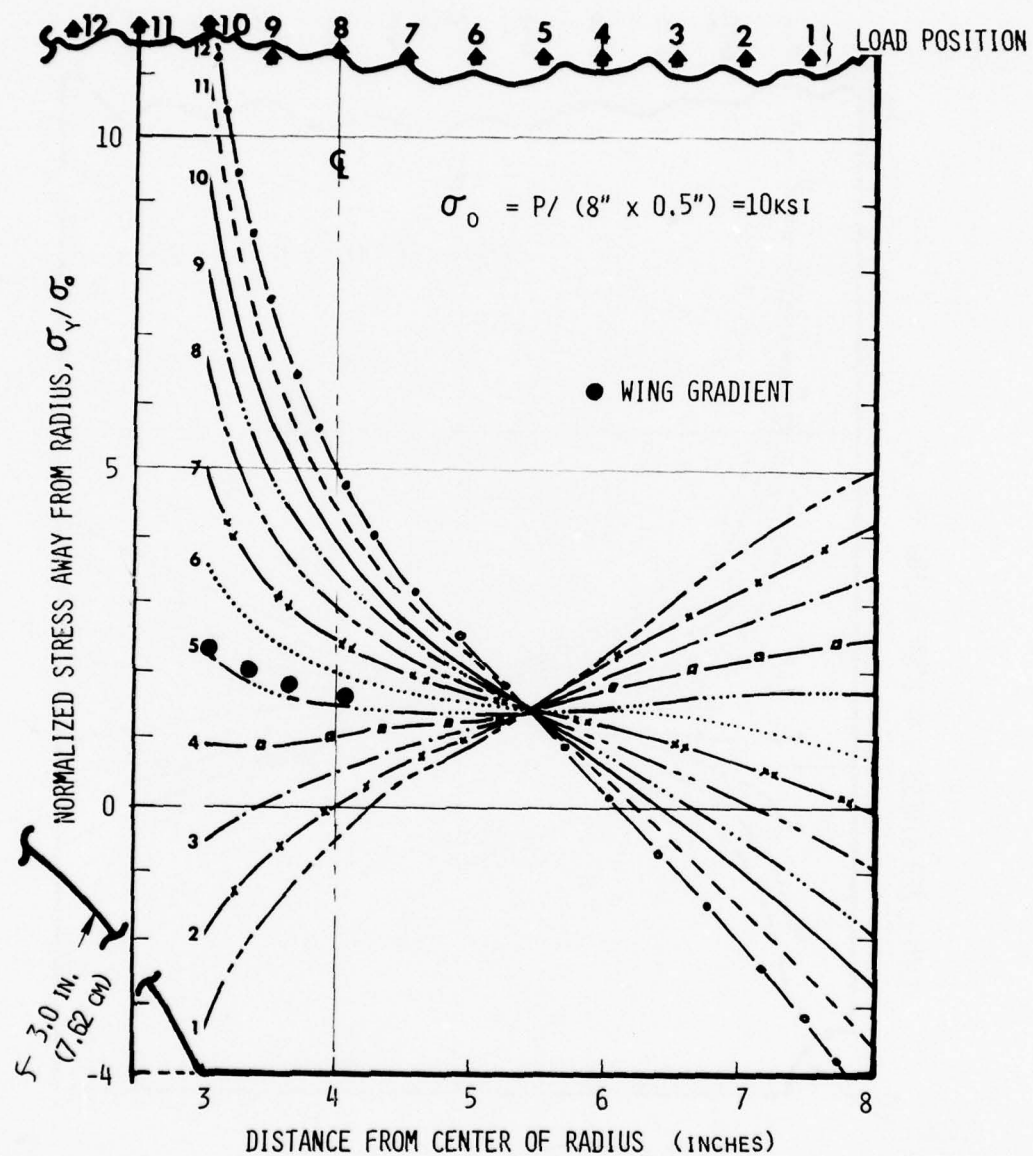


FIGURE 17. COMPARISON OF STRESS GRADIENT FOR 7.62cm RADIUS

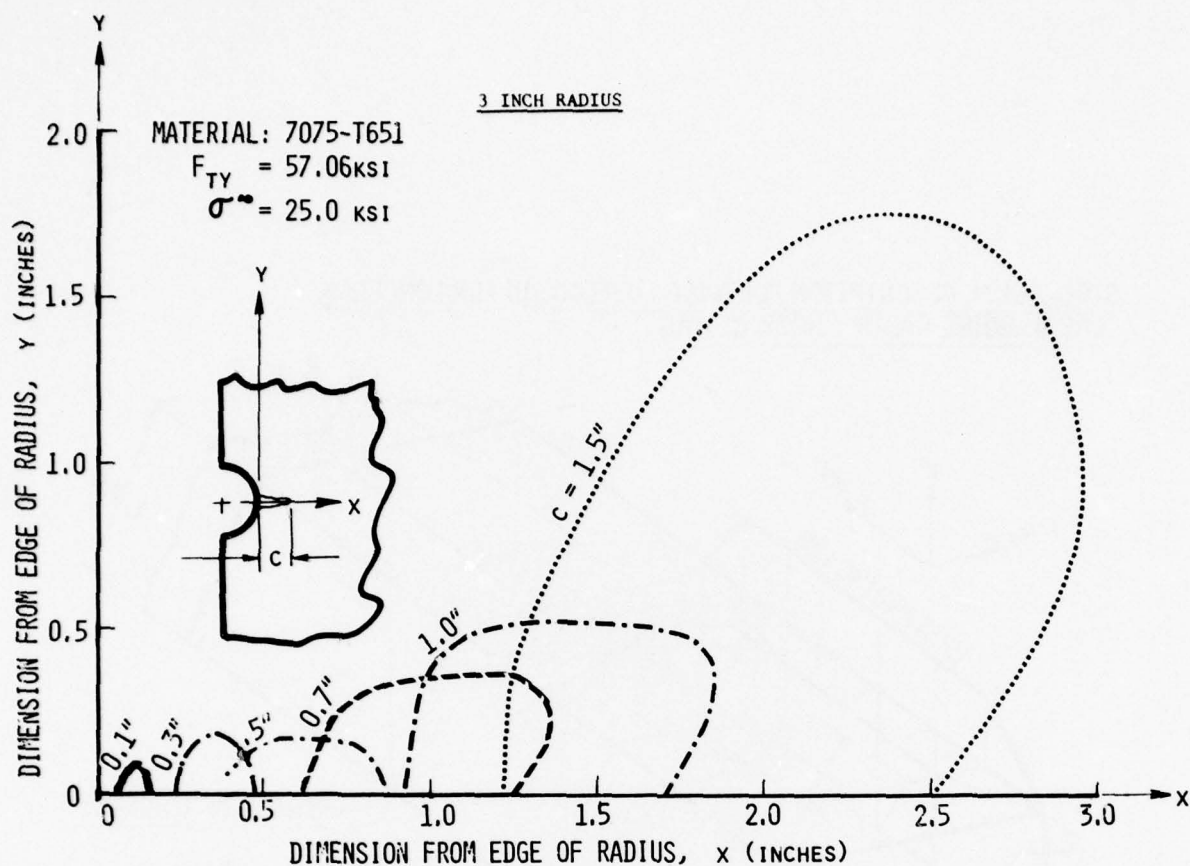


FIGURE 18. PLASTIC ZONE ANALYSIS FOR 7.62cm RADIUS

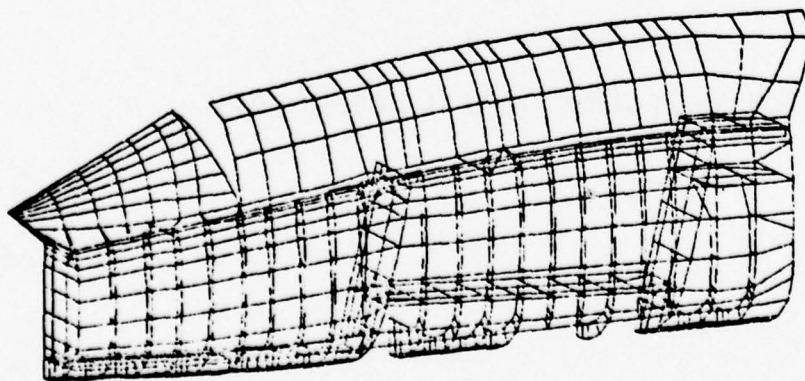


FIGURE 19. FINITE ELEMENT MODEL OF FORWARD FUSELAGE



STRUCTURAL DESCRIPTION FORWARD FUSELAGE UPPER LONGERON  
LOCAL MODEL CANOPY HOOK CUTOUT

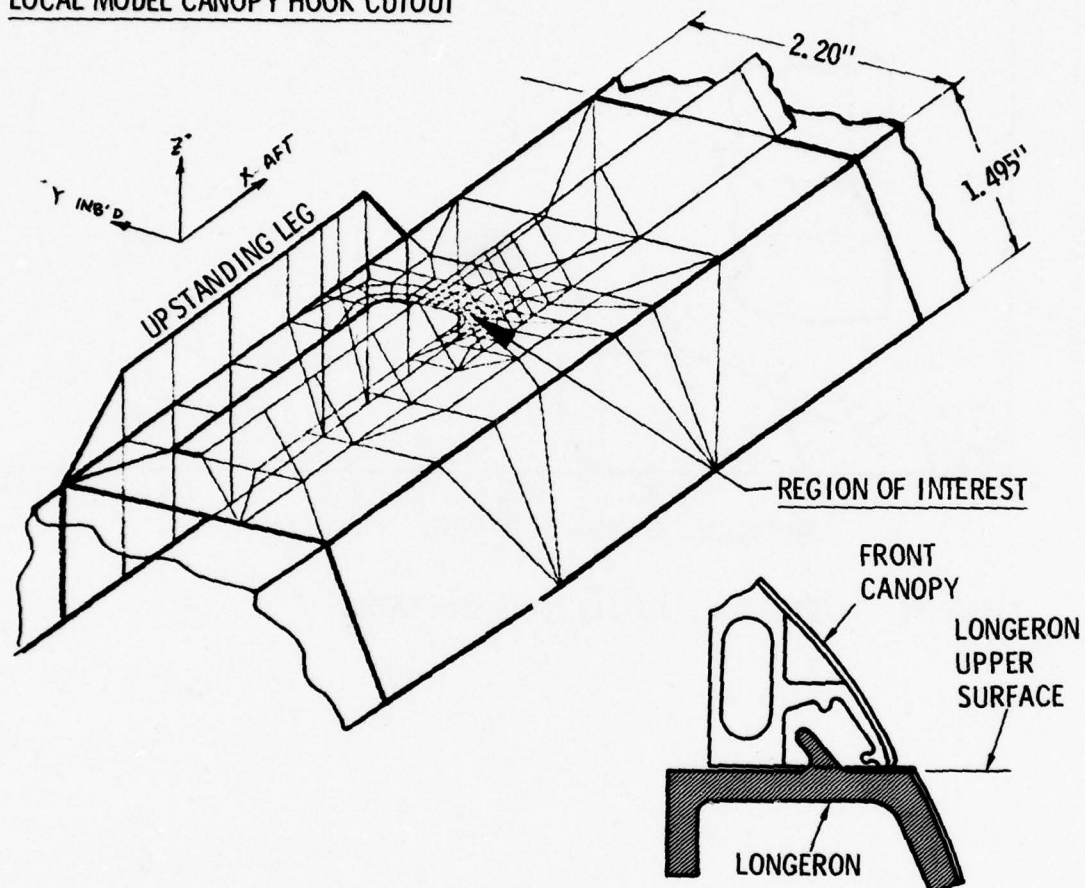


FIGURE 20. LOCAL FINITE ELEMENT MODEL OF LONGERON CUTOUT

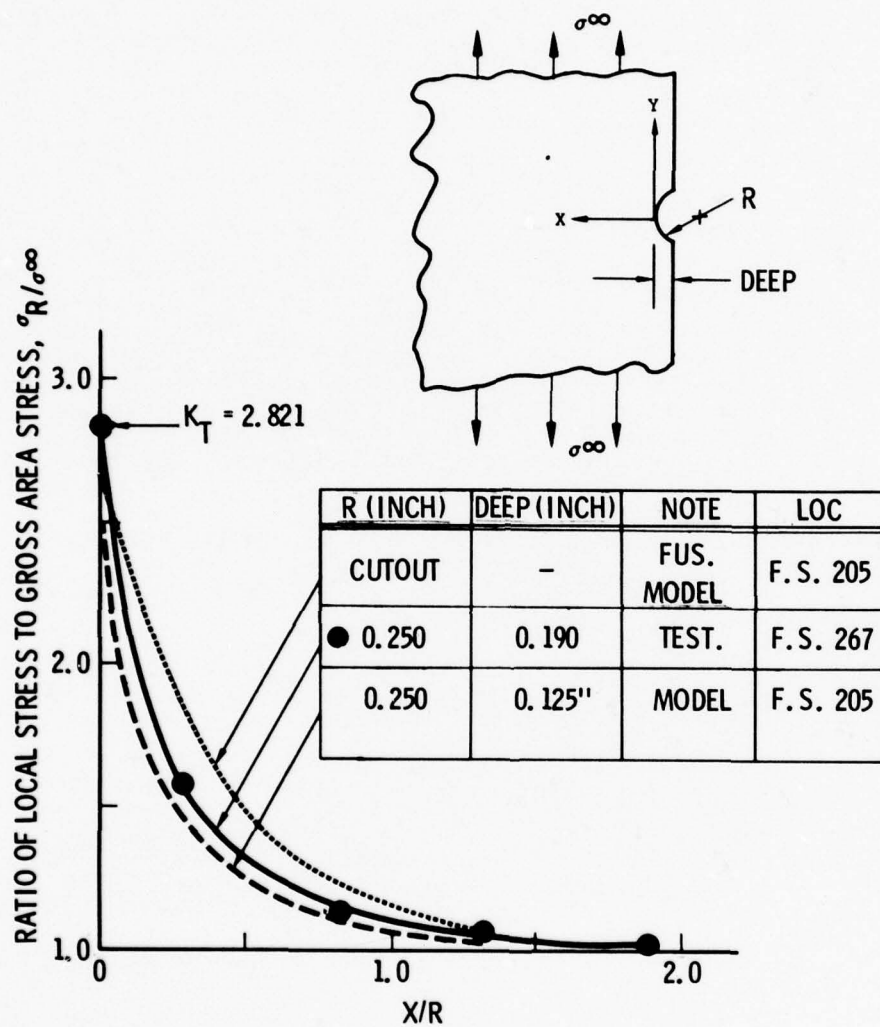


FIGURE 21. STRESS GRADIENT FOR CUTOUT STUDIES

## DAMAGE TOLERANCE ANALYSIS OF REDUNDANT STRUCTURES

By  
T. Swift

Douglas Aircraft Company  
McDonnell Douglas Corporation  
Long Beach, California 90846

### SUMMARY

A modern transport aircraft contains wide expanses of basic redundant structure which must be designed with some damage tolerance capability. Reliable and economical analytical procedures are therefore required to ensure the most efficient design which will meet these damage tolerance requirements.

Several kinds of analytical approaches are described herein including finite-element, energy release rate, and displacement compatibility methods. Each of these methods can be used to calculate the crack tip stress intensity and stiffener stress concentration factors necessary for the damage tolerance design of stiffened structure. The role that stiffeners play in reducing the crack tip stress intensity factor to a level which can arrest cracks after rapid propagation is described. The effects of variations in geometry on the crack tip stress intensity factor, stiffener stress, and residual strength are presented, including the results of a parametric study. Finally, analytical procedures are described which account for fastener nonlinear shear displacement and the effects of stiffener plasticity.

### 1. INTRODUCTION

Considerable effort is expended during the early design phases of modern aircraft structures to ensure a crack-free fatigue life. In the early layout stages, this effort starts by using simplified analytical methods together with working stress levels obtained from past experience. As the design progresses and fatigue-sensitive areas become more clearly defined, the analysis of these areas becomes more sophisticated. Cumulative damage calculations are performed based on spectra developed from the expected utilization of the aircraft. This analysis is supported by information gained from large component development tests of structure simulating actual critical components. Finally, the design is verified by full-scale fatigue testing to at least twice the expected service life. The flight-by-flight loading applied in these tests simulates the actual service loading as closely as is economically feasible. Nevertheless, all of this effort cannot guarantee that fatigue cracking will not occur in at least some aircraft in the fleet. The structure must therefore be designed to be tolerant of some fatigue cracking in service. Further, to ensure safe operation of the fleet, any such cracking must be detectable during scheduled inspections before it reaches critical proportions. Structure can be designed in more than one way to achieve this. For example, safety can be achieved in single-load-path structure by ensuring that crack propagation will be slow enough to be detected before unstable cracking to failure occurs. This type of structure has become known as "slow crack growth" structure. Moreover, structure can be designed with either redundant load paths or crack-arrest capability so that if failure of one or more elements occurs, some load can still be carried. This type of structure is, of course, known as "fail-safe structure." The critical crack size for "slow crack growth" structure is usually small and not easy to detect. On the other hand, much larger and thus more easily detectable damage can usually be sustained in fail-safe type structures. When one considers that a modern jet transport aircraft can contain over 15,000 square feet of basic structure, it becomes obvious that greater safety will be ensured if these large expanses of basic structure are designed to be redundant and thus fail-safe. Good analytical procedures are required for economical design to meet fail-safe requirements for redundant structures. These procedures must be capable of performing parametric studies in an economical way so that the most efficient geometrical configurations can be selected. This paper will be devoted to a review of analytical methods used for the fracture analysis of built-up redundant structures.

### 2. BASIC PRINCIPLES OF STIFFENERS AS CRACK ARRESTERS

#### 2.1 General Discussion

The structure of a modern transport aircraft is essentially a thin shell with stiffening elements. In the case of the wing, skins are designed to react shear loads and spanwise stringers are provided for stability under compressive loads. Chordwise ribs break these stringers into short lengths to increase compressive allowable stresses and also react air loads and crushing loads due to wing bending curvature. In the case of the fuselage, longerons provide stability for fuselage bending loads and frames transfer payloads into the skins which react shear and pressurization loads, as indicated by Figure 1. These stiffening elements, provided essentially for static strength, are sometimes adequate as skin crack arresters. Quite often though, geometrical changes are required to optimize the stiffeners for damage tolerance. To obtain a clear understanding of the role that stiffeners play in the damage tolerance of structures, it will be useful to look at their effect on crack tip stress intensity factor.

#### 2.2 Effect of Stiffeners on K

It has been shown previously that both crack propagation and residual strength are functions of the crack tip stress intensity factor,  $K$ . In unstiffened panels,  $K$  increases as the crack length increases for constant applied stress. In this case, when the crack reaches a critical length, fast fracture occurs, resulting in complete failure of the panel. Carefully designed stiffening elements, however, such as frames with circumferential crack stopper straps, can provide effective redundant load paths, thus confining damage to a local area.

The stress intensity factor,  $K$ , has been shown to be a function of the stress field ahead of the crack tip. In the case of stiffened panels this stress field is reduced as a large portion of the redistributed load is transferred to the stiffening elements. This is illustrated diagrammatically in Figure 2. Figure 3 shows actual sheet stress distributions,  $\sigma_y$ , ahead of a crack tip in both unstiffened and stiffened panels containing a 17-inch-long crack. The distributions shown are results of finite-element analysis. The stiffeners are shaped as a "Hat" section at 8-inch spacing with a cross-sectional area of 0.5121 square inch. The sheet is 0.071-inch thick. In the case of the stiffened panel, the center stiffener is assumed to be broken. As indicated by the figure, there is a considerable reduction in sheet stress as load is transferred to the unbroken outer stiffeners. The reduction in stress depends on the size and location of the stiffeners and the flexibility of their attachments to the skin. Figure 4 shows the local stress  $\sigma_y$  at a location 0.5-inch ahead of the crack tip as a function

at stiffener area for the same 17-inch-long crack. Again, the center stiffener is assumed to be broken. A greater reduction in stress could be expected with increasing stiffener area if the center stiffeners were assumed to be intact. In this case, a large concentrated load would not be transferred to the sheet at the center of the crack.

It can be shown that the effect of stiffeners on the stress intensity factor in redundant, built-up structures can be expressed as:

$$K = \beta \sigma \sqrt{\pi a} \quad (1)$$

where  $\beta$  is a correction due to all geometrical effects.

The term  $\beta$  is a function of crack length and also represents the following geometrical effects:

- Stiffener spacing
- Stiffener section properties -- area, inertia, neutral axis location
- Stiffener elastic or plastic material properties
- Fastener displacement, either linear or nonlinear
- Skin thickness, modulus, and Poisson's ratio.

The value of  $\beta$  can be less than unity when the crack tip is in the vicinity of an intact stiffener or greater than unity if the stiffener is broken. This is illustrated in Figure 5 which shows  $\beta = K/\sigma\sqrt{\pi a}$  as a function of crack length for the stiffened panel described earlier. It can be seen that when the crack tip is in the vicinity of the broken stiffener, the value of  $\beta$  and thus the stress intensity factor is high due to load redistribution from the broken stiffener into the cracked area. This situation is relieved as the crack tip approaches the outer, intact stiffeners. A large percentage of the load given up by the cracked sheet and broken stiffener is transferred to the intact stiffeners, as indicated by Figure 6 which shows outer stiffener maximum load,  $P$ , as a function of crack length. The effect of stiffeners in increasing or decreasing the stress intensity factor,  $K$ , for the broken or intact stiffener case, respectively, is illustrated in Figure 7, which is merely a plot of Equation (1).

### 2.3 Residual Strength

The equation for crack tip stress intensity factor in stiffened structure can be rearranged in terms of the critical stress,  $\sigma_c$ , critical crack size,  $a_c$ , and the material fracture toughness,  $K_c$  (in the case of plane stress). Thus, Equation (1) becomes

$$\sigma_c = K_c / (\beta \sqrt{\pi a_c}) \quad (2)$$

A residual strength diagram based on skin fracture can be plotted from this equation. At this point, it will be useful to review a simple residual strength diagram.

Consider the skin fracture curve shown in Figure 8a, plotted from Equation (2) for the panel described earlier with a broken central stiffener in which the skin material is 7075-T73. If a crack of length  $2a_1$  exists in the skin, equally spaced about the center stiffener, and a stress  $\sigma_1$  is applied, then fast fracture will occur at point A (neglecting slow growth) and the crack will be arrested at B. The crack is arrested because its tip intensity factor is reduced below  $K_c$  due to transfer of load to the stiffener. The stiffener itself can become critical as it picks up load from the cracked skin and an allowable stiffener strength curve can be plotted as shown also in Figure 8a. Further increase in stress above  $\sigma_1$  would cause stable crack growth to point F where skin fracture would again occur. The crack would rapidly extend to a point at G when stiffener failure would occur with subsequent failure of the panel. This failure would have been precipitated by skin fracture. Any fast fracture above point E would not be arrested. For example, fast fracture at point C with stress level  $\sigma_2$  and crack length  $2a_2$  would cause complete failure at point D due to stiffener overload.

The stiffener strength curve shown in Figure 8a is based on 7075-T6 extruded material having an ultimate test strength of 84 ksi. The effect of reducing the stiffener tension strength on the failure mode is illustrated in Figure 8b where the stiffener strength curve reflects the lower static strength properties of 2024-T3. In this case, the residual strength will not be based on point F of the fracture curve. Any fast fracture at a stress higher than  $\sigma_2$  would cause failure of the panel. For example, if a skin crack existed of length  $2a_1$  and stress  $\sigma_1$  were applied, fast fracture would occur at A. Without further increase in applied stress, the crack would rapidly propagate to point B, where complete failure would occur, precipitated by stiffener overload.

A further criterion for failure of stiffened structure is illustrated in Figure 8c. Elastic analysis indicates that the first rivet in the intact stiffener adjacent to the crack tip can fail and precipitate failure of the panel. In this case, the panel residual strength would be based on stress  $\sigma_2$  of Figure 8c. Any fast fracture at a stress higher than  $\sigma_2$  and lower than  $\sigma_3$ , as in the case of  $\sigma_1$ , would cause failure of the panel precipitated by first rivet failure. For example, for a panel with crack length  $2a_1$  and applied stress  $\sigma_1$ , fast fracture would occur at A and the crack would rapidly extend to B when failure would occur due to first rivet failure. Fast fracture at stress levels above  $\sigma_3$  would cause total panel failure due to stiffener failure. The rivet criteria curve in Figure 8c is based on aluminum rivets of 3/16-inch diameter. The effect of increasing fastener strength is only slight, as indicated by Figure 8d which also shows the effect of increasing stiffener strength and fracture toughness,  $K_c$ .

The fastener strength criteria discussed above is the result of elastic analysis. In practice, the first rivet load is greatly relieved due to yielding. Testing has indicated that fastener failure will precipitate panel failure only at extremely high stress levels (in conventional aircraft structure) when skin fracture toughness is high. Of course, yielding of the first rivet will increase the crack tip stress intensity factor and relieve the stiffener stress. This problem will be addressed later.

### 2.4 Effect of Stiffeners on Crack Propagation

As indicated earlier, it has been shown that the crack propagation rate  $da/dN$  for any material,  $M$ , can be expressed as a function of crack tip stress intensity range,  $\Delta K$ . The number of cycles required to grow a crack from an initial length  $a_0$  to a final length  $a_f$  can then be expressed as

$$N = \int_{a_0}^{a_f} \frac{da}{\Delta K \cdot M \cdot a} \quad (3)$$

In its simplest form for stiffened structure, the term  $\Delta K$  is given by



$$\Delta K = \beta(1 - R)\sigma\sqrt{\pi a} \quad (4)$$

where  $R$  is the stress ratio  $\sigma_{\min}/\sigma_{\max}$ . The term  $\beta$ , which contains all the geometrical effects described earlier, must be calculated for an assessment of the crack growth in stiffened structure.

It has been shown in this section that both residual strength and crack propagation in stiffened structures depend on the value of the geometrical term  $\beta$ . This term is not readily available without a fairly complex stress analysis. The following sections describe several methods for the calculation of  $\beta$  with the relative merits of each.

### 3. DIRECT FINITE-ELEMENT METHODS

#### 3.1 Panel Idealization

This approach for the calculation of  $\beta$  is based on a "lumped parameter" finite-element analysis of an idealized structure representing the panel. The method is based on the force matrix method of structural analysis<sup>(1,2)</sup> and uses the Fortran Matrix Abstraction Technique, FORMAT<sup>(3)</sup>, to solve the necessary matrix operations. It should be noted, however, that any finite-element procedure could be used. The idealized structure is shown in Figure 9. The panel is divided into a series of discrete bars and shear panels. The bars carry axial load and the panels carry shear load. External reactions and loads are applied at the joints. Only one quarter of the panel requires consideration since the crack is assumed to propagate symmetrically about the centerline of the panel. The bar areas are determined by using a width of skin,  $X_s$  or  $Y_s$ , representing half the distance between the two adjacent bars. The stiffeners are idealized by simulation to discrete areas located in such a way that both axial and bending stiffnesses are correctly represented. The fasteners are represented by a continuous shear panel between the idealized stiffener outer cap and the skin. The thickness of this shear panel is chosen to give the same stiffness as the rivets. Correct simulation of the rivet flexibility is essential in any stiffened panel analysis. An empirical relation for rivet elastic displacement which has been successfully used in the past is

$$\delta_R = \frac{P}{ED} \left[ A + C \left( \frac{D}{B_1} + \frac{D}{B_2} \right) \right] \quad (5)$$

where

$\delta_R$  = displacement

$P$  = applied load

$E$  = modulus of sheet material

$D$  = rivet diameter

$B_1, B_2$  = thickness of jointed materials (skin and stiffener crown)

$A$  = 5.0 for aluminum rivets and 1.666 for steel fasteners

$C$  = 0.8 for aluminum rivets and 0.86 for steel fasteners

The displacement of a shear panel simulating the rivet connection is given by

$$\delta_{SP} = \frac{(B_1 + B_2)P}{2 L_{SP} B_{SP} \mu} \quad (6)$$

where

$L_{SP}$  = length of shear panel (rivet spacing)

$B_{SP}$  = thickness of shear panel

$\mu$  = shear modulus of shear panel

Equating Equations (5) and (6) and solving for the simulated shear panel thickness gives

$$B_{SP} = \frac{ED(B_1 + B_2)}{2\mu L_{SP} [A + C(D/B_1 + D/B_2)]} \quad (7)$$

#### 3.2 Simulation of Crack

Loads are applied to the points at the top of the panel to represent a unit stress and reactions at the bottom are disconnected successively to simulate a propagating crack. The crack tip stress is defined as the bar stress adjacent to the last reaction disconnected, as shown in Figure 9. In this type of analysis it is necessary to perform the analysis for both unstiffened and stiffened panels having identical skin idealizations. The effect of the stiffening elements and thus the value of  $\beta$  is determined by taking a ratio between the simulated crack tip stresses,  $\sigma_{yct}$ , for the stiffened and unstiffened panels as follows:

$$\beta = \frac{\sigma_{yct}(\text{stiffened panel})}{\sigma_{yct}(\text{unstiffened panel})} \quad (8)$$

These stresses are of course finite and thus do not reflect the true singularity at the crack tip; however, since stress intensity is related to the stress field near the crack tip, it is reasonable to obtain the value of  $\beta$  from finite stresses near the crack tip.

The finite-element analysis of the stiffened panel provides stresses over the entire panel as a function of crack length. Stiffener stress concentrations and simulated fastener shear loads can thus be obtained and used with their respective allowables to obtain a residual strength diagram.

### 3.3 Typical Results

Table 1 shows values of simulated crack tip stress for a typical analysis of the stiffened panel configuration described earlier. Also shown are outer stiffener, inner and outer cap stresses, and simulated fastener shear panel maximum shear flows. The resulting value of  $\beta$ , obtained from Equation (8), is plotted in Figure 5. Typical residual strength diagrams resulting from this analysis are shown in Figure 8 for various stiffener strength and  $K_c$  values.

This method of analysis has proved completely successful for panel configurations for which the skin materials have comparatively low fracture toughness. However, for skin materials having high fracture toughness, such as 2024-T3, the allowable stress levels become so high that elastic analysis may not provide accurate results.

The main disadvantage to the direct finite-element method is the large amount of computer time consumed. The necessity to perform analyses on both stiffened and unstiffened panels does not help this situation and although plastic analysis is possible with the method, the cost becomes prohibitive.

## 4. FINITE-ELEMENT ENERGY RELEASE RATE METHOD

### 4.1 Method Description

The finite-element energy release rate approach to the determination of stress intensity in stiffened panels offers the advantage that the results can be obtained directly by analysis of the stiffened panel. The unstiffened panel analysis is not required and thus the savings in computer time is 50 percent compared to the direct finite-element approach. The method is based on the determination of stress intensity factor  $K$  from the relation

$$K = \sqrt{\frac{\partial U}{\partial A} E} \quad (9)$$

where  $\partial U/\partial A$  is the rate of change of strain energy  $U$  with respect to crack area  $A$  and  $E$  is the elastic material modulus. The stress intensity factor  $K$  cannot be obtained from a single computer run at one crack length. A series of solutions is required with increasing crack length. This, however, is not a disadvantage since it is rare that results from a single crack length are required. Disconnection of the reactions to simulate the propagating crack is automatic in the program and usually 12 crack lengths are obtained in one computer run. The strain energy can be determined from the deflection at the crack face or displacement of the applied loads. The latter is more convenient since it eliminates the need to apply displacement vectors in addition to reactions along the line representing the crack path. The strain energy  $U$  is thus obtained by summing the input energy of the applied loads using the relation

$$U = \sum_{i=1}^{i=n} \frac{P_i \delta_i}{2} \quad (10)$$

Figure 10 illustrates the concept. The relation between the energy change  $U$  and the crack area  $A$  is differentiated numerically in the program to determine  $K$  through Equation (9).

### 4.2 Correlation with Classical Solutions

The energy-release-rate approach has been correlated with classical solutions for simple problems. One such correlation is illustrated in Figure 11 for an unstiffened panel. The energy solution is shown compared to the classical solutions of Isida and Irwin. One advantage to this method is that the grid size in the idealization need not be very fine. The solution illustrated in Figure 11, for example, used a 2-inch grid size along the crack path.

### 4.3 Correlation with Two-Panel Solution

The energy-release-rate approach, as previously mentioned, represents a 50 percent savings in computer time and produces results within 1.5 percent of the two-panel solution. A fairly comprehensive structural idealization was computerized to compare the energy and two-panel solution. This idealization is shown in Figure 12 and represents a panel 0.071-inch thick with frames at 24-inch spacing. The results of this analysis are shown in Figure 13.

### 4.4 Complex Structural Configurations

One of the main advantages in the energy solution is the ability to analyze complex configurations not possible with known classical solutions. A typical example of this is in a pressurized fuselage shell, stiffened by frames and titanium crack stopper straps. At the location of a floor beam support, the frame bending moments are extremely high due to input of floor load into the frame. The frame bending induces local stresses in the skin, causing a nonuniform stress distribution across the bay when superimposed on the hoop stresses due to pressure. The calculation of crack tip stress intensity factor in the skin would thus be extremely difficult with any analytical method other than the energy-release approach. This problem is illustrated in Figure 14 which shows a skin crack in the vicinity of a floor beam support. The idealization representing a quarter of the structure is shown in Figure 14. Stresses created by a cabin differential pressure of 8.6 psi were applied together with concentrated loads to simulate the floor beam support and proper frame bending moments. The center crack stopper is assumed to be broken. A residual strength diagram for this structure is plotted in Figure 15 as a function of allowable frame bending moment. The diagram indicates that with a half crack length of 20 inches in the skin, a frame bending moment of 52,000 inch-pounds would cause failure.

## 5. DISPLACEMENT COMPATIBILITY METHOD

### 5.1 Method Description

This method is based on compatibility of displacement between the cracked sheet and the stiffeners after accounting for fastener displacement as illustrated in Figure 16. This approach can result in computer time savings of up to 50 to 1 when compared to the direct finite-element method. The main savings are attributable to pseudoanalytical techniques resulting in a relatively small matrix inversion compared to the finite-element method.

### 5.2 Sheet Displacements

Displacements in the cracked sheet are based on the theory of elasticity using the complex Airy stress function approach of Westergaard<sup>(4)</sup>. The differential equations of equilibrium and compatibility can be satisfied by taking any stress function  $(x,y)$  and using the expressions

$$\sigma_x = \frac{\partial^2 \phi}{\partial y^2}, \quad \sigma_y = \frac{\partial^2 \phi}{\partial x^2}, \quad \tau_{xy} = -\frac{\partial^2 \phi}{\partial x \partial y} \quad (11)$$

Westergaard found that choosing an Airy stress function

$$\phi = \operatorname{Re} \bar{Z} + y \operatorname{Im} \bar{Z} \quad (12)$$

where

$$\bar{Z} = \frac{d\bar{Z}}{dz}, \quad Z = \frac{dZ}{dz} \quad \text{and} \quad Z' = \frac{dZ}{dz}$$

would satisfy the equilibrium and compatibility equations for any problem.

$\operatorname{Re}$  and  $\operatorname{Im}$  are real and imaginary portions of each function of  $Z$ .  $Z$ , a complex function of  $z = x + iy$ , is chosen to satisfy the boundary conditions for each specific problem. Differentiation of Equation (12) and substitution in Equation (11) yields the following equations for stress.

$$\begin{aligned} \sigma_x &= \operatorname{Re} Z - y \operatorname{Im} Z' \\ \sigma_y &= \operatorname{Re} Z + y \operatorname{Im} Z' \end{aligned} \quad (13)$$

Substitution of Equation (13) into the biaxial equation for strain in the  $y$  direction results in the following equation for strain

$$\epsilon_y = \frac{1}{E} [(1 - \nu) \operatorname{Re} Z + (1 + \nu) y \operatorname{Im} Z'] \quad (14)$$

Integration of Equation (14) gives the following equation for displacement.

$$V = \frac{1}{E} [2 \operatorname{Im} \bar{Z} - (1 + \nu) y \operatorname{Re} Z] \quad (15)$$

As an example, consider the two-bay skin-crack case with a broken central stiffener. The cracked skin displacement is obtained by superposition of the four cases shown in Figure 17. Displacements due to these four cases are:

- $V_1$ , the displacement in the cracked sheet due to overall gross stress.
- $V_2$ , the displacement in the uncracked sheet due to outer stiffener rivet loads.
- $V_3$ , the displacement in the uncracked sheet due to center stiffener rivet loads.
- $V_4$ , the displacement in the cracked sheet due to a stress applied to the crack face equal and opposite to the stress caused by the rivet forces.

For an infinite biaxially loaded cracked sheet, the complex stress function  $Z$  obtained by Westergaard<sup>(4)</sup> is given by

$$Z = \sigma z / (z^2 - a^2)^{1/2} \quad (16)$$

Substitution of this stress function into Equation (15) yields the following equation for displacement:

$$V_1 = \sigma \left\{ 2 \sqrt{r_1 r_2} \sin(\theta_1 + \theta_2)/2 - (1 + \nu) y r [\cos(\theta - \theta_{1/2} - \theta_{2/2})] / \sqrt{r_1 r_2} + \nu y \right\} / E \quad (17)$$

The stress  $\sigma_y$  and displacement  $V_F$  in an uncracked plate due to a single concentrated force  $F$  can be derived from the work of Love<sup>(5)</sup> and expressed, respectively, as:

$$\sigma_y = \frac{F y (1 + \nu)}{4 \pi B (x^2 + y^2)} \left[ \frac{3 + \nu}{1 + \nu} - \frac{2 x^2}{x^2 + y^2} \right] \quad (18)$$

where

$$V_F = \frac{F (1 + \nu)}{4 \pi B E} \left[ \frac{(3 - \nu)}{2} \log(x^2 + y^2) + \frac{(1 + \nu) x^2}{x^2 + y^2} \right] + C \quad (19)$$



$x$  and  $y$  are measured from the load point and  $C$  is a constant of integration. The singularity, contained in Equation (19), at the load point can be removed by distributing the point force over the rivet diameter  $D$ . Using Equation (19) to obtain the displacement for an elemental load and integrating across the rivet diameter will yield an equation for displacement free from the singularity at the load center. This equation can then be used to obtain an equation for the displacement  $V_2$  in the uncracked sheet for a system of four forces, as shown in Figure 17. Thus,  $V_2$  can be expressed as:

$$V_2(x_i, y_i, x_j, y_j) = \frac{(1+\nu)(3-\nu)}{16\pi EB} \left( (X_A + 1) \operatorname{Log} \left\{ \frac{(X_A + 1)^2 + Y_A^2}{(X_A + 1)^2 + Y_B^2} \right\} \right. \\ - (X_A - 1) \operatorname{Log} \left\{ \frac{(X_A - 1)^2 + Y_A^2}{(X_A - 1)^2 + Y_B^2} \right\} + (X_B + 1) \operatorname{Log} \left\{ \frac{(X_B + 1)^2 + Y_A^2}{(X_B + 1)^2 + Y_B^2} \right\} \\ - (X_B - 1) \operatorname{Log} \left\{ \frac{(X_B - 1)^2 + Y_A^2}{(X_B - 1)^2 + Y_B^2} \right\} + 4 \left( \frac{1-\nu}{3-\nu} \right) \left[ Y_A \operatorname{Tan}^{-1} \left\{ \frac{2Y_A}{Y_A^2 + X_A^2 - 1} \right\} \right. \\ \left. + Y_A \operatorname{Tan}^{-1} \left\{ \frac{2Y_A}{Y_A^2 + X_B^2 - 1} \right\} - Y_B \operatorname{Tan}^{-1} \left\{ \frac{2Y_B}{Y_B^2 + X_A^2 - 1} \right\} - Y_B \operatorname{Tan}^{-1} \left\{ \frac{2Y_B}{Y_B^2 + X_B^2 - 1} \right\} \right] \right) \quad (20)$$

Similarly, the displacement  $V_3$ , in the uncracked sheet due to a system of two rivet loads is given by:

$$V_3(x_i, y_i, y_j) = \frac{(1+\nu)(3-\nu)}{16\pi EB} \left( \left( \frac{2x_i}{D} + 1 \right) \operatorname{Log} \left\{ \frac{\left( \frac{2x_i}{D} + 1 \right)^2 + Y_A^2}{\left( \frac{2x_i}{D} + 1 \right)^2 + Y_B^2} \right\} \right. \\ - \left( \frac{2x_i}{D} - 1 \right) \operatorname{Log} \left\{ \frac{\left( \frac{2x_i}{D} - 1 \right)^2 + Y_A^2}{\left( \frac{2x_i}{D} - 1 \right)^2 + Y_B^2} \right\} + 4 \left( \frac{1-\nu}{3-\nu} \right) \left[ Y_A \operatorname{Tan}^{-1} \left\{ \frac{2Y_A}{Y_A^2 + \frac{4x_i^2}{D^2} - 1} \right\} \right. \\ \left. - Y_B \operatorname{Tan}^{-1} \left\{ \frac{2Y_B}{Y_B^2 + \frac{4x_i^2}{D^2} - 1} \right\} \right] \right) \quad (21)$$

where

$$X_A = \frac{2}{D} (x_i - x_j) \quad X_B = \frac{2}{D} (x_i + x_j) \\ Y_A = \frac{2}{D} (y_i - y_j) \quad Y_B = \frac{2}{D} (y_i + y_j)$$

Similarly, by transfer of axis and superposition using Equation (18), the stress distribution along the  $x$  axis of the uncracked sheet, as shown in Figure 18, due to a system of outer stiffener and inner stiffener rivet forces is given in general by:

$$\sigma_y(x, 0) = - \frac{(1+\nu)y_i}{2\pi B} \left\{ F_j \alpha(x_j, y_j, b) + P_j \beta(y_j, b) \right\} \quad (22)$$

where

$$\alpha(x_j, y_j, b) = \left( \frac{3+\nu}{1+\nu} \right) \left\{ \frac{1}{(b-x_j)^2 + y_j^2} + \frac{1}{(b+x_j)^2 + y_j^2} \right\} - \frac{2(b-x_j)^2}{\{(b-x_j)^2 + y_j^2\}^2} - \frac{2(b+x_j)^2}{\{(b+x_j)^2 + y_j^2\}^2} \quad (23)$$

$$\beta(y_j, b) = \left( \frac{3+\nu}{1+\nu} \right) \left( \frac{1}{b^2 + y_j^2} \right) - \left( \frac{2b^2}{(b^2 + y_j^2)^2} \right) \quad (24)$$

The displacement  $V_4$  is obtained by applying an equal and opposite stress distribution over the crack face to cancel out the stress distribution  $\sigma_y(x, 0)$  caused by the rivet forces  $F$  and  $P$ .

This is achieved as follows: The displacement anywhere in the cracked sheet due to a system of equal and opposite concentrated forces  $P$  applied to the crack face as shown in Figure 19 can be determined from Equation (15) in which for this case the stress function, due to Irwin<sup>(6)</sup>, is given by



$$Z = \frac{2Pa}{B\pi(z^2 - b^2)} \left[ \frac{1 - (b/a)^2}{1 - (a/z)^2} \right]^{1/2} \quad (25)$$

Substituting  $\sigma_y(x,0)tdb$  for  $P$  and integrating over half the crack length will yield an expression for displacement  $V_4$  in general terms as follows:

$$V_4 = - \frac{(1 + \nu)y_1}{2\pi^2 EB} \left\{ F_j \int_0^a \alpha(x_j, y_j, b) \epsilon(x_i, y_i, b) db + P_j \int_0^a \beta(y_j, b) \epsilon(x_i, y_i, b) db \right\} \quad (26)$$

where  $\alpha$  and  $\beta$  are given by Equations (23) and (24) and  $\epsilon$  is given by:

$$\begin{aligned} \epsilon(x_i, y_i, b) = \log & \left[ \frac{(a^2 - b^2) + (a^2 - b^2)^{1/2} (BC + AD) + r_1 r_2}{(a^2 - b^2) - (a^2 - b^2)^{1/2} (BC + AD) + r_1 r_2} \right] \\ & - \frac{y_i(1 + \nu)(a^2 - b^2)^{1/2}}{r_1 r_2 r_3^2 r_4^2} \left[ (x_i^2 - b^2 - y_i^2) \{x_i(AC - BD) + y_i(BC + AD)\} \right. \\ & \left. - 2x_i y_i \{x_i(BC + AD) - y_i(AC + BD)\} \right] \end{aligned} \quad (27)$$

where

$$A = (r_1 + x_i - a)^{1/2} \quad B = (r_1 - x_i + a)^{1/2}$$

$$C = (r_2 + x_i + a)^{1/2} \quad D = (r_2 - x_i - a)^{1/2}$$

It is necessary to solve Equation (26) numerically.

The total displacement of a point on the cracked sheet due to gross area stress and system of rivet forces is

$$V_{Total} = V_1 + V_2 + V_3 + V_4$$

### 5.3 Stiffener Displacements

Stiffener extension at the fastener shear face is determined due to axial loads and bending from fastener loads and direct loads due to axial stresses. The stiffeners are considered supported over several frames and bend due to fastener loads being offset from the stiffener neutral axis. The intact stiffener is considered supported on three frames and the average bending moment between each fastener, obtained through use of the three-moment equation, is given by:

$$M_{A_i} = \sum_{j=i}^{j=2n} CF_j - \left\{ \frac{3C}{2L^3} \sum_{j=n+1}^{j=2n} F_j (2Ly_j - y_j^2) \right\} \left\{ L - \frac{y_{(i-1)} + y_i}{2} \right\} \quad (28)$$

Stiffener displacement due to bending is given by

$$\delta_{M_i} = \frac{C}{EI} \sum_{i=n+1}^{i=1} M_{A_i} (Y_i - Y_{(i-1)}) \quad (29)$$

Outer stiffener displacement due to direct load is given by

$$\delta_{D_i} = \frac{1}{AE} \sum_{j=n+1}^{j=i} F_j y_j + \frac{y_i}{AE} \sum_{j=i+1}^{j=2n} F_j \quad (30)$$

Outer stiffener displacement due to gross stress is given by

$$\delta_{G_i} = \frac{\sigma y_i}{E}$$

where

$C$  = distance from shear face to neutral axis

$I$  = stiffener inertia

$L$  = distance between supports

$n$  = number of active fasteners per stiffener

$y$  = rivet coordinate from crack centerline

Similarly, each half of the central failed stiffener from the crack centerline is reacted on three frame supports and the average bending moment between each fastener is given generally by

$$M_{A_i} = \sum_{j=1}^{j=i} CP_j - \left\{ \frac{C}{L} \sum_{j=1}^{j=n} P_j \left( \frac{5}{4} - \frac{3Y_j}{4L^2} \right) \right\} \left\{ \frac{y_{(i+1)} + y_i}{2} \right\} \quad (31)$$

Center stiffener displacement due to bending is given by

$$\delta_{M_i} = \frac{C}{EI} \sum_{i=1}^{i=n-1} M_{A_i} (y_{(i+1)} - y_i) \quad (32)$$

Center stiffener displacement due to direct load is given by

$$\delta_{D_i} = \frac{1}{AE} \sum_{j=1}^{j=i} P_j (y_n - y_i) + \frac{1}{AE} \sum_{j=i+1}^{j=n-1} P_j (y_n - y_j) \quad (33)$$

#### 5.4 Fastener Displacements

As load is transferred from the cracked sheet to the stiffener, the effect of fastener displacement is an extremely important consideration in the fracture analysis of stiffened structure. If this is neglected, errors up to 50 percent in the calculation of  $K$  can result. It has been determined by tests that the elastic displacement in shear can be represented by the following empirical relation:

$$\delta_R = \frac{F}{ED} \left[ A + C \left( \frac{D}{B_1} + \frac{D}{B_2} \right) \right] \quad (34)$$

where the terms in this equation are the same as those following Equation (5).

Figure 20 illustrates the importance of fastener flexibility. A panel containing a crack of a half length of 5.0 inches is stiffened by a strap having a cross-sectional area of 0.375 in<sup>2</sup>. The strap is fastened to the panel by one rivet on each side of the crack. The skin displacement under load at the rivet locations equals the displacement of the fastener plus the displacement of the strap. The figure illustrates that 75 percent of the combined rivet and strap displacement is contributed by the rivet. It can easily be seen therefore that fastener displacement is important in the calculation of  $K$ .

#### 5.5 Compatibility of Displacement

The solution to the stiffened panel problem using the compatible displacement method is obtained by the simultaneous solution of a series of compatibility equations. In the case being considered here as an example, compatibility at the center broken stiffener is given generally by:

$$\begin{aligned} & \sum_{j=n+1}^{j=2n} F_j \left\{ v_2(x_n, y_n, x_j, y_j) - \frac{(1+\nu)y_j}{2\pi^2 EB} \int_0^a \alpha(x_j, y_j, b) \epsilon(x_n, y_n, b) db \right\} \\ & - \sum_{j=1}^{j=n} P_j \left\{ v_3(x_n, y_n, y_j) - \frac{(1+\nu)y_j}{2\pi^2 EB} \int_0^a \beta(y_j, b) \epsilon(x_n, y_n, b) db \right\} \\ & + \delta R_n - \delta D_i - \delta M_i - \delta R_i \\ & - \sum_{j=n+1}^{j=2n} F_j \left\{ v_2(x_i, y_i, x_j, y_j) - \frac{(1+\nu)y_j}{2\pi^2 EB} \int_0^a \alpha(x_j, y_j, b) \epsilon(x_i, y_i, b) db \right\} \\ & + \sum_{j=1}^{j=n} P_j \left\{ v_3(x_i, y_i, y_j) - \frac{(1+\nu)y_j}{2\pi^2 EB} \int_0^a \beta(y_j, b) \epsilon(x_i, y_i, b) db \right\} \\ & = \sigma v_1(x_i, y_i) - \sigma v_1(x_n, y_n) \end{aligned} \quad (35)$$

Compatibility at the outer, intact stiffener is given generally by:

$$\begin{aligned} & \delta D_i + \delta M_i + \delta R_i - \sum_{j=n+1}^{j=2n} F_j \left\{ v_2(x_i, y_i, x_j, y_j) - \frac{(1+\nu)y_j}{2\pi^2 EB} \int_0^a \alpha(x_j, y_j, b) \epsilon(x_i, y_i, b) db \right\} \\ & - \sum_{j=1}^{j=n} P_j \left\{ v_3(x_i, y_i, y_j) - \frac{(1+\nu)y_j}{2\pi^2 EB} \int_0^a \beta(y_j, b) \epsilon(x_i, y_i, b) db \right\} = \sigma v_1(x_i, y_i) - \delta G_i \end{aligned} \quad (36)$$

A compatibility matrix is formulated from these equations of size  $2n \times 2n$ . The number of active fasteners,  $n$ , on each side of the crack depends on the configuration. It is economically advantageous to make the value of  $n$  as small as possible, but accuracy is lost if it is made too small. A value of 15 is usually adequate for the case where the center stiffener is failed. A curve of  $K$  is shown in Figure 6 of Reference 7 as a function of the number of effective fasteners. The compatibility matrix is inverted by computer to solve for fastener loads.

### 5.6 Crack Tip Stress Intensity Factor

Crack tip stress intensity factors caused by each pair of center stiffener fastener loads, as shown by case a in Figure 21, are given by

$$K_{CS} = \frac{\sqrt{a} P}{2B\sqrt{\pi}} \left[ \frac{2a^2 + (3 + \nu)Y_1^2}{(a^2 + Y_1^2)^{3/2}} \right] \quad (37)$$

Similarly, for each set of outer stiffener fastener loads, as shown in case b of Figure 21, the stress intensity is given by:<sup>(8)</sup>

$$K = \frac{2FY_1\sqrt{\pi a}}{\pi B} \left[ \left( \frac{3 + \nu}{2} \right) I_1 - (1 + \nu)I_2 \right] \quad (38)$$

where

$$I_1 = \frac{\beta}{Y_1 \sqrt{(Y_1^2 + a^2 - x_1^2)^2 + 4x_1^2 Y_1^2}} \quad (39)$$

$$I_2 = \frac{[(a^2 + x_1^2)Y_1^2 + (a^2 - x_1^2)^2] \beta^2 + x_1^2 Y_1^2 (Y_1^2 - a^2 + x_1^2)}{2Y_1 \beta [(Y_1^2 + a^2 - x_1^2)^2 + 4x_1^2 Y_1^2]^{3/2}} \quad (40)$$

$$\beta = \frac{1}{\sqrt{2}} \left[ (Y_1^2 + a^2 - x_1^2) + \sqrt{(Y_1^2 + a^2 - x_1^2)^2 + 4x_1^2 Y_1^2} \right]^{1/2} \quad (41)$$

Total stress intensity is obtained by superposition of the effects of all active fastener loads, paying strict attention to the direction of the loads, and the effects of overall gross stress.

## 6. CORRELATION BETWEEN DISPLACEMENT COMPATIBILITY AND DIRECT FINITE-ELEMENT METHODS

The displacement compatibility method is considered to be more accurate than the direct finite-element approach. This is mainly due to the fasteners being properly represented as concentrated loads distributed over their diameters instead of simulation to a shear panel as described earlier. It will be noticed in Figure 9 that the gridwork of the finite-element model becomes fairly coarse as the distance from the crack path increases. This is done to save computer time. The shear panel load is applied to the center of its adjacent bar as a concentrated load with the stiffness of the connection appropriate for the length of the panel. For the model shown in Figure 9, there are 10 such shear panel loads for each stiffener at varying distances from the crack. If the correct shear panel stiffnesses and locations from the crack are correctly input into the displacement compatibility program, the correlation shown in Figure 22 will result for the example problem of the two-bay crack with the center stiffener broken. It is apparent that the displacement compatibility method results in higher crack tip stress intensity factors in the region of the broken stiffener but when the crack tips are in the vicinity of the intact stiffener, correlation is good.

## 7. EFFECTS OF STRUCTURAL GEOMETRY

### 7.1 Parametric Study

The effects of structural geometry can best be illustrated by conducting a parametric study. The displacement compatibility method is most suitable for this due to its ease of application and comparatively short computer running times when compared to finite-element methods. The two-bay crack configuration with a broken central stiffener was chosen as the most interesting case. Figure 23 shows the structural configurations considered. The effects of varying the stiffener area and spacing are considered initially and therefore sheet thickness and fastener spacing are held constant at 0.063 and 1.0 inch, respectively. The stiffener depth is held constant at 1.25 inches and the flanges are varied in thickness to achieve section property variation. The results of this parametric study are shown in Tables 2 through 5. The values of  $\beta$  and stress concentration factors in the outer stiffener outer flange and outer stiffener inner flange are given by:

$$SCFO = \sigma_{STO} / \sigma \quad (42)$$

$$SCFI = \sigma_{STI} / \sigma \quad (43)$$

where

$\sigma_{STO}$  = outer stiffener outer flange stress

$\sigma_{STI}$  = outer stiffener inner flange stress



$\sigma$  = panel remote gross stress

## 7.2 Effect of Stiffener Area Variation

For illustration purposes, values of skin  $K_c$  and stiffener  $F_{tu}$  were chosen as 120 ksi/ $\sqrt{\text{in}}$  and 82 ksi respectively. Skin fracture strength, based on Equation (2), is shown in Figure 24 for Cases 13 and 16. Stiffener strength is based on  $F_{tu}/\text{SCFO}$ . The panel residual strength values for a two-bay crack with a broken central stiffener are based on points A and B at the intersection of the skin fracture and stiffener strength curves. Any skin fast fracture at higher stresses than these values would cause failure. In Figure 24, for Case 16, where the stiffener has the largest cross-sectional area, it may be noted that fast fracture at any stress level will occur at a shorter crack length than for the smaller stiffener. This is due to the higher load from the broken stiffener being transferred to the skin in the vicinity of the crack. However, the gross residual strength for the panel with larger area will be higher due to the strength capability of the outer, intact stiffener. The boxed area shown in Figure 24 has been replotted in Figure 25 to a larger scale with Cases 14 and 15 added. It is indicated that the residual strength of the panel will decrease with decreasing stiffener area.

## 7.3 Effect of Stiffener Spacing Variation

The effect on residual strength of varying the stiffener spacing is illustrated in Figure 26 for Cases 4, 8, 12, and 16. The stiffener area for these cases is constant at 0.4113 in<sup>2</sup>. It is evident that the residual strength, defined by points A, B, C, and D, decreases with increasing stiffener spacing. The residual strength for Cases 8, 12, and 16 is based on stiffener strength criteria while that for Case 4 is skin fracture-critical as indicated by point A at the peak of the skin fracture curve. However, it will be noted that in all cases the design would be very well balanced since the intersection of the stiffener strength and skin fracture curves occurs almost at the peak of the skin fracture curve. A  $K_c$  value of 120 ksi/ $\sqrt{\text{in}}$  was chosen to illustrate this point. The case illustrated in Figure 8a is not a balanced design since the stiffener is overstrength in relation to the skin fracture toughness. Figure 8b illustrates a case where the stiffener is under strength.

## 7.4 Combined Effects of Stiffener Spacing and Area

The results of varying stiffener area and spacing are illustrated in Figure 27 for the cases considered, where skin  $K_c$  is 120 ksi/ $\sqrt{\text{in}}$  and stiffener ultimate strength  $F_{tu}$  is 82 ksi. Increasing stiffener spacing and decreasing stiffener area cause decreases in residual strength.

## 7.5 Effects of Skin Fracture Toughness and Stiffener Material Strength

The effect on residual strength of varying the skin fracture toughness is illustrated in Figure 28. Case 16, where stiffener area and spacing are 0.4113 in<sup>2</sup> and 12.0 inches, respectively, is the condition considered. Also illustrated on Figure 28 is the effect of varying the stiffener material strength. In the case of the stronger stiffener with  $F_{tu} = 82$  ksi corresponding to 7075-T6 extrusion, the residual strength is given by points A, B, and C as the skin fracture toughness is reduced from 150 to 90 ksi/ $\sqrt{\text{in}}$ . Points A and B correspond to stiffener-precipitated failure and point C represents failure caused by skin fracture. In the case of the weaker stiffener, the residual strength is given by points D, E, and F as  $K_c$  drops from 150 to 90 ksi/ $\sqrt{\text{in}}$ . All of these failures would be precipitated by stiffener strength criteria although in the case of point F, the stiffener and skin criteria are almost the same.

## 7.6 Effect of Rivet Spacing

The effect of stiffener-to-skin rivet spacing is illustrated in Cases 17, 18, 19, and 20 for the two-bay crack with a broken stiffener of Figure 23. In this case, the stiffener spacing considered was 8 inches and the stiffener area was 0.2538 in<sup>2</sup> with a flange thickness of 0.10 inch. The skin thickness remains constant at 0.063 inch. The results of this parametric study are given in Table 6. Residual strength curves for Cases 17, 18, and 19 are shown plotted in Figure 29. At the intersection points A, B, and C it is indicated that increasing rivet spacing causes a decrease in residual strength. Also illustrated in Figure 29 is the effect of fastener spacing on fast-fracture crack length in the vicinity of the broken central stiffener. A decrease in rivet spacing causes a decrease in fast-fracture crack length. This is due to higher fastener loads at the broken central stiffener when rivet spacing is small, causing higher crack-tip stress-intensity factors at short crack lengths.

## 7.7 Effect of Fastener Stiffness

The effect of variations in fastener stiffness is determined from Cases 6, 21, and 22. Case 6 is for 3/16-inch aluminum rivets, Case 21 is for 1/4-inch aluminum rivets, and Case 22 for 3/16-inch steel rivets. Results for Cases 21 and 22 are shown in Table 7. All of these cases consider the stiffener area and spacing to be 0.2538 in<sup>2</sup> and 8.0 inches, respectively. The fastener spacing is 1.0 inch in each case. Figure 30 shows residual strength for Cases 6 and 22. Case 21 lies between these two, and has been omitted for clarity. As indicated by the figure, a slight loss in residual strength occurs with decreasing fastener stiffness.

# 8. SLOW STABLE CRACK GROWTH

## 8.1 Threshold of Slow Growth

Consider a panel made from a fairly ductile material such as 2024-T3 containing a center crack of half length  $a$  installed in a tensile testing machine. If the load is gradually increased from zero, slow stable tearing will start to occur at some gross stress level prior to reaching a failure stress. It has been shown that the onset of slow stable growth is a function of past loading history and not merely dependent on material.<sup>(9)</sup> If the crack had been generated at a constant gross stress  $\sigma$ , then slow stable growth will start when reloaded to a value of  $\sigma$ . It has been hypothesized that slow stable growth starts when the residual compressive stress at the crack tip, created by the plastic zone from a previous cycle, is completely eliminated.<sup>(9)</sup> Consider Figure 31a, where a high load cycle A has been applied, followed by constant amplitude cycles. Slow, stable crack growth will start to occur in cycle B when the plastic zone boundary ahead of the crack tip matches the boundary created by cycle A; that is, slow, stable growth will start at a stress intensity factor  $K_n$  obtained from

$$a_n + \frac{1}{2\pi} \left( \frac{K_n}{\sigma_{YS}} \right)^2 = a_A + \frac{1}{2\pi} \left( \frac{K_A}{\sigma_{YS}} \right)^2 \quad (44)$$



where

$a_n$  is the current half crack length

$a_A$  is crack half length at previous high load

$K_A$  is stress intensity at previous high load

$\sigma_{YS}$  is material yield strength

This equation of course assumes the classical plastic zone size for plane stress conditions.

Let  $K_{SG}$  be the stress intensity factor at the threshold of slow stable crack growth on the high load cycle B. Then, to satisfy Equation (44)

$$K_{SG} = \sigma_{YS} \sqrt{2\pi[a_A - a_n + 1/2\pi(K_A/\sigma_{YS})^2]} \quad (45)$$

The stress intensity factor range from the point at which slow, stable growth starts to the peak of the cycle is given by

$$(\Delta K)_\beta = K_B - K_{SG}$$

Figure 31b gives crack extension  $\Delta a$  as a function of  $(\Delta K)_\beta$  and  $K_{SG}$  for 2024-T3 sheet.<sup>(9)</sup>

## 8.2 Effect of Slow, Stable Growth on Residual Strength Diagram

Consider Figure 32. The skin fracture curve x was calculated using the direct finite-element approach described in Section 3. The case considered was a two-bay crack with broken central stiffener. The skin material was 2024-T3, 0.071-inch thick, having  $K_c$  value of 192.43 ksi  $\sqrt{\text{in}}$ . The stiffeners were shaped as a "Hat" Section with a gross area of 0.312 in.<sup>2</sup> Curve Y is plotted using the same  $\beta$  values but with  $K_{SG} = 57 \text{ ksi}\sqrt{\text{in}}$ . This value of  $K_{SG}$  is the lowest value observed during test.

Consider the hypothetical case where the crack had been propagated at a gross constant amplitude maximum stress of 20.4 ksi to a half crack length of 1.5 inches. On increasing the gross stress level, slow growth will start at 20.4 ksi (as shown by point A of Figure 32) and follow curve AB (obtained using data from Figure 31b) until point B is reached, where fast fracture will occur. If, on the other hand, the previous maximum constant amplitude stress was 32.0 ksi, the slow growth would not start until 32.0 ksi had been reached at point C in Figure 32 and would follow curve D. This hypothesis is substantiated to some extent by the results of testing the panel described. A crack had been propagated to a half length of 2.69 inches at a maximum gross stress of 22.0 ksi. Static load was gradually applied from zero and slow crack growth started to occur at 23.32 ksi shown by point G in Figure 32. Theoretically, to satisfy Equations (44) and (45), slow growth should have occurred at 22 ksi at point E, but the error is small. It did not, however, start at E on curve Y which was plotted using the lowest observable  $K_{SG}$ . Slow growth continued as the gross stress was increased (as shown by test points in Figure 32) until at point H, fast fracture occurred and the crack was arrested at point I. Curve Y, then, is not entirely material-dependent but is based on a value of  $K_{SG}$  which depends on the load history used to generate the fatigue crack.

## 9. EFFECTS OF PLASTICITY

### 9.1 Fastener Plasticity

Fastener failure as a criterion for panel failure was described in Section 2.3 and illustrated in Figure 8c. Testing experience on conventional structure has shown that this mode of failure is not a problem when skin fracture toughness is below about 100 ksi  $\sqrt{\text{in}}$ . Even though elastic analysis may show the panel to be critical for first fastener criteria, as illustrated by Figure 8c, the first rivet usually will yield without too much effect on the crack-tip stress-intensity factor. However, when fracture toughness values are high, resulting in high allowable stresses as in the case of 2024-T3 material, panel failure may be precipitated by rivet failure.

Although this paper has been confined to analysis, the rivet failure phenomenon can best be described by referring to a test. Figure 33a shows a stiffened panel containing a two-bay skin crack extending beyond the intact stiffeners adjacent to a broken central stiffener. The panel was made from 2024-T3 skin, 0.071 inch thick, with 7075-T6 Hat Section stiffeners spaced 8 inches on center with a cross-sectional area of 0.5471 square inch. The crack had propagated beyond the intact stiffeners by cyclic loading. Static loading was applied in increments and failure occurred at 39.74 ksi gross area stress with a half crack length of 9.88 inches. Inspection of the failed parts revealed that the fasteners in the two adjacent stiffeners had failed over their entire length, indicating that failure was precipitated by fastener failure.

Elastic analysis was performed using the displacement compatibility approach described in Section 5. The results of this analysis are plotted in the form of a residual strength diagram in Figure 33b. The fracture toughness value  $K_c$  used for the diagram was 197.87 ksi  $\sqrt{\text{in}}$ , obtained from fast fracture of another panel having different stiffener area. In this case, elastic analysis using the displacement compatibility approach was performed to obtain the critical stress intensity factor. The crack length at fast fracture was small enough so that fastener yielding did not affect the  $K_c$  value. Figure 33b indicates that at the failure crack length of 9.88 inches, total panel failure should have occurred due to rivet failure at a gross stress of 11.50 ksi. Failure stress due to stiffener and skin fracture are 32.58 ksi and 53.58 ksi, respectively. Since the panel failed at 39.74 ksi, the elastic analysis resulting in a simple residual strength curve similar to Figure 33b is insufficient to accurately predict failure. Obviously, the first rivet yields, causing the next rivets to be overloaded until they over yield. This yielding will occur until the first rivet reaches its failure displacement value. At this point, the crack-tip stress-intensity factor increases due to loss in effectiveness of the stiffener caused by yielding and subsequent failure of the first rivet. Panel failure will occur only then if the increase in crack-tip stress-intensity factor is sufficient to reach a critical value. If this is not the case, further increase in load will be required to cause total failure.

The displacement analytical approach was modified to account for fastener yielding. Any other method such as the finite-element method would not be economically feasible due to high costs of iterating the solution. Load displacement tests were conducted on simple lap splices placed back-to-back to cancel out bending. Correct materials and thicknesses were used. The resulting

load displacement curve was simulated by a trielastic model shown in Figure 34. The computer program was also modified to include the capability to disconnect rivets. An elastic solution is first obtained and each rivet load compared to the elastic-plastic model to determine its appropriate flexibility, depending on which leg of the curve is consistent with the rivet load. The rivet flexibility matrix is then regenerated and a second solution obtained. This procedure is automatically repeated until the crack-tip stress-intensity change between iterations is less than a certain value. Figure 35 shows rivet displacement as a function of gross stress. The lower curve represents the first rivet displacement. The next higher curve represents the second rivet after the first has been disconnected and so on. It will be noticed that considerable difference exists between the elastic and plastic solutions. When all rivets are intact, yielding first starts to occur at 6.808 ksi. The lines AB and EF represent the lower and upper bounds of rivet failure displacement, while line CD represents the average of several tests. Figure 36 shows crack-tip stress-intensity factor as a function of gross stress for various numbers of failed rivets. Again, considerable difference is indicated between elastic and plastic analyses. The vertical line AB represents the critical stress intensity factor of  $197.87 \text{ ksi}\sqrt{\text{in.}}$ . The vertical line CD represents a  $K_{Ic}$  value of 215, used for illustration purposes later. Figure 37 shows a cross plot of the intersection of line CD in Figure 35 with the rivet displacement curves. This curve is titled "Rivet Failure Curve." The intersection of line AB with the stress intensity lines of Figure 36 is plotted in Figure 37 and titled "Skin Fracture Curve  $K_{Ic} 197.87 \text{ ksi}\sqrt{\text{in.}}$ " Also, the intersection of line CD with the stress intensity lines of Figure 36 is plotted in Figure 37 and titled "Skin Fracture Curve  $K_{Ic} = 215 \text{ ksi}\sqrt{\text{in.}}$ "

Figure 37 represents the residual strength diagram at a half crack length of 9.88 inches. To illustrate how this diagram works, assume for a moment that the skin  $K_{Ic}$  value is  $215 \text{ ksi}\sqrt{\text{in.}}$ . Load is increased slowly and the first rivet, adjacent to the crack, fails at point A. The panel allowable from the skin fracture standpoint immediately drops from point B to C. Total failure does not, however, occur because the panel allowable based on second rivet failure has increased to point D since the rivet is farther away from the crack and thus less critical. Also, the load level is still only at 39.5 ksi, represented by point E, and therefore lower than either C or D. If loading is now increased, total panel failure will occur due to skin fast fracture at point C. Of course, as the skin crack rapidly extends beyond the stable value of  $a = 9.88$  inches, the rivet failure curve drops drastically. This results in all rivets failing as the crack extends. For our panel in question, though, the fracture toughness was only  $197.87 \text{ ksi}\sqrt{\text{in.}}$ . As soon as the first rivet fails at 39.5 ksi, represented by point A, the skin fracture allowable drops from point F to point G, which is below the load existing on the panel. Instant failure therefore occurs when the first rivet fails at 39.5 ksi. This value is less than 1 percent lower than the actual failure stress of 39.74 ksi. Variation in rivet failure displacement represented by the lower bound line AB and the upper bound line EF of Figure 35 would give a variation of panel failure between points G and F of Figure 37. The explanation for this is that at the lower bound point G of Figure 35, failure of the first rivet would occur at 37.5 ksi. This is lower than point G in Figure 37 so that load could further be increased to 39 ksi, represented by point G of Figure 37. Consider the upper bound point H of Figure 35 where the first rivet would fail at 42 ksi. In this case, the panel failure stress would be limited to 41 ksi, represented by point F of Figure 37. This, then, represents a spread between 39 and 41 ksi equivalent to minus 1.86 and plus 3.17 percent of the actual failure stress.

## 9.2 Stiffener Plasticity

For conventional aircraft structures in the basic wing or fuselage, the effects of stiffener plasticity may not be a problem. Usually, the panel strength, for the types of damage considered, will be limited by the rivet or skin fracture strength, as in the case described in Section 9.1. In the case of a higher-strength fastening system, however, such as steel HiLoks or adhesive bonding, stiffener plasticity can play an important role.

Again, the stiffener plasticity phenomenon can best be described by referring to a residual strength panel test. Figure 38 shows a 2024-T3 panel containing a center crack which has been propagated beyond two adhesively bonded Z-section 7075-T6 stiffeners. Static loading was applied to the panel, and failure occurred at a gross area stress of 30.6 ksi with a half crack length of 8.2 inches. During the failure process, the stiffeners became completely disbonded from the panel and were permanently deformed in the vicinity of the skin crack without themselves failing. Elastic analysis of this test panel had predicted gross failure stress levels of 17.07, 22.77, and 51.86 ksi for adhesive, stiffener, and skin fracture criteria, respectively. The normal procedure would have been to use the lower figure for an allowable, but in fact the panel failure stress was almost double the value.

A computer program was developed, based on the displacement compatibility approach. Details of this development are contained in the literature.<sup>(10)</sup> The adhesive was divided into a discrete number of segments as illustrated in Figure 39. Nonlinear shear distortion of the adhesive, obtained by napkin ring torsion tests, was simulated by the trielastic-plastic model shown in Figure 40a. The stress strain behavior of the stiffener material was also simulated by a trielastic-plastic model shown in Figure 40b. Figure 41 shows the resulting adhesive strain as a function of gross area stress for different degrees of adhesive disbond. The vertical line AB represents the average failure strain of the adhesive and lines DE and FG represent the lower and upper scatter band for adhesive failure strain. Figure 42 shows crack-tip stress-intensity factor as a function of gross area stress for different amounts of adhesive disbond. Line AB is the critical stress intensity factor obtained from unstiffened panels having the same width as this panel. Figure 43 shows stiffener strain as a function of gross area stress for different amounts of adhesive disbond. The line AB represents the failure strain for 7075-T6 extruded material.

Consider the adhesive strain curve of Figure 41 for all adhesive intact. As loading on the panel is increased, the adhesive starts to yield at about 10-ksi gross area stress. Loading is further increased and adhesive disbond starts to occur at point C, assuming average failure strain values. The points defined by the intersection of line AB with the adhesive strain lines can be cross plotted, giving a curve of gross stress versus amount of adhesive failed. This curve is shown as line ABFC in Figure 44. Similarly, the points defined by the intersection of line AB with the stress intensity factor lines can be cross plotted, giving a curve of gross stress at skin fracture for different amounts of adhesive disbond. This line is shown as curve DGE in Figure 44. The intersection of these two lines gives the panel allowable stress. Further explanation of the residual strength diagram given in Figure 44 is as follows. Loading is increased from zero and adhesive yielding starts to occur at about 10 ksi as shown in Figure 41. Loading is further increased and adhesive disbond occurs at point A and rapidly extends to point B without further increase in load. Load is again increased to point F, causing slow adhesive disbond. At this point, the stiffener is losing effectivity and has caused the panel allowable from a skin fracture point of view to drop from D to G. Further increase in load causes additional disbond and final failure occurs at 30.6 ksi, which correlates exactly with the test. If, however, the average failure properties of the adhesive are used, the stiffener will not yield, as shown by point H in Figure 41 being beyond point C. If the adhesive failure strain is increased slightly, as indicated by line LM, passing through point H in Figure 41 and well within the scatter band of lines DE and FG, the panel allowable increases only by 0.1 ksi to 30.7 ksi. This would cause permanent deformation of the stiffener, which did result during the test. If the analysis is repeated using the lower and upper bounds of adhesive failure strain, the predicted allowable would change to plus or minus 3 percent of the failure gross stress obtained in the test. It is indicated by points H, I, J, and K in Figure 41 that as soon as the stiffener yields, the adhesive no longer transfers load. This is also



reflected in Figure 43 which shows considerable reduction in stiffener strain as soon as the adhesive starts to disbond. Figure 43 also indicates that the stiffener failure strain is never reached due to adhesive disbond. This is also reflected in the test, which results in stiffener yielding near the skin crack but no failure.

# REFERENCES

1. Denke, P. H., A General Digital Computer Analysis of Statically Indeterminate Structures. Douglas Aircraft Company, Paper 834, September 1959.
2. Denke, P. H., A Computerized Static and Dynamic Structural Analysis System; Part III, Engineering Aspects and Mathematical Formulation of the Problem. Douglas Aircraft Company, Paper 3213, presented to SAE International Automotive Congress and Exposition, January 1965.
3. Pickard, J., and Morris, R. C., FORMAT II - Second Version of Fortran Matrix Abstraction Technique. AFFDL-TR-66-207, Volumes I and III, December 1966.
4. Westergaard, H. M., Bearing Pressures and Cracks. Journal of Applied Mechanics, Trans. ASME, vol. 6, No. 1, 1939, pp. A49-53.
5. Love, A. E. H., A Treatise on the Mathematical Theory of Elasticity. Fourth ed. (First American Printing), Dover Publications, 1944, p. 209.
6. Irwin, G. R., Analysis of Stresses and Strains Near the End of a Crack Traversing a Plate. Journal of Applied Mechanics, Trans. ASME, Vol. 24, 1957, pp. 361-364.
7. Swift, T., The Effects of Fastener Flexibility and Stiffener Geometry on the Stress Intensity in Stiffened Cracked Sheet, in Prospects of Fracture Mechanics. Noordhoff International Publishing, 1974, pp. 419-436.
8. Paris, P. C., Application of Muskhelishvili's Method to the Analysis of Crack Tip Stress Intensity Factors for Plane Problems, Part III. Lehigh University, 1960.
9. Swift, T., The Application of Fracture Mechanics in the Development of the DC-10 Fuselage, in Fracture Mechanics of Aircraft Structures, AGARD-AG-176, 1974, pp. 227-287.
10. Swift, T., Fracture Analysis of Adhesively Bonded Panels. ASME Paper No. 77-WA/Mat-2, 1977.

# ACKNOWLEDGMENT

The author wishes to express his appreciation to R. E. Darling and S. F. Y. Gee for their work on the finite-element energy-release-rate analysis.

TABLE 1  
CRACK TIP AND STIFFENER STRESSES FOR EXAMPLE PROBLEM  
USING DIRECT FINITE METHOD

HALF CRACK LENGTH a (IN.)	UNSTIFF. PANEL $\sigma_{yct}$	STIFFENED PANEL $\sigma_{yct}$	$\beta$	OUTER STIFFENER OUTER CAP STRESS	OUTER STIFFENER INNER CAP STRESS	MAX FASTENER PANEL SHEAR FLOW
0		2.259		1.064	1.091	0.00024
1.5	1.866	2.734	1.4652	1.094	1.119	0.00030
2.5	2.291	3.113	1.3588	1.132	1.151	0.00036
3.5	2.663	3.417	1.2831	1.189	1.193	0.00045
4.5	3.009	3.660	1.2164	1.271	1.246	0.00060
5.5	3.342	3.835	1.1475	1.394	1.306	0.00100
6.5	3.670	3.896	1.0616	1.591	1.372	0.00287
7.5	3.996	3.556	0.8899	1.955	1.432	0.01447
8.5	4.307	3.017	0.7005	2.637	1.444	0.07486
9.5	4.085	2.686	0.6575	3.043	1.465	0.10146

STRESSES QUOTED ARE FOR UNIT-APPLIED GROSS AREA STRESS.

TABLE 2  
RESULTS OF PARAMETRIC STUDY,  
STIFFENER SPACING 6.0 INCHES

a (IN.)	CASE 1: STIFF. AREA 0.189 IN. <sup>2</sup>			CASE 2: STIFF. AREA 0.2538 IN. <sup>2</sup>		
	$\beta$	SCFO	SCFI	$\beta$	SCFO	SCFI
0.1875	1.5900	1.0356	1.0350	1.7763	1.0445	1.0440
0.3750	1.5509	1.0375	1.0366	1.7253	1.0465	1.0457
0.5625	1.5014	1.0405	1.0390	1.6608	1.0497	1.0483
0.7500	1.4524	1.0444	1.0422	1.5968	1.0538	1.0517
1.500	1.3133	1.0693	1.0614	1.4145	1.0792	1.0716
2.250	1.2365	1.1094	1.0895	1.3130	1.1189	1.1001
3.000	1.1847	1.1693	1.1255	1.2445	1.1768	1.1361
3.750	1.1423	1.2587	1.1678	1.1887	1.2613	1.1780
4.500	1.1003	1.3965	1.2129	1.1341	1.3882	1.2231
5.250	1.0452	1.6258	1.2518	1.0646	1.5926	1.2637
6.000	0.9318	2.0272	1.2630	0.9298	1.9355	1.2828
6.750	0.8052	2.5085	1.2496	0.7863	2.3290	1.2816
7.500	0.7611	2.9060	1.2455	0.7374	2.6461	1.2865
8.250	0.7453	3.2373	1.2538	0.7203	2.9079	1.3004

a (IN.)	CASE 3: STIFF. AREA 0.3788 IN. <sup>2</sup>			CASE 2: STIFF. AREA 0.4113 IN. <sup>2</sup>		
	$\beta$	SCFO	SCFI	$\beta$	SCFO	SCFI
0.1875	2.1017	1.0592	1.0592	2.1899	1.0623	1.0624
0.3750	2.0312	1.0613	1.0610	2.1139	1.0645	1.0643
0.5625	1.9419	1.0647	1.0637	2.0174	1.0679	1.0671
0.7500	1.8530	1.0691	1.0673	1.9215	1.0723	1.0710
1.500	1.5977	1.0948	1.0876	1.6458	1.0982	1.0914
2.250	1.4537	1.1336	1.1156	1.4901	1.1368	1.1194
3.000	1.3557	1.1886	1.1496	1.3843	1.1910	1.1536
3.750	1.2763	1.2664	1.1881	1.2987	1.2672	1.1921
4.500	1.1999	1.3800	1.2278	1.2166	1.3773	1.2319
5.250	1.1071	1.5563	1.2610	1.1176	1.5464	1.2661
6.000	0.9421	1.8380	1.2713	0.9449	1.8131	1.2796
6.750	0.7765	2.1460	1.2630	0.7737	2.1010	1.2755
7.500	0.7203	2.3873	1.2611	0.7158	2.3250	1.2768
8.250	0.7001	2.5838	1.2679	0.6951	2.5069	1.2855

SCFO = STIFFENER STRESS CONCENTRATION FACTOR AT OUTER FIBER  
NEAR THE SKIN

SCFI = STIFFENER STRESS CONCENTRATION FACTOR AT INNER FIBER



TABLE 3  
RESULTS OF PARAMETRIC STUDY  
STIFFENER SPACING 8.0 INCHES

a (IN.)	CASE 5: STIFF AREA 0.189 IN. <sup>2</sup>			CASE 6: STIFF AREA 0.2538 IN. <sup>2</sup>		
	$\beta$	SCFO	SCFI	$\beta$	SCFO	SCFI
0.250	1.5824	1.0232	1.0267	1.7679	1.0291	1.0336
0.500	1.5219	1.0251	1.0288	1.6889	1.0311	1.0357
0.750	1.4563	1.0279	1.0320	1.6033	1.0342	1.0391
1.000	1.3999	1.0317	1.0362	1.5297	1.0382	1.0436
2.000	1.2657	1.0552	1.0612	1.3529	1.0623	1.0691
3.000	1.1982	1.0939	1.0991	1.2635	1.1008	1.1068
4.000	1.1535	1.1535	1.1494	1.2043	1.1588	1.1562
5.000	1.1167	1.2457	1.2113	1.1558	1.2467	1.2165
6.000	1.0794	1.3956	1.2816	1.1071	1.3858	1.2849
7.000	1.0285	1.6646	1.3489	1.0426	1.6271	1.3523
8.000	0.9029	2.2156	1.3742	0.8940	2.0968	1.3872
9.000	0.7618	2.9031	1.3556	0.7360	2.6526	1.3860
10.000	0.7288	3.4266	1.3587	0.7000	3.0656	1.3994
11.000	0.7197	3.8505	1.3811	0.6907	3.3972	1.4270

a (IN.)	CASE 7: STIFF AREA 0.3788 IN. <sup>2</sup>			CASE 8: STIFF AREA 0.4113 IN. <sup>2</sup>		
	$\beta$	SCFO	SCFI	$\beta$	SCFO	SCFI
0.250	2.0942	1.0389	1.0453	2.1827	1.0411	1.0477
0.500	1.9848	1.0412	1.0477	2.0647	1.0434	1.0502
0.750	1.8659	1.0444	1.0513	1.9363	1.0467	1.0539
1.000	1.7631	1.0487	1.0559	1.8254	1.0510	1.0585
2.000	1.5138	1.0732	1.0819	1.5560	1.0757	1.0847
3.000	1.3859	1.1108	1.1188	1.4175	1.1133	1.1215
4.000	1.3004	1.1659	1.1658	1.3252	1.1677	1.1682
5.000	1.2309	1.2472	1.2215	1.2501	1.2475	1.2234
6.000	1.1622	1.3723	1.2826	1.1763	1.3691	1.2842
7.000	1.0754	1.5810	1.3391	1.0837	1.5696	1.3412
8.000	0.8947	1.9646	1.3610	0.8949	1.9325	1.3670
9.000	0.7153	2.3928	1.3496	0.7102	2.3312	1.3617
10.000	0.6744	2.7017	1.3533	0.6682	2.6170	1.3688
11.000	0.6635	2.9467	1.3699	0.6571	2.8432	1.3874

TABLE 4  
RESULTS OF PARAMETRIC STUDY,  
STIFFENER SPACING 10.0 INCHES

a (IN.)	CASE 9: STIFF. AREA 0.189 IN. <sup>2</sup>			CASE 10: STIFF. AREA 0.2538 IN. <sup>2</sup>		
	$\beta$	SCFO	SCFI	$\beta$	SCFO	SCFI
0.3125	1.5710	1.0157	1.0205	1.7537	1.0197	1.0256
0.6250	1.4902	1.0175	1.0229	1.6484	1.0217	1.0281
0.9375	1.4150	1.0201	1.0265	1.5500	1.0245	1.0319
1.2500	1.3573	1.0236	1.0312	1.4743	1.0282	1.0369
2.5000	1.2321	1.0456	1.0601	1.3091	1.0508	1.0656
3.7500	1.1721	1.0823	1.1049	1.2295	1.0874	1.1101
5.0000	1.1326	1.1402	1.1664	1.1772	1.1439	1.1699
6.2500	1.0999	1.2324	1.2452	1.1340	1.2323	1.2459
7.5000	1.0661	1.3884	1.3393	1.0900	1.3780	1.3365
8.7500	1.0183	1.6858	1.4369	1.0291	1.6465	1.4320
10.0000	0.8833	2.3818	1.4803	0.8697	2.2394	1.4862
11.2500	0.7332	3.2821	1.4574	0.7030	2.9609	1.4859
12.5000	0.7089	3.9242	1.4714	0.6771	3.4634	1.5109
13.7500	0.7045	4.4342	1.5114	0.6733	3.8597	1.5548

a (IN.)	CASE 11: STIFF. AREA 0.3788 IN. <sup>2</sup>			CASE 12: STIFF. AREA 0.4113 IN. <sup>2</sup>		
	$\beta$	SCFO	SCFI	$\beta$	SCFO	SCFI
0.3125	2.0766	1.0265	1.0346	2.1643	1.0281	1.0364
0.6250	1.9305	1.0286	1.0374	2.0066	1.0302	1.0393
0.9375	1.7936	1.0317	1.0415	1.8587	1.0333	1.0434
1.2500	1.6874	1.0356	1.0466	1.7441	1.0373	1.0486
2.5000	1.4530	1.0584	1.0760	1.4906	1.0603	1.0781
3.7500	1.3384	1.0941	1.1191	1.3665	1.0959	1.1208
5.0000	1.2625	1.1477	1.1759	1.2845	1.1491	1.1770
6.2500	1.2002	1.2295	1.2464	1.2172	1.2295	1.2467
7.5000	1.1374	1.3610	1.3279	1.1497	1.3575	1.3212
8.7500	1.0552	1.5939	1.4094	1.0620	1.5817	1.4085
10.0000	0.8624	2.0764	1.4459	0.8608	2.0379	1.4494
11.2500	0.6754	2.6254	1.4825	0.6688	2.5477	1.4436
12.5000	0.6462	2.9966	1.4439	0.6390	2.8903	1.4589
13.7500	0.6418	3.2859	1.4727	0.6346	3.1568	1.4895

TABLE 5  
RESULTS OF PARAMETRIC STUDY,  
STIFFENER SPACING 12.0 INCHES

a (IN.)	CASE 13: STIFF. AREA 0.189 IN. <sup>2</sup>			CASE 14: STIFF. AREA 0.2538 IN. <sup>2</sup>		
	$\beta$	SCFO	SCFI	$\beta$	SCFO	SCFI
0.375	1.5571	1.0110	1.0158	1.7360	1.0138	1.0197
0.750	1.4592	1.0126	1.0183	1.6082	1.0156	1.0224
1.125	1.3795	1.0151	1.0222	1.5039	1.0183	1.0264
1.500	1.3230	1.0183	1.0272	1.4297	1.0217	1.0315
3.000	1.2070	1.0388	1.0581	1.2762	1.0427	1.0624
4.500	1.1529	1.0737	1.1074	1.2044	1.0774	1.1106
6.000	1.1175	1.1294	1.1772	1.1574	1.1319	1.1780
7.500	1.0880	1.2202	1.2699	1.1184	1.2192	1.2670
9.000	1.0668	1.3788	1.3859	1.0776	1.3682	1.3780
10.000	1.0115	1.6968	1.5144	1.0199	1.6568	1.5020
12.000	0.8690	2.5324	1.5796	0.8519	2.3686	1.5786
13.500	0.7133	3.6489	1.5536	0.6801	3.2575	1.5804
15.000	0.6957	4.4038	1.5822	0.6621	3.8447	1.6196
16.500	0.6948	4.9953	1.6425	0.6623	4.3018	1.6821

a (IN.)	CASE 15: STIFF. AREA 0.3788 IN. <sup>2</sup>			CASE 16: STIFF. AREA 0.4113 IN. <sup>2</sup>		
	$\beta$	SCFO	SCFI	$\beta$	SCFO	SCFI
0.375	2.0532	1.0185	1.0266	2.1393	1.0196	1.0279
0.750	1.8757	1.0205	1.0296	1.9477	1.0216	1.0310
1.125	1.7300	1.0233	1.0338	1.7904	1.0246	1.0353
1.500	1.6255	1.0269	1.0392	1.6774	1.0282	1.0407
3.000	1.4068	1.0480	1.0702	1.4408	1.0495	1.0717
4.500	1.3028	1.0816	1.1170	1.3282	1.0831	1.1181
6.000	1.2344	1.1332	1.1811	1.2542	1.1342	1.1812
7.500	1.1778	1.2142	1.2637	1.1931	1.2139	1.2626
9.000	1.1197	1.3488	1.3640	1.1306	1.3452	1.3613
10.500	1.0413	1.5999	1.4709	1.0470	1.5874	1.4673
12.000	0.8385	2.1777	1.5248	0.8356	2.1335	1.5259
13.500	0.6477	2.8475	1.5102	0.6400	2.7541	1.5206
15.000	0.6276	3.2771	1.5317	0.6197	3.1498	1.5460
16.500	0.6281	3.6077	1.5745	0.6205	3.4539	1.5901

TABLE 6  
EFFECTS OF RIVET SPACING

a (IN.)	CASE 17: RIVET SPACING 0.5 IN.			CASE 18: RIVET SPACING 1.0 IN.		
	$\beta$	SCFO	SCFI	$\beta$	SCFO	SCFI
0.25	2.1906	1.0194	1.0095	1.7679	1.0291	1.0335
0.50	1.9331	1.0218	1.0107	1.6889	1.0311	1.0357
0.75	1.7613	1.0252	1.0125	1.6033	1.0342	1.0391
1.00	1.6489	1.0294	1.0147	1.5297	1.0382	1.0435
2.00	1.4271	1.0542	1.0277	1.3529	1.0623	1.0691
3.00	1.3247	1.0940	1.0477	1.2635	1.1008	1.1068
4.00	1.2568	1.1549	1.0760	1.2043	1.1588	1.1562
5.00	1.2005	1.2498	1.1131	1.1558	1.2467	1.2165
6.00	1.1430	1.4058	1.1577	1.1071	1.3858	1.2849
7.00	1.0655	1.6938	1.1992	1.0426	1.6271	1.3523
8.00	0.8338	2.3808	1.1793	0.8940	2.0968	1.3872
9.00	0.6264	3.1463	1.1089	0.7360	2.6526	1.3860
10.00	0.6189	3.6152	1.0865	0.7000	3.0656	1.3994
11.00	0.6267	3.9822	1.0846	0.6907	3.3972	1.4270

a (IN.)	CASE 19: RIVET SPACING 1.5 IN.			CASE 20: RIVET SPACING 2.0 IN.		
	$\beta$	SCFO	SCFI	$\beta$	SCFO	SCFI
0.25	1.5360	1.0389	1.0333	1.4461	1.0397	1.0366
0.50	1.5061	1.0408	1.0345	1.4308	1.0414	1.0377
0.75	1.4664	1.0438	1.0364	1.4087	1.0441	1.0394
1.00	1.4251	1.0478	1.0389	1.3829	1.0479	1.0418
2.00	1.2990	1.0732	1.0543	1.2862	1.0722	1.0565
3.00	1.2265	1.1143	1.0768	1.2201	1.1121	1.0785
4.00	1.1774	1.1754	1.1052	1.1732	1.1712	1.1065
5.00	1.1374	1.2660	1.1379	1.1346	1.2577	1.1390
6.00	1.0978	1.4042	1.1718	1.0963	1.3871	1.1732
7.00	1.0455	1.6302	1.1987	1.0471	1.5893	1.2032
8.00	0.9416	2.0091	1.2023	0.9645	1.8968	1.2196
9.00	0.8243	2.4609	1.1866	0.8727	2.2609	1.2240
10.00	0.7782	2.8467	1.1775	0.8229	2.5973	1.2298
11.00	0.7612	3.1732	1.1789	0.8001	2.8931	1.2421

STIFFENER AREA 0.2538 IN.<sup>2</sup>  
STIFFENER SPACING 8.0 IN.

TABLE 7  
EFFECTS OF FASTENER STIFFNESS

a (IN.)	CASE 21: 1/4-IN. ALUM RIVETS			CASE 22: 3/16-IN. STEEL FASTENERS		
	$\beta$	SCFO	SCFI	$\beta$	SCFO	SCFI
0.25	1.7844	1.0291	1.0337	1.8062	1.0290	1.0338
0.50	1.7014	1.0312	1.0360	1.7176	1.0312	1.0362
0.75	1.6119	1.0343	1.0394	1.6230	1.0344	1.0398
1.00	1.5355	1.0384	1.0439	1.5429	1.0385	1.0444
2.00	1.3543	1.0628	1.0699	1.3559	1.0633	1.0714
3.00	1.2637	1.1017	1.1083	1.2640	1.1027	1.1099
4.00	1.2040	1.1605	1.1583	1.2036	1.1622	1.1608
5.00	1.1551	1.2498	1.2193	1.1543	1.2532	1.2227
6.00	1.1059	1.3924	1.2883	1.1045	1.3998	1.2923
7.00	1.0402	1.6428	1.3553	1.0372	1.6617	1.3586
8.00	0.8842	2.1377	1.3864	0.8713	2.1901	1.3843
9.00	0.7196	2.7159	1.3793	0.6986	2.7967	1.3695
10.00	0.6860	3.1382	1.3887	0.6683	3.2299	1.3738
11.00	0.6789	3.4757	1.4133	0.6642	3.5740	1.3947

STIFFENER AREA 0.2538 IN.<sup>2</sup>  
STIFFENER SPACING 8.0 IN.  
FASTENER SPACING 1.0 IN.



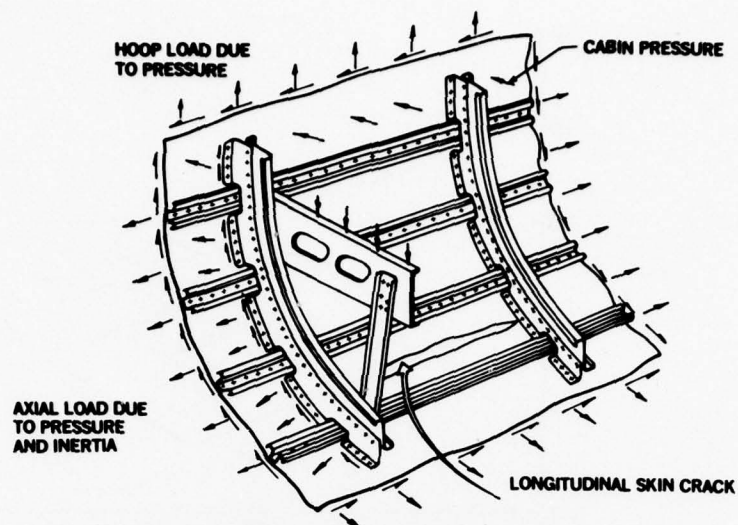


FIGURE 1. FUSELAGE COMPLEX STRUCTURAL CONFIGURATION

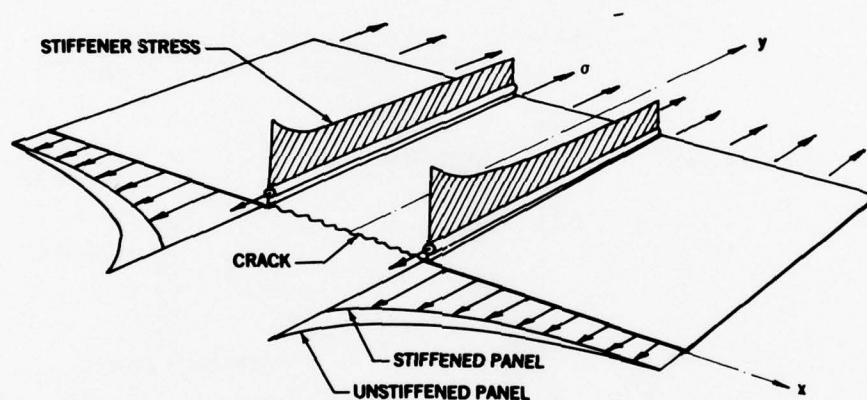


FIGURE 2. STRESS DISTRIBUTION IN A CRACKED PANEL

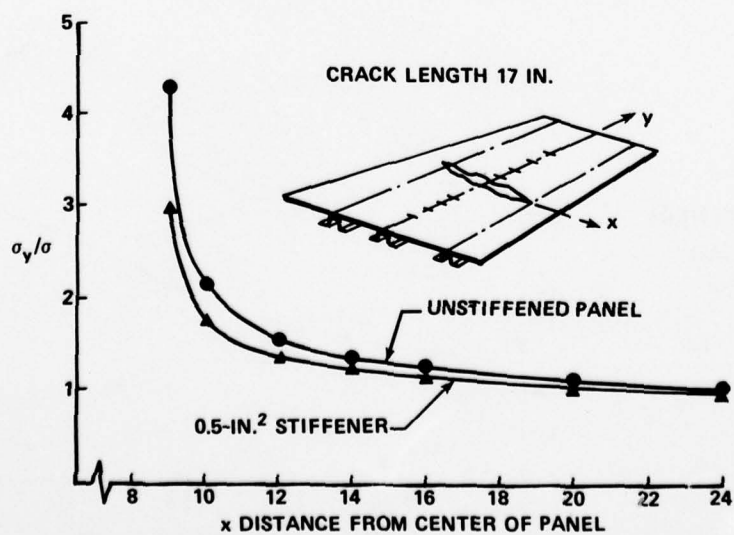


FIGURE 3. STRESS DISTRIBUTION AHEAD OF A CRACK TIP

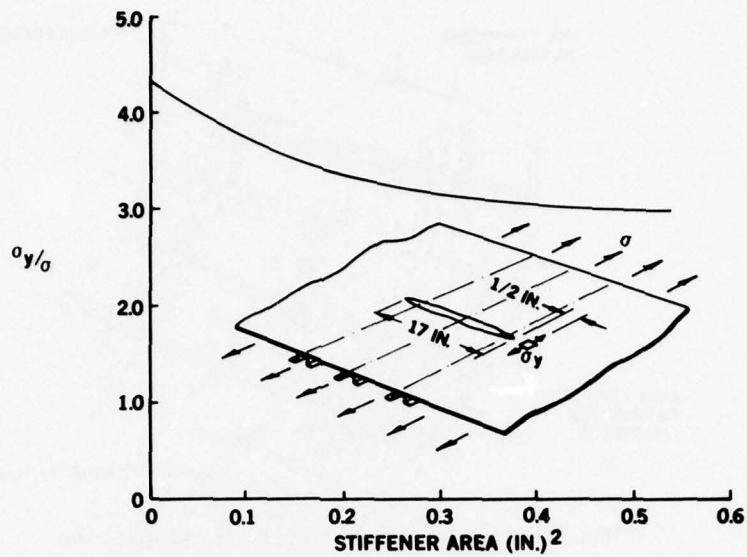


FIGURE 4. EFFECT OF STIFFENER AREA ON STRESS AHEAD OF CRACK TIP

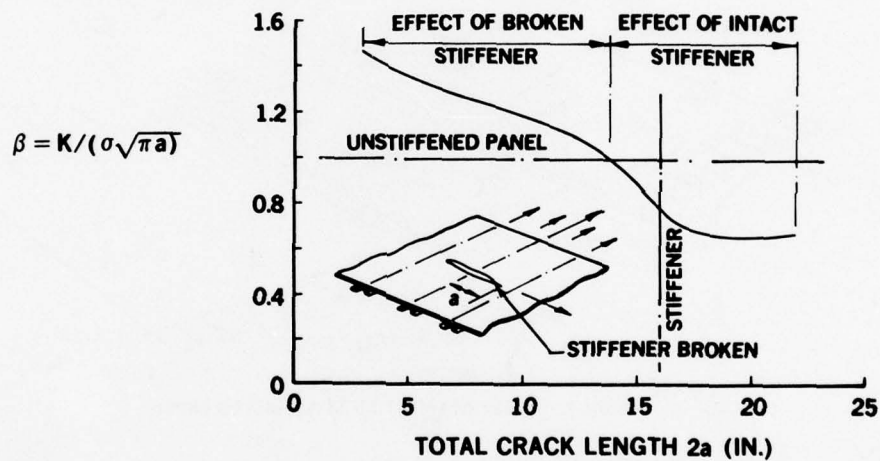


FIGURE 5. EFFECT OF STIFFENING ON BETA

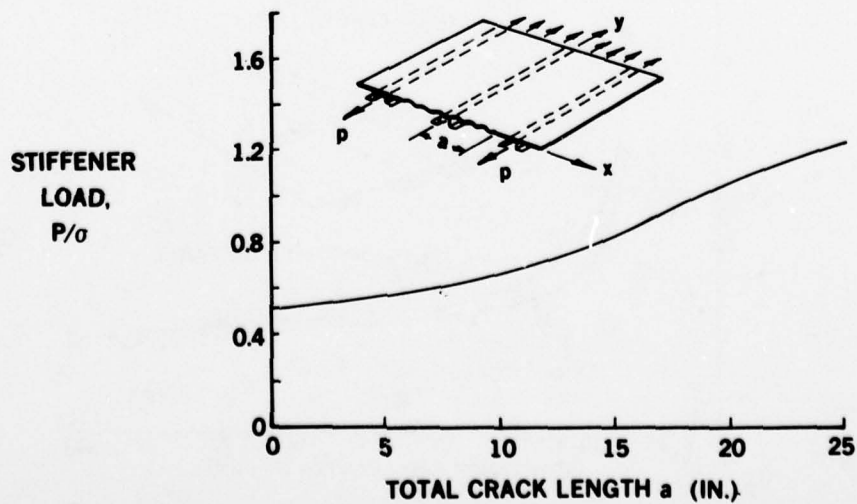


FIGURE 6. OUTER STIFFENER LOAD P

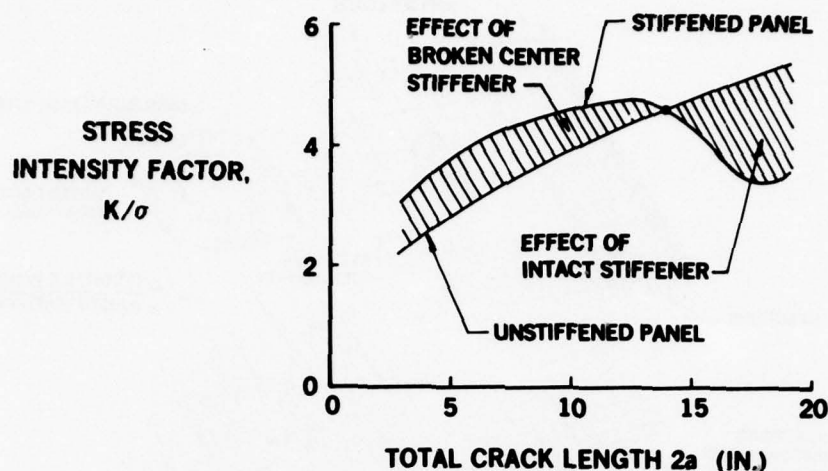
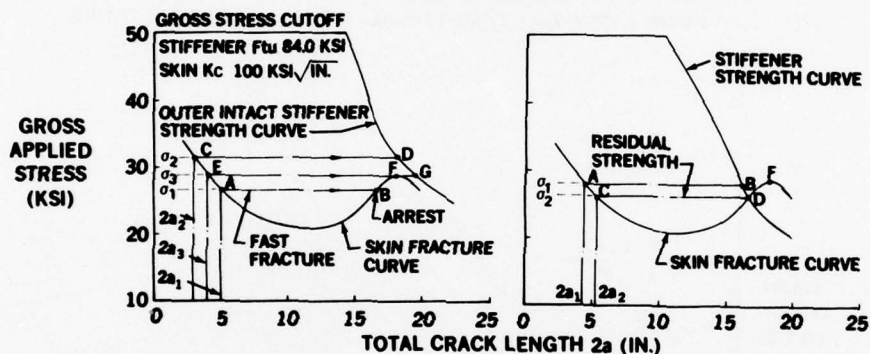
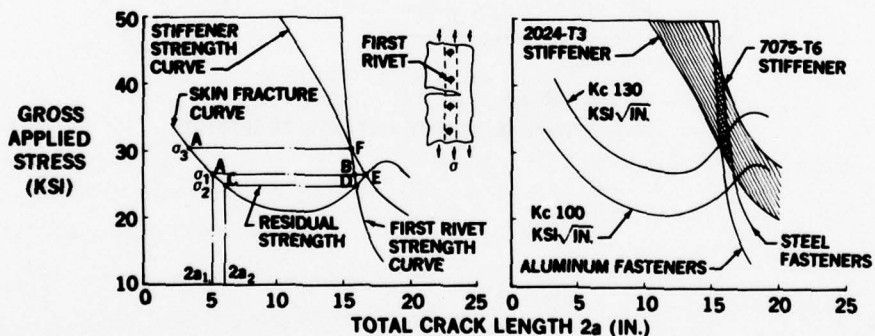


FIGURE 7. UNIT STRESS INTENSITY IN CRACKED STIFFENED PANEL



(a) EFFECT OF STRONG STIFFENER (b) EFFECT OF WEAKER STIFFENER



(c) FIRST RIVET FAILURE CRITERION (ELASTIC ANALYSIS) (d) SKIN, STIFFENER, AND FASTENER STRENGTH ENVELOPE

FIGURE 8. TYPICAL STIFFENED PANEL RESIDUAL STRENGTH DIAGRAMS

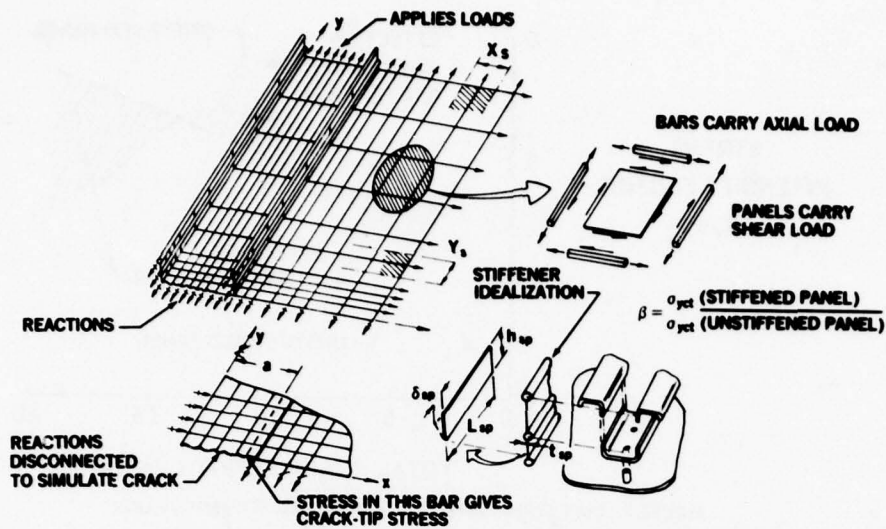


FIGURE 9. STIFFENED CRACKED PANEL FINITE-ELEMENT IDEALIZATION

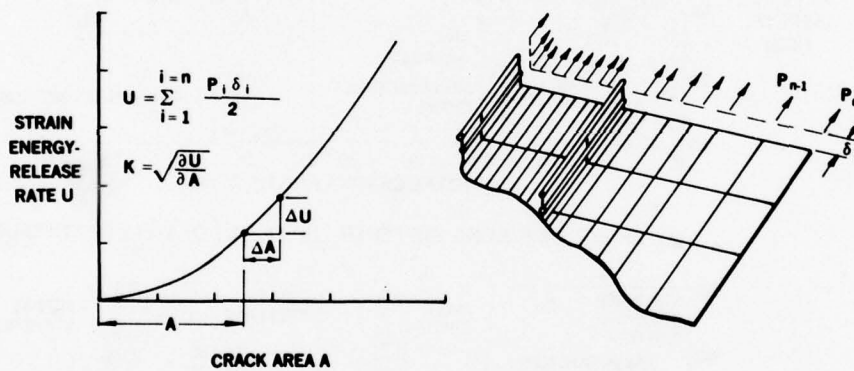


FIGURE 10. ENERGY-RELEASE-RATE SOLUTION

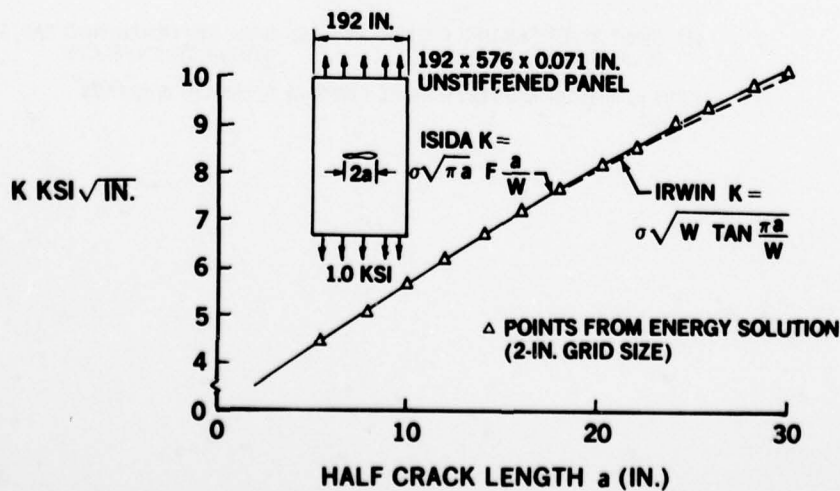


FIGURE 11. CORRELATION OF ENERGY-RELEASE-RATE WITH CLASSICAL SOLUTION



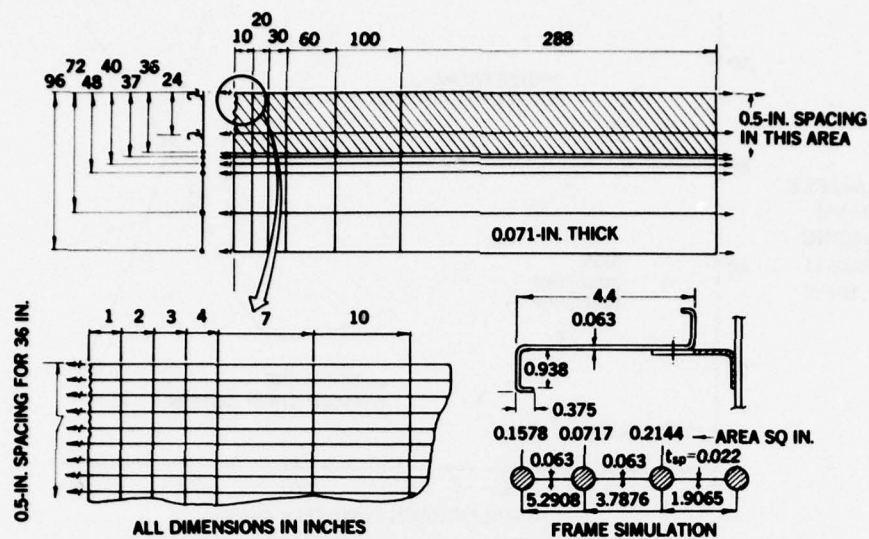


FIGURE 12. IDEALIZATION FOR ENERGY VERSUS TWO-PANEL SOLUTION CORRELATION

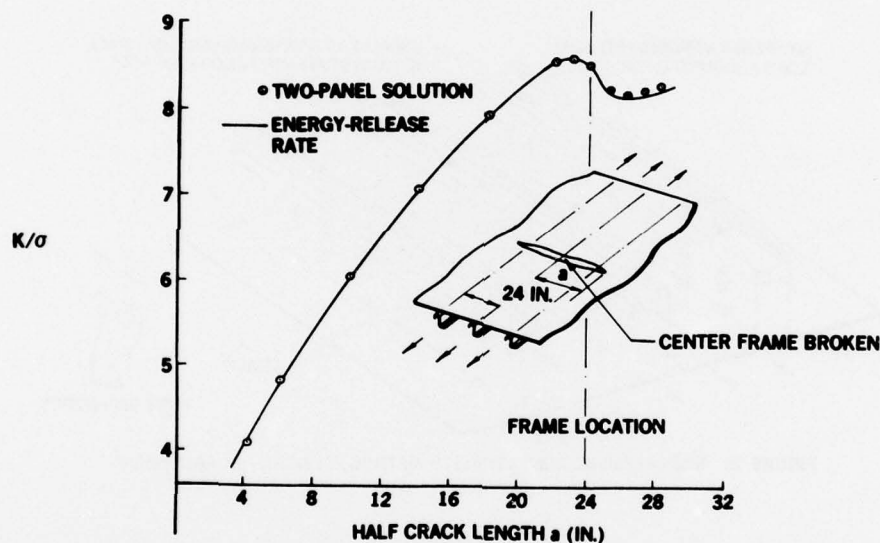


FIGURE 13. ENERGY-RELEASE-RATE VERSUS TWO-PANEL SOLUTION CORRELATION

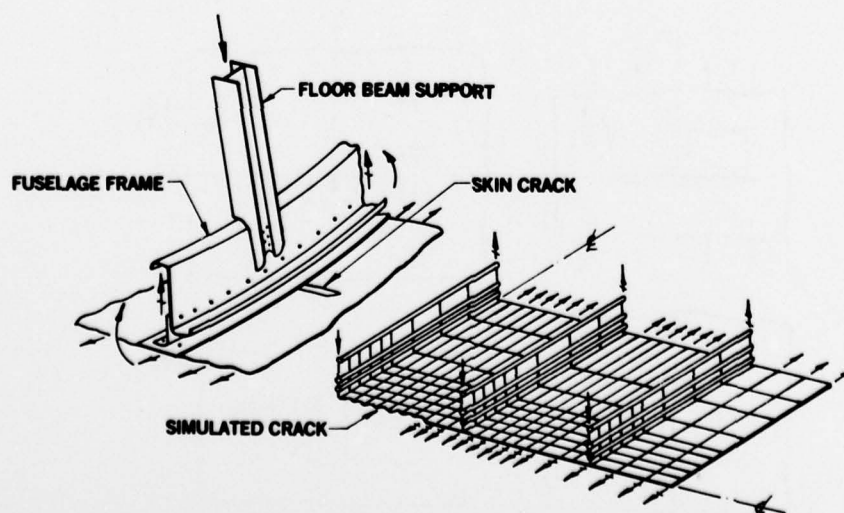


FIGURE 14. IDEALIZATION FOR ENERGY-RELEASE-RATE SOLUTION OF COMPLEX STRUCTURE

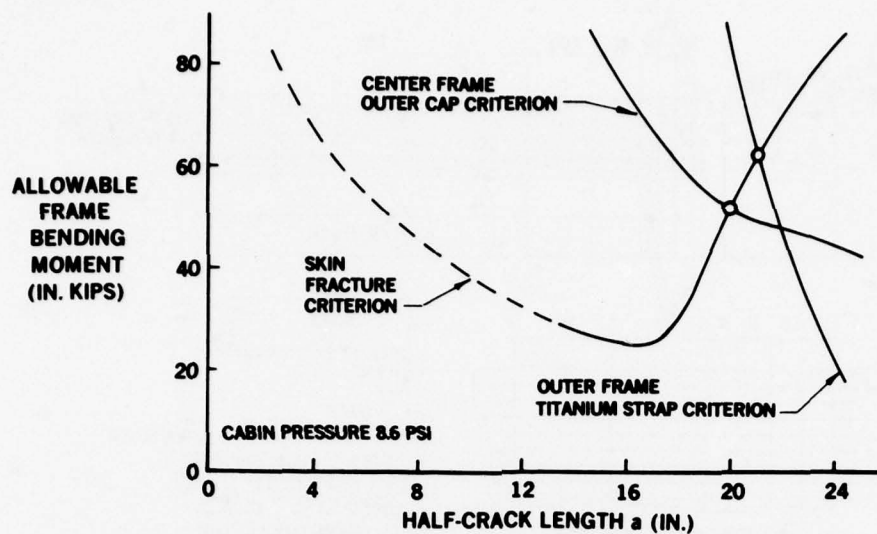


FIGURE 15. RESIDUAL STRENGTH DIAGRAM FOR COMPLEX STRUCTURAL ARRANGEMENT

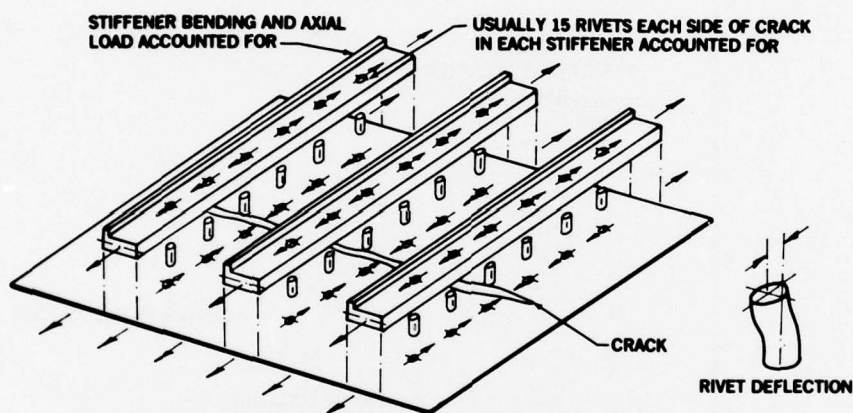


FIGURE 16. DISPLACEMENT COMPATIBILITY METHOD, TYPICAL ARRANGEMENT

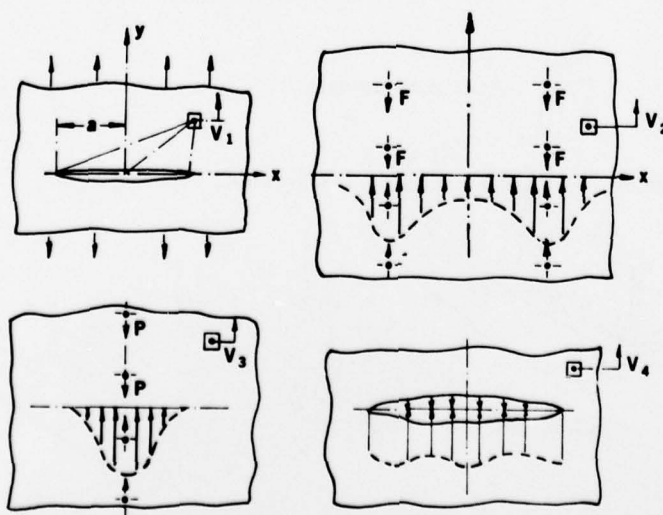


FIGURE 17. DEFLECTIONS WHICH ARE SUPERIMPOSED TO DETERMINE TOTAL SHEET DISPLACEMENT

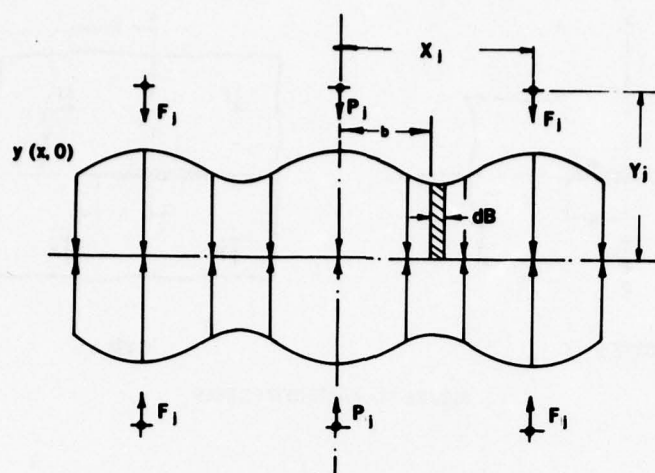
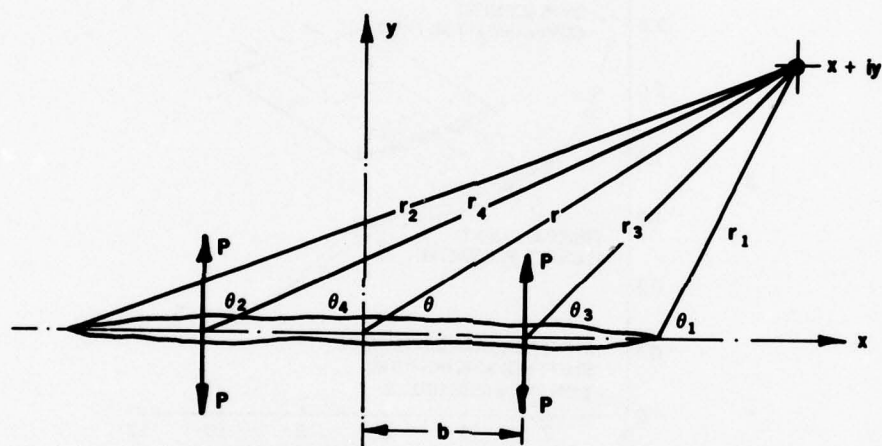
FIGURE 18. STRESS DISTRIBUTION AT  $y = 0$  DUE TO RIVET FORCES

FIGURE 19. CONCENTRATED LOADS APPLIED TO CRACK FACE

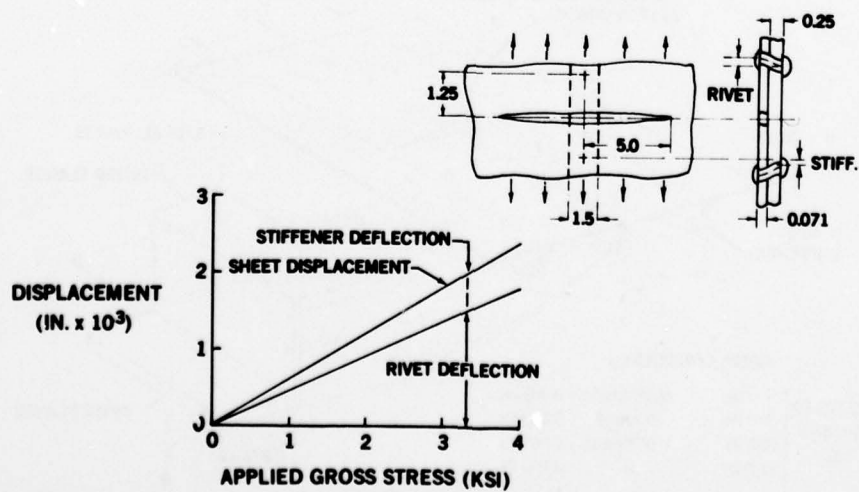


FIGURE 20. RIVET VERSUS STIFFENER DISPLACEMENT

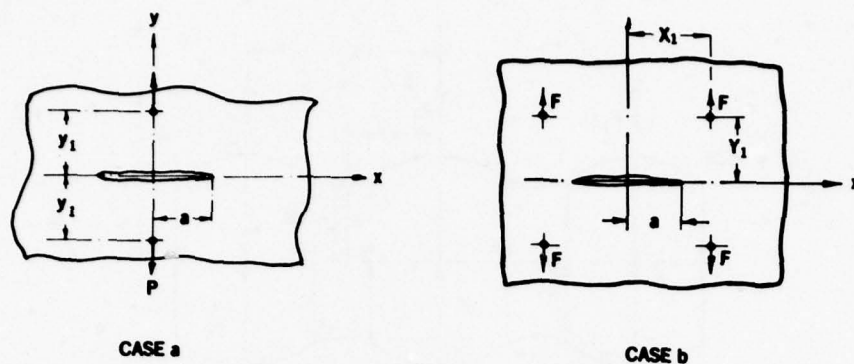


FIGURE 21. FASTENER FORCES

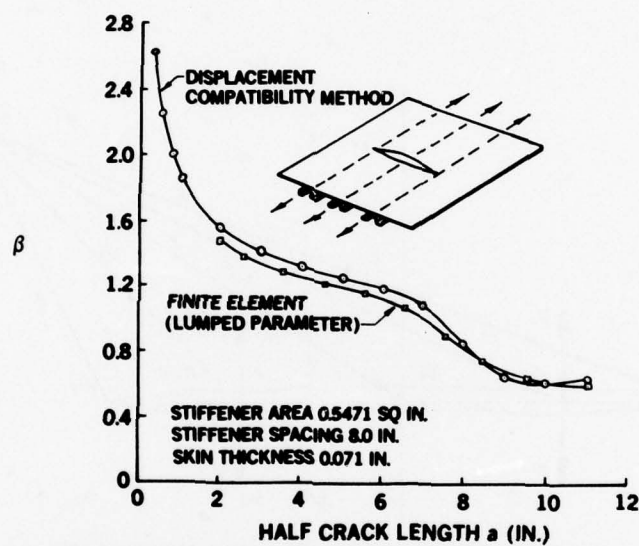


FIGURE 22. CORRELATION OF LUMPED PARAMETER VERSUS DISPLACEMENT COMPATIBILITY APPROACHES

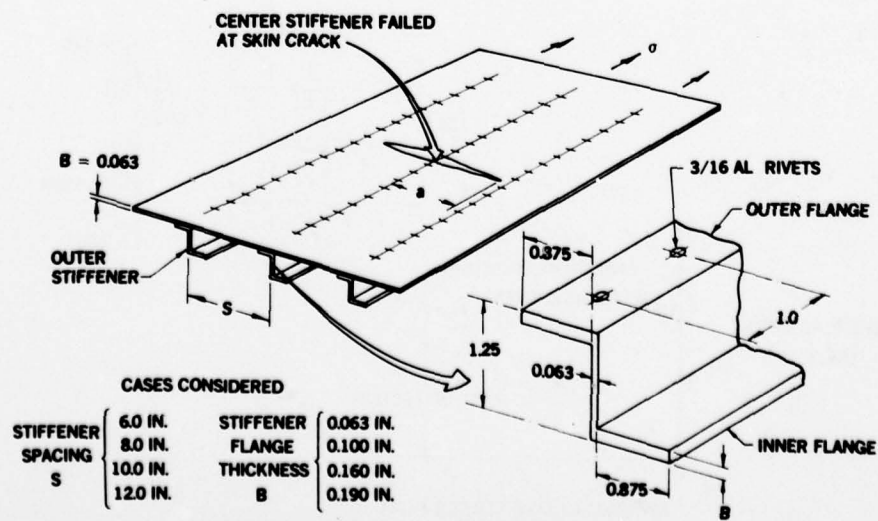


FIGURE 23. CONFIGURATION FOR PARAMETRIC STUDY



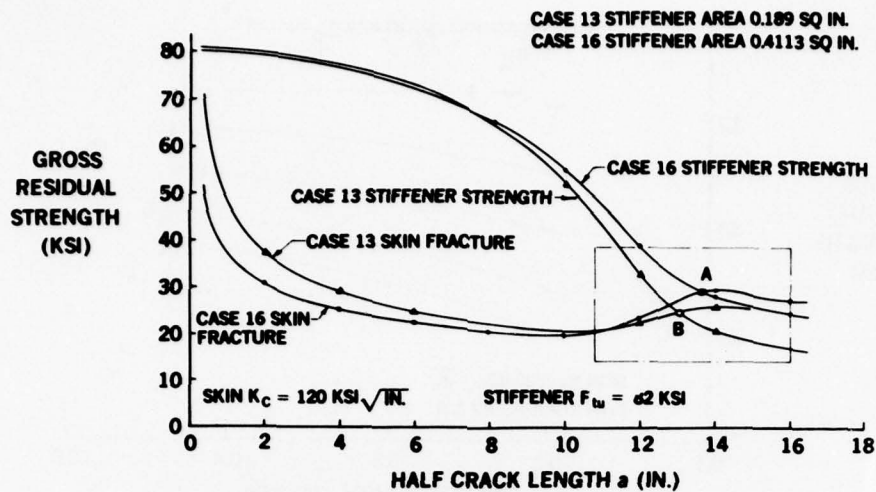


FIGURE 24. RESIDUAL STRENGTH DIAGRAM - STIFFENER SPACING, 12.0 INCHES

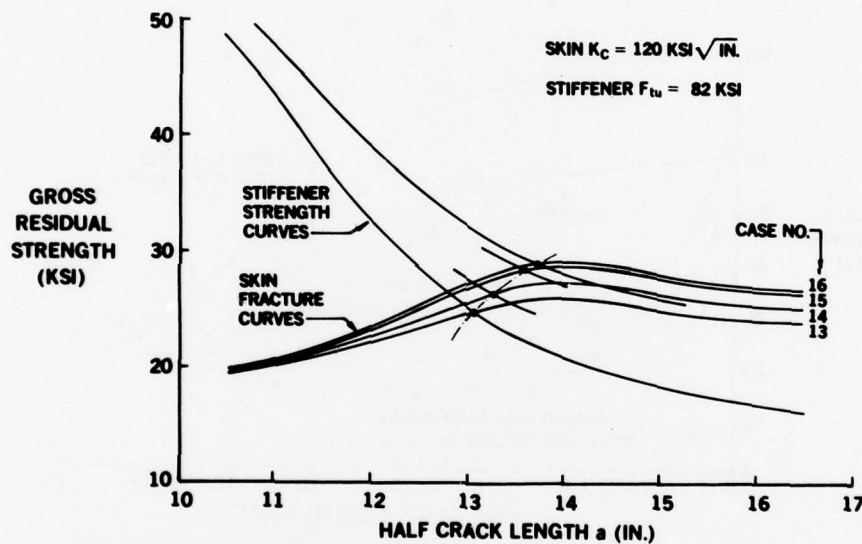


FIGURE 25. RESIDUAL STRENGTH DIAGRAM CASES 13, 14, 15, AND 16

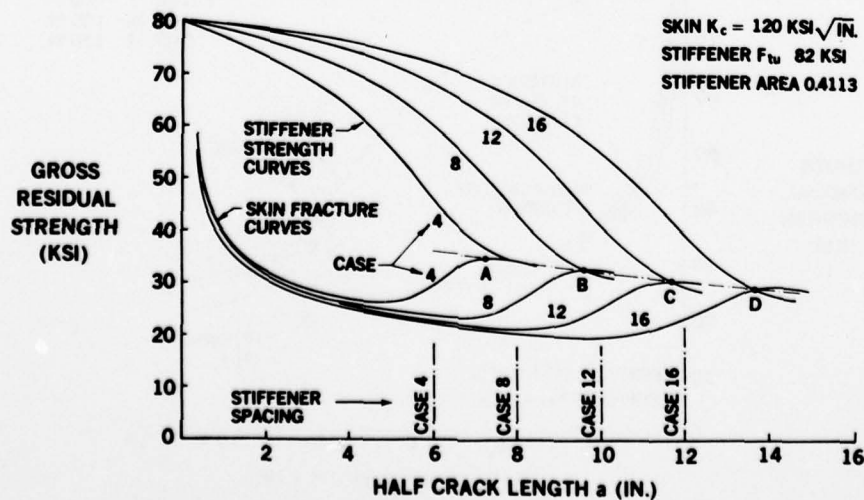


FIGURE 26. EFFECT OF STIFFENER SPACING ON RESIDUAL STRENGTH

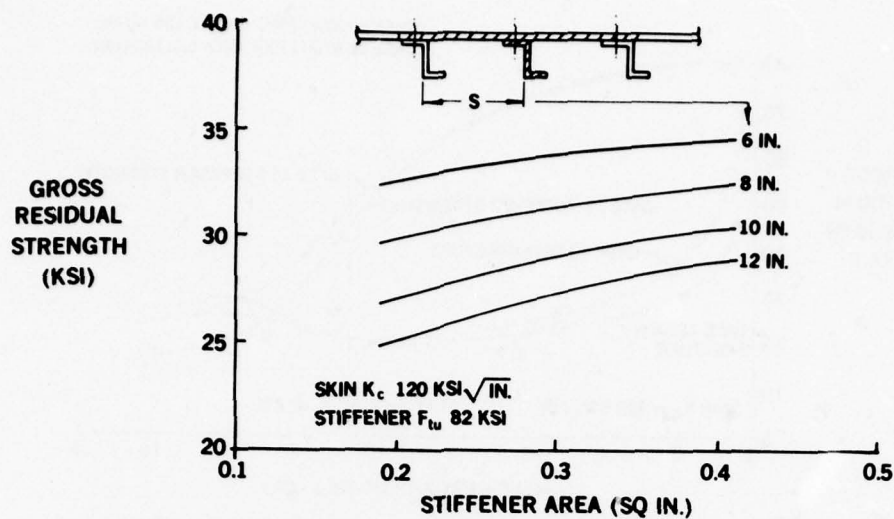


FIGURE 27. EFFECT OF STIFFENER AREA AND SPACING ON RESIDUAL STRENGTH

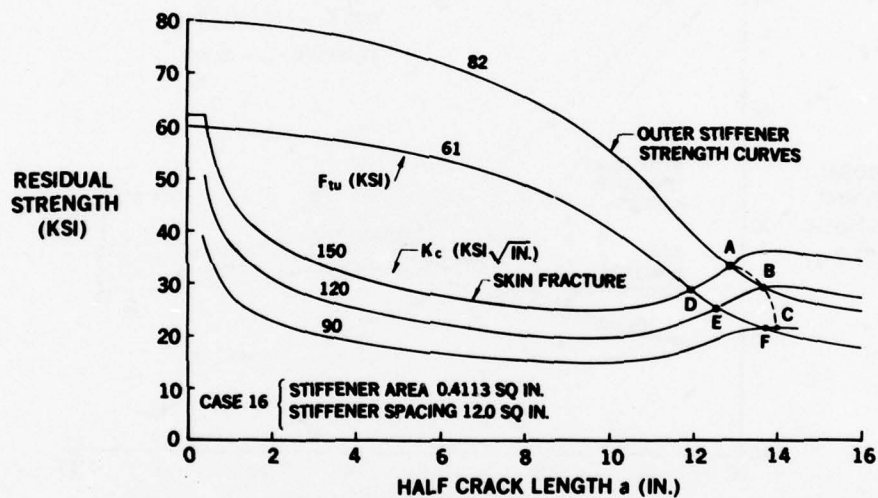
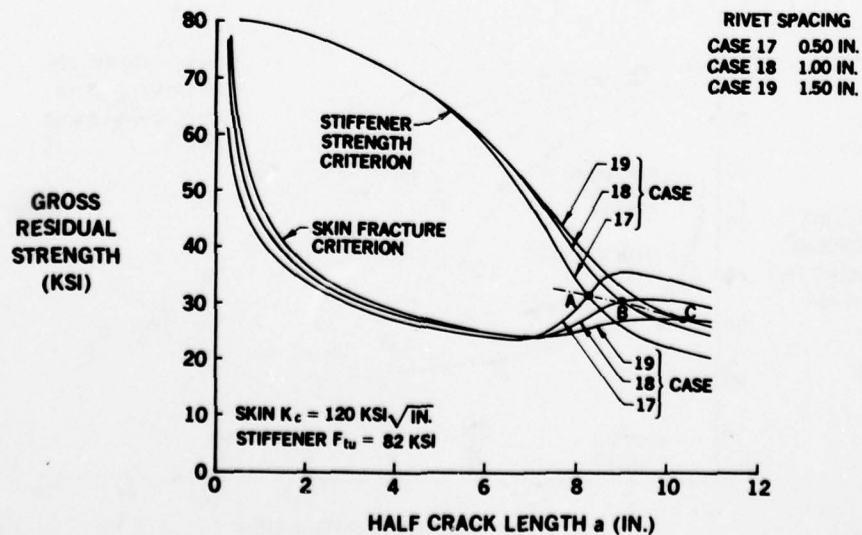
FIGURE 28. EFFECT OF VARIATION IN SKIN  $K_c$  AND STIFFENER MATERIAL STRENGTH

FIGURE 29. EFFECT OF RIVET SPACING ON PANEL RESIDUAL STRENGTH

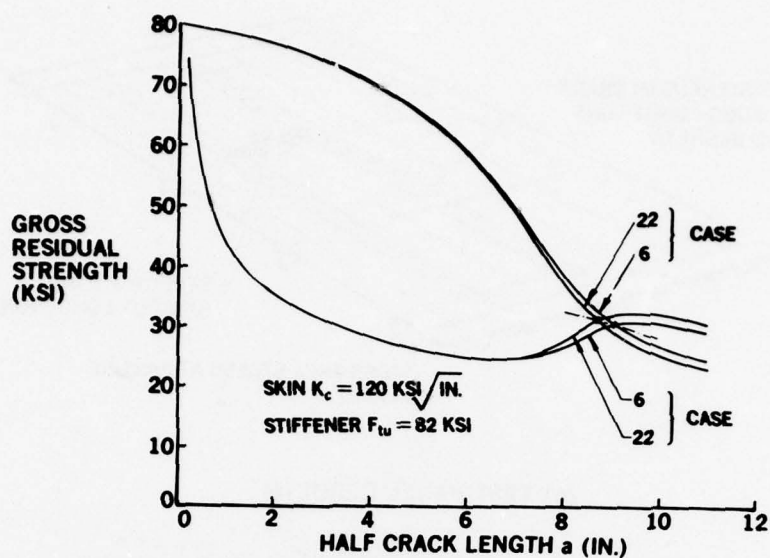


FIGURE 30. EFFECT OF FASTENER STIFFNESS ON RESIDUAL STRENGTH

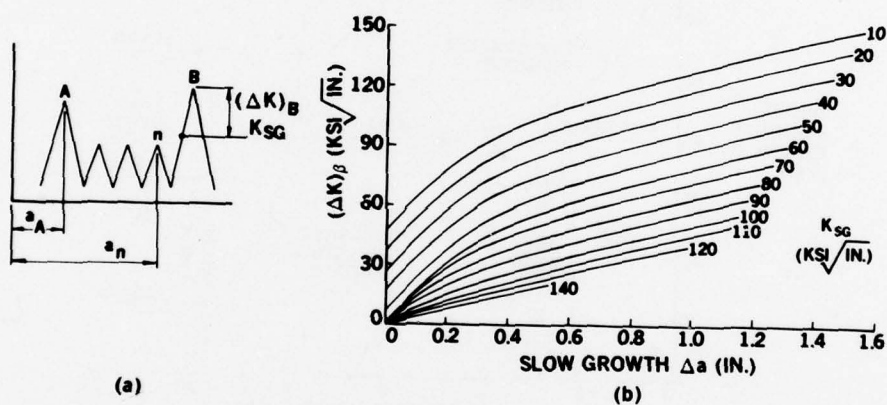


FIGURE 31. SLOW CRACK GROWTH VERSUS STRESS-INTENSITY-FACTOR RANGE

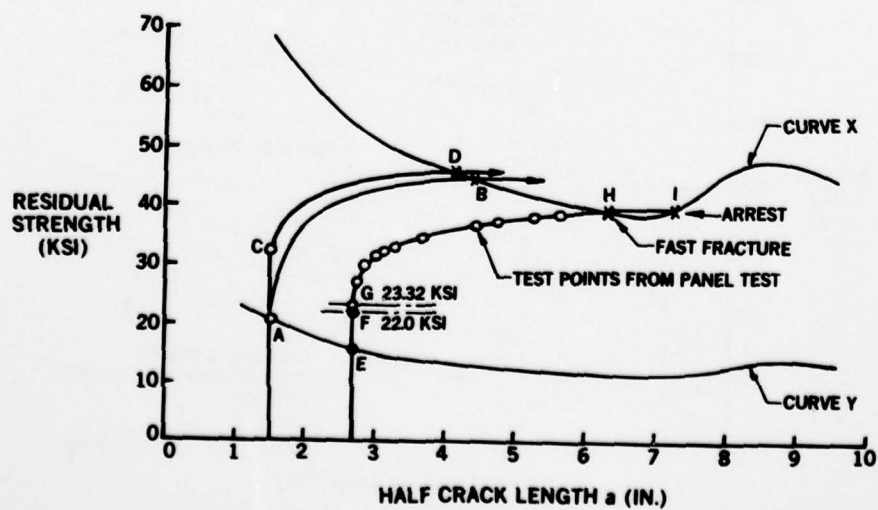
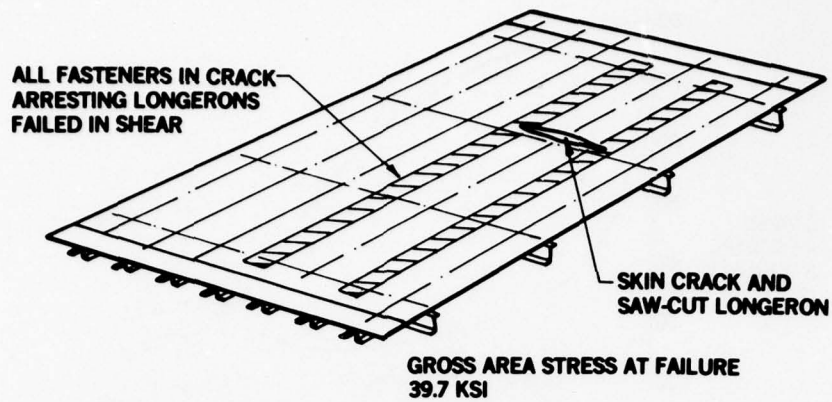
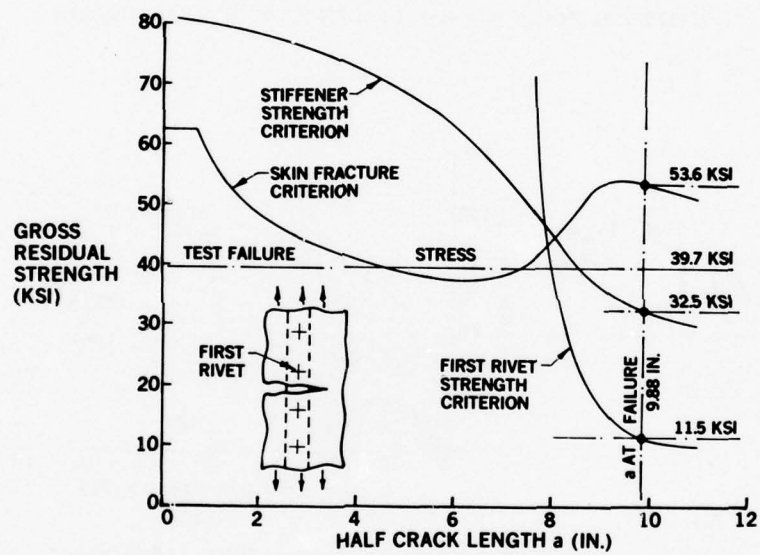


FIGURE 32. RESIDUAL STRENGTH AND THRESHOLD OF SLOW CRACK GROWTH



(a) TEST PANEL RESULTS



(b) RESIDUAL STRENGTH DIAGRAM

FIGURE 33. FIRST RIVET FAILURE PHENOMENON BASED ON ELASTIC ANALYSIS

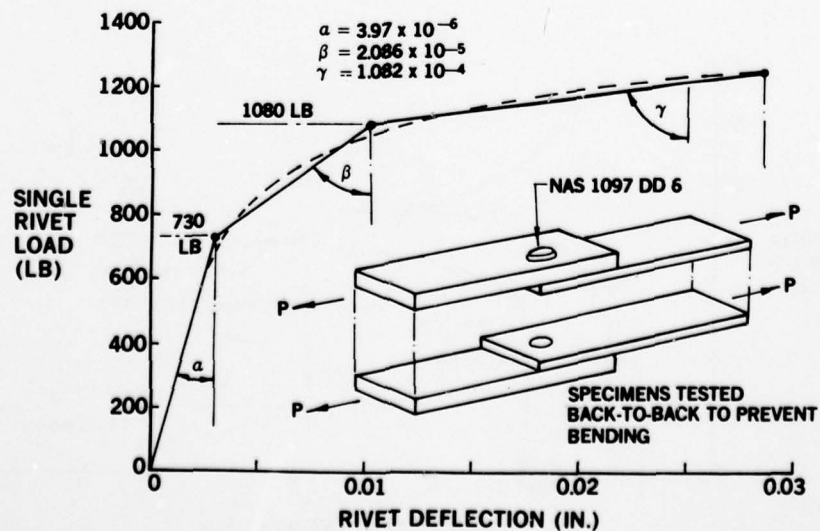
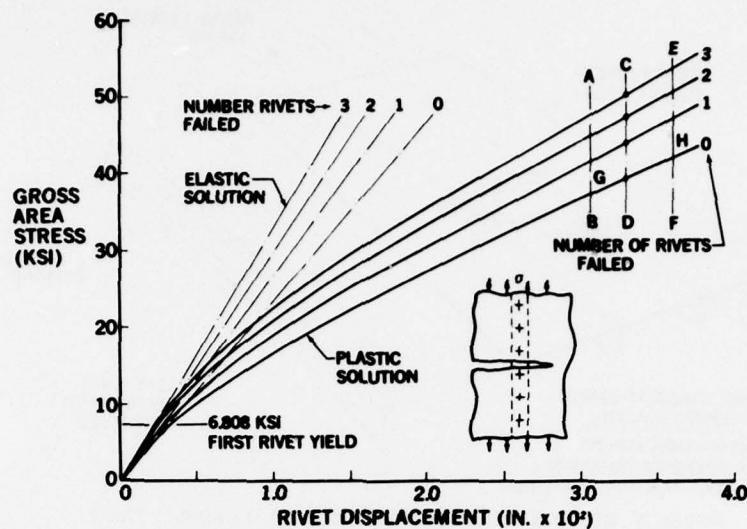
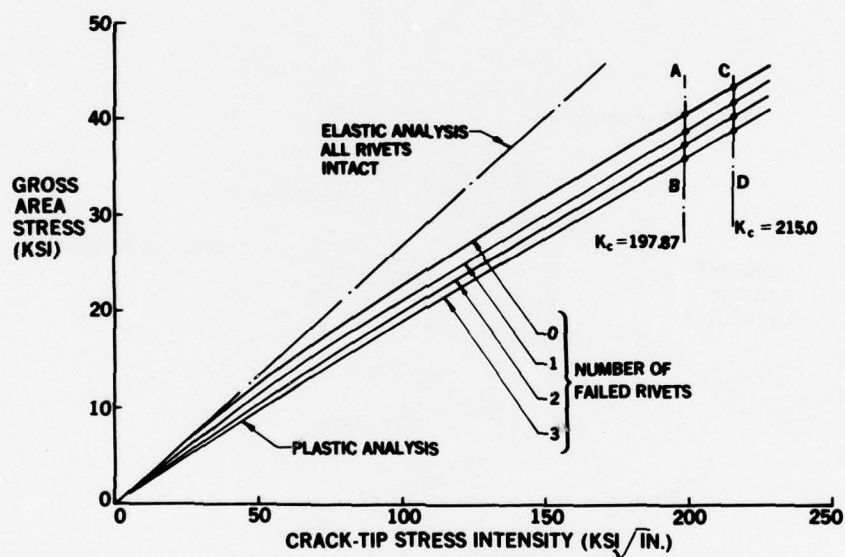
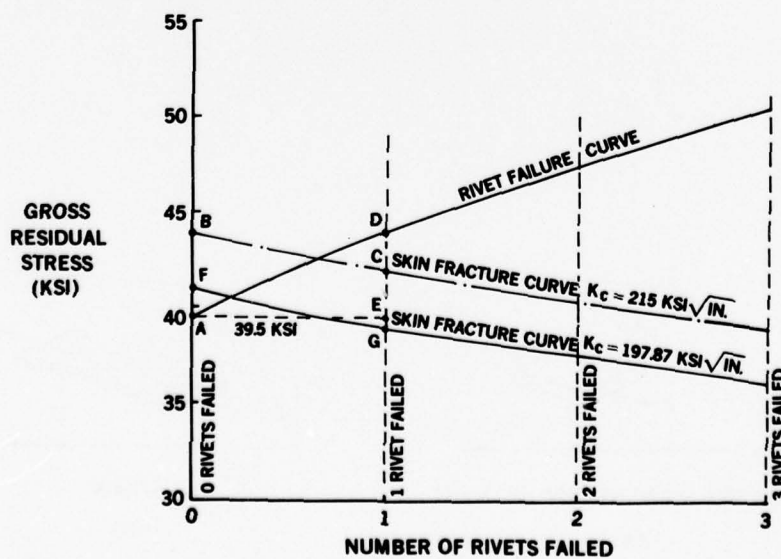


FIGURE 34. SIMULATED RIVET LOAD DISPLACEMENT CURVE



FIGURE 35. RIVET DISPLACEMENT VERSUS GROSS STRESS ( $a = 9.88$  INCHES)FIGURE 36. CRACK-TIP STRESS INTENSITY VERSUS GROSS STRESS ( $a = 9.88$  INCHES)FIGURE 37. RESIDUAL STRENGTH DIAGRAM ( $a = 9.88$  INCHES)

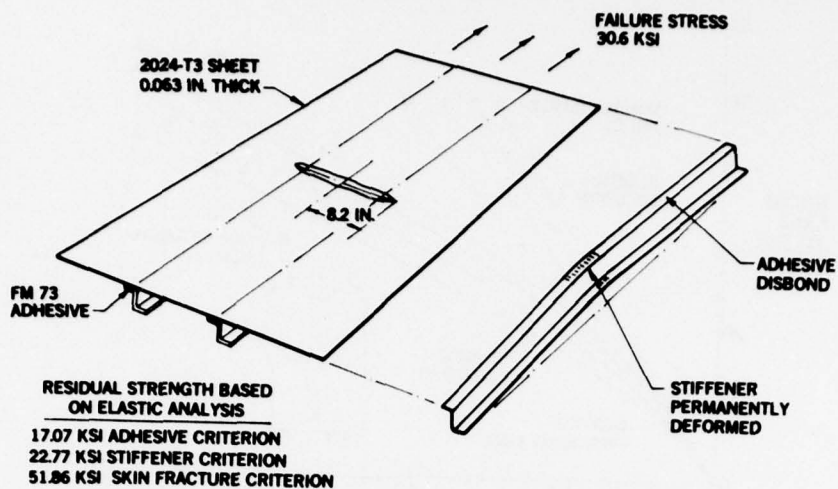


FIGURE 38. RESIDUAL STRENGTH TEST OF ADHESIVELY BONDED PANEL

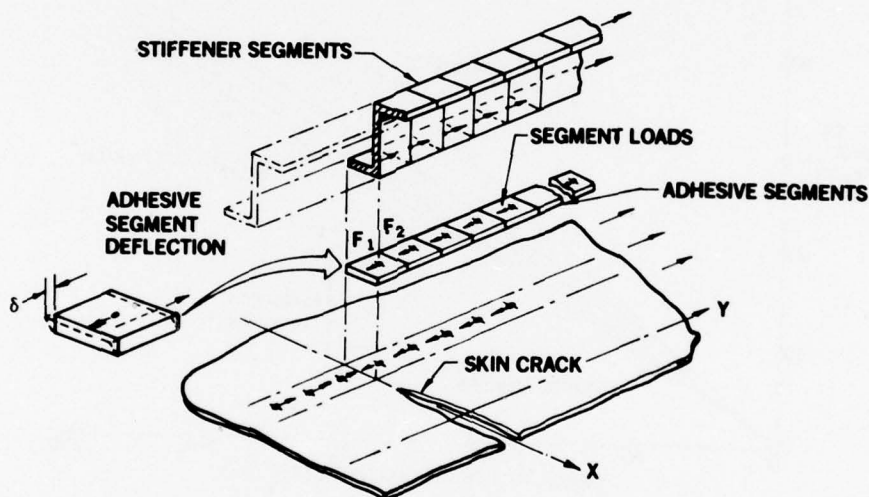


FIGURE 39. DISPLACEMENT COMPATIBILITY MODEL FOR ADHESIVELY BONDED PANEL

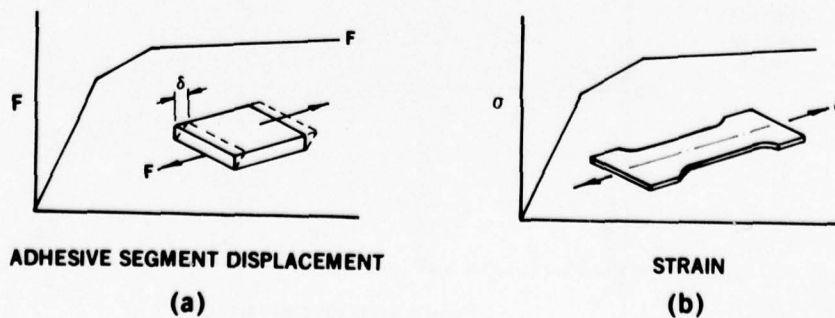


FIGURE 40. ELASTIC-PLASTIC MODELS FOR ADHESIVE AND STIFFENER MATERIALS

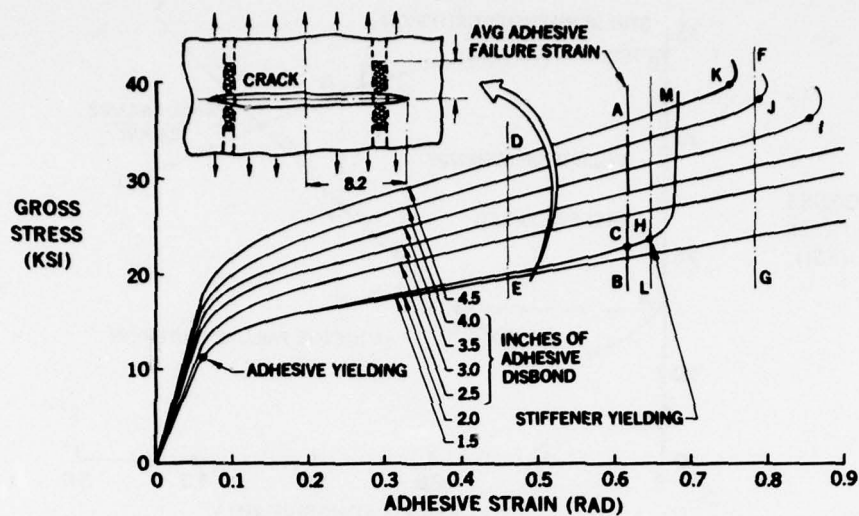


FIGURE 41. ADHESIVE STRAIN VERSUS GROSS STRESS AND AMOUNT OF DISBOND

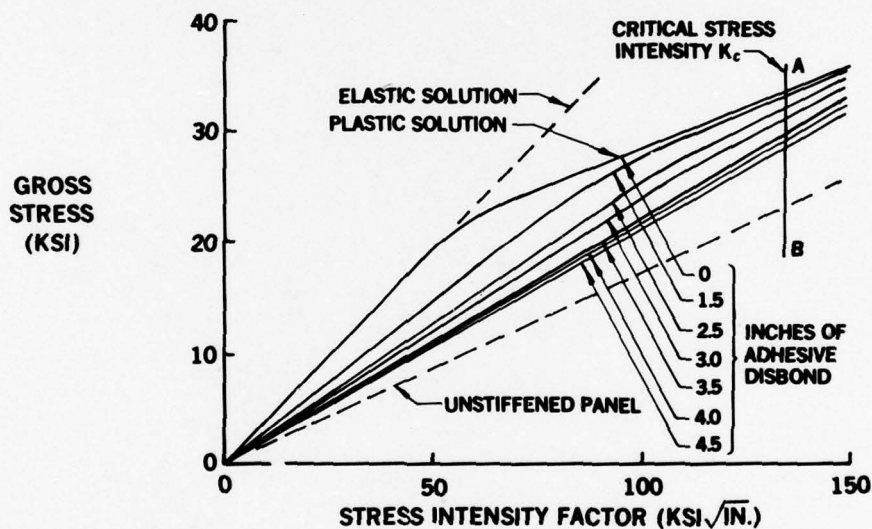


FIGURE 42. STRESS INTENSITY VERSUS GROSS STRESS AND AMOUNT OF DISBOND

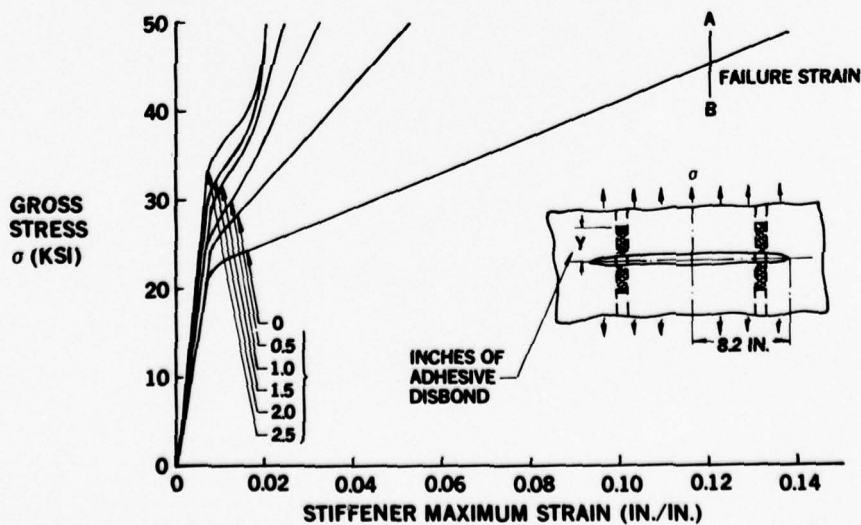


FIGURE 43. STIFFENER MAXIMUM STRAIN VERSUS GROSS STRESS AND AMOUNT OF DISBOND

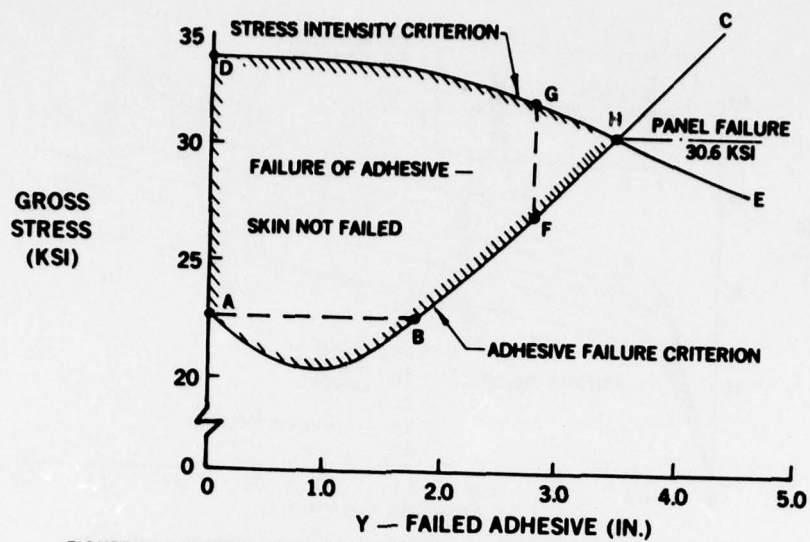


FIGURE 44. RESIDUAL STRENGTH DIAGRAM OF ADHESIVELY BONDED PANEL



## FATIGUE CRACK GROWTH ANALYSIS

David Broek  
 Battelle's Columbus Laboratories  
 505 King Avenue  
 Columbus, Ohio 43201

## 1. INTRODUCTION

Basically, damage tolerance means that (real or assumed) cracks do not grow, within a certain defined period, to a size that would cause loss of the aircraft at a specified load. Damage-tolerance assessment involves analysis of (1) fatigue and environmentally assisted growth of an initial flaw under the anticipated service loading and (2) residual strength characteristics of the cracked structure.

In principle, present-day fracture mechanics and modern stress-analysis techniques permit the prediction of residual strength characteristics of many structures. Techniques for dealing with random or quasi-random service-load histories were recently proposed. The adequacy of these new techniques for crack-growth predictions is the subject of this paper. Since the load spectrum and the stress history are the most important ingredients of a crack growth analysis, the development of an adequate stress history will be discussed extensively.

## 2. RETARDATION MODELS

2.1. Semiempirical Models

A fatigue cycle preceded by a load of higher magnitude produces less crack propagation than it does in the absence of the higher preload. This retardation phenomenon is usually attributed to a combination of compressive residual stresses and crack closure due to residual stresses (e.g., References 1, 2).

At least five models have been proposed<sup>(3-7)</sup> to treat retardation in a quantitative fashion. They have been discussed in detail in the literature.<sup>(2,8,9,10)</sup> None of the models has a solid physical basis, and most are semiempirical, and contain one or more constants to be derived from variable-amplitude crack-growth experiments.

The two best known models are by Wheeler<sup>(3)</sup> and by Willenborg, et al<sup>(4)</sup>, the essentials of which will be briefly presented.

Wheeler introduces a crack-growth reduction factor,  $C_p$ ,

$$\frac{da}{dN} = C_p f(\Delta K) \quad , \quad (1)$$

where  $f(\Delta K)$  is the usual crack-growth function. The retardation factor,  $C_p$ , is given as (see Figure 1):

$$C_p = \left( \frac{r_{pi}}{a_o + r_{po} - a_i} \right)^m = \left( \frac{r_{pi}}{s - a_i} \right)^m \quad , \quad (2)$$

where  $r_{pi}$  = current plastic zone in the  $i$ th cycle under consideration

$a_i$  = current crack size

$r_{po}$  = size of the plastic zone generated by a previous overload

$a_o$  = crack size at which that overload occurred

$m$  = empirical constant (retardation exponent).

At any given crack size,  $a_i$ , only that previous overload is of importance for which  $s = a_o + r_{po}$  (Figure 1) is the largest, i.e., its plastic zone extends beyond the plastic zone of all previous overloads.

The size of the plastic zone is

$$r_{pi} = \frac{K_{max,i}^2}{\alpha \sigma_{ys}^2} = \frac{(\Delta K)_i^2}{(1-R)^2 \alpha \sigma_{ys}^2} ; r_{po} = \frac{K_{max,o}^2}{\alpha \sigma_{ys}^2} \quad (3)$$

where  $K_{max}$  is the maximum stress intensity in a given cycle,  $\alpha = 2\pi$  for plane stress, and  $\alpha = 6\pi$  for plane strain. Since  $a_o \approx a_i$ , it does not make much difference which value is taken for  $\alpha$ , because  $\alpha$  cancels out in Equation (2) if  $a_o = a_i$ .

There is retardation as long as the current plastic zone size is contained within a previously generated plastic zone. If  $r_{pi} > (s - a_i)$ , the reduction factor,  $C_p$ , is equal to one. The retarded crack-growth rate can be determined from the baseline (constant amplitude) crack-growth rate as

$$\left( \frac{da}{dN} \right)_{\text{retarded}} = C_p \left( \frac{da}{dN} \right)_{\text{linear}} \quad , \quad (4)$$

where  $(da/dN)_{\text{linear}}$  follows from constant amplitude data.

The Willenborg model makes use of an effective stress-intensity factor. The maximum stress intensity in the  $i$ th cycle [ $K_{\max,i} = \Delta K_i / (1 - R)$ ], is reduced to  $K_{\max,eff}$  as:

$$K_{\max,eff} = K_{\max,i} - \left\{ K_{\max,o} \sqrt{1 - \frac{a_i - a_o}{r_{po}}} - K_{\max,i} \right\}$$

also,

$$K_{\min,eff} = K_{\min,i} - \left\{ K_{\max,o} \sqrt{1 - \frac{a_i - a_o}{r_{po}}} - K_{\max,i} \right\}, \quad (5)$$

in which the symbols are defined by Figure 1.

Since  $K_{\max}$  and  $K_{\min}$  are reduced by the same amount, the overload does not change  $\Delta K$  but causes only a reduction of the cycle ratio,  $R$ , as long as  $K_{\min,eff} > 0$ . When  $K_{\min,eff} < 0$ , it is set at zero. In that case  $R = 0$  and  $\Delta K = K_{\max,eff}$ .

The two models do not account for (a) the reduction of the retardation effect by negative overloads and (b) the difference in retardation caused by single and multiple overloads. The crack-closure model by Bell and Creager<sup>(7)</sup> attempts to overcome these shortcomings. It is based on a crack-rate equation using an effective stress intensity, which is the difference between the applied stress intensity and the stress intensity for crack closure. The latter is determined semiempirically. The final equation contains several empirical constants.

In essence, all retardation models require a cycle-by-cycle integration of crack growth. During the  $i$ -th cycle at crack size  $a_i$ , a stress range  $\Delta\sigma_i$  is applied. The stress intensity is  $\Delta K_i = 8\Delta\sigma_i/\sqrt{\pi a_i}$ . The linear crack-growth rate follows from constant amplitude data as  $(da/dN)_{linear}$ . Application of one of the retardation models gives the retarded crack-growth rate  $(da/dN)_{retarded}$ . This means that the crack extends to

$$a_{i+1} = a_i + \Delta a = a_i + 1 \times \left( \frac{da}{dN} \right)_{retarded} \quad (6)$$

Then,  $\Delta K_{i+1} = 8\Delta\sigma_{i+1}/\sqrt{\pi a_{i+1}}$  so that the process can be repeated for the next cycle.

Several computer routines for the integration of crack growth have been developed. The use of a particular routine is largely a matter of personal choice, available facilities, and computational efficiency. When properly programmed, the success of a computer routine depends primarily upon the retardation models and very little on the integration scheme.

## 2.2. Comparison of Models

Reference 11 presents calculated crack-growth curves for a flight-by-flight fighter spectrum and a comparison with experiments on central cracks, using a linear integration (no retardation), the Wheeler model with various values of  $m$ , the Willenborg model, and the closure model. Most cases were done twice - once with average crack-growth data and once with upper bound data (upper boundary of scatter band). Examples of the results are presented in Figure 2 for a 7075-T73 aluminum alloy. Depending upon the model, the baseline crack-growth data and the empirical constants used in the retardation model, practically any answer can be arrived at. A linear computation can be just as far off as a Wheeler or Willenborg calculation.

It was checked<sup>(11)</sup> whether disregard of the effect of negative loads by the Willenborg and Wheeler models was of any consequence. Therefore, these models and the closure model were examined for cases with and without GAG (ground-air-ground) cycles. The Wheeler and Willenborg models predict the same result for both cases, however, in the cases considered there were few negative loads in the spectrum and the closure model also gave predictions which were so close that the difference did not show in a plot.

Some models contain adjustable constants, the value of which can be varied by trial and error until the predictions cover the test results. Once the computation is adjusted on the basis of a number of spectrum crack-growth experiments, reasonable predictions can be made for other cases. The Wheeler model and the closure model are preferable because they can be adjusted independent of baseline crack-growth data. The Willenborg model can be adjusted only by selecting another set of crack-growth data. Since the baseline crack-growth data comprise the only undisputable input to the predictions, the use of arbitrary data introduces an unnecessary artificiality. Of the two adjustable models, the Wheeler model is more attractive because of its simplicity. Therefore, the Wheeler model was selected as the vehicle for further comparisons, in Reference 11, as discussed below.

The ratio of predicted and experimental crack-growth life is plotted as a function of the retardation exponent in Figure 3 for spectrum tests on Ti-6Al-4V. This figure shows that  $m = 1.6$  gives the best fit for Ti-6Al-4V subjected to a fighter spectrum. A value of  $m = 1.4$  was found for 7075-T73. Obviously, this cannot be generalized to other types of spectra (e.g., gust) and other materials; but for such cases,  $m$ -values can be determined in the same way. Since the data were for four different crack-growth intervals, they indicate that the relative accuracy is independent of the interval.

When all Wheeler predictions made in Reference 11 are considered for both the aluminum and the titanium alloy at the best values of  $m$ , the distribution shown in Figure 4 is obtained. The mean value is practically equal to 1, the standard deviation is 0.13. These values should be kept in mind when judging the computed curves, presented later, which are all based on  $m = 1.4$  for 7075-T73 and  $m = 1.6$  for Ti-6Al-4V. Retardation factors are determined only by the largest previous plastic zone size. In other words, if the highest load levels occur often enough, crack growth will be nearly independent of the load sequence. This was shown experimentally by several investigators. For example, Schijve<sup>(12)</sup> showed that random loading gives

essentially the same result as a low-high-low order of loads within a flight. Only large-block program loading gives results with no bearing to service loading.

Figure 5 shows the sensitivity of computational results to block size. This case is the same as the one shown in Figure 2. The curve labeled "ordered mix" is the original curve using the exact test sequence. In order to obtain the 100 flight low-high-low block, all load cycles for 100 flights combined into one large 100 flight low-high-low block. The random mix was obtained simply by shuffling the deck of punched cards with the load information.

Obviously, use of the 100-flight block would still be permissible for the computations. The total crack-growth life is only 5 percent less than for the original ordered mix; this percentage is within the general accuracy of the predictions. Crack growth in 100 flights was about 5 to 10 percent of the instantaneous crack size throughout the larger part of the crack growth curve. If it is possible to obtain useful test results with block sizes that cause crack increments of the order of 5 percent, then similar step sizes can be used in the computations. It also means that the frequency of occurrence of the highest load levels should be such that they appear in each block of this size, or during every 5 percent increment in crack size. The advantage of the incremental crack-growth procedure is that it combines all cycles of equal magnitude within the block. Since the crack size is assumed constant over the increment, the stress intensity will not change. Hence, each cycle will cause the same amount of growth. This means that all  $n$  cycles of equal magnitude can be treated as one cycle to give:

$$\Delta a = n \frac{da}{dN} \quad (7)$$

There exist other possibilities for more efficient integration schemes. However, their use is largely determined by the type of stress history that has to be integrated. For example, for a flight-by-flight load history it is possible to then determine the crack extension per flight as

$$\frac{da}{dF} = \sum_{i=1}^n \left( \frac{da}{dN} \right)_i \quad (8)$$

if there are  $n$  cycles in the flight. This is done for a number of crack sizes and for all the different flight types (e.g., missions) in the sequences. Then a diagram is constructed of  $da/dF$  versus  $a$  for each flight type, which can be integrated on a flight-by-flight basis or on a crack-increment basis.

The simplicity of the Wheeler model, relative accuracy, and permissible block size open possibilities for simplified computations. For example, a semilinear analysis, presented in Reference 11, performs a linear integration over 100-flight blocks, using Equation (7) and applies a retardation factor to the resulting crack growth curve from a comparison with an adjusted Wheeler calculation. This semilinear analysis can be easily performed on a programmable pocket calculator. A large series of these semilinear calculations for flight-by-flight stress histories of various types on both 7075-T73 and Ti-6Al-4V. The results are compared in Figure 6 with the actual Wheeler calculations for the same cases. As in the foregoing, four different crack increments were considered. In most cases, the Wheeler result was almost exactly reproduced for any of the  $m$ -values used.

Further comparisons<sup>(13)</sup> of predicted and actual crack growth are presented in Figures 7 and 8. It appears that the accuracy depends strongly upon the spectrum, but in general reasonable predictions are obtained with an adjusted retardation model, more so than with linear integration (curves labeled "Forman" in Figures 7 and 8). Although the linear integration is generally conservative because of the neglect of retardation, the degree of conservatism can vary and is generally unknown.

### 3. STRESS HISTORIES

#### 3.1. Exceedance Spectra

In order to predict the crack-growth behavior of an aircraft structure, the designer needs to know the stress history. For a new design the stress history can only be estimated on the basis of measurements made on existing aircraft systems. As pointed out in the previous sections, the stress history, or more specifically the sequence of low and high stresses is of great influence on the predicted crack-growth life. Not only the magnitude of the stresses is of significance, also the sequence in which they occur is of importance. Measurements made on existing airplanes do give fairly accurate information as to the aircraft loads, but the information on the sequence of loads is only rudimentary. Nevertheless, assumptions have to be made regarding the stress history in order to enable crack-growth predictions. This section gives a discussion of the problems involved.

The load information for an aircraft structure is usually in the form of an exceedance spectrum. Typical exceedance spectra are given in Figure 9 for a transport wing, bomber wing, and fighter wing. The ordinate can either be accelerations or stresses (in some cases gust velocities). The abscissa represents the number of times a level on the vertical axis is exceeded. That is, in Figure 10(a) level A is exceeded  $n_1$  times; level B is exceeded  $n_2$  times. This means that there will be  $n_1 - n_2$  events of a load between levels A and B. These loads will be lower than B, but higher than A. The exact magnitude of any one of the  $n_1 - n_2$  loads remains undetermined.

Basically, there are an infinite number of load levels between A and B. However, there are only  $n_1 - n_2$  occurrences, which means that the number of load levels to be encountered is finite; not every arbitrary load level will be experienced. As a consequence, the spectrum must be approximated by a finite number of levels (as in Figure 10). The larger the number of levels the better the spectrum is approximated. The smaller the number of levels the easier the crack growth analysis. Results of computations and test<sup>(11)</sup> shown in Figure 11 show different approximations of the same spectrum. The curve labeled "Basic spectrum" is for 212 levels, the curve labeled "coarse" is for 8 positive levels, whereas the curves in between are for 12 positive levels (+ 5 negative). The results show that a number of 10 to 12 levels is adequate.



Selection of the lowest level is of importance, because it determines the total number of cycles in the crack-growth analysis. Within reasonable limits this lower truncation level has only a minor effect on the outcome of the crack-growth life. Therefore that this level should be selected on the basis of exceedances rather than on stresses. A number of  $10^5 - 5 \times 10^6$  exceedings per 1000 flights seems reasonable. The selection of the highest load level (clipping level) will be discussed later.

### 3.2. Conversion to Stresses

The load spectrum has to be converted into stress. Usually the following steps are involved:

- Missions are defined and broken up in different mission segments which are characterized by altitude, airspeed, and aircraft weight.
- Load factor data are obtained for the various mission profiles.
- The load factor exceedance data are converted into external load exceedance data. In principle this requires a systems analysis, accounting for speed, altitude weight, and aircraft configuration in the various mission segments.
- A conversion into internal load and stress exceedance data can then be made. Formally, this would require a detailed internal load and stress analysis for a given aircraft configuration in a certain mission segment.
- The stress exceedance data for a mission are then approximated by a number of discrete levels. The number of occurrences of each level is determined and the individual stress cycles are put in a random or idealized sequence for each mission and flight.

Numerous variations and refinements of this process exist. The most common variation is that the external load exceedance diagram for each mission is described by discrete levels. These discrete external load levels are then converted into internal loads and stresses. Of course, each external load level will result in a different stress for each different mission. As a consequence, if there are ten different missions and the load spectrum of each mission is discretized by ten levels, the final stress history consists of 100 different stress levels. Further refinement is sometimes obtained by discretizing the load exceedance data for each mission segment. If there are seven mission segments in each mission, the final stress history consists of 700 different stress levels.

Another variation involves a pairing of maximum and minimum stresses on a random basis such that the stress ranges are of the right size and a fairly representative random sequence is obtained. However, to some extent it defeats the use of mission segments, which imply a deterministic aspect of load sequence within a mission. It may even defeat the deterministic aspect of the individual flights and landings.

The complexity of the procedure and of the stress history and the use of refined computer programs suggest a high level of sophistication and accuracy. It is advisable however, to keep in mind the following approximations and limitations:

- (a) The primary input data, i.e., load factor data for missions and mission segments are a projection, only, and are approximate.
- (b) The conversion of load factor data into loads is also approximate, to varying degrees. For gust loads, load analysis is based on some idealization of the gust; in the simplest case this could be a single-degree-of-freedom response to a  $(1-\cos)$  gust with some gust alleviation factor. For maneuvers, a particular maneuver is assumed and the aircraft equilibrium forces are then determined for that assumed maneuver. In addition, load factors are often determined for symmetric gusts and symmetric maneuvers only, which is another approximation.
- (c) The mix of flights and missions, the random sequence, and the random pairing of positive and negative loads is only an apparent randomness. It becomes deterministic when the sequence is used in a test or computation. The actual aircraft will, of course, never experience this "representative" sequence but may experience something similar.
- (d) Even the loads associated with the deterministic events (e.g., landing and taxiing) in a flight-by-flight history are often only roughly approximated, both in sequence and magnitude.
- (e) The particular distribution of missions is only a basis for design. In all likelihood only very few aircraft will be subjected to the same mission mix. Besides different pilots will fly the same mission in a different manner.

### 3.3. The Requirements for the Stress History

From the foregoing, the question arises how elaborate a stress history for crack-growth analysis should be. To some extent this depends upon the purpose of the crack growth analysis, which can be threefold:

- (a) A rapid analysis for preliminary design. Once the general outline of the aircraft is known from aerodynamic and performance requirements, the main airframe has to be roughly dimensioned. It is determined whether a structure of adequate strength and durability can be built within the confinements of the aerodynamic configuration and the weight constraints set by the performance requirements. At this time, it is also necessary to check whether a structure can be built compliant with adequate damage tolerance and whether it can be optimized with regards to damage tolerance. During this design stage trade-off studies are made that must lead to the optimum design with regard to cost, weight, and performance. Different design



concepts and material selections will be evaluated. Configurations may still change in this stage, thus the procedure may have to be repeated several times.

Obviously, many crack growth computations will have to be made in this stage. Thus a rapid crack growth scheme is required. Load spectra are only known approximately on the basis of design-load-factors. No accurate stress analysis is available. As a consequence, there is no justification for a complicated crack growth scheme which can cope with a complex flight-by-flight stress history. Yet the scheme should be general, independent of material, spectrum type and design stress. In addition, it should operate with a minimum of input data. Therefore, the computation should make use of a general but reliable interaction model and of the simplest possible flight-by-flight characterization.

- (b) An accurate analysis to be used in the final design stage where structure and structural details are being finalized and stress analysis is complete and accurate. In this stage the structure must be shown to satisfy the imposed damage tolerance requirements as related to crack growth life and residual strength. The analyses performed during the final design are usually detailed and complex. Therefore, the crack analysis scheme should also be permitted to have the level of complexity necessary for a reliable result. However, the large number of crack growth analyses necessary for a complete aircraft system may preclude the slow and costly use of cycle-by-cycle analyses.
- (c) A parametric analysis procedure to be used for tail number tracking and fleet management. The spectrum and flight-by-flight histories used during design are the standard design cases. Actual usage of the airplanes may be substantially different. When actual usage data become available, the behavior of possible cracks can be evaluated on the basis of actual load experience. The growth of possible cracks can be tracked and on this basis, management decisions can be made as to maintenance and inspection schemes for individual aircraft and the fleet (ensuring a high level of combat readiness), aircraft usage (assigning different usage to certain aircraft to extend life or maintenance intervals), and retirement.

The large number of aircraft, aircraft systems, and critical locations to be tracked preclude the use of an involved crack growth computation scheme. The method must permit easy determination of crack growth for different locations (stresses), aircraft usage (mission mix, spectrum variations, weight, etc.), and aircraft components. This system can be as simple as a set of parametric charts or it may involve an easy and quick computation of a large number of cases.

It is unlikely that the parametric scheme will give absolute answers. Rather, it will provide relative values if certain parameters change. Therefore, it will be necessary to do more involved computations for a few control points. This more involved computation could be the one discussed above.

### 3.4. Derivation of a Simple Stress History

So far, the spectra considered were applicable primarily for airplane wings. Fin and stabilizer experience a combined gust and maneuver spectrum that is usually as complicated as that of the wing. However, for both structures the ground-air-ground cycles are of little significance. The derivation of a stress history for these parts follows the same rules as for the wing. Parts with relatively simple spectra are the flap structure components. These experience one cycle during takeoff, and one cycle during landing. Maneuvering and gust cycles are superposed to them, but they are so small as compared to the primary loading, that they can usually be neglected. Fuselage structures are subjected to torsional and bending loads due to maneuvering and gust loads on the control surfaces, aerodynamic loads, and pressurization cycles. The latter will be the only significant loading for many locations in the fuselage.

The foregoing discussions have shown the complexity of the stress history derivation, but it has become clear also, that in many cases a relatively simple stress history will suffice for crack growth analyses. The following paragraphs present a rationale for the development of such a history. It is assumed that an exceedance diagram for load factors is available. Taking the 1-g stress level and assuming all stress levels at a given location are proportional to g-level, the exceedance diagram can be converted into a stress exceedance diagram by means of a proportionality factor.

Consider the stress exceedance spectrum for 1000 flights shown in Table 1. Instead of selecting stress levels for the stepped approximation, it is much more efficient to build the steps by selecting exceedances. Since a large number of levels is not necessary in this stage, six levels were chosen in the example. The procedure would remain the same if more levels were to be selected.

The exceedings in the example were taken at 10, 100, 1,000, 10,000, 100,000, and 500,000. Verticals are raised at these numbers and the stepped approximation made. This leads to the positive excursion levels,  $S_1 - S_6$  and the negative excursion levels,  $T_1 - T_6$  (Table 1). The stress levels and exceedances are given in columns 1 and 2 of Table 1. Subtraction gives the number of occurrences in column 3.

The highest stress level is likely to occur only once in the severest mission. Therefore, a mission A spectrum is devised as in column 4 in which  $S_1$  occurs once and lower levels occur more frequently in accordance with the shape of the total spectrum. In order to use all 10 occurrences of level  $S_1$ , it is necessary to have 10 missions A in 1000 flights. These 10 missions A will use the numbers of cycles given in column 5. When the 10 missions A are subtracted from the total number of occurrences in column 3, the remaining load containment of the remaining 990 flights is as given in column 6.

The next severest mission is likely to have one cycle of level  $S_2$ . Hence, the mission B spectrum in column 7 can be constructed in the same way as the mission A spectrum. There remain 60 cycles of  $S_2$ .

Hence, mission B will occur 60 times in 1000 flights. The 60 missions B will use the cycles shown in column 8. Therefore, the cycles remaining for the remaining 930 flights are as given in column 9.

Level  $S_3$  will occur once in a mission C, which is constructed in column 10. There remain 570 cycles  $S_3$ , so that there will be 570 missions C. These will use the cycles given in column 11. The remaining cycles are given in column 12.

There will be 10 missions A, 60 missions B, and 570 missions C in 1000 flights. This means that there remain 360 flights. Dividing the remaining cycles in column 12 by 360, a mission D spectrum is found automatically as in column 13. Consequently, all cycles have been accounted for.

A mission mix has to be constructed now. With mission A occurring 10 times per 1000 flights, a 100-mission block could be selected. However, a smaller block would be more efficient. In the example, a 33-mission block can be conceived as shown in Table 1. After 3 repetitions of this block (99 flights) one mission A is applied.

The cycles in each mission are ordered in a low-high-low sequence, which is permissible as was discussed earlier. The negative excursion  $T_1 - T_0$  are accounted for by combining them with the positive excursions of the same frequency of occurrence:  $T_1$  forms a cycle with  $S_1$ ,  $T_2$  with  $S_2$ , etc. In this way the range of a cycle is S-T, instead of S-mean stress, which is conservative.

Once a spectrum of this type is established, design trade-off studies are easy. Selecting different materials or different design stress levels merely means an adjustment of the ordinate of the exceedance diagram. The stress levels  $S_1 - S_8$  and  $T_1 - T_8$  can be determined and the flight-by-flight spectrum is ready (Table 1). Selection of a different design stress level results in a new set  $S_1 - S_8$ . This requires only the exchange of a few cards in the computer program and the calculation can be rerun.

This shows the versatility of the spectrum derivation of Table 1. It is a result of choosing exceedings to arrive at the stepped approximation of the spectrum, which means that the cycle content is always the same. Thus, the stress history once derived does not change. If stress levels had been selected instead for the stepped approximation, a change in spectrum shape or stress levels would always result in different cycle numbers. In that case, the whole procedure to arrive at the spectrum of Table 1 would have to be repeated and many more changes would have to be made to the computer program.

Of course, Table 1 is an example only. The spectrum could be approximated by more levels, more different missions could be designed, but the same procedure could still be used. However, in view of the comparative nature of the calculations in the early design stage, many more levels or missions are not really necessary.

Figure 12 shows an example of a stress history for a fighter spectrum, which was derived in much the same manner as discussed above.

### 3.5. Standard Spectra

In a cooperative effort between Holland and Germany, standard spectra have been developed for fighters<sup>(14)</sup> and civil transports<sup>(15)</sup> to be used in design trade off-studies and testing. These spectra are also adopted by Switzerland and England. A 4000 flights load history was generated for the transport, whereas the fighter spectrum consists of a 200 flights history. The load histories are random, the ways to convert to a stress history are given. Both spectra are more sophisticated than the one derived in Table 1. They are available as card decks and on tapes to anyone, ready for use in calculations or as an input to a testing system.

## 4. CLIPPING AND TRUNCATION

### 4.1. Clipping

Apart from the sequencing problems addressed in the previous sections, there is a sequence problem associated with retardation. It was pointed out that sequencing of deterministic loads (GAG cycles) should be done in accordance with service reality; probabilistic loads can be sequenced randomly, but a low-high-low order per flight is acceptable.

The sequencing effect caused by retardation is largely dependent on the ratio between the highest and lowest loads in the spectrum and their frequency of occurrence. As a result, it will depend upon spectrum shape. Compare, for example, the fighter spectrum with the transport spectrum in Figure 9. The relatively few high loads in the transport spectrum may cause a more significant retardation effect. As a result, their magnitude and the point at which they occur has a large effect on crack growth. In the fighter spectrum, there are so many high loads that their exact magnitude and sequence becomes of less importance.

The selection of the highest loads in the load history is critical to obtain a reliable crack-growth prediction. It is not realistic to include loads that occur less frequently than about 10 times in 1000 flights, because some aircraft in the fleet may never experience these high loads, so that including them retardation would be dangerously unconservative. Therefore, the spectrum is clipped at 10 exceedings per lifetime. No load cycles are omitted. Only those higher than the clipping level are reduced in magnitude to the clipping level. The effect of clipping on retardation and crack-growth life was demonstrated in experiments by Schijve<sup>(12)</sup>

The question remains whether proper selection of a realistic clipping level is as critical for a crack-growth prediction as it is for an experiment. In this respect, it is important to know which retardation model is the most sensitive to clipping level, which may also depend upon spectrum shape. This was checked by running crack-growth calculations for different clipping levels, different spectrum shapes, and two retardation models<sup>(10,11)</sup>.



Calculations were made for the four significantly different spectra, using the flight-by-flight history developed in Table 1. The cycles in each flight were ordered in a low-high-low sequence. Crack-growth curves were calculated using the clipping levels  $S_2$ ,  $S_3$ ,  $S_4$ , and  $S_5$  in Table 1. The results for all spectra are compiled in Figure 13. Test data for gust spectrum clipping<sup>(12)</sup> are also shown.

The figures allow the following observations:

- The two models give largely different crack-growth lives for all spectra, except C. The differences are not systematic and since there are no test data for comparison, the correct answers are not known. However, by changing the retardation exponent, the Wheeler calculations could be adjusted to give the correct answer.
- With one exception the two models essentially predict the same trend with respect to clipping levels. This shows that they both have equal capability to treat retardation, but the Wheeler model may have greater versatility for different spectrum shapes provided the retardation exponent is adjusted.
- The steep fighter and bomber spectra are less sensitive to clipping level, since the damage of the many high cycles outweighs their retardation effect.
- At low clipping levels the analysis attains more the character of a linear analysis.
- Bringing the clipping level down from 10 exceedances (top data points) to 100 exceedances (second row of data points) reduces the life by about 10 percent or less for all spectra.

#### 4.2. Truncation

Truncation of the lower load levels is important for the efficiency of crack-growth calculations. Truncation is the cut off of the lower level of the stepped spectrum approximation at a given number of cycles. The smaller this number, the fewer cycles will be included in the computations. This number is sometimes taken very small. The argument is that low stress excursions do not contribute much to crack growth, especially in view of the retardation effect.

Schijve<sup>(12)</sup> presents experimental data regarding the effect of truncation. Although these data are somewhat misleading, because truncation was not carried out properly - the lowest load levels of a complete stress history were simply omitted, without a correction of the stress history - they indicate that truncation is not very critical. Therefore, truncation levels are generally taken at approximately  $10^5$  exceedances per 1000 flights.

### 5. PREDICTIONS FOR PRACTICAL CASES

#### 5.1. Spectrum Variations

In the early design stage there may still be uncertainty about the exact shape of the spectrum. Thus design studies may have to be made to evaluate the effects of slight changes in the spectrum. Using the stress history approximation procedure discussed in section 3.4, permits such a study through a simple adjustment of the stress levels, so that the steps fit the new spectrum shape (note that some levels will change more than others, but cycle numbers and history remain the same). The question is whether crack-growth analysis will show the proper trends.

The effect of slight changes in spectrum shape was studied for a fighter spectrum<sup>(11)</sup> using similar but somewhat more refined procedures as in section 3.4. The Wheeler retardation model was used, which was first properly adjusted as shown in Figures 3 and 4. The results are shown in Figures 14 and 15 for 7075-T73, where they are compared with test data. Similar trends were observed for Ti-6Al-4V. Although the differences in spectrum shape are small, they cause drastic differences in crack growth. Yet the computed curves show very good agreement with the experiment, indicating that crack-growth analysis will produce the proper trends. Obviously, this cannot be generalized for all types of spectra, e.g., analysis of a gust spectrum would require a readjustment of the Wheeler model.

Another spectrum variation is caused by a change in design stress level. In the design stage, a trade-off study may be made to assess the effect of changing the design allowables, which would represent such a case. Another example is that different points in a wing will be subjected to different stresses. Again, using the simple tool presented in section 3.4, the assessment can easily be made (note that all stress levels will now be affected by the same factor, but the history and cycle numbers remain the same). Results for this case<sup>(11)</sup> are shown in Figure 16. Once more, it can be concluded that the right trends are predicted.

#### 5.2. Structural Variations

Accurate prediction of crack growth in center-cracked panels does not automatically ensure reliable predictions of crack growth in complex structural geometries. Proof is required that the computational schemes can be generalized.

The most common case of a structural crack is a crack at a hole. Two experiments were performed<sup>(11)</sup> on 7075-T73 specimens 0.5-inch thick. One specimen contained two holes of 0.2-inch diameter, each hole having a through-the-thickness crack at one side. The second specimen contained two holes of 0.5-inch diameter, each with a single corner crack. Test data and computed crack-growth curves are shown in Figure 17. The curves result from semilinear analysis with the Bowie solution for a crack at a hole.

Admittedly, the evidence is only meager, but it seems that reasonable predictions can be made, provided the proper stress intensity factor and properly adjusted crack integration scheme is used.

## 6. RELIABILITY OF PREDICTIONS

The reliability of predictions depends on four factors:

- (1) Integration models and computational schemes
- (2) Material behavior
- (3) Stress-intensity factors
- (4) Spectrum generation.

Using a well-adjusted crack-growth model, experimental data can be predicted within about 30 percent<sup>(11)</sup>, regardless of material and spectrum. This holds if changes are made to the spectrum, even if these changes cause largely different crack growth behavior. Obviously, the use of a different type of spectrum requires empirical readjustment of the retardation model.

Clearly, the discrepancies reflect both the inaccuracies of the computation model as well as the variations in material behavior. The discrepancy between a certain prediction and the test data need not always be due to a wrong prediction. It can also be a result of erratic material behavior in the test. However, the test data are always considered unique when the accuracy of computed curves is examined. Thus, the variations in material behavior are included in the percent of deviation.

Modern stress analyses with either analytical or finite-element techniques provide accurate stress-intensity factors, and it seems safe to assume that the calculated stress intensity for a crack in complex geometry will be within 10 percent. Assuming an average fourth-power dependence on  $K$ , the inaccuracies in the stress-intensity factor may cause deviations of about 50 percent in the computed crack-growth curves. These deviations are larger than those associated with the crack growth computation and material variability.

Establishing a spectrum for a new airplane is a difficult task, involving much guesswork. Yet the spectrum shape is of paramount importance; a slight deviation in spectrum shape can easily cause a difference of a factor of 2 in crack-growth life, as can be seen in Figures 14 and 15. The conversion of the load spectrum into a stress spectrum is also critical. An inaccuracy in the estimated stress level at a given location can easily yield a difference of 50 percent in crack-growth life, as shown in Figure 16.

Thus, crack-growth predictions in the design stage could be a factor of 1.5 - 2 in error, due to inaccuracies in the stress spectrum. This proves the significance of in-flight measurement of the stress spectrum. All crack-growth calculations can be repeated with the actual flight spectrum and do not require additional tests. Hence, crack-growth information can be updated reliably both during test flying and later when service load information becomes available.

Only minor significance should be attached to the stress history (sequence) within one spectrum, as long as loading is of the flight-by-flight type. It was also shown that a spectrum can be represented with about 10 positive stress levels. Block sizes of 100 flights seem to be adequate.

In conclusion, it can be stated that crack-growth predictions are feasible. In particular, the computed crack growth behavior shows the right trend for the effects of spectrum variation, design stress level, and structural geometry. This is a very important achievement because it permits the conduction of trade-off studies. Although the absolute crack growth lives found from computations may not be reliable, the effects of changes in stress level and structural details can be evaluated in a relative sense by simple means, so that optimization becomes possible.

Obviously, extreme caution should be exercised when using the predictions in an absolute sense, because the actual number can be grossly in error. However, once again it is stressed that a substantial part of the error is not due to the crack growth analyses per se, but a result of inaccuracies in spectrum evaluation, stress analyses and of anomalous material behavior. Therefore, safety factors should be applied, if the predictions are to be used in an absolute sense (safety factor application is discussed in the last lecture). Moreover, extensive component testing and the full scale test should be employed to check the adequacy of the analytical predictions. Such testing is still indispensable in proving that the structure has adequate damage tolerance.

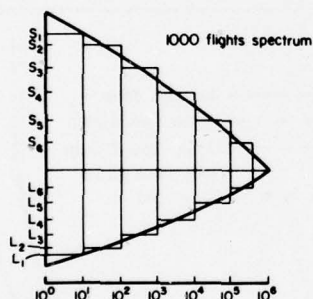
## 7. REFERENCES

1. Schütz, W., Lecture III of this Series.
2. Broek, D., Elementary Engineering Fracture Mechanics, Noordhoff, Leyden Holland (1974)
3. Wheeler, O. E., "Spectrum Loading and Crack Growth", J. of Basic Engineering, 94 D (1972) p 181.
4. Willenborg, J. D., et al, "A Crack Growth Retardation Model Using an Effective Stress Concept, AFFDL-TM-71-1 FBR (1971).
5. Habibie, B. J., "Fatigue Crack Growth Prediction" (In German), Messerschmidt-Bolkow-Blohm, Report No. Uh-03-71 (1971).
6. Hanel, J. J., "Crack Growth Prediction Under Variable Amplitude Loading on the Basis of a Dugdale Model" (In German), German Society for Materials Testing (1973).
7. Bell, P. D., and Creager, M., "Crack Growth Analysis for Arbitrary Spectrum Loading", AFFDL-TR-74-129, (1975).
8. Various Authors, "Fracture Mechanics of Aircraft Structures", AGARDograph No. 176 (1974).



9. Gallagher, J. P., "A Generalized Development of Yield Zone Models", AFFDL-TM-FBR 74-28 (1974).
10. Broek, D., and Smith, S. H., "Damage Tolerance Design Guidelines", Forthcoming AFFDL publication.
11. Broek, D., and Smith, S. H., "Spectrum Loading Fatigue Crack Growth Predictions and Safety Factors", NADC Report 76383-30. Abbreviated version to be published in Engineering Fracture Mechanics.
12. Schijve, J., et al, "Crack Propagation in Aluminum Alloy Sheet Materials Under Flight Simulation Loading", AFFDL-TR-69-50 (1970).
13. Schütz, W., "Calculation Methods for Fatigue Life and Crack Propagation", Section 4 of Fatigue Design of Fighters, a forthcoming AGARD publication.
14. VanDijk, G. M., DeJonge, J. B., "Introduction to a Fighter Aircraft Loading Standard for Fatigue Evaluation 'Fallstaff'", NLR MP 75017 (1975).
15. DeJonge, J. B., Schütz, D., Nowak, H., and Schijve, J., "A Standardized Load Sequence for Flight Simulation Testing", NLR TR 73029, or LBF FB-106, or RAE TR 73183 (1973).

TABLE 1. SIMPLE FLIGHT-BY-FLIGHT SPECTRUM FOR EARLY DESIGN ANALYSIS AND TRADE-OFF STUDIES



## MISSION MIX

33 FLIGHTS  
BLOCK

- 6 TIMES MISSION D
- 1 TIME MISSION B
- 19 TIMES MISSION C
- 1 TIME MISSION B
- 6 TIMES MISSION D

REPEAT BLOCK; EVERY THIRD BLOCK  
APPLY 1 TIME MISSION A.

COMBINE:  $S_1$  WITH  $L_1$  TO ONE CYCLE  
 $S_2$  WITH  $L_2$  TO ONE CYCLE  
ETC.

SEQUENCE: LO-HI-LO IN FLIGHT.

			Mission A		Mission B			Mission C			Mission D			
①	②	③	④	⑤	⑥	⑦	⑧	⑨	⑩	⑪	⑫	⑬	⑭	⑮
Level	Exceedings	Occur- rences	Occur- rences	10X	Remainder 3 - 5	Occur- rences	60X	Remainder 6 - 8	Occur- rences	57X	Remainder 9 - 11	Occur- rences	360X	Remainder 12 - 14
S <sub>1</sub>	10	10	1	10	--	--	--	--	--	--	--	--	--	--
S <sub>2</sub>	100	90	3	30	60	1	60	--	--	--	--	--	--	--
S <sub>3</sub>	1,000	900	15	150	750	3	180	570	1	570	--	--	--	--
S <sub>4</sub>	10,000	9,000	48	480	8,520	17	1,020	7,500	10	5,700	1,800	5	1,800	--
S <sub>5</sub>	100,000	90,000	300	3,000	87,000	200	12,000	75,000	100	57,000	18,000	50	18,000	--
S <sub>6</sub>	500,000	400,000	1,900	19,000	381,000	1,500	90,000	291,000	400	228,000	63,000	175	63,000	--

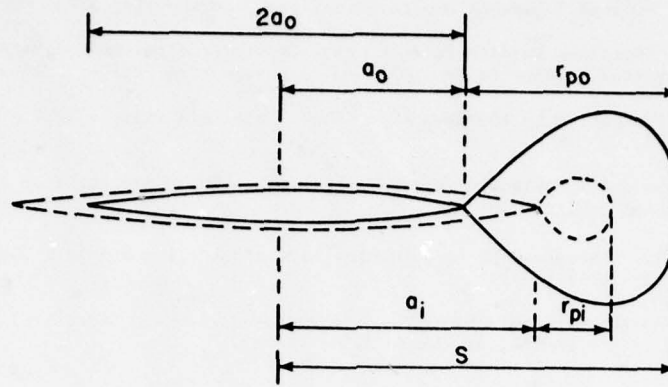


FIGURE 1. YIELD ZONE DUE TO OVERLOAD ( $r_{p0}$ ), CRACK SIZE AT OVERLOAD ( $a_0$ ), CURRENT YIELD ZONE ( $r_{pi}$ ), AND CURRENT CRACK SIZE ( $a_i$ )

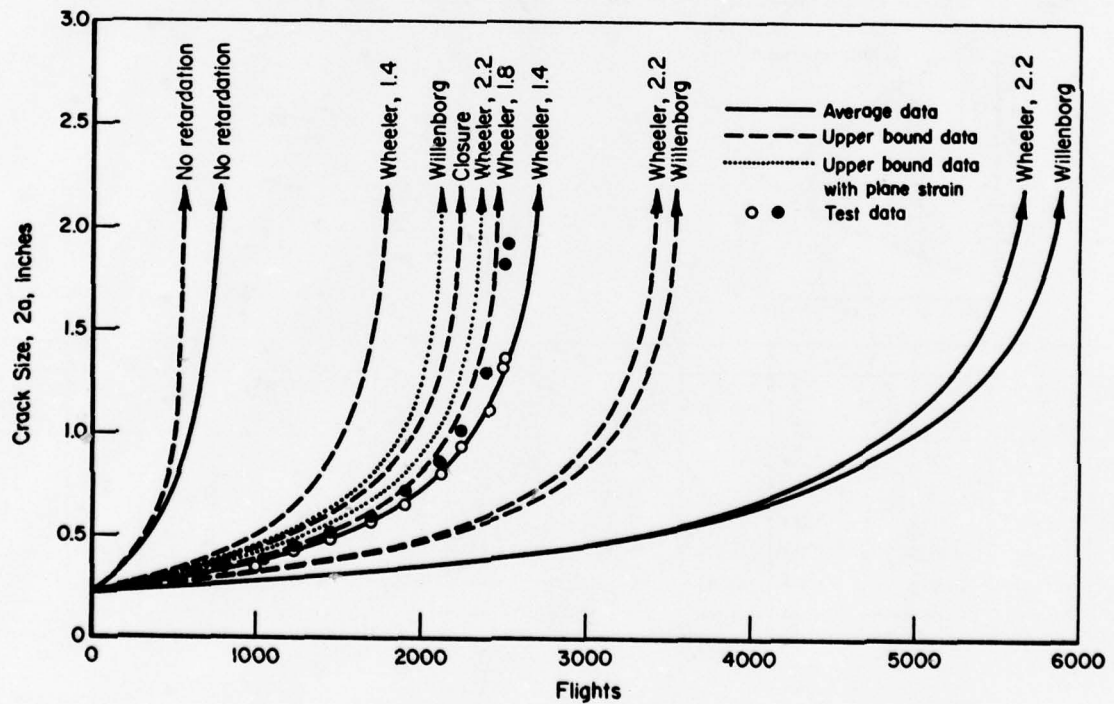


FIGURE 2. VARIOUS PROCEDURES FOR CRACK-GROWTH CALCULATION COMPARED FOR 7075-T73

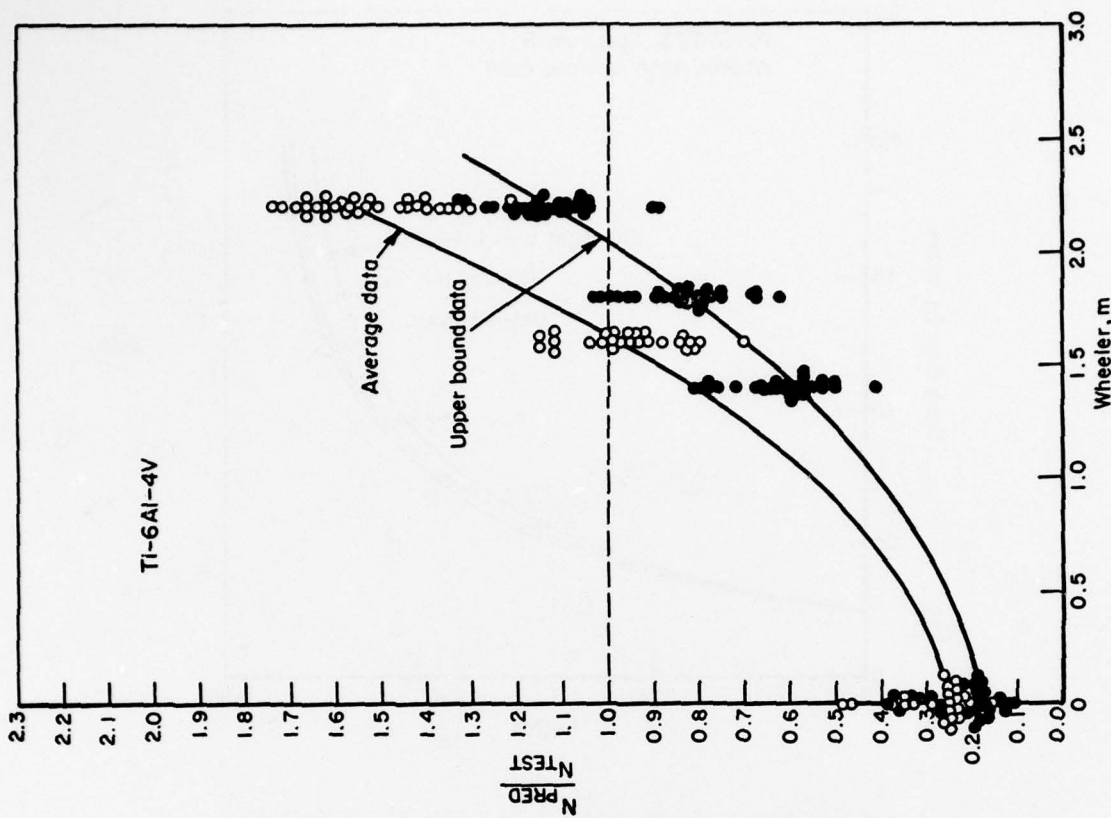


FIGURE 4. EFFECT OF WHEELER EXPONENT ON CRACK-GROWTH LIFE PREDICTIONS

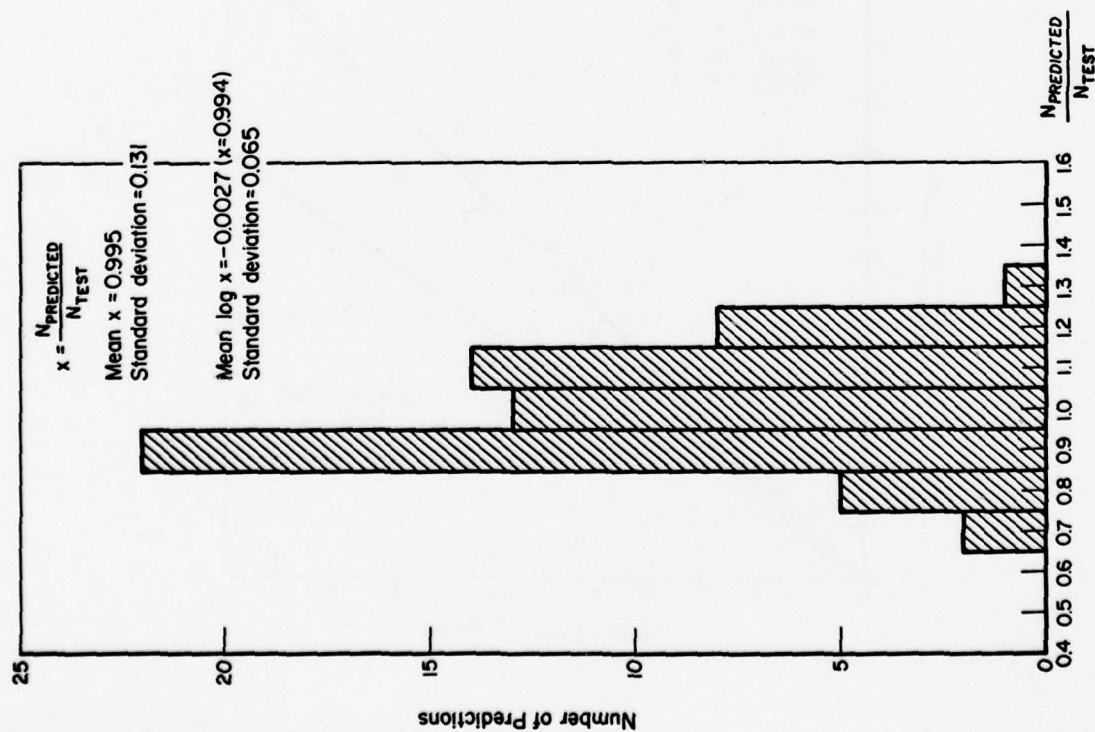


FIGURE 3. HISTOGRAM OF RATES BETWEEN BEST WHEELER PREDICTION AND TEST RESULT FOR BOTH THE TITANIUM AND THE ALUMINUM ALLOY

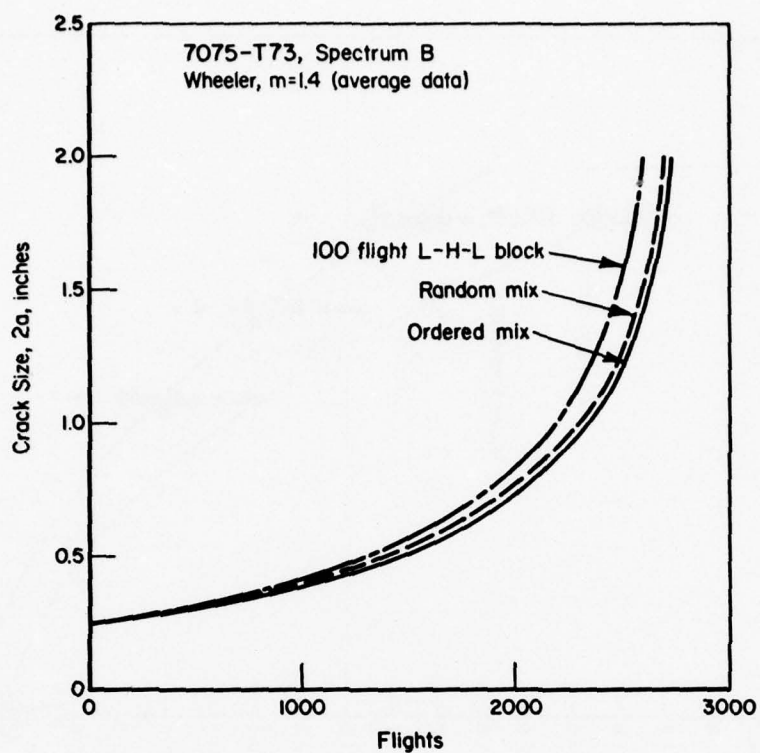


FIGURE 5. EFFECT OF LOAD SEQUENCE ON PREDICTED CRACK GROWTH

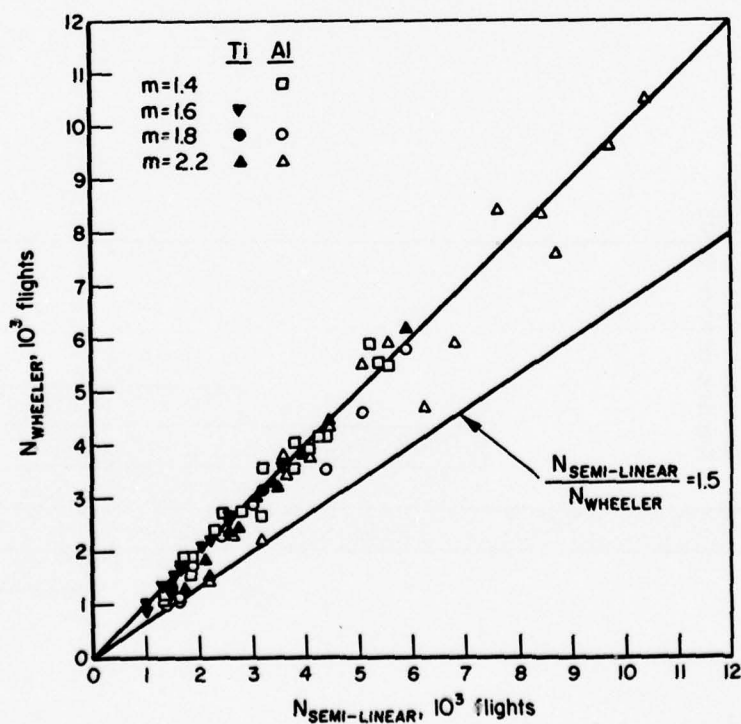


FIGURE 6. COMPARISON OF BEST WHEELER PREDICTIONS WITH APPROXIMATE SEMILINEAR PREDICTIONS



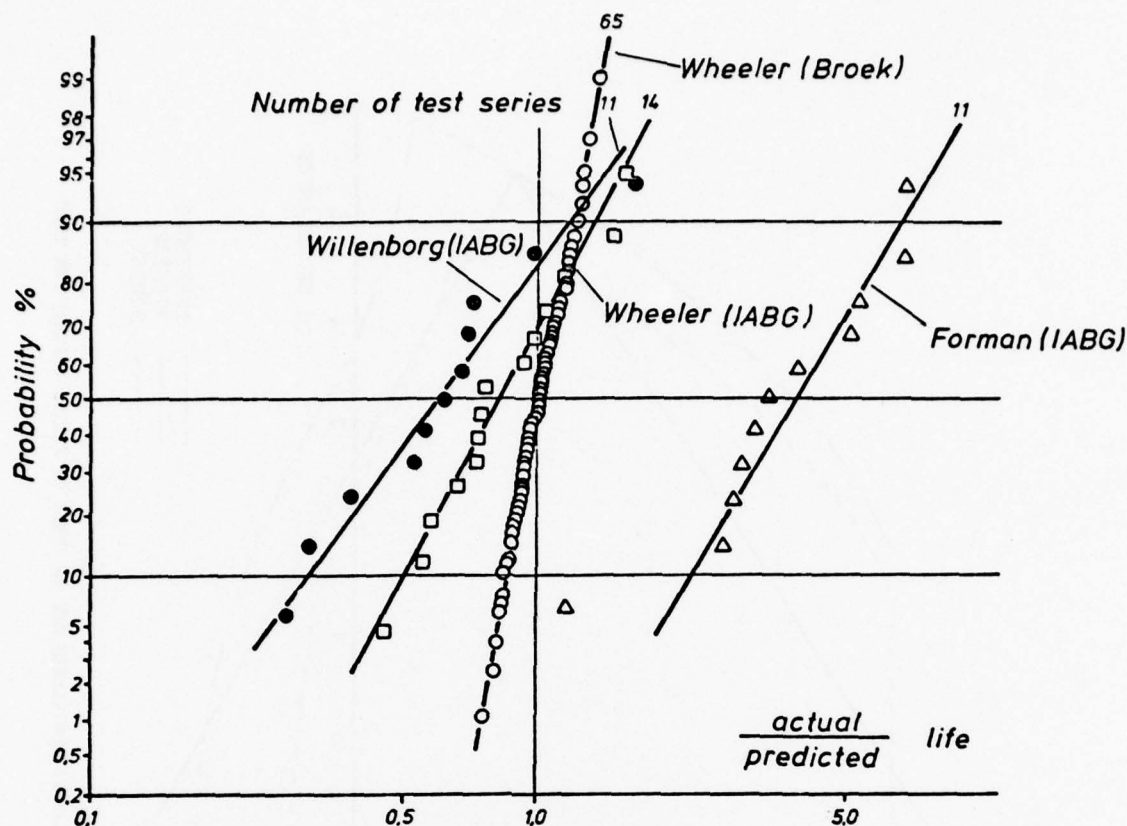


FIGURE 7. COMPARISON OF PREDICTED AND EXPERIMENTAL CRACK GROWTH<sup>(13)</sup> NOTE: WHEELER  $m$  FOR IABG RESULTS WAS TAKEN SAME AS FOR BROEK'S RESULTS

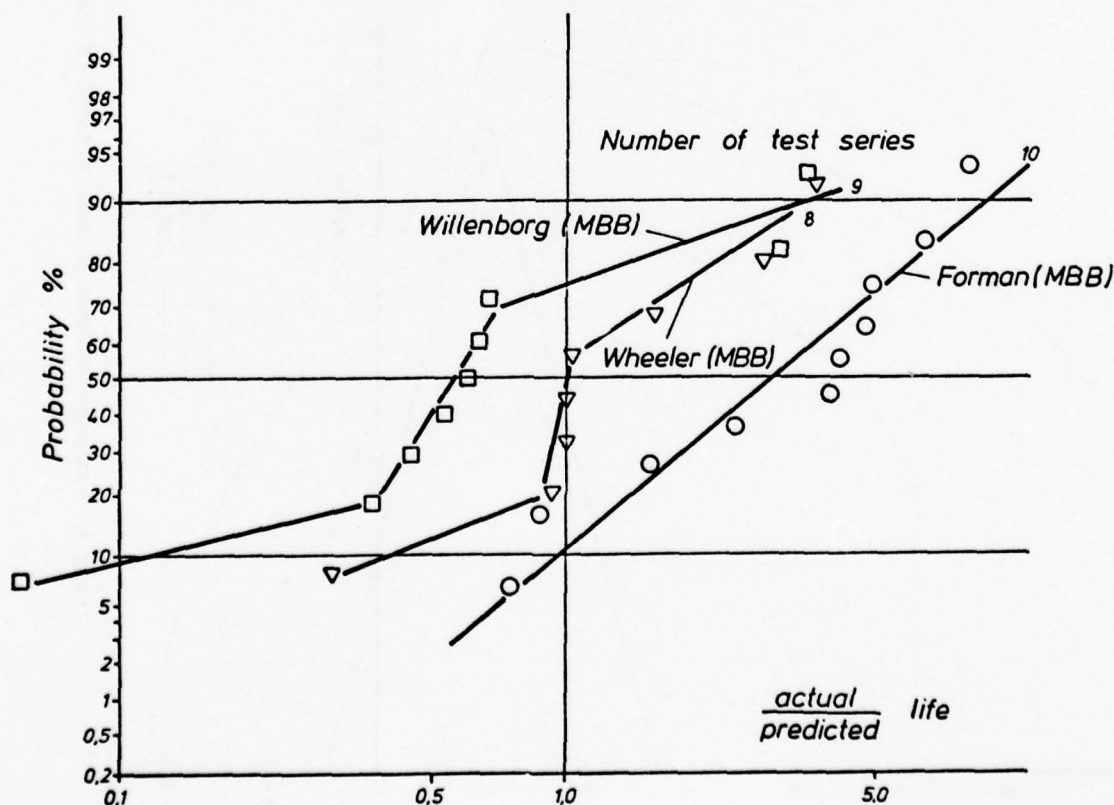


FIGURE 8. COMPARISON OF PREDICTED AND EXPERIMENTAL CRACK GROWTH FOR TACTICAL AIRCRAFT. FITTED  $m$ . NOTE: EXTREME UNCONSERVATIVE RESULTS WERE FOR TESTS WITH MANY COMPRESSIVE STRESSES

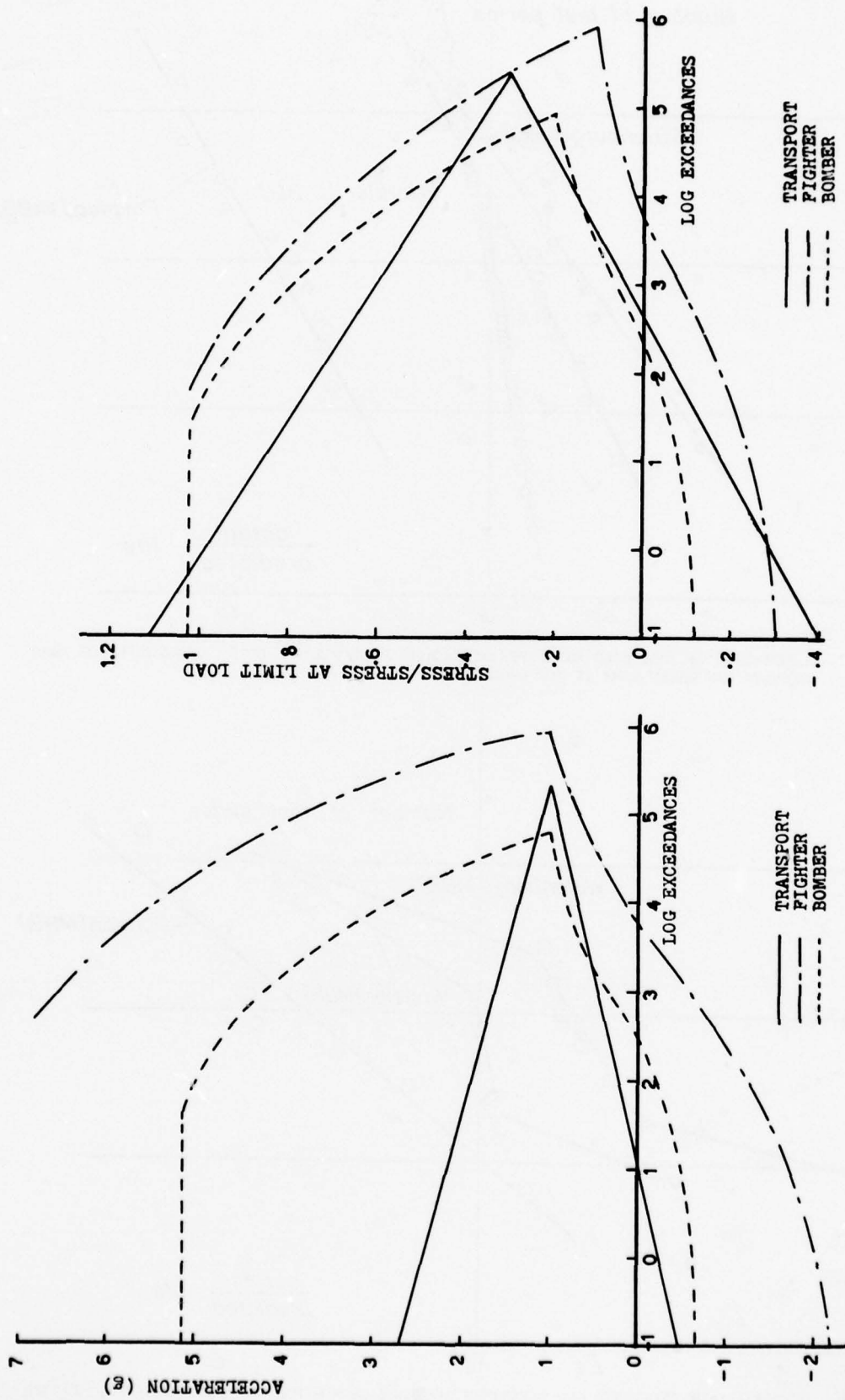
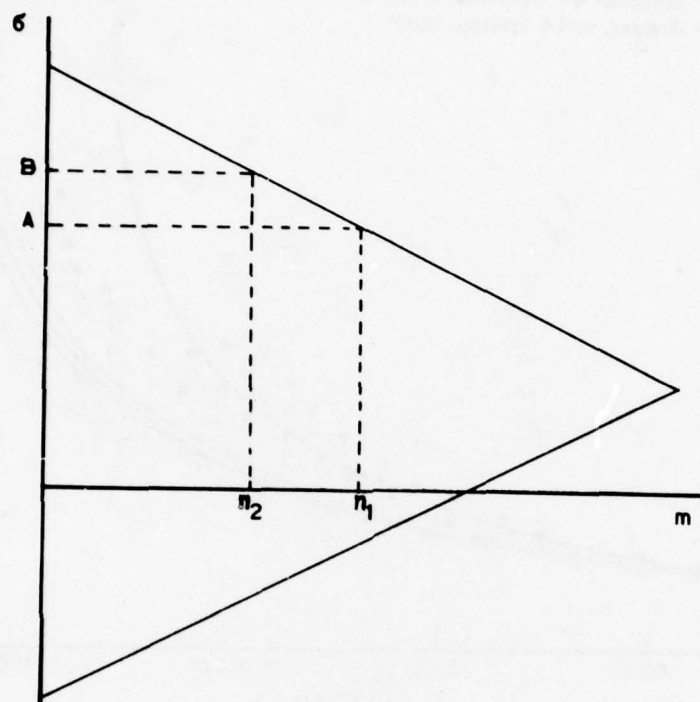
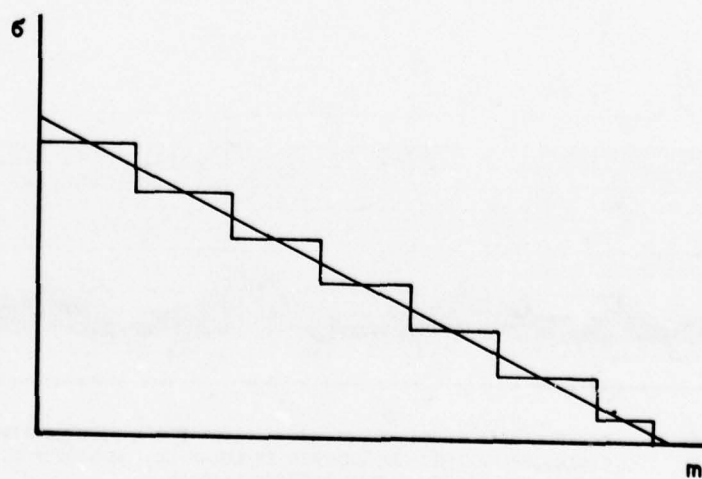


FIGURE 9. EXCEEDANCE SPECTRUM IN TERMS OF CENTER OF GRAVITY ACCELERATION (LEFT) AND IN TERMS OF STRESS (RIGHT) FOR 1000



(a) Occurrences between two load levels



(b) Stepwise approximation

FIGURE 10. SPECTRUM APPROXIMATION

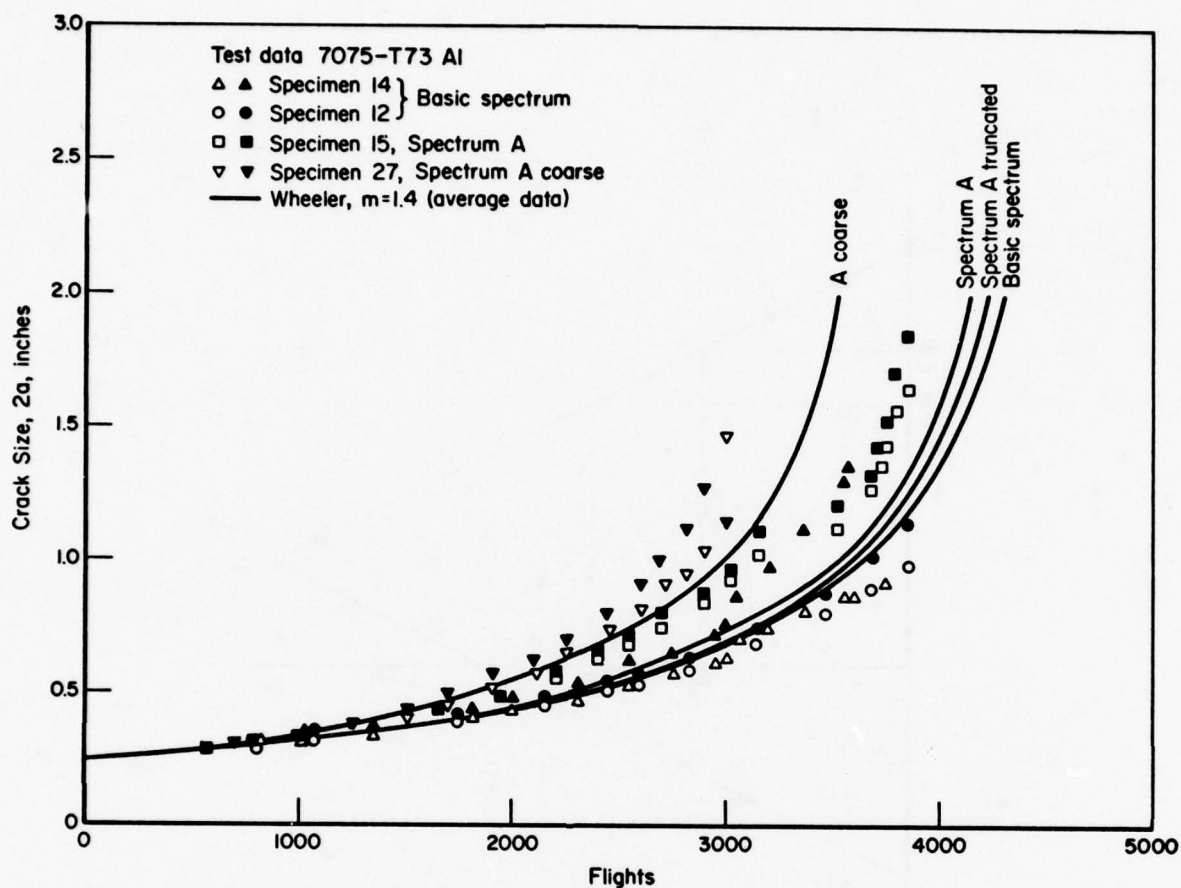


FIGURE 11. COMPARISON OF WHEELER CALCULATIONS WITH TEST RESULTS FOR THE BASIC SPECTRUM AND THREE VERSIONS OF SPECTRUM A IN 7075-T73

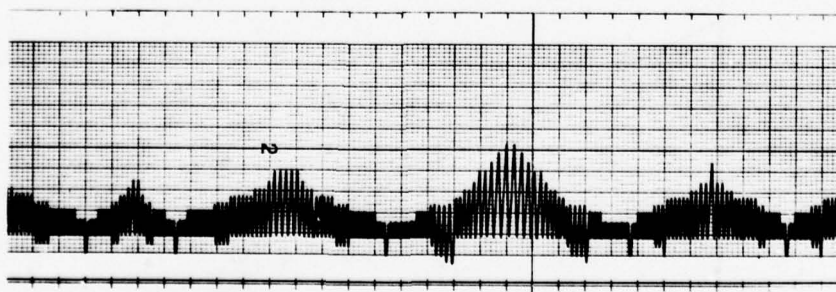


FIGURE 12. EXAMPLE OF A FLIGHT-BY-FLIGHT HISTORY FOR A FIGHTER AIRPLANE. CYCLES PER FLIGHT ARE ORDERED IN LOW-HIGH-LOW SEQUENCE. NOTE GROUND-AIR-GROUND CYCLES BETWEEN FLIGHTS



Symbol	Spectrum	Linear Analysis (Flights)
a ▲ Willenborg △ Wheeler, 2.3	Fighter	270
b ● Willenborg ○ Wheeler, 2.3	Trainer	460
c ■ Willenborg □ Wheeler, 2.3	B-1 class bomber	140
d ▼ Willenborg ▽ Wheeler, 2.3	C-transport	1270

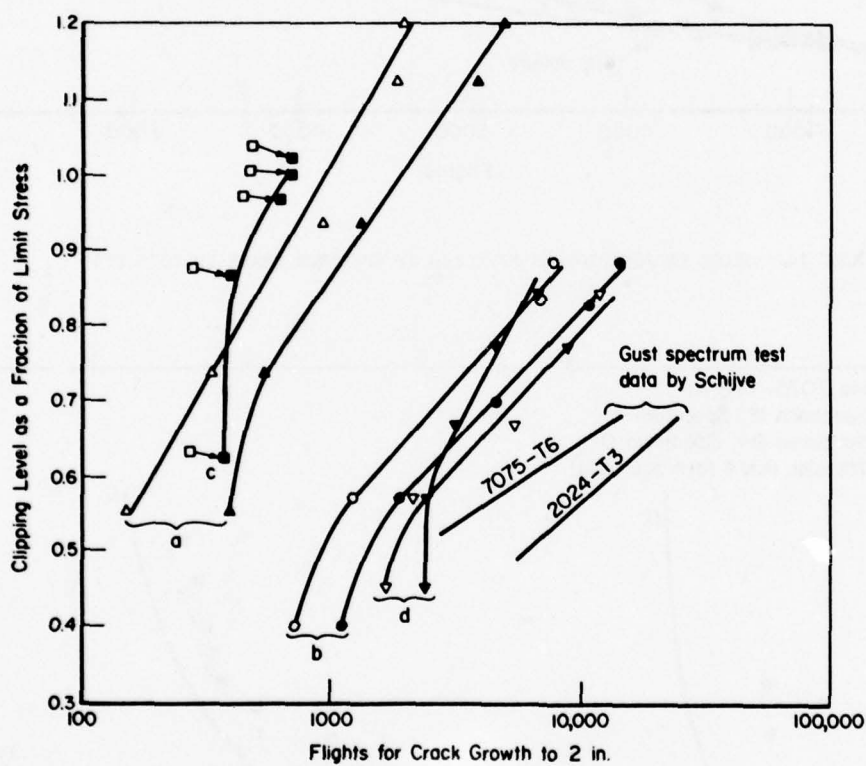


FIGURE 13. EFFECT OF CLIPPING FOR VARIOUS SPECTRA

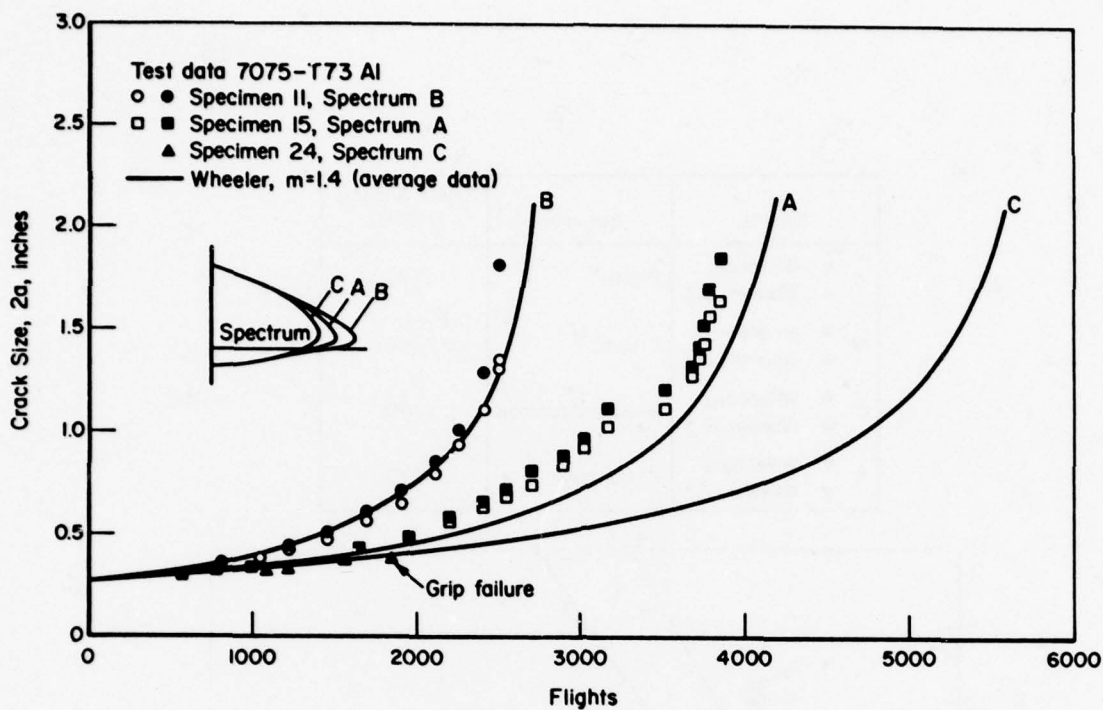


FIGURE 14. CRACK PROPOGATION AS AFFECTED BY SPECTRUM SHAPE IN 7075-T73

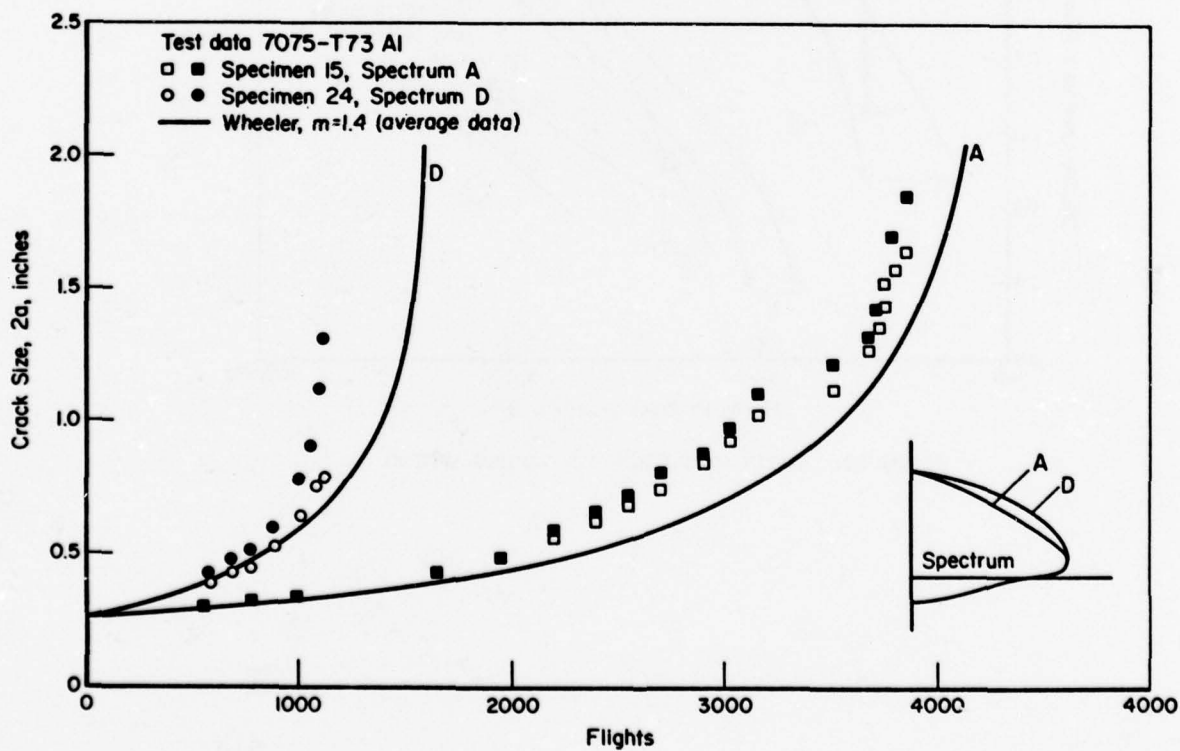


FIGURE 15. CRACK PROPAGATION AS AFFECTED BY SPECTRUM SEVERITY IN 7075-T73

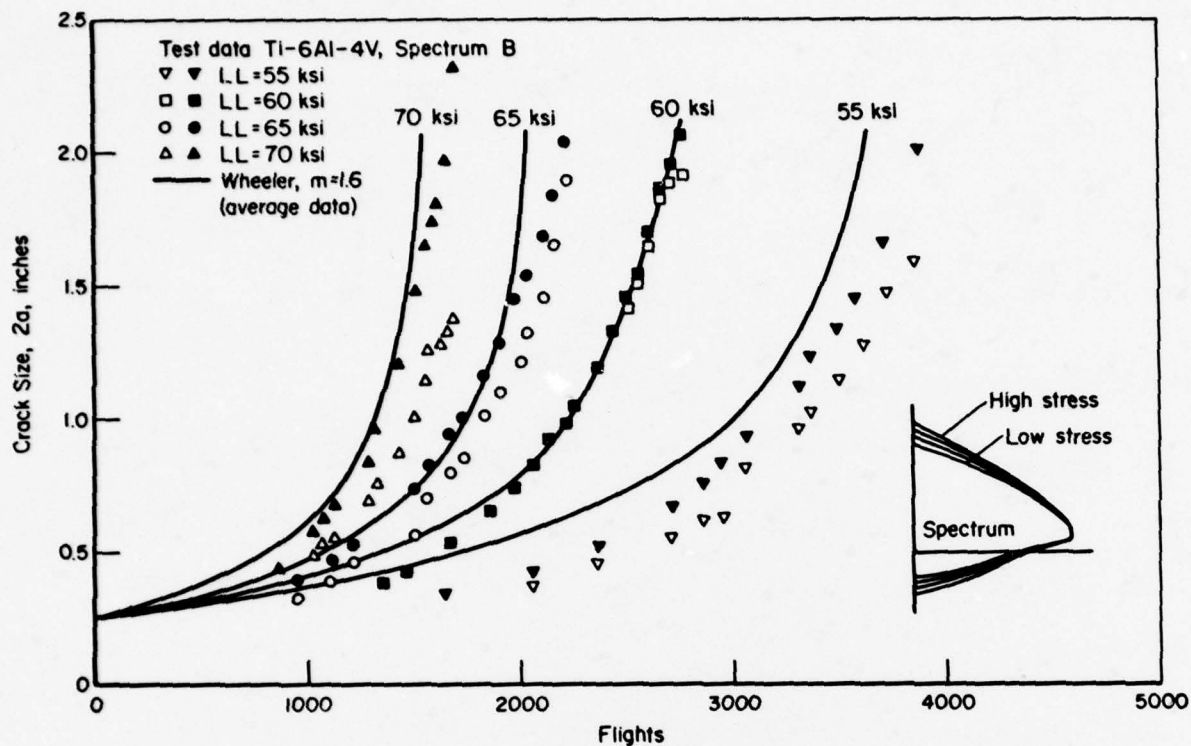


FIGURE 16. CRACK PROPAGATION AS AFFECTED BY DESIGN STRESS LEVEL IN Ti-6Al-4V

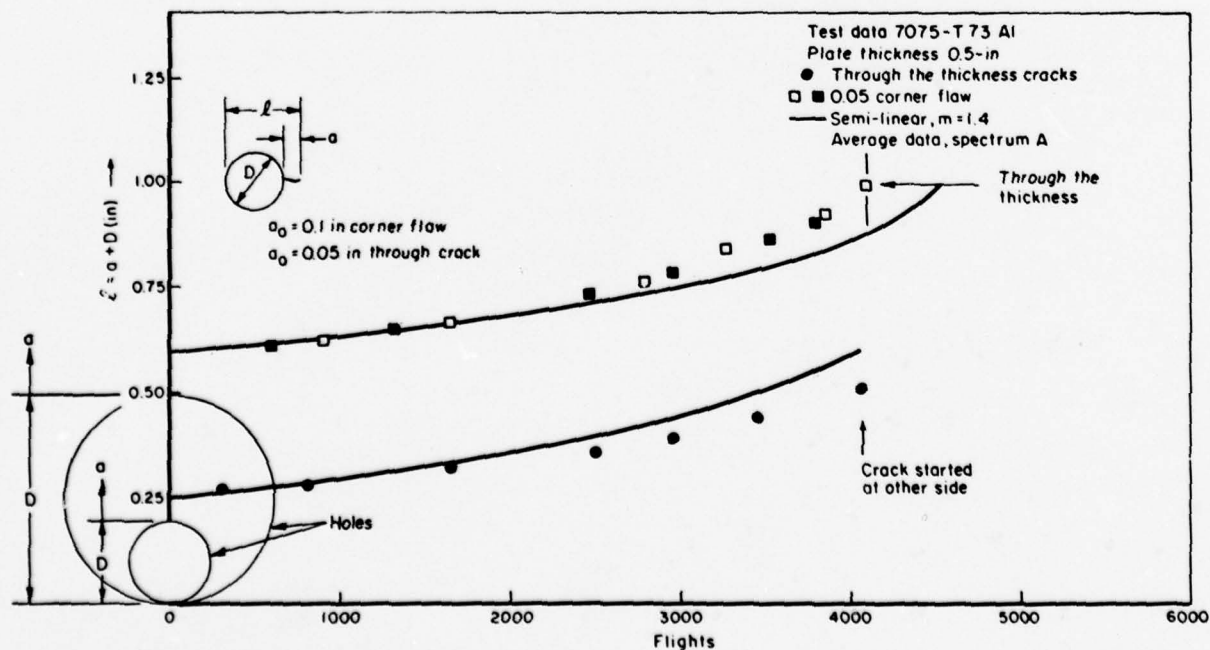


FIGURE 17. CRACKS AT HOLES IN 7075-T73 UNDER BASIC SPECTRUM

**SESSION III**

**DAMAGE TOLERANCE DESIGN**



# DESIGN OF HEAVY SECTIONS

by

Dr.-Ing. Walter Schütz

Industrieanlagen-Betriebsgesellschaft mbH  
Einsteinstraße 20, 8012 Ottobrunn, Germany

## 1. INTRODUCTION

Most highly loaded heavy section airframe components are manufactured either from plate or from forgings, the crack propagation and residual static strength properties of which are therefore of interest to the designer, the certification authorities and the operator.

If heavy section components are made from plate their final shape is obtained by machining-interrupting the grain flow. For many forgings the original shape is hardly changed by machining. However, there may be differences in grain flow between individual forgings.

One might intuitively expect both effects to lead to difficulties in predicting the above materials properties and in a larger-than-normal scatter of these properties. In the present paper the available fracture mechanics data of plate or forged aircraft materials are reviewed; finally some qualitative suggestions and quantitative results are given which, it is hoped will be of use to the designer of heavy sections.

## 2. FRACTURE MECHANICS FOR HEAVY SECTIONS

### 2.1 General Remarks

The structure of modern aircraft, especially military aircrafts, contains a large number of heavy section components made from forgings or plates<sup>1)</sup>. Such components usually have a single load path, and were formerly designed to the "safe life" philosophy, more recently to the "slow crack growth" philosophy. A failure of a single load path component usually results in an accident.

Therefore it is especially important to be able to calculate residual static strength and crack propagation properties of heavy sections using fracture mechanics procedures. In principle it should be easier to use these procedures for heavy sections because

- the sections are thick enough for plane strain conditions and
- the formulae for the stress intensity factor  $K$  are simple compared to those for typical differentially stiffened structures.

However, one might expect the materials properties to be a problem, because

- the thick sections of plates and forgings are not worked as uniformly as, for example, thin sheets,
- the grain flow may be disturbed in forgings or disrupted in components machined from plate and
- many heavy section components are large and are machined from large plates or forgings, which may result in large differences of fracture toughness properties even within one plate.

So it would appear that the problems of using fracture mechanics for typical heavy section components come not so much from the fracture mechanics side, but from the materials properties side. In other words, the difficulties lie not in the calculation procedures, but in the input data - as in many other engineering problems and there might be especially large differences in fracture toughness behaviour between specimens and components.

A considerable amount of fracture toughness and crack propagation data can be found in the literature (1 - 15)). However, these are mostly specimen data from standard ASTM specimens (16) or center notched crack propagation specimens. Data on fracture toughness or crack propagation tests on components are almost completely lacking - the author has found only a few such programs (6, 17-19) - probably because of the enormous cost of such components. In view of the problems mentioned above this is especially critical.

<sup>1)</sup> An example of a thick section component from another field is a forged gun barrel.

## 2.2 Fracture Toughness and Crack Propagation Data

Data available from the literature were evaluated as to the following parameters:

- Mean fracture toughness  $\overline{K_{IC}}$  of forged or plate specimens
- Scatter of fracture toughness
- Crack propagation as above
- Comparison of specimen data with component data.

The following qualitative results were obtained (for quantitative data some figures are included):

### Specimen data:

- The mean fracture toughness of forgings is, if anything, higher than that of plate material of nominally identical heat treatment and composition (1, 2, 3a, 9, 13). This is true for aluminum, titanium and steel. (For a comparison between a Ti6Al4V plate and a forging, see Figures 2 and 3).
- If the forging procedure results in thorough working of the material - as for example with gun barrel forgings - extremely high fracture toughness is obtainable (15).
- The scatter of fracture toughness of plate and forging materials is not significantly different (see Part II for more detail). This is in contrast to the MIL HDBK 5 (2).
- The typical scatter of fracture toughness is lower for aluminum plate and forgings than for titanium plate and forgings (for details see Part II).
- If very extensive forging process control is used, as for titanium compressor disc forgings (3a), the mean fracture toughness will be high and the scatter very low, compare Figures 2 and 3.
- The same is true for so-called high-integrity forgings (5) of aluminum and titanium and for the newer aluminum plates (3), see Figure 4.
- The crack propagation properties of Ti6Al4V plate and forgings are similar, see Figure 5.
- Crack propagation retardation effects due to high loads in a load sequence are smaller in plate and forging specimens than in thin sheets (7). This may be due to the thickness, but in addition also to metallurgical differences.

### Comparison between specimen and component data:

(These conclusions are based on only one test program with 7075-T6 forgings (16)).

- The fracture toughness of the complete forged component was higher in all three locations than that of specimens taken out of the forgings at these locations.
  - The scatter of fracture toughness was much larger for the forgings than for the specimens, see Figure 6. This scatter of the forgings could not be explained by the usual metallographic procedures.
  - Nominally identical forgings with cracks of very similar dimensions can have grossly different ultimate failing loads.
  - Crack propagation was considerably slower under a landing gear spectrum than predicted by the Willenborg retardation model. In other test programs with sheet or plate specimens the Willenborg model always gave unconservative results.
  - The scatter of
    - fatigue life to failure as well as
    - the crack initiation and
    - the crack propagation period
 was extremely large for the forgings under two realistic load sequences, see Figure 7.
  - Forgings with a long fatigue life can have very short crack propagation periods and vice versa.
  - The fracture surfaces and crack shapes in forgings may be highly irregular.
  - The residual static strength, fatigue life and crack propagation life of forgings may be subject to an extremely large scatter, much larger than for sheet or plate components. In order to attain equal probabilities of survival, larger safety coefficients would therefore have to be observed for forgings than for sheet or plate components.
- For a fatigue test on a structure considering of forgings and of sheet and plate components, there obviously exists a dilemma:  
 If the test is stopped at some multiple (say 4) of the required lifetime, the demonstrated structural reliability (at least in a statistical sense) is higher for the sheet and plate components than for the forgings.
- Even if an aircraft is manufactured in several countries, the important forgings should come from one supplier only.

- A long fatigue life of a forged component in test is no guarantee for a long crack propagation period. This again has obvious implications for the full scale fatigue test. Forgings are often used in internal structures and are therefore difficult to inspect. Every effort should be made to improve NDI techniques for such applications.
- The application of fracture mechanics to aluminum forgings is difficult, to say at least. This does not reflect so much on fracture mechanics itself, but results from peculiar forging characteristics, like large scatter of properties even in one location, much more so in different locations.

The following conclusion is based on another test program (19):

- The scatter of crack propagation rate may be much higher in integrally machined panels than in simple specimens.

### 3. REFERENCES

1. N.N., "Damage Tolerant Design Handbook, Parts 1 and 2" MCIC-HB-01.
2. N.N., "Military Standardization Handbook. Metallic Materials and Elements for Aerospace Vehicles" MIL-HDBK-5B (1974).
3. Zenner, H., and Schütz, W., "Bauteilspezifische Werkstoffuntersuchungen. Untersuchungen am Halbzeug 7050-T73651" IABG-Report TF-621.3 (1976).
- 3a. Zenner, H., and Schütz, W., "Bauteilspezifische Werkstoffuntersuchungen. Untersuchungen an Triebwerksscheiben aus Ti6Al4V" IABG-Report TF-676.3 (1977).
4. Schimmelbusch, H.W., "Metallurgical Evaluation of 7175-T736 and 7175-T66 Die Forgings" The Boeing Company, Report D6-24480.
5. Hyatt, M.V., Pasley, D.H., Goodlet, I., and Yohn, C.P., "High Integrity Forgings of Aluminum and Titanium Alloys" AFML-TR-77-81.
6. Larsson, S.E., "Fatigue Experience from Tests Carried out with Forged Beam and Frame Structures in the Development of the Saab Aircraft Viggen" in: Advanced Approaches to Fatigue Evaluation NASA SP 209.
7. Wahnhill, R.J.H., Schijve, J., Jacobs, F.A., and Schra, L., "Environmental Fatigue under Gust Spectrum Loading for Sheet and Forging Aircraft Materials" NLR MP 75037 U, (Oct. 1975).
8. Wagner, W., "Werkstoffuntersuchungen an verschiedenen Ti- und Al-Legierungen" MBB-Report UFE-710-71.
9. Oberparleiter, W., and Schütz, W., "Bauteilspezifische Werkstoffuntersuchungen. Untersuchungen am Halbzeug Ti6Al4V-Platte" IABG-Report TF-675.3 (1977).
10. Oberparleiter, W., and Schütz, W., "Rißfortschritt an 7075-T7351-Platten unter Einzelflugbelastung" IABG-Report TF-482 (1975).
11. Oberparleiter, W., and Schütz, W., "Rißfortschrittsverhalten von 7075-T7351, HP 9-4-30, 300 M und Ti6Al4V unter Einzelflug- und Einstufenbelastung" IABG-Report TF-549 (1975).
12. N.N., "Statistische Auswertung der 1975 und 1976 an ungeknickten Trägerplatten ermittelten Bruchzähigkeitswerte" Krupp Metall- und Schmiedewerke, Essen (1977).
13. Oberparleiter, W., Kratzer, H., and Schütz, W., "Zusammenstellung bruchmechanischer Kennwerte" IABG-Report TF-645 (1977).
14. Oberparleiter, W., and Schütz, W., "Rißfortschritts- und Restfestigkeitsversuche an 6 mm dicken Titanplatten" IABG-Report TF-360 (1973).
15. Oberparleiter, W., and Schütz, W., "Bruchzähigkeits- und Rißfortschrittsverhalten des Geschützrohrstahles 35 NiCrMoV 14 6" IABG-Report TF-436 (1974).



16. N.N., "Standard Method of Test for Plane Strain Fracture Toughness of Metallic Materials"  
ASTM Designation E-399-74, American Society for Testing and Materials Annual Book of Standards, Part 31 (1974).
17. Zola, J.C., "Analysis of Heavy Lift Helicopter Rotor Hub Lower Lug" in: Case Studies in Fracture Mechanics  
AMMRC MS 77-5.
18. Schütz, W., "Crack Propagation and Residual Static Strength of Typical Aircraft Forgings" in: Fracture Mechanics Design Methodology  
AGARD-CP-221 (1977).
19. Heath, W.G., Nicholls, L.F., and Kirkby, W.T., "Practical Applications of Fracture Mechanics Techniques to Aircraft Structural Problems" in: Fracture Mechanics Design Methodology  
AGARD-CP-221 (1977).



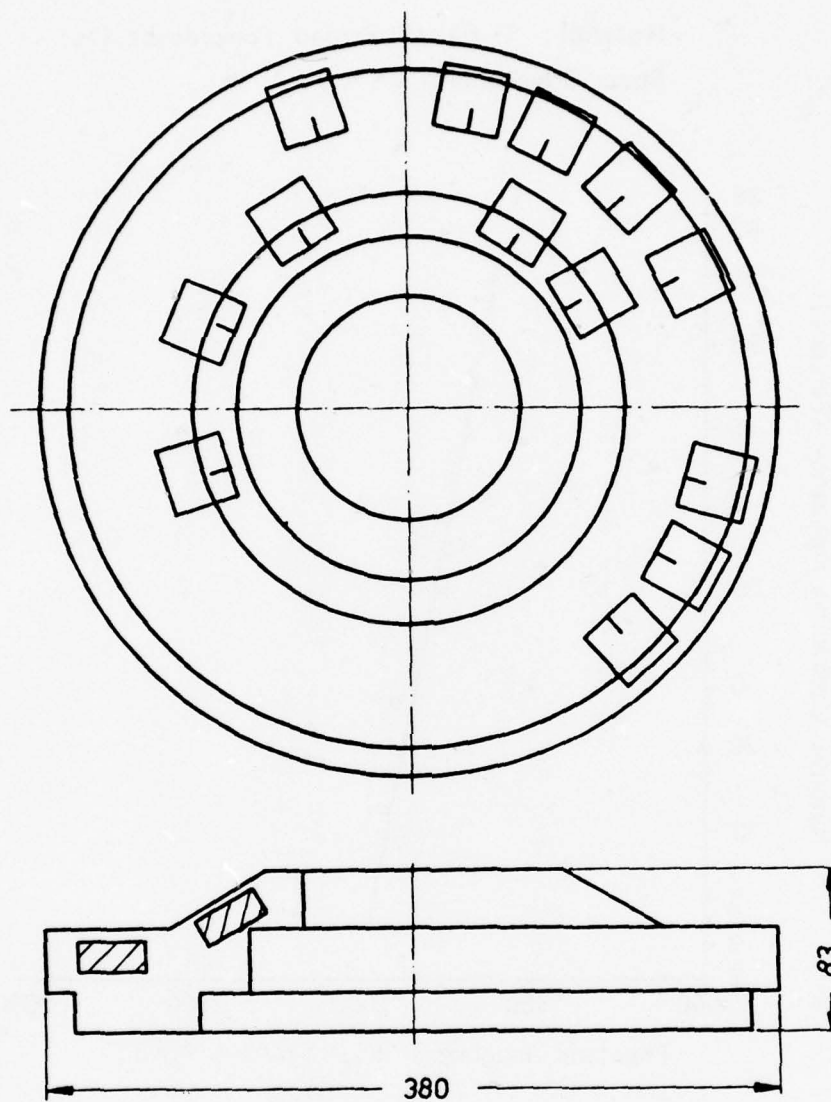
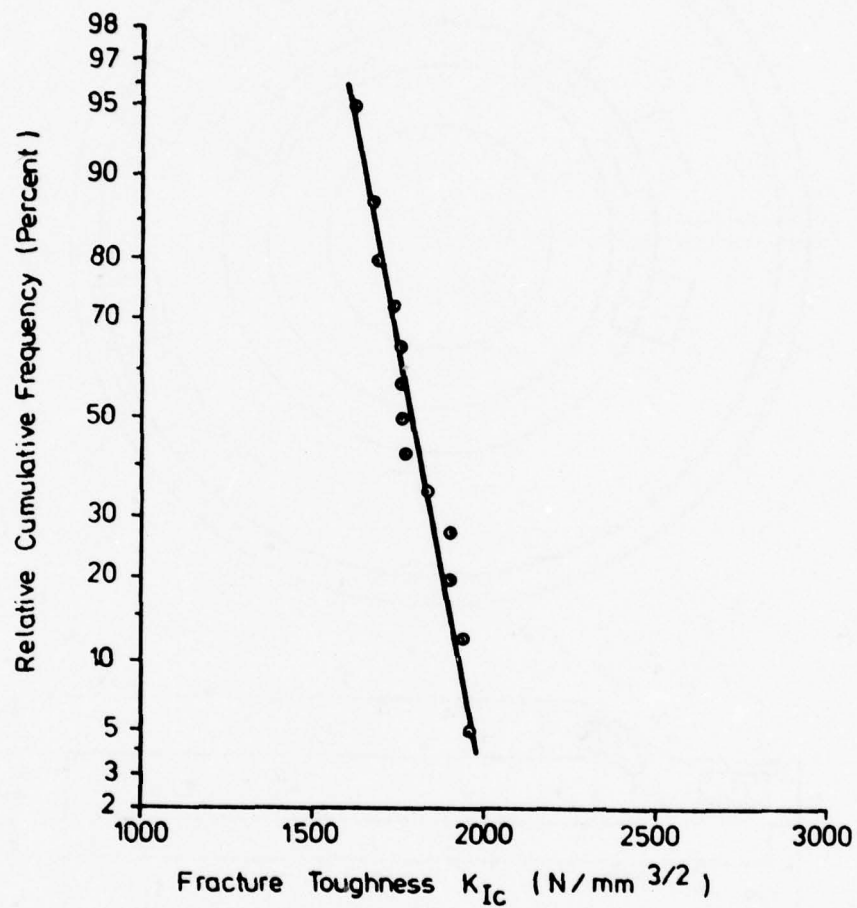


FIGURE 1. FORGED COMPRESSOR DISC OF Ti6AL4V  
SPECIMEN ORIENTATION

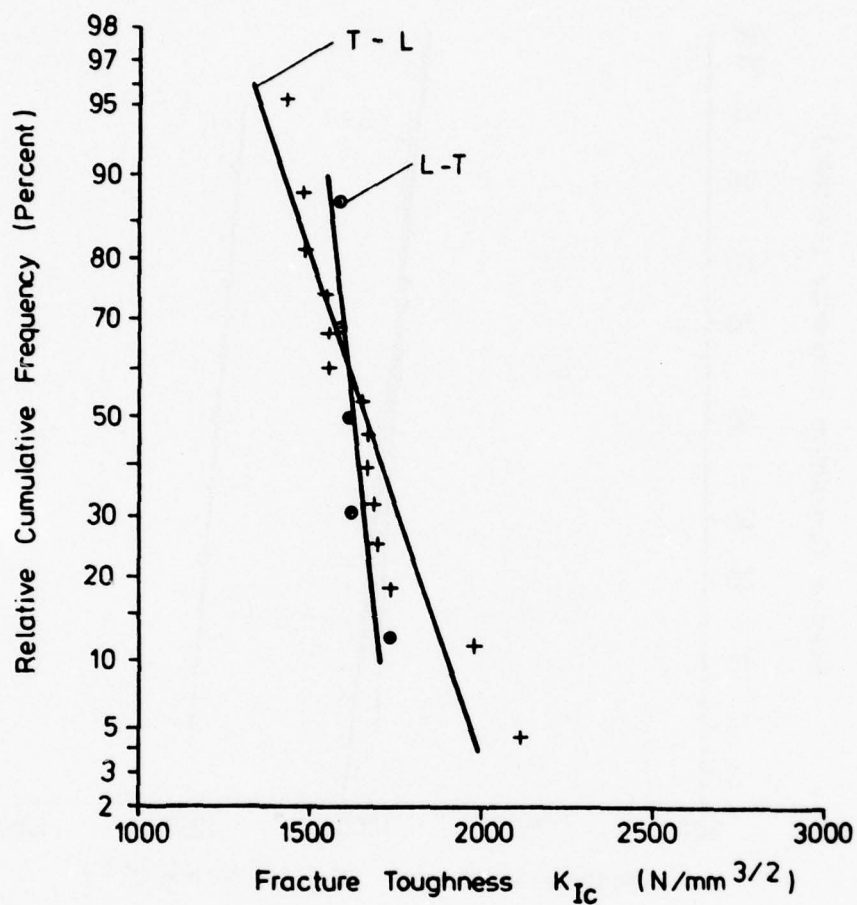
Material : Ti 6Al 4V Forged Compressor Disc  
Spec. Orientation : C - R



○  $\overline{K_{IC}}$  (50 Percent) = 1790 N/mm<sup>3/2</sup>  $v = 0.06$

FIGURE 2. STATISTICAL EVALUATION OF FRACTURE TOUGHNESS

Material : Ti 6Al 4V - Plate 1920 x 720 x 78 mm



- o  $\overline{K_{Ic}}$  (50 Percent) = 1623 N/mm<sup>3/2</sup>  $v = 0,037$   
 +  $\overline{K_{Ic}}$  (50 Percent) = 1660 N/mm<sup>3/2</sup>  $v = 0,12$

FIGURE 3. STATISTICAL EVALUATION OF FRACTURE TOUGHNESS

Material : 7050 - T 73651 - Plate  
2000 × 1000 × 110mm

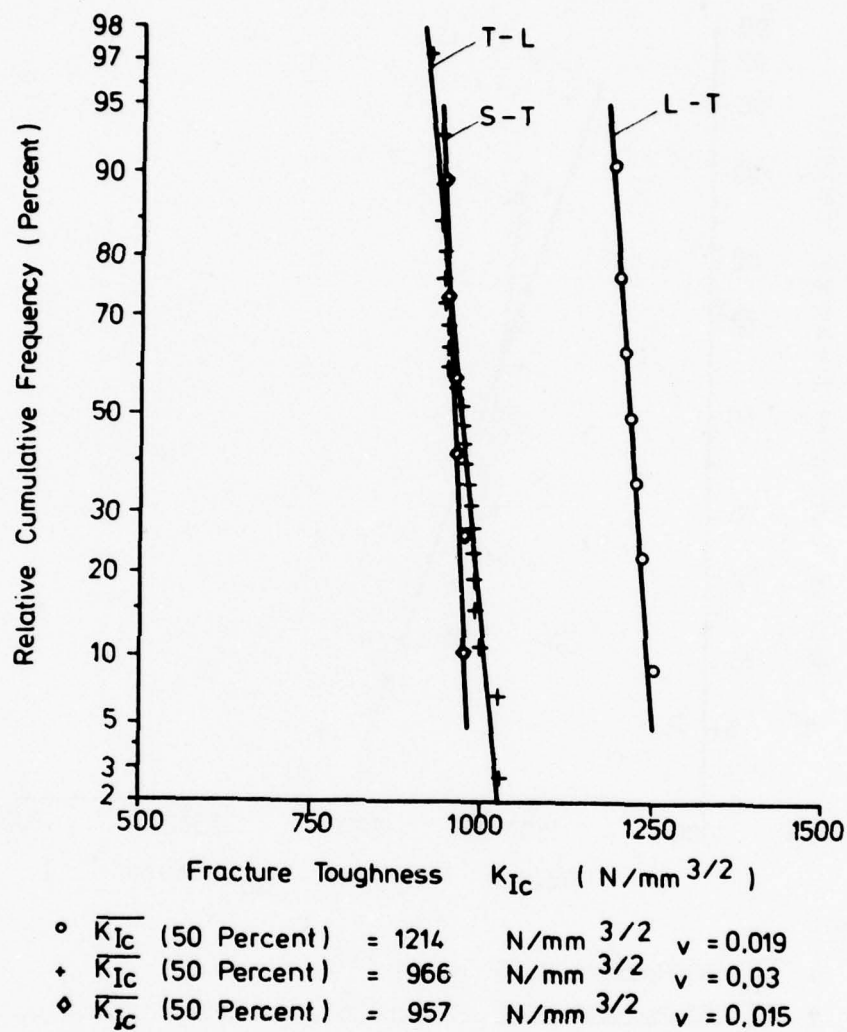


FIGURE 4. STATISTICAL EVALUATION OF FRACTURE TOUGHNESS



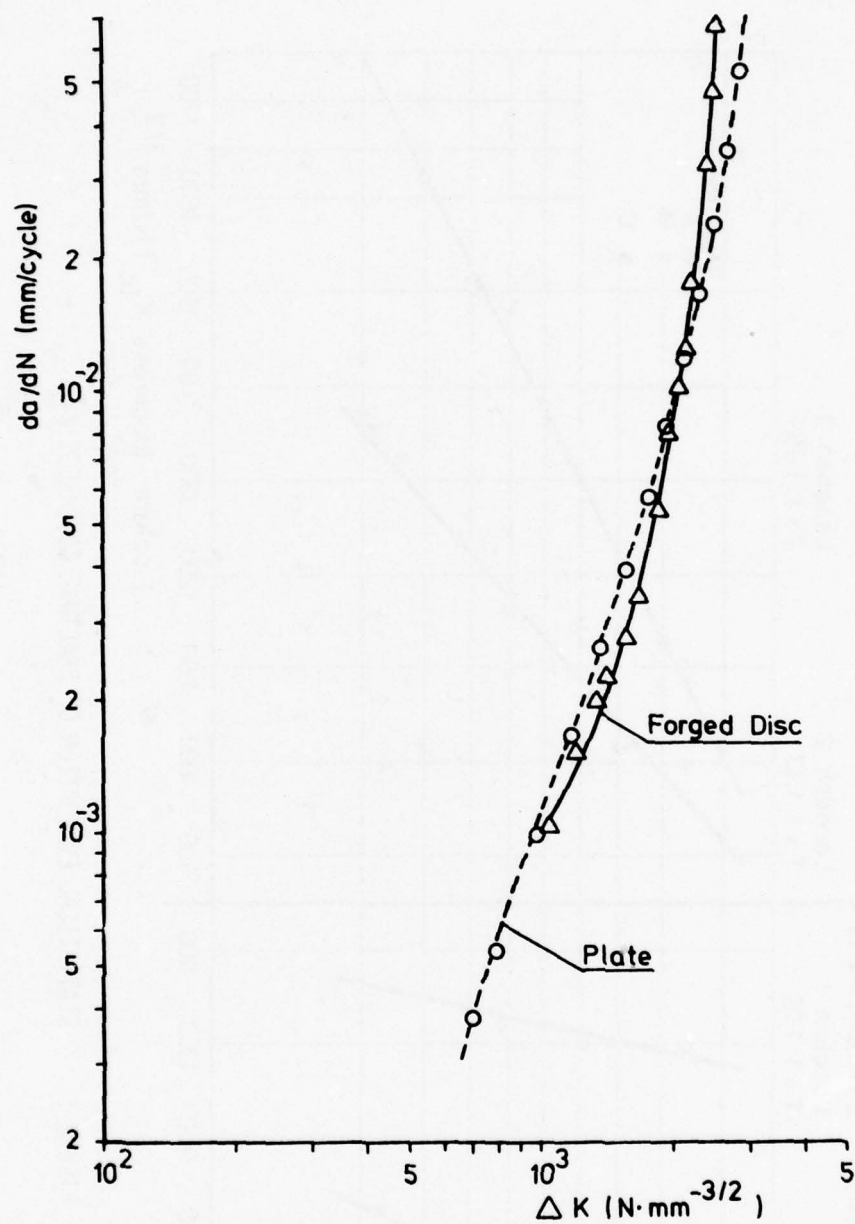
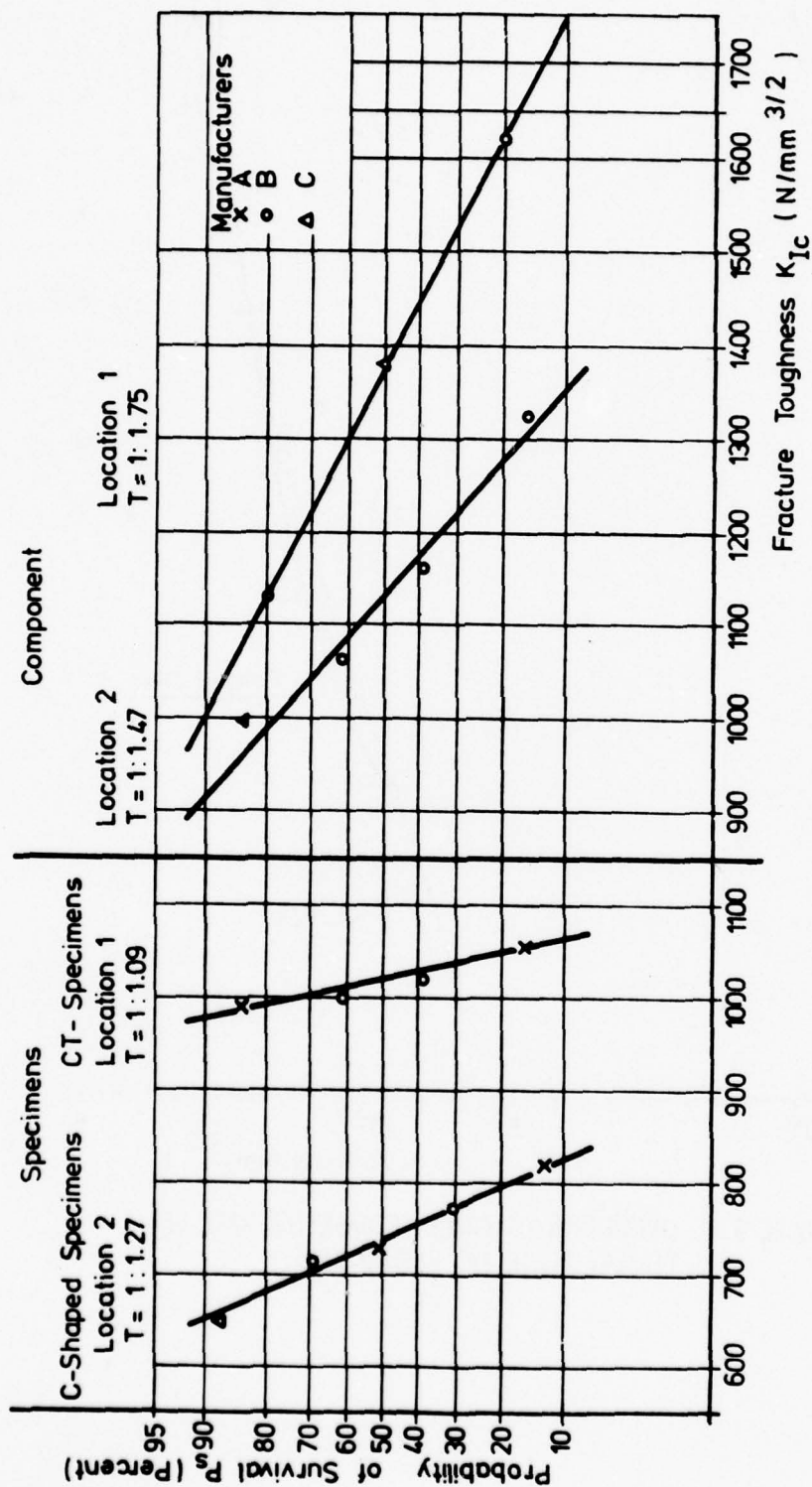


FIGURE 5. COMPARISON OF CRACK PROPAGATION RATE OF  
Ti6AL4V PLATE AND FORGED DISC

FIGURE 6. STATISTICAL EVALUATION OF FRACTURE TOUGHNESS  $K_{IC}$

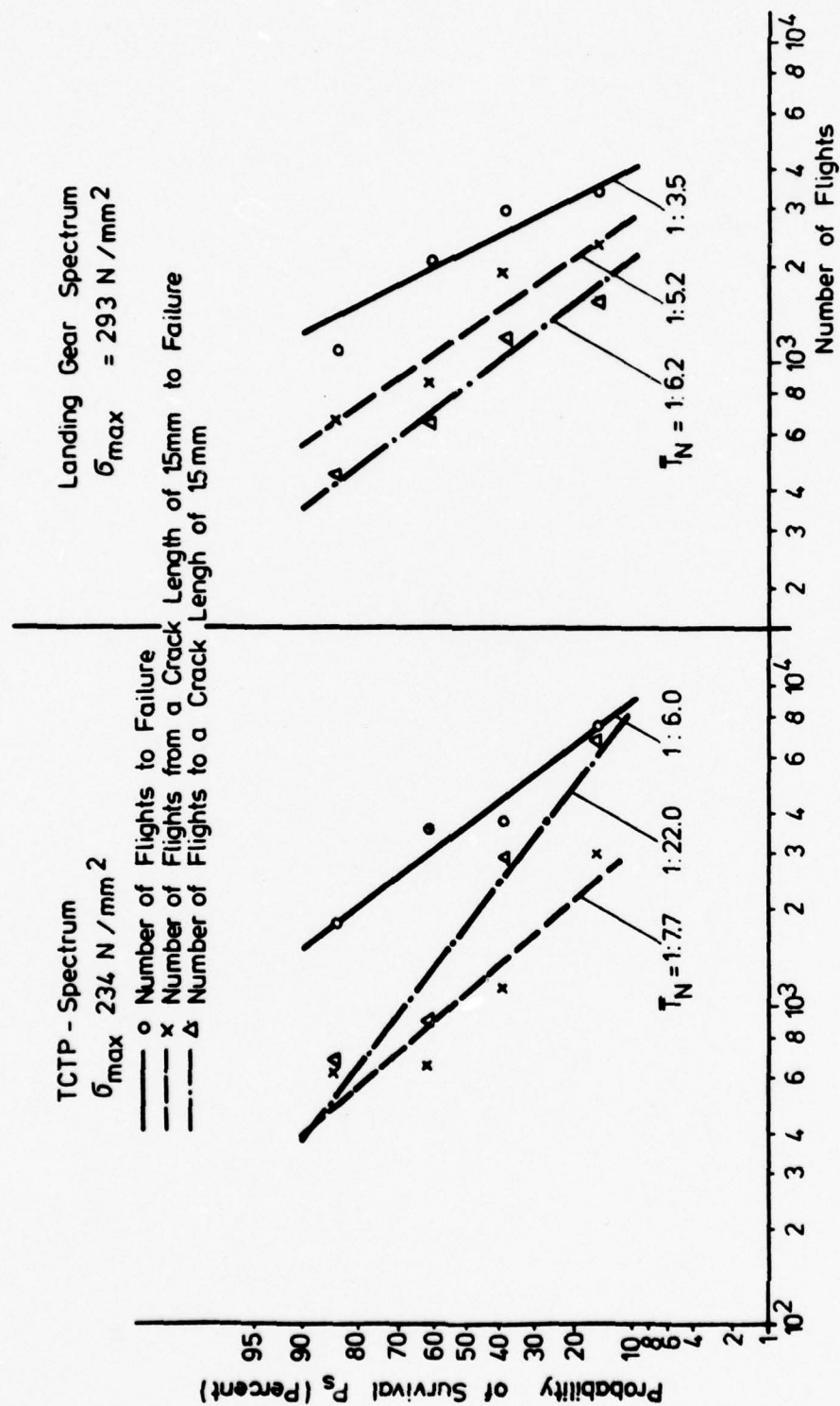


FIGURE 7. STATISTICAL EVALUATION OF CRACK PROPAGATION TESTS

# TREATMENT OF SCATTER OF FRACTURE TOUGHNESS DATA FOR DESIGN PURPOSES

by

Dr.-Ing. Walter Schütz

Industrieanlagen-Betriebsgesellschaft mbH  
Einsteinstraße 20, 8012 Ottobrunn, Germany

## 1. INTRODUCTION

The numerical values used in fracture mechanics calculations (i.e.  $K_{IC}$ ,  $da/dN$ ) depend on material properties. Therefore they have an inherent scatter - like all material data. For design purposes, this scatter must be accounted for either by "safety factors" or by suitable statistical procedures.

The mathematical procedures as such are relatively simple and well known; it is, however, a most difficult question which numerical values to use in such a calculation, for example for the coefficient of variation of fracture toughness  $K_{IC}$ ; this is so because such numerical values are still very scarce, as they are much more difficult and expensive to determine than, for example,  $F_{tu}$ -values.

Also, fracture toughness may be much more sensitive to slight variations in heat treatment than the normal mechanical properties; this may result in large differences of fracture toughness between different heats of a nominally identical material. This may be another reason why in most cases only "typical" values for  $K_{IC}$  are given in handbooks (1).

## 2. TREATMENT OF SCATTER IN FRACTURE MECHANICS CALCULATION

### 2.1 General Remarks

Numerical values of mechanical properties determined by tests cannot be used directly for design purposes because that would imply a large percentage of failures: They have to be lowered, that is a certain "safe" distance has to be kept between the stress endured by the test specimen(s) and the stress allowable for design. Historically this "safe" distance was obtained by a consensus of the parties concerned and called a "safety factor". This factor was assumed to cover all eventualities so that practically no failure would occur. Two examples are the factor of 1.5 against ultimate strength for aircrafts and of 1.5 against yield strength for ships. This factor usually has to be kept against the "book value" of the mechanical property concerned, which may be a minimum value, as in the Federal Republic of Germany's Aircraft Materials Handbook (2) or, as in the MIL-HDBK 5 (1), a statistical value assigned a certain probability with a certain confidence.

In recent years the probabilistic approach has gained acceptance which recognises that a certain probability of failure is inherent in any engineering structure and that by proper use of statistics this probability can be calculated - in contrast to the safety factor approach - and therefore kept at an acceptably low level.

However, it should be kept in mind that any statistical calculation requires as input numerical constants - for example the coefficient of variation of  $K_{IC}$  - and therefore depends on the degree of accuracy of these input data and assumptions. In other words: The real difficulties lie not so much in the mathematics of the problem, but in using correct input data and in making the right assumptions - as in many other engineering problems. In the end, even when a high-grade statistical treatment is employed, engineering judgment will be decisive - as it was with the old "safety factor" approach. Therefore the advantage of using a probabilistic approach is smaller than one would at first think.

Nevertheless in this paper some numerical values to be used as input data for fracture toughness calculations will be suggested which in the author's opinion can be used for design purposes. They were collected from the literature and from IABG data.

Also some suggestions will be made as to other necessary assumptions, i.e. the required probabilities of survival, the kind of distribution to use, etc.

### 2.2 Necessary Input Data and Assumptions

Theoretically the mean, the scatter (standard deviation or coefficient of variation) and the distribution are necessary to be able to calculate the necessary factor by which the mean value must be reduced in order to arrive at the required probability of survival.



### The Distribution

The determination of the distribution requires an extremely large number of tests, which will certainly not be available for fracture toughness data for a long time to come, if ever. Therefore it is necessary to assume the distribution. Usually the Normal distribution is used for strength of materials, for example for the tensile strength or the fatigue strength <sup>+</sup>). For fatigue life on the other hand, the log-normal distribution is often employed and will therefore be used in this paper for probabilistic crack propagation calculations.

One disadvantage of the normal distribution is that for high probabilities of survival very low allowable stresses are calculated if the scatter, i.e. the coefficient of variation, was high. One example: The often-used "mean minus three sigma" value, corresponding to a probability of survival of about 99.8 per cent is half as high as the mean value for a coefficient of variation of .166. For still higher probabilities of survival and coefficients of variation the allowable stress would become zero or even negative.

Therefore many statisticians have developed distributions which give a lower limit at which the probability of survival reaches 100 per cent, for example the Weibull distribution, the arc sin  $\sqrt{P}$  distribution developed by Rossow and co-workers<sup>(3)</sup> or a distribution developed by the IABG<sup>(4)</sup>. The latter results in a probability of survival of 100 per cent at "mean minus 2.75 sigma" and will be used later for a special purpose.

However, in the region between 50 and 95 per cent probability of survival there is no practical difference between any of the above distributions and for simplicity's sake the Normal distribution is therefore suggested as good enough for fracture toughness calculations and will be used in this paper.

### The Mean

The mean fracture toughness can be calculated as arithmetic mean from a small number of tests, say from two to three valid results, according to E-399-74<sup>(5)</sup>. This is then the mean of a (small) sample which has to be reduced to the mean of the population using normal statistical procedures<sup>(6)</sup>!

In a strength of materials problem one always has to make the conservative assumption that the mean of the population is lower than the mean of the sample. For this calculation the coefficient of variation is necessary. Its numerical value should not be the one determined from the sample (even if it were large enough), rather it should be a "typical" or even an "upper limit" coefficient of variation, see below, and section 3 and 4.

### The Coefficient of Variation

If more than 4 fracture toughness tests are carried out on one heat of a material for one specimen orientation, a statistical evaluation is possible and should be done according to the formula

$$P_s = \frac{3m - 1}{3n + 1} \cdot 100 \text{ (per cent),}$$

where  $P_s$  : probability of survival

$m$  : order number, where

$m = 1 \hat{=}$  highest fracture toughness of the series

$m = n \hat{=}$  lowest fracture toughness of the series

$n$  : number of tests.

Plotting this on Normal probability paper will result in a more or less straight line. From this the standard deviation  $\sigma$  can be taken and the coefficient of variation  $v$  calculated as

$$v = \frac{\sigma}{\bar{x}}$$

where  $\bar{x}$  = arithmetic mean fracture toughness.

( $P_s = 50$  per cent).

This then is a measure of the scatter of the one heat of material tested, i.e. of the sample.

There is another kind of scatter between different heats of a nominally identical material. If all the fracture toughness tests on different heats of a nominally identical material in one specimen orientation are evaluated together, one is assuming they belong to one population. There are statistical procedures to test this assumption<sup>(6, 7)</sup>.

Finally it must be recognized that the ASTM-standard method itself may have an inherent scatter, probably due to its many requirements which will be met in varying degrees in one test series. That is, even if a number of specimens of one sample actually had identical fracture toughness, the results would certainly still show some scatter due to the inherent weaknesses of the ASTM standard.

<sup>+</sup>) The well known staircase or up-and-down method assumes a Normal distribution for the fatigue strength.

### 3. NUMERICAL DATA FOR THE COEFFICIENT OF VARIATION OF FRACTURE TOUGHNESS AND CRACK PROPAGATION

#### 3.1 Procedure and Data for $K_{IC}$

The literature known to the author (2, 8-23) was screened for test series with five or more nominally identical specimens in one specimen orientation resulting in valid ASTM-standard tests. Most data were obtained from the Damage Tolerant Design Handbook, Part 1 (9), some test series with British alloys from (9a); a larger number of suitable test series was also obtained from IABG reports (8, 13-15, 21-23). Each series was evaluated by computer, using the formula given above in section 2.2 and the coefficient of variation was obtained. Some examples of these evaluation are given in Figures 1, 2 and 4, which were taken from IABG tests, Figure 1 from (3), Figure 2 from (15); (Figure 3 shows the forged compressor disc) and Figure 4 from (14).

The coefficients of variation (65 for aluminum alloys, 46 for titanium alloys and 64 for steels) were then plotted against  $\sigma_y$  specifying the following parameters:

- type of alloy (Ti 6-4, Ti 8-1-1 etc.)
- type of product (plate, forging etc.)
- specimen orientation
- miscellaneous (temperature, corrosion etc.)

One example of such a plot is shown in Figure 5 for Ti-alloys.

It became apparent that none of these parameters influenced the coefficient of variation within one class of materials, with one (well known) exception: D6AC steel showed a larger-than-normal scatter. According to MIL-HDBK 5B data (1) Al-forgings have a larger scatter (defined as minimum/maximum fracture toughness) than Al-plate. However, this cannot be confirmed from the data in (2 and 8-23).

Next the coefficients of variation were evaluated statistically for Al-, Ti- and Fe-alloys according to the formula in Section 2.2, see Figures 6 - 8. However, the 23 test series for D6AC steel were evaluated separately, see Figure 9. In these statistical evaluations the distribution developed by the IABG (4) and mentioned above was used in lieu of the Normal distribution

- because it results in a probability  $P_s = 0$  at a coefficient of variation  $v > 0$ ; this is obviously a necessary requirement, because zero scatter of fracture toughness is physically impossible and
- because it gives a probability  $P_s = 100$  per cent at a sensible coefficient of variation.

In the following Table 1 the results of Figures 6 - 9 are condensed.

TABLE 1

Material	Al-alloys	Ti-alloys	Steels except D6AC	D6AC
coefficient of variation $v$				
at 50	0.03	0.05	0.05	0.1
90	0.06	0.12	0.10	0.22
100 per cent probability	0.14	0.27	0.22	0.4

$v = 0.14$  at 100 per cent probability for Al-alloys means that using the assumed distribution (4) 100 per cent of the test series had a lower coefficient of variation than 0.14; 0.05 at 50 per cent probability for steels means that the fracture toughness of half of the steel test series had a lower coefficient of variation than 0.05.

As can be seen from Table 1 the scatter of fracture toughness  $K_{IC}$  is lower for Al-alloys than for Ti-alloys and steels. Table 1 also shows numerical values of the coefficient of variation to be expected for the different classes of material and at different probabilities.

Another important numerical value is the mean fracture toughness  $\bar{K}_{IC}$  of different heats of a certain alloy in a certain specimen orientation and its scatter. This was obtained in two ways:

- All test series with five or more valid ASTM tests of one specific alloy and specimen orientation were extracted from the literature and their arithmetic mean fracture toughness  $\bar{K}_{IC}$  determined. These values were then evaluated statistically using the formula given in Section 2.2. Some examples are shown in Figures 10 - 13.
- All the valid test results in (9) for one specific alloy and specimen orientation were evaluated together, even if only one or two valid tests per heat were available. The result is given in Figure 14 for 7050-T73651 (9) in the L-T-direction.

Figures 10 - 14 show the mean fracture toughness to be expected from several heats of one material, that is (at 50 per cent probability) its "typical" fracture toughness. They also show the coefficient of variation to be expected between different heats of a material. This coefficient of variation is again lower for the Al-alloy than for Ti-alloy, while D6AC is highest.

### 3.2 Procedure and Data for $K_{IC}$

As there is no universally agreed method to determine  $K_{IC}$ , it is not intended to give numerical data here. However, should such a method be available some day, the procedures presented in Section 3.1 can also be used. It might even be possible to use the numerical data shown in Section 3.1 for the coefficient of variation of fracture toughness  $K_{IC}$  also for  $K_{IC}$  because in the author's opinion there is no valid reason why the scatter should be different.

### 3.3 Procedure and Data for Crack Propagation

A somewhat similar picture exists with regard to crack propagation data: While for  $K_{IC}$  it was the lack of an agreed method, for crack propagation it is the lack of data which makes it almost impossible to give reliable numerical values. This statement may need some explanation in view of the very large amount of  $da/dN$  data which is available, for example, from Part II of the Damage Tolerant Design Handbook (24) alone or from a large round robin-program described in (25): All these data were determined under constant stress amplitudes and cannot be used to derive numerical values for the scatter of crack propagation data under realistic loading. (This is a well known fact from normal fatigue testing). Therefore crack propagation tests under stochastically or deterministically varying load sequences are necessary; for aircraft design purposes these would typically be flight-by-flight sequences. Such data are available only in very limited numbers, even if only three crack propagation tests per parameter were considered enough for a statistical evaluation. To the author's knowledge only IABG data are available (11, 13, 26-29) fulfilling even this meagre requirement. Only two test series were carried out on two different heats of a nominally identical material (13). The IABG data are for actual forgings (not specimens) (11), for thin Ti6Al4V sheet specimens (27), for thick 7075-T7351 (28, 29) and Ti6Al4V (13, 29) plate specimens and for thick steel specimens machined from bar stock (29). The specimens had center notch crack starters. All these data were evaluated statistically. An example for 8 test series of Ti6Al4V sheet (27) is given in Figure 15, the complete data are condensed in Table 2.

TABLE 2

Material	Coefficient of variation of log numbers of flights from a crack length of 5 mm to complete failure			number of test series
	minimum	mean	maximum	
Ti6Al4V sheet	0.008	0.02	0.046	8
Ti6Al4V plate	0.028	0.07	0.11	5
7075-T7351 plate	0.02	0.04	0.07	9
300 M bar	0.11	0.12	0.13	2
7075-T6 forging (11) (complete component!)	0.27	0.30	0.32	2

It appears that the coefficient of variation of log numbers of flight from a crack length of 5 mm to complete failure

- is quite low for Ti6Al4V sheet specimens
- is higher for plate specimens than for sheet specimens
- is extremely high for the forgings.

## 4. RECOMMENDED VALUES OF FRACTURE TOUGHNESS PROPERTIES FOR DESIGN PURPOSES

### 4.1 General Remarks

When using the data described in section 3.1 (or similar specimen data) for the derivation of numerical fracture toughness values for the purpose of designing components, one implicitly assumes that the scatter of specimens fracture toughness is identical with the scatter of the component fracture toughness.

This assumption is not always correct as was shown by the author in (11) (see the Part I of this paper): Whereas the scatter of fracture toughness of standard ASTM specimens taken from a forged component was quite normal, the scatter of the component fracture toughness was much higher.



Nevertheless the above assumption must be made, otherwise one could not use specimen data for the design of components.

For designing a component using probabilistic fracture mechanics the necessary probability of survival must be selected according to engineering judgement. In strength of materials problems often the "mean minus three sigma" value is used ( $\approx P_s = 99.8$  per cent); in certain standards for fatigue of welded bridges the "mean minus two sigma" value is employed, corresponding to 97.7 per cent probability of survival assuming a Normal distribution. The author is aware of only one suggestion of a similar nature for fracture mechanics: Odorico showed in an AGARD paper (12) that the Aerospatiale company of France uses the "mean minus two sigma" fracture toughness for calculating critical crack length etc. The other numerical values necessary, the mean fracture toughness  $\overline{K_{IC}}$  and the standard deviation  $\sigma$  are obtained in the following way according to (12): All the available ASTM tests on one material in one condition and one specimen orientation that is from several heats, are statistically evaluated together. As the various Al-alloys have different scatter, different standard deviations are used.

#### 4.2 Procedure and Numerical data for $K_{IC}$

In the present paper a slightly different procedure is proposed:

- the coefficient of variation is equal within one class of material, namely
  - 0.06 for Al-alloys
  - 0.12 for Ti-alloys      for normal applications
  - 0.10 for steels
- and
  - 0.14 for Al-alloys
  - 0.27 for Ti-alloys      for critical applications
  - 0.22 for steels

These numbers correspond to probabilities of 90 per cent for normal and 100 per cent for critical applications according to Table 1.

The above coefficients of variation are applicable in principle to all semifinished products, that are plates, bars, extrusions and forgings. With Al-forgings there may be the problem of using specimen data for design of components, as mentioned above, see also Part I.

For mean fracture toughness  $\overline{K_{IC}}$  either the actual test results available for the specific problem can be used; if such data are not available  $\overline{K_{IC}}$  can be taken from the literature (for example from (2, 8, 9-15)) using all valid test results available i.e. from many different heats. It must be understood that this  $\overline{K_{IC}}$  is in both cases the mean of a sample, which must be reduced to the mean of the population, using the coefficients of variation given above.

#### 5. REFERENCES

1. N.N., "Military Standardization Handbook. Metallic Materials and Elements for Aerospace Vehicle Structures" MIL-HDBK-5B (1974).
2. N.N., "Werkstoffhandbuch der Deutschen Luftfahrt" Beuth-Vertrieb, Köln.
3. Dengel, D., "Die arc sin  $\sqrt{P}$  - Transformation - ein einfaches Verfahren zur grafischen und rechnerischen Auswertung geplanter Wöhlerversuche" Zeitschrift für Werkstofftechnik, Heft 8 (1975).
4. Hück, M., "Ansatz und Auswertung von Treppenstufenversuchen im Dauerfestigkeitsbereich" IABG-Report B-TF-742 B.
5. N.N., "Standard Method of Test for Plane-Strain Fracture Toughness of Metallic Materials" ASTM Designations E-399-74. Annual Book of ASTM Standards, Part 31 (1974).
6. Little, R.E., "Manual on Statistical Planning and Analysis" ASTM STP 588 (1975).
7. N.N., "Comparison of Samples" ESDU ITEM No. 68016, Engineering Sciences Data Unit, London (1968).
8. Oberparleiter, W., Kratzer, H., Schütz W., "Zusammenstellung bruchmechanischer Kennwerte" IABG-Report TF-645 (1977).

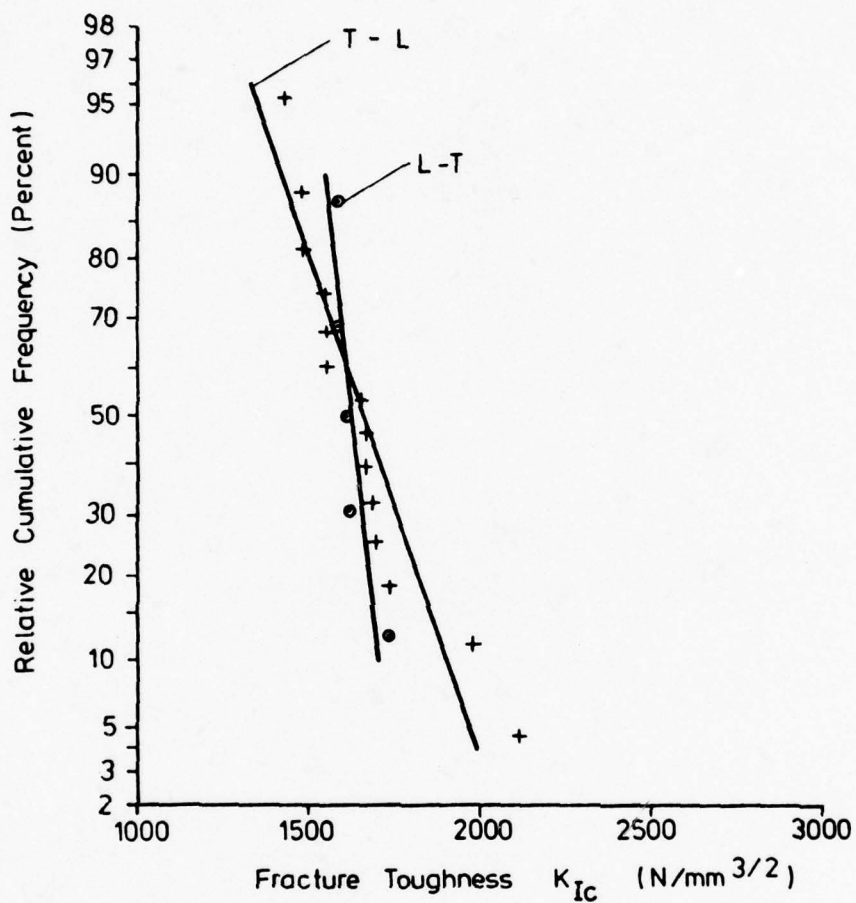


9. N.N., "Damage Tolerant Design Handbook. A Compilation of Fracture and Crack-Growth Data for High-Strength Alloys. Part 1" MCIC-HB 01.
- 9a. Kirkby, W., "Fracture Toughness Test Results", in: Fracture Mechanics of Aircraft Structures AGARD-AG-176 (1975) ed. by H. Liebowitz.
10. N.N., "Statistische Auswertung der 1975/76 an ungeknickten Trägerplatten ermittelten Bruchzähigkeitswerte" Krupp Metall- und Schmiedewerke, Essen (1977).
11. Schütz, W., "Crack Propagation and Residual Static Strength of Typical Aircraft Forgings" AGARD-CP-221 (1977).
12. Odorico, J., "Application de la Mechanique de la Rupture à la Selection des Alliages d'Aluminium" AGARD-CP-221 (1977).
13. Oberparleiter, W., "Bauteilspezifische Werkstoffuntersuchungen. Untersuchungen am Halbzeug Ti6Al4V-Platte" IABG-Report TF-675.3 (1977).
14. Zenner, H., "Bauteilspezifische Werkstoffuntersuchungen. Untersuchungen am Halbzeug 6060-T73651" IABG-Report TF-621.3 (1976).
15. Zenner, H., "Bauteilspezifische Werkstoffuntersuchungen. Untersuchungen am Halbzeug Ti6Al4V-Schreiben" IABG-Report TF-676.3 (1978).
16. Schütz, W., "Fatigue Life Prediction of Aircraft Structures - Past, Present and Future" Eng. Fracture Mechanics, Vol. 6, No. 3 (1976) pp 671-699.
17. Witzke, W.R., Stephens, J.R., "Comparison of Equivalent Energy and Energy Per Unit Area Data with Valid Fracture Toughness Data for Iron, Aluminum, and Titanium Alloys" JTEVA, Vol. 6. No. 1 (1978) pp 75-79.
18. May, J.M., "British Experience with Plane Strain Fracture Toughness ( $K_{IC}$ ) Testing" ASTM STP 463 (1970) pp 41-62.
19. Heyer, R.H., and McCabe, D.E., "Evaluation of a Method of Test for Plane Strain Fracture Toughness Using a Bend Specimen" ASTM STP 463 (1970) pp 22-41.
20. Brown, W.F., Jr., "Review of Developments in Plane Strain Fracture Toughness Testing" ASTM STP 463 (1970).
21. Kratzer, H., Oberparleiter, W., and Schütz, W., "Ergänzende bruchmechanische Untersuchungen an Flugzeugbauwerkstoffen" IABG-Report TF-560 (1976).
22. Oberparleiter, W., Kratzer, H., and Schütz, W., "Bruchzähigkeit verschiedener Luftfahrtwerkstoffe bei - 50° C" IABG-Report TF-513 (1975).
23. Kratzer, H., Oberparleiter, W., and Schütz, W., "Bestimmung der Bruchzähigkeit verschiedener Luftfahrtwerkstoffe" IABG-Report TF-492 (1975).
24. N.N., "Damage Tolerant Design Handbook, Part II" MCIC-HB-01 (1975).
25. Clark, W.G., Jr., and Hudak, S.J., "Variability in Fatigue Crack Growth Rate Testing" JTEVA, Vol. 3, No. 6 (1976) pp 454-476.
26. Oberparleiter, W., and Schütz, W., "Berechnung des Rißfortschritts an Bauteilen bei veränderlichen Spannungsamplituden" IABG-Report TF-508 (1976).
27. Zenner, H., and Schütz, W., "Rißfortschritt an Titanblechen im Einzelflugversuch" IABG-Report TF-224 (1972).

28. Oberparleiter, W., and Schütz, W., "Rißfortschritt an 7075-T7351 Platten unter Einzelflugbelastung"  
IABG-Report TF-482 (1975).
29. Oberparleiter, W., and Schütz, W., "Rißfortschrittsverhalten von 7075-T7351, HP 9-4-30, 300 M und Ti6Al4V unter Einzelflug- und Einstufenbelastung"  
IABG-Report TF-549 (1975).

28. Oberparleiter, W., and Schütz, W., "Rißfortschritt an 7075-T7351 Platten unter Einzelflugbelastung"  
IABG-Report TF-482 (1975).
29. Oberparleiter, W., and Schütz, W., "Rißfortschrittsverhalten von 7075-T7351, HP 9-4-30, 300 M und Ti6Al4V unter Einzelflug- und Einstufenbelastung"  
IABG-Report TF-549 (1975).

Material : Ti 6Al 4V - Plate 1920 x 720 x 78 mm



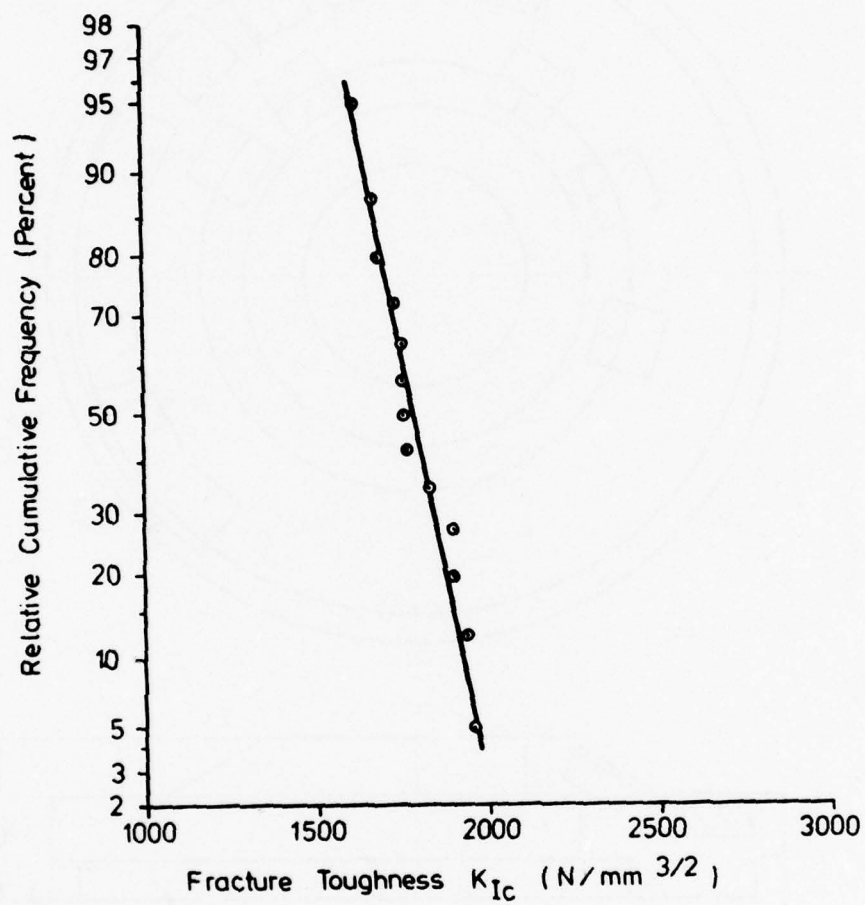
o  $\overline{K_{Ic}}$  (50 Percent) = 1623 N/mm<sup>3/2</sup>  $v = 0,037$

+  $\overline{K_{Ic}}$  (50 Percent) = 1660 N/mm<sup>3/2</sup>  $v = 0,12$

FIGURE 1. STATISTICAL EVALUATION OF FRACTURE TOUGHNESS



Material: Ti 6Al 4V Forged Compressor Disc  
Spec. Orientation: C - R



°  $\overline{K_{Ic}}$  (50 Percent) = 1790 N/mm<sup>3/2</sup>     $v = 0,06$

FIGURE 2. STATISTICAL EVALUATION OF FRACTURE TOUGHNESS

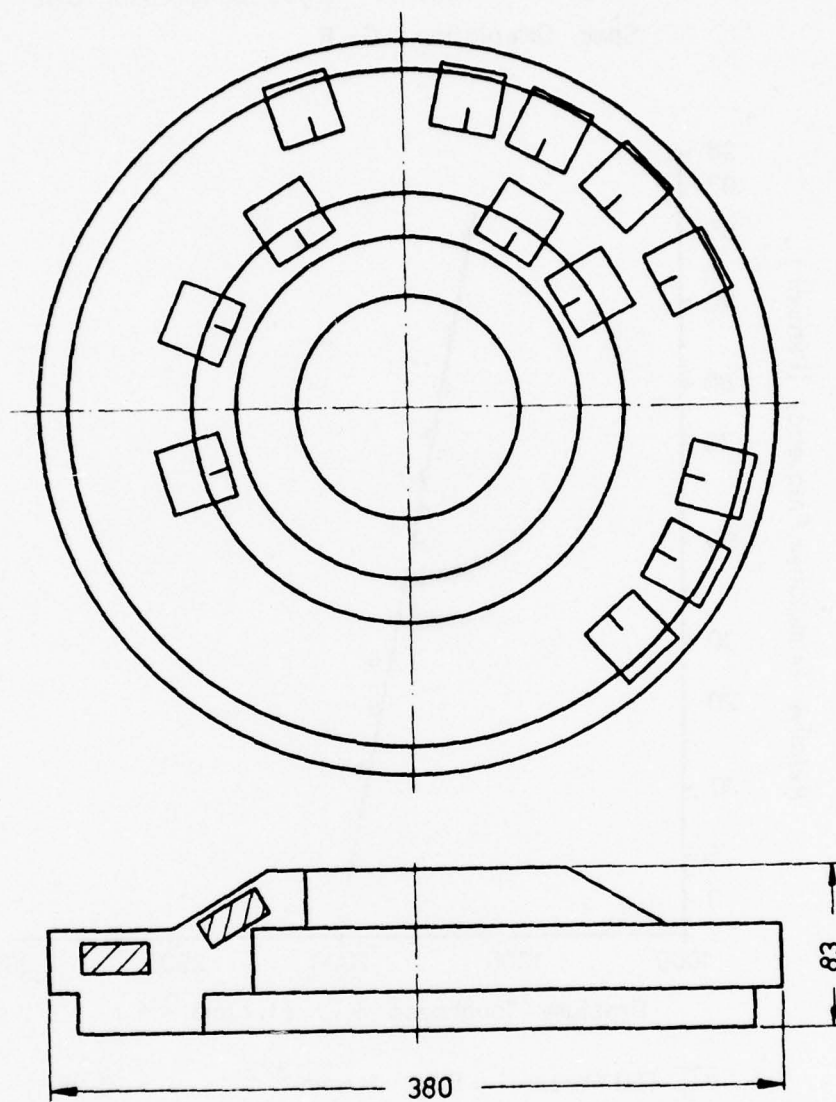
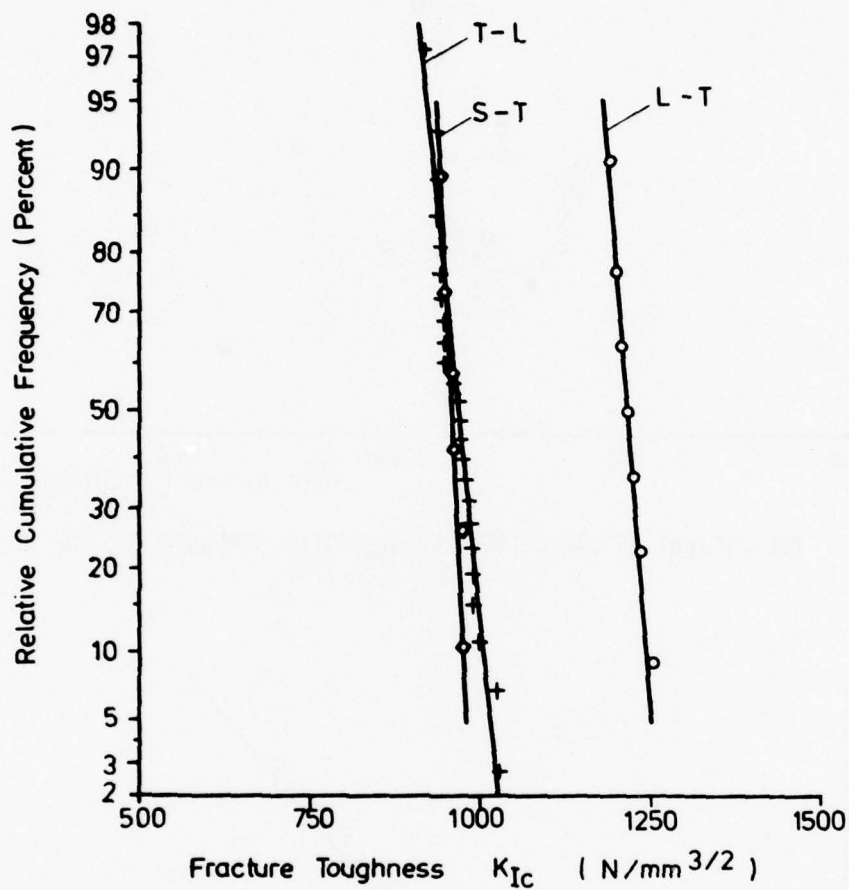


FIGURE 3. FORGED COMPRESSOR DISC OF T16AL4V  
SPECIMEN ORIENTATION

Material : 7050 - T 73651 - Plate  
2000 x 1000 x 110mm



◊ $\overline{K_{IC}}$ (50 Percent)	= 1214	$N/mm^{3/2}$	$\nu = 0,019$
+ $\overline{K_{IC}}$ (50 Percent)	= 966	$N/mm^{3/2}$	$\nu = 0,03$
◊ $\overline{K_{IC}}$ (50 Percent)	= 957	$N/mm^{3/2}$	$\nu = 0,015$

FIGURE 4. STATISTICAL EVALUATION OF FRACTURE TOUGHNESS

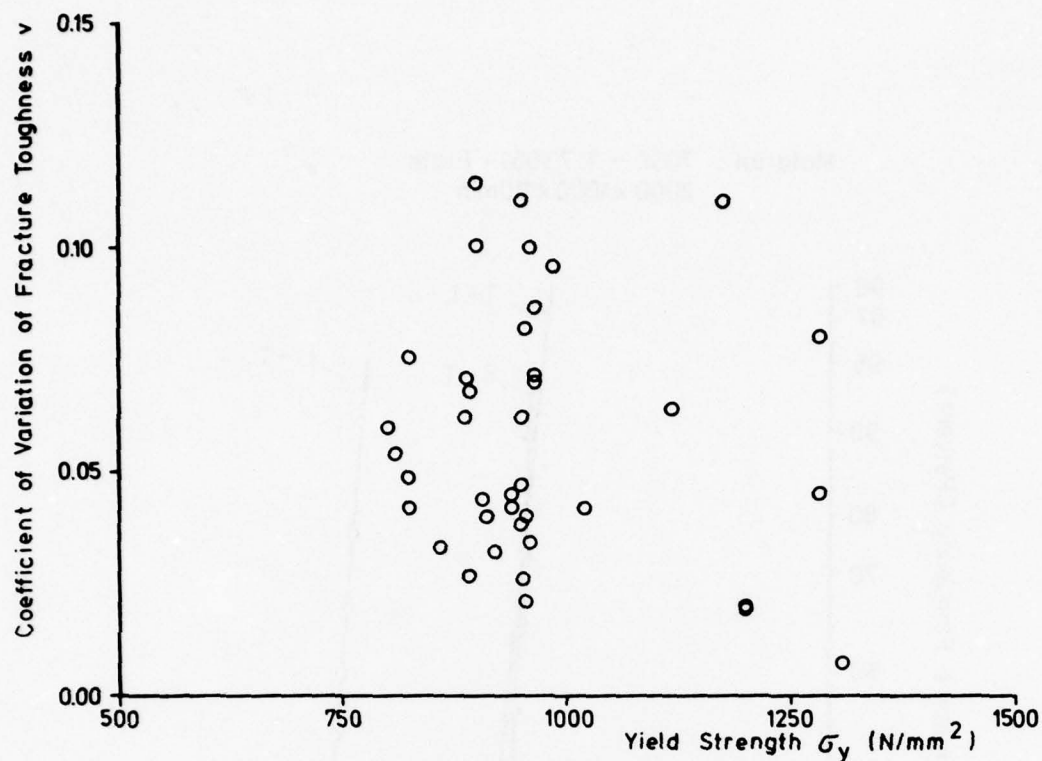
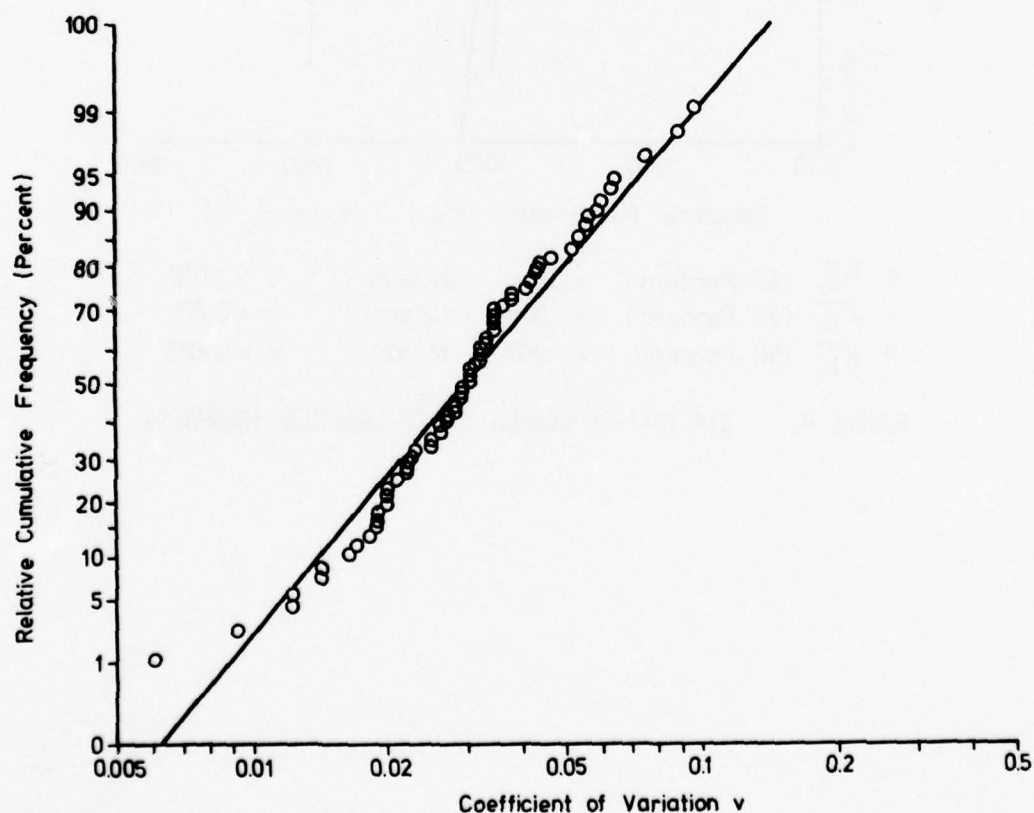
FIGURE 5. COEFFICIENT OF VARIATION  $v$  VERSUS YIELD STRENGTH  $\sigma_y$  FOR TI-ALLOYS

FIGURE 6. STATISTICAL EVALUATION OF THE COEFFICIENT OF VARIATION OF AL-ALLOYS



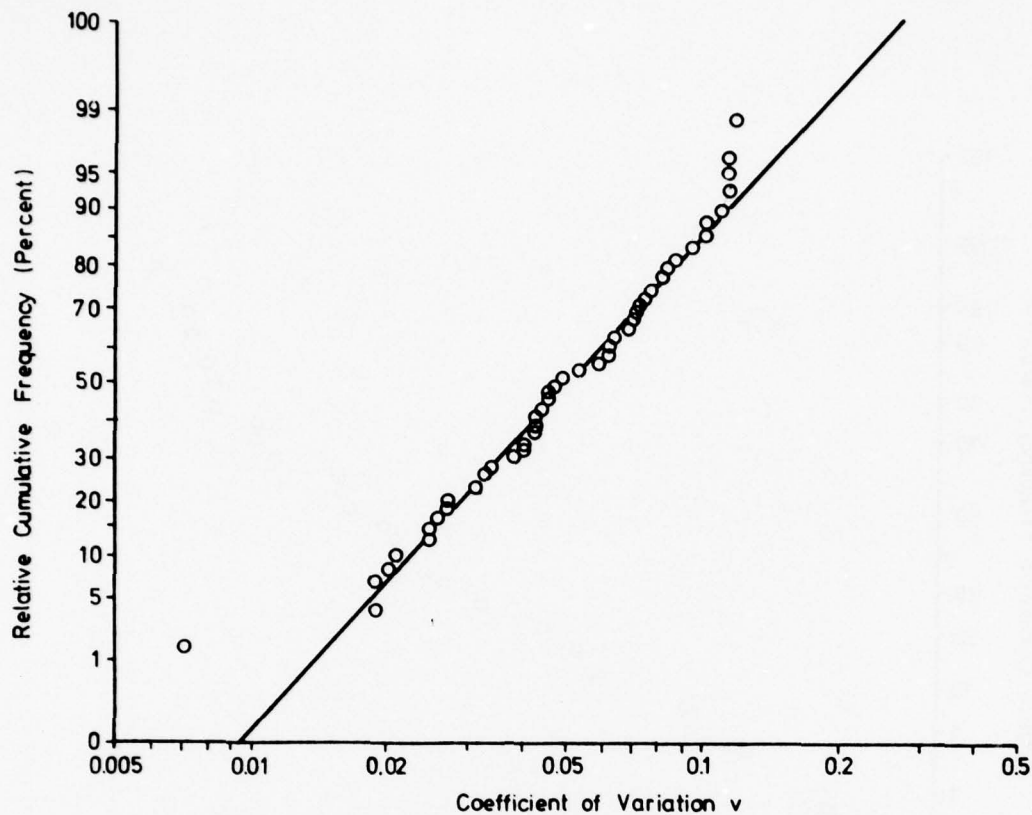


FIGURE 7. STATISTICAL EVALUATION OF THE COEFFICIENT OF VARIATION OF TI-ALLOYS

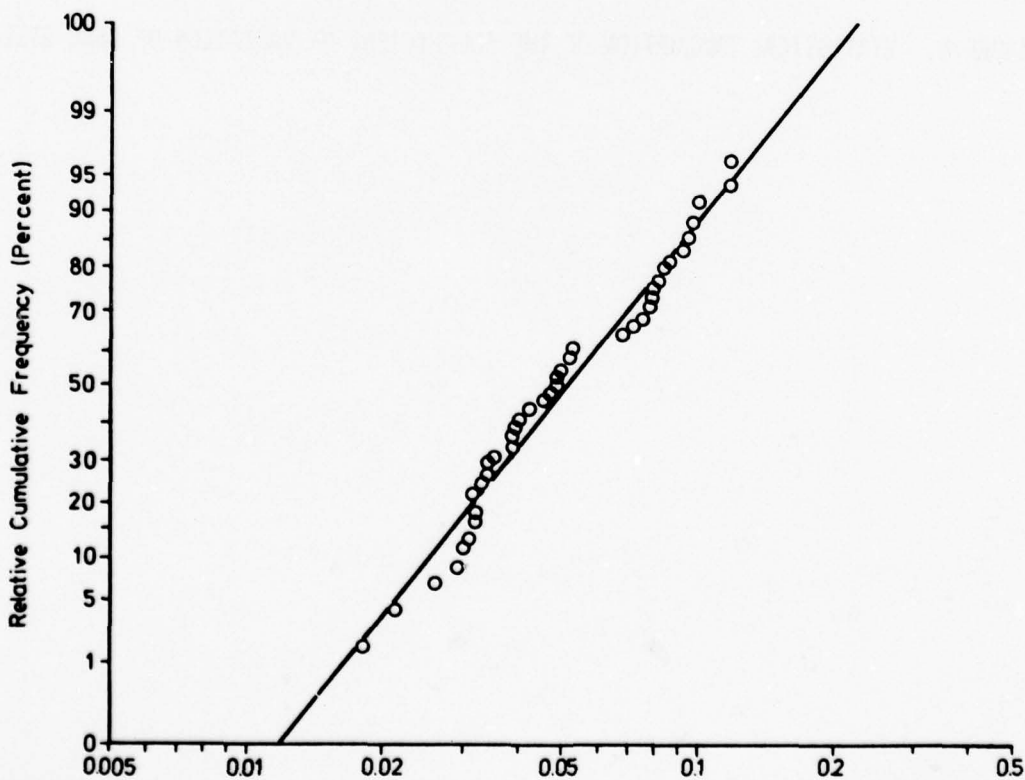


FIGURE 8. STATISTICAL EVALUATION OF THE COEFFICIENT OF VARIATION OF STEELS, EXCEPT D6AL

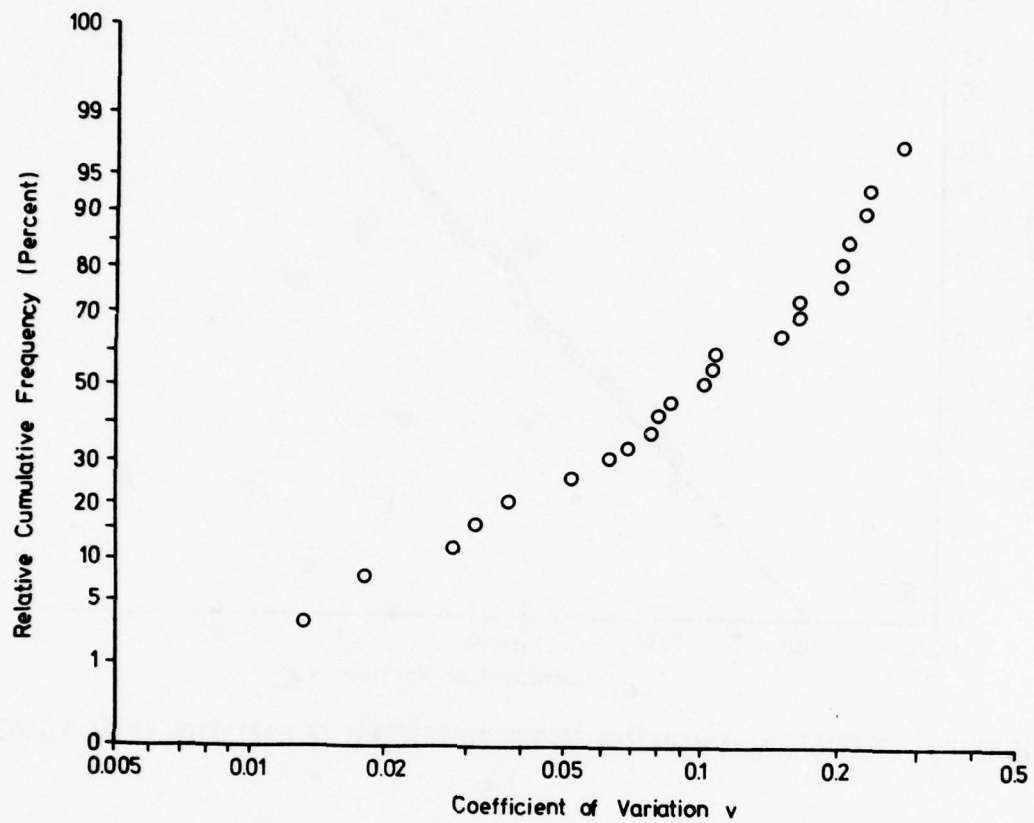
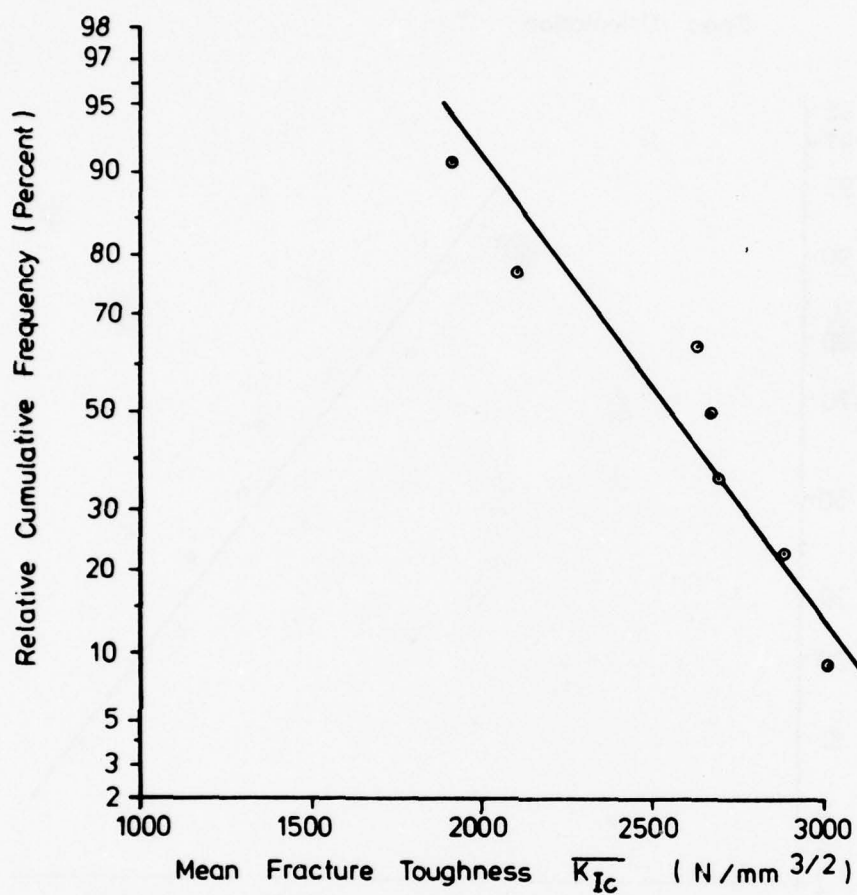


FIGURE 9. STATISTICAL EVALUATION OF THE COEFFICIENT OF VARIATION OF D6AC-STEEL

Spec. Orientation : L - T



$$\overline{K_{Ic}} (50 \text{ Percent}) = 2560 \text{ N/mm}^{3/2} \quad v = 0.16$$

FIGURE 10. STATISTICAL EVALUATION OF MEAN FRACTURE TOUGHNESS OF 7 DIFFERENT HEATS OF TI6AL4V

Spec. Orientation : T - L

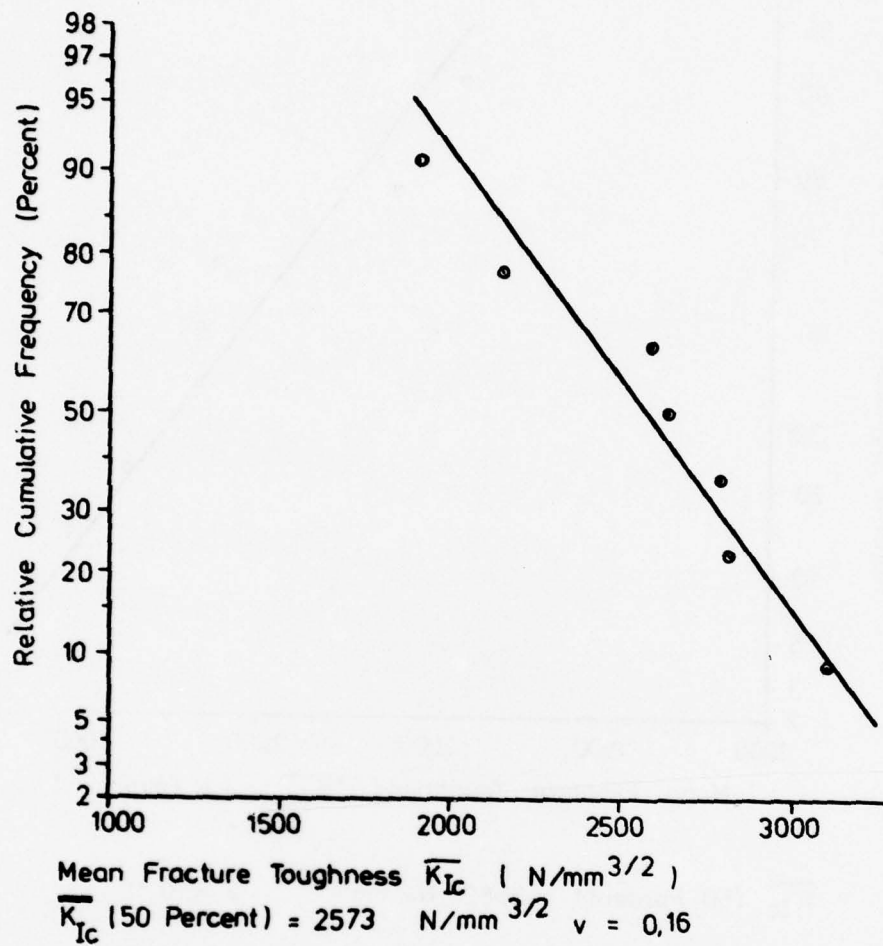
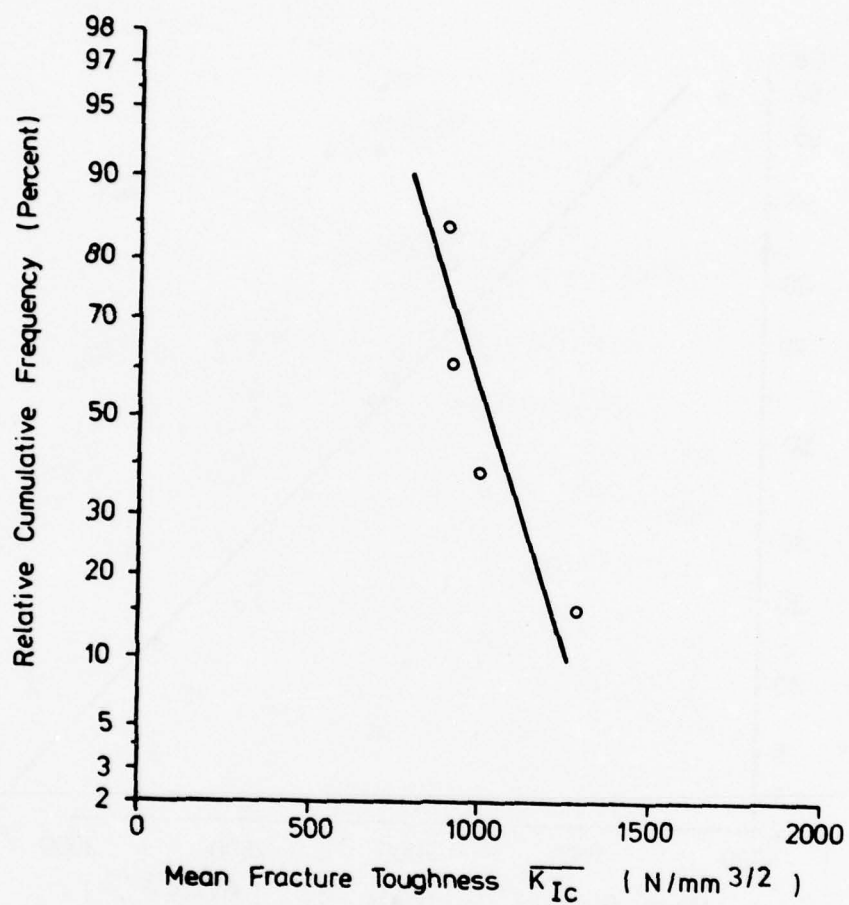


FIGURE 11. STATISTICAL EVALUATION OF MEAN FRACTURE TOUGHNESS OF 7 DIFFERENT HEATS OF TI6AL4V



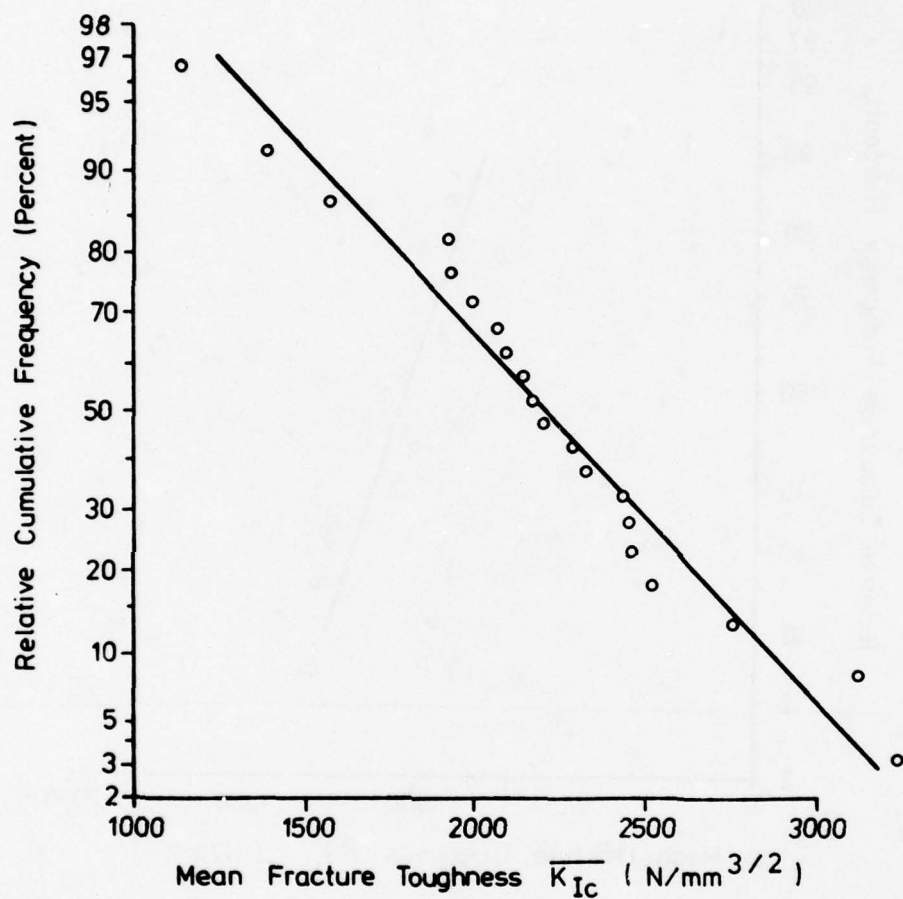
Spec. Orientation : T - L



◦  $\overline{K}_{IC}$  (50 Percent) = 1028 N/mm<sup>3/2</sup>  $v = C, 17$

FIGURE 12. STATISTICAL EVALUATION OF MEAN FRACTURE TOUGHNESS OF 4 DIFFERENT HEATS OF 7050-T73651

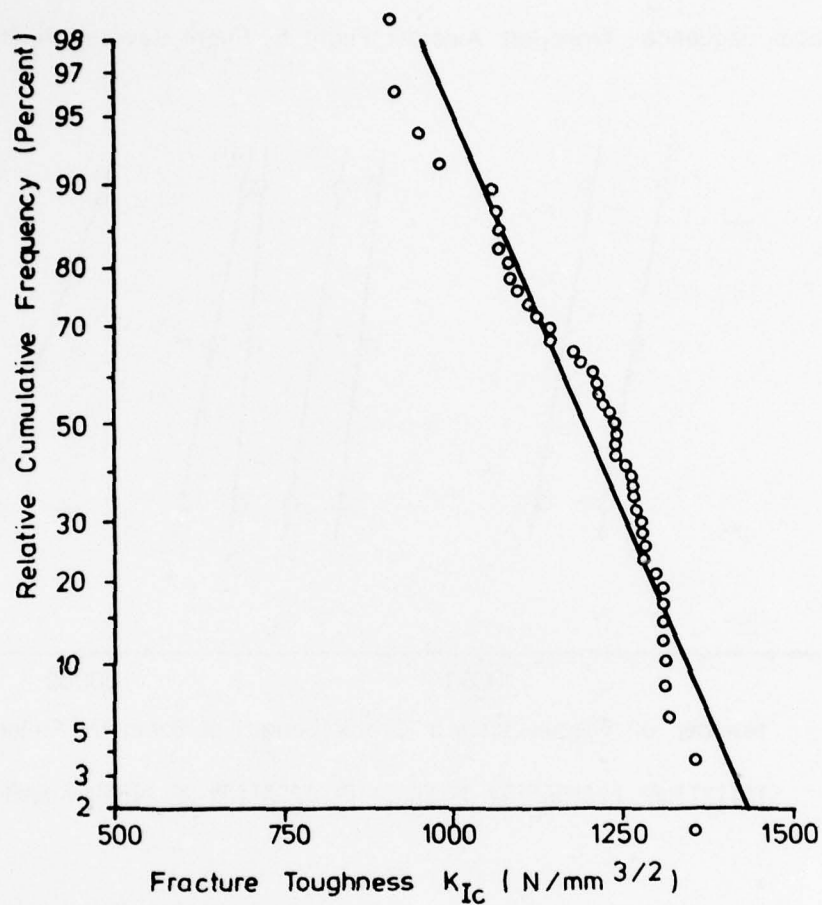
Spec. Orientation L - T



•  $\overline{K_{IC}}$  (50 Percent) = 2215 N/mm<sup>3/2</sup>  $\nu = 0,23$

FIGURE 13. STATISTICAL EVALUATION OF MEAN FRACTURE TOUGHNESS OF 20 DIFFERENT HEATS OF D6AC

Spec. Orientation : L - T



○  $\overline{K_{Ic}}$  (50 Percent) = 1195 N/mm<sup>3/2</sup>  $\nu = 0.1$

FIGURE 14. STATISTICAL EVALUATION OF FRACTURE TOUGHNESS  
OF 17 DIFFERENT HEATS OF 7050-T73561 PLATE

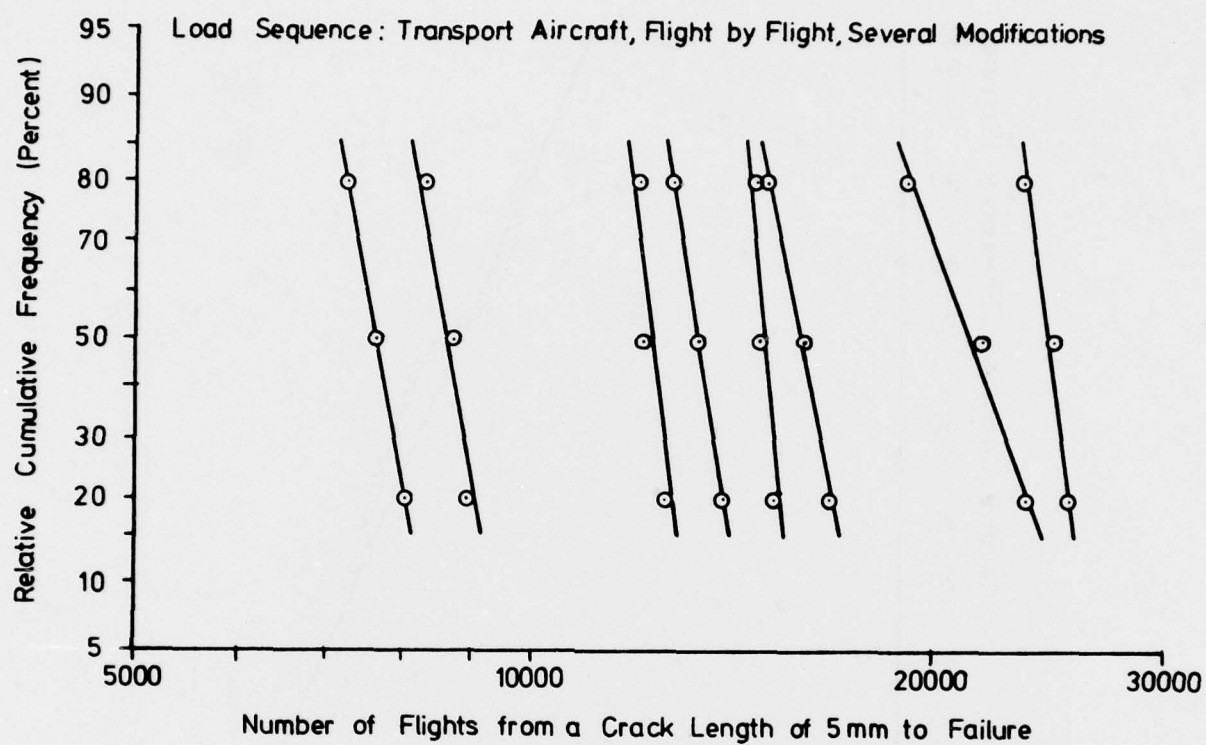


FIGURE 15. STATISTICAL EVALUATION OF CRACK PROPAGATION OF TI6AL4V SHEET SPECIMENS



## DESIGN OF REDUNDANT STRUCTURES

by  
T. Swift

Douglas Aircraft Company  
McDonnell Douglas Corporation  
Long Beach, California 90801

### SUMMARY

The selection of damage sizes to be used in the design of a large commercial transport aircraft are discussed in this paper. Development tests are described which assess the capability of different materials and structural configurations to meet the selected criteria. Correlation of various analytical methods is shown for varying degrees of damage for both fuselage and wing structural arrangements. A limited number of tests are described which verify the chosen inspection intervals for externally detectable damage after internal member failure.

### 1. INTRODUCTION

During the early design phases of an aircraft structure, decisions must be made on possible damage sizes to be sustained at limit load. These possible damage sizes can usually be defined by reviewing the structural configuration and loading environment. Once the damage size has been selected and design stress levels chosen, then candidate materials and structural configurations must be evaluated to meet the requirements. Trade studies must be performed followed by development testing to determine which combinations of material and structural arrangement will satisfy the requirements in the most economical way. One of the prime objectives of a development test program is the correlation of analytical methods. When one considers the many structural arrangements which exist in a large transport aircraft, it becomes obvious that tests cannot be conducted for each configuration. Verification of the damage tolerance criteria for most of the structure must be performed analytically. The methods must, however, be verified by a minimum of testing. Final verification of the residual strength capability as well as inspection interval selected should be determined by component testing of just a few selected areas of the structure. Inspection intervals must be set with enough margin of safety so that fatigue damage will be found before catastrophic failure. When this final selection is made, it must be remembered that the best analytical tools will result in some variations due to material scatter and the lack of ability to account for every local effect which may be present.

### 2. DAMAGE TOLERANCE DESIGN LIMITS

#### 2.1 Damage Sizes for Fuselage Residual Strength

Redundant structures are not necessarily inherently fail-safe. Commercial aircraft fail-safe requirements state simply that catastrophic failure should not occur after failure of a single principal structural element. However, if this single element failure remains undetected and the redistributed load eventually causes fatigue failure of a second element, resulting in catastrophic failure of the aircraft, then this structure, although redundant, cannot be classified as fail-safe. Detectability then becomes one of the basic elements in the design of fail-safe redundant structures. Further, when one considers the vast structural expanse of a modern transport aircraft and realizes that the majority of main structural elements are covered with insulation and furnishings, it becomes obvious that for these large expanses of basic structure, external detectability prior to catastrophic failure should be a prime design factor. The structural designer does have some control over this. For example, the upper crown of a fuselage structure is primarily designed for down-bending tension loads. The smaller, negative bending compression loads could easily be taken care of by a few large longerons spaced widely apart. If a fatigue crack developed in one of these members and the crack could not be detected because the view of the crack was blocked by inside furnishings, it could rapidly propagate to failure. The designer can improve this situation considerably by spreading out the longeron area into smaller, more closely spaced stiffeners, so that if one fails and causes a skin crack, the transfer of load from the broken longeron is not immediately catastrophic.

In order to specify the size of external damage to be designed for, one needs to consider possible sources of fatigue cracking. For the case of the fuselage basic shell, consider Figure 1. When the cabin is pressurized, radial growth of the skin is resisted by frames and longerons, causing local bending along the rivet lines. Where the skin attaches to the frame shear clips, this local bending is superimposed onto axial stresses caused by pressure and inertia bending loads, which could cause one-bay cracking between longerons at point A.

Local skin bending also occurs along the rivet line attaching the longeron to the skin. The hoop stress due to cabin pressure varies across the bay and is superimposed onto the local bending stress, causing a critical location halfway between frames. Thus, a one-bay longitudinal crack could develop between frames at point B.

At the attachment of the longeron to the frames, the local bending stresses in the longeron are superimposed onto the axial stresses due to pressure and inertia. This could cause longeron failure at C. After failure of the longeron, which is not critical if the design practices previously mentioned are followed, the skin stresses increase by a factor of about 2.2, depending on the longeron area. This increase in stress can cause a skin crack at the next attachment which could propagate into both adjacent bays, thus creating a two-bay circumferential crack at point D. In a large transport fuselage, there is usually considerable variation in bending moment around a frame due mainly to transfer of payload into the shell. This frame bending, in locations that create tension in the outer cap, will cause local increases in skin stress over the frame which are superimposed onto hoop stresses due to cabin pressure. This situation is aggravated by the discontinuous shear clip, and skin cracking could occur which would propagate into both adjacent bays, creating a two-bay longitudinal crack at E.

If there is a tendency for fast fracture to occur, the adjacent members must be designed to arrest the crack. In the case of a two-bay circumferential crack, the arrested crack size is usually 16 to 20 inches long and the two-bay longitudinal crack is 40 to 45 inches long. If there is a crack stopper strap at a frame location, fatigue crack growth in the skin will be almost completely retarded until the crack stopper itself fails. This failure may go undetected due to lack of internal visibility. The design should therefore include the capability to allow this member to fail without causing catastrophic propagation of the skin crack.

The two-bay damage quoted above is quite large and should be easy to detect by loss of cabin pressure, internal noise created by pressure escaping through the crack, or nicotine from smoking passengers and oxidization stains on the skin due to fretting.

The fuselage structure then should be designed at least to sustain the damage shown in Figure 2 for limit load application. In addition, there is a possibility of damage due to foreign objects such as parts from disintegrating engines. A section of a turbine blade, for example, could pierce the fuselage shell, resulting in a fast fracture in the skin. The damage sustained from this discrete source could also cause a frame member to fail. This damage would be obvious to the flight crew, however, and the aircraft need only be designed for those loads likely to be encountered during return to the airport. This loading is usually that associated with 1.5 g plus cabin pressure. Thus, the design should include the capability to sustain two bays of skin cracked with a broken central frame member at the loads just mentioned.

## 2.2 Damage Size for Wing Residual Strength

Accessibility to the internal wing structure for inspection purposes appears easier than in the fuselage case. However, access doors must be removed and the tanks purged with inert gas to remove fuel fumes prior to inspection. Thus, it is not as easy as merely inspecting the wing externally. There may be several locations in the wing basic internal structure which are more fatigue-sensitive than external structure such as the fuel transfer slots in the wing stringers, as illustrated in Figure 3. Also at the intersection of a wing rib with the stringer, secondary loads are introduced due to distribution of airload and rib-crushing loads caused by curvature from wing deflection. In the event of stringer failure, the skin becomes overloaded locally due to load transfer from the broken stringer, and skin cracking in two adjacent skin bays will eventually occur. The structure must therefore be designed so that the skin damage can be found externally prior to catastrophic failure. In the event that fast fracture of the crack occurs, the adjacent stiffeners must be sized to arrest the crack. The wing basic structure is therefore designed to sustain a two-bay skin crack with a broken central stiffener at limit load, as shown in Figure 3.

## 3. DESIGN DETAILS

### 3.1 Fuselage Design Features

At this point, it will be useful to note just a few features of basic fuselage detail design which can help improve the fail-safe characteristics. Figure 4a shows a DC-10 basic fuselage frame member with a separate shear clip attached to the skin. The cutout in the shear clip allows the longeron members to pass through, and is a fatigue-sensitive location: Fatigue cracking can occur in the corner of the cutout. However, if this does occur, only the shear clip cracks, leaving the frame member intact to perform its main function. In the case of the design in Figure 4b, a crack starting at this cutout would rapidly propagate through the frame, resulting in loss of bending capability.

A crack stopper strap located at the frame position as in Figure 4a will relieve the stress concentration at the first rivet in the shear clip and provide continuity across the cutout, resulting in a vastly improved fatigue life. The strap can also work as frame-bending material in addition to arresting large fatigue cracks.

Figure 4c shows a basic circumferential skin splice with internal splice plates and finger doublers. This splice is designed in such a way that fatigue cracking will always occur in the skin at the row of attachments through the finger doubler. A crack in the internal splice plate as shown would not be externally detectable. Considerable testing has been performed to perfect this design feature while maintaining more than six times the required life. Similarly, in the case of a horizontal splice, as shown in Figure 4d with both internal and external splice plates, fatigue cracking will always occur in a location which is externally visible.

### 3.2 Wing Design Features

Crack propagation tests of stiffened panels indicate that if the path of a fatigue crack, passing through a row of rivets, is greater than one fastener head diameter away from the fastener countersink, then the crack will pass near the hole without arresting in the hole. This is illustrated in Figure 5a. On the other hand, if the crack path is less than one diameter from the countersink, then the crack will certainly arrest in the hole as shown in Figure 5b. If two rows of fasteners are required, then it is an advantage to stagger the rows and make sure the distance between countersinks is less than twice the diameter, as illustrated in Figure 5c. This will ensure that the crack will always enter a rivet hole, resulting in immediate loss of the stress intensity factor. The DC-10 wing is designed to include this feature and all stringers are attached with two rows of staggered rivets at a spacing which will guarantee propagation toward a rivet hole, as shown in Figure 5d.

## 4. DESIGN STRESSES

### 4.1 Basic Fuselage Shell

The DC-10 will be considered here as an example for the damage tolerance assessment of a large transport aircraft. In the case of the basic fuselage shell structure, there are many design requirements to be met apart from the damage tolerance criteria. As indicated previously in the section on damage tolerance analysis of redundant structures, higher residual strengths can be obtained by spacing stiffeners closer together. Close spacing, however, may not result in a minimum-weight design. For example, the most efficient circumferential frame spacing for a shell radius of 118.5 inches is 20.0 inches. This has been determined from considerations of general and local instability together with payload redistribution. Similarly, the most efficient longeron spacing for the size of shell varies from 6.5 inches at the bottom to 8 inches at the top. These dimensions are more a function of material elastic modulus than any other parameter. Even though the fracture mechanics specialist may desire different dimensions to optimize his own criteria, he is forced to be realistic about this and consider other criteria as well as his own. However, damage criteria must be met and he has several options at his disposal such as choice of skin material, use of crack stoppers, or stiffener configurations, apart from stiffener spacing. The fuselage shell minimum gage is determined primarily from fatigue life considerations due to local effects of cyclic pressure.

After the damage size has been decided upon as indicated on Figure 2, a review of expected stress levels is required. Figure 6 shows the limit P/A stress levels at the crown of the shell from both cabin pressure and inertia bending. This location is the most critical for circumferential damage. It will be noted that the highest stresses are in the aft fuselage. Much of the fuselage is minimum gage which explains the lower stresses in the forward section. The most critical location for longitudinal damage is in a minimum-gage area where the shear stresses are highest and where the axial stresses are zero. This, again, is in the aft fuselage. The actual stress distribution in a fuselage shell due to pressure and shear is extremely complex to determine, and a conservative approach must be taken when considering allowable residual stresses for longitudinal damage. The hoop stress halfway between longerons varies between 65 percent of

Pr/B at the frame and 82 percent of Pr/B at midbay, defined by points A and B in Figure 6, and is fairly constant at 75 percent of Pr/B at the longeron, defined by line CD. Nominal cabin pressure is 8.6 psi with a valve tolerance of 0.5 psi, making a limit pressure of 9.1 psi. The maximum principal limit stress due to the average hoop stress and shear is about 20,000 psi in the minimum gage area at the side of the aircraft, as indicated in Figure 6. At 1.5 g plus pressure, this figure is approximately 15,500 psi. These values reduce to about 11,400 psi hoop stress only at the crown of the shell. This, of course, exists only in the skin because the frames do not react shear loads. It has been determined by residual strength tests on cracked cylinders subjected to internal pressure and shear<sup>(1)</sup> that using principal stress  $\sigma_p$  based on the following expression is about 8 percent conservative.

$$\sigma_p = \sigma_h/2 + \left[ (\sigma_h/2)^2 + \tau^2 \right]^{1/2} \quad (1)$$

where

$\sigma_h$  = average hoop stress

$\tau$  = shear stress

In general, the fuselage residual strength requirements were a two-bay circumferential crack at 34.0 ksi and a two-bay longitudinal crack at 20.0 ksi. It was decided to conservatively apply this principal stress normal to the direction of a longitudinal crack.

#### 4.2 Basic Wing Structure

The design limit stress level generally used for lower wing surface from a static viewpoint is limited to approximately 34 ksi. This is simply based on the ultimate material strength, considering a conservative fastener hole factor of 1.25 (based on past experience and tests) for 2024-T3 material, which is the prime candidate for a lower wing surface. The limiting gross area stress level to be used for residual strength with the chosen damage size is then simply two-thirds of  $64/1.25 = 34$  ksi. If this stress level could be met at the damage size decided upon, then no weight penalty would be incurred. This limit stress is also an approximate upper bound to meet fatigue life requirements.

### 5. FUSELAGE TRADE STUDIES

#### 5.1 Circumferential Crack

As stated earlier, the circumferential damage size to be sustained at a gross limit stress of 34 ksi is two bays of skin with a broken central stiffener. The stiffener spacing in the most critical location for this type of damage at the fuselage crown is 8.0 inches. The only design variables left are stiffener geometry and material, fastener spacing and type, and skin material. The skin material is the most important. Early testing had determined fracture toughness values for four candidate skin materials: 2024-T3 material, having an apparent  $K_{Ic}$  value in the region of 158 ksi $\sqrt{\text{in.}}$ , appeared to be superior. Values for other candidate materials were 52.7 to 63.5 ksi $\sqrt{\text{in.}}$  for 7075-T6, 70 ksi $\sqrt{\text{in.}}$  for 2014-T6, and 90.0 ksi $\sqrt{\text{in.}}$  for 7075-T73. All of these values were for T-L load versus crack orientation direction. Analysis was performed, using the "lumped parameter finite-element" approach, for the four candidate materials and 8-inch longeron spacing. Two sizes of hat-section longerons were chosen to be generally representative of the critical area, with a single row of rivets and two sizes of tee sections having two rows of fasteners. Geometrical details of these stiffeners have been previously published<sup>(2)</sup>. The two rows of fasteners in the tee stiffeners were simulated by a single shear panel having the same stiffness as the two rows. Figures 7 and 8 show the results for the small and large sections, respectively. Stiffener material considered was always 7075-T6 for its high strength.

The results of this study indicated a higher residual strength could be attained with tee-type stiffeners due primarily to the two rows of fasteners. A slight increase could also be expected for the tee section due to slightly lower bending stresses in tee stiffeners because their neutral axes are closer to the fastener shear face. This is illustrated in Figure 9 which shows a residual strength comparison for two configurations having Z section stiffeners. In both cases, the stiffener has the same cross section, but in case A it is assembled with the heaviest section attached to the skin. A substantial increase in strength is indicated for configuration A compared to B. Of course, the effect has been exaggerated to illustrate this point.

The most dramatic effect illustrated in Figures 7 and 8 is due to skin material. It appears that 7075-T6 and 2014-T6 materials resulted in allowables substantially lower than the requirements. Panels made from 2024-T3 appeared to be more than adequate while those made from 7075-T73 had less than desired strength but were more promising than 7075-T6 and 2014-T6 panels. It was decided to test 7075-T73 and 2024-T3 panels with the stiffener sizes referred to in Figures 7 and 8.

#### 5.2 Fuselage Longitudinal Crack

There were several questions concerning structural requirements for the longitudinal crack. First, the relative merits of configurations with and without crack stopper straps, as shown in Figure 4(a), needed to be investigated. Material requirements from a skin fracture standpoint required evaluation. Lumped parameter finite-element analyses were then performed for several structural configurations to obtain a first approximation of the effects of these variables.

In curved shells subjected to internal pressure, longitudinal crack tips are affected by a bulging phenomenon. The bulge, caused by loss of hoop tension reaction to the pressure loading, in turn causes local bending at the crack tips, which increases the effective crack-tip stress-intensity factor, as shown in Figure 10a. Work performed by Paul Kuhn<sup>(3)</sup> on this problem indicated that a factor could be applied to the stress intensity factor given by:

$$\beta_B = 1 + 5(2a)/R \quad (2)$$

where

$\beta_B$  = a bulge coefficient due to pressure and curvature



$a$  = half crack length

$R$  = shell radius.

Observations from previous water cycle tests on curved panels indicated the bulge effect was eliminated when the crack tips were in the vicinity of a frame. It was assumed, however, for the two bay crack case that maximum bulge would occur halfway between frames, but because the crack center was held by the center frame, the  $2a$  in Equation (2) would be as shown in Figure 10b. Thus for frame spacing of 20 inches the value of  $2a$  in Equation (2) would be 10. It was also assumed that the bulge would be reduced as a cosine function in the vicinity of frames, starting out as a factor of 1 at the center frame, reaching a maximum when the tip was midbay, and decreasing to 1 again at the frame. The assumed bulge factor was therefore

$$\beta_B = 1 + \frac{5(10)}{2R} \left[ 1 + \cos \pi \left( 1 + \frac{2a}{L} \right) \right] \quad (3)$$

where  $R$  is the shell radius (118.5 inches) and  $L$  is the frame spacing (20.0 inches).

The residual strength curve from a skin fracture standpoint is thus determined from

$$\sigma_c = \frac{K_c}{\beta \beta_B \sqrt{\pi a}} \quad (4)$$

where

$\beta$  = geometrical effects of stiffening

$\beta_B$  = the bulge effect

Figure 11a shows a residual strength curve for the case with crack stoppers under the frames when the center crack stopper is broken. Figure 11b shows the effect of also breaking the center frame while Figure 12 represents the case of frames without crack stoppers when the center frame is intact. A summary table of allowables for skin fracture is shown in Figure 12 based on the peak of the residual strength fracture curves. It should be noted that the stiffener criteria cannot be plotted directly on these diagrams since their loadings are complex and include such effects as bending from payload distribution. Also, the additional component of principal stress due to shear is not reacted by the frames and so their allowables cannot be plotted on the same diagram. This will be considered later.

Figure 12 indicates that only 2024-T3 material would be adequate for configurations without crack stoppers. With crack stoppers included and the center frame intact but with the center crack stopper broken, Figure 11a indicates that only 7075-T6 would be inadequate at the design principal stress. For the case where center frame and crack stopper are broken, both 2014-T6 and 7075-T6 would be inadequate. Again, as in the case of the circumferential crack, it was decided to test 2024-T3 and 7075-T73 as candidate skin materials. The two other materials, 2014-T6 and 7075-T6, were eliminated as candidates.

## 6. FUSELAGE FLAT PANEL TEST PROGRAM

### 6.1 Tests for Circumferential Crack Case

Several flat-60-inch-wide by 120-inch-long stiffened panels were tested under uniaxial loading to obtain early damage tolerance verification data. Two skin materials, 2024-T3 and 7075-T73, both 0.071-inch thick, were tested in combination with the four longeron configurations shown in Figures 7 and 8. The primary purpose of these tests was to determine their residual strength for the damage size shown in Figure 2. Longerons were initially saw cut, and half-inch saw cuts were made in the skins. Figure 13 shows one of these panels after failure. This figure also illustrates the saw cut longeron and a skin crack arrested after fast fracture. The skin cracks were propagated to predetermined lengths under constant-amplitude loading. Static loading was then applied to cause fast fracture. Two tests were performed on each panel. The first test area was repaired before the second test was conducted, which was always a test to failure. Tests conducted on the 2024-T3 panel with large hat stiffeners indicated an allowable much higher than required for the specified damage size. The second tests on each of the remaining 2024-T3 panels were modified to include two saw-cut longerons and a three-bay crack. This was done to obtain further verification and information considered useful for the foreign object damage case. Table 1 shows final failure gross area stresses and final crack lengths for these panels.

The test results for the 7075-T73 panel with large tee longerons were not straightforward, and it will be useful to follow the failure process. A skin crack over the saw-cut central longeron was propagated at a constant amplitude stress of 15.5 ksi with a stress ratio ( $R$ ) of 0.05. Static load was applied and fast fracture occurred at 24.8 ksi with a total crack length of 3.21 inches. The crack was arrested as shown in Figure 14a. Cycling was continued at 18.0 ksi,  $R = 0.05$ , and after 181 cycles, the crack was  $1/8$  inch out of the left rivet hole, as shown in Figure 14b. Static load was again applied and fast fracture occurred at 23.59 ksi in the second hole on the left, as shown in Figure 14c. Cycling was continued at 18 ksi,  $R = 0.05$ , and after 167 cycles, the crack had extended 0.42 inch from the second hole on the left and into the second hole on the right, as shown in Figure 14d. Static load was again applied and fast fracture occurred at 27.8 ksi, arresting as shown in Figure 14e. Static load was increased to 31.6 ksi when fast fracture again occurred from longeron 4 to 5, as shown in Figure 14f. At this point, four rivets had failed as noted in Figure 14f. The load was further increased and failure occurred at a gross area stress of 36.05 ksi.

### 6.2 Correlation of Circumferential Crack Cases

Because of the variability in material fracture toughness,  $K_c$  at fast fracture was calculated directly from the stiffened panel test results. Analysis then correlates with test results if arrest and final failure occur as predicted using these  $K_c$  values. Residual strength



$$\sigma_c = K_c / \left[ \beta \sqrt{\pi a} \left( \sec \frac{\pi a}{W} \right)^{1/2} \right] \quad (5)$$

where  $W$  is the panel width.

The results of tests performed on the 7075-T73 panels are shown correlated with lumped parameter finite-element analysis in Figures 15 and 16. The calculated stiffener strength curves are based on ultimate strength of the average stiffener material with coupons cut from the failed panels. Better correlation at failure was obtained generally with the tee-section stiffeners. In the case of the small hat section, Figure 17 shows test correlation using the displacement compatibility method. The prediction at final failure is better and appears to be due to this method predicting slightly lower stiffener stresses.

The only 2024-T3 panel failed from a two-bay crack was the one with a large hat longeron. Correlation of this failure was not very satisfactory using elastic analysis as described in the paper entitled "Damage Tolerance Analysis of Redundant Structures" and illustrated in Figure 33 of that paper. Through elastic-plastic analysis, however, the failure was correlated within 1 percent, as illustrated in Figure 37 of the paper just mentioned.

The only occurrence of fast fracture in the 2024-T3 panels was with the small, hat-section longeron. This occurred at an average half-crack length of 6.205 inches and a gross area stress of 39.3 ksi. Analysis based on the displacement compatibility method gave a  $K_c$  value of  $197.87 \text{ ksi}\sqrt{\text{in}}$ . This value was used to correlate the large-hat case using elastic-plastic analysis. Figure 18 shows how this crack was arrested before reaching a longeron on the left. It is interesting to note that the crack on the right passed through a rivet hole and was out of the other side before it arrested. The skin damage was extended on the left by saw cut across another bay to match the crack on the right. In addition, a second longeron was saw-cut, making the total damage three bays of skin with two saw-cut longerons. Static load was increased and failure occurred at a gross stress of 27.92 ksi with a half-crack length of 12.845 inches. A computer program, based on the displacement compatibility approach, was developed and a residual strength diagram obtained based on the  $K_c$  value of  $197.87 \text{ ksi}\sqrt{\text{in}}$ , and a stiffener ultimate strength of 86 ksi, obtained by testing coupons from the failed longerons. This diagram is shown in Figure 19. Correlation of this test was very good as indicated by the stiffener-precipitated failure in Figure 19. The failure stress level was much lower than for the large-hat section stiffener case with the two-bay damage previously mentioned. This is apparently the reason why the elastic analysis gave good correlation. This explanation is also apparently true in the case of the small- and large-tee longeron tests in combination with 2024-T3 skin material. In the case of the small-tee longeron, the skin damage was again extended into three bays and a second longeron saw-cut. The analysis was performed by simulating the two rivet rows to a single row having double stiffness. The correlation of analysis and test was reasonable with the displacement compatibility approach as indicated by Figure 20. It would have been expected from analysis that additional slow growth would have occurred to approximately half-crack length of 12.0 inches, with failure at the intersection of the two curves at 33.0 ksi. The same procedure was used with the large-tee longeron, and correlation in this case was exact, as indicated by Figure 21. It must be pointed out that some variation can be expected if standard handbook stiffener strength values are used. In the case here, it was the purpose to correlate the analytical method and so in each case the stiffener strength values were those taken from coupon tests of the failed parts.

### 6.3 Tests for Longitudinal Crack Case

Several flat, 120-inch-wide stiffened panels were tested under uniaxial loading to obtain early damage tolerance verification data for the longitudinal crack case. One of these panels is illustrated in Figure 22 after failure. Again, 0.071-inch-thick 7075-T73 and 2024-T3 materials were chosen as skin candidates. The panels were stiffened by frames and longerons representing full-scale construction. At least two tests were conducted on each panel. Three of the more interesting tests will be discussed as typical examples. In the case of the first panel, made from 7075-T73 material with 7075-T6 frames and longerons, a 3-inch saw cut was made in the skin normal to and over one of the frames in the region of the shear clip cutout, shown in Figure 4a. The frames were spaced 20 inches apart and did not include titanium crack stoppers.

Cyclic load was applied to propagate the crack to a predetermined length and then static load was applied up to a gross area stress of 17 ksi. This was done several times and eventually fast fracture occurred at a half-crack length of 17.5 inches and the crack was arrested in rivet holes at the two adjacent frames. Half-crack length at arrest was 19.63 inches. Cycling was continued at a gross area stress of 14.04 ksi,  $R = 0.05$  to propagate the cracks out of the rivet holes. The number of cycles to form a fatigue crack and propagate to a length of 0.2 inch beyond the hole edge was 43. Static load was again applied and failure occurred at a gross stress of 18.1 ksi with a half-crack length of 20.97 inches. Analysis, based on the lumped parameter finite-element approach together with a  $K_c$  value of  $92.76 \text{ ksi}\sqrt{\text{in}}$ , based on the fast fracture, resulted in the residual strength diagram in Figure 23.

As explained earlier, it was the intention to assume the principal stress caused by shear and hoop loads acted normal to the longitudinal crack. In practice, though, the frames would only react loads induced by the hoop component. The residual strength diagram in Figure 23 indicates that the strength criteria for the center intact frame and the skin fracture criteria at the failure crack length were nearly the same. In the case of the second test panel, of similar construction, the center frame was reinforced to be sure that it did not influence the failure from a skin fracture standpoint, which was the primary test purpose. The results of this test and analysis are shown in Figure 24. The failure stresses for the two panels are nearly identical, indicating that the center frame influence was not great. The failure stresses were, however, lower than the 20-ksi goal.

A third panel, still made from 7075-T73 but including titanium crack stopper straps, was tested. A 4-inch-long saw cut was made normal to and over a crack stopper strap. Constant amplitude cyclic loading was applied to give 15.0 ksi with  $R = 0.05$ . After 13,125 cycles, a crack 2.78 inches long was noticed in the 3-inch-wide titanium crack stopper. The skin half-crack length was 3.3 inches at this point. After 14,866 cycles, the crack stopper was broken and the skin average half-crack length was 9.01 inches long. The center frame outer cap was reinforced, leaving the crack stopper broken. As in the case of previous panels, static load was applied at various crack lengths and eventually fast fracture occurred at 20.14 ksi with a half-crack length of 10.285 inches. The crack was arrested in a rivet hole at both adjacent frames. Cycling was continued to reinitiate the cracks at a gross area stress of 13.18 ksi,  $R = 0.05$ , and after 894 cycles, the cracks had propagated to approximately 0.4 inch beyond the hole edges. Static load was applied and failure occurred at 25.12 ksi with a half-crack length of 20.06 inches. As before, lumped parameter finite-element analysis resulted in the residual strength diagram shown in Figure 25. The outer crack stopper strength is based on specimens cut from the crack stoppers on the failed panel. In this case, correlation was exact.

## 7. WING FLAT PANEL TEST PROGRAM

Several large panels were tested to simulate the wing lower surface. These panels were made using 2024-T351 plate and 7075-T6 J-section stiffeners with two rows of fasteners. The material in this case had been previously selected, based on unstiffened, center-cracked panel tests. A typical panel is shown in Figure 26 mounted in a large fatigue-testing machine. The panel shown measures 8 feet wide by 17 feet long. The skin was 0.267-inch thick and stiffeners, spaced at 6.0 inches, were 0.732 in.<sup>2</sup> in area. This panel is considered comparatively light. The center stiffener was saw-cut, and a saw-cut was made in the skin over the saw-cut stiffener. A fatigue crack was propagated into both adjacent skin bays under constant-amplitude loading. Again, as in the case of fuselage panels, the primary objective here was to determine the residual strength with two-bay damage. Several applications of fail-safe load were applied up to 34.0 ksi at increasing crack lengths without fast fracture. The panel finally failed at 33.8 ksi with a half-crack length of 6.5 inches. Analysis was performed using the elastic compatible displacement approach. In this case, the fasteners were individually represented at their appropriate locations. However, all fastener loads were referred to the stiffener neutral axis so that stiffener bending only in one plane was considered. Fracture toughness values for this material and loading direction were available only for 30-inch-wide panels, which was not considered wide enough to give valid  $K_{Ic}$  values for this material. In the absence of these data, the value of 198 ksi $\sqrt{\text{in.}}$  was used, based on fuselage test results. The resulting correlation is shown in Figure 27 and the prediction is within 6-1/2 percent of the test value using the elastic analysis approach.

Figure 28 shows a test panel representative of the lower wing surface in a location requiring a heavy cross-sectional area. The skin was 0.7-inch-thick 2024-T351 plate with stiffeners spaced at 9.5 inches and having a cross-sectional area of 3.34 in.<sup>2</sup>. The center stringer was saw-cut, and, again, a saw cut was made in the skin which was propagated into both skin bays. A fail-safe load, identical to the previous test, was applied. The panel failed at a gross area stress of 34 ksi with a half-crack length of 10.19 inches. Again, elastic compatible displacement analysis was performed using a  $K_{Ic}$  value of 198 ksi $\sqrt{\text{in.}}$ . Note that this value was not reduced due to increased skin thickness. The resulting residual strength diagram is shown in Figure 29. This correlation is apparently extremely close, and failure is predicted due to skin fracture. However, in practice, the panel failure was precipitated by rivet failure in the two-crack arresting stiffeners, as illustrated in Figure 30. Based on the elastic analysis, this phenomenon would occur at a gross stress of 14.25 ksi, which of course is far from the truth. A plastic analysis was conducted using the bielastic model shown in Figure 31a for rivet load displacement characteristics. The rivets were assumed to be in a single row with double stiffness. The compatible displacement analysis resulted in the first rivet load versus panel gross stress, as shown in Figure 31b. This figure shows that the rivet would fail at a gross stress of 35 ksi rather than 14.25 ksi for the elastic analysis. Actual failure occurred, as mentioned, at 34 ksi. This again illustrates the need for plastic analysis to predict the correct gross stress at rivet failure. However, it should be noted that the elastic approach will predict failure stress fairly closely, as has been demonstrated here for panels with various configurations and sizes.

## 8. FUSELAGE CURVED PANEL TESTS

### 8.1 Test Description

Several large, curved panels were tested under constant-amplitude loading which simulated internal cabin pressure plus inertia bending loads. The simulated cabin pressure was provided by a vacuum chamber, fitted with a pressurized rubber seal, which was lowered onto the panel. Pressure loading was reacted by whiffletrees along the edge of the panel, and axial loads, simulating longitudinal pressure and inertia loads, were applied to the ends of the panels by hydraulic jacks. The concept is illustrated in Figure 32. Fatigue tests were conducted on these panels, followed by damage tolerance tests. In some cases, saw cuts were made in the skins and propagated under cyclic loads to form fatigue cracks. Residual strength tests were also performed for both longitudinal and circumferential damage.

### 8.2 Correlation of Bulge Factor

One out of six curved panels tested was made from 7075-T73 material; all others were 2024-T3. This panel was the only one in which a fast fracture could be simulated. The high fracture toughness of the 2024-T3 material made it impossible to cause a fast fracture under representative cabin pressure loads in these panels. A 6-inch-long saw cut was made in the 7075-T73 panel over a frame and a longitudinal skin crack propagated into adjacent skin bays under cyclic pressure loads. At several crack lengths, static pressure load was increased to cause fast fracture. This eventually occurred at a half-crack length of 12.5 inches and simulated cabin pressure of 10.45 psi, which corresponds to an average hoop stress of 12.17 ksi, based on stress equations which account for frame and longeron stiffening<sup>(4)</sup>. The critical stress at fast fracture was calculated from an equation similar to (4) but with the secant panel width correction factor. The value of  $\beta_B$  was determined from Equation (3) and  $\beta$  was obtained by lumped parameter finite-element analysis. The value of  $K_{Ic}$  used was 92.25 ksi $\sqrt{\text{in.}}$ , an average from flat panel tests illustrated in Figures 23 and 24. The resulting calculated stress at fast fracture was 12.96 ksi, 6 percent higher than the actual stress. The arrested crack was repaired and the test repeated. The results of these two tests are shown in Table 2.

### 8.3 Test Results of 2024-T3 Curved Panel

Space limitations made it difficult to describe all tests performed on the curved panels, a typical example of which is shown in Figure 33 after failure from a circumferential crack. However, one longitudinal crack test used to verify the damage tolerance size requirements is worth reporting. After 92,975 constant-amplitude load cycles, simulating a GAG case, a 3-inch-longitudinal saw cut was made over an intact titanium crack stopper strap. Cyclic pressure of 9.3 psi was applied, and after 8,654 cycles, a noticeable fatigue crack was detected at the ends of the saw cut. After 20,000 cycles, the center crack stopper had not broken and little crack growth had occurred. Cyclic pressure was increased to 10.73 psi (to include effects of skin shear). At 32,157 cycles, the crack stopper was still intact and since little skin growth had occurred, it was decided to saw-cut the crack stopper. Cycling was continued at 10.73 psi until the total skin crack length  $2a$  was 16.9 inches. Static pressure was increased to 14.34 psi to check for fast fracture. The crack extended to a total length  $2a$  of 17.22 inches but remained stable. Cycling was continued until the total crack length  $2a$  was 18.96 inches, 38,019 cycles after the start. Static pressure was again increased to 14.44 psi and the crack extended to a total length of 19.1 inches but remained stable. Cycling was continued until the crack was 20.05 inches long, after 48,511 cycles. At this point, the skin crack was saw-cut to a total length of 23.03 inches to make it symmetrical about the center frame. The crack had extended about 2 inches longer on one side than the other. Cycling was again continued until the total crack length was 24.89 inches. Static pressure was applied to 14.49 psi and the crack extended to a total length of 25.28 inches. Cycling was again continued until the crack length was 31.03 inches. Static pressure was again applied, and at 12.06 psi the center frame failed. The crack extended to 32.83 inches total but remained



stable, as shown in Figure 34. The pressure was increased to 14.59 psi and the crack extended to 34.94 inches but remained stable. At this point, the crack was heading for the center of a shear clip which was not the most critical position. It was therefore decided to extend the crack by saw-cut toward the shear clip cutout, shown in Figure 4(a). The resulting configuration is shown in Figure 35. Static pressure was increased to 12.88 psi when the two outer crack stoppers failed. The skin crack was still stable but extended to 45.56 inches. At this point, a crack was detected in one of the outer frames, adjacent to the broken central frame, and was arrested in a rivet hole, as shown in Figure 36. Pressure was reapplied and complete failure occurred at 13.13 psi. The total number of pressure cycles applied to this panel was 141,574, representing 94 years of airline service at the current utilization rate of 2 hours per flight and 3000 hours per year. A lumped parameter finite-element analysis was performed for the failure skin crack length.

The frame crack into the rivet hole illustrated in Figure 36 was simulated by reduction in area of an idealized bar in the appropriate location. The resulting skin crack-tip stress-intensity factor at failure was  $107.4 \text{ ksi}\sqrt{\text{in}}$ . Values as high as  $130 \text{ ksi}\sqrt{\text{in}}$  had been applied during the test so that skin-precipitated failure was ruled out. The finite-element analysis predicted an outer-frame outer-cap stress at failure to be 73.9 ksi. Coupons cut from the broken frame gave ultimate strength values varying between 73.16 and 74.02 ksi. It was therefore concluded that final failure was precipitated by outer frame failure. The results of this test are shown in Figure 37.

## 9. FUSELAGE SKIN MATERIAL SELECTION

Tests on flat 7075-T73 panels for the circumferential crack case confirmed the analysis and indicated that the desired gross stress of 34.0 ksi could not be met with this material, as shown in Table 1. The choice of 2024-T3 material would easily satisfy the requirements. With crack stopper straps, the longitudinal damage requirements could be met with 7075-T73, as indicated by Figure 25, but the question of frame bending, adding local skin stresses, could cause the crack to extend beyond the frame. However, with 2024-T3 skin and crack stoppers, Figure 12 indicates an allowable of 51.2 ksi for skin fracture, which would amply cover the frame bending condition at limit stress since the static ultimate strength of the skin would limit the limit stress to about 41.3 psi. In view of this, 2024-T3 was chosen for the skin.

## 10. FUSELAGE DAMAGE TOLERANCE SIZE VERIFICATION ANALYSIS

The choice of 2024-T3 skins easily satisfied the damage size requirements of Figure 2. This is illustrated in Figure 11. However, it must be shown that the crack arresting outer members remain intact. A simple residual strength diagram will not show this due to the complexity of the stiffener loading. In the case of the DC-10 aircraft, stiffening elements of the entire shell were checked for the loading shown in Figure 38 to be sure they would remain intact. The skin crack was assumed to be  $(40 + 30B)$ , where  $B$  is the skin thickness. This was to allow for any crack extension due to increased skin stress from frame bending.

## 11. EFFECTS OF STIFFENING ON CRACK GROWTH

It has been shown from a residual strength standpoint that the calculation of  $\beta$  by both finite-element and compatible displacement methods appears to be fairly accurate. The variation of  $\beta$  in stiffened panels can also be experimentally determined and compared to analysis. Several center-cracked stiffened panels were tested under constant-amplitude loading. The panels, made from 0.063-inch-thick 2024-T3 and measuring 48 by 48 inches, were fitted with crack stoppers 15 inches apart. The crack stoppers were made from 0.063, Ti6Al-4V titanium 2.25 inches wide, riveted with two rows of rivets at 1-inch spacing. Cracks in the panels were propagated between rivets. Crack growth rates for both stiffened and unstiffened control panels were plotted against half-crack length  $a$ . A curve of  $da/dN$  versus  $\Delta K$  was obtained for the unstiffened panel. At various crack lengths,  $da/dN$  was obtained for the stiffened panel. The values of  $\Delta K$  were then obtained from the curve of  $\Delta K$  versus  $da/dN$ . The value of  $\beta$  was then obtained from:

$$\beta = \frac{\Delta K (\text{unstiffened panel})}{\Delta K (\text{stiffened panel})} \quad (6)$$

Analysis of the stiffened panels was performed to obtain  $\beta$ , using the displacement compatibility approach. Two methods of idealizing the strap were used. The first one assumed only one row of fasteners in the strap at its center but with double stiffness. The second treated the strap as two separate straps with areas centered on the rivet rows. The straps were uncoupled. Figure 39 shows correlation between analysis and test for three of the panels.

## 12. INSPECTION PROGRAM

The structural inspection plan for a large commercial aircraft such as the DC-10 is defined in the Maintenance Review Board report. This document outlines the basic requirements for an approved initial maintenance program for the aircraft. The report is developed by a Maintenance Steering Committee composed of the airframe manufacturer, the engine manufacturer, and the operating airline, and is based on Handbook MSG-2, "Airline Manufacturer Maintenance Program Planning Document." The program is a constant density sampling that requires participation of all airplanes in a fleet defined for each carrier or group of carriers sharing inspection resources. The structures program includes 100 percent inspection of specified interior and exterior items, as well as sample inspection of fractions of each operator's fleet which must be done by a specified time. The structure is divided into zones which include structurally significant items (SSI's). Three types of SSI's are specified in the structures program: external, internal, and internal with external visibility. The sampling program is conducted in the following manner. For example, if an SSI is selected for the sampling program at 20,000 hours and the sampling fraction is one-fifth, then one-fifth of all operators' fleets must be inspected prior to 20,000 hours. SSI's considered to be more critical are given 100 percent inspection - that is every aircraft in each operator's fleet is inspected. There are 543 SSI's in the DC-10 inspection program. The 100 percent program includes 287 of these, and 306 are in the sampling program. Inspection intervals are basically 4000, 8000, 12,000, 16,000, and 20,000 hours. The 100 percent inspection program is broken down as follows:

36 external items inspected every 4000 hours  
94 external items inspected every 8000 hours  
119 external items inspected every 12,000 hours

10 internal items inspected every 4000 hours  
28 internal items inspected every 8000 hours

The sampling program includes only internal items as follows:

18 items, 1/7<sup>th</sup> inspected every 16,000 hours  
6 items, 1/6<sup>th</sup> inspected every 16,000 hours  
2 items, 1/5<sup>th</sup> inspected every 16,000 hours  
131 items, 1/7<sup>th</sup> inspected every 20,000 hours  
102 items, 1/6<sup>th</sup> inspected every 20,000 hours  
47 items, 1/5<sup>th</sup> inspected every 20,000 hours

In addition to these inspections, A and C checks are made. The A check consists of walk-around inspection of special items every 250 hours. The C check consists of a condition check of installations by zones, and is performed at 2000-hour intervals. Operators performing inspections must be equipped with inspection techniques such as X-ray, sonic, inspection, or eddy current radio isotope.

### 13. WING INSPECTION INTERVAL VERIFICATION

As previously noted, it is highly desirable for damage in basic structure to be externally detectable prior to reaching critical proportions. Crack growth tests were performed to verify that after failure of an internal member, an externally detectable skin crack would not propagate to a critical length within two inspection intervals. An example of one such test is described here. A panel similar to the one illustrated by Figure 28 was tested under flight-by-flight spectrum loading. The center stiffener, having dimensions identical with those shown in Figure 29, was completely saw-cut and a saw cut made in the skin, as shown in Figure 40. Constant-amplitude cyclic loading was applied initially to generate a crack from the saw cut prior to the application of flight-by-flight loading. Analysis was performed to correlate the test. The effects of the broken stiffener were obtained by the compatible displacement approach and  $\beta$  values were thus obtained from the analysis used to generate the residual strength diagram of Figure 29. These  $\beta$  values were corrected to account for the hole using the Bowie correction factors for a through crack at a hole. The Bowie factors were multiplied by the  $\beta$  values obtained from compatible displacement analysis. Forman's equation for 2024-T3 material was used to determine the crack growth rate as a function of  $\Delta K$ <sup>(5)</sup>. Cycle-by-cycle analysis was performed without accounting for any retardation effects, using a computerized crack growth rate integration program. The resulting correlation is shown in Figure 40. It should be pointed out that the  $K_{Ic}$  value used in Forman's equation was 83 ksi, whereas the value used to correlate residual strength tests having long cracks was 198 ksi $\sqrt{\text{in}}$ . The results of this test and analysis indicated that the initially detectable crack would not become critical for at least two external inspection intervals.

### 14. FUSELAGE INSPECTION VERIFICATION

Verification of inspection intervals for critical damage tolerance areas in the fuselage basic shell structure was obtained generally from curved panel testing. Some information was also obtained during full-scale fatigue testing. As an example of this verification testing, a test on one of the large curved panels, described in Section 8.3, will be discussed here. This example will also serve to illustrate the external detectability philosophy used for basic shell structure.

During fatigue testing of a large curved panel, similar to the one illustrated in Figure 33, a 7075-T6 longeron was found to be cracked at 63,600 equivalent flight hours. The test was being conducted under biaxial loading conditions to simulate a GAC cycle, including the effects of cabin pressure combined with fuselage bending stresses. Axial applied P/A stress was 15.5 ksi and simulated cabin pressure was 9.3 psi. Equivalent flight length was 1.43 hours. The longeron failed completely 26,180 hours after the initial crack was discovered. To form a skin crack of 0.5-inch detectable length over the failed longeron required 38,600 hours. An additional 30,600 hours were required to propagate the skin crack to a two-bay length, considered critical at limit stress. Axial load was applied to give a gross skin stress of 36 ksi at this crack length (17.8 inches) without causing the panel to fail. This sequence of events is illustrated in Figure 41. In this case, at least four 16,000-hour internal inspections have been made before a detectable crack has formed in the skin. Seven external inspections are made between externally detectable and critical crack lengths.

No attempt was made to correlate the longeron crack growth, subjected to bending caused by cabin pressure and axial stresses from fuselage bending. However, it was possible to predict formulation of the skin crack using conventional fatigue analysis methods. Lumped parameter finite-element analysis predicts the stress distribution in the vicinity of a broken longeron, as shown in Figure 42.

The first rivet load, adjacent to the failed longeron, is also shown. Using the stress severity concept<sup>(6)</sup> for this geometric configuration gave an effective stress  $\sigma_{eff}$  as follows

$$\sigma_{eff} = 0.51 \sigma_{br} + \sigma_{bp} \quad (7)$$

where

$\sigma_{br}$  = Bearing stress at rivet

$\sigma_{bp}$  = Bypass stress (unloaded side of rivet)

Axial skin stress<sup>(4)</sup>  $\sigma$  was 16.92 ksi ( $R = 0.18$ ). Bearing stress  $\sigma_{br}$  was 26.0 ksi. The bypass stress on the unloaded side of the rivet was 1.331 (16.92) giving 22.52 ksi. Thus, the effective stress  $\sigma_{eff}$  became 35.78 ksi. Fatigue Sn data for basic fuselage construction is shown in Figure 43. A fatigue crack could be expected in the skin at 29,000 cycles (41,470 hours). This overestimates the test result by 7 percent, which is considered very close. The scatter in results could generally be expected to be much greater than this. After failure of the longeron and formulation of the skin crack as described above, 30,600 hours of testing were required to reach a two-bay length. This crack growth was correlated using Forman's equation (5) for 2024-T3 together with  $\beta$  values obtained by finite-element analysis. These  $\beta$  values are published for a small hat-section longeron<sup>(1)</sup> as in Case 15. The analysis predicts that the skin crack will grow to a two-bay length in 17,160 hours, which is only a little over half the time taken in the test. In this case, therefore, the analysis was conservative to a considerable degree. A possible explanation for this is that the test panel was biaxially loaded whereas this was not accounted for in the analysis.



## REFERENCES

1. Swift, T., The Application of Fracture Mechanics in the Development of the DC-10 Fuselage, in Fracture Mechanics of Aircraft Structures, AGARD-AG-176, 1974, pp. 227-287.
2. Swift, T. and Wang, D. Y., Damage Tolerance Design-Analysis Methods and Test Verification of Fuselage Structure. AFFDL-TR-70-144, 1970.
3. Kuhn, P., Notch Effects on Fatigue and Static Strength, in Current Aeronautical Fatigue Problems. Proceedings of ICAF Symposium held in Rome, 1963.
4. Flugge, W., Stress Problems in Pressurized Cabins, NACA TN2612, August 1965.
5. Forman, R. G., Kearny, V. E., and Engle, R. M., Numerical Analysis of Crack Propagation in Cyclic Loaded Structures, Journal of Basic Engineering, Trans of ASME, Vol. 89, Sept 1967.
6. Jarfall, L., Fatigue Cycling of Bolted Joints, FFA Report HF-1239, May 1967. (NTIS N68-37213)

## ACKNOWLEDGMENT

The author wishes to express his appreciation to D. Y. Wang for his help in conducting the tests described herein.

TABLE 1  
CIRCUMFERENTIAL CRACK FLAT PANEL TEST RESULTS

SKIN MATERIAL	LONGERON TYPE	LONGERON NET AREA (SQ IN.)	DAMAGE TYPE	FAILURE STRESS (KSI)	FAILURE CRACK LENGTH $2a$ (IN.)
7075-T73	HAT	0.3029	2 BAY	31.20	16.31
	HAT	0.5121	2 BAY	29.60	16.70
	TEE	0.2895	2 BAY	29.61	17.81
	TEE	0.4865	4 BAY	36.05	32.00 (1)
2024-T3	HAT	0.3029	3 BAY	27.92	25.69 (2)
	HAT	0.5121	2 BAY	39.74	19.76
	TEE	0.2895	3 BAY	30.97	23.27 (2)
	TEE	0.4865	3 BAY	34.29	24.21 (2)

(1) CENTER STIFFENER SAW CUT, OTHERS INTACT PRIOR TO FAILURE

(2) TWO CENTER STIFFENERS SAW CUT

TABLE 2  
CORRELATION OF STRESS AT FAST FRACTURE  
IN 0.08-INCH 7075-T73 STIFFENED CURVED PANEL

$a_c$ (IN.)	$\beta$ (1)	$\beta_B$ (2)	CALCULATED $\sigma_c$ (KSI) (3)	TEST $\sigma_c$ (KSI)	PRESSURE $P_c$
12.5	0.8163	1.36	12.96	12.17	10.45
12.1	0.8264	1.378	13.02	12.58	10.8

(1) LUMPED PARAMETER FINITE-ELEMENT ANALYSIS

(2) EQUATION (3)

(3) EQUATION (4) MODIFIED BY SECANT TERM FOR WIDTH EFFECT

$K_c = 91.43 \text{ KSI/IN. (FLAT PANELS)}$

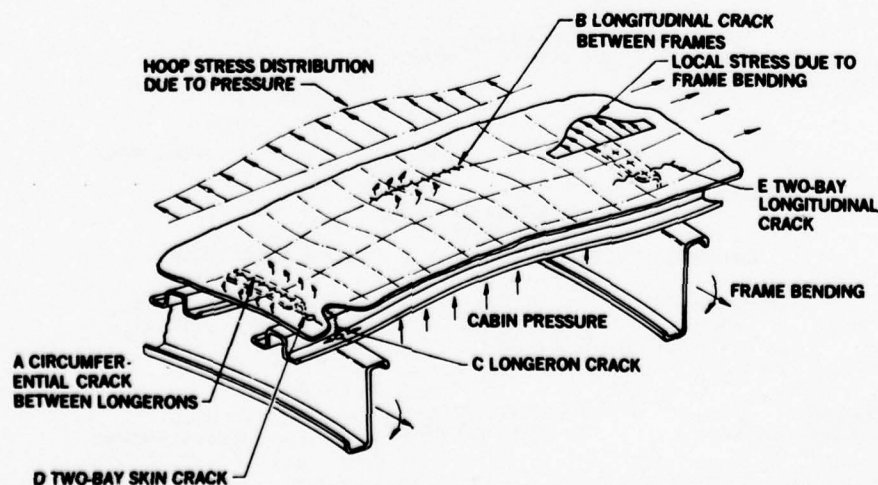


FIGURE 1. FATIGUE-SENSITIVE AREAS IN FUSELAGE BASIC SHELL STRUCTURE

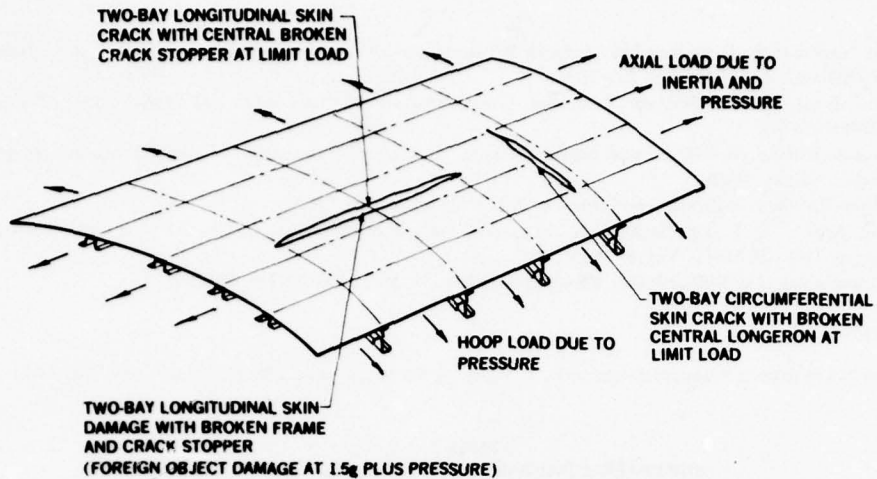


FIGURE 2. FUSELAGE DAMAGE TOLERANCE SIZES FOR STRUCTURAL DESIGN

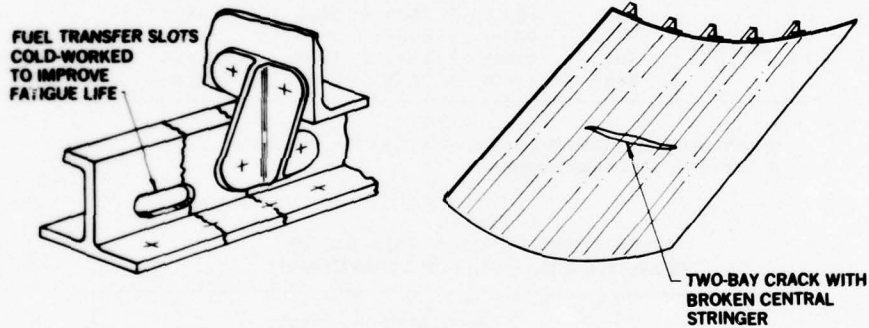


FIGURE 3. WING DAMAGE TOLERANCE SIZES

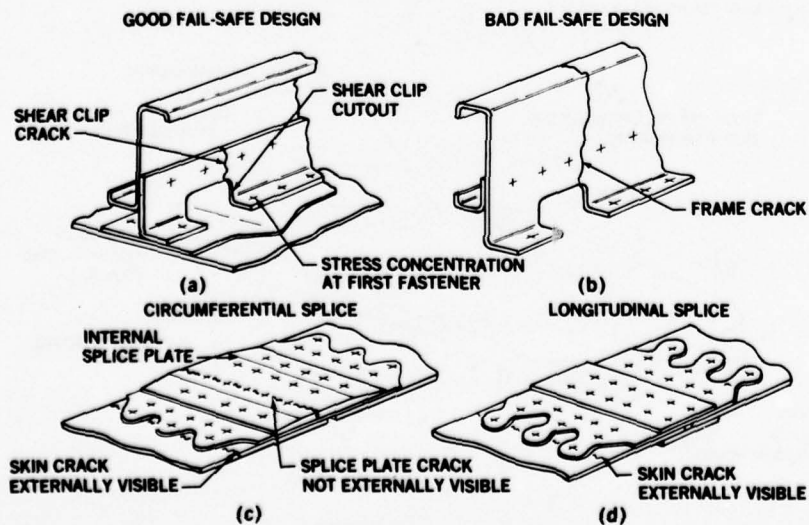


FIGURE 4. FUSELAGE STRUCTURAL DESIGN DETAILS

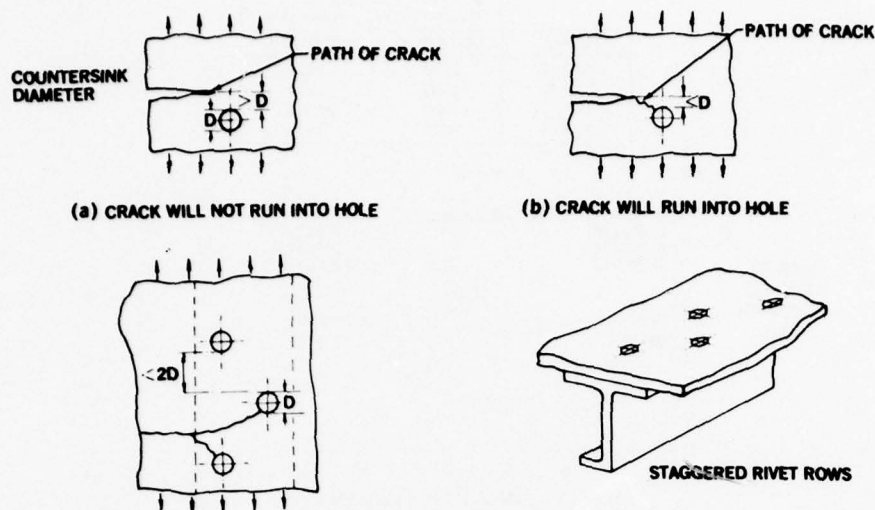


FIGURE 5. WING DESIGN FEATURE

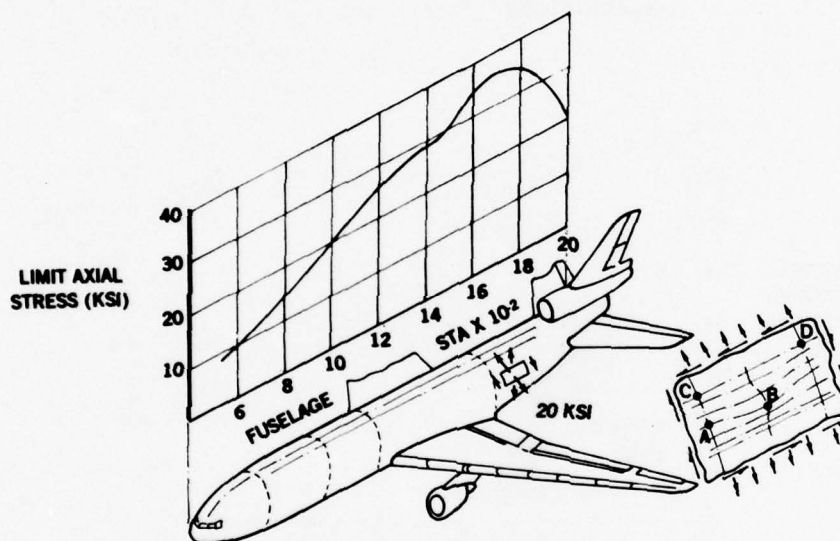


FIGURE 6. FUSELAGE SHELL CROWN AXIAL P/A STRESS DISTRIBUTION

MATERIAL	CALCULATED ALLOWABLE (KSI)	
	SMALL TEE	SMALL HAT
7075-T6	16.48	13.60
2014-T6	21.60	18.40
7075-T73	27.68	23.32
2024-T3	39.20	36.48

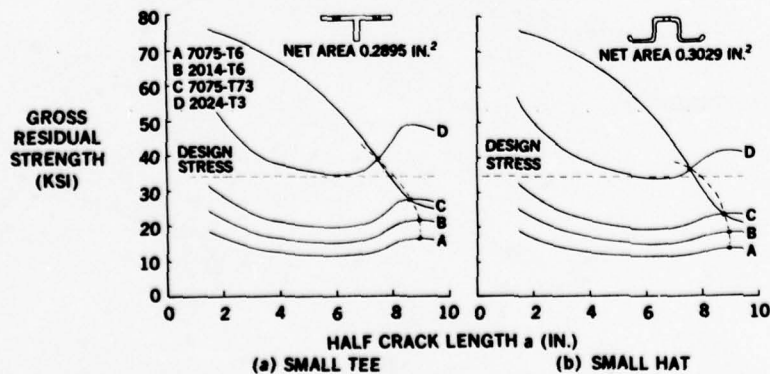


FIGURE 7. RESIDUAL STRENGTH FOR TWO-BAY CRACK WITH FAILED CENTRAL SMALL STIFFENERS

MATERIAL	CALCULATED ALLOWABLE (KSI)	
	LARGE TEE	LARGE HAT
7075-T6	17.28	14.72
2014-T6	22.88	19.52
7075-T73	29.60	25.28
2024-T3	42.56	38.72

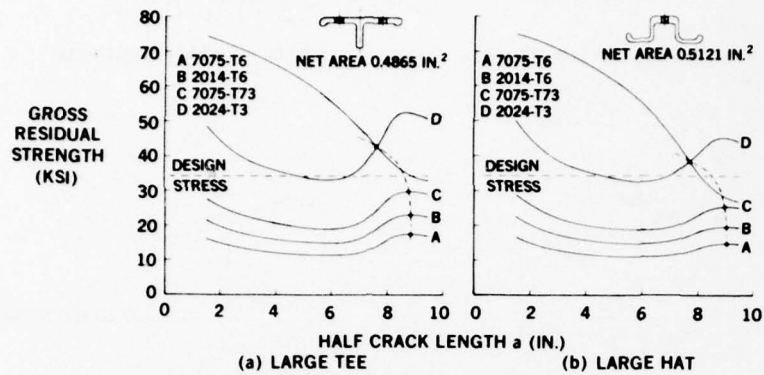


FIGURE 8. RESIDUAL STRENGTH FOR TWO-BAY CRACK WITH FAILED CENTRAL LARGE STIFFENERS

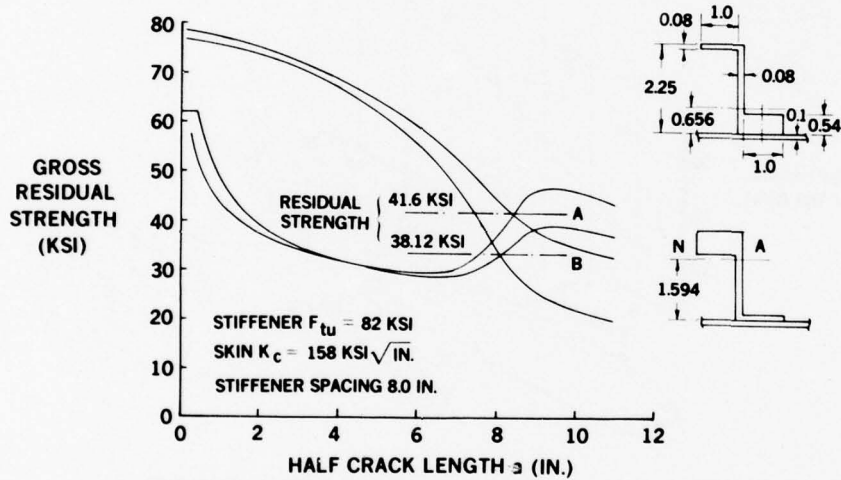


FIGURE 9. RESIDUAL STRENGTH COMPARISON - TWO-BAY CRACK WITH CENTER STIFFENERS FAILED

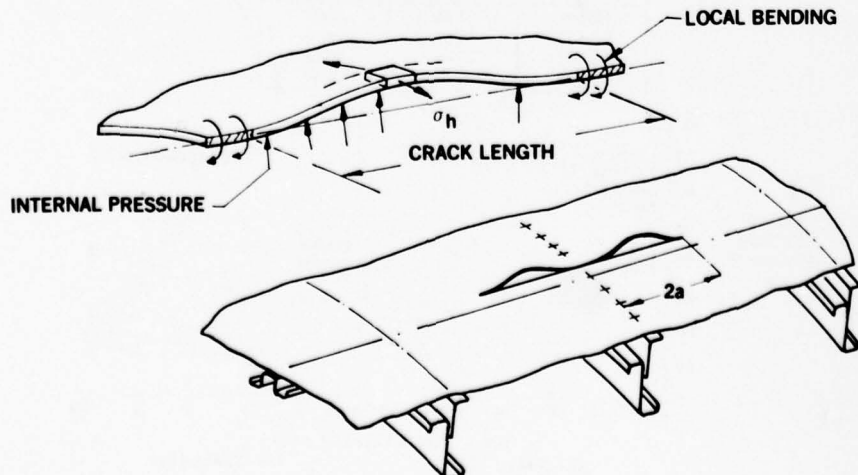


FIGURE 10. EFFECT OF BULGING DUE TO PRESSURE AND CURVATURE



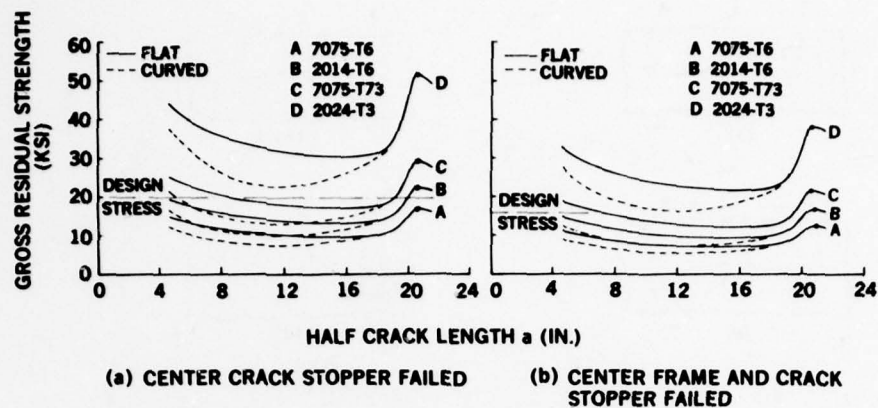


FIGURE 11. RESIDUAL STRENGTH DIAGRAM - FRAMES WITH CRACK STOPPERS

	RESIDUAL STRENGTH (KSI)			
	7075-T6	2014-T6	7075-T73	2024-T3
WITH CRACK STOPPER CENTER CRACK STOPPER FAILED	16.96	22.56	29.12	51.20
CENTER FRAME AND CRACK STOPPER FAILED	12.80	16.80	21.60	37.76
NO CENTER CRACK STOPPER CENTER FRAME INTACT	11.52	15.20	19.20	34.40

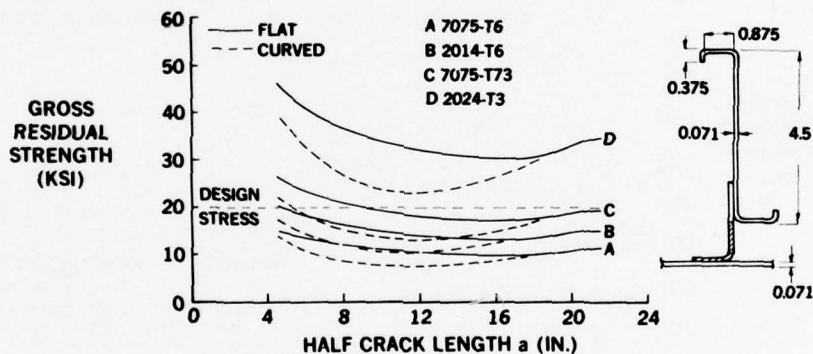
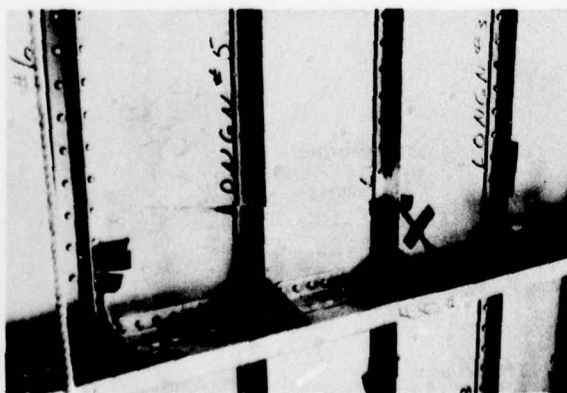
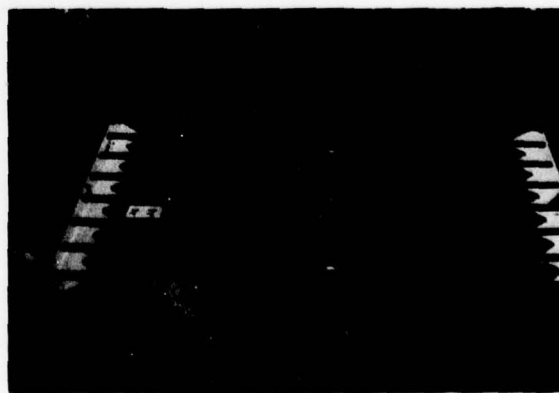


FIGURE 12. TWO-BAY LONGITUDINAL CRACK FRAMES, ONLY CENTER FRAME INTACT



(a) TWO-BAY CRACK CENTER STIFFENER SAW-CUT



(b) AFTER FINAL FAILURE

FIGURE 13. FLAT CIRCUMFERENTIAL CRACK TEST PANEL

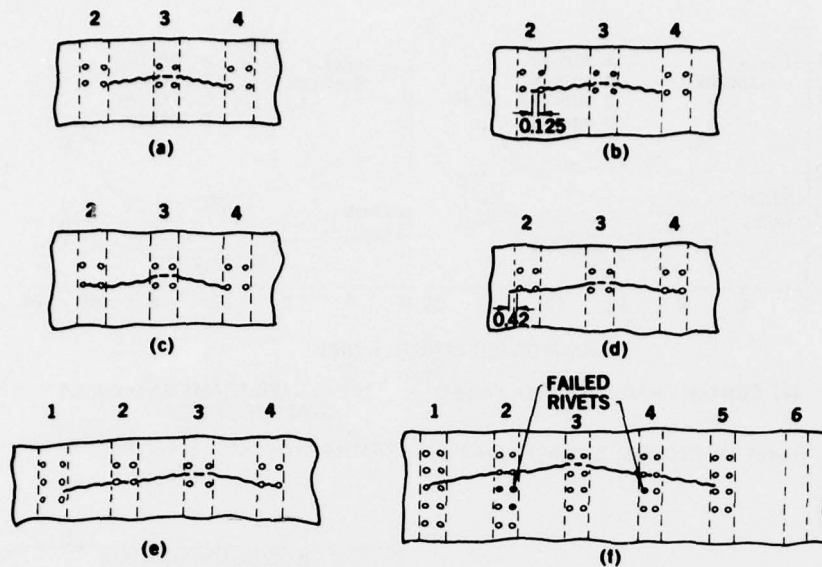


FIGURE 14. TEST RESULTS - LARGE TEE LONGERON, 7075-T73 SKIN

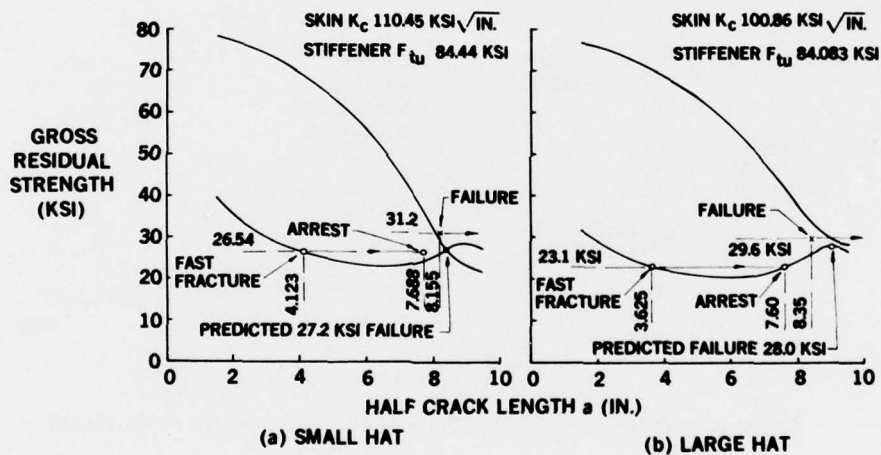


FIGURE 15. RESIDUAL STRENGTH TEST CORRELATION - HAT SECTION LONGERONS

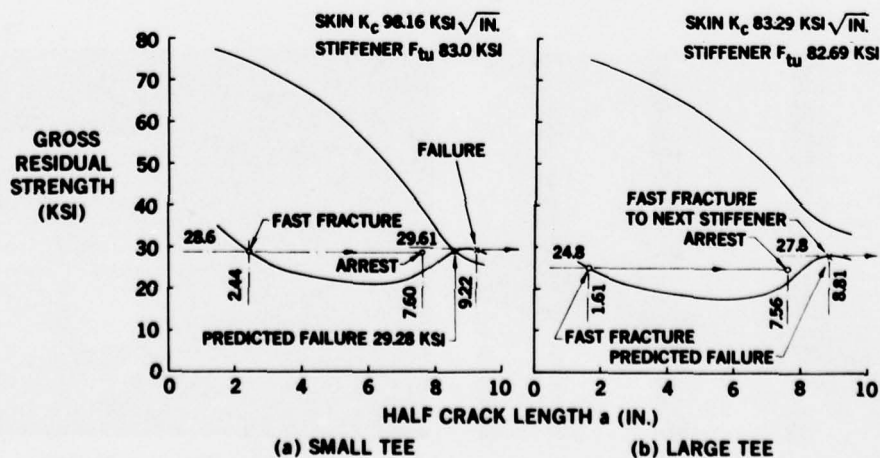


FIGURE 16. RESIDUAL STRENGTH TEST CORRELATION - TEE SECTION LONGERONS

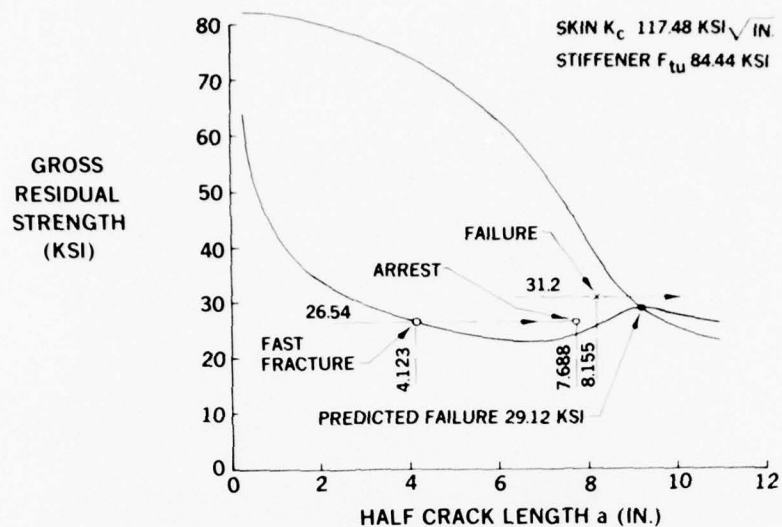


FIGURE 17. RESIDUAL STRENGTH TEST CORRELATION - SMALL HAT LONGERON (DISPLACEMENT COMPATIBILITY METHOD)

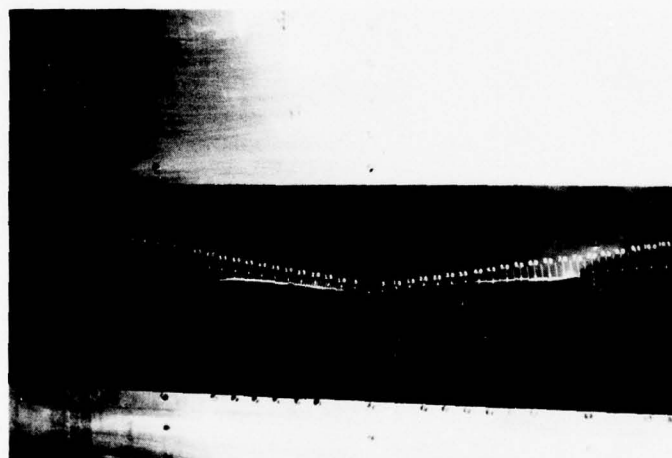


FIGURE 18. ARRESTED TWO-BAY CRACK - CENTER LONGERON SAW-CUT

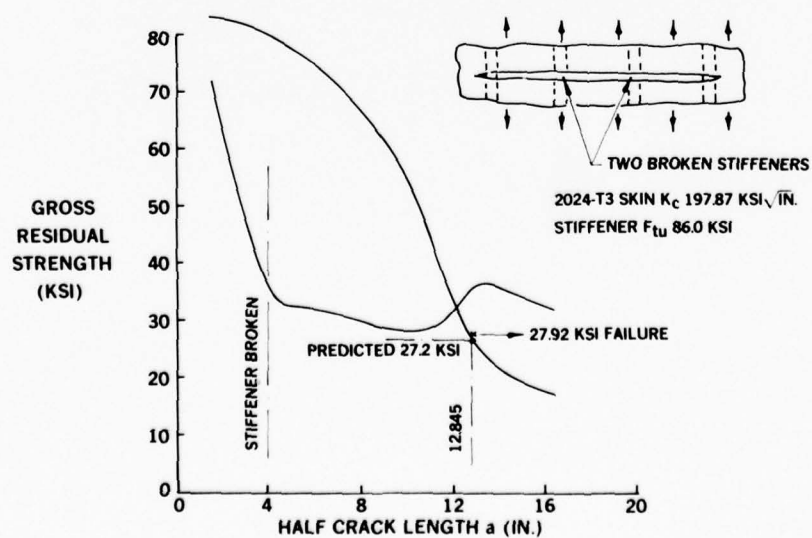


FIGURE 19. CORRELATION OF ANALYSIS AND TEST - THREE-BAY CRACK WITH TWO SAW-CUT LONGERONS (SMALL HAT - 2024-T3 SKIN)

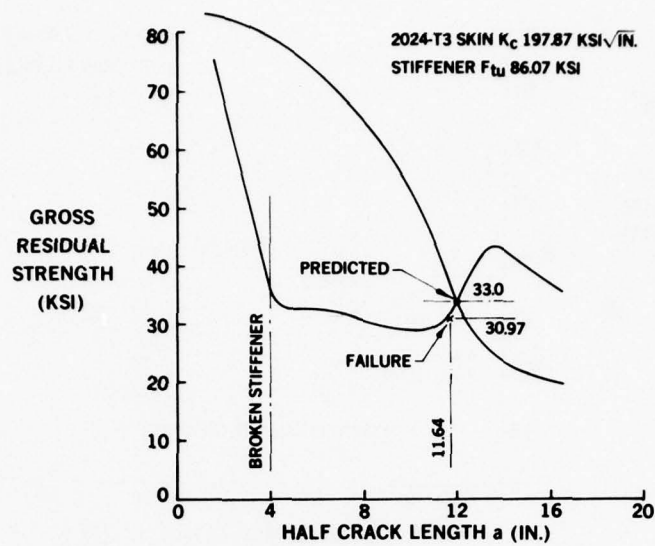


FIGURE 20. CORRELATION OF ANALYSIS AND TEST - THREE-BAY CRACK WITH TWO SAW-CUT LONGERONS (SMALL TEE - 2024-T3 SKIN)

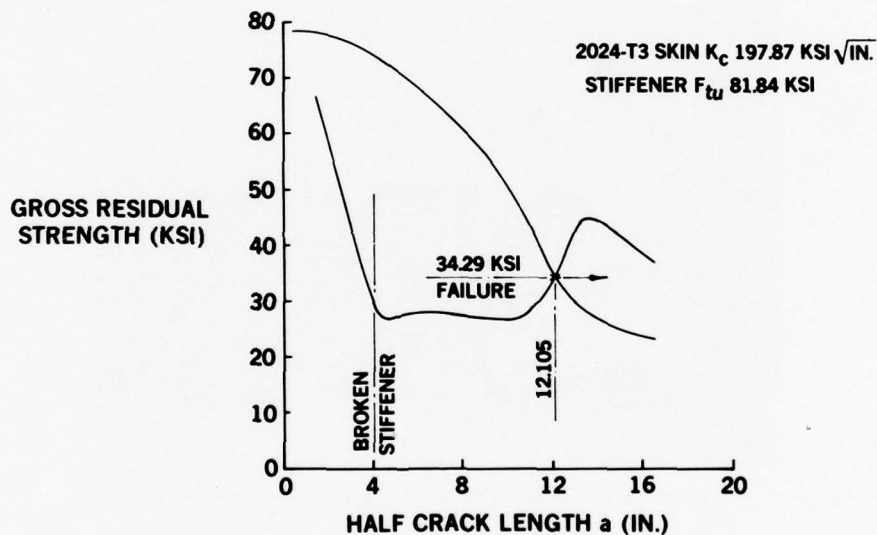


FIGURE 21. CORRELATION OF ANALYSIS AND TEST - THREE-BAY CRACK WITH TWO SAW-CUT LONGERONS (LARGE TEE - 2024-T3 SKIN)

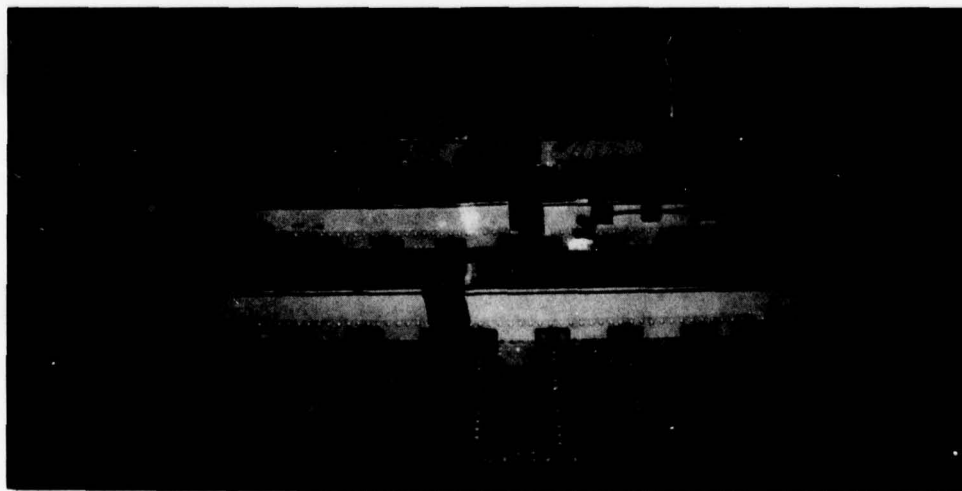


FIGURE 22. 120-INCH-WIDE, FLAT, LONGITUDINAL CRACK TEST PANEL



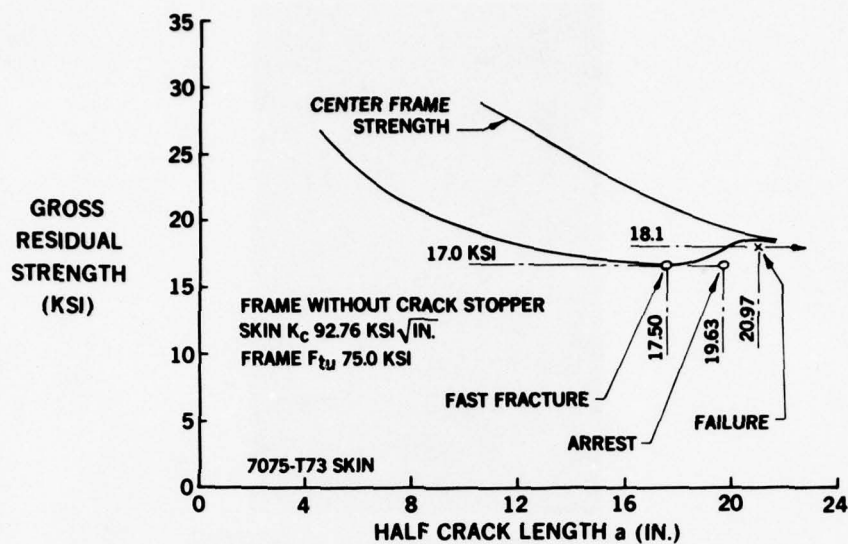


FIGURE 23. RESIDUAL STRENGTH TEST CORRELATION - FRAMES WITHOUT CRACK STOPPERS, CENTER FRAME INTACT

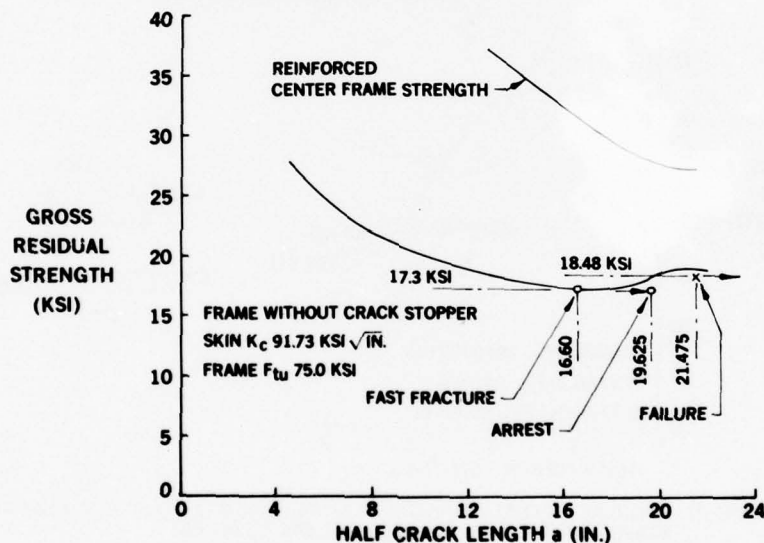


FIGURE 24. RESIDUAL STRENGTH TEST CORRELATION - FRAMES WITHOUT CRACK STOPPERS, INTACT CENTER FRAME REINFORCED

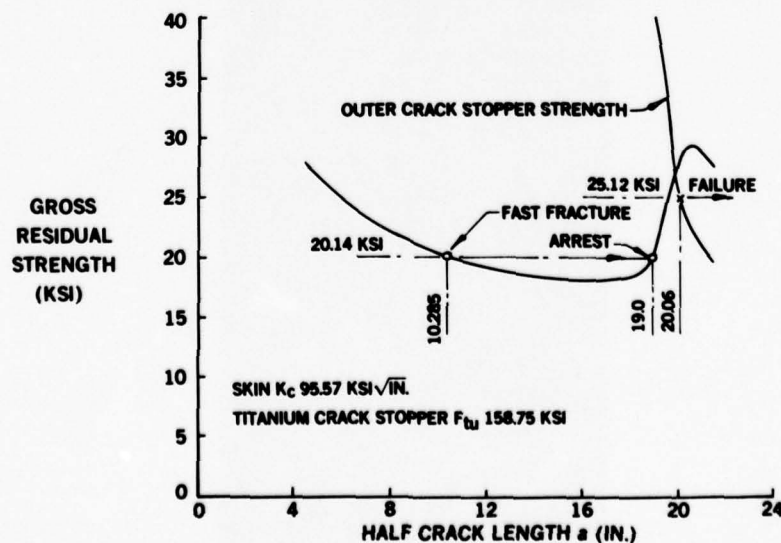


FIGURE 25. RESIDUAL STRENGTH TEST CORRELATION - FRAME WITH CRACK STOPPERS, CENTER CRACK STOPPER FAILED, CENTER FRAME REINFORCED

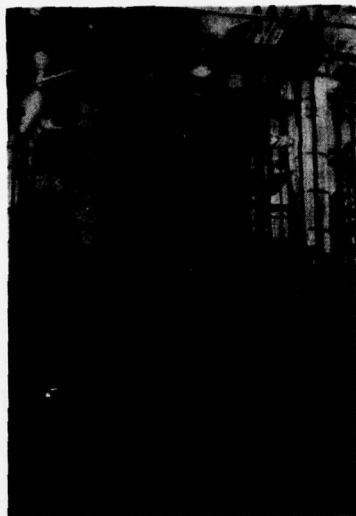


FIGURE 26. DC-10 WING LOWER SURFACE TEST PANEL

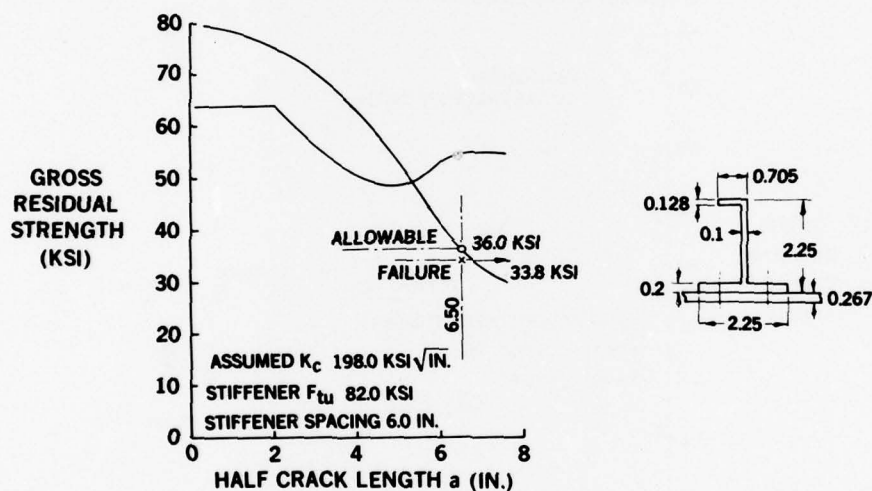


FIGURE 27. RESIDUAL STRENGTH TEST CORRELATION - TWO-BAY CRACK WITH SAW-CUT CENTER STRINGER (WING PANEL LIGHT CONSTRUCTION)



FIGURE 28. LOWER WING SURFACE RESIDUAL STRENGTH TEST PANEL (HEAVY SECTION)

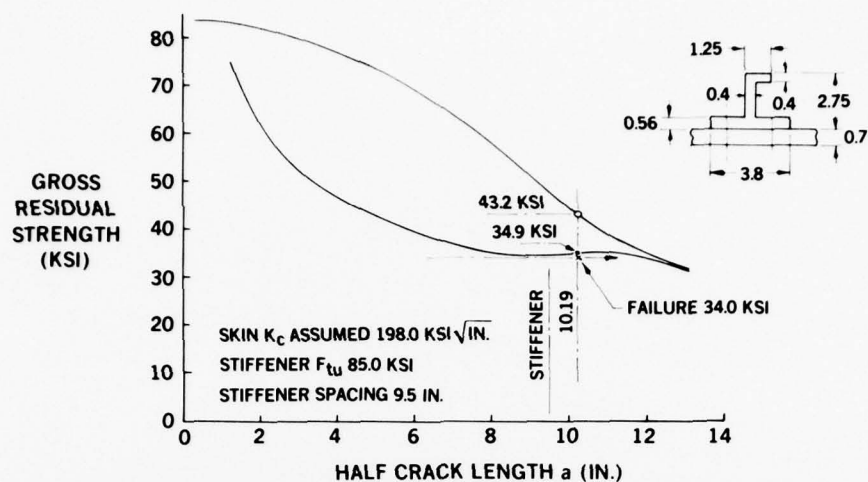


FIGURE 29. RESIDUAL STRENGTH TEST CORRELATION - TWO-BAY CRACK WITH BROKEN CENTRAL STRINGER (WING PANEL HEAVY CONSTRUCTION)

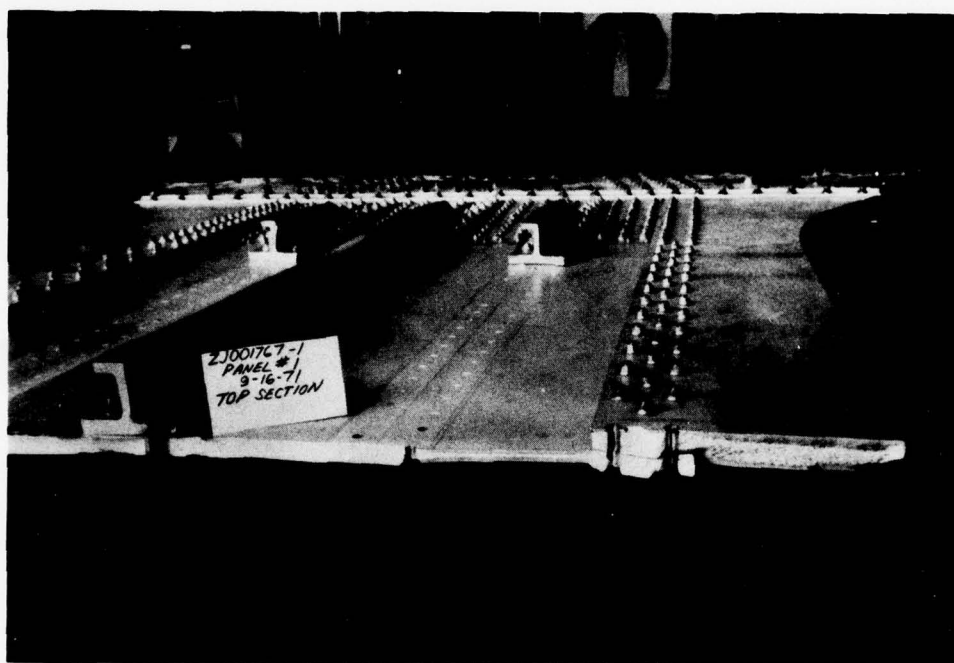


FIGURE 30. WING PANEL RIVET PRECIPITATED FAILURE

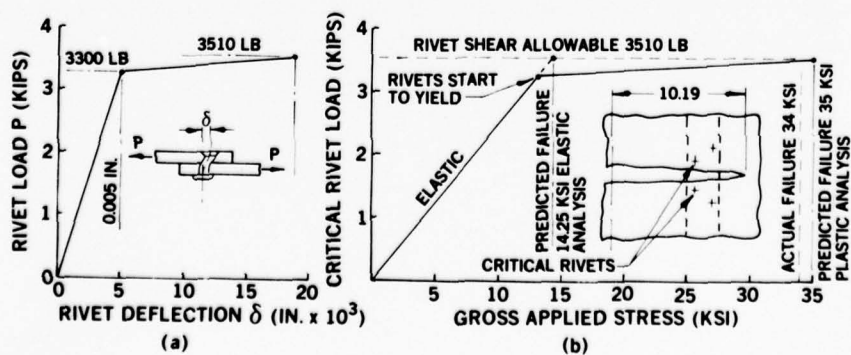


FIGURE 31. WING PANEL RIVET LOAD DISPLACEMENT AND RESIDUAL STRENGTH DIAGRAM

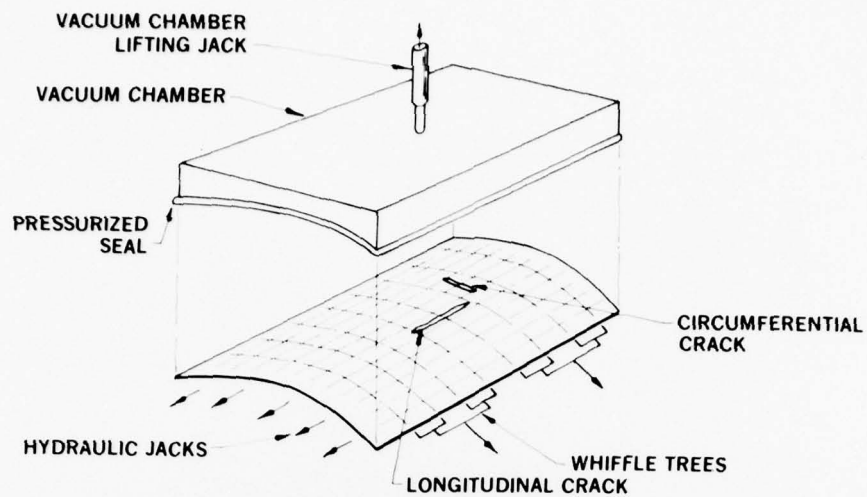


FIGURE 32. CURVED PANEL TESTS

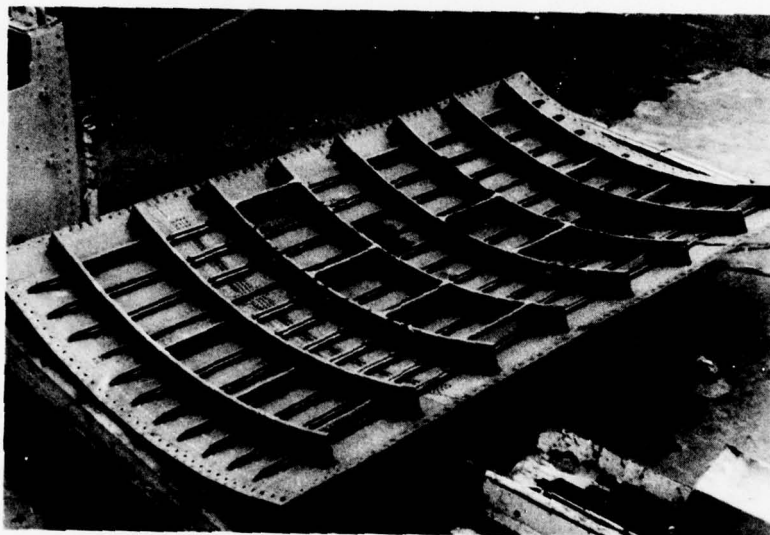


FIGURE 33. TYPICAL 2024-T3 CURVED TEST PANEL

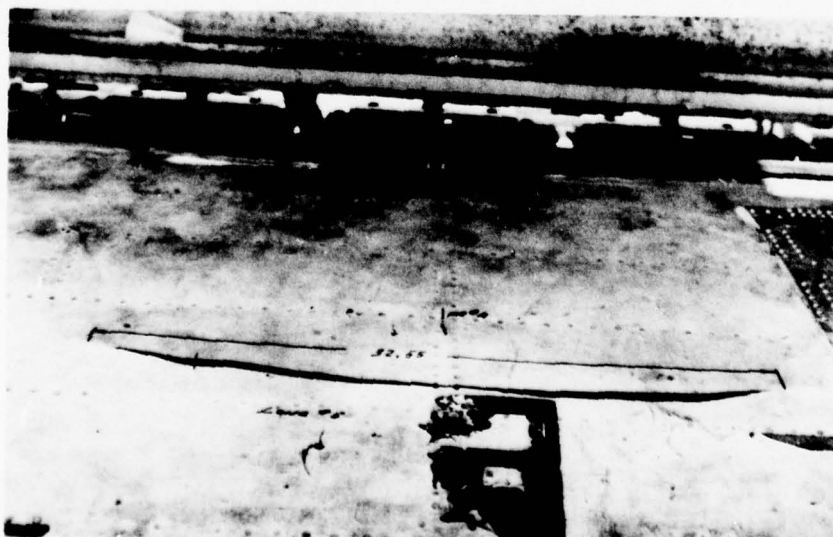


FIGURE 34. TWO-BAY CRACK AFTER CENTER FRAME FAILURE (CURVED PANEL TEST)



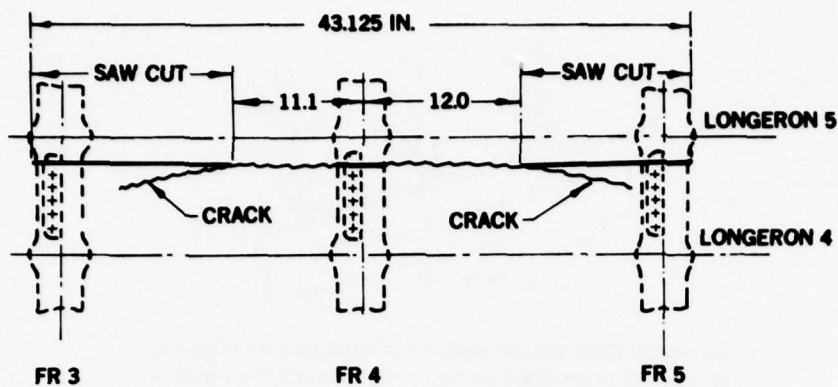


FIGURE 35. SAW-CUT TOWARD HOLE IN SHEAR CLIP

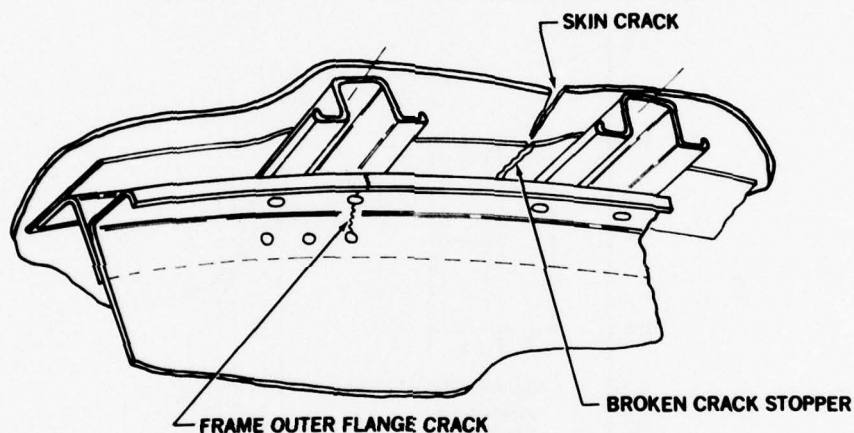


FIGURE 36. FATIGUE CRACK IN OUTER FRAME ARREST IN RIVET HOLE

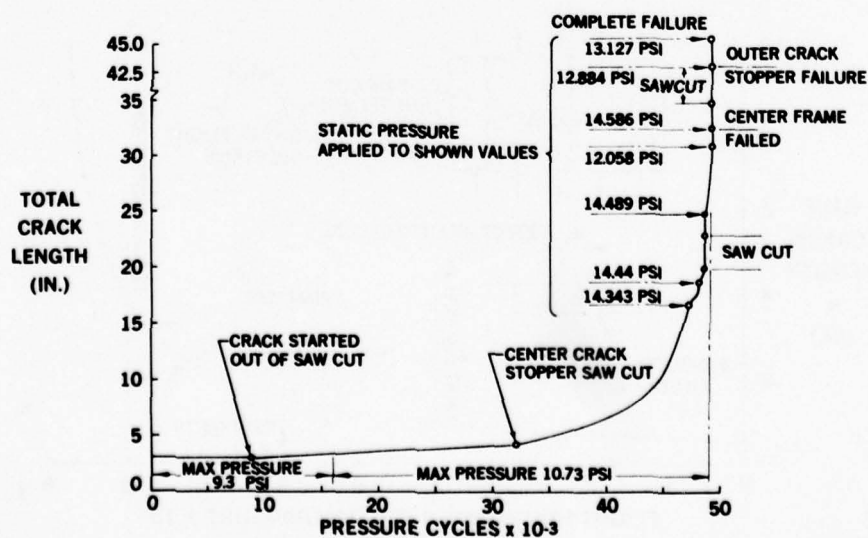
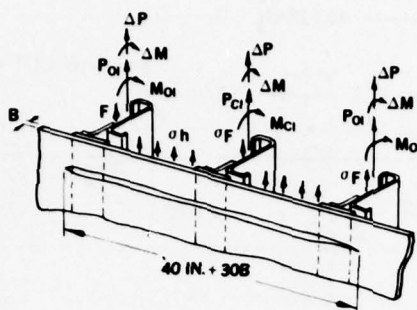


FIGURE 37. RESULTS OF 2024-T3 PANEL LONGITUDINAL CRACK TEST



$M_{OI}$  = OUTER FRAME BENDING MOMENT DUE TO INERTIA PLUS PRESSURE  
 $M_{CI}$  = CENTER FRAME BENDING MOMENT DUE TO INERTIA PLUS PRESSURE  
 $P_{OI}$  = OUTER FRAME INERTIA LOAD  
 $P_{CI}$  = CENTER FRAME INERTIA LOAD  
 $\Delta M$  = FRAME BENDING MOMENT DUE TO SKIN CRACK  
 $\Delta P$  = FRAME LOAD DUE TO SKIN CRACK  
 $\sigma_F$  = INITIAL FRAME STRESS DUE TO PRESSURE FOR INTACT STRUCTURE  
 $\sigma_h$  = SKIN AVERAGE HOOP STRESS DUE TO PRESSURE

FIGURE 38. SHELL LOADING FOR RESIDUAL STRENGTH CHECK

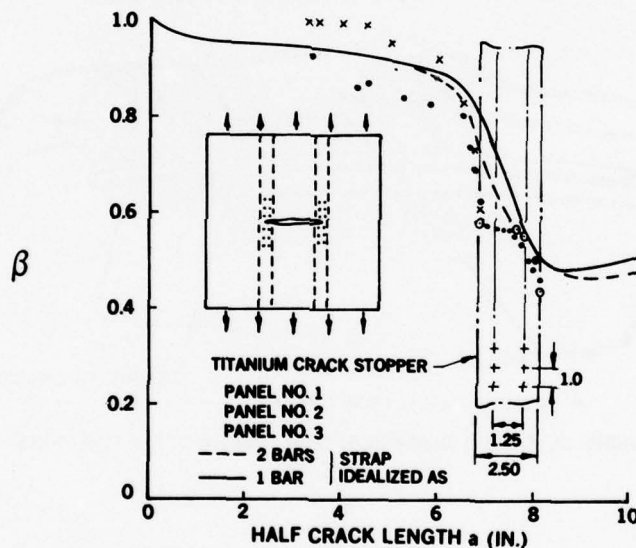
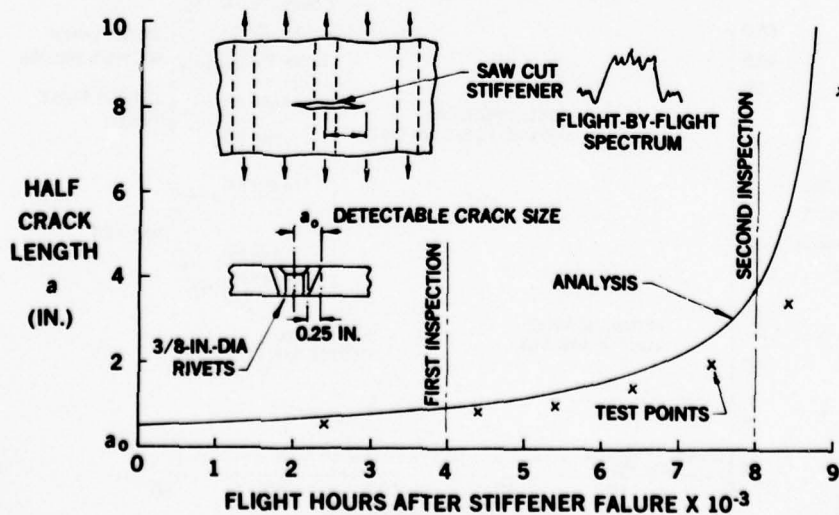
FIGURE 39. CORRELATION OF  $\beta$  FROM ANALYSIS AND CRACK GROWTH TESTS

FIGURE 40. WING PANEL CRACK GROWTH ANALYSIS CORRELATION

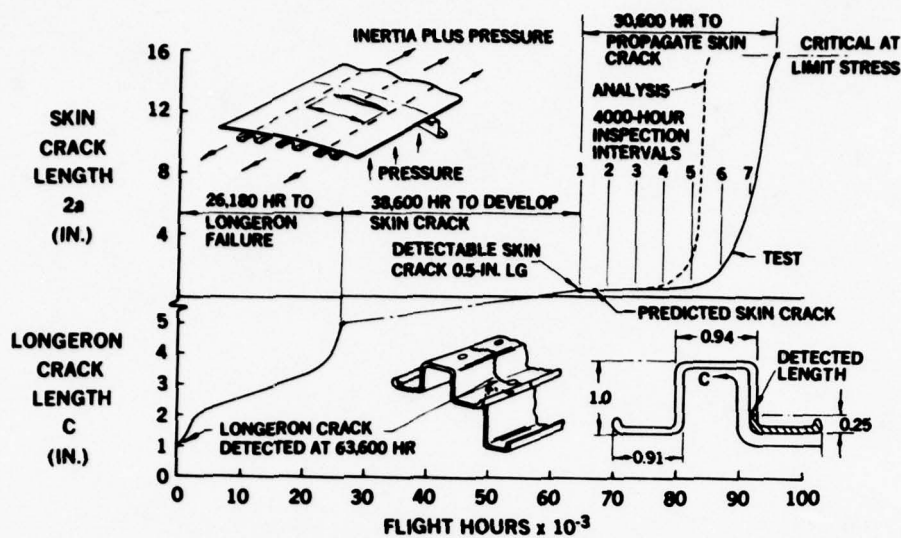


FIGURE 41. CRACK PROPOGATION IN FUSELAGE LONGERON AND SKIN (COMPONENT TEST)

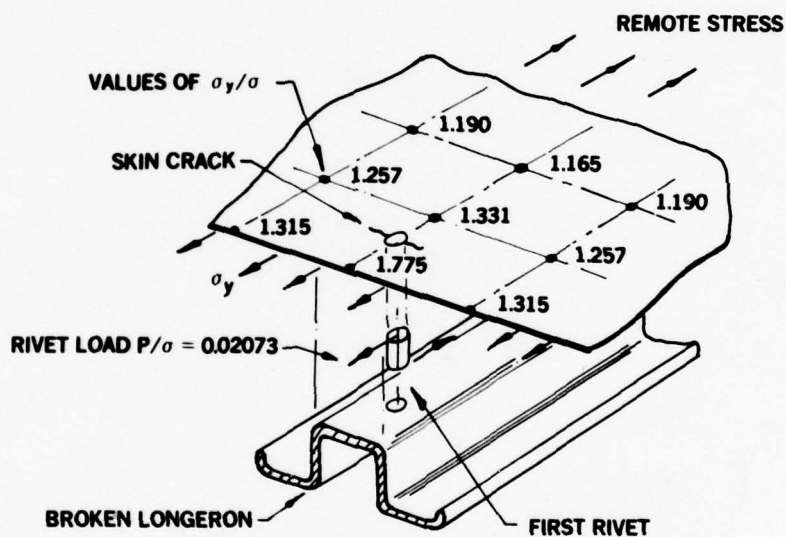


FIGURE 42. SKIN STRESS DISTRIBUTION IN VICINITY OF BROKEN LONGERON

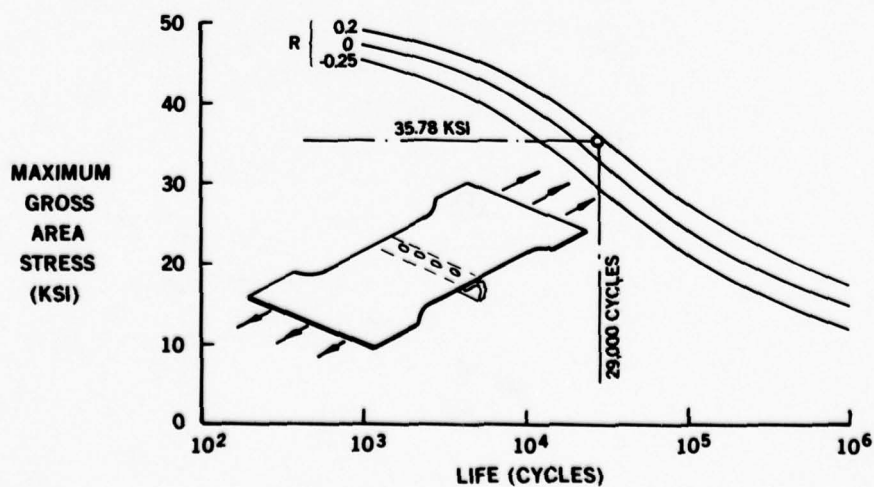


FIGURE 43. BASIC FUSELAGE STRUCTURE FATIGUE DATA

# ANALYSIS OF AIRCRAFT STRUCTURE USING APPLIED FRACTURE MECHANICS

D.P. Wilhem  
Northrop Corporation  
Aircraft Group  
3901 West Broadway  
Hawthorne, California 90250

## SUMMARY

In many instances, an aircraft designed and analyzed for a particular set of usages is placed in a service environment which is more severe than originally planned. The consequence of this occurrence is that many design details such as cutouts, holes, etc., are placed in a spectrum of loads which result in higher operating stresses. In the original full scale fatigue test, a different (design usage) spectrum is usually employed, and can only indicate fatigue critical areas. Using the finite element approach with stress intensity values and usage spectra, estimates are made of the crack growth life for a part-through-crack at a cutout. These data are then used to establish inspection intervals. Three (3) distinct spectra were developed to represent usage, and analytical/experimental correlation was made for those spectra. In the majority of cases, good agreement was obtained. For these cases where the correlation is not good, refinements need to be made to the stress intensity solutions and/or the crack growth model. The reliance on more than one method of analysis is recommended for stress intensity evaluation (i.e., analytical, finite element, semi-empirical, etc.) of fatigue and fracture-critical areas. A comparison of the methods used in determining crack growth parameters sometimes indicates that the added cost of a more complex technique is not warranted, particularly when parametric design studies are involved. The use of a newer approach to the prediction of both fatigue crack growth and residual strength, employing a wide range resistance curve, is promising. Its usefulness in pinpointing differences in the cutout problem is given.

## 1. INTRODUCTION

Evaluating a fatigue or fracture critical part involves many disciplines. Once external loads are determined, they must be translated to internal loads. Then the spectrum of loads can be developed, depending on mission, mission-mix, etc. Examination of service structure can give an insight into the areas which are prone to cracking, and at which initial crack length to start the analysis. Due to changes in the spectrum, areas which were fatigue sensitive can become fracture critical. Evaluations of redesigns (fixes) must be assessed so that inspection intervals can be established. With confidence in the analysis, it is possible to experimentally check the validity of the analysis and establish inspection intervals. Differences not previously observed between through-the-thickness and part-through-thickness cracks are shown using a fatigue crack growth resistance approach.

## 2. LOADS/SPECTRUM AND EQUIVALENT CRACK GEOMETRIES

### 2.1 Influence of Loading Variables on Spectra and Loads

High performance aircraft loads are generally derived from the following:

- ° Symmetric and Unsymmetric Maneuvers
- ° Abrupt Pitch Maneuvers
- ° Gusts
- ° Store Ejection
- ° Landing
- ° Ground Handling (Taxi, Braking, Turning, etc.).

In new systems, loads data are based on past experience with similar type aircraft. The mission sequencing of the loads is initially derived from military standards or federal regulations. Many times, fatigue cracking problems arise due to usage changes and result in more severe usage than originally intended and/or designed for.

Figure 1 shows composite maneuver spectra for one aircraft type. There are small differences in load factor occurrences at low load factor, for various usages. At load factors  $>5G$  there are large differences. These are reflected in typical lower wing skin stress (at some area near the main box) noted in Figure 2. Fatigue and subsequent fracture problems occur when an aircraft initially designed, and full scale fatigue tested to a training spectrum, is placed in an aerobatic role, for example. A change in environment of this type can possibly lead to a 20 fold increase in occurrences of limit design stress. The establishment of inspection intervals for new usage is most important. Areas which are prone to cracking must be analyzed by fracture mechanics techniques. This also applies to any "fixes" or life improvements which may be proposed to increase service life.

### 2.2 Inspection Summaries

Much information can be gained from destructive inspections of any structure. This procedure is becoming more common to provide QC the frequency, size, and other data on crack sites. Data obtained from one wing evaluation, where 212 holes were destructively split open, indicated the trends shown below after



fractographic examination. Total fatigue spectrum loading sequences were on the order of four (plus) lifetimes.

- ° 86% < 0.005-Inch Deep
- ° 9% 0.006-0.010 Inch Deep
- ° 3% 0.011-0.020 Inch Deep
- ° 2% > 0.020-Inch Deep

Ten cracks deeper than 0.010 inch:

- ° 8 Fastener holes, 0.043"max.
- ° 2 Drain holes, 0.037"max.

Most cracks near center of hole, not at skin-substructure interface.

Most importantly, of ten (10) fastener holes located in a fatigue critical area, seven (7) contained cracks which were considered as too small for NDI detection. This breakdown is typical of the inspection done on high performance aircraft wings. Information of this type can be used to establish initial flaw sizes for analysis, setting NDI limits, etc.

### 3. NONLINEAR FRACTURE MECHANICS ANALYSIS AND TEST

#### 3.1 Root Radius of Wing Skin-Linear Elastic Analysis

A problem area under consideration is a lower wing skin, cracking in the area of the wing to fuselage attach rib. The original geometry consisted of a 1.27 cm radius shown as the dashed line in Figure 3, which was subsequently changed to a 7.62 cm radius. Details of this area are shown in Figure 4.

As an initial effort, LEFM analysis was attempted of this area since spectrum analysis indicated fatigue problems in the region along with in-service data. In addition, the usage had changed and produced a more critical condition. Large panel spectrum testing was planned, and predictions were required for those data. Closer examination of Figure 4 indicates that a true radius is not the actual condition. Therefore, an "active chord" was chosen for the analysis. This chord was selected to have a length equal to the radius, in both cases. A chord can be treated as a notch, and since cracks at radii solutions are not available, the deep notch solution was used from Reference 1. The solution required modification to treat the part-through-thickness crack (PTC), occurring in practice. Stress intensity values were obtained for the PTC condition, using superposition principles, i.e., "active chord," through-the-thickness crack (TTC) solution (Reference 1), modified for PTC behavior and back surface magnification. The details of this procedure are given in Reference 2. A PTC in the 1.27 cm radius ( $a/c = 1.0$ ) produces the normalized stress intensities (Betas) shown in Figure 5. It is of interest to compare the TTC geometry solution for this problem with other solutions, assuming a full 1.27 cm radius to evaluate the severity of the problem. Figure 6 shows these data. A cracked finite element solution compared to the Reference 1 solution, shows good agreement. However, large stress intensities for short crack lengths are observed, which is indicative of the influence of the full radius on K. It was believed that the more realistic case was to use a chord geometry.

#### 3.2 Root Radius of Wing Skin - LEFM Prediction and Test Data

Several large panel tests of the geometry shown in Figure 7 were tested using offcenter loading in spectrum fatigue to produce a gradient in the radius. There was no preflaw, but cracking was measured from the radius after initiation. These panels were 2.4m long and 0.3m wide with two (2) 7.6cm radii simulating the wing, to determine the design life improvement. Details of these tests are reported in Reference 2. A prediction was made of crack growth (without retardation), using the K's obtained by superposition in the manner just described, changing the active chord to 7.6cm. The predictions, assuming a TTC and PTC of 0.005 inches is shown in Figure 7, along with the test data. Note the long life for the PTC prediction. The test data is better fitted by the TTC prediction. Examination of the strain gage data provided the explanation for this trend in rapid crack growth.

The panel test stress gradient was established as determined from a local NASTRAN finite element model of the areas between the root rib to gear rib of the aircraft. It did not contain the substructure in the model, and as a result, gave a larger than anticipated edge (radius) stress. This area was remodeled, including all substructure, and a more realistic gradient was obtained. The test gradient and new gradient (dashed line) are shown in Figure 8. Note that the stress is in terms of local limit stress. Even though the new model gives lower limit stress, it is at the material yield strength on the radius edge. The indications obtained analytically, i.e., plastic behavior for peak spectrum stresses were confirmed from the strain gage test data on large panels shown in Figure 9. This strain-time plot, recorded at zero load, indicates plastic behavior as far as 0.8 inch from the radius edge.

These data indicated that an elastic-plastic analysis was necessary. This analysis was given in the first lecture. Its application to the fatigue crack growth problem is presented next.

#### 3.3 Coupon Geometries and Gradient Matching



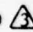
The NASTRAN finite element models for the 1.27 and 7.62cm radii were selected to match the wing structural model stress gradients. An intermediate radius of 3.81cm was also selected for analysis, to determine trends between varying radii. The stress gradient results obtained from the model of the coupons for the geometries shown in Figure 10 were compared with strain gage data on the actual test coupon. Seven (7) gages were placed in line along the centerline of the radius. The comparison between model gradient and coupon stress gradient is shown in Figure 11. The agreement is considered quite good. Also note that the edge stress for all coupons is quite large ( $K_t > 2.2$ ), and emphasizes the need for an elastic-plastic analysis. The 7.62cm radius shows a lower stress gradient than the two (2) smaller radii. This is due


to the offcenter loading of the model and coupon. The coupon geometries are shown in Figure 12, and matrix of test coupons and loading conditions in Table 1. In explanation of Table 1, the following parameters were under study.


- ° Two (2) alloys of 7075
- ° Part-through and through cracks
- ° Three (3) radii
- ° Constant amplitude and spectrum loading.


Fatigue crack growth data would be obtained from specimens 1 through 9 in a nonlinear stress field. Edge stress was selected to be half way between the yield and ultimate. Some modification of the LEFM crack growth equations would be necessary to treat nonlinear fatigue stress.

TABLE 1 - TEST SPECIMEN MATRIX

CAN/ SPECIMEN NO.	MATERIAL	TYPE OF CRACK 	RADIUS (inch)	THICKNESS (inch)	WIDTH (inch)	MAXIMUM LOAD (kips)	MAXIMUM STRESS  (psi)	INITIAL CRACK LENGTH (inch)	INITIAL CRACK DEPTH (inch)
1	7075-T651	PTC	0.50	0.422	6.00	65.0	25622	0.016	0.087
2	7075-T651	TTC	0.50	0.422	6.00	65.0	25622	0.020	---
3	7075-T7351	PTC	0.50	0.521	6.00	63.5	20313	0.002	0.009
4	7075-T7351	TTC	0.50	0.521	6.00	63.5	20290	0.007	---
5	7075-T7351	TTC	1.50	0.521	6.00	46.0	14710	0.013	---
6	7075-T7351	TTC	3.00	0.523	8.00	105.0	25095	0.065	---
7	7075-T7351	PTC	3.00	0.521	8.00	105.0	25191	0.016	---
8	7075-T7351	PTC	3.00	0.515	8.00	105.0	25485	0.050	0.050
9	7075-T7351	TTC	3.00	0.524	8.00	105.0	25047	0.047	---
10 	7075-T7351	PTC	3.00	0.514	8.00	58.5	14226	0.051	0.056

 PTC Corner Crack at the radii  
TTC Through-the-thickness crack at the radii

 Gross area stress

 Spectrum Test

### 3.4 Application of J-Integral to Fatigue Crack Growth Prediction

The analysis of fatigue crack propagation in isotropic, homogeneous structural elements, has been accomplished with varying success by a number of investigators. The method often employed, involves the fatigue testing of standard specimen configuration such as a compact (CS) or center cracked tension specimen (CCT). The coupon is repeatedly loaded sinusoidally at a particular frequency, constant amplitude load level and stress ratio. The crack length is measured at intervals during the test. From this data the crack growth rate  $da/dN$ , that is, the crack extension per cycle can be calculated. If the crack growth rate is described as a function of a crack growth index such as stress intensity factor range ( $\Delta K$ ), a crack growth model can be formulated that will relate the index parameter to the crack growth rate.

The success of any crack growth life prediction technique is measured by its ability to reproduce the crack growth behavior of the tests on which it is based. To date, over one hundred (100) crack growth models have been proposed. Most of the models emphasize certain crack growth factors such as environment, frequency, or stress ratio over other factors. Nearly all of the models contain constants in their equations that must be mathematically fitted to the test data. These constants are usually material dependent so that a different set of constants are needed for each material or product form under consideration.

The crack growth rate in aluminum alloys is particularly susceptible to the influence of stress ratio  $R$ , ( $R = \sigma_{min} / \sigma_{max}$ ) where "R" is the ratio of minimum to maximum stress in a cycle. The environment surrounding the crack tip also effects the crack growth rate. FitzGerald (Reference 3) has proposed a model that accounts for both of these factors. The crack growth rate may be expressed as:

$$\frac{da}{dN} = C K_{max}^m [(K_{max} + K_{env})(1-R)]^2 \quad (1)$$

C and m in the above equation are material constants and  $K_{env}$  is an environmental factor that is a function of  $K_{max}$ , the test environment and the material. It has been noted that  $K_{env}$  can be separated into three (3) regions of crack growth rate, a linear varying lower region, a plateau, and an exponentially increasing upper portion. In this program, it was found that this equation matched the crack growth rate data in the upper portion of the curve better than the more widely used model such as that proposed by Forman (Reference 4). Fatigue crack growth data for 7075-T7351 and 7075-T651 aluminum plate were obtained from compact specimens at a stress ratio of 0.10 in the linear elastic range. Equation 1 was fitted to the data measured from these tests.

In linear elastic fracture mechanics, the stress intensity factor is commonly used as the index parameter

for crack extension. The stress intensity factor for an edge crack in a semi-infinite sheet subjected to tension has been determined using series type mapping functions with the complex variable stress-function method. For Mode I crack extension  $K$  may be expressed as:

$$K_I = 1.12 \sigma \sqrt{\pi a} \quad (2)$$

The free surface correction factor for this geometry is 1.12.

As shown previously, finite element analysis may be used to calculate the J-integral or  $\mathcal{G}$ , the strain energy release rate. For small values of applied stress, the results of the J-integral analysis may be equated to the stress intensity factor  $K$  where:

$$J = \frac{K^2}{E} \quad (3)$$

$$\text{or } K = \sqrt{JE} \quad (4)$$

An effective stress intensity factor  $K_{\text{eff}}$  can be calculated where:

$$K_{\text{eff}} = \sigma \sqrt{\pi a} \phi(\sigma, K_e) \lambda(a) \gamma \quad (5)$$

where  $\phi(\sigma, K_e)$  = plasticity correction factor  $K_p/K_e$

$\lambda(a)$  = correction factor for the stress concentration (Figures 5-4)

$\gamma$  = front free surface correction factor.

This effective stress intensity factor can be used directly as the index in the crack growth rate equation thus:

$$\frac{da}{dN} = C (K_{\text{max}})_{\text{eff}}^m \left[ (K_{\text{max}})_{\text{eff}} + K_{\text{env}} \right] (1-R)^2 \quad (6)$$

where the constants  $C$ ,  $m$  and  $K_{\text{env}}$  are the same as those defined previously.

The effective stress intensity factor for a corner crack can be developed in a similar manner. A shape parameter  $Q$  is introduced that adjusts the through-crack solution to treat a surface crack.  $Q$  is the square of an elliptic integral of the second kind. Newman, Reference 5, has developed a simple approximation of  $Q$  which is used here. The elastic stress intensity factor for a quarter elliptical crack will vary along its periphery. For  $a/c$  ratios greater than 1., the point of maximum stress intensity will occur near the surface of the plate. At this point,  $K$  may be expressed as:

$$K = \sigma \sqrt{\frac{\pi a}{Q}} \gamma \quad (7)$$

Near the surface of the plate, the back surface has been found to have little effect on the magnitude of the stress intensity factor and, therefore, its effect has not been included. If the applied stress exceeds linear elastic fracture mechanics limits, then an additional factor to account for the effect of plasticity must be introduced. The stress intensity factor for this case is:

$$K_{\text{eff}} = \sigma \sqrt{\frac{\pi a}{Q}} \phi(\sigma, K_e) \lambda(a) \gamma \quad (8)$$

The functions  $\phi(\sigma, K_e)$  and  $\lambda(a)$  are the correction factors for plasticity and stress concentration respectively. The procedure used here is similar to that of "Compounding Stress Intensity Factors" (Reference 6). Note that the procedure requires a modification for PTC behavior. If:

$$K_{\text{elastic}}(\text{TTC}) = J_{\text{elastic}}(\text{TTC}) \times E \quad (9)$$

and

$$K_{\text{plastic}}(\text{TTC}) = J_{\text{plastic}}(\text{TTC}) \times E \quad (10)$$

for a given stress then:

$$K_{\text{plastic}}(\text{TTC}) = K_{\text{elastic}}(\text{TTC}) \sqrt{\frac{J_{\text{elastic}}}{J_{\text{plastic}}}} \quad (11)$$

In Equation 11,  $\sqrt{\frac{J_e}{J_p}}$  is the plasticity correction to be multiplied by the elastic  $K$  for a PTC at a given stress level.

### 3.5 Constant Amplitude Fatigue Crack Growth Data Correlation

Figure 13 is a summary of the test data for the various radii specimens. The following conclusions can be made regarding these data.

\* 7075-T651 aluminum shows a more rapid fatigue crack growth than 7075-T7351 (CAN 2, 4 and 1, 3) for the same flaw geometry.

\* The presence of a part-through-the-thickness (PTC) crack will result in a factor of ten increase in fatigue life over a through-the-thickness crack (TTC), regardless of 7075 alloy temper (i.e., compare CAN's 1 & 2, 3 & 4, 6 & 7, 8 & 9).



As an example of the type of correlations obtained in this study, Figure 14 and 15 shows the 1.27cm radius results. The differences shown in these two (2) figures is due to material alloy. A typical LEFM based prediction is shown in Figure 14. Note the long life prediction which occurs. The elastic-plastic prediction is shown to agree quite well with the data.

### 3.6 Spectrum Fatigue Crack Growth and Variations

The stress gradient was used in the analysis, as shown in Figure 11, for the 7.62cm radius. Stress intensities were computed as described in 3.4. The correlation for this spectrum test is shown in Figure 16, which appears to be quite good.

Using the pin loading gradient of Figure 11 for the 1.27cm radius (all coupons were clamp loaded), predictions of spectrum loading were made. This prediction is shown for a typical training spectrum in Figure 17, along with the results obtained from strain gage gradient. Good correlation is noted for analysis, thus, proving confidence in the analytical technique. Also indicated in Figure 17 is the analytical prediction from a more severe spectrum for the same material. This large decrease in crack life should be considered in planning inspection intervals.

### 4.0 USE OF CRACK GROWTH RESISTANCE TO EXPLAIN PTC AND TTC BEHAVIOR

The constant amplitude fatigue crack growth data from CAN 3 - 9 (see Table 1) was analyzed using the method described in Reference 7 to determine the resistance to fatigue crack growth. These data have been separated into thru-thickness and PTC data, and are shown in Figure 18. The method of analysis will not be described in detail here, but essentially assumes that fatigue crack growth per cycle is similar to the static crack extension resistance curve when stress ratio is near zero. The elastic/plastic data of Figure 18 shows differences between the TTC and PTC data. Theory indicates that there be no difference between resistance curves for a given material, thickness and test environment - as long as the stress intensity is computed correctly. The differences in resistance curves of Figure 18 can be explained by the assumptions used in the development of the stress intensities for the elastic/plastic PTC. Comparison of the fatigue crack growth resistance data obtained for the TTC specimens of this study with those data obtained from LEFM data (same material, compact specimens), indicate similarity of curves. Therefore, the higher, PTC resistance curve indicates that the elastic/plastic "K's" would need to be modified for other factors such as flaw shape change, back surface magnification, etc., which would alter the stress intensity. The reduction in K required to produce similarity in resistance curves is on the order of the differences noted in life predictions.

### 5.0 PREDICTION OF SPECTRUM CRACK GROWTH AT COCKPIT LONGERON

The cockpit longeron cutout analyzed in both coupon and structural models using finite elements, was spectrum tested. The results of the coupon tests are shown in Figure 19. Note that the same procedure was used here to predict spectrum growth as was used for the larger radii coupons. The prediction using retarded growth is not in agreement with the data. In fact, the agreement using unretarded growth is not good. Several factors are influencing the prediction of this data. Many have been mentioned already, i.e., varying a/c with crack growth, inability to accurately predict PTC - K's, etc. However, it is apparent from this lack of correlation that more research is needed in developing a more accurate retardation model. This becomes more important when other than plane strain behavior (i.e., mixed mode) occurs as in this cut-out situation.

### 6.0 CONCLUSIONS

A J-integral approach, with modified stress intensities, can be successfully used to predict elastic-plastic fatigue crack growth.

Using finite element data, structural stress gradients can be matched by coupon testing, using finite element models of the coupon. These gradients (analytical or experimental) can then be used in predicting the fatigue crack growth behavior for the structure in question.

More research is required into the fatigue crack growth model to predict those structures which show mixed mode cracking.

### 7.0 REFERENCES

1. Tada, H., et.al., "The Stress Analysis of Cracks Handbook," Del Research Corporation, Hellertown, Pa, 1973.
2. NOR 77-58, "T-38 Thick Skinned Wing Study," Northrop Corporation, Aircraft Group, Hawthorne, CA, March 1977.
3. FitzGerald, J.H., "Empirical Formulations for the Analysis and Prediction of Trends for Steady-State Fatigue Crack Growth Rates," American Society for Testing and Materials, Journal of Testing and Evaluation, Volume 5, No. 5, pp. 343-353.
4. Forman, R.G. et.al., "Numerical Analysis of Crack Propagation in Cyclic Loaded Structures." Journal of Basic Engineering, Volume 89, September 1967, pp. 459-464.
5. Newman, Jr., J.C., "Predicting Failure of Specimens with Either Surface Cracks or Corner Cracks at Holes," NASA TND-8244, June 1976.
6. Cartwright, D.J. and Rooke, D.P., "Approximate Stress Intensity Factors Compounded from Known Solutions," Engineering Fracture Mechanics, 6, 563, 1974.
7. Wilhem, D.P. and Ratwani, M.M., "Application of the R-Curve Concept to Fatigue Crack Growth," ASME Journal of Engineering Materials and Technology, October 1978, pp. 416 - 420.



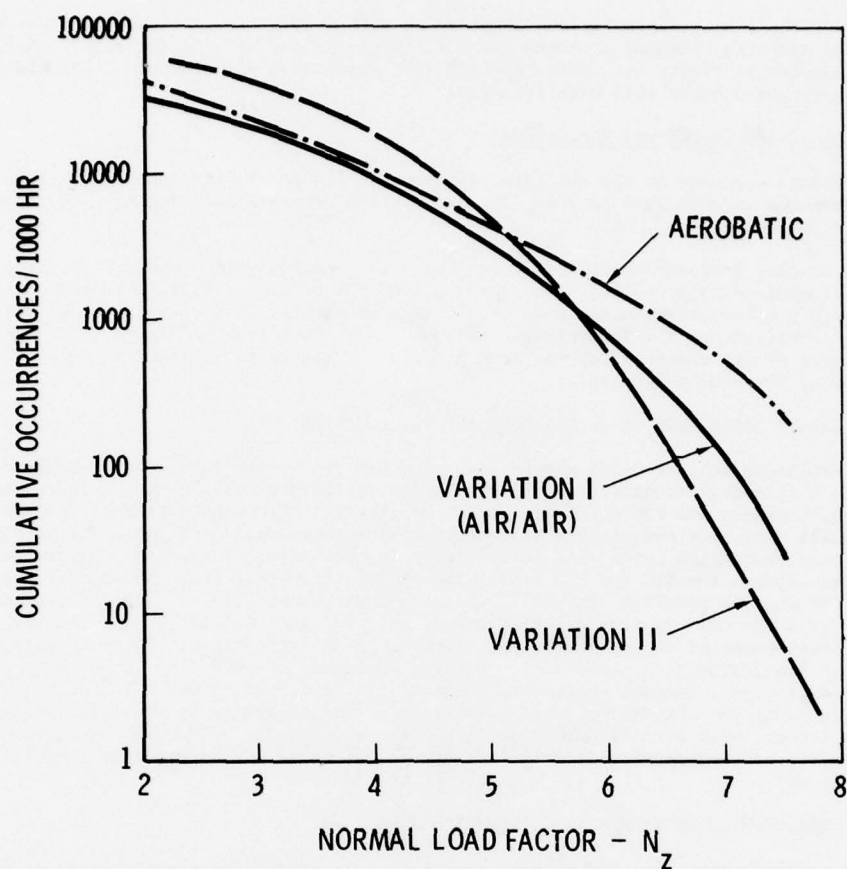


FIGURE 1. TYPICAL COMPOSITE MANEUVER SPECTRA

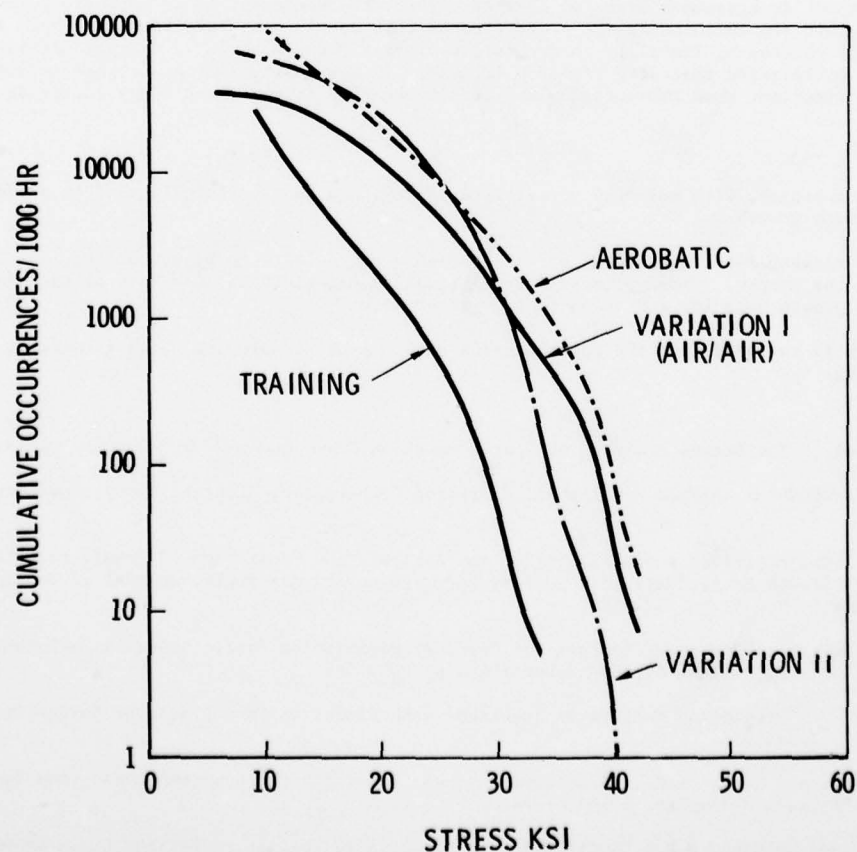


FIGURE 2. TYPICAL LOWER WING SKIN STRESS WITH SPECTRUM VARIATION

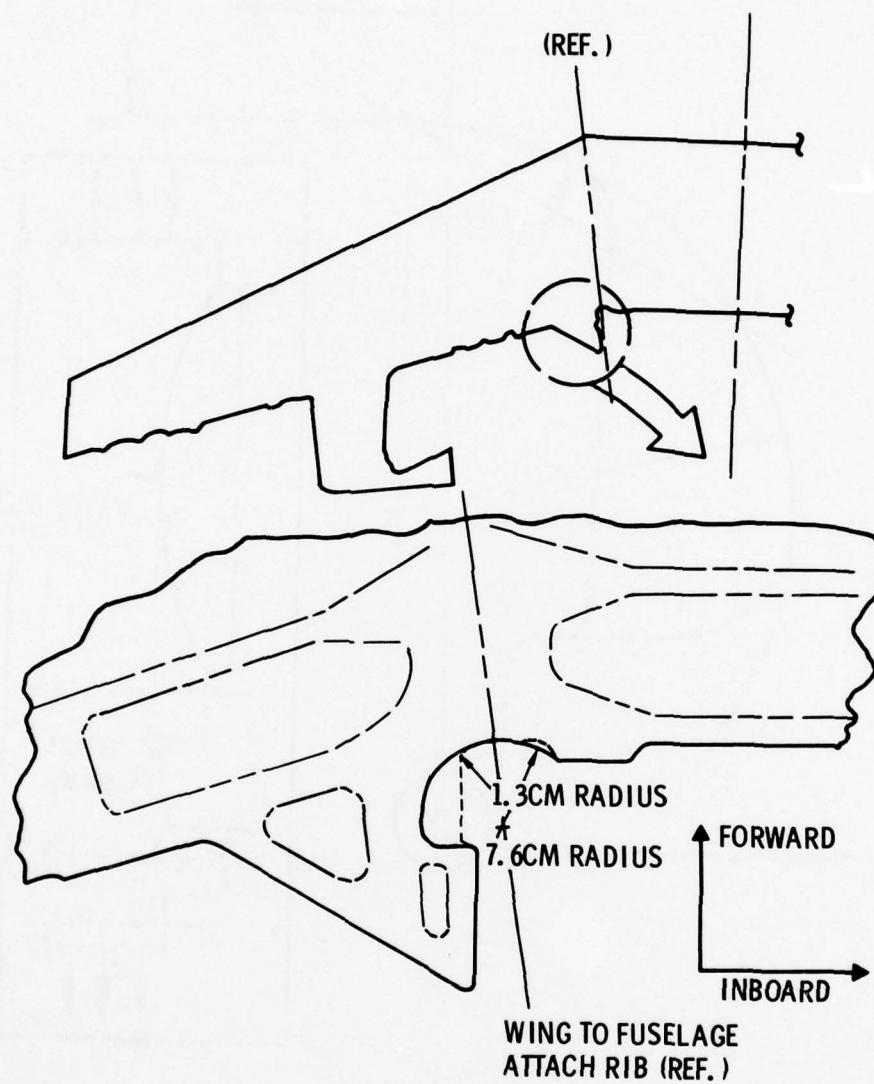


FIGURE 3 RADII CONFIGURATION IN WING ROOT STUDY

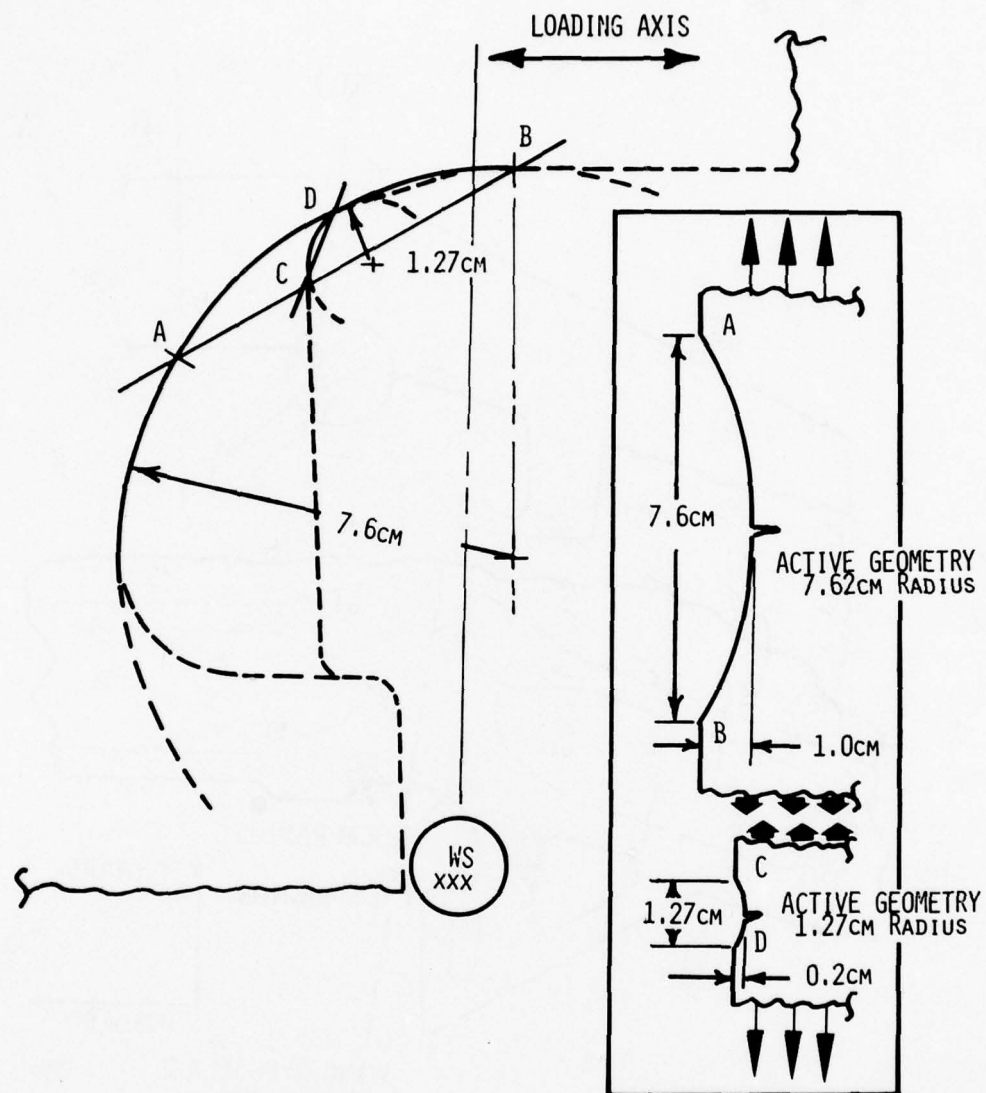


FIGURE 4. ACTUAL AND SIMULATED GEOMETRIES FOR RADIUS STUDY

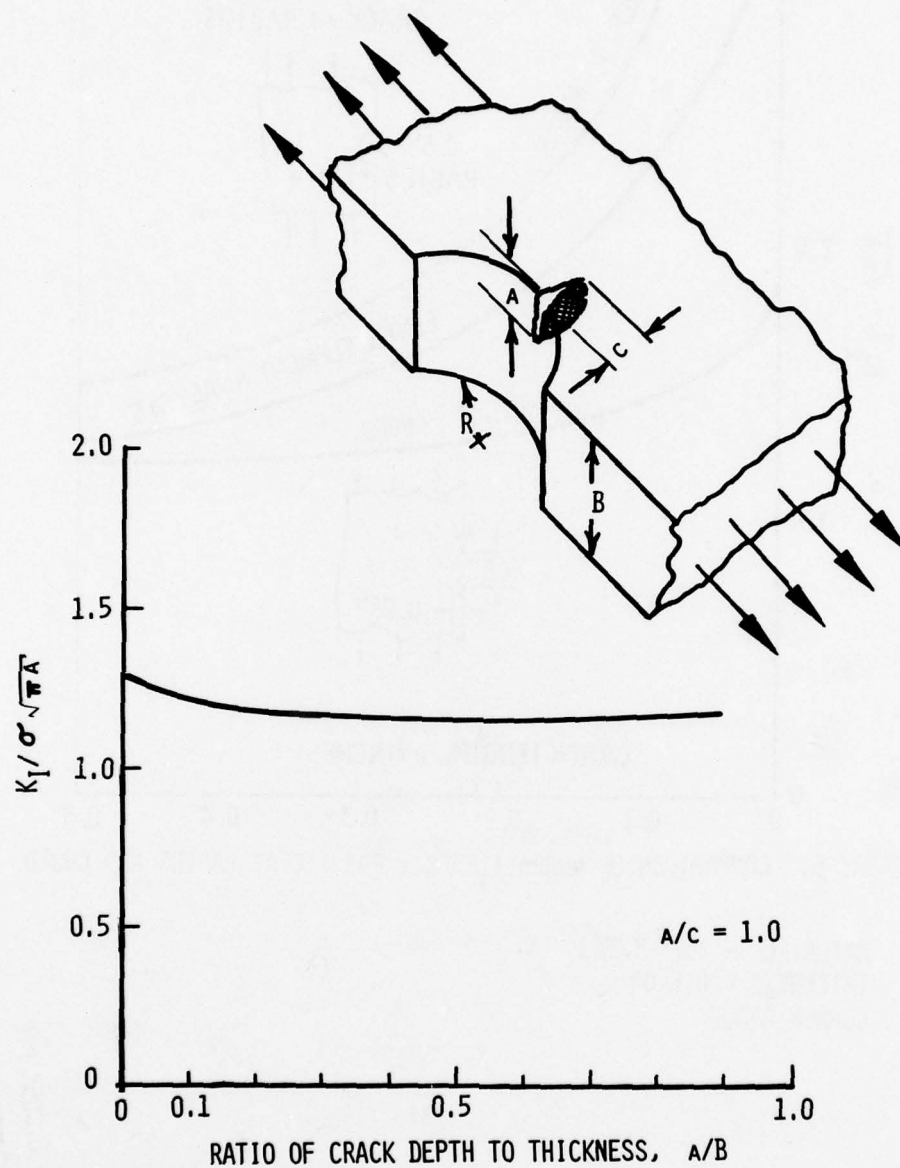


FIGURE 5. NORMALIZED STRESS INTENSITY FOR A PTC AT A CHORD OF A 1.27cm RADIUS



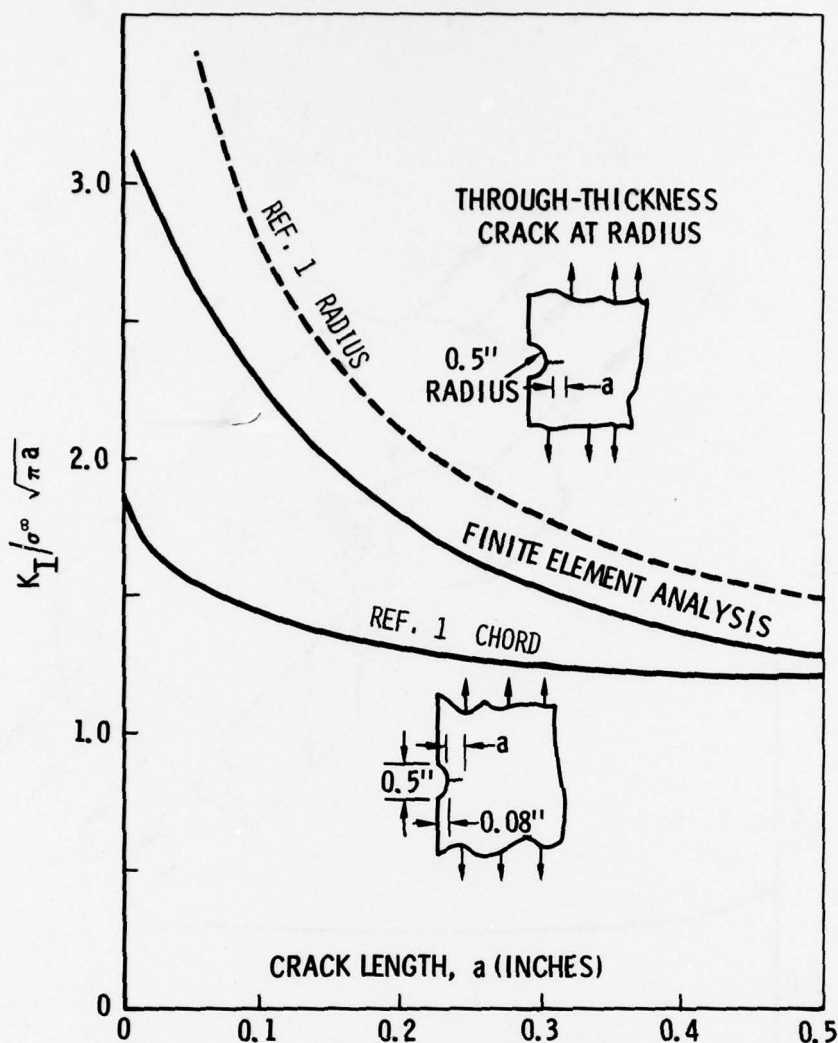


FIGURE 6. COMPARISON OF NORMALIZED K's FOR TTC AT RADIUS AND CHORD

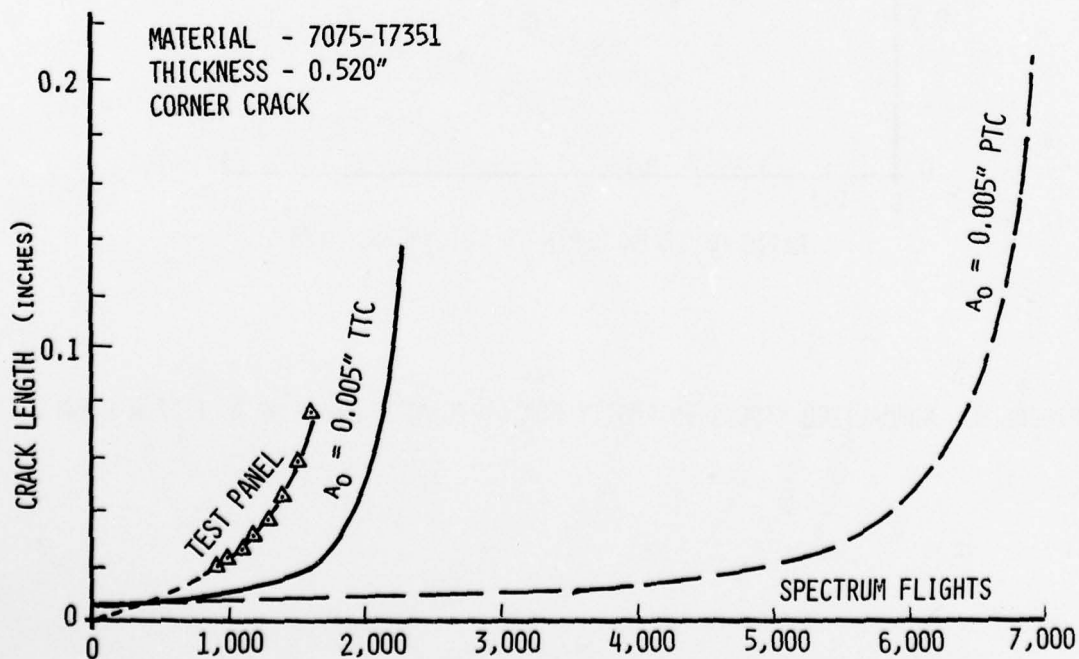


FIGURE 7. SPECTRUM FATIGUE CRACK GROWTH AT RADIUS WITH PREDICTIONS

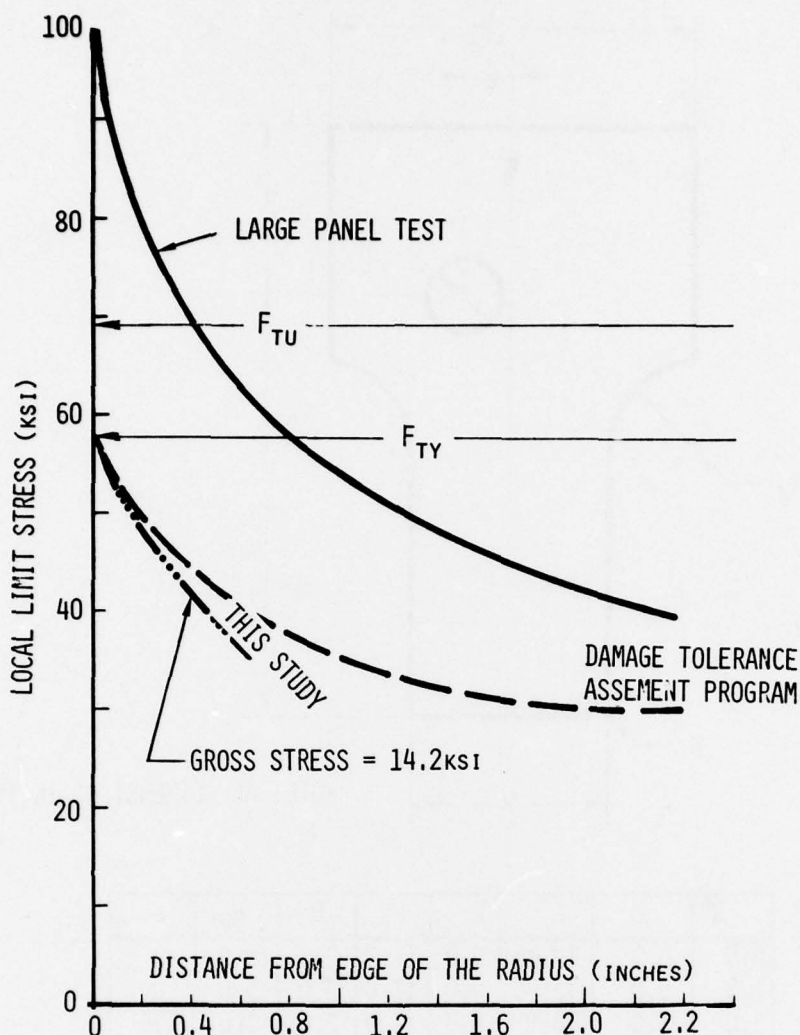


FIGURE 8. STRESS GRADIENT COMPARISON AT 7.62cm RADIUS USING LIMIT STRESS

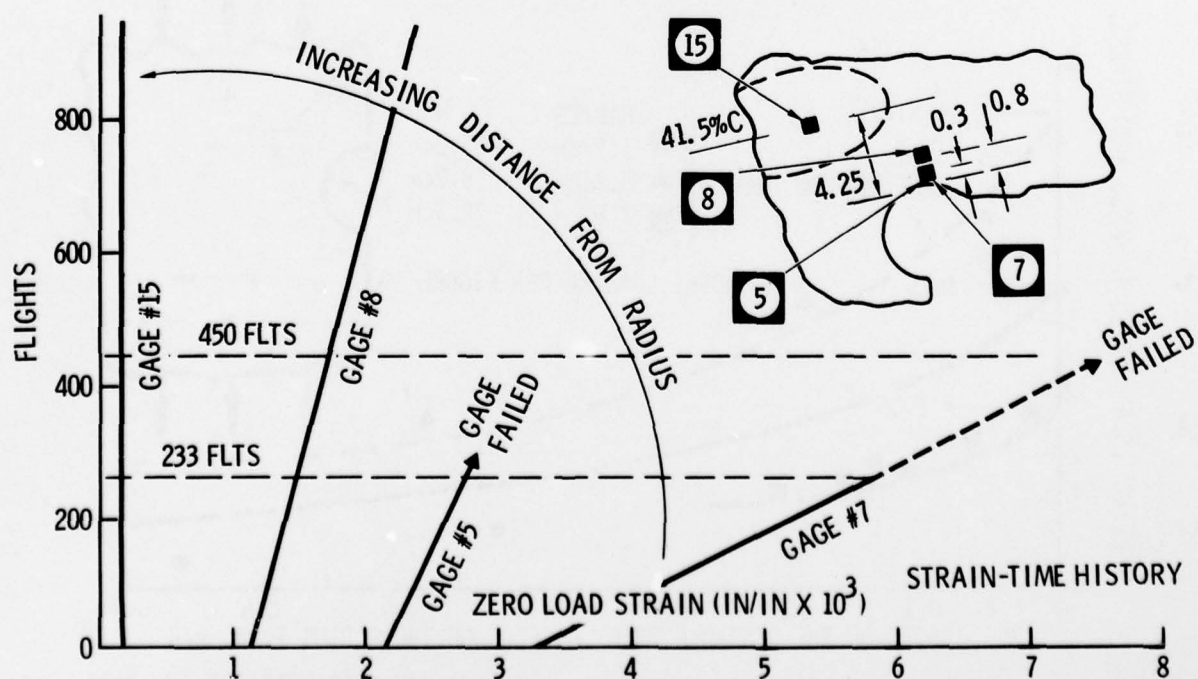
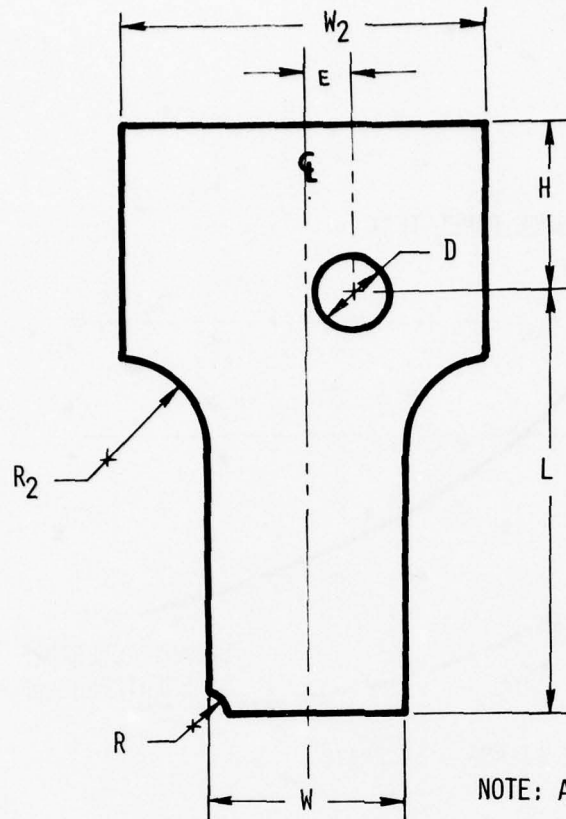


FIGURE 9. STRAIN - TIME HISTORY AT ZERO LOAD IN RADIUS AREA



NOTE: ALL DIMENSIONS IN INCHES

R	H	L	W	W <sub>2</sub>	D	R <sub>2</sub>	E
0.5	5.0	12.75	6.0	11.0	2.0	3.0	0
1.5	5.0	12.75	6.0	11.0	2.0	3.0	0
3.0	5.0	16.0	8.0	12.0	2.0	3.0	1.5

FIGURE 10. GEOMETRIES USED IN TEST AND ANALYSIS

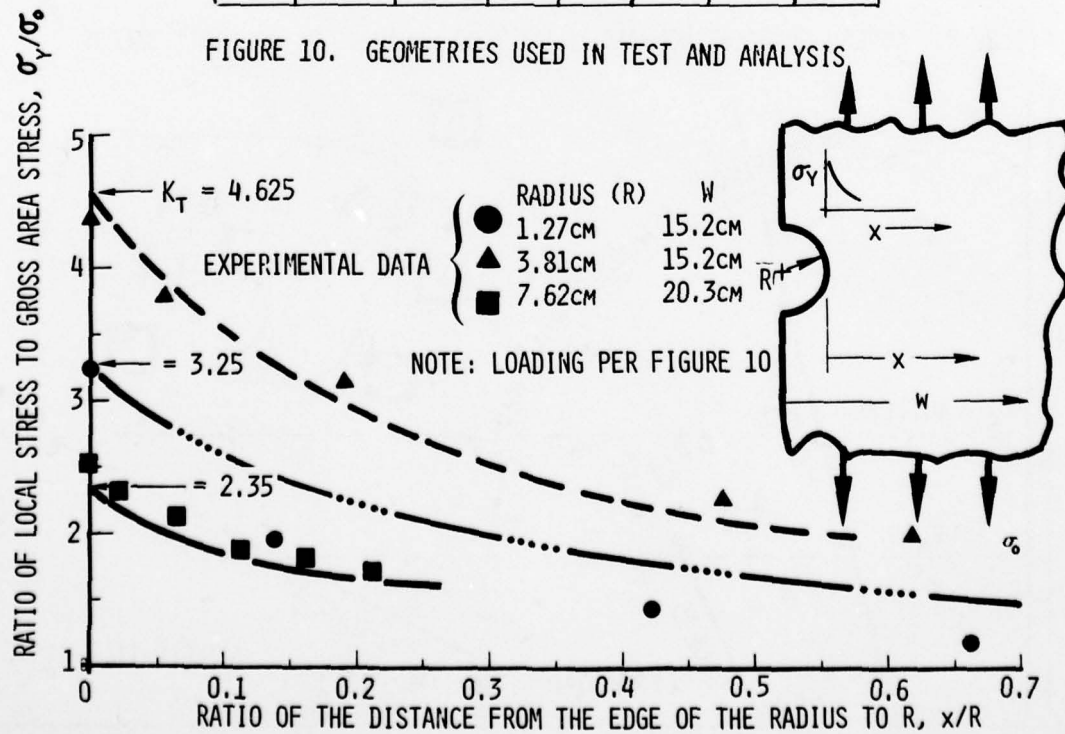
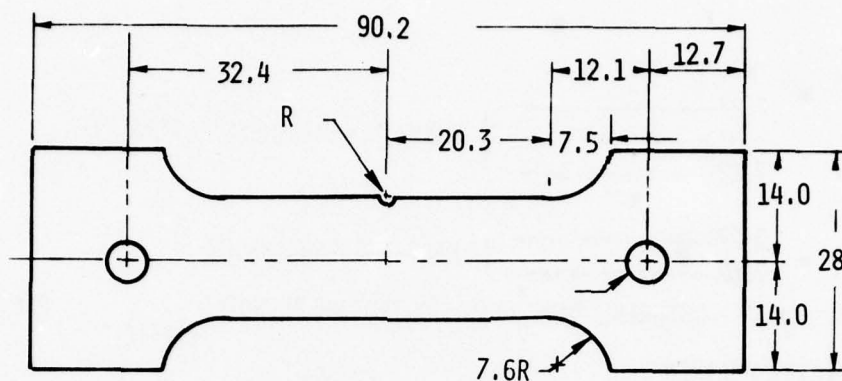
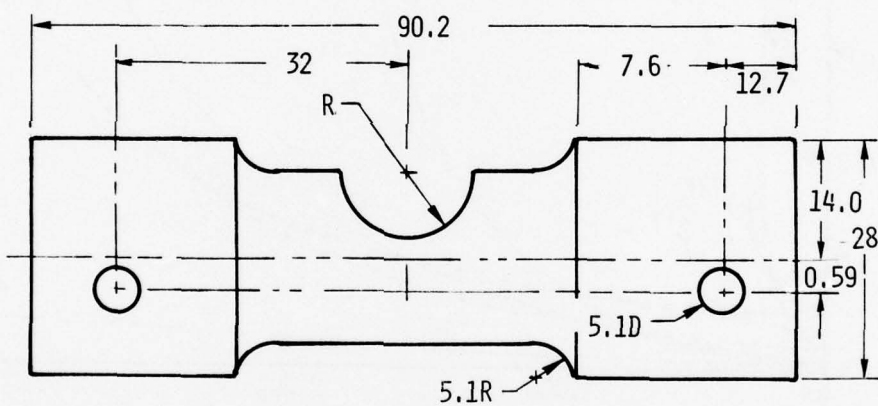


FIGURE 11. COMPARISON OF STRAIN GAGE RESULTS vs ANALYTICAL GRADIENTS FOR THE THREE RADII



1.27 AND 3.81cm RADII COUPONS

ALL DIMENSIONS IN CM



7.62cm RADIUS COUPON

FIGURE 12. TEST COUPON GEOMETRIES





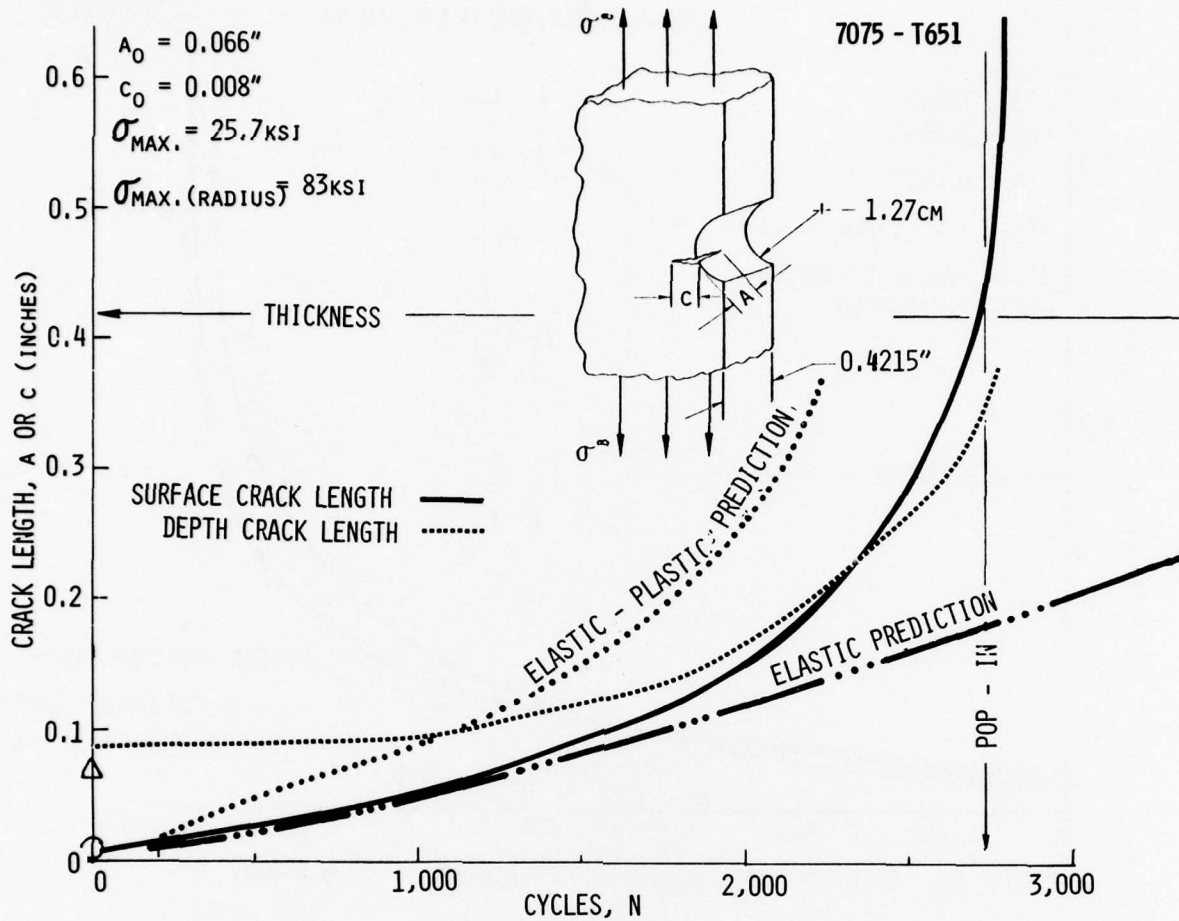


FIGURE 14. COMPARISON OF PREDICTED AND MEASURED CRACK GROWTH, 7075-T651

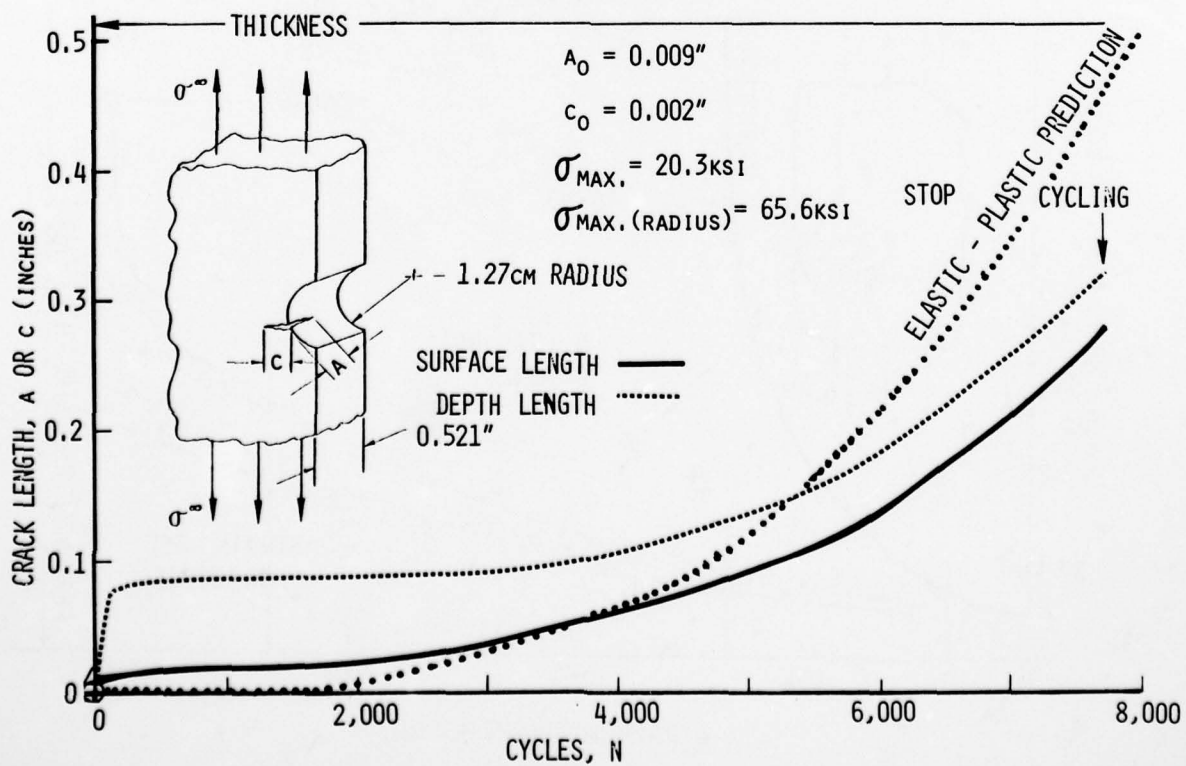


FIGURE 15. COMPARISON OF PREDICTED AND MEASURED CRACK GROWTH, 7075-T7351

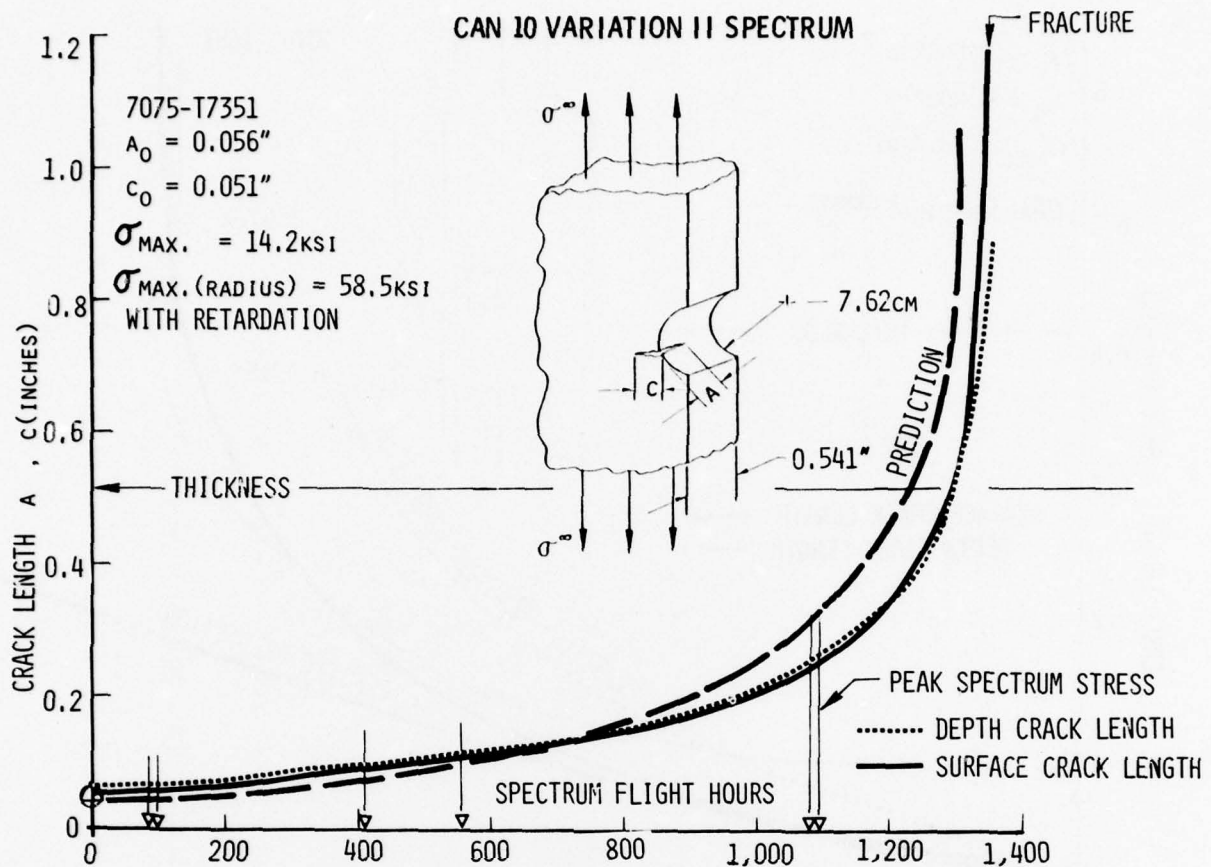


FIGURE 16. SPECTRUM CRACK GROWTH AND PREDICTION, 7.62cm RADIUS

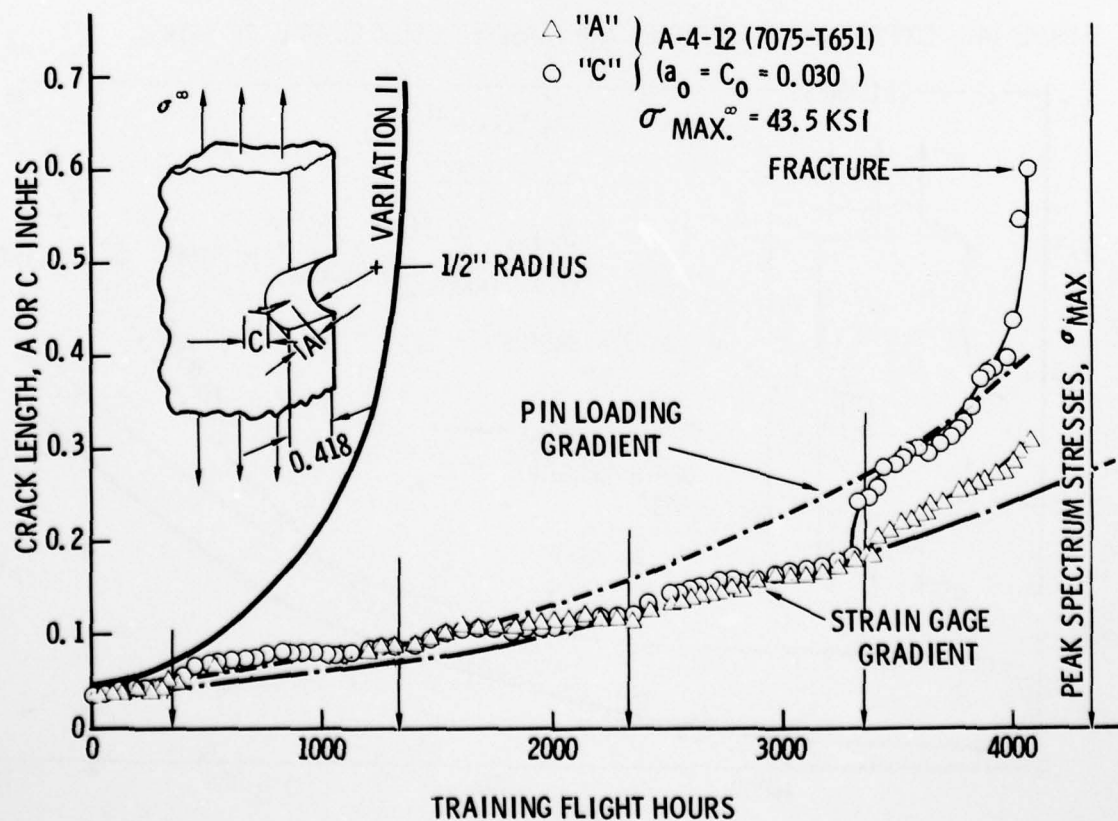


FIGURE 17. RESULT OF SPECTRUM VARIATION AND LOADING ON CRACK GROWTH

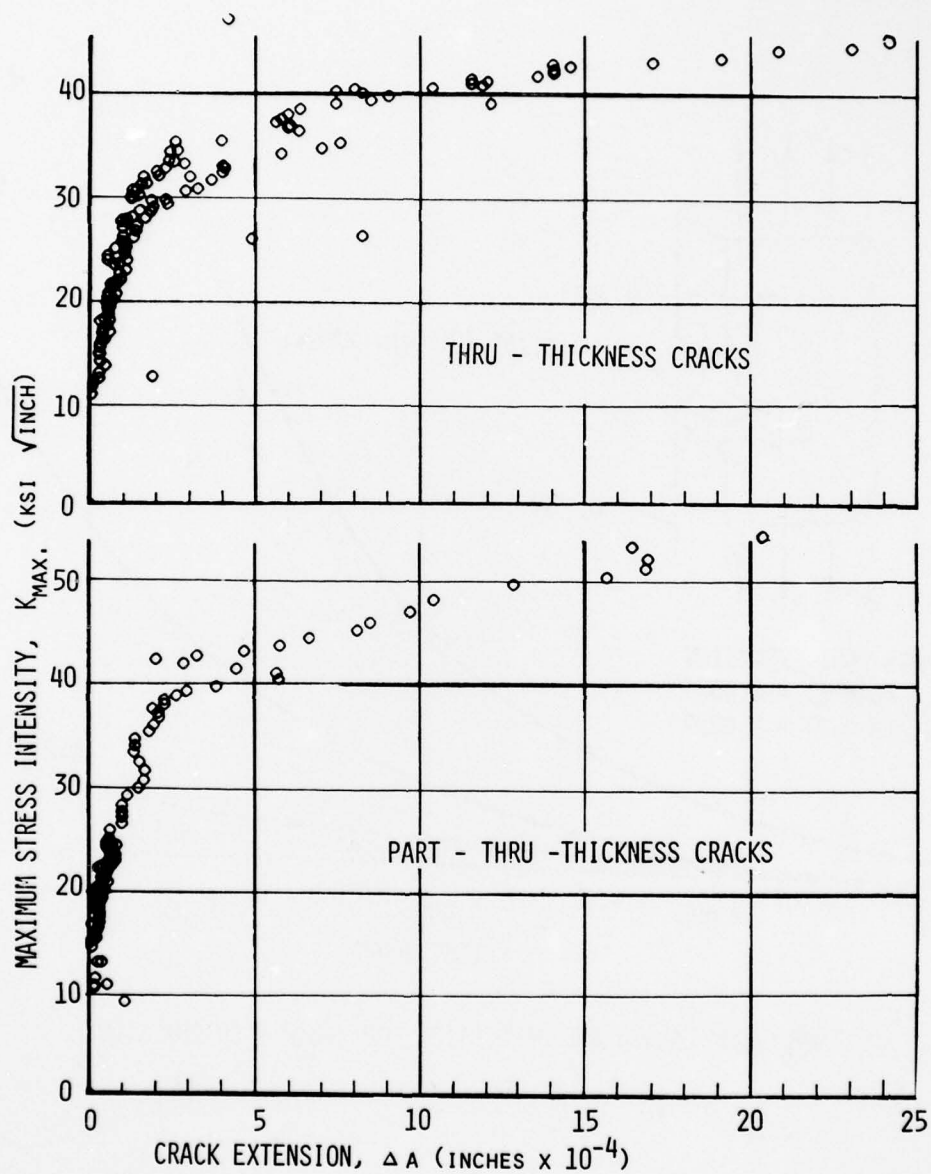


FIGURE 18. FATIGUE CRACK GROWTH RESISTANCE DATA FOR TTC AND PTC AT RADII



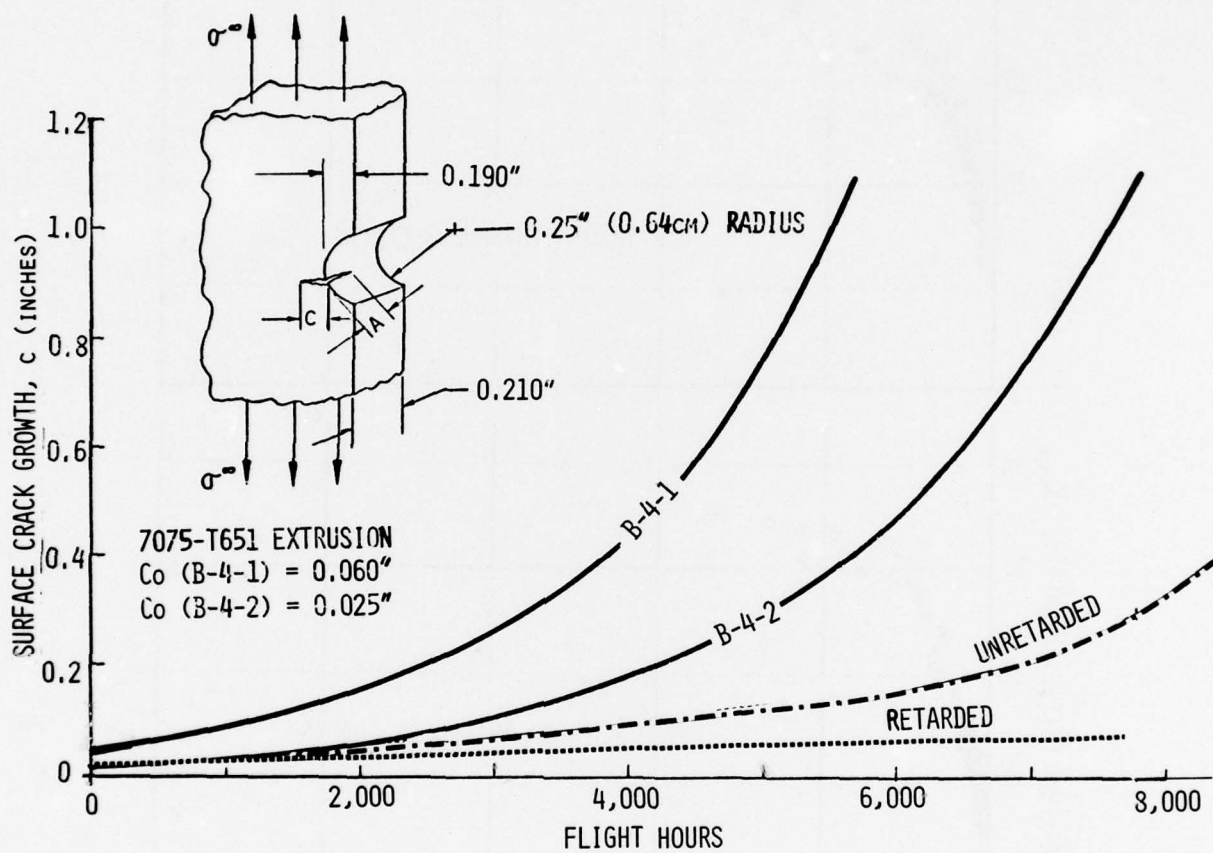


FIGURE 19. SPECTRUM CRACK GROWTH AND PREDICTION FOR COCKPIT CUTOUT STUDY

## DAMAGE TOLERANCE IN PRACTICE

David Broek  
 Battelle's Columbus Laboratories  
 505 King Avenue  
 Columbus, Ohio 43201

## 1. INTRODUCTION

This paper discusses some practical aspects in the application of damage tolerance criteria in the design and operation of aircraft, including the complete fracture control plan. Various authorities have issued rules specifying the required damage tolerance of the airplane structure. These rules will be briefly discussed first. Thereafter, the problem of the application of safety factors will be addressed once more, particularly from the point of view of crack-growth predictions. This will lead to the conclusion that substantial testing is still necessary (and also required by the authorities). Therefore, a brief discussion of damage tolerance testing will follow. Finally, the potentials of fleet monitoring will be addressed, because this practice offers a possibility for a continuous updating of the predictions of life expectancy, which facilitates management decisions. Fleet monitoring is a logical extension of the fracture control plan.

## 2. DAMAGE TOLERANCE REQUIREMENTS

2.1. Civil Airworthiness Requirements

The implementation of damage-tolerance requirements presents many practical problems. The requirements should be rational in

- Specifying a degree of safety that reasonably can be met in design
- Making assumptions as to damage development sequences and initial damage.

Present-day airplanes with good safety and economy records should meet the requirements.

The U. S. Federal Aviation Administration has recently adopted new rules in FAR 25 for damage tolerance of civil airplanes<sup>(1)</sup>. These rules can be found in Reference 2, together with several other proposed rules, the most important of which, are those put forward by the JAR Committee, a joint committee of European Airworthiness Authorities. FAR and JAR rules differ in details but not greatly in their intention. The major differences are in the Means of Compliance provided as an Appendix to both sets of rules and giving an interpretation of those rules. The actual rules can be summarized in a few sentences:

If fail-safe (damage tolerant) design is impractical, adequate fatigue life should be shown by analysis and tests. The residual strength shall always be sufficient to sustain Ultimate Load.

In all other cases, the structure should be shown fail-safe (damage tolerant) by analysis or tests or a combination of analysis and tests. In principle, the residual strength shall always be sufficient to sustain Limit Load. The extent of damage for residual strength evaluation shall be consistent with the initial detectability and subsequent growth under repeated loads. Emphasis is on detection. Realistic load sequences should be used.

The rules leave most of the necessary assumptions and assessments to the designer. Obviously, the Authorities will have the option to challenge such assumptions. The appendices to the rules clearly show the intent of the regulations: where reasonably possible the structure should remain safe if cracks develop, the crack growth period should be sufficiently long so that the cracks can be detected during scheduled inspections at reasonably long intervals. Naturally, a long inspection interval is economically more attractive to the operator. Thus the manufacturer will strive to attain sufficiently low growth rates to allow long inspection intervals, because this will add a sales argument.

2.2. The USAF Requirements

The USAF is in the process of implementing a general and overall fracture control plan. The back bones of the plan are the "Aircraft Damage Tolerance Requirements" of Military specification MIL-A-83444<sup>(3)</sup> and the "Airplane Structural Integrity Program" of Military Standard MIL-STD-1530<sup>(4)</sup>. The first document specifies the design criteria for aircraft with respect to damage tolerance, the second document provides the principles of the fracture control plan and specifies the information required from the manufacturer to permit implementation of the plan by the USAF.

The requirements distinguish three types of structures -

- (1) Slow-crack growth (SCG). Sudden failure by unstable crack extension at a high load would cause loss of the airplane.
- (2) Multiple-Load Path (MLP). Sudden failure of one member (one load path) is not catastrophic. Other members share the extra load.
- (3) Crack-Arrest Fail-Safe (CAFS). Sudden rapid crack extension at a high load is not catastrophic. Crack arrest will occur in reinforced areas (e.g., at stringers).

A structure can be either inspectable or noninspectable. For an inspectable structure, it has to be assumed that a crack of a certain size can be missed during an inspection. This crack may not grow to critical at a

specified load within a certain period. For the case where the crack would terminate, e.g., in a hole before it becomes critical, continuing damage is assumed at the other side of the hole.

A summary of the USAF requirements is presented in Table 1. It is specified that an initial crack of 0.005 inch shall be assumed at every structural hole. At the critical locations a crack of 0.05 inch must be assumed if the structure is of the slow crack growth type, whereas a 0.02-inch crack must be assumed if the structure provides for multiple load paths or crack arresters. Depending upon inspectability and type of structure these cracks may not grow to critical within a specified period at a specified load. If the cracks are inspectable, it must be assumed that a crack of a certain size can escape detection. The required life of this crack to critical is also specified. Since critical cracks may occur in multiple load path and crack arrest structure, requirements are also given for remaining life and strength after a crack instability.

In all cases existing damage is based on assumptions - which are rather arbitrary. Since small cracks grow slowly and large cracks more rapidly, the resulting crack-growth life is extremely sensitive to the initial damage assumptions. As the basis for the initial flaw assumptions is weak, there is no way to estimate the built-in degree of conservatism. Therefore, SCG structure may be unduly penalized by the requirement of both a longer crack life and a larger initial flaw. The penalty should rather be in the life requirement only.

Due to the continuing damage assumptions, it appears difficult to satisfy the postinstability requirements for MLP and CAFS structure, even if these structures amply meet the primary requirements. In that case, the primary requirements become more or less superfluous.

A rationalization of these requirements could be attained if

- The damage assumptions were abolished
- Necessary crack-growth calculations were immediately backed up by a number of specified tests
- Inspectability were to be proven
- The postinstability requirements were relieved
- As far as possible, only natural damage developments were considered
- The requirements would rely heavily on tests.

It should be noted that if a structure is qualified as noninspectable, the requirements do hardly more than specifying a SAFE LIFE requirement instead of a FAIL-SAFE or damage-tolerance requirement. The only difference is that the SAFE LIFE has to be determined on the basis of a crack growth analysis with an assumed initial crack, instead of a conventional fatigue analysis. However, this would be reasonable if crack growth analysis were more accurate than fatigue analysis.

### 3. SAFETY FACTORS

Safety factors are required in a damage-tolerance analysis to account for possible variability due to unknowns, and due to inaccuracies. A decision has to be made not only on the magnitude of these safety factors but also on how and when they should be applied. Various possibilities exist:

- (1) Safety factor on fatigue stresses
- (2) Safety factor on baseline data
- (3) Safety factor on initial crack size
- (4) Safety factor on final life.

A safety factor on fatigue stresses is very unattractive because of the complex nature of fatigue and fatigue-crack growth. Calculated crack-growth rates would have no straightforward relation with actual crack growth, and the calculated and actual retardation effects would be different. Thus, the effect of the safety factor would be a variable, dependent upon geometry and spectrum.

A safety factor on baseline data would have similar drawbacks. In the simplest case, a constant factor, e.g., of 2, would be taken, independent of crack size. This means that a crack of a given size would grow twice as fast in the calculation than in reality. Since the plastic zone size at this crack length would not change, retardation would be effective over approximately half the number of cycles. Stresses of a given magnitude would also occur at different crack sizes than with average data, i.e., at a different K-level. Thus, their associated growth rate would not simply be increased by a factor of 2, but the increase would depend on the entire previous history. As a consequence, the effect of the safety factor would vary for different stress histories. The "safety" would also change for cases with different K-crack length relations.

The situation would become more complex if the factor on growth rate would change with crack size, as would occur with upper bound data. Moreover, it is difficult to give an unambiguous definition of upper bound data. In the  $da/dN$  versus  $\Delta K$  plot of one constant amplitude test, a few outlying data points will be found. These may have been caused by erroneous measurements, but may also be real if the crack showed a somewhat faster growth locally. The data sets for the next tests will give a few more outlying points; thus causing the scatterband in the  $da/dN$  versus  $\Delta K$  plot. In each experiment there were a few anomalous places where crack growth was different from "normal". These anomalies are not reflected in the total crack growth life. Using the scatterband to determine upper bound data is tacitly assuming anomalous behavior throughout the crack-growth life.



A safety factor on initial crack size seems an attractive possibility and needs to be explored. Figure 1 shows computed crack propagation curves(5) for a fighter spectrum for various crack configurations in plates of different thicknesses. The curves were started at a 0.02-inch initial flaw. For reasons of safety, one might want to assume a larger initial crack size, e.g., 0.05 inch instead of 0.02 inch. Then the curves would start at 0.05 inch. The question is whether this would be more conservative, or not.

Let the degree of conservatism be defined as

$$C = \frac{N_{0.2}}{N_{0.5}}$$

where  $N_{0.2}$  is the crack growth life of a 0.02-inch initial flaw to failure and  $N_{0.5}$  is the growth life of a 0.05-inch initial flaw to failure. The ratios  $N_{0.2}/N_{0.5}$  were derived from Figure 1 and are plotted in Figure 2. It appears that the degree of conservatism would vary from 2.25 for a surface flaw in 0.125-inch plate to 1.1 for a corner crack at 0.5-inch diameter hole in 1-inch plate. This results from different flaw geometries having a different K-crack size dependence, which in turn yield different initial growth rates.

It follows that taking a safety factor on initial crack size results in different degrees of conservatism for different crack cases, with less conservatism for more dangerous cracks. An arbitrary increase of the initial crack size for particular structural configurations results in unknown conservatism which may be as low as 0.1. By the same token, a fixed initial flaw size for all cases and all materials does not always result in the same conservatism either. Therefore, the application of a safety factor by assuming a large initial crack size for all cases should be rejected.

The remaining possibility is a safety factor on crack-growth life. Obviously, a safety factor on life will more nearly give the same degree of conservatism for life expectancy, independent of structural configuration, crack geometry, and spectrum. The safety factor would be applied at the end of the calculation procedure by dividing the life at all crack sizes by the same factor; this would constitute the "safe" crack-growth curve. The "safety" or the degree of conservatism would be quantifiable.

#### 4. DAMAGE TOLERANCE TESTING

##### 4.1. Necessity of Tests

The major limitations of fracture mechanics and damage-tolerance analysis were amply discussed in this Lecture Series. It has become clear that an important drawback is the limited accuracy. However, the accuracy of predictions is limited by the variability in properties and by the unknowns in load and stress history more than by anything else. Thus the limited accuracy is not intrinsic to the analysis procedures in the cases that linear elastic fracture mechanics apply. Nevertheless, the limited accuracy remains a technical limitation which will not disappear if more refined analysis procedures are developed. Generally speaking, an answer of limited accuracy is better than no answer at all, provided adequate safety factors are taken into account. Comparative use of the information to judge how various measures effect the fracture risk will be a more satisfactory approach. Tests on full scale components and the complete airframe will always remain necessary, although there still remains the problem of how accurately a test simulates actual service experience.

Two types of damage tolerance tests can be distinguished namely: design development test and full-scale demonstration tests. These two types will be considered in the following subsections.

##### 4.2. Design Development Tests

Design development testing may have many objectives other than those associated with damage-tolerance performance. Therefore, the discussions in this section may not always be fully applicable. In view of the scope of this Lecture Series, it will be assumed that the testing will be for damage tolerance substantiation only.

Under these restrictions, the objective of design development testing is to obtain the longest life and the best damage tolerance at the lowest weight and lowest cost. In this respect, different design concepts, design details, and structural materials are compared.

Design development testing by nature is comparative testing. That means that the test conditions do not always have to be an exact simulation of service conditions as long as the variables considered are tested the same way. How closely the test conditions have to resemble service conditions depends upon the predictability of the effect of a change in conditions. Consider, e.g., the way of load application for the case of crack growth. If there were minor differences with the service circumstances, the results could still be translated if a proper K solution is available for the two cases. However, major differences could still give results opposite from those obtained in service, especially when the difference in test results are relatively small.

It is recommended that a data analysis be made along the lines of the damage tolerance analysis discussed in previous lectures. This has the advantage that some of the design development tests can serve also as analysis substantiation tests and damage tolerance demonstration tests. (In connection to this, it is useful to have at least some of the design development test specimens strain gauged for an additional check of the stress analysis and K analysis.)

##### 4.3. Full-Scale Demonstration Tests

The objective of this task is to verify the structural integrity of the basic design and any necessary modifications. Damage tolerance demonstration tests are part of the full-scale testing program. Their purpose is to demonstrate that the airplane structure has damage tolerance properties in compliance with the applicable Damage Tolerance Requirements, as for crack growth and residual strength.



Crack growth and residual strength test will usually be performed on the full-scale fatigue airframes at the conclusion of the fatigue evaluation. The amount of full-scale damage tolerance testing depends upon the extent to which damage tolerance is demonstrated during design development tests. Usually it is the manufacturer's option whether the full-scale tests are performed on a complete airframe or on separate major assemblies thereof (wing, fuselage, empennage, etc.), provided proper care is taken that load input and reactions are the same as in the complete airframe. Testing components introduces some extra problems as to load reactions and load interactions with other components. As an example, for separate tests on wing and fuselage, the load reactions of the fuselage on the wing should be simulated by supports or appropriate stiffness at the wing fuselage joints. When testing the complete airframe, an extremely complicated loading system is required and the different load histories of the various components have to be simulated simultaneously. The changes of malfunctioning increase with the test complexity, so that the expected down time is large.

From the point of view of damage tolerance testing per se, there are advantages in performing separate tests on major components. This pertains specifically to residual strength and crack arrest tests. In those cases, the critical locations can be tested one by one. Tests on different components could go on simultaneously. Failures would only affect the component in which they occur.

In order to achieve the complex loading condition of both the ground and in-flight situation, local as well as distributed loads have to be applied. The local loads (e.g., those from power plants) can be applied at the appropriate fittings. The distributed loads pose problems because the structure does not provide for load application points. Therefore, these have to be built in, which may require minor modifications of the structure. Details of various possible systems can be found in the literature<sup>(6-10)</sup>.

The load history has to be a flight-by-flight simulation. Deterministic loads are to be applied in the flight segment in which they occur. Probabilistic loads may be ordered or randomized. In the case of ordering, a low-high-low sequence per flight is recommended in accordance with previous discussions, which are applicable also to clipping and truncation questions.

In a successful full-scale test, cracks should be detected at the earliest possible time. This is crucial for obtaining crack-growth records of the critical locations, but it is also of importance for secondary cracks and nuisance cracks. This means that thorough inspections should be scheduled that cover the complete test article.

The full-scale test is also a learning period. Areas of potential service problems are identified. More important, the best possible way of inspection should be established. Therefore, a variety of inspection techniques should be evaluated for their effectivity at various locations.

Records can be made of the natural development of cracks and the progression of damage. The damage development will, in generally, be different from the assumed damage development in the damage tolerance analysis. An evaluation of the natural damage along the same lines as used in the damage tolerance analysis, will prove or disprove the validity of the previous damage tolerance calculations. It will appear whether a reassessment of the damage tolerance analysis has to be made. More important is that it will give a direct proof of the adequacy of crack-growth life with respect to the applicable requirements.

If cracks do not develop during the period of durability testing, damage tolerance tests may be performed by artificial crack starters at the critical locations. Usually, only one or two of a number of similar locations of equal criticality will be selected. All critical locations of different design will be selected, however, unless some can be waived on the basis of the results of design development tests. Provided interaction of cracks does not occur, all selected locations can be precracked simultaneously to save testing time.

The predictability of fracture and arrest is somewhat better than of fatigue-crack growth. Therefore, the results of the design development tests and the residual strength analysis will often be a sufficient proof of compliance with the applicable residual strength requirements. However, it is advisable to do some fracture testing under the complex loading situation of the full-scale test articles. In view of the high risk of losing the test article, these fracture tests should not be conducted until all the crack-propagation data are satisfactorily analyzed to ensure that no further crack-growth testing is desirable. Essentially, only one fracture test can be performed. However, a fair amount of information can be obtained with the proper test plan. For example, all cracks but one can be repaired in a provisory manner. The remaining crack is loaded to 90 percent of the expected failure load. It is then repaired, while the repair of another crack is removed and the procedure repeated. Finally, the most critical crack is taken to failure.

It is advisable to perform a teardown inspection at the end of the full-scale test including any scheduled damage tolerance tests. The inspection involves a complete disassembly and laboratory-type inspection of all critical areas, including those not anticipated in the design but revealed by the tests.

## 5. AIRCRAFT SAFETY

### 5.1. Final Damage Tolerance Analysis

During and after completion of the damage tolerance testing, a final evaluation of the compliance with the applicable Damage Tolerance Requirements can be made. The test data provide direct information on crack growth and residual strength for the case of natural damage development under the specific circumstances of the tests. It shows whether crack-growth life is adequate to cover the specified inspection intervals.

A reprediction of the test data by means of the analysis procedures used throughout the design provides a final proof of the adequacy of the analysis. Necessary changes and corrections can be made, which then allow a final analytical proof of compliance with the damage tolerance criteria.

If the "actual" and "assumed" aircraft usages are reasonably similar, the design damage-tolerance analysis provides practically all the information for the planning of inspections and repairs to ensure safety of the aircraft. However, this ideal situation never occurs because, in practice,

- (1) The aircraft is assigned new tasks - different from those anticipated
- (2) The aircraft is flying many more of a specific mission than was foreseen
- (3) The load spectrum derived from experience with other aircraft systems for particular missions appears to be significantly different for the new system, as a result of a different aircraft response or as the result of a change in logistics or training habits.

Apart from the differences in aircraft usage, individual aircraft within a fleet may be subject to usage patterns substantially different from the average assumed spectrum for that fleet. This may adversely affect aircraft safety. Therefore, a continued updating of the damage tolerance analysis may be warranted for a complete fracture control plan. This can be accomplished by *fleet monitoring and aircraft monitoring*.

### 5.2. Fleet Monitoring

A different usage spectrum may significantly affect crack propagation. Thus, the initially determined safe crack-growth intervals must be continually adjusted because the future usage spectrum will continue to deviate from the anticipated. The information obtained for actual crack-growth damage is essential to

- (1) Ensure safe operation of individual aircraft
- (2) Establish safe operational envelopes of the weapon system
- (3) Schedule inspection and repairs for individual aircraft and for the whole fleet, such as to ensure a smooth maintenance schedule for the weapon system
- (4) Schedule major retrofits and judge their efficiency and schedule retirement and replacement
- (5) General system management to maintain a rational degree of combat readiness to which structural integrity is one of the contributing factors.

The adjustment and monitoring of safe crack-growth intervals on the basis of actual aircraft usage has to be based on a combination of the results of a parametric study and of records of actual aircraft usage. Analysis of this data package will provide information relative to the damage status of individual aircraft and of the fleet to permit an appraisal of the safe crack-growth interval under certain conditions of continued usage.

The USAF has established a detailed fracture control plan in the Aircraft Structural Integrity Program (ASIP)(4) which describes five tasks that must be undertaken to ensure structural integrity. These tasks are summarized in Figure 3. Tasks I through IV are conducted by the aircraft manufacturer; Task V is the responsibility of the Air Force. The compilation of the fleet management data package (Task IV) provides the USAF with the necessary information for an efficient fleet management (Task V). As outlined in the foregoing paragraphs, the monitoring of fatigue-crack growth is an essential part of the fleet management. The parts of Tasks IV and V constituting the elements of the monitoring procedure are shown in the heavy-framed boxes in Figure 3.

Apart from conducting the parametric analysis, the aircraft manufacturer has to make provisions for instrumentation and data recording to permit records of aircraft usage. These provisions are twofold.

- (1) Comprehensive instrumentation for a few aircraft to allow a loads/environment spectra survey. The survey is necessary to assess the applicability of the design spectrum.
- (2) Simpler instrumentation for all other aircraft for routine mission monitoring. Interpretation of data records is facilitated by the results of (1). It is this instrumentation, together with the parametric analysis results, that is to be used for the service monitoring program (as part of Task V).

Although fatigue monitoring has been done in the past to some extent, the monitoring of fatigue-crack propagation has not been practiced on a rational basis. The application of the ASIP requirements involves many problems as shown in Figure 4. A methodology that can achieve this with sufficient accuracy on an economical basis includes at a minimum,

- (1) A rationale for a parametric analysis of crack growth
- (2) Guidelines for flight data records as to the scale and nature of the quantities to be measured
- (3) Procedures to obtain information from the data records and the parametric analysis in a relatively simple way
- (4) Establishment of logistics to ensure flawless and economic handling and processing of data records under the restrictions set by a complex system of aircraft operations.

### 5.3. Aircraft Monitoring

The basic data for fatigue-crack monitoring are to be obtained for the fleet and the individual aircraft. In principle, these data should be the stress histories actually experienced at each of the critical



locations of each individual aircraft. However, this is difficult, if not impossible, for the following reasons:

- (1) Monitoring the stresses at a large number of different locations is costly and not very practical
- (2) Direct stress recording is not possible. Another quantity has to be measured from which the stresses can be derived for critical locations
- (3) Continuous recording of analog signals is costly. Since some counting (or data reduction) procedure will have to be used anyway, it is usually preferable to have this counting done on a real time basis by the recording instrument.

Therefore, a decision has to be made on (1) the quantity to be measured, (2) the location(s) of measurement, and (3) the presentation of data (e.g., counting procedure).

As for the quantity to be measured, there is not much choice. Ideally, it would be the stress at all critical locations, because the stress is the quantity that has to be used in the crack-growth analysis. However, if records can be made of only one location (which may not be critical), the measurement of stresses becomes dubious. For example, there is not a unique relation between the stresses in the wing and the tail; hence, the stress record of a location in the wing would give no information about the stress history of the fin or the stabilator.

Moreover, the stress history of a certain location in the wing cannot always be derived unambiguously from the record of another location. The distribution of bending moments in the wing changes, e.g., due to fuel consumption from the wing tanks or the disposal of external stores. If these occurrences were recorded simultaneously, the stress at a certain location could be derived from the stress measured at another location.

The alternative for stress measurement is the measurement of acceleration. Taking an extreme case, the accelerations experienced by the wing tip do not bear much information regarding the stresses in the wing. The center of gravity accelerations do, but there is no unique relation between these accelerations and the stresses at some location in the aircraft.

It follows that acceleration records would have to be complemented by records of speed, altitude, aircraft configuration (stores, fuel, flaps, landing gear, spoilers). A complete description of a situation would require measurement of acceleration along the three axes of translation and information about roll, yaw, and pitch rates. Then a large number of variables has to be recorded. Moreover, the data reduction cannot be done easily by the recording instrument because going from accelerations to stresses is a complicated procedure.

Hence, it may seem more attractive to record strain directly at a fairly large number of locations, since this would eliminate the conversion problem. Alternatively, some additional data may be required for purposes other than fatigue monitoring and would have to be recorded anyway. The final decision then becomes largely a matter of economics, availability of multichannel recorders, and costs of data reduction. However, a parametric analysis of crack growth may indicate that for a particular aircraft system, or a category of aircraft systems, only limited information is required if strains are recorded and more if accelerations are recorded, or vice versa.

Usually, only a few aircraft in a fleet will be equipped with instrumentation for the elaborate flight measurements described. All other aircraft of the fleet will be monitored by a simpler device where only a few locations will be strain gauged or only center of gravity accelerations in Z-direction will be measured.

An important problem is the number of discrete levels that should be counted in order to obtain a reasonable coverage of the whole spectrum. In this respect, the spectrum shape is of relevance. Also, it is necessary to know which particularities of the spectrum should not be missed for proper crack monitoring. Answers will be obtained from the parametric analysis.

Secondly, the levels themselves have to be set. Here, a problem of truncation is involved. The choice of the lowest level will be derived for the total number of counts that is made. The setting of the highest level determines what will be the highest loads that will be applied in the analysis. The settings of the levels have to be selected on the basis of how well the total spectrum (including upper and lower ends, the tails, and the GAG cycles) could be established on the basis of the counts and on the basis of the most significant damage levels found in the analysis.

Finally, the counting procedure will have to be selected. The load history recordings that form the basis for aircraft monitoring and the techniques of data reduction (counting procedures) are decisive for the reliability of fleet management. Although there is a firm knowledge on how well a certain counting strategy describes the spectrum, there is little information on how well it describes the important parameters for crack growth; neither is there much information about the number of levels to use and the height of the levels.

#### 5.4. Parametric Analysis

Whether or not an intensive fleet monitoring program is carried out, the fact remains that aircraft usage may be substantially different from the assumptions made in the damage tolerance analysis. Therefore, a parametric crack growth analysis to assess the effect of different usage is always in place.

Several schemes for parametric analysis have been proposed. Gallagher and Bader<sup>(11)</sup> showed that if a plot is made of  $a/a_c$  (instantaneous crack size over critical crack size) versus  $N/N_c$  (cycles or flights at crack size  $a$ , over total crack life) all data fall in a relatively small scatterband, regardless of spectrum and geometry. This would provide a normalized growth curve for all conditions (Figure 5), useful for

parametric evaluations. Gallagher and Bader showed mathematically that this result should be expected, but their analysis can be easily defeated and it can be shown that their result was fortuitous.

Alternatively, it has been suggested by many authors that crack growth can be analyzed on the basis of a parameter that is descriptive for the spectrum. For example, the stresses in the spectrum could be adequately described in certain cases on the basis of their root mean squares (RMS) value. Thus at a given crack size  $a$  one can define

$$\Delta K_{RMS} = B \Delta K_{RMS} \sqrt{\pi a} \quad (1)$$

Using similarity argument one can then postulate that

$$\frac{da}{dN} = f(\Delta K_{RMS}) \quad (2)$$

The function  $f(\Delta K_{RMS})$  could be obtained empirically from a small number of experiments with random loading. Subsequently, the crack growth behavior for a different spectrum could be easily obtained by directly integrating Equation (2). No retardation model would be necessary, the integration would be linear and could be performed in seconds on a pocket calculator. Unfortunately, Equation (2) is only applicable when all conditions for similarity are fulfilled. This is nearly so when the spectrum is stationary Gaussian with a relatively small period. Obviously it is not so when the spectrum contains many discrete events (such as GAG cycles) and when the spectrum contains relatively few high loads.

A third possibility is to use an integration based on  $da/dF$ , the crack extension per flight. For each parameter variation the crack extension per flight would be calculated at five to ten different crack sizes, using for example 100 flight increments at each crack size and applying an appropriate retardation model. The resulting  $da/dF$  data can then be plotted as a function of crack size which permits establishment of a  $da/dF$  curve. Linear integration of this curve provides the crack growth curve. Since cycle-by-cycle integration would only be conducted at a few crack sizes, the calculations can be fast enough to permit parametric studies.

A final possibility is to use the simple spectrum evaluation technique discussed in a previous lecture, combined with the semilinear integration discussed in the same lecture. Such a scheme would probably be the most expeditious while it would still have acceptable accuracy. (Note that the parametric analysis is of a comparative nature.)

## 6. CLOSURE

On a multitude of occasions during this meeting, the shortcomings were pointed out of damage tolerance analysis because of its presumable inaccuracy. This pertains in particular to crack-growth computations and to a lesser extent to residual strength calculations. Admittedly, the analysis procedures have shortcomings and further developments are required. However, the accuracy of the analyses should be judged against the background of the level of accuracy that can reasonably be expected from any engineering analysis. Furthermore, the inaccuracies due to the analysis procedure should be clearly distinguished from those due to the data input, since the combination of the two constitutes the accuracy of the final result. If the inaccuracy in the input data predominates in the end result, the inadequacies of the analysis become of secondary importance.

To consider the accuracy of an engineering analysis, the classical static strength analysis of the new (undamaged) structure will be taken as an example. In this analysis, the modulus, the yield strength, and ultimate tensile strength of the material are usually considered as reliable data input. Nevertheless, in setting the design allowables a substantial margin is taken with respect to the values actually observed. The static strength analysis is considered a sophisticated design tool. Yet, when it comes to the full-scale test of the complex structure, it turns out that the difference between the actual static strength and the calculated strength can easily be as much as 10 percent. (In this respect, it should also be recognized that the structure fails at only one place.) In view of this discrepancy and in view of possible misjudgment of the maximum loads, a substantial safety factor is taken on the calculated strength.

It is difficult to understand why a damage tolerance analysis is demanded to have a better accuracy than a conventional static strength analysis. It was shown during this meeting that the residual strength of cracked complex structure can be predicted within about 10 percent also. This proves the adequacy of the analysis at least for those applications. It was also shown at this meeting (W. Schütz) that in some cases the residual strength of a forged component can be largely different than predicted. However, this was due to the inconsistency of the properties of the material, rather than due to inadequate analysis. Obviously, in that case a residual strength test could not give more reliable information than an analysis, nor would a more sophisticated analysis improve the prediction. Against this background, the anomalies in the analysis methods per se, become of secondary importance. A further sophistication of these methods would not largely improve the end result if the accuracy of the input data is not improved.

Apparently, reasonable crack-growth predictions for flight-by-flight loading can be made provided the input data are reliable. During the progress of the design, the input data gradually become better defined. In the early design stages, their accuracy is low. Nevertheless, computed crack-growth information can be used in a comparative way in parametric studies, to evaluate the relative crack-growth performance resulting from certain design changes.

At the time of component testing and full-scale testing, some actual crack-growth information becomes available. On the basis of these data the models can be adjusted and subsequently all predictions for other cases and other locations can be updated. As a consequence, these predictions have approximately the same accuracy as the experimental data.



When in-flight spectrum measurements become available, a final updating of the crack-growth predictions can be made. At that time, a final safety-factor on crack-growth life can be taken to establish inspection intervals. (It is emphasized that safety factors anywhere else in the computations, i.e., on cyclic stresses or on baseline data, do not permit evaluation of the margin of safety; moreover the margin of safety will be different for different configurations. Taking a safety factor on the final outcome of the computation is the only way to factor all computations to the same extent.) The effects of different aircraft usage can also be evaluated. In particular, the problem of the occurrence of high loads can be analyzed, since also the effects of spectrum truncation and clipping can be adequately predicted with a well-adjusted crack-growth model.

Crack-growth computations may be costly, because of the long computer times involved. However, for the application to specific cases much more efficient computation routines can be followed, permitting the use of desk computers or even pocket calculators.

Present-day knowledge of fracture mechanics and modern stress-analysis techniques permit the prediction of damage tolerance (crack growth and residual strength) of most of the airplane structure. The techniques still have shortcomings. Also, the data required as input to the analysis do not always have the desirable accuracy. However, shortcomings can be pointed out in the guesswork associated with any new design. In general, designing is a projection in the future of past experience, using more or less approximate models for stress analysis and estimating the unknowns. Confidence in the design procedures is based upon experience and apparent adequacy in the past. The magnitude of the applied safety factors reflects the degree of confidence.

Hence, the shortcomings of damage tolerance analysis can hardly be an excuse for postponing the application to design, although the lack of past experience asks for some caution. In the absence of experience, some confidence in the methodologies can be obtained from an application to existing designs, where a comparison with service behavior can be made directly. Otherwise, confidence can only be built by accumulating experience through cautious application.

Sometimes damage-tolerance analysis is almost categorically rejected as inadequate. The alternative is to rely entirely on tests. However, tests suffer from some of the same inadequacies (i.e., spectrum input, material variability). Of course, tests will always be necessary (even static strength is demonstrated by experiment), but tests provide information for a few cases only. A combination of analysis and tests allows evaluation of other critical locations with the possibility of updating the results. Damage-tolerance analysis does have shortcomings. It is not yet generally applicable. Research will continue to improve the procedures. However, postponing application of the present technology - until these new developments materialize - is no longer justified.

#### 7. REFERENCES

1. Anon., Federal Aviation Regulations FAR 25 - in particular FA 25.571.
2. Anon., Regulatory Review Program, Part 25, Conference Agenda, March 1977. U. S. Department of Transportation.
3. Anon., "Airplane Damage Tolerance Requirements", MIL-A-83444.
4. Anon., "Aircraft Structural Integrity Program - Airplane Requirement", MIL-STD-1530 (USAF).
5. Broek, D., and Smith, S. H., "Spectrum Loading Fatigue Crack Growth Predictions and Safety Factor Analysis", NADC Report No. 76383-30 (1976). Summary to be published in Eng. Fract. Mech.
6. Nelson, L. W., Meleon, M. A., and Simons, H., "The L-1011 Fatigue and Fail-Safe Development Program", RAE TR 73183 Paper 1.3.
7. Fonk, G. J., "Investigation of the Fail-Safe Properties of Civil Aircraft", RAE TR 73183 Paper 1.4.
8. Plantema, F. J., and Schijve, G., Editors, Full-Scale Fatigue Testing of Aircraft Structures, Pergamon (1961).
9. Schijve, J., and Broek, D., et al, "Fatigue Tests With Random and Programmed Load Sequences. A Comparative Study on Full-Scale Wing Center Sections", AFFDL-TR-66-143 (1966).
10. Ripley, E. L., "The Philosophy Underlying the Structural Tests of a Supersonic Transport Aircraft With Particular Attention to the Thermal Cycle", NASA SP 309 (1972) pp 1-91.
11. Gallagher, J. P., and Bader, A. M., "A Normalization Scheme for Describing Crack-Growth Behavior", AFFDL-note, undated.

TABLE 1. SUMMARY OF USAF AIRPLANE DAMAGE TOLERANCE REQUIREMENTS

	Slow Crack Growth Structure	Multiple Load Path and Crack Arrest Structure
<u>Noninspectable Crack</u>		
Assumed initial crack	0.05 in.	0.02 in.
Required life	2 airplane lives	1 airplane life
Required residual strength	Load occurring once in 20 lives	Load occurring once in 20 lives
<u>Inspectable Cracks</u>		
Assumed crack after inspection		
After special NDI inspection	0.05 in.	0.02 in.
After normal NDI inspection	0.25 in.	0.25 in.
After visual inspection	2 inches	2 inches
Required growth period	$\frac{1}{2}$ airplane life	$\frac{1}{2}$ airplane life
Required residual strength	Load occurring once in 5 lives	Load occurring once in 5 lives
<u>After Instability (and Arrest)</u>		
Required Growth Period		1 Flight to $\frac{1}{2}$ life depending upon detectability

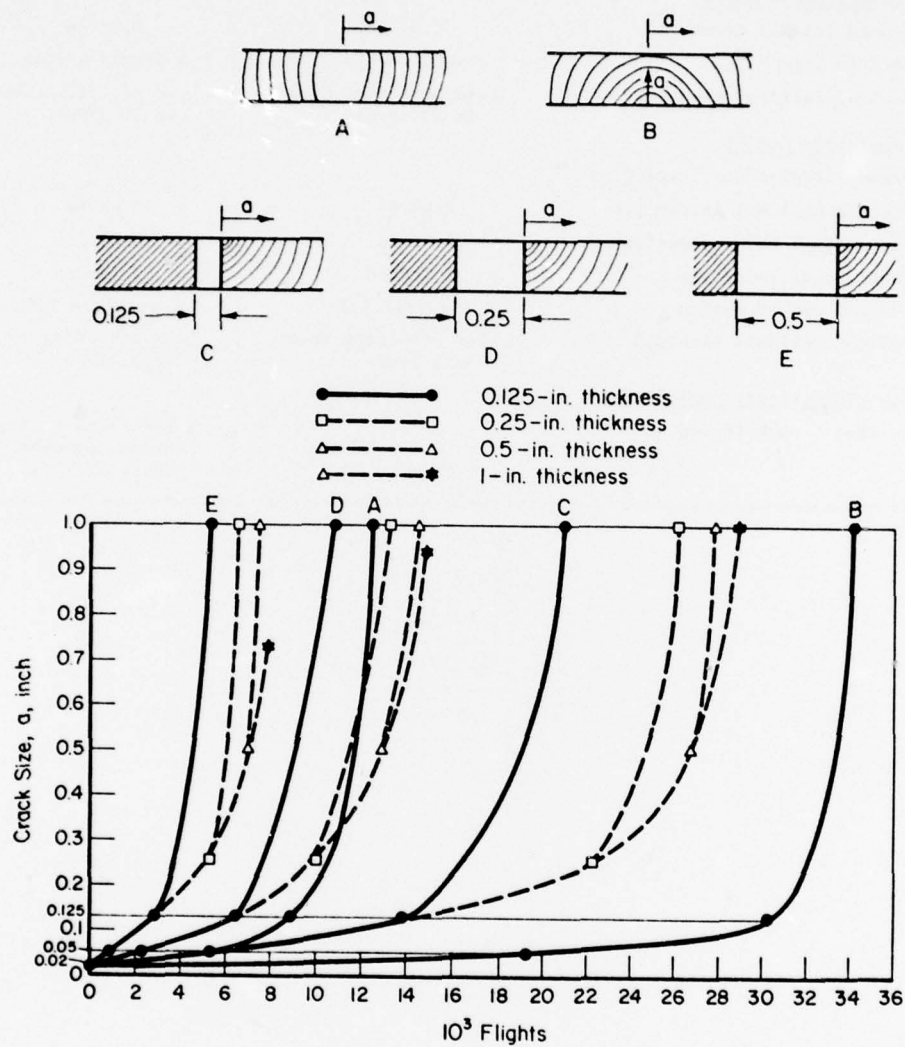


FIGURE 1. CRACK GROWTH FROM .02 AND .05 INCH INITIAL FLAW SIZES FOR VARIOUS CONFIGURATIONS

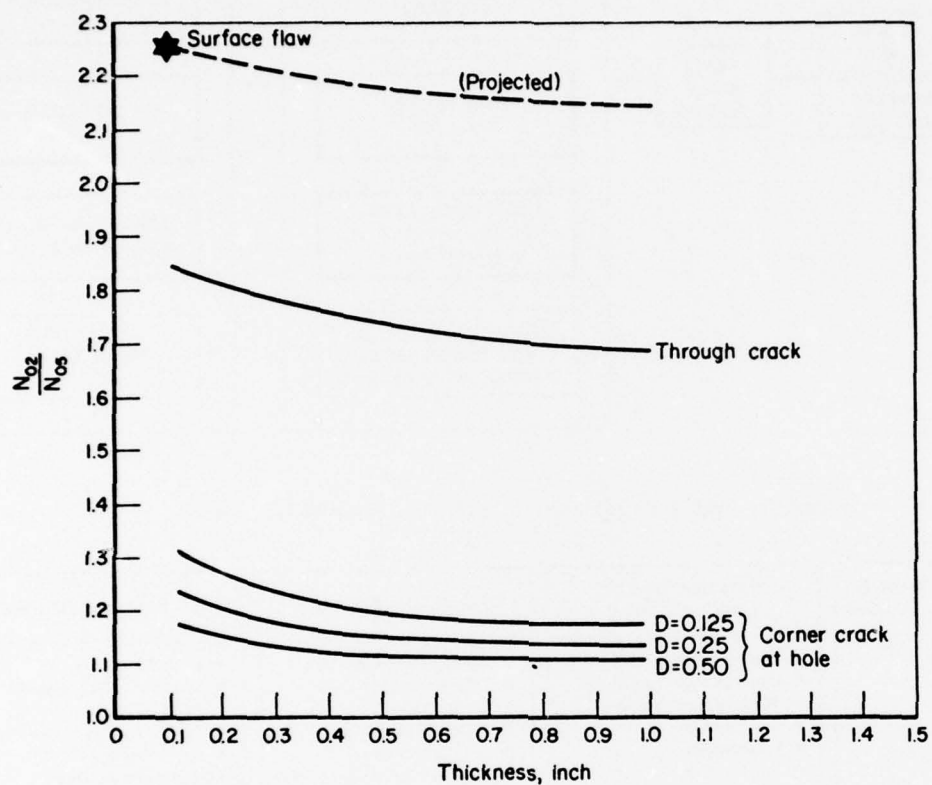


FIGURE 2. RATIO OF CRACK GROWTH LIVES FROM .02 and .05 INCH INITIAL FLAWS TO FAILURE FOR VARIOUS CONFIGURATIONS AS A FUNCTION OF THICKNESS



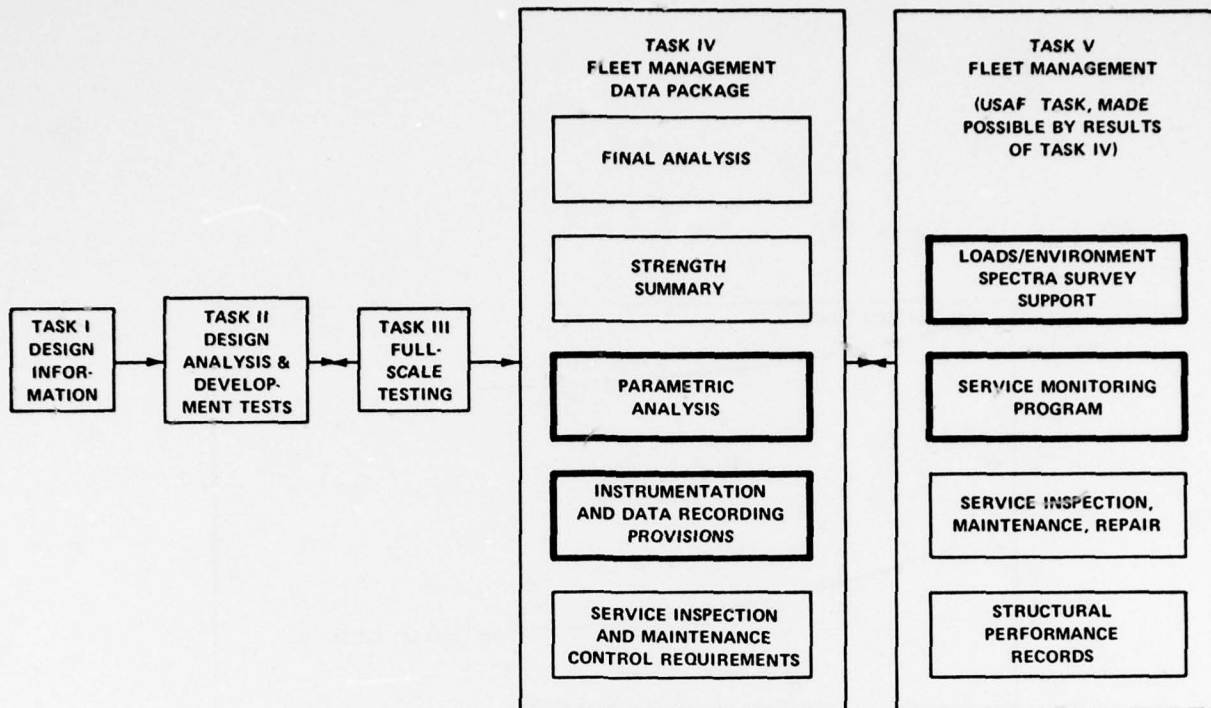


FIGURE 3. TASKS IN AIRCRAFT STRUCTURAL INTEGRITY PROGRAM

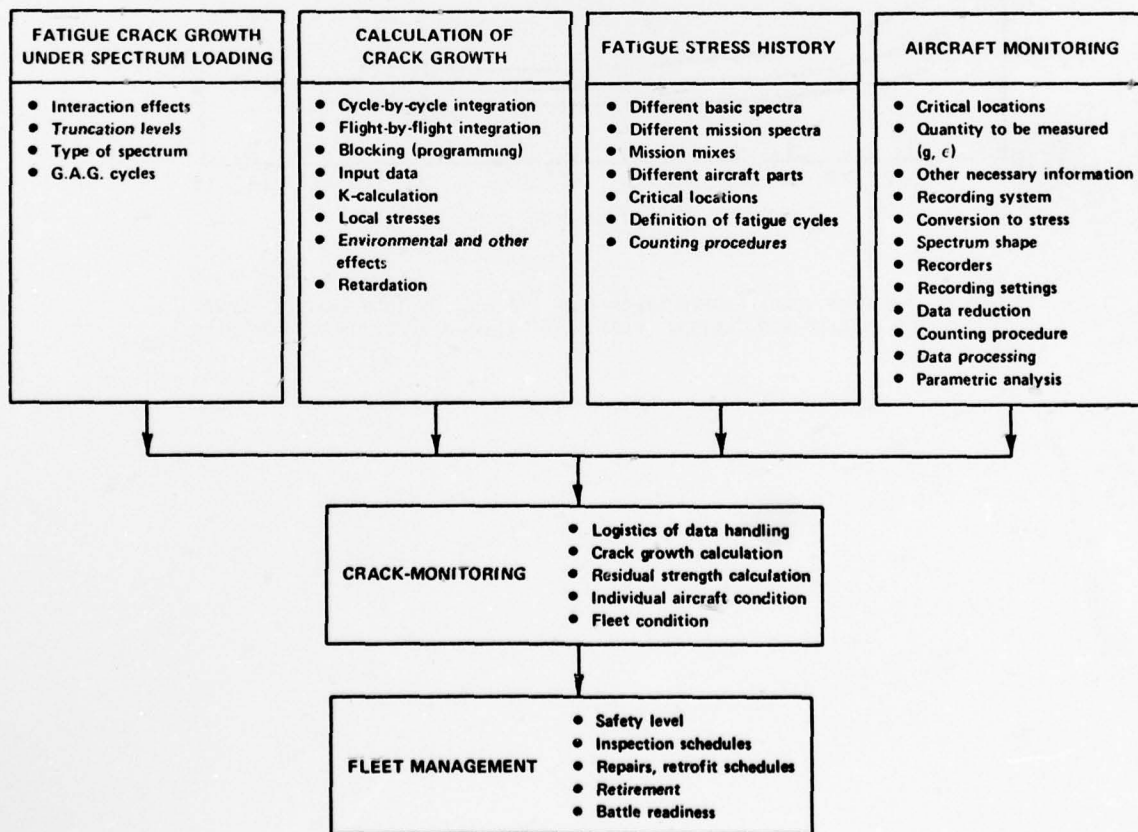


FIGURE 4. PROBLEM AREAS AND DETAIL PROBLEMS INVOLVED IN FLEET MONITORING

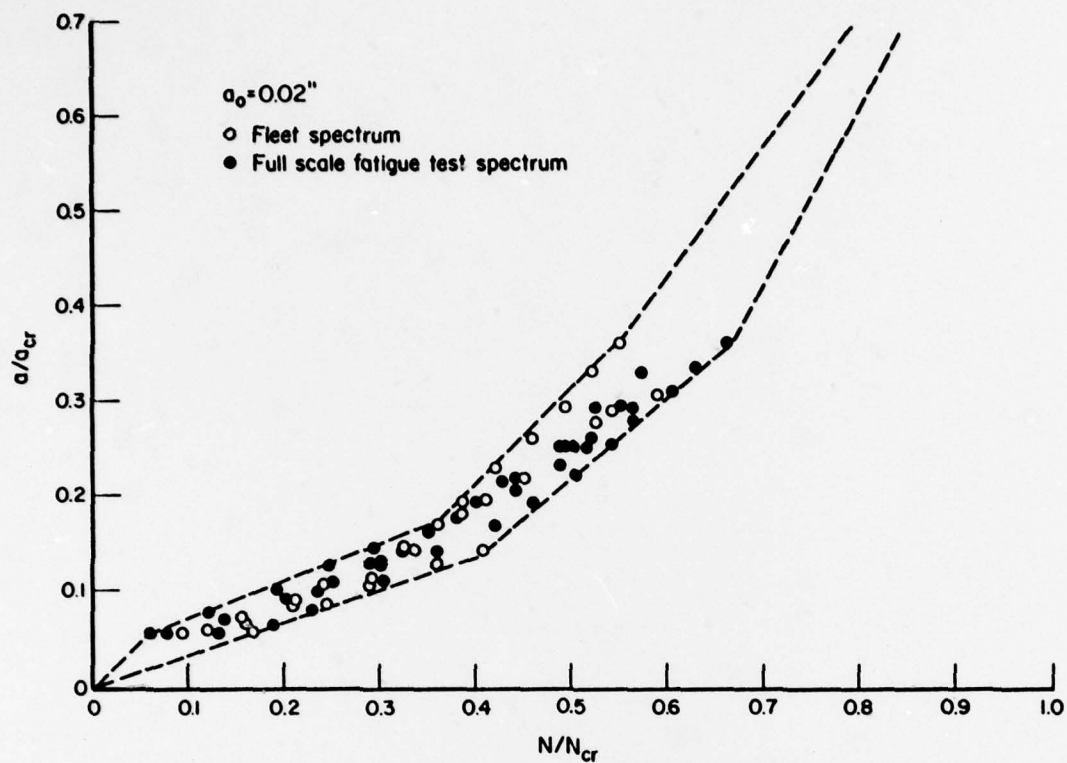


FIGURE 5. NORMALIZED CRACK-GROWTH CURVE FOR VARIOUS CRITICAL LOCATIONS OF A TRANSPORT WING - GROUPED TOGETHER

## SELECTIVE BIBLIOGRAPHY

The bibliography which follows has been prepared by the AGARD Technical Information Panel and is a compilation of references selected specially to suit this particular Lecture Series; it is not intended to be comprehensive. It is regretted that AGARD cannot undertake to provide copies of the documents listed. These should be sought from the organizations which published them.

	Page
CATEGORY A	
FRACTURE MECHANICS DATA AND DATA ANALYSIS	B-1
CATEGORY B	
STRESS INTENSITY FACTORS AND STRESS ANALYSIS OF CRACKS	B-3
CATEGORY C	
FRACTURE MECHANICS AND DAMAGE TOLERANCE ANALYSIS	B-6
CATEGORY D	
APPLICATIONS TO SPECIFIC AIRPLANES	B-13
CATEGORY E	
FATIGUE CRACK GROWTH PREDICTION	B-16
CATEGORY F	
STATISTICS AND RELIABILITY	B-21
CATEGORY G	
MISCELLANEOUS, INCLUDING FRACTURE MECHANICS OF COMPOSITES	B-23
CATEGORY H	
FRACTURE CONTROL	B-28

# CATEGORY A - FRACTURE MECHANICS DATA AND DATA ANALYSIS

76/00/00 77N77913

ENERGY UTILIZATION IN THE US IRON AND STEEL INDUSTRY: A LINEAR PROGRAMMING ANALYSIS  
Missirian, G.  
California Univ., Berkeley.

AD-A039785 NA-74-862-Vol-2 AFML-TR-76-137-Vol-2 76/10/00 77N29288

FRACTURE MECHANICS EVALUATION OF B-1 MATERIALS. VOLUME 2: FATIGUE CRACK GROWTH DATA  
Ferguson, R.; Berryman, R.C.  
Rockwell International Corp., Los Angeles, Calif. (B-1/ Div.)

A total of 1,764 fracture mechanics tests were conducted on fourteen alloys to develop property data for use in the B-1 design. Tests were performed on aluminum alloys 2024, 2124, 2219, 7049, 7050, 7075 and 7175; titanium alloy Ti-6Al-4V; steel alloys 9Ni-4Co-.20C, 9Ni-4Co-.30C and 300M; corrosion resistant steel Ph13-8Mo; nickel alloy INCONEL 718; and nickel-cobalt alloy MP 35N. The effects of product form, heat-to-heat variability, grain orientation, and heat treat condition on fracture behavior were investigated. The results of the tests are presented in tables and graphs in detailed and summarized forms. The effects of the various material and testing variables on fracture behavior are discussed. ABA GRA.

AD-A039883 NA-74-862-Vol-1 AFML-TR-76-137-Vol-1 76/10/00 77N29287

FRACTURE MECHANICS EVALUATION OF B-1 MATERIALS. VOLUME 1: TEXT  
Ferguson, R.; Berryman, R.C.  
Rockwell International Corp., Los Angeles, Calif. (B-1 Div.)

A total of 1,764 fracture mechanics tests were conducted on fourteen alloys to develop property data for use in the B-1 design. Tests were performed on aluminum alloys 2024, 2124, 2219, 7049, 7050, 7075 and 7175; titanium alloy Ti-6Al-4V; steel alloys 9Ni-Co-.20C, 9Ni-4Co-.30C and 300 M; corrosion resistant steel Ph13-8Mo; nickel alloy INCONEL 718; and nickel-cobalt alloy MP 35 N. The effects of product form, heat-to-heat variability, grain orientation, and heat treat condition on fracture behavior were investigated. In addition, the fracture properties of welds in Ti-6Al-4V, Ph13-8Mo and 9-4-.20 alloys and of diffusion bonds in Ti-6Al-4V were determined. Testing variables were temperature, specimen thickness, environment, cyclic frequency and R factor for the DA/DN tests. The results of the tests are presented in tables and graphs in detailed and summarized forms. The effects of the various material and testing variables on fracture behavior are discussed. ABA GRA.

77/02/00 77N22564

APPLICATION OF FRACTURE MECHANICS TO THE SELECTION OF ALUMINUM ALLOYS. PART 2: RESULTS  
Bathias, C.

Société Nationale Industrielle Aérospatiale, Paris (France). (Lab. Central.)  
In AGARD Fracture Mech. Design Methodology, 13p (see N77-22554 13-39)

Three approaches in the application of fracture mechanics to the selection of aluminum alloys are presented, and their behavior is determined. Principal results are shown and discussed along with various means of investigation. ABA Transl. by B.B.

77/02/00 77N22563

APPLICATION OF FRACTURE MECHANICS TO THE SELECTION OF ALUMINUM ALLOYS, PART 1  
Odorico, J.

Société Nationale Industrielle Aérospatiale, Paris (France). (Lab. Central.)  
In AGARD Fracture Mech. Design Methodology, 7p (see N7722554 11-39)

The essential properties to guarantee the safety, availability and longevity of aircraft structures are considered. These properties consist of some of the following: (1) residual static resistance of pre-cracked test material; (2) sensitivity to corrosion under tension; (3) resistance to fatigue; and (4) protection against corrosion for the maintenance of the structures. Results acquired for these different properties are presented. ABA Transl. by B.B.

NASA-CR-141695 MDC-E1153 74/10/00 75N18397

FRACTURE MECHANICS DATA FOR 2024-T861 and 2124-T851 ALUMINUM  
Pionke, L.J.; Linback, R.K.  
McDonnell-Douglas Astronautics Co., St Louis, Mo.

The fracture toughness and fatigue flaw growth characteristics of 2024-T861 and 2124-T851 aluminum were evaluated under plane stress conditions. Center cracked tension specimens were employed to evaluate these properties under a number of different test conditions which include variations in specimen thickness, specimen orientation, test environment, and initial flaw size. The effect of buckling was also investigated for all tests of thin gage specimens, and the effect of frequency and stress ratio was evaluated for the cyclic tests. Fracture toughness test results were analyzed and presented in terms of fracture resistance curves; fatigue flaw growth data was analyzed using empirical rate models. The



results of the study indicate that both fracture toughness and resistance to fatigue crack growth improve with buckling during testing of thin gage panels was found to degrade the resistance to fatigue flaw growth only at elevated temperatures. ABA author.

AD-774487 NRL-7650 73/12/21 74N21567

SOME FRACTURE MECHANICS RELATIONSHIPS FOR THIN SHEET MATERIALS

Sullivan, A.M.; Stoop, J.

Naval Research Lab., Washington, D.C.

The fracture resistance parameter KC has been determined for a number of aluminum, titanium, and steel alloy sheet materials over a thickness range of 0.032 to 0.25 in (0.8 to 6.25 mm). The KC parameter is found to depend inversely upon the material yield stress. Further, a relationship can be established between KC and fracture appearance. Analysis of the data has also disclosed that the amount of crack extension, i.e., final crack length appears to be influenced by the initial crack length. A straight-line curve in logarithmic coordinates relates the ratio of initial to final crack length. The development of these relationships can be of real assistance in the design of a standard initial screening test for KC. (Modified author abstract.) ABA GRA.

NASA-CR-134209 MCR-74-43 74/01/00 74N20127

DEVELOPMENT AND FRACTURE MECHANICS DATA FOR 6Al-6V-2Sn TITANIUM ALLOY

Fiftal, C.F.; Beck, E.J.

Martin Marietta Corp., Denver, Colo.

Fracture mechanics properties of 6Al-6V-2Sn titanium in the annealed, solution-treated, and aged condition are presented. Tensile, fracture toughness, cyclic flaw growth, and sustained-load threshold tests were conducted. Both surface flaw and compact tension-specimen geometries were employed. Temperatures and/or environments used were  $-65^{\circ}\text{F}$  (220 K) air, ambient,  $300^{\circ}\text{F}$  (422 K) air, and room-temperature air containing 10 and 100% relative humidity. ABA author.

AD-757654 NRL-7460 72/12/29 73N23933

A REVIEW OF THE PLANE-STRESS FRACTURE MECHANICS PARAMETER KC DETERMINED USING THE CENTER CRACKED TENSION SPECIMEN

Sullivan, A.M.; Freed, C.N.

Naval Research Lab., Washington, D.C.

The report discusses the current status of the center-cracked tension (CCT) specimen as a means of determining the plane-stress fracture-mechanics parameter KC. The effect of specimen geometry (width and crack length) together with that of specimen thickness is illustrated by examples from NRL research. The experimental parameters employed at NRL are detailed together with those in use at other laboratories for the purpose of assisting in the development of a standard procedure for such testing so that data can be reliably compared. ABA author (GRA).

# CATEGORY B - STRESS INTENSITY FACTORS AND STRESS ANALYSIS OF CRACKS

76/00/00 76A38387

## ON THE PRINCIPLE OF SUPERPOSITION FOR STRESS INTENSITY FACTORS

Aamodt, B.; Bergan, P.G.

(Norske Veritas, Oslo, Norway); (Norges Tekniske Hogskole, Trondheim, Norway)

Engineering Fracture Mechanics, Vol.8, No.2, 1976, p.437-440.

The principle of superposition as applied for stress intensity factors for different types of loading is discussed. Using an energy formulation, it is shown that stress intensity factors for different loading types are additive provided all loading types tend to open the crack. Negative part contributions to the stress intensity factor may also be superimposed if the associated loads tend to close the crack along the entire crack front. ABA (author).

75/00/00 76A22567

## AN ASSUMED DISPLACEMENT HYBRID FINITE ELEMENT MODEL FOR THREE-DIMENSIONAL LINEAR-FRACTURE-MECHANICS ANALYSIS

Atluri, S.; Kathiresan, K.

(Georgia Institute of Technology, Atlanta, Ga.)

In Society of Engineering Science, Annual Meeting, 12th, Austin, Tex., October 20-22, 1975, Proceedings. (A76-22551 09-31) Austin, University of Texas, 1975, p.391-399.

An 'embedded singularity' finite element procedure for the computation of mixed modes I, II, and III stress intensity factors, which vary along an arbitrarily curved crack front in three-dimensional problems, is presented. The finite element method is based on a 'hybrid displacement model' which enforces the displacement and traction continuity between near-field 'singular' elements and far-field 'regular' elements (with regular polynomial variation of the field variables) through a modified variational principle of potential energy. Stress intensity factors are calculated directly, along with the structure's nodal displacements. The problem of a through crack in a finite thickness plate subjected to symmetric loading is studied, and results are reported for the variation of the  $K_I$  stress intensity factor through the plate thickness. ABA (author).

76/00/00 76A17327

## ON THE USE OF ISOPARAMETRIC FINITE ELEMENTS IN LINEAR FRACTURE MECHANICS

Barsoum, R.S.

(Combustion Engineering, Inc., Windsor, Conn.)

International Journal for Numerical Methods in Engineering, Vol.10, No.1, 1976, p.25-37.

Quadratic isoparametric elements which embody the inverse square root singularity are used in the calculation of stress intensity factors of elastic fracture mechanics. Examples of the plane eight noded isoparametric element show that it has the same singularity as other special crack tip elements, and still includes the constant strain and rigid body motion modes. Application to three-dimensional analysis is also explored. Stress intensity factors are calculated for mechanical and thermal loads for a number of plane strain and three-dimensional problems. ABA (author).

75/04/00 75A28234

## AN ASSUMED DISPLACEMENT HYBRID FINITE ELEMENT MODEL FOR LINEAR FRACTURE MECHANICS

Atluri, S.N.; Kobayashi, A.S.; Nakagaki, M.

(Georgia Institute of Technology, Atlanta, Ga.); (Washington University, Seattle, Wash.)

International Journal of Fracture, Vol.11, Apr. 1975, p.257-271.

This paper deals with a procedure to calculate the elastic stress intensity factors for arbitrary-shaped cracks in plane stress and plane strain problems. An assumed displacement hybrid finite element model is employed wherein the unknowns in the final algebraic system of equations are the nodal displacements and the elastic stress intensity factors. Special elements, which contain proper singular displacement and stress fields, are used in a fixed region near the crack tip; and the interelement displacement compatibility is satisfied through the use of a Lagrangean multiplier technique. Numerical examples presented include: central as well as edge cracks in tension plates and a quarter-circular crack in a tension plate. Excellent correlations were obtained with available solutions in all the cases. A discussion on the convergence of the present solution is also included. ABA (author).

74/00/00 75A18195

## PROPAGATION OF ELLIPTICAL SURFACE CRACKS AND NONLINEAR FRACTURE MECHANICS BY THE FINITE ELEMENT METHOD

Aamodt, B.; Bergan, P.G.

(Norges Tekniske Hogskole, Trondheim, Norway)

In Conference on Dimensioning and Strength Calculations, 5th and Congress on Material Testing, 6th, Budapest, Hungary, October 28 - November 1, 1974, Proceedings. Volume 1. (A75-18192 06-39) Budapest, Akademiai Kiado, 1974, p.1-31 to 1-42.

A technique reported by Aamodt et al. (1973) is used to study the growth of semielliptical surface cracks in a Ni-steel plate. The approach makes use of a multilevel superelement formulation for elastoplastic analyses. A numerical study

of crack propagation is conducted and the finite element method is applied in a problem of nonlinear fracture mechanics. The formulation of the superelement technique for elastoplastic problems is discussed along with the numerical study of a doubly edge-cracked thick plate. ABA G.R.

74/00/00 75A15997

**UNIMOD - AN APPLICATIONS ORIENTED FINITE ELEMENT SCHEME FOR THE ANALYSIS OF FRACTURE MECHANICS PROBLEMS**

Nair, P.; Reifsnider, K.L.

(Virginia Polytechnic Institute and State University, Blacksburg, Va.)

In Fracture Analysis; Proceedings of the National Symposium on Fracture Mechanics, College Park, Md., August 27-29, 1973, Part 2. (A75-15989 04-39) Philadelphia, Pa., American Society for Testing and Materials, 1974, p.211-225.

A new concept in elastic-plastic analysis using finite element techniques is analyzed. The resulting procedural scheme, called UNIMOD, is found to be an effective method of performing stress analysis of complex elastic-plastic defect problems which cannot be handled by classical elastic fracture mechanics. Advantages of the UNIMOD scheme include extreme versatility, universal applicability to existing programs and conceptual as well as operational simplicity. ABA (author).

74/00/00 74A41254

**FRACTURE MECHANICS**

Benzley, S.E.; Parks, D.M.

(Sandia Laboratories, Albuquerque, N. Mex.); (Brown University, Providence, R.I.)

In Structural Mechanics Computer Programs: Surveys, Assessments, and Availability; Proceedings of the Symposium, University of Maryland, College Park, Md., June 12-14, 1974. (A74-41251 21-32) Charlottesville, University Press of Virginia, 1974, p.81-102. AEC-supported research.

Some fracture mechanics computer programs currently being used are surveyed. Most of this software represents very recent developments in computational fracture mechanics. Included are brief abstracts of computer programs that treat the characteristic near field singularity that is present at the tip of a crack. A critical review of computational fracture mechanics is offered, and some suggestions are given as to the proper selection of fracture mechanics software for a particular problem. In addition, a discussion of future trends in this field is presented.

73/00/00 74A17777

**COMPUTATIONAL FRACTURE MECHANICS**

Rice, J.R.; Tracey, D.M.

(Brown University, Providence, R.I.)

In Numerical and Computer Methods in Structural Mechanics. (A74-17756 06-32) New York, Academic Press, Inc., 1973, p.585-623.

Numerical procedures for accurate determination of elastic stress intensity factors for the general two-dimensional crack problem are reviewed. The elastic perfectly plastic state of crack tip deformation is studied by a finite element procedure. Elastic-plastic fields in the immediate vicinity of a crack tip are determined numerically by finite element procedures based on asymptotic studies of crack tip singularities in plastic materials. The small-scale yielding problem is modeled, and expressions for crack tip opening displacement, shear singularity amplitude, and plastic zone extent are derived. A finite element solution to the large-scale yielding of a circumferentially cracked round tension bar is obtained. The three-dimensional aspects of flawed structures and numerical methods of treating them are studied. Ductile fracture mechanisms, in particular crack tip fracture on the microscale, are discussed. ABA V.P.

73/09/00 73A43812

**ANALYSIS OF STRESS INTENSITY FACTORS FOR THE TENSION OF A CENTRALLY CRACKED STRIP WITH STIFFENED EDGES.**

Isida, M.

(National Aerospace Laboratory, Tokyo, Japan)

Engineering Fracture Mechanics, Vol.5, Sept. 1973, p.647-665.

Theoretical analysis of the stress intensity factor for the tension of a centrally cracked strip reinforced with stringers along its edges. The method is based on the Laurent expansions of the complex stress potentials, and the perturbation technique is applied in determining their coefficients from the boundary conditions. Formulas for the crack tip stress intensity factors are given in the form of 36-term power series of  $\lambda^2$ , where  $\lambda$  is the ratio of the crack length to the plate width. The analysis covers, as special cases, a centrally cracked strip with free edges, a centrally cracked strip with clamped edges, and a wide plate stiffened by parallel stringers and containing a crack between every two adjacent stringers. Numerical calculations are performed for various combinations of the extensional and bending rigidities of the stringers, and their stress-relieving effects are examined in detail. The present method is considered to give practically exact values for  $\lambda < 0.95$ , regardless of other parameters. ABA (author).



71/00/00 73A28231

## ANALYSIS OF STRESS INTENSITY FACTOR FOR SURFACE-FLAWED TENSION PLATE.

Miyamoto, H.; Miyoshi, T.

(Tokyo University, Tokyo, Japan)

In High Speed Computing of Elastic Structures; Proceedings of the Symposium, Liege, Belgium, August 23-28, 1970. Volume 1. (A73-28226 13-32) Liege, Universite de Liege, 1971, p.137-155.

Consideration of the stress intensity factor for a semielliptical surface flaw in a plate of finite thickness subjected to tension. There is no exact solution to this problem in three-dimensional theory of elasticity, and the approximate solutions obtained by Irwin (1962) and Kobayashi and Moss (1969) are reexamined. ABA M.V.E.

AD-A021280 ASRL-TR-177-1 AFFDL-TR-75-51 76/01/00 76N29650

## FUTURE MECHANICS ANALYSIS OF AN ATTACHMENT LUG

Orringer, O.

Massachusetts Inst. of Tech., Cambridge. (Aeroelastic and Structures Research Lab.)

This report documents a finite-element analysis procedure for computation of mode 1 and mode 2 stress intensity factors associated with a sharp crack in an attachment lug detail. The procedure is a complete Fortran-4 Program which generates and parametrically analyzes the lug, based on designer-oriented input data. The formulation of a special crack-containing element is reviewed and its performance is summarized. A detailed description of the lug analysis procedure covers the physical problem, modeling, program flow and options, input/output conventions, execution times and limitations which must be observed. Results from example analyses of some attachment lugs are presented. ABA GRA.

SLA-74-5181 Conf-740604-1 73/00/00 74N34372

## FRACTURE MECHANICS

Benzley, S.E.; Parks, D.M.

(Brown Univ.) Sandia Labs., Albuquerque, N. Mex.

Presented at the Intern. Symp. on Structural Mech. Software, College Park, Md., 12-14 June 1974.

Some fracture mechanics computer programs currently being used are surveyed. Most of this software represents very recent developments in computational fracture mechanics. Included are brief abstracts of computer programs that treat the characteristic near-field singularity that is present at the tip of a crack. A critical review of computational fracture mechanics is offered and some suggestions are given as to the proper selection of fracture mechanics software for a particular problem. *Future trends in this field are presented.* ABA author (NSA).

AD-778098 TR-0074 SAMSO-TR-74-89 74/04/05 74N28416

## USE OF FINITE ELEMENT ANALYSIS IN FRACTURE MECHANICS

Atchley, C.E.; Raymond, L.

Aerospace Corp., El Segundo, Calif. (Lab. Operations.)

Many problems in fracture mechanics are not readily amenable to analytical treatment. Stress distributions and stress intensity factors cannot always be calculated easily for a given structural geometry and loading condition. However, finite element methods offer an accurate, versatile, and conceptually simple means by which a given structure can be analyzed. They allow a general application of classical crack propagation analysis whereby the necessary estimates of the stress intensity factor may be calculated. The report presents the development of a general finite element method commonly used in structural mechanics and several finite element approaches employed specifically in fracture mechanics for computing stress and displacement functions, and stress intensity factors for a cracked structure. (Modified author abstract) ABA GRA.



## CATEGORY C - FRACTURE MECHANICS AND DAMAGE TOLERANCE ANALYSIS

76/00/00 77A24916

### THE CONSIDERATION OF DAMAGE TOLERANCE IN THE DESIGN OF JOINTS

Circle, R.L.

(Lockheed-Georgia Co., Marietta, Ga.)

In *Advances in Joining Technology: Proceedings of the Fourth Army Materials Technology Conference*, Boston, Mass., September 16-19, 1975. (A77-24901 10-31) Chestnut Hill, Mass., Brook Hill Publishing Co., 1976, p.455-469.

Damage tolerance is defined as the ability of a structure to sustain an injury that might come from a variety of sources. In order to be truly damage tolerant, a structure must possess a satisfactory ability to sustain damage, be inspectable enough so that damage can be readily detected, and have an adequate combination of slow rate of crack growth and long critical lengths so that it will endure long enough for damage to be discovered. Joints involving special problems in meeting these objectives are discussed. Among the analysis problems that need to be addressed are load-path eccentricities and high bearing stresses resulting from load transfer. One of the best design practices is to limit the number of joints to an absolute minimum, along with design of a multi-load-path structure with inherent damage-arresting characteristics. Several techniques such as high clamp-up, cold expansion, and interference fit fasteners can be used to improve joint damage tolerance. ABA S.D.

76/12/00 77A20991

### DESIGN USING ELASTIC-PLASTIC FRACTURE MECHANICS

Sumpter, J.D.G.; Turner, C.E.

(Naval Construction Research Establishment, Dunfermline, Scotland); (Imperial College of Science and Technology, London, England)

*International Journal of Fracture*, Vol.12, Dec. 1976, p.861-871. Research supported by the Science Research Council.

Current usage of crack opening displacement and proposed usage of the J contour integral in the design of structures experiencing significant plasticity are examined in the light of data from test piece geometries in which uncontained yielding occurs ahead of the crack tip, at general yield. This behavior is contrasted with several 2D structural models of cracks at holes in plates or in thick walled cylinders. In the structural situations, plasticity ahead of the crack is normally contained by an outer elastic field and in these circumstances estimates of J based on linear elastic fracture mechanics with plastic zone correction are adequate. Only when plasticity ahead of the crack is uncontained, as for buried or part through cracks with shallow remaining ligaments, is a plasticity estimate of J necessary. ABA (author).

76/11/00 77A15855

### FRACTURE MECHANICS OF AEROSPACE MATERIALS

Schwalbe, K.-H.

(Deutsche Forschungs- und Versuchsanstalt fuer Luft- und Raumfahrt, Institut fuer Werkstoff-Forschung, Porz-Wahn, West Germany)

*DFVLR-Nachrichten*, Nov. 1976, p.775-778. In German.

Fractographic and fracture mechanics analysis techniques are reviewed and assessed in application to aerospace materials, with emphasis on the behavior of cracks in nucleation and propagation. The importance of stress intensity as a parameter is emphasized. Crack-tip processes, trade-off between fracture toughness and strength, the width of lines on the fracture surface, and the cost effectiveness of fracture mechanics safety analyses are discussed. Limitations on fracture safety predictions are indicated (scatter of materials properties parameters, inadequate knowledge of stress loading patterns, time variability of amplitude and mean value of stresses on aerospace parts). ABA R.D.V.

76/02/00 76A28607

### USE OF FRACTURE MECHANICS IN ESTIMATING STRUCTURAL LIFE AND INSPECTION INTERVALS

Kaplan, M.P.; Reiman, J.A.

(USAF, Aeronautical Systems Div., Wright-Patterson AFB, Ohio)

*Journal of Aircraft* Vol.13, Feb. 1976, p.99-103.

As structural efficiency of aircraft has increased in the recent past, the Air Force has found it necessary to include, in the newer systems, damage tolerance criteria for fracture critical parts. These criteria are explained briefly, and sample calculations indicating methods for determining component structural life are demonstrated. Implicit in this calculation is the definition of inspection intervals. The second portion of this discussion details some of the assumptions that go into this analysis and their sensitivity. A large portion centers on stress spectrum definition. It is shown that, from one set of occurrence data, alternative spectra may be derived which have substantial differences in life. ABA (author).

75/10/00 76A15799

### YIELDING FRACTURE MECHANICS

Turner, C.E.

(Imperial College of Science and Technology, London, England)

*Journal of Strain Analysis*, Vol.10, Oct. 1975, p.207-216.

Yielding fracture mechanics seeks to find a relationship between applied stress, crack size and material toughness that is

independent of the geometry of a component when fracture occurs after significant degree of yielding. The crack opening displacement, and the J contour integral are two proposals for describing the stresses and deformation at the tip of a sharp crack embedded in a region of yielding material. J can be expressed as the product of uniaxial yield stress and the crack opening displacement and a factor with a value between about 1 and 2.5. The concepts are still under development. Either term can be chosen as a measure of the severity of crack tip deformation in a given material with the onset of crack growth in monotonic loading occurring at a critical value, for a given thickness. Experimental evidence so far is in broad support of this picture but there remains uncertainty over the degree to which critical crack opening displacement or J is independent of geometry and the extent to which stable crack growth prevents the usage of one simple criterion of fracture for all structural configurations. ABA (author).

75/09/00 75A47591

#### APPLICATION OF FRACTURE MECHANICS TO AIRCRAFT STRUCTURAL SAFETY

Wood, H.A.

(USAF, Flight Dynamics Laboratory, Wright-Patterson AFB, Ohio)

(Japan Society for the promotion of Science and National Science Foundation, United State-Japan Seminar on Combined Nonlinear and Linear Fracture Mechanics - Applications to Modern Engineering Structures, Sendai, Japan, Aug. 12-16, 1974.)

Engineering Fracture Mechanics, Vol.7, Sept. 1975, p.557-564.

Design requirements have been developed to insure structural safety for current and future USAF aircraft. New structure is assumed to be flawed. Materials, stress levels and structural arrangements are chosen so as to prevent damage from growing to catastrophic size prior to detection. Safety from damage induced through service usage is insured by providing inspection capability and by meeting specific residual strength and safe crack growth requirements. Compliance with these requirements implies the capability to predict growth rates under complex loadings and to calculate the fracture strength of structures fabricated of relatively tough materials which may exhibit large amounts of crack tip plasticity prior to failure. This paper reviews significant factors leading to the development of damage tolerance criteria and illustrates the role of fracture mechanics in the analysis and testing aspects necessary to satisfy these requirements. ABA (author).

75/06/00 75A41909

#### ON FRACTURE MECHANICS UNDER COMPLEX STRESS

Toor, P.M.

(Lockheed-Georgia Co., Marietta, Ga.)

Engineering Fracture Mechanics, Vol.7, June 1975, p.321-329.

The majority of linear elastic fracture mechanics investigations since the pioneering work of Irwin and Paris have been carried out under tension-tension loading conditions in sheet metal. However, built up structures have generally been under complex stress conditions and to date very scanty information is available on fracture mechanics parameters under complex stress conditions. The current state of the art for mixed mode crack tips deformation is reviewed. In order to use linear elastic fracture mechanics methodology to predict crack growth rate in shear webs, an experimental program was initiated. Initial tests on 7075-T6 aluminum alloy sheet, using a picture frame type specimen, were conducted. The critical stress intensity factors and the rate of crack growth under aforementioned condition are established. ABA (author).

ASME Paper 75-GT-79 75/03/00 75A34628

#### A FRACTURE MECHANICS APPROACH TO TURBINE AIRFOIL DESIGN

Linask, I.; Dierberger, J.

(United Aircraft Corp., Pratt and Whitney Aircraft Div., East Hartford, Conn.)

American Society of Mechanical Engineers, Gas Turbine Conference and Products Show, Houston, Tex., Mar. 2-6, 1975, 8 p.

An analytical study was conducted using fracture mechanics principles to model turbine airfoil cracking. It was found that crack initiation can be related to calculated residual strains in the airfoil coating and that coating properties are an important consideration in determining crack location and orientation. The coating crack subsequently propagates into base material according to basic fracture mechanics laws. A comparison with engine tested blade experience is made. It is concluded that the presented model provides a rational method for design life prediction but its general application requires definition of new types of material property information. ABA (author).

74/00/00 75A25191

#### ELEMENTARY ENGINEERING FRACTURE MECHANICS

Broek, D.

(Delft, Technische Hogeschool, Delft, Netherlands)

Leiden, Noordhoff International Publishing, 1974. 417 p.

Mechanisms of fracture and crack growth are considered along with the elastic crack-tip stress field, the crack tip plastic zone, the energy principle, questions of dynamics and crack arrest, plane strain fracture toughness, plane stress and transitional behavior, the crack opening displacement criterion, fatigue crack propagation, and the fracture resistance of materials. Applications of fracture mechanics are also discussed, giving attention to fail-safety and damage tolerance,

the determination of stress intensity factors, practical problems, the fracture of structures, and stiffened sheet structures. ABA G.R.

74/00/00 75A15987

#### PROPOSED FRACTURE MECHANICS CRITERIA TO SELECT MECHANICAL FASTENERS FOR LONG SERVICE LIVES

Grandt, A.F., Jr; Gallagher, J.P.

(USAF, Materials Laboratory, Wright-Patterson AFB, Ohio); (USAF Flight Dynamics Laboratory, Wright-Patterson AFB, Ohio)

In Fracture Toughness and Slow-stable Cracking; Proceedings of the National Symposium on Fracture Mechanics, College Park, Md., August 27-29, 1973. Part 1. (A75-15976 04-39) Philadelphia, Pa., American Society for Testing and Materials, 1974, p.283-297.

It is proposed that long service lives may be attained by selecting a fastener system which keeps the stress intensity range during service below the threshold stress intensity range. Using this criterion one may specify the maximum flaw size (from prior damage or initiated by fretting) which will be permanently retained by the residual stress field surrounding the fastener. An analytical procedure which can be employed to obtain stress intensity factors for practical fastener crack configurations is demonstrated with results for open holes, cold-worked holes, interference fit fasteners, and pinloaded holes. In addition, threshold stress intensity factor data are taken from the literature and presented in a form convenient for use by the design engineer. ABA (author).

74/09/00 74A46221

#### RANGE OF VALIDITY AND APPLICATION OF FRACTURE MECHANICS

Radaj, D.

(Daimler Benz AG, Stuttgart, West Germany)

Zeitschrift fuer Werkstofftechnik, Vol.5, Sept. 1974, p.317-323. In German.

The range of validity and application of linear-elastic and electro-plastic fracture mechanics is determined according to practicable quantitative criteria. The former is applicable to the low stress brittle fracture in brittle materials, the latter is applicable to the higher stress brittle and tear fracture in tougher materials. The real continuum mechanics fracture criterion is not yet determined. Linear-elastic fracture mechanics is widely applicable to fatigue fractures. Taking into account the interaction and sequence effect of low and high load amplitudes is necessary. The fracture mechanics approach to brittle and fatigue fracture is compared with traditional testing techniques. ABA (author).

AIAA Paper 74-347 74/04/00 74A26661

#### EVALUATION OF DAMAGE TOLERANCE IN AIRCRAFT STRUCTURES

McHenry, H.L.; Hensley, E.K.

(General Dynamics Corp., Convair Aerospace Div., Fort Worth, Tex.)

AIAA, ASME, and SAE, Structures, Structural Dynamics and Materials Conference, 15th, Las Vegas, Nev., Apr. 17-19, 1974, AIAA 11 p.

The specific requirements and the evaluation procedures used to qualify the damage tolerance of two competing wing carrythrough structure designs are reviewed. One design is principally  $\beta$ -processed 6Al-4V titanium in a fail safe configuration, and the other is principally 10 Ni steel in a monolithic configuration. Fail safe analyses were conducted using finite element models with individual elements reduced in size or eliminated to simulate failure. Crack arrest was evaluated experimentally on panels with brazed stiffeners. Crack growth analyses were based on extensive test data and the Wheeler retardation model. ABA (author).

73/00/00 74A14461

#### FRACTURE MECHANICS AIRCRAFT STRUCTURAL DESIGN APPLICATION AND RELATED RESEARCH

Wood, H.A.; Tupper, N.

(USAF, Flight Dynamics Laboratory, Wright-Patterson AFB, Ohio); (USAF, Materials Laboratory, Wright-Patterson AFB, Ohio)

In International Congress on Fracture, 3rd, Munich, West Germany, April 8-13, 1973, Reports. Part 9. (A74-14384 03-32) Dusseldorf, Verein Deutscher Eisenhuettenleute, 1973, p.VIII-523.1 to VIII-523.6.

Description of fracture control procedures employed by the US Air Force in the design of current and future aircraft to ensure safety by reducing the probability of catastrophic failure due to undetected damage. Attention is given to fracture-safety related aspects of material and process selectivity, material procurement and control, nondestructive inspection, and damage tolerance analyses and testing. Applications of fracture mechanics criteria to aircraft design have helped to clarify the importance of research in identifying the basic metallurgical mechanisms of fracture. Knowledge gained from such research is judged necessary for improving resistance to crack growth and for developing alloys which are relatively insensitive to chemical environments in which aircraft operate. ABA T.M.



AD-A046151 NOR-75-86 AFFDL-TR-73-42-PT-3 77/08/00 78N14436  
 DEVELOPMENT AND EVALUATION OF METHODS OF PLANE STRESS FRACTURE ANALYSIS. PART 3.  
 APPLICATION OF THE RESIDUAL STRENGTH PREDICTION TECHNIQUE TO COMPLEX AIRCRAFT  
 STRUCTURE

Ratawani, M.M.; Wilhem, D.P.  
 Northrop Corp., Hawthorne, Calif. (Aircraft Div.)

Using the residual strength technique, uniaxially loaded, angle stiffened wing panels were analyzed and fracture strengths determined. Excellent correlation was obtained between experimental and analytical data for an initially intact and broken central stringer for a six bay aluminum panel with thin skin, a thick (0.193 inch) skin aluminum panel, and an all titanium panel. Both crack arrest and fracture could be predicted using the tangency conditions between the crack driving force curves (sq. rt. of  $J$ ) and the crack growth resistance curve (sq. rt. of  $J_R$ ). The influence of biaxial load ratio (tension fields) on crack opening displacement, plastic zone size and load transfer was examined for an all aluminum fuselage panel with a crack in the skin located normal to the longerons and parallel to the frames. Comparisons are made between analytical and experimental strain and residual strength data for biaxially loaded structure. AGA GRA.

NLR-TR-75129-U 75/09/00 77N25584  
 USER'S MANUAL OF ARREST. A COMPUTER ROUTINE FOR PREDICTION OF RESIDUAL STRENGTH OF  
 CRACKED STIFFENED PANELS

Vlieger, H.; Sanderse, A.  
 National Aerospace Lab., Amsterdam (Netherlands). (Structures and Materials Div.)

A detailed description is given of the computer program arrest and of the execution of it in determining the residual strength diagram of cracked stiffened panels. The essentials of the computer program are dealt with whereas the derivation of the equations together with the program flow charts and the program listing are given in Appendices. An example of computation is given to illustrate the preparation of the computer input and the treatment of the computer output data in order to determine the residual strength diagram. The procedure to find the fail-safe stress level from this residual strength diagram is outlined in a reference which accompanies this user's manual. ABA author (ESA).

77/02/00 77N22559  
 APPLICATION OF FRACTURE MECHANICS IN DESIGNING BUILT-UP SHEET STRUCTURES

Vlieger, H.  
 National Aerospace Lab., Amsterdam (Netherlands).  
 In AGARD Fracture Mech. Design Methodology, 18 p (see N77-22554 13-39)

Different analyses that are relevant to the design of a fail-safe aircraft structure are discussed: the static strength, the crack initiation and propagation and the residual strength analyses. The application of fracture mechanics in the crack propagation and residual strength analyses is given particular attention. Theoretical results of an investigation carried out in this field and verification of these results by experiments are shown. Finally, some guidelines for aircraft structural applications are presented. ABA author.

77/02/00 77N22555  
 PRACTICAL APPLICATIONS OF FRACTURE MECHANICS TECHNIQUES TO AIRCRAFT STRUCTURAL  
 PROBLEMS

Heath, W.G.; Nicholls, L.F.; Kirkby, W.T.  
 (British Aircraft Corp., London); (RAE, Farnborough). Hawker Siddeley Aviation Ltd., London (England).  
 In AGARD Fracture Mech. Design Methodology, 22 p (see N77-22554 13-39)

Experience gained in the UK in the application of fracture mechanics techniques to problems arising in the design, testing and operation of aircraft is outlined. Design examples are taken from studies of crack behavior in stiffened wing panels and also from pressure cabin design, including areas subject to combined mechanical and thermal stresses. Problems of testing are illustrated by reference to the use of COD, and other measurements, in residual strength tests to predict approach to unstable crack growth. Test data are given which illustrate scatter in crack growth in stiffened panels. In addition, the nature of the difficulties that have been encountered in applying fracture mechanics analysis to failures arising in aircraft in service is discussed. ABA author.

AGARD-CP-221 ISBN-92-835-1090-X 77/02/00 77N22554  
 FRACTURE MECHANICS DESIGN METHODOLOGY

Advisory Group for Aerospace Research and Development, Paris (France).  
 Presented at the 43rd Meeting of the AGARD Structures and Materials Panel, London, 28-29 Sept. 1976.

NLR-MP-76024-U 76/09/09 77N21481  
 APPLICATION OF FRACTURE MECHANICS IN DESIGNING BUILT-UP SHEET STRUCTURES

Vlieger, H.  
 National Aerospace Lab., Amsterdam (Netherlands). (Structures and Materials Div.)  
 Presented at the AGARD Specialists' Meeting on Fracture Mech. Design Methodology, London, 28-29 Sept. 1976.

Different analyses (static strength, crack initiation and propagation, and residual strength) relevant to the design of a



fail-safe aircraft structure are discussed in order to restrict the occurrence of cracks and to guarantee some specified life of the aircraft if cracks nevertheless arise. The crack propagation and residual strength analyses are discussed with respect to application of fracture mechanics principles and sheet structures. The factors that influence the effectiveness of a fail-safe design and ways in which fail-safe properties can be improved are discussed. ABA ESA.

AD-A032034 ASRL-TR-177-2 AFFDL-TR-75-70 76/04/00 77N20528

**FRACTURE MECHANICS ANALYSIS OF CENTERED AND OFFSET FASTENER HOLES IN STIFFENED AND UNSTIFFENED PANELS UNDER UNIFORM TENSION**

Stack, G.

Massachusetts Inst. of Tech., Cambridge. (Aeroelastic and Structures Research Lab.)

This report documents a finite-element analysis procedure for computation of mode I and mode II stress intensity factors associated with one or two sharp cracks emanating from a fastener hole in a panel under uniform tension. The fastener hole may be offset from the panel centerline, and one or both edges of the panel may be integrally stiffened. The formulation of a special assumed-stress hybrid element for the region near the fastener hole is presented. A detailed description of the programming covers the physical problem, modelling, program flow and options, input/output conventions, execution times, and limitations which must be observed. Results are presented for performance tests of the special element, and for some example analyses of cracked panels. ABA GRA.

ARL/STRUC-TM-245 76/08/00 77N20478

**FRACTURE MECHANICS FUNDAMENTALS WITH REFERENCE TO AIRCRAFT STRUCTURAL APPLICATIONS**  
Hoskin, B.C.

Aeronautical Research Labs., Melbourne (Australia).

To be presented at the A.R.L. Symp. on Aircraft Structural Fatigue

Fracture mechanics is being increasingly applied to problems associated with cracked, or potentially cracked, aircraft structures. Such applications include assessment of the residual strength of cracked components and also the prediction of fatigue crack growth. However, fracture mechanics is still very much a developing subject even as regards its fundamentals and, hence, in any application, it is important to bear in mind the limitations associated with some of its results. A survey is made of basic fracture mechanics, with emphasis on those limitations likely to be of importance in aircraft structural applications. ABA author.

AD-A032045 ASRL-TR-177-3 AFFDL-TR-75-71 76/04/00 77N20452

**FRACTURE MECHANICS ANALYSIS OF SINGLE AND DOUBLE ROWS OF FASTENER HOLES LOADED IN BEARING**

Orringer, O.; Stalk, G.

Massachusetts Inst. of Tech., Cambridge. (Aeroelastic and Structures Research Lab.)

This report documents a finite-element analysis procedure for computation of mode I and mode II stress intensity factors at a cracked fastener hole in a single row or a double staggered row of fastener holes on a tension panel. The panel is loaded by cosine bearing pressure distributions applied to each fastener hole. Different bearing forces may be specified for each hole, and any hole may be designated as the damaged hole. The physical structure, finite-element model, program flow and options, input/output conventions, execution times, and limitations are discussed. Results of some example analyses are presented. ABA GRA.

76/01/00 76N19477

**DAMAGE TOLERANCE OF SEMIMONOCOQUE AIRCRAFT**

Haskell, D.F.

Ballistic Research Labs., Aberdeen Proving Ground, Md.

In AGARD Specialists' Meeting on Impact Damage Tolerance of Struc., 12 p (see N76-19471 10-39)

The simple theoretical method which was developed may be used to predict deformation, strain, and fracture of aircraft skin subjected to blast attack. Test results and predictions of the theory compare favorably. The method is used to analytically delineate the factors that significantly affect skin damage tolerance. For the conditions studied, these factors, in decreasing order of influence, are standoff distance, panel width, skin thickness, aspect ratio, skin ultimate strength, rivet spacing, and rivet hole diameter to skin thickness ratio. Test results of two types of semimonocoque helicopter tail booms damaged by bare explosive charges and small-caliber, high-explosive projectiles while under simulated maximum flight load show that both skin and the skin stiffening system are important in the damage tolerance of these structures. Damage tolerance of these structures is proportional to the section modulus of the undamaged section and inversely proportional to the amount of skin removed from the structure by the damaging agent. It is also demonstrated that large increases in damage tolerance can be achieved by increasing longitudinal stiffness. ABA author.

AGARD-CP-186 ISBN-92-835-0154-3 76/01/00 76N19471

**SPECIALISTS' MEETING ON IMPACT DAMAGE TOLERANCE OF STRUCTURES.**

Advisory Group for Aerospace Research and Development, Paris (France).

Paper presented at 41st Meeting of the Structures and Materials Panel, Ankara, 28 Sept. - 3 Oct. 1975.

75/10/00 76N16460

**BASIC CONCEPTS IN FRACTURE MECHANICS**

Eftis, J.; Jones, D.L.; Liebowitz, H.

George Washington Univ., Washington, D.C. (School of Engineering and Applied Sciences).

In AGARD Non-Destructive Inspection Practices, Vol. I, p.11-25 (see N76-16458 07-38)

The linear elastic fracture mechanics approach to design against fracture of structural components, basically a stress intensity approach which establishes criteria for fracture instability in the presence of a crack, is presented. Emphasis is placed on design of aerospace structures. Factors discussed include the fail-safe or fracture safe philosophy of damage tolerant structures; critical crack size; and fatigue crack growth under constant amplitude fatigue loading and variable amplitude fatigue loading. Examples are given. ABA J.M.S.

74/03/00 75/N22536

**PRACTICAL APPLICATION OF FRACTURE MECHANICS FOR JUDGEMENT OF THE SPACELAB MODULE STRUCTURE**

Walter, J.

ERNO Raumfahrttechnik GmbH, Bremen (West Germany).

In ESRO Large Struct. for Manned Spacecraft, p.489-495 (see N75-22504 14-31)

The application of fracture mechanics to thin-walled metallic structures, especially for internally pressurized structures in the presence of small defects (inclusions, surface flaws, embedded flaws, etc.) is demonstrated. The brittle fracture behavior yield stress due to sustained load stresses (environments, stress-corrosion cracking) and cyclic stresses is shown and the leak-before-burst criterion explained. Computation methods for obtaining critical flaw sizes from experimental specimen data and tolerable flaw sizes, as well as the necessary nondestructive detection methods, are discussed. ABA author (ESRO).

NASA-CR-134597 SD73-SH-0171-Vol-2 74/08/00 74N35280

**FRACTURE CONTROL METHODS FOR SPACE VEHICLES. VOLUME 2: ASSESSMENT OF FRACTURE MECHANICS TECHNOLOGY FOR SPACE SHUTTLE APPLICATIONS**

Ehret, R.M.

Rockwell International Corp., Downey, Calif. (Space Div.)

The concepts explored in a state of the art review of those engineering fracture mechanics considered most applicable to the space shuttle vehicle include fracture toughness, precritical flaw growth, failure mechanisms, inspection methods (including proof test logic), and crack predictive analysis techniques. ABA author.

74/01/00 74N23417

**THE USE OF FRACTURE MECHANICS PRINCIPLES IN THE DESIGN AND ANALYSIS OF DAMAGE TOLERANT AIRCRAFT STRUCTURES**

Wood, H.A.

Air Force Flight Dynamics Lab., Wright-Patterson AFB, Ohio.

In AGARD Fracture Mechanics of Aircraft Structures, p.18-31 (see N74-23413 14-32)

The application of fracture control principles to aircraft design in order to produce safer structures is discussed. The mechanical and physical properties of the construction materials which are capable of modification to produce the desired strength are discussed. The selection of materials for airframes is based on requirements established through actual failure experience and service life data. The nature of the requirements and allowances in their application are defined. Tables of data are provided to show the inspection requirements for cases of: (1) slow crack growth structure, (2) crack arrest structure, and (3) fail-safe structure. ABA author.

AGARD-AG-176 AGARDograph-176 74/01/00 74N23413

**FRACTURE MECHANICS OF AIRCRAFT STRUCTURES**

Liebowitz, H.

(George Washington Univ.)

Advisory Group for Aerospace Research and Development, Paris (France).

NASA-TM-X-71925 74/01/31 74N21545

**FRACTURE MECHANICS**

Hardrath, H.F.

National Aeronautics and Space Administration. Langley Research Center, Langley Station, Va.

Presented at AIAA 12th Aerospace Sci. Meeting, Washington, D.C., 31 July 1974.

Fracture mechanics is a rapidly emerging discipline for assessing the residual strength of structures containing flaws due to fatigue, corrosion or accidental damage and for anticipating the rate of which such flaws will propagate if not repaired. The discipline is also applicable in the design of structures with improved resistance to such flaws. The present state of the design art is reviewed using this technology to choose materials, to configure safe and efficient structures, to specify inspection procedures, to predict lives of flawed structures and to develop reliability of current and future airframes. ABA author.

AD-767614 NOR-72-32-PT-1 AFFDL-TR-73-42-PT-1 73/05/00 74N13262

DEVELOPMENT AND EVALUATION OF METHODS OF PLANE STRESS FRACTURE ANALYSIS. PART 1:  
REVIEW AND EVALUATION OF STRUCTURAL RESIDUAL STRENGTH PREDICTION TECHNIQUES

Verette, R.M.; Wilhem, D.P.

Northrop Corp., Hawthorne, Calif. (Aircraft Div.)

The treatment of residual strength prediction for aircraft structures having through flaws is considered in this report. A discussion of the circumstances which normally give rise to plane stress or mixed mode fracture is presented along with a summary of those elements which would constitute an ideal residual strength method. This method would be capable of prescribing the remaining strength possessed by a broad variety of flawed aircraft structures under actual service environments. Currently available prediction techniques fall considerably short of the desired goal, and the strong and weak points of existing methods, as well as comparisons with test results, are presented. A recommended technique is described for residual strength prediction which bridges the gap between the existing methods and the ideal. The recommended approach will account for slow crack growth and plasticity. It appears that the approach will utilize the  $J$  integral in combination with a modified form of the crack growth resistance curve in making residual strength predictions. ABA author.

73/05/00 73/N29928

THE USE OF FRACTURE MECHANICS PRINCIPLES IN THE DESIGN AND ANALYSIS OF DAMAGE TOLERANT  
AIRCRAFT STRUCTURES

Wood, H.A.

Air Force Flight Dynamics Lab., Wright-Patterson AFB, Ohio.

In AGARD Fatigue Life Prediction for Aircraft Struct. and Mater., 13 p (see N73-29924 20-32)

Current trends in the usage of high strength structural materials for aerospace applications are reviewed. The manner in which fracture control procedures may be implemented to achieve a higher degree of damage tolerance are discussed. The application of fracture requirements to two current designs is related. These experiences have contributed to the formulation of specifications for use across the board on all new systems. Important aspects of the proposed USAF damage tolerance criteria, including initial damage assumption and crack growth analyses, are discussed. ABA author.



# CATEGORY D - APPLICATIONS TO SPECIFIC AIRPLANES

AIAA 77-464 77/00/00 77A25770

## DAMAGE TOLERANCE PROGRAM FOR THE B-1 COMPOSITE STABILIZER

Waggoner, G.; Erbacher, H.

(USAF, Aeronautical Systems Div., Wright-Patterson AFB, Ohio); (Grumman Aerospace Corp., Bethpage, N.Y.)  
In Structures, Structural Dynamics and Materials Conference, 18th, March 21-23, 1977, and Aircraft Composites:  
The Emerging Methodology for Structural Assurance, San Diego, Calif., March 24, 25, 1977, Technical Papers. Volume  
A. (A77-25726 10-39) New York, American Institute of Aeronautics and Astronautics, Inc., 1977, p.388-395.

The procedure used by the USAF to achieve damage tolerance in airframe structures is reviewed. The paper then describes how these procedures were interpreted and applied to boron and graphite epoxy composite subcomponents representative of the B-1 horizontal stabilizer. The information presented includes the establishment of program goals; the selection of test specimens; the procedure used to define and locate flaws in critical areas of the structure; the determination and application of test loads and environments; and test results. ABA (author).

76/00/00 77A24917

## DAMAGE TOLERANCE ANALYSIS OF AN AIRCRAFT STRUCTURAL JOINT

Smith, S.H.; Simonen, F.A.

(Battelle Columbus Laboratories, Columbus, Ohio)

In Advances in Joining Technology: Proceedings of the Fourth Army Materials Technology Conference, Boston, Mass.,  
September 16-19, 1975. (A77-24901 10-31) Chestnut Hill, Mass., Brook Hill Publishing Co., 1976, p.471-502.

The new US Air Force specification, MIL-A-83444, on damage-tolerance requirements was applied to a typical structural joint on the wing structure of a military cargo aircraft. Detailed structural analysis of a chordwise structural joint was performed considering load transfer and finite-element structural models. Work energy and crack-surface-displacement methods of linear elastic-fracture mechanics were used to determine the variation of crack-tip stress-intensity factors with crack size. Fatigue-crack-propagation behavior analysis of the full-scale fatigue-test spectrum and reported flight-by-flight service usage spectrum was determined for the structural joint. From initial assumed corner crack sizes at the fastener holes, the fatigue-crack-propagation behavior analysis was utilized to establish the required inspection intervals for depot- or base-level inspection. The structural crack-growth lives to clean-up size at holes of the structural joint were determined. ABA (author).

ICAS Paper 76-26 76/10/00 76A47372

## THE ROLE OF FRACTURE MECHANICS AND FATIGUE IN THE DESIGN OF ADVANCED AEROSPACE VEHICLES

Antona, E.; Giavotto, V.; Salvetti, A.; Vallerani, E.

(Torino, Politecnico, Turin, Italy); (Milano, Politecnico, Milan, Italy); (Pisa, Università, Pisa, Italy); (Aeritalia Spa, Naples, Italy)

International Council of the Aeronautical Sciences, Congress, 10th, Ottawa, Canada, Oct. 3-8, 1976, 17 p. Consiglio Nazionale delle Ricerche.

The fracture and fatigue behavior of fittings and structural elements of spacelab are investigated and research guidelines are laid down. Flaws and cracks incubating and propagating to defects of critical lengths are defined and discussed, fatigue stress spectra and fracture toughness criteria are described. Precritical crack growth and crack growth induced by cyclic loads, leakage before burst and burst before leakage, treatment of through cracks and part-through cracks, non-destructive inspection techniques, and acceptance testing and proof testing are discussed. Fracture analysis and fracture control procedures are defined and outlined, and applicability of statistical energy methods is examined. ABA R.D.V.

AIAA Paper 76-904 76/09/00 76A45390

## DAMAGE TOLERANCE ASSESSMENT OF F-4 AIRCRAFT

Pinckert, R.E.

(McDonnell Aircraft Co., St Louis, Mo.)

American Institute of Aeronautics and Astronautics, Aircraft Systems and Technology Meeting, Dallas, Tex., Sept. 27-29, 1976. 12 p.

The damage-tolerance-assessment phase of two F-4 aircraft structural-integrity programs has been completed. Methods were developed to determine the operational limits of the fracture critical areas and to incorporate initial flaw assumptions, crack-growth computations, and operational limits into the F-4 fleet tracking program. In this paper, the following subjects are covered: (1) development of fatigue spectra to represent service usage; (2) development of a crack-growth prediction technique; (3) determination of the initial quality of F-4 aircraft structure represented by equivalent initial flaw sizes; (4) establishment of baseline aircraft assumptions and the prediction of operational limits; (5) the development of a 'damage index' system to track crack growth at one critical location on an aircraft and determine the damage at other locations; and (6) the development of stress-life curves to convert counting accelerometer data into damage related to crack growth. ABA (author).



SAWE Paper 1043 75/05/00 75A47482

**FATIGUE AND DAMAGE TOLERANCE EFFECTS ON PRELIMINARY DESIGN WING WEIGHTS**

Stephens, R.E.

(Lockheed-Georgia Co., Marietta, Ga.)

Society of Allied Weight Engineers, Annual Conference, 34th, Seattle, Wash., May 5-7, 1975, 20 p.

The purpose of this study is to assess the effect of current design criteria and advanced technology on an existing structure. The structure chosen for the study was the C-141 inner wing box. The design criteria include the new fatigue and damage tolerance criteria which will probably be required on any new air force aircraft. The advanced technology includes new materials and new structural configurations. Two alternate box configurations are presented showing the effects of material properties and cover configurations on the wing weight. Prediction of some trends based on these results is presented. ABA (author).

AIAA Paper 75-805 75/05/00 75A33763

**ANALYTICAL PREDICTION OF FATIGUE CRACK GROWTH AT COLD-WORKED FASTENER HOLES**

Chang, J.B.

(Rockwell International Corp., Los Angeles, Calif.)

AIAA, ASME, and SAE, Structures, Structural Dynamics, and Materials Conference, 16th, Denver, Colo., May 27-29, 1975, AIAA 7 p. Research sponsored by the Rockwell International Independent Research and Development Program.

A methodology for the quantitative prediction of crack growth behavior at cold-worked fastener holes under fatigue cyclic loading has been developed. The proposed analytical prediction technique is based on an effective stress field concept which accounts for the amount of the compressive residual stress existing at the edge of the cold-worked hole. Stress intensity factor ranges ( $\delta$ -K) and crack growth rates (DA/DN) are all formulated in terms of the effective stress field. An existing fatigue crack growth analysis computer program has been modified to account for these changes. This program was subsequently used to study the B-1 fracture mechanics design development test data. Good correlations have been obtained. ABA (author).

AIAA Paper 74-29 74/01/00 74A18738

**APPLICATION OF DAMAGE TOLERANCE TECHNOLOGY TO ADVANCED METALLIC FIGHTER WING STRUCTURE**

Jeans, L.L.; La Rose, R.L.

(Northrop Corp., Aircraft Div., Hawthorne, Calif.)

American Institute of Aeronautics and Astronautics, Aerospace Sciences Meeting, 12th, Washington, D.C., Jan. 30-Feb. 1, 1974, 10 p.

Current air force damage tolerant criteria requirements were developed to ensure that proper emphasis is given in new aircraft structural systems to flaw initiated failure analysis. In this study damage tolerant criteria were analytically investigated in an indepth preliminary design environment on wing components representative of metallic materials and design concepts applicable to future fighter aircraft. Direct comparisons with static and fatigue strength considerations were made. Crack growth analysis was completed for the most critical structure using the Willenborg retardation model and appropriate material crack growth rate and toughness data. ABA (author).

77/02/00 77N22567

**DAMAGE TOLERANCE AND DURABILITY ASSESSMENTS OF UNITED STATES AIR FORCE AIRCRAFT**

Coffin, M.D.; Tiffany, C.F.; Bader, R.

Air Force Systems Command, Wright-Patterson AFB, Ohio.

In AGARD Fracture Mech. Design Methodology, 21 p (see N77-22554 13-39)

A program to conduct damage tolerance and durability assessments of 'in-service' aircraft to assure structural safety and economic life management is discussed. The F-4C/D assessment serves as a classic example to illustrate the objectives, the approach, and the results desired. The general methodology associated with the accomplishment of the technical tasks is presented and discussed. The modification and inspection program resulting from this assessment is described. ABA author.

77/02/00 77N22558

**NORTHROP/UNITED STATES AIR FORCE DURABILITY AND DAMAGE-TOLERANCE ASSESSMENT OF THE F-5E/F AIRCRAFT**

Munrane, S.R.; Stronge, T.D.; Davenport, O.B.

(Aeronautical Systems Div., Wright-Patterson AFB, Ohio) Northrop Corp., Hawthorne, Calif. (F-5 Technology Dept.)

In AGARD Fracture Mech. Design Methodology, 33 p (See N77-22554 13-39)

Fatigue test failures experienced during a complete airframe flight-by-flight fatigue test are reviewed, including the application of fracture mechanics employed during resolution of these failures. Damage-tolerance analyses and specimen tests for other primary structure are discussed. State-of-the-art analytical crack growth rate predictions for flight-by-flight spectra are compared with specimen test results. Compliance of the F-5E/F airframe structure with the USAF damage-tolerance requirements is discussed, along with recommendations for the application of fracture mechanics to future aircraft design. ABA author.

77/02/00 77N22557

## APPLICATION OF FRACTURE MECHANICS TO THE F-111 AIRPLANE

Buntin, W.D.

General Dynamics/Fort Worth, Tex.

In AGARD Fracture Mech. Design Methodology, 12 p (see N77-22554 13-39)

Safe service operations of critical steel components in the F-111 aircraft are assured by analyses and tests developed using principles of fracture mechanics. A unique flaw in a major fitting which forms the inboard section of the wing caused the loss of an airplane in flight. Subsequent analytical and experimental investigations are described which thoroughly investigated the fracture characteristics of all critical steel components in the airframe. Fracture analysis tools were developed and used as essential elements in interpreting experimental data and in describing the damage tolerance of the F-111 fleet. The methodology which was evolved is compared with current airplane damage tolerance requirements. ABA author.

AD-785196 AFFDL-TR-74-5 74/05/00 75N11955

## A SPECTRUM TRUNCATION AND DAMAGE TOLERANCE STUDY ASSOCIATED WITH THE C-5A OUTBOARD PYLON AFT TRUSS LUGS

Gallagher, J.P.; Stalnaker, H.D.; Rudd, J.L.

Air Force Flight Dynamics Lab., Wright-Patterson AFB, Ohio.

A simplified lug specimen configuration is subjected to two load spectra derived from the same exceedance data: (1) a 17 level block loading program, and (2) a 14-mission flight-by-flight loading program. Crack growth data from the two spectra for this PH 13-8Mo material are compared on a life basis; each spectrum contained an equal number of ground air ground (GAG) cycles per lifetime. An analysis of the effect associated with the degree of truncation to which the flight spectrum could be subjected was performed using the conservative no retardation — no load interaction crack growth model and the Willenborg crack growth retardation model. The stress intensity factor calibration developed using finite element techniques is supplemented with stress intensity factor values obtained using the Anderson — James inverse approach. Additional tests on 7075-T6 aluminum are described which investigate the importance of load redundancy. ABA author (GRA).

AD-781809 AFFDL-TR-73-50-Vol-4 73/07/00 74N33464

## ADVANCED METALLIC STRUCTURES: AIR SUPERIORITY FIGHTER WING DESIGN FOR IMPROVED COST, WEIGHT AND INTEGRITY. VOLUME 4: BASELINE DAMAGE TOLERANCE EVALUATION

Davis, D.F.

General Dynamics/Fort Worth, Tex. (Convair Aerospace Div.)

The basic objective of this study was to provide an updated analysis of the F-111F baseline wing box reflecting the latest proposed Air Force version of damage tolerance criteria. In addition, sensitivity and trade studies were made on the baseline. The effect on allowable stress and service life due to variation in KIC, DA/DN, initial damage assumptions, and service usage were determined. NDI experience, thermal and chemical environment, and the impact of a fracture control plan were studied. Baseline data on inspection experience was compiled. The impact on stress levels and life of varying the residual strength load requirement was determined. ABA GRA.

74/01/00 74N23428

## THE APPLICATION OF FRACTURE MECHANICS IN THE DEVELOPMENT OF THE DC-10 FUSELAGE

Swift, T.

Douglas Aircraft Co., Inc., Long Beach, Calif.

In AGARD Fracture Mechanics of Aircraft Structures, p.226-287 (see N74-23413 14-32)

The degree of damage tolerance used in the design of the DC-10 fuselage pressure shell is discussed with reasons for its selection. Analysis methods are presented for the prediction of the residual strength of damaged, stiffened panels, based on the matrix force solution of an idealized structure combined with fracture mechanics equations. The effects of attachment flexibility, which play an important part in the residual strength of damaged structure, are accounted for. Crack growth retardation due to the plastic zone formed on high load cycles and its effect on propagation under spectrum loading is discussed. It is shown that the stress intensity at the threshold of slow stable growth is not only a material property but depends almost entirely on past load history. A description of the development test program to verify the analytical techniques and to substantiate the fail-safe strength of the fuselage shell is given together with the results of many of the tests. ABA author.

## CATEGORY E - FATIGUE CRACK GROWTH PREDICTION

ONERA, TP No. 1977-78 77/00/00 77A50986

## FATIGUE CRACK GROWTH MODEL PREDICTION WITH TWO COUPLED DIFFERENTIAL EQUATIONS

Pellas, J.; Baudin, G.; Robert, M.

(ONERA, Chatillon-sous-Bagneux, Hauts-de-Seine, France)

(Fracture 1977; Proceedings of the Fourth International Conference on Fracture, Waterloo, Ontario, Canada, June 19-24, 1977, p.1353-1360.) ONERA, TP No. 1977-78, 1977. (p.1353-1360) 9 p.

The Wheeler crack propagation model is criticized on the grounds that the exponent that is supposed to be characteristic of each material is not intrinsic, that it takes into account only the loading history after the last overload, and does not incorporate the existence of the crack arrest phenomenon. To remedy this situation, a new parameter is introduced in the fatigue crack growth law: the crack propagation threshold. The new crack propagation law thus consists of two coupled differential constitutive equations connecting crack propagation rate, stress intensity factor, and loading history by means of the crack propagation threshold. Some predictions based on this model are in good agreement with experimental data from tests on a bending specimen for a single overload and for two-level loading. ABA P.T.H.

77/09/00 77A49265

## EMPIRICAL FORMULATIONS FOR THE ANALYSIS AND PREDICTION OF TRENDS FOR STEADY-STATE FATIGUE CRACK GROWTH RATES

Fitzgerald, J.H.

(Northrop Corp., Aircraft Div., Hawthorne, Calif.)

Journal of Testing and Evaluation, Vol.5, Sept. 1977, p.343-353. Research sponsored by Northrop Corp.

The general characteristics of steady-state fatigue crack growth rates are discussed. An empirical formulation is described where two constants form a basic crack growth rate versus maximum stress intensity  $K_{max}$  curve, which is a straight line on a log-log graph. The constants that form the base curves for various materials are correlated to Young's modulus. A third parameter that is sensitive to material alloy and environment is described and methods for obtaining this value are presented. Crack growth rate data for several stress ratios can then be projected to the basic modulus-dependent curve, where straight line scatter bands and statistical information pertaining to the overall accuracy of the formulations can be determined. ABA (author).

77/09/00 77A47508

## PREDICTION OF FATIGUE CRACK GROWTH RATES - THEORY, MECHANISMS, AND EXPERIMENTAL RESULTS

Irving, P.E.; McCartney, L.N.

(Aeronautical Research Council, National Physical Laboratory, Teddington, Middx., England)

(Metals Society, Fatigue Conference, Cambridge, England, Mar. 28-30, 1977.) Metal Science, Vol.11, Aug. - Sept. 1977, p.351-361.

Two kinds of continuum-based crack growth laws are reviewed. Those based on instantaneous values of cyclic crack-opening displacement with a stress range intensity factor exponent equal to two, and those based on damage or strain accumulation which have a stress range intensity factor exponent of four and which predict the onset of rapid crack acceleration as the stress-intensity factor approaches the fracture toughness value. A third type of law, based on energy-balance concepts within a crack tip process zone, predicts, for the exponent value, a gradient lying between two and four depending on the size of the reversed plastic zone. A comparison of theoretical and experimental results suggests that exponent-4 laws provide better agreement for data gathered in inert environments. The use of experimental data for determining a mechanism or choosing a model is discussed. ABA M.L.

76/00/00 77A36222

## APPLICATION OF FRACTURE MECHANICS TO THE PREDICTION OF CRACK GROWTH DAMAGE ACCUMULATION IN STRUCTURES

Wood, H.A.; Gallagher, J.P.; Engle, R.M., Jr

(USAF, Flight Dynamics Laboratory, Wright-Patterson AFB, Ohio)

In Mechanics of Fracture; Proceedings of the Annual Winter Meeting, New York, N.Y., December 5-10, 1976. (A77-36214 16-39) New York, American Society of Mechanical Engineers, 1976, p.171-190.

This paper provides a summary of current practice on predicting crack growth damage accumulation with specific applications to current USAF policies on safety and durability. Analytical procedures are required to determine safe crack growth. The life prediction methodology is examined to illustrate the major effects of the structural parameters, material parameters and loading. Examples are cited to give indication of confidence in making life predictions. ABA (author).



77/01/00 77A21598

**PHENOMENOLOGICAL EQUATION FOR THE DETERMINATION OF FATIGUE CRACK GROWTH RATES BASED ON FRACTURE MECHANICS PARAMETERS**

Marci, G.

(Babcock-Brown-Bower-Reaktor GmbH, Mannheim, West Germany)

Materialpruefung, Vol.19, Jan. 1977, p.17-21. In German.

A fracture mechanics equation for the determination of fatigue crack growth rates is developed under consideration of the geometric model of closure and the partition of the stress and strain range in the vicinity of the crack tip. Experimental data are presented which show that the range of tensile stress and strain has to be reduced by a constant range. The range of tensile stress and strain which corresponds to this range is set equal to the compressive stresses and strains in their effect on the fatigue damage. ABA (author).

77/02/00 77A21276

**REVIEW OF FATIGUE-CRACK-GROWTH PREDICTION METHODS**

Nelson, D.V.

(General Electric Co., Sunnyvale, Calif.)

(Society for Experimental Stress Analysis, Spring Meeting, Chicago, Ill., May 11-16, 1975.) Experimental Mechanics, Vol.17, Feb. 1977, p.41-49.

Empirical relations for describing constant-amplitude crack-growth behavior are reviewed. The effect of stress ratio (mean stress) on crack growth is illustrated through the use of plots analogous to constant-lifetime fatigue diagrams. Experimentally observed load-sequence effects, such as crack retardation due to tensile overloads, acceleration due to compressive overloads, the interaction between tensile and compressive overloads, etc. are summarized. The crack-closure phenomenon is reviewed, since it seems to provide a plausible physical explanation for many sequence effects. Methods of predicting crack growth under variable-amplitude loading (including irregular loadings representative of actual service) are reviewed and some of their limitations noted. ABA (author).

76/00/00 77A13294

**SPECTRUM CRACK GROWTH PREDICTION METHOD BASED ON CRACK SURFACE DISPLACEMENT AND CONTACT ANALYSES**

Dill, H.D.; Saff, C.R.

(McDonnell Aircraft Co., St Louis, Mo.)

In Fatigue Crack Growth under Spectrum Loads; Proceedings of the Symposium, Montreal, Canada, June 23, 24, 1975. (A77-13278 03-39) Philadelphia, Pa., American Society for Testing and Materials, 1976, p.306-317; Discussion, p.317-319.

A method for prediction of crack growth behavior has been developed, based on evaluations of stress intensity caused by crack surface contact. The potential interference of the crack surfaces is determined from analyses of elastic displacements during loading and unloading and of the permanent deformation left in the wake of a growing crack. The potential interference is treated as a wedge acting behind the crack tip and the contact stresses created by this wedge are computed through an elastic-plastic analysis. The effective stress intensity range used for crack growth prediction is found by subtracting the stress intensity caused by these contact stresses from the applied stress intensity range. Comparisons of crack growth behavior predicted by this method and that measured in constant amplitude tests, with and without high loads, and in block spectrum tests have shown that the method accounts for load interaction effects in these cases. These effects include delayed retardation following high loads, crack growth acceleration during high loads, and dependence of growth rates on number of high loads. ABA (author).

76/00/00 77A13292

**PREDICTION OF FATIGUE CRACK GROWTH UNDER IRREGULAR LOADING**

Nelson, D.V.; Fuchs, H.O.

(General Electric Co., Sunnyvale, Calif.); (Stanford University, Stanford, Calif.)

In Fatigue Crack Growth under Spectrum Loads; Proceedings of the Symposium, Montreal, Canada, June 23, 24, 1975. (A77-13278 03-39) Philadelphia, Pa., American Society for Testing and Materials, 1976, p.267-286; Discussion, p.287-291. Research supported by the Association of American Railroads, Deere and Co., and NSF.

Data obtained from constant-amplitude tests permit the calculation of crack growth under irregular loading. A new method for prediction of fatigue crack growth behavior is proposed which has the ability of accounting for important load sequence effects due to both tensile and compressive overloads. The effect of compressive loadings which cause gross yielding is given special consideration. All predictions are made using a linear elastic fracture mechanics approach. Two crack growth relations are used: (1) the Forman relation in conjunction with condensed load histories and full histories with range-by-range growth calculation; and (2) a relation based on an effective stress intensity range concept which tries to account for possible sequence and stress ratio effects. Predictions by the second method were much better for the suspension history when gross yielding in compression occurred. ABA S.D.



76/00/00 77A13279

**OBSERVATIONS ON THE PREDICTION OF FATIGUE CRACK GROWTH PROPAGATION UNDER VARIABLE-AMPLITUDE LOADING**

Schijve, J.

(Delft, Technische Hogeschool, Delft, Netherlands)

In *Fatigue Crack Growth under Spectrum Loads*; Proceedings of the Symposium, Montreal, Canada, June 23, 24, 1975. (A77-13278 03-39) Philadelphia, Pa., American Society for Testing and Materials, 1976, p.3-23.

The paper starts with a discussion on loads in service, after which a survey is given of various types of variable-amplitude loading as applied in test programs. The various phenomenological aspects of fatigue damage associated with fatigue cracks are indicated. Interaction effects between cycles of different magnitudes are defined. Methods for measuring interaction effects, examples of interaction effects, and possible explanations are reviewed. This includes both tests with simple types of variable-amplitude loading (overloads and step loading) and more complex load-time histories (program loading, random load, and flight-simulation loading). New evidence on crack closure is presented. Various types of prediction methods are discussed. The paper is primarily a survey of the present knowledge, with an analysis of the consequences for prediction techniques. ABA (author).

75/11/00 76A12166

**AN ANALYSIS OF THE INFLUENCE OF MEAN STRESS INTENSITY AND ENVIRONMENT ON FATIGUE CRACK GROWTH IN A NEW HIGH STRENGTH ALUMINUM ALLOY**

Branco, C.M.; Culver, L.E.; Radon, J.C.

(Imperial College of Science and Technology, London, England)

Journal of Testing and Evaluation, Vol.3, Nov. 1975, p.407-413. Research supported by the Ministry of National Education of Portugal.

The effects of the mean stress intensity factor and the range of the stress intensity on fatigue crack propagation during wholly tensile loading cycles in the aluminum alloy RR58 in laboratory air and in a 3.5% NaCl solution have been studied using contoured double-cantilever beam specimens. In general the fatigue crack growth rate in NaCl solution was greater than in air under similar conditions except for tests in which high values of the maximum stress intensity factor were used when no significant difference was observed. Based on the experimental data a relation between the cyclic crack growth rate and the tensile loading levels has been proposed. ABA (author).

AIAA Paper 75-1311 75/09/00 75A45691

**FRACTURE MECHANICS LCF LIFE PREDICTION SYSTEM WITH APPLICATION TO AN ADVANCED GAS TURBINE ALLOY**

Hurchalla, J.; Johnson, H.E.; Wallace, R.M.

(United Technologies Florida Research and Development Center, West Palm Beach, Fla.)

American Institute of Aeronautics and Astronautics and Society of Automotive Engineers, Propulsion Conference, 11th, Anaheim, Calif., Sept. 29-Oct.1, 1975, AIAA 9 p.

The basic philosophy and application of fracture mechanics concepts to the design of advanced rotating hardware employing a high-strength alloy are reviewed. Turbine disk lug fractures occurring during engine development endurance testing are examined. A fracture mechanics life prediction technique is found to be suitable for design of high-temperature cyclic rupture of a disk notch. A general approach to LCF life prediction using only a fracture mechanics crack growth mechanism is shown to be a viable method, although offering no benefit in accuracy over traditional LCF design methods. A combined life prediction system is identified as representing the best approach based on prediction scatter. ABA S.D.

ASME Paper 75-MAT-N 75/07/00 75A38730

**PREDICTIONS OF THE EFFECT OF YIELD STRENGTH ON FATIGUE CRACK GROWTH RETARDATION IN HP-9Ni-4Co-30C STEEL**

Petrak, G.J.; Gallagher, J.P.

(Dayton, University, Dayton, Ohio); (USAF, Flight Dynamics Laboratory, Wright-Patterson AFB, Ohio)

(American Society of Mechanical Engineers, 1975.) ASME, Transactions, Series H - Journal of Engineering Materials and Technology, Vol.97, July 1975, p.206-213.

Baseline mechanical property data, constant amplitude fatigue crack growth rate data, and single-peak overload test data are presented for HP-9Ni-4Co-30C steel heat treated to three strength levels. These data are then used to evaluate a new model proposed for defining the instantaneous crack growth rate following an overload. The constant amplitude crack growth rates are affected by the strength level of the material with the higher strength exhibiting the faster cracking rates. The magnitude of retardation following an overload cycle is also shown to be influenced by the strength of the material. The lower strength steel displayed significantly more retardation for the same load levels. A general yield zone model is used to predict retarded growth rates. These predictions are shown to correlate quite well with the test data. The model successfully accounts for the different amounts of retardation associated with the different strength levels of the material. ABA (author).

ASLE Preprint 74LC-5A-2 74/10/00 75A12181

**DETERMINING FATIGUE CRACK PROPAGATION RATES IN LUBRICATING ENVIRONMENTS THROUGH THE APPLICATION OF A FRACTURE MECHANICS TECHNIQUE**

Polk, C.J.; Murphy, W.R.; Rowe, C.N.

(Mobil Research and Development Corp., Princeton, N.J.)

American Society of Lubrication Engineers and American Society of Mechanical Engineers, Joint Lubrication Conference, Montreal, Canada, Oct. 8-10, 1974, ASLE 8 p.

73/12/00 74A22503

**A REVIEW OF SOME DAMAGE TOLERANCE DESIGN APPROACHES FOR AIRCRAFT STRUCTURES**

Toor, P.M.

(Lockheed-Georgia Co., Marietta, Ga.)

(Symposium on Fracture and Fatigue, George Washington University, Washington, D.C., May 3-5, 1972.)

Engineering Fracture Mechanics, Vol.5, Dec. 1973, p.837-880.

The properties of available methods for residual strength analysis in aircraft structures are assessed with attention to their limitations. Various linear and nonlinear crack propagation laws and loading effects in crack propagation are discussed. Fracture mechanics methods are applied to several types of structural components under spectrum-loading conditions. A comparison of test and analysis data for complex structures under loads indicated that simple methods of fracture mechanics should be effective in determining the damage tolerance strength and crack growth rates in aircraft components. More studies of the effectiveness of fracture mechanics methods on full-scale structural testpieces are urged to support positive laboratory evaluations of such methods. ABA V.Z.

72/12/00 73A18482

**METHOD OF ANALYSIS AND PREDICTION FOR VARIABLE AMPLITUDE FATIGUE CRACK GROWTH**

Porter, T.R.

(Boeing Co., Research and Engineering Div., Seattle, Wash.)

(Symposium on Fracture and Fatigue, George Washington University, Washington, D.C., May 3-5, 1972.)

Engineering Fracture Mechanics, Vol.4, Dec. 1972, p.717-736.

In this analysis method, the crack growth rate is evaluated for each load cycle using a modification of the fracture mechanics correlation technique. The crack growth for each cycle was evaluated as a function of the stress intensity factor excursion with a correction factor for the maximum and minimum peak stress levels in the test spectrum. The fatigue crack growth correction for the peak stresses in the spectrum is given as a growth rate correction factor  $R$ . The relationship for  $R$ , is termed the 'fatigue crack growth rate interaction model'. For verification, the interaction model was applied to test data from spectrum loading tests. The correlation obtained for the example, indicated that the model properly predicts the interaction effects and its use could significantly improve the accuracy of crack growth life calculations for programmed spectrum tests. ABA (author).

72/09/00 73/A15298

**FATIGUE CRACK PROPAGATION IN TERMS OF FRACTURE MECHANICS CONCEPTS**

Castagna, M.

(Centro Sperimentale Metallurgico, Rome, Italy)

(Associazione Italiana di Metallurgia, Convegno Nazionale, 15th, Bologna, Italy, June 1972.) Metallurgia Italiana, Vol.44, Sept. 1972, p.407-413; Discussion, p.413, 414. In Italian.

Treatment of the problem of fatigue fracture of a structural element on the basis of an analysis of the processes of growth of a crack from an initial dimension to a final or critical dimension. It has been shown experimentally that the main parameter controlling the propagation velocity of a fatigue crack is the cycle variation of the stress intensification factor, in terms of which a formula expressing the resistance of a material to crack propagation due to cyclic or, more generally, time-variable stresses is obtained. This type of characterization is performed on various types of steel and, in particular, on 38NiCrMo4 tempered at various temperatures after quenching in such a way as to obtain various resistance levels. ABA A.B.K.

AD-A044420 FR-8101 AFML-TR-76-176 77/04/00 78N12092

**CUMULATIVE DAMAGE FRACTURE MECHANICS AT ELEVATED TEMPERATURES**

Sims, D.L.; Annis, C.G., Jr; Wallace, R.M.

Pratt and Whitney Aircraft, West Palm Beach, Fla. (Government Products Div.)

The interpolative hyperbolic sine model for mission-mix crack growth was used to predict the propagation histories and cycles-to-failure for two specimen geometries (compact tension and surface crack) at two temperatures (1000°F and 1200°F). Results were encouraging with an average prediction error of less than 15%. ABA author (GRA).

AD-A002554 ASD-TR-74-24 74/06/00 75N20777

**FRACTURE MECHANICS OF TINY CRACKS NEAR FASTENERS**

Anderson, W.E.

Battelle Columbus Labs., Ohio

This report deals with the question of how tiny a crack might be in aluminum alloys of high strength and still be

analytically treated by the methods of linear elastic fracture mechanics (LEFM). These techniques are used to obtain estimates of the expected rate of crack extension. Under simple cyclic loadings, LEFM-based predictions are usually within a factor of two from measured experimental results. ABA GRA.

73/05/00 73N29932

A SUMMARY OF CRACK GROWTH PREDICTION TECHNIQUES

Wood, H.A.

Air Force Flight Dynamics Lab., Wright-Patterson AFB, Ohio.

In AGARD Fatigue Life Prediction for Aircraft Struct. and Mater. 31 p (see N73-29924 20-32)

The use of material growth rate data and analytical retardation models in predicting crack growth under variable amplitude loading is reviewed. Retardation models of current interest are discussed and compared. An effective stress model is described, including the mathematical formulation, applicability and usage limitations. Comparison of analyses and tests for typical spectra are shown. A primary factor in the accurate prediction of spectrum crack growth behavior is the proper representation of basic growth rate data including consideration of R factor shift and possible limit, threshold levels of stress intensity, closure effects and environment. The relative significance of each of these parameters on total crack growth life is discussed. ABA author.



## CATEGORY F - STATISTICS AND RELIABILITY

77/08/00 77A46729

## PROBABILISTIC FRACTURE MECHANICS

Besuner, P.M.; Tetelman, A.S.

(Failure Analysis Associates, Palo Alto, Calif.)

Nuclear Engineering and Design, Vol.43, No.1, Aug. 1977, p.99-114. Research sponsored by the Electric Power Research Institute.

Probabilistic fracture mechanics (PFM) analysis of structural components exhibiting crack-like imperfections is developed as a tool for predicting and enhancing structural reliability, and PFM methodology and applications are discussed. PFM is subsumed under engineering probability and reliability analysis, and leans on deterministic stress analysis and material models in estimating residual static strength or fatigue lifetime of cracked structures. A nomographic technique for selecting the mean yield strength of an alloy minimizing failure probability for a hypothetical component with yielding and brittle fracture failure modes, Monte Carlo simulation programs, computation of fatigue failures stemming from crack-like flaws in the uniformly stressed region of a typical turbine rotor spindle are discussed, and computation of the initiation cycles required to generate an actual fatigue crack, are discussed. ABA R.D.V.

76/00/00 77A13293

## STRUCTURAL RELIABILITY PREDICTION METHOD CONSIDERING CRACK GROWTH AND RESIDUAL STRENGTH

Varanasi, S.R.; Whittaker, I.C.

(Boeing Commercial Airplane Co., Seattle, Wash.)

In Fatigue Crack Growth under Spectrum Loads; Proceedings of the Symposium, Montreal, Canada, June 23, 24, 1975. (A77-13278 03-39) Philadelphia, Pa., American Society for Testing and Materials, 1976, p.292-305.

An analysis method to estimate structural reliability based on crack growth and residual strength of aircraft structures is presented. The method is based on linear elastic fracture mechanics theory and allows for the variability of crack initiation and growth found in the experimental data of various metals. At a reference stress intensity factor, the central tendency and the variance values of material crack-growth parameters are determined. Combinations of these parameters are selected by Monte Carlo simulation techniques, and are used to describe the characteristically stochastic behavior of crack growth in a material. This description of material crack-growth behavior is then applied to the typical case of built-up skin-stringer configuration of fail-safe type airplane structures to predict the number and size of cracks in a fleet at any time during its life. Thus, inspection routines may be established, based on realistic fleet performance, to provide suitable levels of structural reliability for a fleet of airplanes during its operational lifetime. ABA (author).

ACS Paper 53-BE-75F 76/10/00 76A46282

## AN ERROR ANALYSIS OF FAILURE PREDICTION TECHNIQUES DERIVED FROM FRACTURE MECHANICS

Wiederhorn, S.M.; Fuller, E.R., Jr.; Mandel, J.; Evans, A.G.

(National Bureau of Standards, Institute for Materials Research, Washington, D.C.); (Rockwell International Science Center, Thousand Oaks, Calif.)

(American Ceramic Society, Fall Meeting, Indianapolis, Ind., Sept. 21-24, 1975.) American Ceramic Society, Journal, Vol.59, Sept.-Oct. 1976, p.403-411.

Three principal methods of failure prediction for brittle materials are analyzed statistically. Each method depends on fracture mechanics for its predictive value; hence the variance of the failure time depends on the scatter in the fracture-mechanics data and the scatter in the estimate of the initial size of the strength-limiting crack. The variance is used to calculate confidence limits for the prediction of failure for glass and sic. Procedures for the collection and analysis of data are discussed, and the implications of the analysis for lifetime prediction are evaluated. ABA (author).

75/04/00 75A34145

## STATISTICAL CONSIDERATIONS IN LINEAR ELASTIC FRACTURE MECHANICS

Lende, E.M.; Neal, D.M.; Spiridigliozzi, I.

(US Army, Army Materials and Mechanics Research Center, Watertown, Mass.)

(US Air Force, US Navy, US Army, and NASA, Symposium on Propulsion System Structural Integration and Engine Integrity, Monterey, Calif., Sept. 3-6, 1974.) Journal of Aircraft, Vol.12, Apr. 1975, p.411-420. ARPA-supported research.

Critical defect-size distributions are estimated for various metals and for hot-pressed silicon nitride using the Monte Carlo method. With regard to the critical flaw-size computation, results obtained for the numerous materials are compared to the sensitivity or probability of detection of particular flaw sizes based on existing nondestructive evaluation techniques. In several instances, defect detection is the limiting factor. Comparison of flaw estimates for the silicon nitride to fractographic observations demonstrates capability of order-of-magnitude accuracy. The technique is also used to explore the influence of variable parameters in a simple crack-growth law. An important result was the nonnormality of life estimates, even though normal distributions were used for input variables. The consequence is a much lower probability of occurrence for the modal value of the life distribution than might be anticipated. With regard to the Monte Carlo method, the paper demonstrates that selection of the appropriate number of simulations must rely on consideration of third- and higher-order moments of the resulting statistical distributions. ABA (author).



NASA-CR-150301 E-16-646 77/06/00 77N27178

**PROBABILISTIC FRACTURE MECHANICS AND OPTIMUM FRACTURE CONTROL ANALYTICAL PROCEDURES FOR A REUSABLE SOLID ROCKET MOTOR CASE**

Hanagud, S.; Uppaluri, B.

Georgia Inst. of Tech., Atlanta. (School of Aerospace Engineering.)

A methodology for the reliability analysis of a reusable solid rocket motor case is discussed. The analysis is based on probabilistic fracture mechanics and probability distribution for initial flaw sizes. The developed reliability analysis is used to select the structural design variables of the solid rocket motor case on the basis of minimum expected cost and specified reliability bounds during the projected design life of the case. Effects of failure prevention plans such as non-destructive inspection and the material erosion between missions are also considered in the developed procedure for selection of design variables. The reliability-based procedure can be modified to consider other similar structures of reusable space vehicle systems with different failure prevention plans. ABA author.

PB-248910/2 NBSIR-75-952 75/12/00 76N22307

**AN ERROR ANALYSIS OF FAILURE PREDICTION TECHNIQUES DERIVED FROM FRACTURE MECHANICS**

Wiederhorn, S.M.; Fuller, F.R., Jr; Mandel, J.; Evans, A.G.

(Rockwell Intern. Corp., Thousand Oaks, Calif.)

National Bureau of Standards, Washington, D.C. (Inst. for Materials Research.)

Three principal methods of failure prediction for brittle materials are analyzed statistically. Each method depends on fracture mechanics for its predictive value and hence, the variance of the failure time is found to depend on the scatter in the fracture mechanics data and the scatter in the estimate of the initial size of the strength limiting crack. The variance is used to calculate confidence limits for the prediction of failure for two materials, glass and silicon carbide. Procedures for the collection and analysis of data are discussed, and the implications of the analysis for lifetime prediction are evaluated. ABA GRA.

PB-246255/4 FAA-75-4-6 EPRI-217-1-TR-4 75/07/00 76N20269

**PROBABILISTIC FRACTURE MECHANICS**

Besuner, P.M.; Tetelman, A.S.

Failure Analysis Associates, Palo Alto, Calif.

Methodology is developed for probabilistic fracture mechanics analysis (PFM) of structural components with crack-like imperfections. Details are given for the development and application of both a simple nomographic method and a basic numerical tool for PFM applications. Two illustrative applications based on linear elastic fracture mechanics are included to demonstrate the utility of PFM. The first example selects the mean yield strength of an alloy in order to minimize the probability of failure for a hypothetical component with two failure modes, yielding and brittle fracture. The second example points out the need for and current unavailability of required input data. ABA GRA.

# CATEGORY G - MISCELLANEOUS, INCLUDING FRACTURE MECHANICS OF COMPOSITES

77/01/00 77A22871

## CRITICAL LOOK AT CURRENT APPLICATIONS OF FRACTURE MECHANICS TO THE FAILURE OF FIBRE-REINFORCED COMPOSITES

Kanninen, M.F.; Rybicki, E.F.; Brinson, H.F.

(Battelle Columbus Laboratories, Columbus, Ohio); (Virginia Polytechnic Institute and State University, Blacksburg, Va.)  
Composites, Vol.8, Jan. 1977, p.17-22.

While successful for failure analysis of many commonly used structural materials, fracture-mechanics applications to fibre-reinforced composites have so far not been as effective. The paper explores some basic reasons for this. A brief review of the micromechanical events involved in composite fracture is given first. then a critical appraisal is made of various analytical contributions that have appeared in the literature. It is found that these are generally empirical extensions of linear elastic fracture mechanics that are not capable of coping with the complexity of the crack-extension process as seen from the micromechanical point of view. It is concluded that innovative fracture-mechanics techniques are required; one possibility is suggested. ABA (author).

75/00/00 76A22466

## LIMITATIONS OF FRACTURE MECHANICS AS APPLIED TO COMPOSITES

Smith, C.W.

(Virginia Polytechnic Institute and State University, Blacksburg, Va.)

In *Inelastic Behavior of Composite Materials*; Proceedings of the Winter Annual Meeting, Houston, Tex., November 30-December 5, 1975. (A76-22460 09-24) New York, American Society of Mechanical Engineers, 1975, p.157-175.

The evolution of the fracture mechanics analysis of composite materials is reviewed. The modified Griffith-Irwin fracture mechanics is described, with emphasis on the role of the stress intensity factor and the strain energy release rate for both isotropic and anisotropic materials. Fatigue crack growth in isotropic materials is treated. A micromechanical approach is presented for modeling crack-fiber-bond line interactions in infinite media. Current macromechanical approaches to this problem are described. These include the critical volume and strain energy density theories, the hybrid theory and the strip yield model, and the approximate theories of hypothetical crack and critical distance. All of these theories require the exclusion of a nonlinear zone near the crack tip in which significant material damage may occur. ABA B.J.

76/02/00 76A20533

## FRACTURE MECHANICS OF METAL MATRIX-METAL FIBRE COMPOSITES

Arkhangelska, I.N.; Mileiko, S.T.

(Akademii Nauk SSSR, Institut Fiziki Tverdogo Tela, Chernogolovka, USSR)

Journal of Materials Science, Vol.11, Feb. 1976, p.356-362.

A model of the metal matrix-metal fiber composite has been constructed. The critical stress intensity coefficient has been estimated taking into account the increase of the energy absorbing capacity of a fiber surrounded by a plastic matrix due to the increase of the elongation at rupture of the fiber under these conditions. The results of experiments carried out on aluminum matrix-steel fibers composites support the validity of the model. The effect of conditions at the fiber-matrix interface on the fracture toughness of the composite has also been studied. ABA (author).

75/00/00 76A16817

## A FINITE-ELEMENT PROGRAM FOR FRACTURE MECHANICS ANALYSIS OF COMPOSITE MATERIAL

Atluri, S.N.; Kobayashi, A.S.; Nakagaki, M.

(Georgia Institute of Technology, Atlanta, Ga.); (Washington, University, Seattle, Wash.)

In *Fracture Mechanics of Composites*; Proceedings of the Symposium, Gaithersburg, Md., September 25, 1974. (A76-16813 05-39) Philadelphia, Pa., American Society for Testing and Materials, 1975, p.86-98.

A hybrid displacement model is proposed for solving two-dimensional fracture mechanics problems for rectilinear-anisotropic materials. This finite-element procedure uses four singular elements surrounding the crack tip and regular elements occupying the remaining region. The applications discussed deal with a center crack in a bimaterial tension plate, a center crack orthotropic tension plate, a double edge-cracked tension plate, a three-point bend specimen, and a slanted-crack orthotropic tension plate. The relative merits of the hybrid displacement method are included. ABA S.D.

75/00/00 76A16813

## FRACTURE MECHANICS OF COMPOSITES

Proceedings of the Symposium, Gaithersburg, Md., September 25, 1974. Symposium sponsored by the American Society for Testing and Materials. Philadelphia, Pa., American Society for Testing and Materials (ASTM Special Technical Publication, No.593), 1975, 235 p.

This collection of papers is concerned with a state-of-the-art review of analysis methods for studying the complex phenomena related to the fracture processes in composite laminates, along with fracture toughness data on commonly used high-performance composites and adhesives. Particular attention is paid to crack arrestment of laminated composites and to crack arrestment strip concepts. Featured topics discuss three-dimensional stress distribution in the vicinity

of through-the-thickness crack with and without crack tip damage, determination of stress intensity factors for cracks in laminates modeled as homogeneous solids, a fracture theory used to explain the fracture behavior of laminates containing both circular and sharp notches, crack size effect in composites, and characterization of a structural adhesive used in bonding materials. Individual items are announced in this issue. ABA S.D.

74/09/00 74A45810

#### FRACTURE MECHANICS OF PLASTIC-FIBER COMPOSITES

Sih, G.C.; Chen, E.P.; Huang, S.L.

(Lehigh University, Bethlehem, Pa.); (US Naval Material Command, Naval Air Development Center, Warminster, Pa.)  
Engineering Fracture Mechanics, Vol.6, Sept. 1974, p.343-359.

The concept of fracture mechanics is introduced to characterize the toughness of fiber-reinforced composites which should be distinguished from tensile strength. A material may have a high tensile strength but a low toughness, meaning that it has a low resistance to crack extension. Depending on the analytical model used, the same experimental data may report different fracture toughness values. In general, the combination of crack propagation in directions parallel and perpendicular to the fibers makes the composite problem very difficult to analyze. Composites with well-aligned fibers are more susceptible to crack propagation parallel than perpendicular to the fibers and can be analyzed with a reasonable degree of accuracy by using the existing KC or SC theory in fracture mechanics. The KC or SC values for several composites are reported and applied to solve various example problems illustrating the advantage of fiber reinforcement. ABA (author).

73/00/00 73A43629

#### FRACTURE MECHANICS FOR FIBROUS COMPOSITES.

Sih, G.C.; Hilton, P.D.; Badaliance, R.; Shenberger, P.S.; Villarreal, G.

(Lehigh University, Bethlehem, Pa.)

In Analysis of the Test Methods for High Modulus Fibers and Composites; Proceedings of the Symposium, San Antonio, Tex., April 12, 13, 1972. (A73-43626 23-18) Philadelphia, American Society for Testing and Materials, 1973, p.98-132.

In the present paper, a combined theoretical and experimental research report for investigating the application of fracture mechanics to composite systems is carried out. Preliminary results are presented which include the development of two fiber reinforced composite crack models (one with a low-fiber-volume fraction and the other a high-fiber-volume fraction) and corresponding experimental data. The qualitative features of the theoretical prediction are in agreement with the experimental data indicating that there exists an optimum fiber volume fraction for which the composite achieves maximum fracture toughness. Tests were performed on unidirectional fiber reinforced composites with the crack running parallel to the fibers. For this arrangement, the current theory of fracture mechanics is shown to apply with good accuracy for glass fiber composites. ABA (author).

73/00/00 73A43628

#### FRACTURE MECHANICS AND COMPOSITE MATERIALS — A CRITICAL ANALYSIS

Zweben, C.

(Du Pont de Nemours and Co., Inc., Wilmington, Del.)

In Analysis of the Test Methods for High Modulus Fibers and Composites; Proceedings of the Symposium, San Antonio, Tex., April 12, 13, 1972. (A73-43626 23-18) Philadelphia, American Society for Testing and Materials, 1973, p.65-97.

The emergence of advanced filamentary composite materials as a structural material comes at a time of increasing concern over reliability. This places increasing emphasis on the ability to characterize the fracture and fatigue behavior of these materials. This paper discusses what appear to be the three main approaches being pursued. The first applies classical fracture mechanics (CFM) on a macroscopic level, treating composites as homogeneous, anisotropic materials. The second recognizes material heterogeneity and applies CFM to the problems of crack propagation in the matrix and fiber phases and interfaces separately. The third method, which might be called the material modeling approach, uses approximate models in order to represent the major effects of heterogeneity and to simplify the analysis. ABA (author).

ASME Paper 73-DE-20 73/04/00 73A30821

#### FRACTURE MECHANICS OF PLASTIC-FIBER COMPOSITES

Sih, G.C.; Chen, E.P.; Huang, S.L.

(Lehigh University, Bethlehem, Pa.); (US Naval Material Command, Aero Mechanics Dept., Warminster, Pa.)

American Society of Mechanical Engineers, Design Engineering Conference and Show, Philadelphia, Pa., Apr. 9-12, 1973, 12 p.

The concept of fracture mechanics is introduced to characterize the toughness of fiber-reinforced composites which should be distinguished from tensile strength. A material may have a high tensile strength but a low toughness meaning that it has a low resistance to crack extension. Depending on the analytical model used, the same experimental data may report different fracture toughness values. In general, the combination of crack propagation in directions parallel and perpendicular to the fibers makes the composite problem very difficult to analyze. Composites with well-aligned fibers are more susceptible to crack propagation parallel to the fibers than perpendicular and can be analyzed with a reasonable degree of accuracy by using the existing KC or SC-theory in fracture mechanics. ABA (author).



72/00/00 73A25813

**FRACTURE MECHANICS FOR CORROSION FATIGUE**

McClintock, F.A.

(MIT, Cambridge, Mas.)

In *Corrosion Fatigue Chemistry, Mechanics and Microstructure; Proceedings of the International Conference*, Storrs, Conn., June 14-18, 1971. (A73-25801 11-17) Houston, Tex., National Association of Corrosion Engineers, 1972, p.289-301; Discussion, p.301, 302.

The stress and displacement fields that correspond to a given stress intensity factor are analyzed, and methods of determining the stress intensity factor for bodies of various shape under various loads are examined. The concepts of the opening displacement and the opening angle at the crack tip are introduced which are relevant to the initiation of growth from a preexisting crack or to crack propagation in the rigid plastic regime. Such characterizations of the stress and displacement fields around a growing corrosion fatigue crack are useful for correlating crack growth rates under test and service conditions. They do not, however, describe the essentially plastic surroundings that are seen by the chemical and dislocation processes on an even finer scale. The nature of a fracture criterion that would serve as an internal boundary condition for an elastic plastic continuum solution is studied on the basis of some fully plastic solutions. The quantitative determination of such a fracture criterion is examined. ABA V.P.

73/02/00 73A23251

**FRACTURE MECHANICS OF BRITTLE MATRIX DUCTILE FIBER COMPOSITES**

Tardiff, G., Jr

(California, University, Livermore, Calif.)

Engineering Fracture Mechanics, Vol.5, Feb. 1973, p.1-10. AEC-sponsored research.

A model to predict the increase in critical flaw size or stable crack growth potential which can occur by the inclusion of ductile fibers in a brittle matrix is considered. The model is based upon the superposition of two known stress intensity solutions; one for the crack opening mode resulting from a remotely applied stress and the second, an opposing stress intensity that results from a crack closing force exerted by unbroken fibers spanning the crack surfaces. The extent of stable growth possible is computed at the ultimate stress of the brittle phase as functions of fiber strength and of volume fraction for various amounts of fiber rupture. A hot pressed beryllium matrix is used as an example. The crack surface displacement over which a given fiber is capable of deforming without rupture is found to be sensitive to the fiber-matrix interface strength. ABA (author).

AD-A046280 NOR-77-41-Vol-1 AFFDL-TR-77-31-Vol-1 77/06/00 78N15513

**CHARACTERIZATION OF FATIGUE CRACK GROWTH IN BONDED STRUCTURES. VOLUME 1: CRACK GROWTH PREDICTION IN BONDED STRUCTURES**

Ratwani, M.M.

Northrop Corp., Hawthorne, Calif. (Aircraft Div.)

This is the first of two volumes that present methods for solving crack problems in the metallic elements of adhesively bonded structures. There are six major sections in the report that cover the following topics: (1) Methods of analysis, namely the finite element method and the integral equation method. Assumptions in the analysis and the influence of various parameters on the analytical results. (2) Criteria for the propagation of a debond. (3) Criterion for the crack transfer to a sound layer. (4) Verification test program. (5) Sensitivity of analysis to various parameters. (6) Limitations of the analysis. The stress intensity factors have been obtained for the geometries of: (1) a cracked sheet with an adhesively bonded stringer, and (2) a two-layer bonded structure with a center crack, an edge crack and a crack at a hole. The influence of finite boundaries, adhesive methods, debond size, and bending on stress intensity factors has been studied. Comparison has been made of actual crack growth life and that based on analytical stress intensity factors. The crack growth life has been predicted analytically within ten percent of actual life. The influence of adhesive and adherend materials and thicknesses on crack growth life has been studied. The predicted debond sizes have been compared with those observed experimentally. A criterion for the cracking of a sound layer, based on load transfer to a sound layer, has been developed. ABA author (GRA).

AD-A045877 AMMRC-MS-77-5 77/06/00 78N13482

**CASE STUDIES IN FRACTURE MECHANICS**

Rich, T.P.; Carwright, D.J.

Army Materials and Mechanics Research Center, Watertown, Mass.

A collection of more than thirty case studies is presented covering a wide range of practical engineering applications of fracture mechanics to design, inspection, maintenance, and failure analysis. The case studies are written by individual specialists within industry, government, and academia from the United States and Great Britain. The collection is divided into five sections corresponding to (1) aerospace, (2) joints and mountings, (3) pressure vessels and rotating machinery, (4) surface vehicles, and (5) materials. Most of the case studies are between twelve and fifteen pages in length and written to a standard format. The interdisciplinary nature of fracture applications is reflected in the case studies, and the reader is brought through a sequential development and solution of actual engineering problems in an interesting and economical manner. ABA author (GRA).



AD-A038936 NADC-76387-30 76/12/14 77N29231

## INVESTIGATION OF DAMAGE TOLERANCE OF GRAPHITE/EPOXY STRUCTURES AND RELATED DESIGN IMPLICATIONS

Adsit, N.R.; Waszczak, J.P.

General Dynamics/Convair, San Diego, Calif.

This investigation was undertaken to evaluate the damage tolerance of typical graphite/epoxy structure to service damage. AS/3501 graphite/epoxy I-stiffened panels and honeycomb panels were fabricated and its tolerance to low-velocity impacts was measured. Three impact threats were investigated; runway stones, a blunt impactor with a tip radius of 0.64 cm (1/4 inch), and a blunt impactor with a tip radius of 2.54 cm (1 inch). Impact parameters were selected that would just cause visual damage. This worked well for the runway stones, but for the tests of the one-inch penetrator on the honeycomb panels visual damage was not easily observed. C-scan damage was, however, easily detectable. Residual strength specimens were cut from the damaged panels and tested. The specimens contained damage at levels of 70, 100, 130% of the level to cause visual (or C-scan) damage. ABA GRA.

75/00/00 76N32582

## LINEAR ELASTIC FRACTURE MECHANICS AS AN AID IN JUDGING SERVICE FAILURES

Vonschuetz, W.

Industrieanlagen-Betriebsgesellschaft mbH, Ottobrunn (West Germany)

Requirements to be met by a crack propagation formula are discussed, and the Formann formula is advocated for crack propagation calculations. Examples of service failures are given in which the fracture mechanics approach was used successfully to judge the causes of failure and to prevent further failures. ABA author.

AD-A001609 SM-74-2 AFML-TR-74-111 74/04/00 75N19372

## EXPLORATORY DEVELOPMENT ON FRACTURE MECHANICS OF COMPOSITE MATERIALS

Cruse, T.A.; Osias, J.R.

Carnegie-Mellon Univ., Pittsburgh, Pa. (Dept of Mechanical Engineering.)

An extended experimental and analytical study of linear elastic fracture mechanics for graphite/epoxy advanced composite laminates is reported herein. The experimental program successfully addresses three topics: the existence of valid fracture toughness testing of composites; the hypothesis that angle-ply fracture strength is governed by fiber tensile strength; and, the fracture strengths of angle-ply laminates can be correlated on the basis of a critical strain energy release rate model. Two independent test specimen geometries are used to show that valid fracture strengths can be obtained, subject to discussed size constraints for specimen geometries. The analytical study makes use of a previously reported stress analysis method for crack tip stress intensity factors using a special form of the boundary-integral equation method. The problems of center notched tensile loaded plates with edge cracks emanating from the notch edges are analyzed in detail. A possible correlation of two strength models for notched laminates is reported. ABA GRA.

74/01/00 74N23442

## AN ANALYSIS OF TEST FATIGUE FAILURE BY FRACTOGRAPHY AND FRACTURE MECHANICS

Peel, C.J.

Royal Aircraft Establishment, Farnborough (England)

In AGARD Fracture Mechanics of Aircraft Structures, p.503-508 (see N74-23413 14-32).

The fracture surfaces of two fatigue cracks, that had caused the failure of an engine impeller during a fatigue substantiation test, were examined by electron microscopy to find the number of fatigue crack growth cycles. This was done by measuring the spacings of fatigue striations on the fracture surface as a function of crack depth and by subsequent integration of the striation spacing versus crack depth expression. The measured striation spacings were compared with laboratory crack growth data to determine the fatigue stress intensity range as a function of crack depth and hence the fatigue stress range. The number of crack initiation cycles was then found by comparing the fatigue stress range and number of crack growth cycles with further laboratory data and the total fatigue life was calculated to have been approximately 50,000 cycles. This identified the fatigue loading that had caused the failure as having been the 29179 cycles of engine acceleration and deceleration that had been applied during the test. ABA author.

NASA-CR-124469 73/05/31 74N10835

## EVALUATION OF STRESS CORROSION CRACKING SUSCEPTIBILITY USING FRACTURE MECHANICS TECHNIQUES, PART I

Sprowls, D.O.; Shumaker, M.B.; Walsh, J.D.; Coursen, J.W.

Aluminum Co. of America, Pittsburgh, Pa.

Stress corrosion cracking (SSC) tests were performed on 13 aluminum alloys, 13 precipitation hardening stainless steels, and two titanium 6Al-4V alloy forgings to compare fracture mechanics techniques with the conventional smooth specimen procedures. Commercially fabricated plate and rolled or forged bars 2 to 2.5 in thick were tested. Exposures were conducted outdoors in a seacoast atmosphere and in an inland industrial atmosphere to relate the accelerated tests with service type environments. With the fracture mechanics technique tests were made chiefly on bolt loaded fatigue precracked compact tension specimens of the type used for plane-strain fracture toughness tests. Additional tests of the aluminum alloy were performed on ring loaded compact tension specimens and on bolt loaded double cantilever beams.

For the smooth specimen procedure 0.125-in dia. tensile specimens were loaded axially in constant deformation type frames. For both aluminum and steel alloys comparative SCC growth rates obtained from tests of precracked specimens provide an additional useful characterization of the SCC behavior of an alloy. ABA author.

## CATEGORY H - FRACTURE CONTROL

77/00/00 77A37645

## ADVANCED NONDESTRUCTIVE INSPECTION TECHNIQUES AS APPLIED TO FRACTURE MECHANICS DESIGN FOR TURBINE ENGINE COMPONENTS

Packman, P.F.

(Vanderbilt University, Nashville, Tenn.)

In *Fatigue Life Technology*; Proceedings of the symposium, Philadelphia, Pa., March 27-31, 1977. (A77-37638 17-07) New York, American Society of Mechanical Engineers, 1977, p.95-116.

The reliability of nondestructive testing techniques in detecting microdefects in gas turbine engine components is examined with particular reference to four techniques which have demonstrated high detection potential. These are high resolution eddy current bolt hole scans; the KET radioactive gas penetrant system; adoptive learning techniques applied to ultrasonics; and acoustic emission flaw characterization. The advantages and drawbacks of each technique are noted. A nondestructive inspection transfer function is proposed which can be used to translate reliability data from simple to complex shapes, thus minimizing the need for expensive demonstration programs on complex shapes. ABA V.P.

74/00/00 75A18202

## FRACTURE MECHANICS EVALUATION METHODICS FOR MAGNETIC PARTICLE INSPECTION AND PENETRATION TESTING

Richter, H.-U.; Ruehe, E.

(NEB Schwermaschinenbau, Magdeburg, East Germany)

In *Conference on Dimensioning and Strength Calculations, 5th and Congress on Material Testing, 6th*, Budapest, Hungary, October 28-November 1, 1974, Proceedings. Volume 1. (A75-18192 06-39) Budapest, Akademiai Kiado, 1974, p.1-459 to 1-469.

Approaches for the comprehensive evaluation of the fracturing properties of a structural component are considered, giving attention to the establishment of acceptable and unacceptable crack parameters. Most of the factors involved can be quantitatively assessed by using the methods of fracture mechanics. The evaluation pattern is considered, taking into account design data, crack size, crack density, and the type of defect. A defect classification scheme can provide the basis for a decision concerning the acceptability of the specimen. ABA GRA.

AIAA Paper 72-383 73/11/00 74A15968

## FRACTURE MECHANICS APPLICATIONS IN MATERIALS SELECTION, FABRICATION SEQUENCING AND INSPECTION

Krupp, W.E.; Hoepfner, D.W.

(Lockheed-California Co., Burbank, Calif.)

(AIAA, ASME, and SAE, Structures, Structural Dynamics, and Materials Conference, 13th, San Antonio, Tex., Apr. 10-12, 1972, AIAA) *Journal of Aircraft*, Vol.10, Nov. 1973, p.682-688.

Description of the use of fracture mechanics concepts in quantitative comparisons of the effects of various alternatives involved in the design, manufacture, assembly, and quality assurance of critical parts and, in particular, of fracture-critical aircraft components. Specific examples are presented for illustration. ABA M.V.E.

74/01/00 74N23437

## NONDESTRUCTIVE TESTING (NDT) AND FRACTURE MECHANICS

Bolis, E.

Aeritalia SPA, Torino (Italy)

In *AGARD Fracture Mechanics of Aircraft Structures*, p.413-417 (see N74-23413 14-32)

The basic concepts of nondestructive testing (NDT) are reviewed in relationship with fracture mechanics concepts. The necessity of correlating basic differences between ordinary destructive mechanical tests and NDT is considered. The use of NDT for assessment of integrity of aircraft components and structures, after fabrication and during service life is discussed. Inherent limitations of NDT and necessity of interdepartmental team work are reviewed. General information on routine and advanced methods is included. ABA author.

74/01/00 74N23418

## BASIC CONCEPTS IN FRACTURE MECHANICS

Eftis, J.; Jones, D.L.; Liebowitz, H.

George Washington Univ., Washington, D.C.

In *AGARD Fracture Mechanics of Aircraft Structures*, p.32-73 (see N74-23413 14-32)

A review of fracture mechanics is presented highlighting the strengths and limitations and establishing some perspective of its relationship to the general fracture process. The importance of nondestructive inspection as one of several potential safeguards against failure by fracture is stressed. The subjects discussed include: (1) macroscopic classification of fracture, (2) linear elastic fracture mechanics, (3) fracture toughness in semibrittle fracture, (4) applications of fracture mechanics concepts, and (5) fatigue crack growth characteristics. ABA author.



NASA-TN-D-7483 E-7570 73/11/00 74N12187

FLIGHT MONITOR FOR JET ENGINE DISK CRACKS AND THE USE OF CRITICAL LENGTH CRITERION OF FRACTURE MECHANICS

Barranger, J.P.

National Aeronautics and Space Administration. Lewis Research Center, Cleveland, Ohio.

A disk crack detector is discussed which is intended to operate under flight conditions. It monitors the disk rim for surface cracks emanating from the blade root interface. An eddy current type sensor, with a remotely located capacitance/conductance bridge and signal analyzer, can reliably detect a simulated crack 3 mm long. The sensor was tested on a spinning turbine disk at 540°C. Tests indicate that the system is useful at disk rim velocities of 460 m/sec by using fracture mechanics, it is shown for INCONEL 718 that a crack operating under a rim stress of  $34 \times 10^7 \text{ N/m}^2$  has a critical length of 18 mm. ABA author.



REPORT DOCUMENTATION PAGE												
1. Recipient's Reference	2. Originator's Reference	3. Further Reference	4. Security Classification of Document									
	AGARD-LS-97	ISBN 92-835-1294-4	UNCLASSIFIED									
5. Originator	Advisory Group for Aerospace Research and Development North Atlantic Treaty Organization 7 rue Ancelle, 92200 Neuilly sur Seine, France											
6. Title	FRACTURE MECHANICS DESIGN METHODOLOGY											
7. Presented	on 5-6 October, 1978 in Delft, The Netherlands, 9-10 October, 1978 in München, Germany, and 12-13 October, 1978 in Sacavem, Portugal.											
8. Author(s)	Various		9. Date January 1979									
10. Author's Address	Various		11. Pages 248									
12. Distribution Statement	This document is distributed in accordance with AGARD policies and regulations, which are outlined on the Outside Back Covers of all AGARD publications											
13. Keywords/Descriptors	<table border="0"> <tr> <td>Fracture mechanics</td> <td>Cracking (fracturing)</td> <td>Strains</td> </tr> <tr> <td>Damage</td> <td>Crack propagation</td> <td>Aircraft</td> </tr> <tr> <td>Design criteria</td> <td>Stresses</td> <td></td> </tr> </table>			Fracture mechanics	Cracking (fracturing)	Strains	Damage	Crack propagation	Aircraft	Design criteria	Stresses	
Fracture mechanics	Cracking (fracturing)	Strains										
Damage	Crack propagation	Aircraft										
Design criteria	Stresses											
14. Abstract	<p>This Lecture Series deals with three related subjects, namely the principles of fracture mechanics, damage tolerance analysis, and damage tolerance design. The first starts with an introduction to the subject and then reviews the criteria for slow crack and fast fracture; discusses fracture toughness data for plane strain and stress; and presents ways of evaluating and using <math>da/dN</math> data. The second deals with stress-intensity analysis of complex structures, techniques for appraising stress-intensity factors, and damage-tolerance analysis of actual aircraft components (forgings, joints, etc). Finally, under damage tolerance design, an evaluation is made of the accuracy of residual strength and crack-growth predictions (from experiments and computations), and consideration given to the subject of safety factors and definition of damage-tolerance requirements.</p> <p>The material in this publication was assembled to support a Lecture Series under the sponsorship of the Structures and Materials Panel and the Consultant and Exchange Programme of AGARD.</p>											

<p>AGARD Lecture Series No.97 Advisory Group for Aerospace Research and Development, NATO FRACTURE MECHANICS DESIGN METHODOLOGY Published January 1979 248 pages, including Bibliography of 117 items</p> <p>This Lecture Series deals with three related subjects, namely the principles of fracture mechanics, damage tolerance analysis, and damage tolerance design. The first starts with an introduction to the subject and then reviews the criteria for slow crack and fast fracture; discusses fracture toughness data for plane strain and stress; and presents ways of evaluating and using <math>da/dN</math> data. The second deals with stress-intensity analysis of complex structures, techniques for appraising</p> <p>P.T.O.</p>	<p>AGARD-LS-97</p> <p>Fracture mechanics Damage Design criteria Cracking (fracturing) Crack propagation Stresses Strains Aircraft</p>	<p>AGARD Lecture Series No.97 Advisory Group for Aerospace Research and Development, NATO FRACTURE MECHANICS DESIGN METHODOLOGY Published January 1979 248 pages, including Bibliography of 117 items</p> <p>This Lecture Series deals with three related subjects, namely the principles of fracture mechanics, damage tolerance analysis, and damage tolerance design. The first starts with an introduction to the subject and then reviews the criteria for slow crack and fast fracture; discusses fracture toughness data for plane strain and stress; and presents ways of evaluating and using <math>da/dN</math> data. The second deals with stress-intensity analysis of complex structures, techniques for appraising</p> <p>P.T.O.</p>	<p>AGARD-LS-97</p> <p>Fracture mechanics Damage Design criteria Cracking (fracturing) Crack propagation Stresses Strains Aircraft</p>
<p>AGARD Lecture Series No.97 Advisory Group for Aerospace Research and Development, NATO FRACTURE MECHANICS DESIGN METHODOLOGY Published January 1979 248 pages, including Bibliography of 117 items</p> <p>This Lecture Series deals with three related subjects, namely the principles of fracture mechanics, damage tolerance analysis, and damage tolerance design. The first starts with an introduction to the subject and then reviews the criteria for slow crack and fast fracture; discusses fracture toughness data for plane strain and stress; and presents ways of evaluating and using <math>da/dN</math> data. The second deals with stress-intensity analysis of complex structures, techniques for appraising</p> <p>P.T.O.</p>	<p>AGARD-LS-97</p> <p>Fracture mechanics Damage Design criteria Cracking (fracturing) Crack propagation Stresses Strains Aircraft</p>	<p>AGARD Lecture Series No.97 Advisory Group for Aerospace Research and Development, NATO FRACTURE MECHANICS DESIGN METHODOLOGY Published January 1979 248 pages, including Bibliography of 117 items</p> <p>This Lecture Series deals with three related subjects, namely the principles of fracture mechanics, damage tolerance analysis, and damage tolerance design. The first starts with an introduction to the subject and then reviews the criteria for slow crack and fast fracture; discusses fracture toughness data for plane strain and stress; and presents ways of evaluating and using <math>da/dN</math> data. The second deals with stress-intensity analysis of complex structures, techniques for appraising</p> <p>P.T.O.</p>	<p>AGARD-LS-97</p> <p>Fracture mechanics Damage Design criteria Cracking (fracturing) Crack propagation Stresses Strains Aircraft</p>

<p>stress-intensity factors, and damage-tolerance analysis of actual aircraft components (forgings, joints, etc). Finally, under damage tolerance design, an evaluation is made of the accuracy of residual strength and crack-growth predictions (from experiments and computations), and consideration given to the subject of safety factors and definition of damage-tolerance requirements.</p> <p>The material in this publication was assembled to support a Lecture Series under the sponsorship of the Structures and Materials Panel and the Consultant and Exchange Programme of AGARD, presented on 5-6 October, 1978 in Delft, The Netherlands, 9-10 October, 1978 in München, Germany, and 12-13 October, 1978 in Sacavem, Portugal.</p> <p>ISBN 92-835-1294-4</p>	<p>stress-intensity factors, and damage-tolerance analysis of actual aircraft components (forgings, joints, etc). Finally, under damage tolerance design, an evaluation is made of the accuracy of residual strength and crack-growth predictions (from experiments and computations), and consideration given to the subject of safety factors and definition of damage-tolerance requirements.</p> <p>The material in this publication was assembled to support a Lecture Series under the sponsorship of the Structures and Materials Panel and the Consultant and Exchange Programme of AGARD, presented on 5-6 October, 1978 in Delft, The Netherlands, 9-10 October, 1978 in München, Germany, and 12-13 October, 1978 in Sacavem, Portugal.</p> <p>ISBN 92-835-1294-4</p>
<p>stress-intensity factors, and damage-tolerance analysis of actual aircraft components (forgings, joints, etc). Finally, under damage tolerance design, an evaluation is made of the accuracy of residual strength and crack-growth predictions (from experiments and computations), and consideration given to the subject of safety factors and definition of damage-tolerance requirements.</p> <p>The material in this publication was assembled to support a Lecture Series under the sponsorship of the Structures and Materials Panel and the Consultant and Exchange Programme of AGARD, presented on 5-6 October, 1978 in Delft, The Netherlands, 9-10 October, 1978 in München, Germany, and 12-13 October, 1978 in Sacavem, Portugal.</p> <p>ISBN 92-835-1294-4</p>	<p>stress-intensity factors, and damage-tolerance analysis of actual aircraft components (forgings, joints, etc). Finally, under damage tolerance design, an evaluation is made of the accuracy of residual strength and crack-growth predictions (from experiments and computations), and consideration given to the subject of safety factors and definition of damage-tolerance requirements.</p> <p>The material in this publication was assembled to support a Lecture Series under the sponsorship of the Structures and Materials Panel and the Consultant and Exchange Programme of AGARD, presented on 5-6 October, 1978 in Delft, The Netherlands, 9-10 October, 1978 in München, Germany, and 12-13 October, 1978 in Sacavem, Portugal.</p> <p>ISBN 92-835-1294-4</p>



**AGARD**

NATO  OTAN

7 RUE ANCELLE · 92200 NEUILLY-SUR-SEINE  
FRANCE

Telephone 745.08.10 · Telex 610176

**DISTRIBUTION OF UNCLASSIFIED  
AGARD PUBLICATIONS**

AGARD does NOT hold stocks of AGARD publications at the above address for general distribution. Initial distribution of AGARD publications is made to AGARD Member Nations through the following National Distribution Centres. Further copies are sometimes available from these Centres, but if not may be purchased in Microfiche or Photocopy form from the Purchase Agencies listed below.

NATIONAL DISTRIBUTION CENTRES

**BELGIUM**

Coordonnateur AGARD – VSL  
Etat-Major de la Force Aérienne  
Quartier Reine Elisabeth  
Rue d'Evere, 1140 Bruxelles

**CANADA**

Defence Scientific Information Service  
Department of National Defence  
Ottawa, Ontario K1A 0Z2

**DENMARK**

Danish Defence Research Board  
Østerbrogades Kaserne  
Copenhagen Ø

**FRANCE**

O.N.E.R.A. (Direction)  
29 Avenue de la Division Leclerc  
92 Châtillon sous Bagneux

**GERMANY**

Zentralstelle für Luft- und Raumfahrt-  
dokumentation und -information  
c/o Fachinformationszentrum Energie,  
Physik, Mathematik GmbH  
Kernforschungszentrum  
7514 Eggenstein-Leopoldshafen 2

**GREECE**

Hellenic Air Force General Staff  
Research and Development Directorate  
Holargos, Athens, Greece

**ICELAND**

Director of Aviation  
c/o Flugrad  
Reykjavik

**UNITED STATES**

National Aeronautics and Space Administration (NASA)  
Langley Field, Virginia 23365  
Attn: Report Distribution and Storage Unit

THE UNITED STATES NATIONAL DISTRIBUTION CENTRE (NASA) DOES NOT HOLD  
STOCKS OF AGARD PUBLICATIONS, AND APPLICATIONS FOR COPIES SHOULD BE MADE  
DIRECT TO THE NATIONAL TECHNICAL INFORMATION SERVICE (NTIS) AT THE ADDRESS BELOW.

**ITALY**

Aeronautica Militare  
Ufficio del Delegato Nazionale all'AGARD  
3, Piazzale Adenauer  
Roma/EUR

**LUXEMBOURG**

See Belgium

**NETHERLANDS**

Netherlands Delegation to AGARD  
National Aerospace Laboratory, NLR  
P.O. Box 126  
Delft

**NORWAY**

Norwegian Defence Research Establishment  
Main Library  
P.O. Box 25  
N-2007 Kjeller

**PORTUGAL**

Direcção do Serviço de Material  
da Força Aérea  
Rua da Escola Politécnica 42  
Lisboa  
Attn: AGARD National Delegate

**TURKEY**

Department of Research and Development (ARGE)  
Ministry of National Defence, Ankara

**UNITED KINGDOM**

Defence Research Information Centre  
Station Square House  
St. Mary Cray  
Orpington, Kent BR5 3RE

PURCHASE AGENCIES

*Microfiche or Photocopy*

National Technical  
Information Service (NTIS)  
5285 Port Royal Road  
Springfield  
Virginia 22161, USA

*Microfiche*

Space Documentation Service  
European Space Agency  
10, rue Mario Nikis  
75015 Paris, France

*Microfiche*

Technology Reports  
Centre (DTI)  
Station Square House  
St. Mary Cray  
Orpington, Kent BR5 3RF  
England

Requests for microfiche or photocopies of AGARD documents should include the AGARD serial number, title, author or editor, and publication date. Requests to NTIS should include the NASA accession report number. Full bibliographical references and abstracts of AGARD publications are given in the following journals:

Scientific and Technical Aerospace Reports (STAR)  
published by NASA Scientific and Technical  
Information Facility  
Post Office Box 8757  
Baltimore/Washington International Airport  
Maryland 21240, USA

Government Reports Announcements (GRA)  
published by the National Technical  
Information Services, Springfield  
Virginia 22161, USA

